IDENTIFICATION OF THE CELLULAR ORIGIN AND "STEMNESS" PHENOTYPE OF MALIGNANT RHABDOID TUMOURS (MRT) MAY REPRESENT A NEW THERAPEUTIC APPROACH IN PAEDIATRIC ONCOLOGY

RAS AZIRA BINTI RAMLI

NORTHERN INSTITUTE FOR CANCER RESEARCH

NEWCASTLE UNIVERSITY

IDENTIFICATION OF THE CELLULAR ORIGIN AND "STEMNESS" PHENOTYPE OF MALIGNANT RHABDOID TUMOURS (MRT) MAY REPRESENT A NEW THERAPEUTIC APPROACH IN PAEDIATRIC ONCOLOGY

RAS AZIRA BINTI RAMLI

Thesis submitted in partial fulfilment of the requirements for the degree of Doctor of Philosophy

NORTHERN INSTITUTE FOR CANCER RESEARCH

SCHOOL FOR MEDICAL SCIENCES

NEWCASTLE UNIVERSITY

JUNE 2018

Abstract

Introduction: Malignant Rhabdoid Tumours (MRT) are especially lethal cancers that predominantly occur in infants and young children. MRT are caused by biallelic inactivation of a single gene; *SMARCB1* which is a component of SWI/SNF chromatin remodelling complex. The tumours can be found almost everywhere in the body and the cell of origin for MRT is still unknown. Expression profiling of primary MRT demonstrates strong overexpression of a large number of stemness/self-renewal genes (PBTG, unpublished). Previous studies have shown that expression of these genes are deregulated by *SMARCB1* and/or larger SWI/SNF complex. Therefore, this project was aimed to uncover the potential cell of origin and to examine if expression of self-renewal genes could potentially contribute towards disease aggressiveness. The understanding of other mechanisms involved in MRT tumourigenesis is essential to identify therapeutic targets that can improve the outcomes of MRT patients.

Methods: I performed a meta-analysis cross-referencing expression profiles from primary MRT (n= 119), and functional models in which *SMARCB1* was re-expressed (n=5 lines) with expression profiles from multiple candidate stem cell types including epithelial, embryonal, neural, mesenchymal and neural crest (n= 446). I developed a lentiviral CRISPR/Cas9 system to efficiently model *Smarcb1* mutation in primary candidate cells of origin *ex vivo*. To understand how *SMARCB1* loss is capable of hijacking active stemness/self-renewal machinery to initiate MRT tumourigenesis, an integrated data analysis was performed to identify stemness/self-renewal genes whose expression are *SMARCB1*-dependent, by cross-referencing a manually curated stemness/self-renewal gene list with existing RNA-seq data from primary MRT and MRT cell lines with and without re-expression of *SMARCB1* and with CRISPR/Cas9 genome-wide screening data from MRT cells with and without re-expression of *SMARCB1*. Finally, the expression of stemness/self-renewal genes and their relevance as a therapeutic target in MRT, specifically the protein BMI1, was studied using shRNA and a small molecular inhibitor.

Results: Bioinformatic analysis of potential cells of origin suggests three putative candidate cell populations within the family of neural crest (NC), neural progenitor and mesenchymal stem cells. The extent of transcriptional overlap clearly reflects differences in tumour location and molecular subgroup. Unlike most cells tested, early neural crest (NC) cells tolerated *Smarcb1* mutation and conferred proliferative advantage resembling human MRT molecularly and immunophenotypically. From my integrated bioinformatic analysis of self-renewal/stemness, *BMI1* was identified as a functional *SMARCB1*-dependent gene. Here, I show that targeted disruption of BMI1 by shRNA or pharmacologic inhibition using PTC209 strongly impairs MRT cell growth, suppresses tumour cell self-renewal, induces apoptosis and senescence. Using functional gene expression analysis, I found that *BMI1* knockdown in MRT cells transcriptionally activates critical genes in MRT such as *p21*, *p16* and *CD44*.

Conclusion: Our findings suggest NC cells as a potential cell of origin for MRT. I describe a system for ranking putative cells of origin and a practical means for inducing *Smarcb1* mutations *ex vivo*. Furthermore, I show evidence that subtypes within MRT have different cells of origin. Here, I also establish the role of *BMI1* in self-renewal and survival of MRT cells. In addition, I show that the effects of *BMI1* knockdown recapitulates the effect of *SMARCB1* re-expression in MRT cells, demonstrating an attractive therapeutic target for MRT.

Declaration

I certify that no part of the material documented in this thesis has previously been submitted for a degree or other qualification in this or any other university. I declare that this thesis represents my own unaided work, carried out by myself, except where it is acknowledged otherwise in the thesis text.

Ras Azira Ramli

June 2018

Acknowledgements

There have been many people who have walked alongside me during the last three years and this thesis becomes a reality with the kind support and help of many individuals. I would like to extend sincere thanks to all of them.

Foremost, I would like to express my sincere gratitude to my supervisors, Dr. Daniel Williamson and Professor Steven Clifford. Their continuous support and their extraordinary knowledge of paediatric cancer and bioinformatics have helped me immensely throughout my research. Thank you for giving me the opportunity to do this project. I would also like to thank my PhD assessors Professor Olaf Heidenreich and Dr. Michael Jackson for their constant guidance, advices and encouragement for the last three years.

My deepest appreciation is extended to Dr Martina Finetti and Dr Matthew Selby. I would never have been able to achieve what I have without your wisdom, support and guidance. Thank you for comforting me during the difficult times of my studies and thank you for believing in me. I would like to express my gratitude to everyone in Paediatric Brain Tumour Research Group, especially Dr Janet Lindsey, Magretta Adiamah, Emma Lishman and Dr Claire Keeling for their voluntary hours to help me polishing this thesis into something presentable. Also, I would like to especially thank Dr Steven Crossier for his tremendous help and guidance in immunohistochemistry. It was a great pleasure working with this team and I really appreciate their ideas, help, good humour and friendship. Special thanks go to all people at Sir James Spence Institute, Herschel and Paul O Gorman for their technical help and support.

My PhD study would not be possible without the financial support from Ministry of Higher Education, Malaysia and Newcastle University, UK. Finally, these acknowledgements would not complete without mentioning my backbone and biggest supporter. My deepest appreciation belongs to my parents and siblings. Without their encouragement I would not have made it.

Dedication

Dedicated

to my inspiring parents,

brother

and sisters,

for being the

pillows, role models, catapults,

cheerleading squad and sounding boards

I have needed.

"The only way to achieve the impossible is to believe it is possible."

-Charles Kingsleigh-

List of Abbreviations

µg	Microgram
µl	Microliter
3' UTR	Three Prime Untranslated Region
A	Adenine
Ab	Antibody
AML	Acute Myelogenous Leukaemia
ARID1A/ BAF250a	AT Rich Interactive Domain 1A (SWI-Like)
ATPase	Adenylpyrophosphatase
ATRT	Atypical Teratoid Rhabdoid Tumour
BAF155	BRG1-Associated Factor 155
BAF170	BRG1-Associated Factor 170
BMI1	BMI Polycomb Ring Finger Oncogene
BMP	Bone morphogenetic proteins
BP	Base Pair
BRAF	V-Raf Murine Sarcoma Viral Oncogene Homologue B1
CDKN1A	Cyclin Dependent Kinase Inhibitor 1A
CDKN2A	Cyclin-Dependent Kinase Inhibitor 2A
cDNA	Complementary DNA
ChIP	Chromatin immumoprecitiation
ChIP	Chromatin Immunoprecipitation
ChIP-seq	Chromatin Immunoprecipitation Sequencing
CNAs	Copy-Number Aberrations
CNN	Copy Number Neutral
CNS	Central Nervous System
Conc	Concentration
CpG	Cytosine-Guanine Dinucleotide
CRISPR	Clustered Regularly Interspaced Short Palindromic Repeats
DMSO	Dimethyl Sulfoxide
dNTPs	Nucleoside Triphosphates Containing Deoxyribose

E. coli	Escherichia Coli
EB	Embroid bodies
ECRT	Extra Cranial Rhabdoid Tumours
EGFR	Epidermal Growth Factor Receptor
ES	Enrichment Score
ESC	Embryonic Stem
EWS	Ewing Sarcoma Breakpoint Region 1
EZH2	Enhancer Of Zeste Homolog 2
FACS	Fluorescent Activated Cell Sorting
FITC	Fluorescein-5-isothiocyanate
Fwd	Forward
g	G-Force
GAPDH	Glyceraldehyde-3-Phosphate Dehydrogenase
GC%	Guanine-Cytosine Content
gDNA	Genomic DNA
GeCKO	Genome-scale CRISPR Knock Out
GEO	Gene Expression Omnibus
GFAP	Glial Fibrillary Acidic Protein
GFP	Green Fluorescent Protein
GLI1	GLI Family Zinc Finger 1
GLI2	GLI Family Zinc Finger 2
GLI2	GLI Family Zinc Finger 2
GLI3	GLI Family Zinc Finger 3
GO	Gene Ontology
GSEA	Gene set enrichment analysis
GSEA	Gene Set Enrichment Analysis
Gy	Gray (Unit)
H&E	Hematoxylin and eosin
H2O	Dihydrogen Monoxide
H3	Histone 3
H3K27me3	Histone 3 Lysine 27 Trimethylation
H3K36me3	Histone 3 Lysine 36 Trimethylation

H3K4me3	Histone 3 Lysine 4 Trimethylation
HATs	Histone Acetyltransferases
HD-SCR	High dose chemotherapy-Stem cell rescue
HDACs	Histone Deacetylase
Hh	Hedgehog
IgG	Immunoglobulin G
IHC	Immunohistochemistry
IMDM	Iscove's Modified Dulbecco's Media
InDel	Insertion-Deletion
INO80	Inositol Requiring 80
IP	Immunoprecipitation
IPA	Ingenuity pathway analysis
iPSC	Induced Pluripotent Stem Cell
ISWI	Imitation Switching Defective
JARID2	Jumonji, AT Rich Interactive Domain 2,
KEGG	Kyoto Encyclopedia of Genes and Genomes
LDA	Limiting Dilution Assay
LOH	Loss of heterozygosity
MB	Medulloblastoma
MB	Medulloblastoma
$MgCl_2$	Magnesium Chloride
mM	MilliMolar
MOI	Multiplicity Of Infection
mRNA	Messenger RNA
MRT	Malignant Rhabdoid Tumours
MSC	Mesenchymal Stem Cell
mV	Millivolts
NaCl	Sodium Chloride
NB	Neuraoblastoma
NC	Neural crest
NGS	Next Generation Sequencing
NMB	Newcastle Medulloblastoma

NMF	Non-negative matrix factorisation
NPC	Neural Progenitor Cell
NSC	Neural Stem Cells
NTC	Non Targeting Control
OCT4	Octamer-Binding Transcription Factor 4
OS	Overall survival
PBTG	Paediatric Brain Tumour Group
PCA	Principal Component Analysis
PCDH	Pcdh-CMV-MCS-EF1-Puro
PcG	Polycomb Group Proteins
PcGs	Polycomb Group Proteins
PCR	Polymerase Chain Reaction
PI	Propidium Iodide
PNET	Primitive neuroectodermal tumour
Pol II	Rna Polymerase Ii
Pol III	Rna Polymerase Iii
PRC1	Polycomb Repressive Complex 1
PRC2	Polycomb Repressive Complex 2
q-PCR	Quantitative Polymerase Chain Reaction
Rev	Reverse
RFP	Red Fluorescent Protein
RNA	Ribonucleic Acid
rpm	Revolutions Per Minute
RPMI	Roswell Park Memorial Institute Medium
RT	Radiotherapy
RT	Reverse Transcriptase
RT-PCR	Reverse Transcriptase PCR
RTK	Rhabdoid Tumour of Kidney
RTPS	Rhabdoid tumour predisposition syndrome
SALL4	Spalt-Like Transcription Factor 4
SDS	Sodium Dodecyl Sulphate
sgRNA	Single Guide RNA

SHH	Sonic Hedgehog
shRNA	Short Hairpin RNA
SNP	Single nucleotide polymorphism
SOX2	SRY (Sex Determining Region Y)-Box 2
SWI/SNF	Switch/sucrose nonfermenting
t-SNE	t-distributed Stochastic Neighbor Embedding
TBP	TATA-Binding Protein
TBS-T	Tween 20 Tris-Buffered Saline
TE	Tris EDTA Buffer
Tm	Melting Temperature
TP53	Tumour Protein P53
TRIS	Tris (Hydroxymethyl) Aminomethane
TSM	TumourSphere completed Media
TSSs	Transcription Start Sites
Vol	Volume
vst	Variance Stabilising Transform
WHO	World Health Organisation
WT	Wild Type
WT1	Wilms Tumour 1
BLAST	Basic Local Alignment Search Tool
PTCH	Patched

Table of contents

List of Tables

List of Figures

Chapter 1 Introduction

1.1 Malignant Rhabdoid Tumours (MRT)

Malignant Rhabdoid Tumours (MRT) are one of the most aggressive paediatric cancers with a poor survival rate (Kato et al., 2003, Reinhard et al., 2008). The tumour was originally described in the kidney by The National Wilms Tumour study in 1978 as a rare rhabdomyosarcomatoid variant of Wilms' tumour (Grupenmacher et al., 2013, Tomlinson et al., 2005, Biegel et al., 2002b, Biegel, 2006). However, tumours with similar rhabdoid morphology were later found in other parts of body such as soft tissues and brain. MRT most commonly occur in the kidney designated as rhabdoid tumours of kidney (RTK) and central nervous system (CNS) termed as Atypical Teratoid/Rhabdoid Tumours (ATRT).

1.1.1 Atypical Teratoid/ Rhabdoid Tumour (ATRT)

Although ATRT was first described as MRT of the central nervous system in 1987, it was recognised as a distinct entity of primary brain and spinal tumours in 1996 (Rorke et al., 1996). This tumour possesses unique characteristic due to its complex immunophenotypes and multi-lineage differentiation potential (e.g neuronal, mesenchymal and glial). In most cases of ATRT, 50% of the tumours arise in the cerebellum or brain stem. Another 40% of ATRT can be found as a mass in the cerebral or suprasellar supratentorial regions.

1.1.1.1 Extracranial Rhabdoid Tumour (ECRT)

MRT that arise outside the brain such as liver, soft tissues, peripheral nerves and others are known as extracranial rhabdoid tumour (ECRT). Despite different anatomical sites and clinical behaviours to ATRT, ECRT is also characterised by biallelic mutation in *SMARCB1* (also known as *SNF5/INI1/BAF47,* hereafter referred to as *SMARCB1* in this thesis) and therefore are related entities. RTK was the first tumour classified as MRT. However, features of typical renal rhabdoid tumour were also found in liver and soft tissue of the chest wall in 1982 (Oda and Tsuneyoshi, 2006) paravertebral region in 1983 and in other soft tissues three years later. Since then, various tumours observed outside the renal which demonstrated similar morphology to RTK has been reported. ECRT can be further divided into renal and extra-renal rhabdoid tumour. This sub-classification is made

as renal tumour tends to develop at early onset and has the capacity to disseminate into the brain. Moreover, patients with ECRT are commonly linked to germline mutations and therefore at high risk of developing multiple primary MRT at different locations in the body.

1.1.1.2 Clinical histology

The histopathological hallmarks of MRT cells are large and round undifferentiated epithelial and mesenchymal cells with prominent nucleoli and eosinophilic cytoplasmic inclusions (Figure 1.1). MRT cells are highly proliferative and mitotic figures are often seen in the nucleus (Sredni and Tomita, 2015). The diagnosis of MRT can be quite difficult due to tumour heterogeneity and several anatomical locations. In contrast to RTK which can easily be identified, ATRT often demonstrates pleomorphic features and sometimes typical rhabdoid cells are either undetected or absent (Bourdeaut et al., 2008). MRT exhibit multiphenotype immune profiles with common expression of vimentin, cytokeratin and smooth muscle antigen (Sigauke et al., 2006).

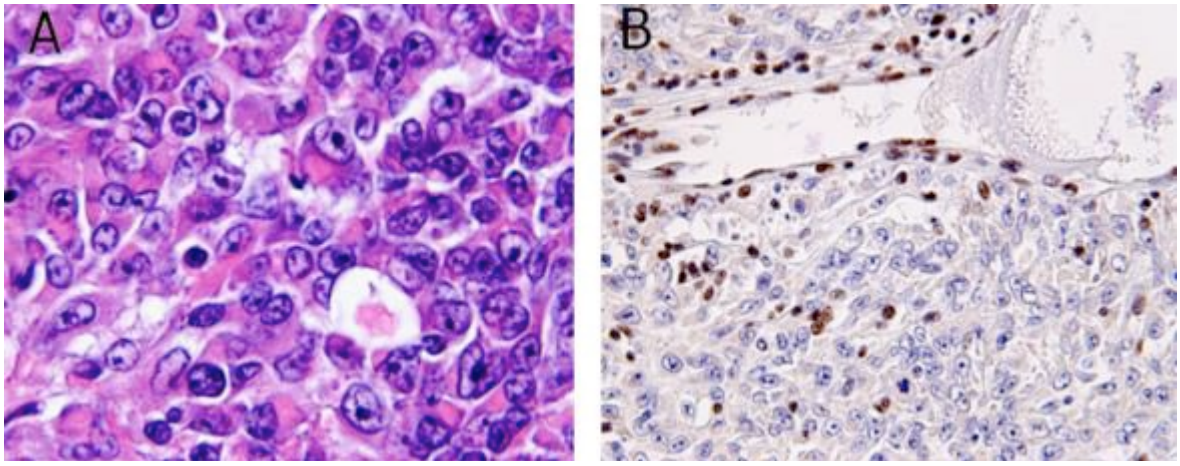

Figure 1.1 ***Immunohistochemistry of Atypical Teratoid/Rhabdoid Tumour*** *A) negative SMARCB1 staining B) SMARCB1 positive staining in endothelial and inflammatory cell. Pictures were taken from Sigauke et al. (2006).*

1.1.1.3 Embryonal central nervous system (CNS) tumours

Despite its unique and well-defined tumour biology, ATRT has been often misdiagnosed as other types of embryonal tumours such as Medulloblastoma (MB), primitive neuroectodermal tumour or choroid plexus carcinoma since the tumour can be found in similar regions of the CNS (Louis et al., 2007).

Embryonal tumours of CNS are the most common paediatric brain tumour characterised by various group of neoplasms in infants and young children less than 36 months of age (MacDonald, 2008). Each type of embryonal tumours is highly homogenous consisting of undifferentiated small round cells with multiple lineages arrangements and often with high mitotic turnover rate. The tumours are quite rare accounting for 3.3% of all brain tumours (McGovern et al., 2014). However, they represent around 15.7% and 4.3% of malignant brain tumours in children (ages 0-14) and adolescents (ages 15-19) respectively. In 2007, The World Health Organization (WHO) includes MB, supratentorial primitive neuroectodermal tumours (sPNETs) and ATRT into CNS classification based on lineage arrangements and location of the primary tumour (Louis et al., 2007). Advances in molecular profiling of these CNS neoplasms have enabled better understanding of the tumour entities especially ATRT which previously had been misdiagnosed as MB but it is now recognised as a distinct entity.

1.1.1.4 Incidence and epidemiology

MRT in infants and children were initially described as a distinct tumour in 1978, arising almost everywhere in the body with high prevalence in the kidney and brain (Venneti et al., 2011a). Regardless of the primary tumour location, the tumours are highly malignant with a tendency to metastasize early and have poor survival rates in comparison to other childhood tumours (Reinhard et al., 2008). The actual incidence in children and infants is yet to be determined due to lack of systematic diagnosis protocol which often associates with inaccurate diagnosis evaluation. However, discovery of genetic alterations that affect the *SMARCB1* locus on chromosome 22 as a leading cause of MRT has advanced the diagnosis accuracy and introduction of specific antibodies against *SMARCB1* (Ab No.612110, BD Transduction Laboratories, San Jose, Calif) offers a better clinical

management since then (Woehrer et al., 2010). It is evident in the population-based study conducted by Austrian Brain Tumour Registry where half of the ATRT was correctly diagnosed after the introduction of WHO classification of CNS neoplasms and prior to the use of antibody against *SMARCB1* in immunohistochemistry (IHC) diagnosis (Figure 1.2). Furthermore, recognised patients (with ATRT) showed better overall 5 years survival compared to unrecognised patients (p-value: 0.00469).

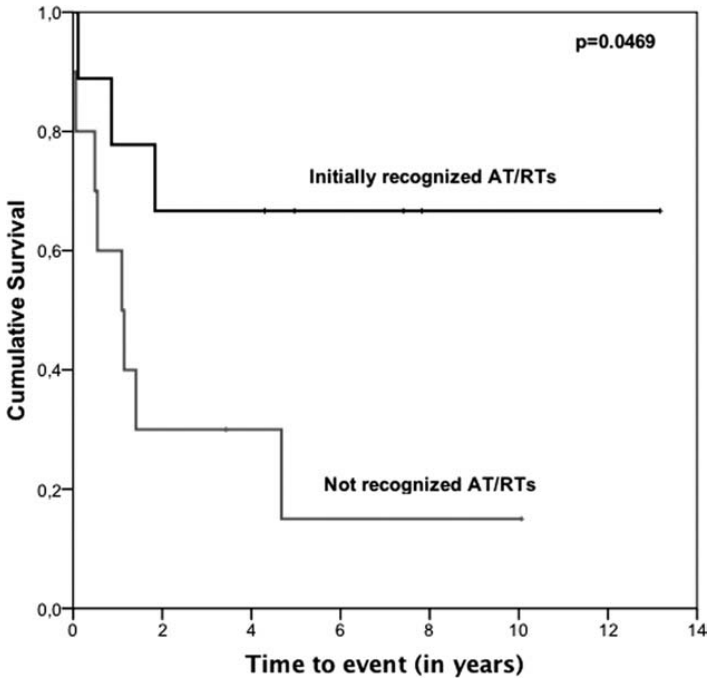

Figure 1.2 ***Kaplan-Meier survival curves of ATRT showing differences in survival of patients of initially recognised ATRT compared to misdiagnosed ATRT tumours before disease stratification using anti-SMARCB1 antibody.*** *The tumours wrongly classified as other types of CNS tumours i.e Medulloblastoma have led to inappropriate treatments to the patients. Consequently, the overall survival of misdiagnosed patients was significantly poor relative to initially recognised ATRT patients (p = 0.0469) (Picture was taken from (Woehrer et al., 2010).*

MRT occur most commonly in infants and young children. Report from Austrian Brain Tumour Registry (1996-2006) study illustrated ATRT as the sixth most common malignant brain tumours with an incidence rate of 1.38 per 1,000,000 person/years and peak incidence from birth to three years of age (median age between 12 and 24 months) with male predominance over female (Woehrer et al., 2010). Of 113 CNS tumours included in the Austrian Brain Tumour Registry, the incidence of ATRT of the brain reported in children aged below 3 years (17.3%) is almost comparable to MB (16%) and PNET (13.3%). Of note, this population-based study also reported low incidence of ATRT in other age groups. Another report from The Central Brain Tumour Registry of the United States also demonstrated the effect of age at time of diagnosis on incidence rate (Ostrom et al., 2014). According to this study, the highest cases were reported among children <1-year old and the rate of incidence decreased with increasing age. Similar to the report by Woehrer et al. (2010), the prevalence of ATRT was higher in children younger than 3 years accounting for 68.4% of all cases. Other studies of ATRT reported the median age at time of diagnosis between 1-3 years old (Lafay-Cousin et al., 2012, Panandiker et al., 2012). Categorization of children according to age of group at time of diagnosis suggests that ATRT occurs more predominantly in patients less than 3 years old (Figure 1.3). To date, only 31 cases of ATRT observed in adults have been reported in the literature (Buscariollo et al., 2012). Altogether, these studies demonstrated that ATRT is more prevalent in children aged 0-2 years old than in other age groups.

Similarly, the incidence of ECRT in children reported in the UK between 1993 and 2010 was five per 1,000,000 in the first year of life and the prevalence decreased in older age groups (Brennan et al., 2013a). Notably, the incidence rate varied depending on age and primary site of which the tumour was diagnosed (Table 1.1). The table shows that the most common tumour location for all age groups was kidney accounting for 51% of reported cases followed by 26% in other parts of bodies such as trunk and arms, 15% of the cases found in the head and neck and 14% of the cases found in liver. However, the incidence of tumours in infants (0-12 months) was higher compared to other age groups (2-4 years and 5-14 years). No cases were recorded in the liver for patients aged 2-14 years old. A comparable early-onset disease was also observed in an institution study in

South Korea which recorded a median age of 9 months of age for 11 patients with ECRT (Hong et al., 2015).

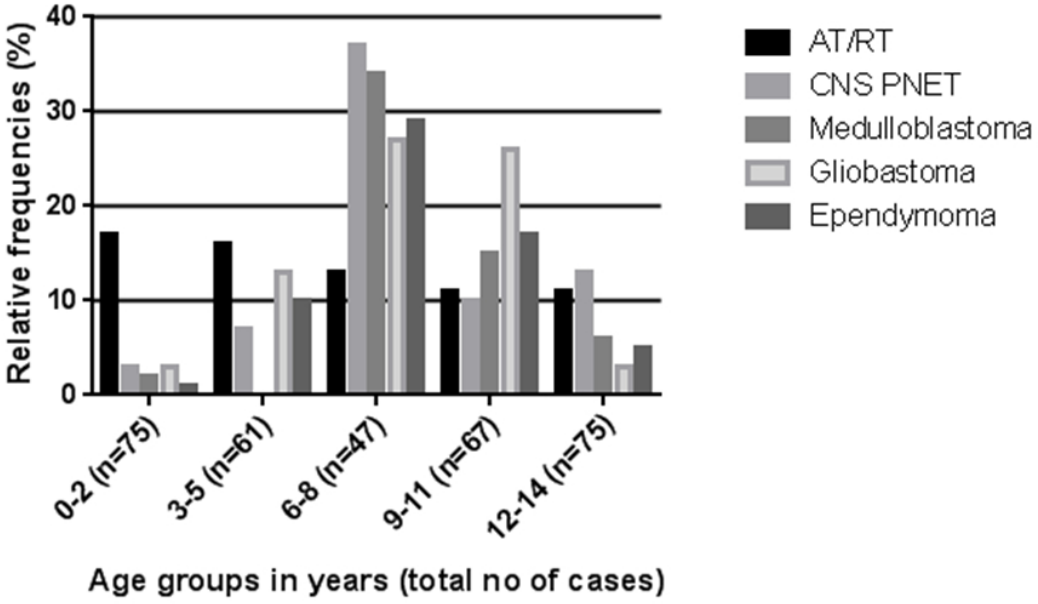

Figure 1.3 ***Population based study demonstrates relative incidence of the 6 most common malignant central nervous system (CNS) tumours in 5 different age groups****. ATRT represents Atypical Teratoid Rhabdoid Tumour where as PNET indicates primitive neuroectodermal tumour. ATRT presents a peak incidence between 0 and 3 years age group in comparison to other CNS tumour entities demonstrating early onset phenotype of disease. The graph was taken from Woehrer et al. (2010).*

Location	Age at diagnosis				Total
	0 years	1 years	2-4 years	5-14 years	
Kidney	33	8	8	2	51
Liver	11	3	0	0	14
Head and neck	7	0	6	2	15
Other	14	4	3	5	26*
Total	65	15	17	9	106

Table 1.1 ***Population based study showing distribution of extracranial rhabdoid tumours in 4 different age groups between 1993 and 2010 in United Kingdom.*** *The tumour locations reported in this study were kidney, liver, head and neck, and others which consist of arm/shoulder (five cases), thorax (nine cases), abdomen/pelvis (five cases), trunk not otherwise specified (four cases), omentum (one case), ovary (one case) and bladder (one case). Data was taken from the National Registry of Childhood Tumours. The table was adapted from (Brennan et al., 2013a).*

MRT are often described as extremely aggressive childhood cancers and show only a little evidence of improving survival rate at presentation (Figure 1.4). The survival analysis of MRT patients indicates that age at time of diagnosis is the prognostic factor. A study by Tomlinson et al. (2005) demonstrated strong correlation of improved OS with increase in age of diagnosis partly due to limitations in treatment received by younger and infant patients. In line with this, analysis of the data collected from SEER program showed the younger patients (0-24 months) have poor prognosis compared to older patients (>18 years old) (Sultan et al., 2010). Similarly, a UK based population study reported worse prognosis in younger patients (0-12 months) than did the patients aged 1 year or older.

	Tomlinson et al., 2005	Hilden et al., 2004	Tekautz et al., 2005	Kodet et al., 1991	Fanburg-Smith et al., 1998
Location	Kidney	Brain	Brain	Soft parts	Soft parts
Number of patients	n = 142	n = 42	n = 31	n = 26	n = 18
Median age at diagnosis	10 months	24 months	12 months	9 months	13 years
Overall survival	23%	16.75%	89% pts >3 years, 17 pts <3 years	5/26 pts	4/11 pts

Table 1.2 ***Clinical presentation of MRT found in various part of the body reported from published studies.*** *Clinical presentation of MRT found in various parts of the body reported from published studies. The overall survival is less than 25% in infants (10 months) and young patients (24 months). This table was adapted from Bourdeaut et al. (2008).*

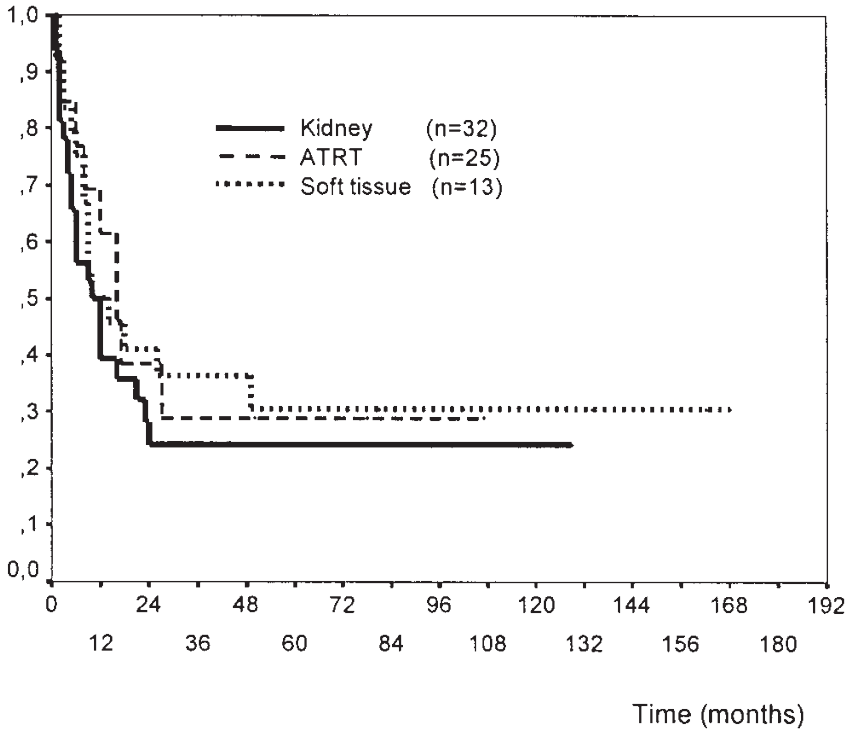

Figure 1.4 ***Kaplan-Meier curves illustrate the overall survival (OS) of patients with MRT, stratified by tumour locations.*** *In general, there is no significant difference in OS between RTK, ATRT and soft tissues (p= 0.64) (Reinhard et al., 2008).*

1.1.1.5 Survival

The factors associated with a poor prognosis in MRT are metastatic disease at time of diagnosis and younger age. Analysis of data from National Cancer Institute (NCI) Surveillance, Epidemiology, and End Results (SEER) showed disease prognosis is poor. The database was utilised to identify 144 patients with ATRT from 1973 to 2008. Overall median survival (OS) for an ATRT cohort was 10 months from time of diagnosis and the year of diagnosis had no effect on survival (Buscariollo et al., 2012). In addition, patients diagnosed as metastatic suffered with remarkably shorter median OS (3 months) relative to patients with focal disease at the time of diagnosis (13 months). Another population-based study from the German HIT database from 1998-2004 demonstrated patients with

77% of patients with ATRT died of disease with 13±5% of 3 years event-free survival (EFS) and 22±6% of the overall survival (OS) (von Hoff et al., 2011). In addition to this, retrospective review from The Hospital for Sick Children showed the median survival of 143 cases reported from 1995 to 2007 was 17.3 months (Athale et al., 2009).

1.1.1.6 Clinical management of MRT and treatment response

Disease management for patients with MRT includes initial therapy for patients with MRT which consists of surgical resection to remove the primary tumour followed by therapy (Bansal and Goel, 2007). The current treatments for MRT include multimodal chemotherapy, radiotherapy (RT) and surgical interventions. Radiotherapy treatment is often delayed and avoided for patients younger than 3 years old due to radio-toxicity which has severe side effects on brain development and endocrine dysfunction (Bansal and Goel, 2007).

The younger patients (age < 3 years old) are often prescribed with a combination of high dose chemotherapy using methotrexate and autologous stem cell transplantation (Gardner et al., 2008). The treatment historical series from St Jude Children's Research Hospital (Memphis, TN, USA) reported an impressive impact of high dose chemotherapy (HDCT) in patients with ATRT (> 3 years old). However, it is worth noting that from this series only one of three patients were alive after receiving RT as their upfront treatment. Interestingly, a new treatment approach using cycles of ifosfamide, carboplatin, etoposide (ICE) was administered in the patients 3 years of age of older. Of 4 patients, 3 of them were successfully recovered from the disease after 5 years of treatment (Tekautz et al., 2005). Prolonged survival (median of 42 months from diagnosis) was also achieved in 5 out 10 patients who received cycles of carboplatin, escalating doses of thiotepa and chemotherapy. Nevertheless, it is still unclear whether the better survival seen in older patients reflects the more aggressive treatment or age-related factors.

The higher incidence of MRT in patients less than 3 years old confers a challenge in clinical management of disease due to prevention of RT in this age group. However, a recent study showed a strong correlation between RT and OS in younger patients (< 3 years)(Buscariollo et al., 2012)(Figure 1.5). Median OS for patients who did not receive

RT as upfront treatment was 6 months. However, the study was not able to measure the actual OS for patients who received RT. Despite controversial issues regarding the adverse effect of RT on neurological sequelae of the youngest patient, this aggressive treatment is still considered the best therapy to cure MRT (Chen et al., 2006, Chi et al., 2009, Tekautz et al., 2005). Particularly, patients with localised tumour can receive more benefit from RT since they can be treated with focal irradiation thus minimizing toxicities.

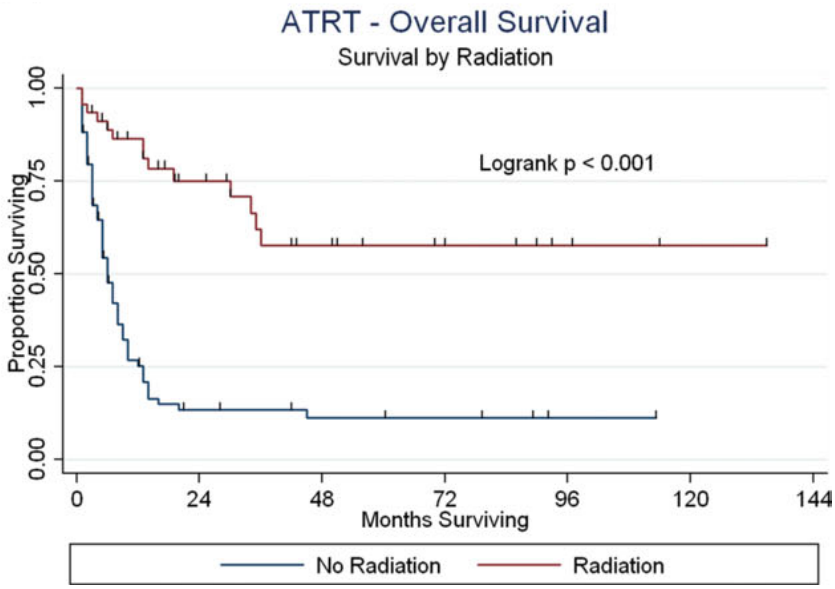

Figure 1.5 ***Kaplan-Meier curves showing overall survival (OS) for patients with ATRT who either received or did not receive radiotherapy (RT) as their upfront treatment.*** *A retrospective review by Buscariollo et al. (2012) showed the positive correlation between RT and overall survival (OS). They reported that the median OS for patients receiving initial radiotherapy was improved as median survival has not yet reached at the time the patients were recorded (from 34 months to not yet reached). In contrast, the median OS for patients who did not receive the RT as initial treatment was 6 months ($p < 0.001$). The plot was reproduced from (Buscariollo et al., 2012).*

High dose chemotherapy is also used in conjunction with analogous stem cell rescue therapy (ASCT) as part of MRT treatment. This intensive chemotherapy was used as an alternative to RT in young children (<3 years old) (Sung et al., 2016). Gidwani et al. (2008) published a single case report of a 4-month old boy who had received high dose myeloablative therapy followed by autologous peripheral blood stem cell transplantation as a treatment for ATRT. Surprisingly, he achieved long-term disease-free survival after treatment although he underwent incomplete tumour resection. Of note, RT was not included in the treatment course at all and no late side effects were recorded. A separate clinical study using the same treatment regimen was conducted in a 21-month-old patient diagnosed with metastatic rhabdoid tumour of kidney (RTK). However, the patient died 9 months after diagnosis due to chemo-resistance as the same agents used in the two courses (cyclophosphamide, etoposide, carboplatin and melphalan). Additionally, a small cohort of ATRT patients in the USA also received myeloablative regimen and stem cell rescue according to CCG-99703 clinical protocol. All the patients were treated with intensive myeloablative chemotherapy followed by ASCT if they were in complete remission. Of 6 patients who received this treatment regimen, 3 of them were reported alive with two of these demonstrating long-term survival (>5 years survival). These studies showed that overall survival of small number of patients with MRT can be improved when treated using HD-ASCT. Nevertheless, the efficacy of this treatment modality needs to be explored further in MRT.

Overall, several reports which have described multiple combinations of treatments for ATRT including intravenous chemotherapy, intrathecal chemotherapy, high-dose chemotherapy followed by autologous stem cell rescue (HD-SCR) and radiotherapy, showed variable results. Since the outcomes from the current treatments are far from satisfactory, novel approaches with fewer or zero side effects are very much needed to improve the survival rates of patients with MRT.

1.1.1.7 Biology and Genetics

1.1.1.7.1 SMARCB1 loss: a classic feature of MRT

Regardless of the anatomical site of the primary tumour, MRT at all sites are classified as the same entity given that they exhibit a common genetic origin, tumour morphology and characteristics (Versteege et al., 1998, Grupenmacher et al., 2013). The first genetic characteristic identified in MRT was monosomy 22 and subsequently translocation and deletions of the 22q11.2 cytoband (Versteege et al., 1998, Biegel et al., 2002b, Biegel et al., 1999). Positional cloning studies revealed the bi-allelic inactivation of *SMARCB1* at this cytoband location was responsible for initiation of MRT (Versteege et al., 1998). *SMARCB1* is universally expressed in all tissues and is a highly conserved subunit of the SWI/SNF chromatin remodelling complex (Versteege et al., 1998, Grupenmacher et al., 2013).

MRT possess unique genetic homogeneity compared to other embryonal tumours as the malignancy is caused by mutation of a single gene and no other mutation (Roberts and Biegel, 2009). High-resolution genomic analysis of ATRT identified no recurrent genomic alterations other than *SMARCB1* (Hasselblatt et al., 2013). Additionally, Lee et al. (2012) described MRT as a "remarkably simple" disease genetically due to extreme low mutation rate identified in 35 MRT with *SMARCB1* as sole event driver. *SMARCB1* mutation was recurrently mutated at very high frequency in this cohort (25 out of 32 cases that were whole exome sequenced). Also, they reported the mean mutation rate of 0.19 mutations per Mb with a minimum of 0 and a maximum of 0.45 mutations per Mb. This rate marked the lowest mutation rate that has ever been reported in comparison with other types of cancers sequenced to date such as prostate and melanoma. Apart from *SMARCB1* mutation, the authors also identified *GABRB2*, *TP53* and *NF2* as recurrently mutated genes. However, these mutations were found in small subclonal populations. Collectively, it highlights the stability of *SMARCB1* in MRT and therefore leads to a question of how such a single underlying cause can result in such a profoundly aggressive childhood cancer. Recent whole-genome sequencing of ATRT showed the locus that was most commonly affected was *SMARCB1* thus corroborating the previous finding that

SMARCB1 is the only recurrent mutation commonly mutated in MRT (Johann et al., 2016).

Mutation analysis of the coding sequencing has identified a few “hot spots” of mutation in *SMARCB1* gene. Deletion or mutation of the *SMARCB1* locus on chromosome 22 have been found in MRT implying the role of *SMARCB1* as tumour suppressor gene (Versteege et al., 1998, Biegel et al., 1999). However, type of mutations and position of mutations vary depending on the location of tumour in the body. ATRT (~50 of cases) has a high frequency of monosomy 22 or a deletion/translocation in the band 22q11.2 (Versteege et al., 1998, Biegel et al., 2002b). On the other hand, most of the ECRT samples present high frequency of homozygous mutation in *SMARCB1* (Biegel et al., 2002b). Furthermore, ECRT tends to harbour unbalanced translocations or deletions of chromosome 22 which are not usually detected in CNS (ATRT)(Biegel et al., 2002b, Biegel et al., 1999).

Coding sequence analysis shows some discrepancy in the distribution of mutation in exons between ATRT and ECRT. Higher frequency of *SMARCB1* mutation for kidney (ECRT) was observed in exon 2, 6 and 7 whereas exons 5 and 9 are frequently mutated in CNS tumour of ATRT (Biegel et al., 2002b) (Figure 1.6). Notably, two hotspot mutations were reported in CNS ATRT cases only including cysteine deletion in exon 9 and a C to T transition in codon 201 in exon 5.

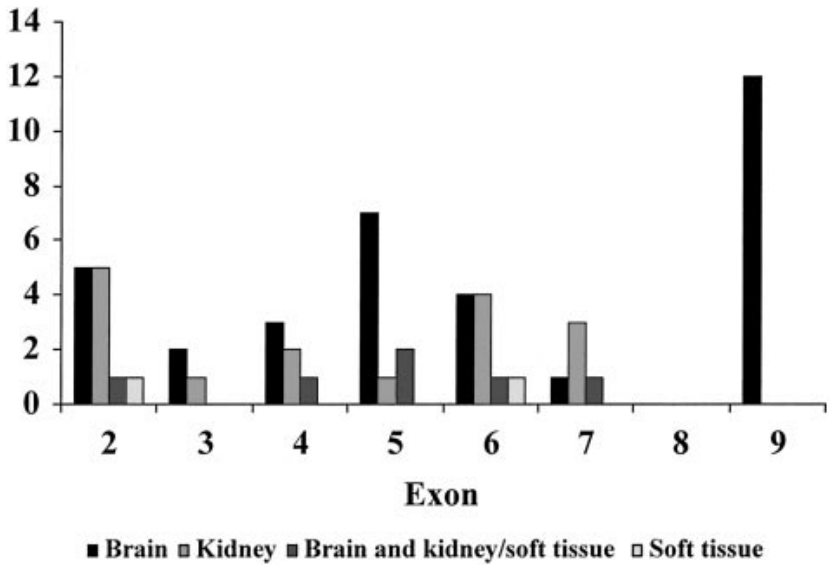

Figure 1.6 ***Coding sequence analysis of 58 primary MRT revealed distribution of mutation in SMARCB1****. Biegel et al. (2002b) identified variation of frequently mutated exon in SMARCB1 between ATRT and ECRT. Notably, no coding sequence mutations were reported for exons 1 and 8 in this study. Despite a small number of kidney tumours analysed in this study, these tumours showed a higher frequency of mutation in exon 7 compared to ATRT (brain). Strikingly, recurrent mutation of cysteine in exon 9 was reported in ATRT (brain) only. The figure was taken from (Biegel et al., 2002b).*

Single nucleotide polymorphism (SNP) array analysis demonstrated the majority of the MRT tumours (50 of 51 samples) have either deletions, mutations or loss of heterozygosity (LOH) on chromosome 22 that leads to the inactivation of *SMARCB1* (Figure 1.7) (Jackson et al., 2009, Lee et al., 2012, Hasselblatt et al., 2013).

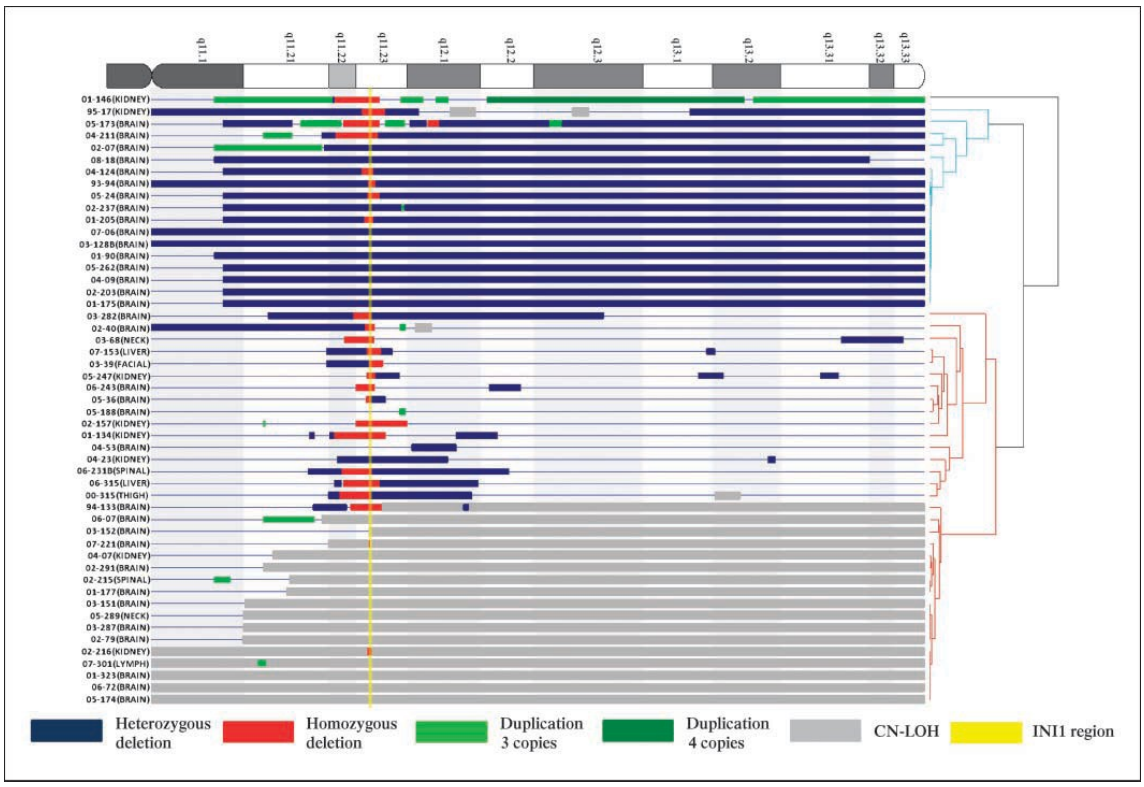

Figure 1.7 ***Jackson et al. (2009) reported copy number alterations (CNA) on chromosome 22 by single nucleotide polymorphism (SNP) array analysis****. There are three major groups; top group represents the large deletions; the middle cluster represents small deletions whereas the bottom cluster represents the large region of copy number LOH. In general, neoplasm with large deletions or large regions of copy number LOH were almost exclusively brain malignancies. Soft tissue tumours were found primarily to contain small deletions. The figure was taken from Jackson et al. (2009).*

1.1.1.7.2 Genetic alteration of SMARCA4 as a second mutational driver in MRT

Patients with MRT are commonly described with bi-allelic inactivation of *SMARCB1*. However, it was discovered, initially in a familial case, that patients could predispose to MRT tumourigenesis while retaining *SMARCB1* expression (Frühwald et al., 2006). In this familial case, two sisters were affected by MRT (a sister with RTK and another sister with ATRT) and demonstrated the typical morphological and clinical features associated with MRT. Nevertheless, molecular studies including CGH and array CGH, FISH, gene

dosage analysis by denaturing high-performance liquid chromatography (dHPLC), and DNA-sequencing showed no evidence for mutation in *SMARCB1*. In addition to this, immunohistochemistry of the tumours also demonstrated positive staining of SMARCB1 within the nuclei of tumour cells. The findings from this familial case ruled out *SMARCB1* as a mutation driver and strongly pointed to the existence of a second locus that contributes to MRT tumourigenesis. SNP array of the tumour samples identified *SMARCA4* nonsense mutation and the tumour cells demonstrated negative immunoreactivity for SMARCA4 by immunohistochemistry. Copy neutral LOH covering the *SMARCA4* locus in 19p13 further supported *SMARCA4* as the second hit in tumour cells (Schneppenheim et al., 2010). After that, a sporadic case of ATRT in 9-month-old boy presented with no genetic alteration in *SMARCB1* and expression of SMARCB1 as evaluated by immunohistochemistry. However, the tumour demonstrated a lack of immunoreactivity for the SMARCA4 antibody. The finding was corroborated by a homozygous mutation in the *SMARCA4* gene (Hasselblatt et al., 2011). These studies provide the evidence that another component of SWI/SNF complex also contributes towards MRT tumourigenesis.

SMARCA4 plays a critical role in the SWI/SNF chromatin remodelling complex as the ATPase subunit (Biegel et al., 2014). This gene is located on the chromosomal region 19p13.2, spanning a total genomic size of about 100Kb. Mutation in *SMARCA4* was found in several human cancers including prostate, breast, lung, pancreas and colon (Medina and Sanchez-Cespedes, 2008). In mouse models, homozygous deletion of *SMARCB1* and *SMARCA4* leads to embryonic lethality, thus establishing its role as tumour suppressor gene (Tolstorukov et al., 2013, Bultman et al., 2000). Gene expression analysis of *SMARCA4* deleted tumour from *SMARCA4* conditional mouse model showed enrichment of cell cycle progression related gene, thus consistent with the association between SWI/SNF complex and tumourigenesis.

Patients with *SMARCA4* mutation have a high tendency to carry germline mutation and present poorer disease prognosis compared to *SMARCB1* deficient patients with known germline status (Figure 1.8) (Hasselblatt et al., 2014).

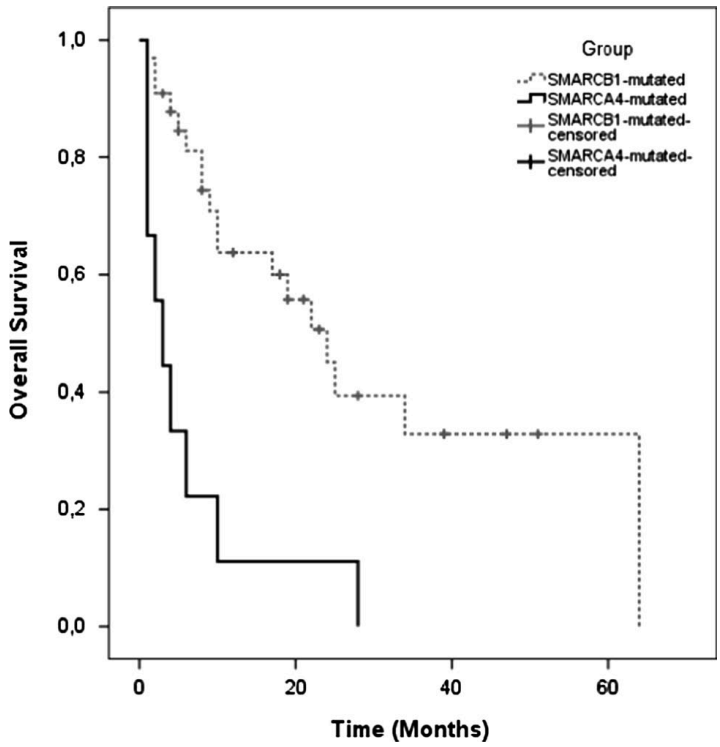

Figure 1.8 ***Overall survival of patients with SMARCA4 mutation (n=9) compared to patients with SMARCB1 deficient (n=33) with known germline status****. Log-Rank test p<0.001. Graph was taken from (Hasselblatt et al., 2014).*

The role of *SMARCA4* in MRT oncogenesis was studied in mouse embryonic fibroblast (MEF) by (Wang et al., 2009). The authors reported the expression of *SMARCA4* is required for tumour formation to compensate *SMARCB1* loss. In this study, *SMARCA4* was found in proliferating cells and was critical for mouse development and mutation in this gene impeded cell proliferation 5 days after deletion. Furthermore, co-inactivation of *SMARCB1* and *SMARCA4* resulted in rapid cell apoptosis.

1.1.1.8 Genetic abnormality

1.1.1.8.1 Rhabdoid tumour predisposition syndrome (RTPS)

Rhabdoid tumour predisposition syndrome (RTPS) was first described in 1999 based on rare familial syndrome cases where two or more family members inferred heterozygous

germline mutations in *SMARCB1* on chromosome 22q11.2 leading to aggressive MRT disease. Sévenet et al. (1999) defined a new hereditary syndrome based on constitutional mutation of *SMARCB1* capable of predisposing to MRT. Additionally, Proust et al. (1999) reported a case of two sisters presenting with ATRT almost simultaneously and died shortly after treatment (14 months and 26 months).

Patients who present multiple primary tumours are inevitably associated with germline mutation (Eaton et al., 2011) and exhibit aggressive clinical behaviour. Older children with RTPS tend to develop multiple schwannomas. (Bourdeaut et al., 2011, Kordes et al., 2010, Bruggers et al., 2011). The possibility of incomplete penetrance and gonadal mosaicism in familial cases may confer challenges for screening of an individual's cancer risk (Eaton et al., 2011). Genetic screening and counselling should be provided to the families with RTPS. Notably, as cases are more readily recognised and diagnosed, favourable outcomes for the familial cases have been reported (Ammerlaan et al., 2008, Kordes et al., 2014, Modena et al., 2013)

1.1.1.8.2 Genetic epidemiology in MRT

RTPS cases exhibited high penetrance due to aggressive nature of MRT and high mortality rate, the tumour predisposition can be observed more than one generation in the family (Janson et al., 2006, Sévenet et al., 1999, Kordes et al., 2010, Taylor et al., 2000). In-depth knowledge of RTPS including its frequency, penetrance and expression as well as family member recurrence risk is critically needed. A retrospective study was performed in 115 tumours by Bourdeaut et al. (2011) has provided genetic epidemiologic information and guidelines for genetic counselling of this disease. High frequency of germline mutation can be found in MRT patients at any group and the patients tend to develop tumours at a very young age; median age at time of diagnosis was 6 months compared to median 8 months at time of diagnosis for patients with wild-type alleles (Figure 1.9). Also, 2-year OS was 7.6% in patients with germline mutation relative to 29.45% for patients with wild-type germline alleles (Figure 1.10a). As previously reported, OS of patients is highly correlated to the age of patients (Tomlinson et al., 2005, Tekautz et al., 2005); in which patients older than 2 years showed better survival than younger patients (Figure 1.10b) (Bourdeaut et al., 2011).

The majority of germline cases occur through *de novo* mutations and the pedigree of inheritance pattern of the *SMARCB1* mutation across the generations is rare (Ammerlaan et al., 2008, Frühwald et al., 2006). It has been reported that *SMARCB1* germline mutation are not always inherited and unaffected adult carriers are known. This situation is known as gonadal mosaicism. In a series of familial cases (100 cases), the parents of children with *SMARCB1* germline mutation are completely unaffected (4 out of 7 inherited cases). Eaton et al. (2011) in her study suggested that familial cases may present incomplete penetrance and gonadal mosaicism i.e the *SMARCB1* mutation must appear within the parental gametes and not somatic cells (Eaton et al., 2011). A familial case study with posterior fossa brain tumours revealed splice mutations of *SMARCB1* in some affected and unaffected family members (Taylor et al., 2000). The proband's parents were healthy. However, the proband's maternal uncle was diagnosed with a posterior fossa choroid plexus carcinoma and died of disease. Additionally, the maternal grandfather's sibling also died from paediatric brain tumour at infancy. Gonadal mosaicism is therefore the most likely explanation for this germline inheritance as the proband's unaffected mother showed absence of disease symptoms.

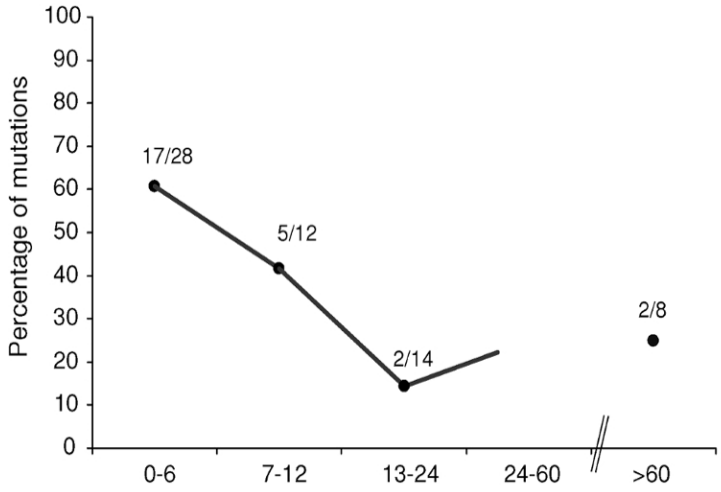

Figure 1.9 ***A retrospective study of germline mutation by Bourdeaut et al. (2011) indicates the incidence of germline mutation at any age****. There are 4 different age clusters and the majority of MRT cases (60%) occur before 6 months of age. The data was presented as a ratio of the number of patients with germline SMARCB1 mutation vs the number of patients with mutated or wild type alleles for SMARCB1 for whom the*

constitutional studies could be performed. The graph was taken from Bourdeaut et al. (2011).

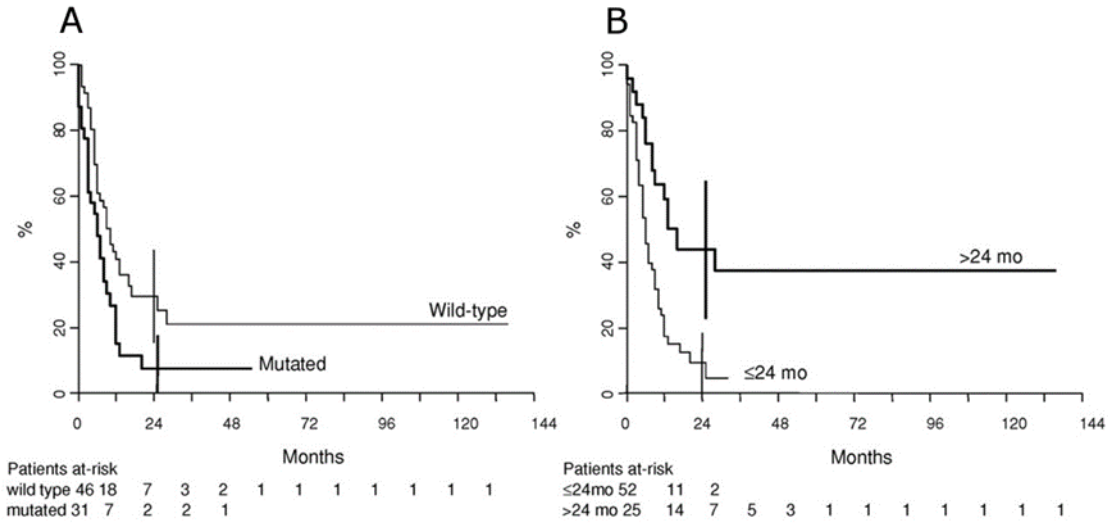

Figure 1.10 ***Bourdeaut et al. (2011) in their retrospective study of 115 tumours revealed a strong correlation of age with disease prognosis for patients with germline mutation****. (a) The overall survival (OS) of patients with germline SMARCB1 mutations was poor relative to patients with wild type SMARCB1. (b) age at time of diagnosis also plays a critical role in conferring disease prognosis according to mutation status. Poor survival was observed in germline patients aged below 2 years old relative to older patients (>2 years old). The graphs were taken from Bourdeaut et al. (2011).*

1.1.1.8.3 Non-rhabdoid SMARCB1-deficient tumours

MRT are commonly defined by alterations of *SMARCB1*. The introduction of a diagnostic antibody has improved the ability to recognise previously misdiagnosed MRT and immunostaining using a monoclonal anti-SMARCB1 antibody presents a gold standard for detection of MRT. However, *SMARCB1* mutations were also found in non-rhabdoid cancers that have composite rhabdoid cells as well as cancers that are lacking typical rhabdoid cell characteristics.

Immunohistochemical analysis of 55 tumours identified four CNS and three peripheral tumours with negative staining for SMARCB1 which only weakly resemble MRT histologically (Bourdeaut et al., 2007). CNS tumours which were found in choroid plexus were diagnosed as choroid plexus carcinomas due to different cell morphology despite a loss of SMARCB1 expression. The three peripheral tumours with negative IHC staining exhibited rare cell features in MRT such as "rosette-like" pattern, spindle or clear cells. Furthermore, the cells demonstrated positive immunoreactivity staining for vimentin and cytokeratin. However, the characteristic of rhabdoid cells such as abundant cytoplasm with inclusion bodies and a big nucleus with prominent nuclei were not detected within the cells. These findings illustrated that peripheral tumours can also exhibit similar patterns as are associated with ATRT.

Close to 80-90% cases with epithelioid sarcomas demonstrated loss of *SMARCB1* regardless of distal or proximal location (Margol and Judkins, 2014). Extra-skeletal myxoid chondrosarcomas also have been reported to exhibit typical rhabdoid cells and negative immunoreactivity for SMARCB1 (Oda and Tsuneyoshi, 2006). These tumours also present aggressive clinical behaviour similar to MRT.

Mutation of *SMARCB1* has also been implicated in familial schwannomas. Patients present both constitutional and somatic mutation of *SMARCB1* and the tumours demonstrated a mosaic pattern of SMARCB1 loss by immunohistochemistry (Patil et al., 2008). Analysis of the coding region of *SMARCB1* by direct sequencing and multiplex ligation-dependent probe amplification (MLPA) of patients with schwannomatosis revealed partial LOH of the *SMARCB1* region. These alterations were found both in tumour samples with and without *NF2* gene expression (Boyd et al., 2008).

Altogether, the cell morphology needs to be interpreted carefully along with immunohistochemistry profiles for characterisation of MRT especially ATRT as *SMARCB1*-deficient tumours can also be found in the same location as other *SMARCB1* negative non-rhabdoid tumours and may share clinical features with MRT including early onset and unfavourable outcomes.

1.1.1.9 MRT: a single entity containing molecularly defined subgroups

MRT arising at different anatomic locations are characterised as the same entity as they share similar cell morphology, biology and clinical behaviours. Previous studies reported MRT harboured very few mutations and a remarkably simple genome (Lee et al., 2012). However, it is not fully understood if ECRT and ATRT are molecularly distinct due to conflicting results from the previous studies (Pomeroy et al., 2002, Grupenmacher et al., 2013). Based on microarray analysis of primary MRT (5 RTK and 5 ATRT), Pomeroy et al. (2002) concluded that MRT which arise from different locations in the body are molecularly distinct. However, studies by Grupenmacher et al. (2013) and Paediatric Brain Tumour Group (PBTG) at Northern Institute for Cancer Research (NICR) illustrated otherwise. Gene expression analysis of primary MRT (10 RTK and 13 ATRT) and cell lines (G401-RTK and MON-AT/RT) demonstrated a separation between two subgroups related to anatomical location (Grupenmacher et al., 2013). However, miRNA expression analysis demonstrated MRT as a single entity regardless of tumour origin. Their findings illustrate that MRT are indeed a single entity that consist of two molecular subgroups. PBTG's work to elucidate the degree of overlapping between expression profiles between ATRT and ECRT further validated the existence of two molecular subgroups related to tumour location in the body. Consensus clustering of non-negative matrix factorisation (NMF) of primary MRT (10 ATRT, 13 ECRT) two subgroups within MRT, one group that is not exclusively ECRT while the other group is made up exclusively of ATRT. To identify if MRT is a single entity regardless of anatomical origins, the expression profiles of MRT were compared with medulloblastoma. Medulloblastoma consists of four molecular subgroups namely Wnt, Shh, Grp3 and Grp 4 (Taylor et al., 2012). NMF clustering of these tumours showed MRT as a single entity regardless of anatomical origin while medulloblastoma retained the four subgroups.

Recent omics studies using whole-genome DNA, RNA, microRNA, ChIP sequencing and genome-wide DNA methylation assays illustrates multiple subgroups within ECRT and ATRT. In 2015, Torchia et al. (2015) reported two molecular subgroups of ATRT with differential gene enrichment profiles, survival and distinct clinicopathlogical characteristics. Following this report, analysis of 450K DNA methylation of 192 primary ATRT demonstrated three distinct subgroups within ATRT that are associated with

SMARCB1 mutations, tumour locations and demographics (Johann et al., 2016). The subgroups are called ATRT-TYR, ATRT-SHH and ATRT-MYC. Whole DNA genome and RNA sequencing analyses in these subgroups revealed no recurrent gene alteration in addition to *SMARCB1*. However, these subgroups are epigenetically very different based on whole-genome bisulfite sequencing and H3K27Ac chromatin-immunoprecipitation sequencing studies. Almost concurrently, Torchia et al. (2016) reported three epigenetic subgroups within ATRT with distinct genomic profiles, chromatin and functional landscape that links to various signalling and epigenetic pathways.

Transcriptional and methylation analysis of ECRT also segregated this tumour into two subgroups. RNA-sequencing analysis of ECRT demonstrated two molecular subgroups associated with organ site called sub-group 1 and sub-group 2 (Chun et al., 2016). Cross-referencing of the differentially expressed genes between MRT subgroups of their cohort with 29 genes reported by Grupenmacher et al. (2013) as overexpressed in ATRT relative to RTK. The cross-referencing analysis showed that sub-group 1 may share a closer expression profile to ATRT while sub-group 2 may be similar to ECRT (Chun et al., 2016).

Molecular subgroups were also observed in mouse models for MRT and reflect the heterogeneity observed in human MRT (Han et al., 2016). Analysis of tumours from *Smarcb1*-deficient mouse models from Smarcb1wt/del_ex$^{1-2}$ and Smarcb1flox/flox;Rosa26-Cre^{ERT2} (lymphomas, intracranial and extra-cranial MRT). Transcription profiles of these mouse models were compared with non-*Smarcb1* deficient mouse models (medulloblastoma and neuroblastoma). Unsupervised hierarchical clustering revealed two major branches; the first branch consists of medulloblastoma, neuroblastoma and intracranial MRT, while the second branch consists of lymphomas and extracranial MRT. NMF consensus clustering on the same dataset (medulloblastoma and neuroblastoma served as the control) showed three subgroups within *Smarcb1*-deficient tumours; one group exclusively CD8(+)T-cell lymphomas, one group exclusively intracranial tumours and the third group contained mixtures of intracranial and extracranial tumours. The intracranial tumours were segregated into two subgroups showed different enrichment of gene expression that possibly related to cell of origin.

Collectively, multi-platform analyses of human and mouse MRT tumours demonstrated molecular subgroups within primary MRT and further segregated into subgroups within ECRT and ATRT.

1.1.1.10 MRT mouse models: history and challenges

Attempts to generate *Smarcb1*-deficient mouse models for MRT have met variable success. Homozygous deletion of *Smarcb1* is associated with early embryonic lethality (E7) (Roberts et al., 2000). However, heterozygous *Smarcb1*+/- engineered mice are capable of developing tumours that resemble human MRT. (Roberts et al., 2000, Guidi et al., 2001, Klochendler-Yeivin et al., 2000). However, these tumours were found almost exclusively in the soft tissue of the neck. Notably, almost no tumours were developed in the brain from this model. More importantly, this model was not practical to study the role of *Smarcb1* in tumourigenesis due to low tumour penetrance and higher latency for tumour development. To circumvent the problems, a conditional inversion of *Smarcb1* in mice was engineered using loxP-Cre system (SMARCB1inv; Mx-Cre model) (Roberts et al., 2002). Nevertheless, most mice died 1 to 3 weeks after induction due to disease aggressiveness and a fully penetrant tumour. The mice were discovered to develop mature CD8+ T cell lymphoma or rarely rhabdoid tumours with a median onset of only 11 weeks. More recently, Han et al. (2016) generated a Smarcb1 flox/flox; Rosa26-CreERT2 mouse model and injected tamoxifen into the mice at various time points to control inactivation of *Smarcb1*. Mutation at an early embryonic stage results in an aggressive neoplasm recapitulating human MRT with full penetrance and with early onset (median 2.5 mo). Importantly, the mouse model used in this study demonstrated phenotypes and expression profiles that resemble human MRT. Findings from this study provide an important insight for discovery of cell of origin as the effect of *SMARCB1* inactivation at different developmental stages towards MRT tumourigenesis could be controlled using tamoxifen injection.

1.2 SWI/SNF chromatin remodelling complex

1.2.1 Introduction of SWI/SNF complex

The SWI/SNF (switch/sucrose nonfermenting) complex was first described in yeast but later was also found in all eukaryotes (Cristofaro et al., 2001, Kaeser et al., 2008, Moshkin et al., 2007). The mammalian SWI/SNF complex consists of at least nine subunits either of two highly homologous ATPase catalytic subunits; *SMARCA4* (*BRG1*) or *SMARCA2* (*BRM*), invariant core subunits including *SMARCB1*, *SMARCC1* (*BAF155*) and *SMARCC2* (*BAF170*) (Prasad et al., 2015, Wilson and Roberts, 2011, Cristofaro et al., 2001, Willis et al., 2012, Weissman and Knudsen, 2009) and 4-8 cellular lineage-restricted subunits. *ARID1A* and *ARID1B* are found in the BAF-A and BAF-B (Brahma Associated Factor) complex respectively, while *ARID2* is found in the PBAF (Polybromo BAF) complex (Figure 1.11).

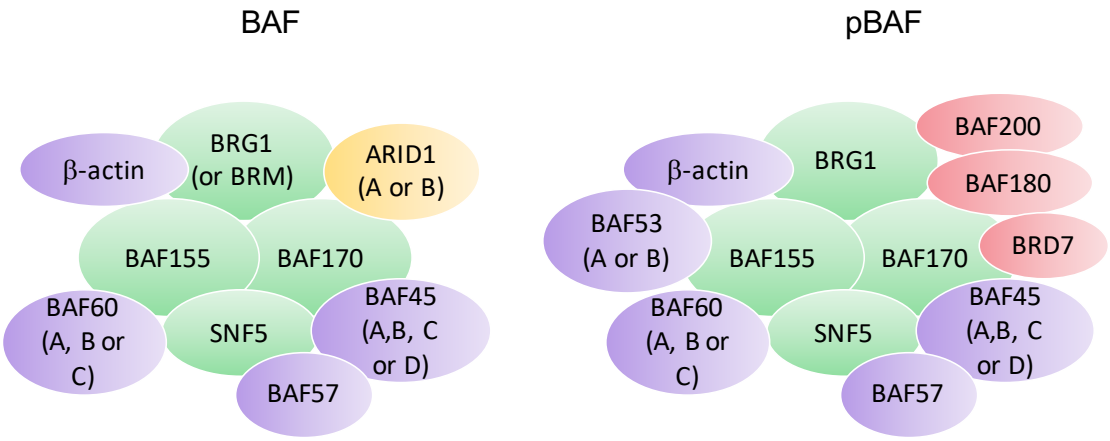

Figure 1.11 ***Two types of SWI/SNF chromatin remodelling complexes in humans.*** *The SWI/SNF complex consists of evolutionary conserved core subunits (green) and variant subunit (purple). BAF represents BRG1 SWI/SNF complex while pBAF represents polybromo BRG1 associated SWI/SNF complex. ARID1 (A or B, in orange) is a unique component for the BAF complex while BAF200, BAF180 and BRD7 are specific for pBAF complex. The figures are reproduced from (Wilson and Roberts, 2011).*

The complex is evolutionarily conserved and present at all developmental stages. The chromatin remodelling complex alters the structure of chromatin during gene regulation in an ATP-dependent manner (Tang et al., 2010, Flaus and Owen-Hughes, 2004). The SWI/SNF complex regulates DNA accessibility through two mechanisms; firstly, translocation of the nucleosome along the DNA during transcriptional regulation and secondly dimer replacement during DNA repair. At present, the mechanism of action of the SWI/SNF complex in chromatin remodelling process is not fully explained. However, two chromatin remodelling models have been proposed so far; one model involves twisting of the DNA helix along the histone octamer using torsion force like a screw in a slot. Repeated twisting and pulling movement allows sliding of the nucleosome (Saha et al., 2006)(Figure 1.12).

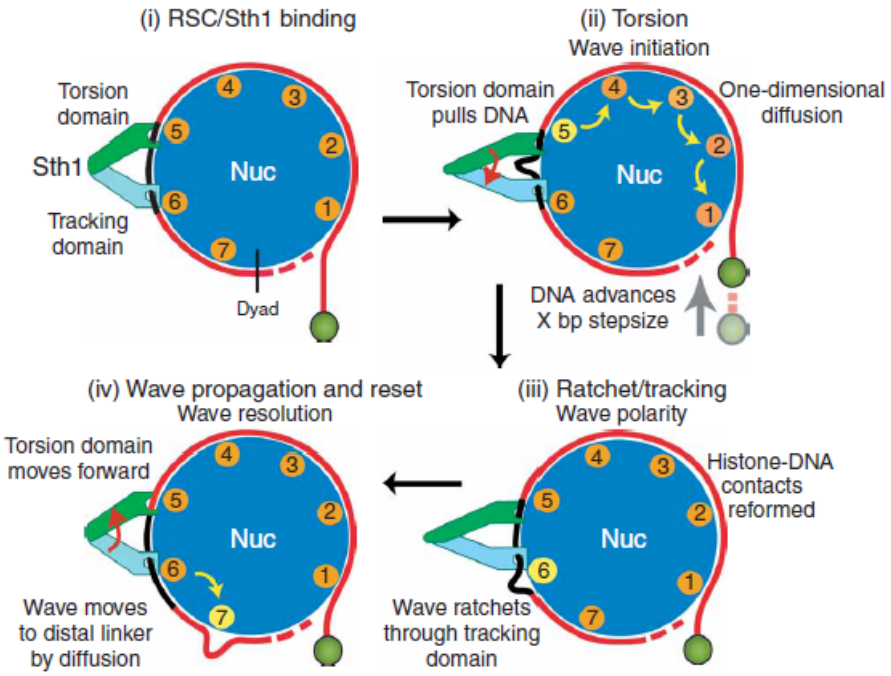

Figure 1.12 ***The wave-ratchet-wave model using torsion force****. A half-nucleosome shown in a top view (blue) and STH1 represent the tracking domain and tension force that twist the DNA helix along the nucleosome. The figures were taken from Saha et al. (2005).*

The second model involves unwrapping DNA from the nucleosome dyad at a histone octamer to form a DNA loop and translocating DNA around the nucleosome in a wave-like formation (Saha et al. (2005)) (Figure 1.13). The second model is by far the most practical rather than just the simple twisting-diffusion mechanism (first theory) because the presence of massive hairpins on DNA will obstruct the twisting and diffusion motion of DNA helix on the histone surface and therefore inhibit the sliding. A study performed by Aoyagi and Hayes (2002) supported the second model that DNA maintains its rotational position during the sliding process and that DNA translocation occurs at minimal contact on histone octamer and partially dissociates from the nucleosome.

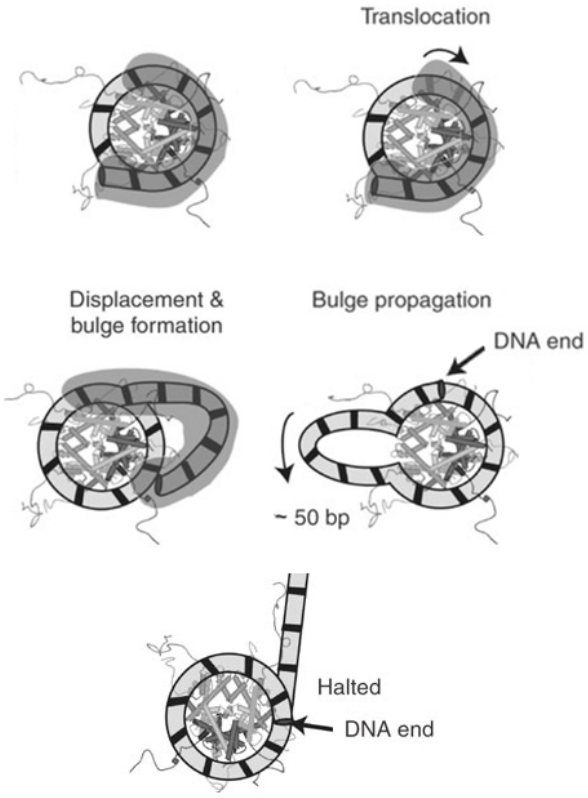

Figure 1.13 ***Bulge theory of nucleosome mobilisation by SWI/SNF complex involving DNA translocation steps along the nucleosome****. The nucleosome is viewed perpendicular to the DNA superhelix, with the location of the DNA represented by black bars. The figures were taken from (Zofall et al., 2006).*

1.2.1 Role of SWI/SNF complex in gene transcription and cellular development

SWI/SNF chromatin remodelling complex executes lots of biological function such as cell differentiation (Gresh, Bourachot et al. 2005), proliferation (Hah, Kolkman et al. 2010), neural development (Yoo and Crabtree 2009, Weinberg, Flames et al. 2013) and tumourigenesis. Studies have illustrated significant roles for SWI/SNF in cell differentiation. The conformation of subunits diverges between type of cells or tissues and it can change during differentiation and developmental stages (Sokpor et al., 2017). *SMARCE1* and *SMARCA4* are both required for activation of CD8 and silencing of CD4 during T-lymphocyte development (Chi et al., 2002). Additionally, the BAF complex also plays a role in maintenance and pluripotency of mouse embryonic stem cells (Ho et al., 2009, Kidder et al., 2009). Mutation of *SMARCA4 in vivo* is associated with early embryonic lethality (Bultman et al., 2000). Chromatin immunoprecipitation (ChIP) analysis revealed that *SMARCA4* binds to promoter regions of self-renewal and pluripotency-related genes such as *OCT4*, *SOX2*, *NANOG* and *SALL4* (Kidder et al., 2009). Additionally, *SMARCA4* also binds to the promoter region of genes that are involved in maintaining an undifferentiated state of cells such as *DNM3L*, *DPPA2*, *FBX15* and *TDGF1*.

In vitro and *in vivo* studies demonstrate that SWI/SNF enzymes have been implicated in gene transcription by facilitating the binding of the transcriptional activators at TATA-binding protein (TBP), formation of RNA polymerase II related pre-initiation complex and elongation (Kim et al., 2005, Kuras and Struhl, 1999, Reppas et al., 2006, Ryan et al., 1998). The study in yeast illustrates that the transcriptional activation of several promoters was required at the SUC2 promoter and mutation in SWI/SNF subunits greatly impaired transcription induction process (Hirschhorn et al., 1992, Neigeborn and Carlson, 1984). Biochemical and genetic analysis provide the evidence that the complex involved in transcription initiation that neutralises the repressive effects of contracting DNA into a chromatin structure (Ryan et al., 1998).

1.2.2 SWI/SNF mutations and silencing in cancer

Chromatin remodelling and tumour suppressor function are reported to play a role in cancer development. A study by Kadoch et al. (2013) has demonstrated that subunits of SWI/SNF chromatin remodelling complex are most commonly mutated in human cancer, accounting for 19.6% of all human cancers that have been reported in 44 exome sequencing studies. The discovery of *SMARCB1* mutation in MRT has elucidated the role of the complex as a tumour suppressor (Roberts et al., 2000, Roberts et al., 2002). Moreover, mutations in at least 8 genes encoding SWI/SNF complex subunits have been implicated in various malignancies (Figure 1.14). Genome-wide analysis of 18 different tumours samples showed a very high mutation frequency in SWI/SNF subunits (20%) and this figure was nearly comparable to that of *TP53* mutation (Agaimy, 2014). In addition to mutation of *SMARCB1*, mutation in other subunits has been discovered including *ARID1A*, *SMARCA4, PBRM1* and *BRD7* subunits. *ARID1A* and *SMARCA4* have been associated with formation of various aggressive cancers such as MB, ovarian clear cell carcinomas (OCCCs), endometrioid carcinomas, lung adenocarcinoma and breast cancer thus suggesting the role of this subunit in different cell or tissue lineages. Heterozygous mutation in *ARID1B* results in Coffin-Siris syndrome which is associated with difficulty in language acquisition and mental retardation (Kadoch et al., 2013, Hodges et al., 2016, Shain and Pollack, 2013).

Although complete loss of function of the genes is commonly associated with tumour formation, several human cancers were identified to harbour heterozygous mutations in SWI/SNF subunits. Reduced expression of the subunits such as *ARID1A* and *SMARCB1* is still capable of driving tumourigenesis and similar events have been found in steroid-refractory acute lymphoblastic leukaemia (Wilson and Roberts, 2011, Kadoch et al., 2013). While exome sequencing studies demonstrated that mutations in specific subunits of SWI/SNF complex have been implicated in tumourigenesis, many subunits which are ubiquitously expressed in cells do not contribute towards either tumour suppression or development (Kadoch et al., 2013). For instance, neuron-specific subunits such as *BAF45c*, *BAF45b* and *BAF53b* did not appear in dividing cells, therefore have no remarkable role in suppressing tumour progression. In addition, BAF53a is a universally expressed subunit that binds directly to *SMARCA4*. Mutation in *SMARCA4* has been

implicated in many tumour formations but mutation in BAF53a is not. Other BAF subunits that are mutated in human cancers are summarised in Figure 1.14.

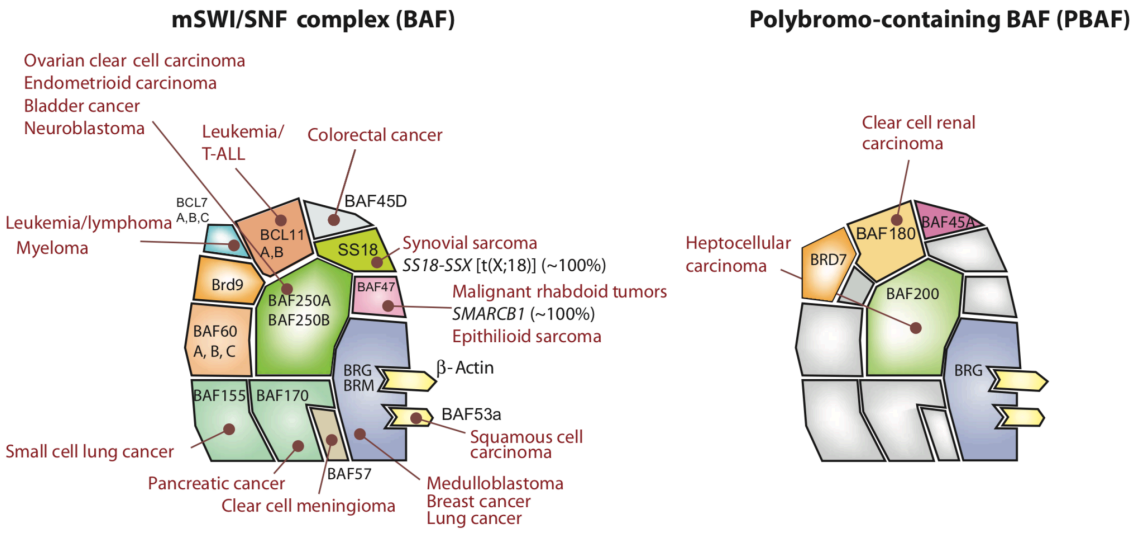

Figure 1.14 ***Mutations in the specific genes encoding SWI/SNF chromatin remodelling complex present in specific malignancies****. Mammalian SWI/SNF complexes are divided into two groups: SMARCA4/2 associated factor (BAF or SWI/SNF-A) and polybromo-associated BAF (PBAF or SWI/SNF-B). Figures were taken from (Kadoch et al., 2013).*

1.2.3 Deregulation in SWI/SNF chromatin remodelers: a central key to MRT tumourigenesis

The first event that linked SWI/SNF complex to tumourigenesis was mutation in *SMARCB1,* discovered in the late 1990s (Versteege et al., 1998). *SMARCB1* is a highly conserved subunit and ubiquitously present in almost every combination of SWI/SNF chromatin remodelling complexes. This subunit was inactivated in most case of MRT by biallelic mutation (Roberts et al., 2002, Versteege et al., 1998, Biegel et al., 2002a).

SMARCB1 may also have a role in DNA damage response, and when mutated lead to an increase in the expression of phosphorylated *p53* and aberrant mitotic features hence

activation of a specific subset of *p53* target genes (Klochendler-Yeivin et al., 2006). Inactivation of the *p53* checkpoint did not rescue cell proliferation but instead decreased apoptosis in *SMARCB1* deficient cells (Isakoff et al., 2005, Klochendler-Yeivin et al., 2006). Heterozygous mutation in these two suppressor genes in mice (*SMARCB1*$^{+/-}$ *p53*$^{-/-}$) increased the frequency of tumour formation and reduced the tumour latency in comparison to *SMARCB1* +/- mice.

Inactivation of *SMARCB1* in MRT has been shown to cause downregulation of many genes including cell cycle-related genes. The expression of *p16Ink4a* is downregulated after inactivation of *SMARCB1* and it has been postulated the aberrant function of *p16* leads to MRT tumourigenesis (Venneti et al., 2011a, Versteege et al., 2002). The situation was reversed following *SMARCB1*-reexpression in MRT cell lines consequently leading to cell cycle arrest in the G1-phase. The *p16* is a tumour suppressor protein that functions as a cyclin-dependent kinases 4 and 6 (*CDK4* and *CDK6*) inhibitor which in turn inhibits phosphorylation of retinoblastoma tumour suppressor protein, RB (Imbalzano and Jones, 2005, Versteege et al., 2002). Re-expression of *SMARCB1* also causes activation of senescence-associated proteins such as Rb, downregulation of E2F (acts as cyclin transcription activator) and Cyclin D1, accompanied by upregulation of both *p16* and *p21* (Versteege et al., 2002, Versteege et al., 1998, Chai et al., 2005, Oruetxebarria et al., 2004, Kia et al., 2008). Inactivation of pRb did not induce cell senescence in *SMARCB1*-deficient cells. However, re-expression of *Rb* or *p21* in these cells restored the normal biological activity of cell senescence. Additionally, the double mutation in *SMARCB1* with *Rb* or *p16* does not increase the cellular proliferation rate. However, the tumour formed following inactivation in *SMARCB1* alone is much faster and occurs at various sites in mice than tumours that arise following mutation in *Rb* and *p16*. Overall, these results indicate the role of *SMARCB1* in cell cycle regulation.

A recent study by Tolstorukov et al. (2013) has identified interaction between SWI/SNF remodelers and chromatin at transcription start site (TSS) in controlling nucleosome occupancy. Deregulation of the subunit of SWI/SNF complex such as *SMARCB1* and *SMARCA4* reduced the occupancy of the complex to nucleosome at TSS and leads to downstream changes in gene expression. SMARCA4 ChIP-seq analysis demonstrated high enrichment of this protein at promoter gene following *SMARCA4* deletion and this

finding is positively correlated with expression level of target genes. Affymetrix microarray analysis of similar samples showed a modest association between nucleosome occupancy and down- or up-regulation of genes in general. However, subsets of genes were remarkably upregulated in *SMARCA4*- and *SMARCB1*-deficient cells. Interestingly, a higher degree of overlap between genes that were downregulated following *SMARCB1* loss and genes that were downregulated following *SMARCA4* loss suggests comparable but not identical effects on gene expression of these two genes. Together, conditional deletion of *Smarcb1 in vivo* demonstrated dependency on *Smarca4* expression to initiate tumourigenesis and co-inactivation of *Smarca4* and *Smarcb1* failed to initiate tumour *in vivo*. These findings suggest two possibilities; 1) dependency on *SMARCA4* to initiate tumourigenesis to compensate for the loss of function of *SMARCB1* and 2) loss of *SMARCB1* activates the hyperactivity of residual *SMARCA4*-containing SWI/SNF complex.

1.3 Mechanisms of tumourigenesis caused by SMARCB1 loss in Malignant Rhabdoid Tumour (MRT)

MRT is considered a remarkably simple genetic disease as there is no second driver to trigger tumour development (Lee et al., 2012). Mutation in tumour suppressor *SMARCB1* is minimally sufficient to initiate tumour formation as shown by MRT mouse model studies (Han et al., 2016, Vitte et al., 2017). However, it is not enough to conclude that the mutation alone can cause such an aggressive and lethal disease. Although the detailed role of *SMARCB1* in malignant transformation is not fully elucidated, it seems that *SMARCB1* loss contributed towards tumourigenesis through p16/Rb/E2F and p53 pathways (Isakoff et al., 2005, Klochendler-Yeivin et al., 2006, Chai et al., 2005). MRT are lethal cancers that strike predominantly in very young patients. Early embryonic lethality was observed when *SMARCB1* was inactivated at E1-E6 with no apparent *SMARCB1* deleted pup (Klochendler-Yeivin et al., 2000, Guidi et al., 2001). However, temporal control of *SMARCB1* inactivation between E6-E10 in Smarcb1flox/flox; Rosa26-CreERT2 mice increased the tumour latency, high penetrance and developed tumours that resemble human MRT (Han et al., 2016). Importantly, low and null penetrance of tumours were observed when tamoxifen injections were given at E8-10 and E11-18 respectively. Notably, *SMARCB1* loss at P2-P3 resulted in growth failure and rapid death. Altogether, these studies demonstrate mutation of *SMARCB1* must occur in a specific window during development to provoke genome-wide chromatin remodelling which interrupts normal cell differentiation thus contributing to disease aggressiveness. Furthermore, mutation of *SMARCB1* in these cells is taught to have the capacity to hijack and aberrantly maintain the inherent “stemness/self-renewal” programme active in these cells and that contributes critically to MRT tumourigenesis. Moreover, *SMARCB1* inactivation in specific cell population resulted in MRT tumourigenesis at various locations in the body. Recent omics and mouse model studies of primary MRT highlight the possibility of MRT derived from either mesenchymal, neural or neural crest cells (Chun et al., 2016, Han et al., 2016). Therefore, this field should be explored further as it may allow better prediction of disease prognosis and development of therapeutic target for MRT.

1.3.1 SMARCB1 tumour suppressor inactivation in the cell of origin potentially contributes to MRT aggressiveness

1.3.1.1 MRT: genetically homogeneous but phenotypically highly heterogeneous

MRT are teratoid in nature containing cells demonstrating morphology and differentiation markers from multiple lineages even within the same tumour (Ho et al., 2000). Re-expression of *SMARCB1* in MRT prompts the individual cells within a population to differentiate towards a variety of lineages such as epithelial, neural and mesenchymal. Different gene enrichment expression profiles of primary MRT were identified in the same tumour highlighting their phenotypic heterogeneity and molecular complexity (Chun et al., 2016, Johann et al., 2016). It is still not fully understood how *SMARCB1* loss activates the MRT cells to become undifferentiated. However, re-expression of *SMARCB1* in MRT cell lines triggered adipocyte (Caramel et al., 2008) and hepatocyte (Gresh et al., 2005) differentiation.

1.3.1.2 Evidence of potential cell of origins in MRT

Numerous opinions of the cell of origin for MRT have been proposed due to the multi-phenotypic nature of the tumours. However, their true cell of origin is still a subject of debate and it is hard to establish due to the various bodily locations of the primary tumours.

Attempting to identify a cell of origin for ATRT, *SMARCB1* and *SMARCA4* were conditionally inactivated in cerebellar granule neurons of Math1-cre:: Smarcb1fl/f and Math1-cre:: Smarca4fl/f mice respectively (Moreno et al., 2014). Although the mice demonstrated severe neurologic defects and hypomorphic cerebellum, no tumour formation within the cerebellum was observed. This result eliminates cerebellar granule precursors as potential cells of origin for MRT. However, cumulative genome-wide profiling of MRT showed dysregulation of neural progenitor stem cell markers and expression of genes that regulate neural progenitor and neural crest cell differentiation thus possibly neural progenitor cells or neural crest origin for MRT (Okuno et al., 2010, Chun et al., 2016). Gene set enrichment analysis (GSEA) of primary MRT showed that

genes that were downregulated in embryonic stem cells (ESC) were significantly downregulated in MRT. In addition to this, the expression of gene sets known to be polycomb targets in ESC were also downregulated in MRT. These analyses suggested the possibility that tumours originate from early types of stem cells where chromatin around specific genes remains dominated by PRC2 histone marking (Gadd et al., 2010).

Recent mouse model studies by Han et al. (2016) and Vitte et al. (2017) have suggested neural crest (NC) cells as potential cell of origin for MRT. Inactivation of *Smarcb1* in protein zero (P0) in neural crest cells developed tumours that phenotypically resembled human MRT (Vitte et al., 2017). In addition, cross-referencing of transcriptome profiles of MRT mouse and human tumours with stem cell expression profiles including embryonic stem cell (GSE44175), neural progenitor (GSE44175 and GSE44175), neuron (GSE46150), oligodendrocytes derived from neural stem cells (GSE9566), astrocytes derived from neural stem cells (GSE9566), ectomesodermal tissue from the palate (GSE9566) and neural crest (GSE11149) suggests neural progenitor and NC as potential cell of origin for MRT (Han et al., 2016). Gene expression analysis of tumours from (Han et al., 2016)'s mouse model reflected the diversity within human MRT. Nevertheless, Han et al. (2016) failed to observe the tumour formation in the CNS although the mouse was modelled for ATRT.

Genome analysis of primary ATRT by Torchia et al. (2016) and Lafay-Cousin et al. (2012) revealed significant enrichment of mesenchymal gene signatures in subgroups within ATRT. Torchia et al. (2016) presented two subgroups within ATRT in which subgroup 1 showed enrichment of neural-related gene expression. Whilst, subgroup 2 demonstrated upregulation of genes that involve in mesenchymal cell lineage and signalling such as BMP and cell differentiation (i.e *ERPINF1, CLDN10, FBN2*). This study provides an indication of two potential cells of origin for ATRT. Likewise, gene expression analysis of primary ECRT also suggested two possible cell of origins which are neural crest cells and mesenchymal stem cells. An experimental study by Caramel et al. (2008) showed re-introduction of *SMARCB1* into MRT cells (ECRT cell lines) provoked differentiation towards the adipocyte lineage thus illustrating the possibility that MRT originate from mesenchymal stem cells.

All these studies outline potential cells of origin for MRT. It remains to be determined through systematic analysis and experimental work if MRT arise at different locations in the body derive from different progenitor cells or share a common cell of origin.

1.3.1.3 Deregulation of self-renewal pathways: A classic tale in cancer

Embryonic stem cells are defined by their properties of self-renewal and multi-lineage differentiation with the capability to develop into every cell, tissue and organs in humans (Hadjimichael et al., 2015). Self-renewal is a process by which stem cells divide asymmetrically to generate two or more daughter cells, perpetuating the stem cell pool throughout life (Shenghui et al., 2009). The process involves the maintenance of the undifferentiated state of stem cells and multipotency or pluripotency, depending on the type of stem cells. Stem cell self-renewal machinery involves a balance of function between tumour suppressor genes (limiting self-renewal activity) and proto-oncogenes (promoting self-renewal activity). Self-renewal machinery is not restricted to only stem cell population as other types of restricted progenitors or differentiated cells including lymphocytes and restricted glial progenitors also possess the capacity to self-renew. The lymphocytes were shown to share at least some self-renewal mechanism similarly to stem cells such as dependence on the *BMI1* proto-oncogene (Van der Lugt et al., 1994). However, stem cells possess extensive self-renewal potential and can be distinguished from the more lineage-restricted progenitor cells which have limited self-renewal capacity (Shenghui et al., 2009). It is important to note, although stem cells have extensive self-renewal potential, this does not essentially mean that the cells continue to self-renew under physiological conditions. For instance, neural crest cells possess substantial potential to self-renew in culture (Kruger et al., 2002), however, the cells can undergo few cycles of cell division before differentiating *in vivo* (Fraser and Bronner-Fraser, 1991, Morrison et al., 1999).

1.3.1.4 Deregulation of classic self-renewal properties of normal stem cells implicated in the development of human cancers

Self-renewal is described as a classic feature of stem cells. The self-renewal genes play a critical role in various cellular activities including embryogenesis, normal tissue repair

and homeostasis (Horne and Copland, 2017). In cancer, normal signalling pathways that are associated with self-renewal such as Wnt, Notch and Hedgehog are often deregulated. The mutation of these signalling pathways may occur in stem cells or progenitor cells that possess self-renewal properties which result in tumourigenesis.

A pathway that is commonly associated with embryogenesis and adult tissue homeostasis is the Wnt pathway (Logan and Nusse, 2004). The pathway is a key regulator of stem cell maintenance and regulation (Reya and Clevers, 2005). Activating the Wnt signalling cascade in many tissue types leads to tumour development by activating self-renewal pathways while inhibiting cell differentiation. For instance, the expression of Wnt3a protein in ESC inhibited cell differentiation in epiblast stem cells and increased self-renewal capacity of cells as illustrated by the increase in the number of colonies (Ten Berge et al., 2011). In the context of neural stem cell, Wnt signalling through β-catenin regulates the cycling and expansion of neural progenitor cells. However, aberration function of this pathway in the spinal cord and brain of mice led to upregulation of neural precursor population and increased the tumour mass of the spinal cord and brain (Zechner et al., 2003, Chenn and Walsh, 2002). Evidently, the mutation in β-catenin has been implicated in medulloblastoma (Zurawel et al., 1998). Mutation in Wnt signalling has been associated with the development of many human cancers including colon cancers, skin cancers and also leukaemia.

Other pathways which also affect normal self-renewal machinery and have also been implicated in cancer when mutated include the Hedgehog (Hh) pathway. This pathway is involved in many fundamental processes associated with embryonic development such as stem cell maintenance, cell differentiation, tissue polarity and cell proliferation (Taipale and Beachy, 2001). Aberrations in the Hh pathway can cause tumourigenesis as seen in medulloblastoma (MB), basal cell carcinoma, lung, breast and prostate cancers. The role of the Hh pathway in mediating stem cell maintenance and cell differentiation was studied in mammary stem/progenitor cells *in vitro*. The experimental study revealed that the components of the Hh pathway such as PTCH and SMO were highly expressed in mammary stem/progenitor cells compared to differentiated cells (Liu et al., 2006b). For instance, mRNA expression of *PTCH* was ~4 fold higher in mammary

stem/progenitor cells relative to the differentiated cells. In another experiment, the mammary epithelial cells were grown as mammospheres in order to measure self-renewal. Overexpression of *GLI1* and *GLI2* (downstream effector of Hh pathways) in mammary epithelial cells increased the number of mammospheres by 49% and 66% respectively compared to uninfected cells. These results indicate the Hh pathways mediates the self-renewal machinery through the downstream effectors such as GLI, PTCH, SMO. In other types of human cancer such as breast cancer and medulloblastoma, the downstream effector of Hh signalling pathway which is BMI1 was found to be upregulated. BMI1 is a subunit of the Polycomb repressive complex 1 and is also known to be the key regulator in the self-renewal pathway (Wang et al., 2012, Srinivasan et al., 2017). Overexpression of BMI1 has been implicated in medulloblastoma tumourigenesis through the Hh pathway (Wang et al., 2012). Chromatin immunoprecipitation (ChiP) study of primary medulloblastoma and cell line (DAOY) showed significant enrichment of *GLI1* and *GLI2* at the *BMI1* promoter, suggesting the expression of *BMI1* is regulated by the Hh pathway. In line with this, small interference RNA (siRNA) targeting *GLI1* showed positive correlation between *BMI1* expression and Hh pathway inhibition by which downregulation of *GLI1* reduced the transcript of *BMI1*. Altogether, findings from this study suggest the role of Hh in mediating self-renewal through the BMI1 pathway.

1.3.1.5 Mechanisms of self-renewal in Malignant Rhabdoid Tumour (MRT)

SMARCB1, a hallmark in MRT is a member of the SWI/SNF chromatin remodelling complex (Roberts et al., 2002, Versteege et al., 1998, Biegel et al., 2002a). Mammalian BAF is reported to play a role in regulating pluripotency during embryogenesis (Ho et al., 2009). The study in mouse embryonic stem cells revealed the involvement of the BAF complex in self-renewal and pluripotency pathways. Knockdown of Brahma related genes (Brg) using shRNA in mice reduced proliferation capacity indicated by a small size of colonies assessed by colony formation assay. Also, *Brg*-deficient cells showed a decrease in expression of self-renewal genes such as *Oct4, Sox2* and *Nanog* (Ho et al., 2009). Findings from these studies describe the role of SWI/SNF complex in self-renewal and pluripotency.

In the context of MRT, *SMARCB1* loss reduced the capacity of SWI/SNF complex to impede the repressive function of EZH2, which is an enzymatic subunit of the histone H3K27 methyltransferase Polycomb complex, PRC2 (Wilson et al., 2010a). Consequently, *SMARCB1*-deficient MRT caused upregulation of PRC2 mediated repression and activation of stem cell-associated programs to facilitate tumour development. In addition, primary MRT also showed expression of embryonic gene signatures (Richer et al., 2017). Transcriptomic analysis of primary MRT showed enrichment of stem cell-related genes such as *SALL4* and *LIN28B*. In addition to this, immunohistochemistry of primary ATRT also provides evidence of MRT expressing stem cell markers involved in self-renewal such as SOX2, NANOG, KLF4, MUSHASHI and OCT4 (Deisch et al., 2011, Venneti et al., 2011b). Given that *SMARCB1* is a member of the SWI/SNF complex and MRT express stem cells markers, it is noteworthy to investigate if mutation in *SMARCB1* causes deregulation in self-renewal and pluripotency mechanisms to initiate tumourigenesis and disease aggressiveness.

RNA-seq analysis of primary MRT and cell lines available in Paediatric Brain Tumour Group (PBTG) demonstrated overexpression of many self-renewal genes such as *GLI2, JAK2, FGF1* and *BMI1*. As previously discussed in section 1.3.1.4, downstream effectors of Hh such as *BMI1* have been implicated in the embryonal tumour, medulloblastoma. From cross-referencing analysis of stemness/self-renewal gene list with genomic data that are available in the group including RNA seq of primary and *SMARCB1* re-expression model cell and CRISPR/Cas9 GeCKO screening with and without *SMARCB1* in MRT cells (detailed in Chapter 2 and 6), *BMI1* was identified as *SMARCB1* dependent gene. Hence, the role of *BMI1* was studied in MRT tumourigenesis.

1.3.1.6 BMI1

Oncogenic transformations are usually associated with the acquisition of developmental programs that resulted in extensive self-renewal and pluripotency, the classic features of stem cells (Suvà et al., 2013). Studies have reported the epigenetic programmes including DNA methylation, histone modification and nucleosome remodelling in regulating many cellular activities that are also fundamental to cancer development such as DNA repair, transcription and replication (Dawson and Kouzarides, 2012). The earliest evidence that

links epigenetic abnormalities to cancer were from gene expression and DNA methylation studies (Feinberg and Vogelstein, 1983). The researchers found a high frequency of methylation at CpG in the normal tissues as opposed to unmethylated CpG regions in cancer tissue. Subsequent experiments using high-performance liquid chromatography revealed global reduction of 5-methylcytosine content in the tumour sample (Gama-Sosa et al., 1983). Following this discovery, many types of epigenetic abnormalities were found in human cancers (Dawson and Kouzarides, 2012). Recently, SWI/SNF chromatin-related components such as polycomb repressive complex (PRC) have been linked to tumourigenesis of *SMARCB1*- and *SMARCA4*-deficient tumours (Januario et al., 2017, Knutson et al., 2013, Alimova et al., 2012).

BMI1 is the most extensively studied Polycomb Repressive Complex 1 (PRC1) subunit because of its significant role as a transcriptional regulator for self-renewal mechanisms in stem cells. The *BMI1* (B cell-specific Moloney murine leukaemia virus insertion site - 1) gene is located on the plus strand of chromosome 10 (10p13) (Alkema et al., 1993, Jiang et al., 2009). The gene extends over a 4.9 kb range and consists of 10 exons and 9 introns (Jiang et al., 2009). The functional promoter region of *BMI1* has not been fully elucidated and most of the studies use a sequence of 20-30 base pairs (bp) upstream of the translational start site as the promoter of this gene (Alkema et al., 1993, Jiang et al., 2009, Abdouh et al., 2009). The BMI1 protein is 37 kDa consisting of 326 amino acids (Alkema et al., 1993).

Inactivation of this gene has been implicated in many types of cancers. It has been shown that *BMI1* expression is required for maintenance of self-renewal machinery and proliferative potential of both normal and leukemic mouse hematopoietic stem cells (Park et al., 2003, Iwama et al., 2004) as well as mouse neural stem cells (Molofsky et al., 2005). *Bmi1* null mice are embryonic lethal and display striking abnormalities including neurological, morphological and haematopoiesis (Park et al., 2004).

Most mouse hematopoietic stem cells (HSC) models express high levels of *Bmi1* and inactivation of this gene *in vivo* results in a 10-fold reduction of the phenotypic hematopoietic stem cells as assessed by flow cytometry (Iwama et al., 2004). To determine the role of *BMI1* in haematopoiesis, the expression of HSC was examined in

Bmi1$^{-/-}$ mice. This study revealed that Bmi1$^{-/-}$ mice have a normal number of HSC. However, the number of HSC was significantly reduced in postnatal Bmi1$^{-/-}$ mice (Van der Lugt et al., 1994). Transplanted bone marrow and fetal liver cells from this Bmi1 null mice gave only transient haematopoiesis. These findings suggest that *Bmi1* loss impairs the maintenance of self-renewing hematopoietic stem cells.

The requirement of *BMI1* for regulating self-renewal also has been studied in mouse neural stem cells (Molofsky et al., 2003). Knockout of *Bmi1* in central nervous system (CNS) stem cells from the telencephalon at embryonic day 14.5 (E14.5) resulted in less primary tumourspheres relative to wild-type accounting for 14-fold smaller volume ($P < 0.01$). Strikingly, less secondary tumourspheres were observed (33-fold fewer ($P < 0.01$)) signifying deficiencies in self-renewal. Notably, there was no significant difference in the number of primary tumourspheres of *BMI1*-deficient neural crest stem cells (NCSCs) derived from the gut at E14.5 (enteric nervous system) compared to wild type. However, secondary tumoursphere formation was abrogated in *BMI1*-deficient neural crest cells (60-fold fewer secondary multipotent neurospheres ($P < 0.01$)). Altogether, this experimental study illustrates the defect of self-renewal machinery following *BMI1* loss in both neural crest cells and CNS.

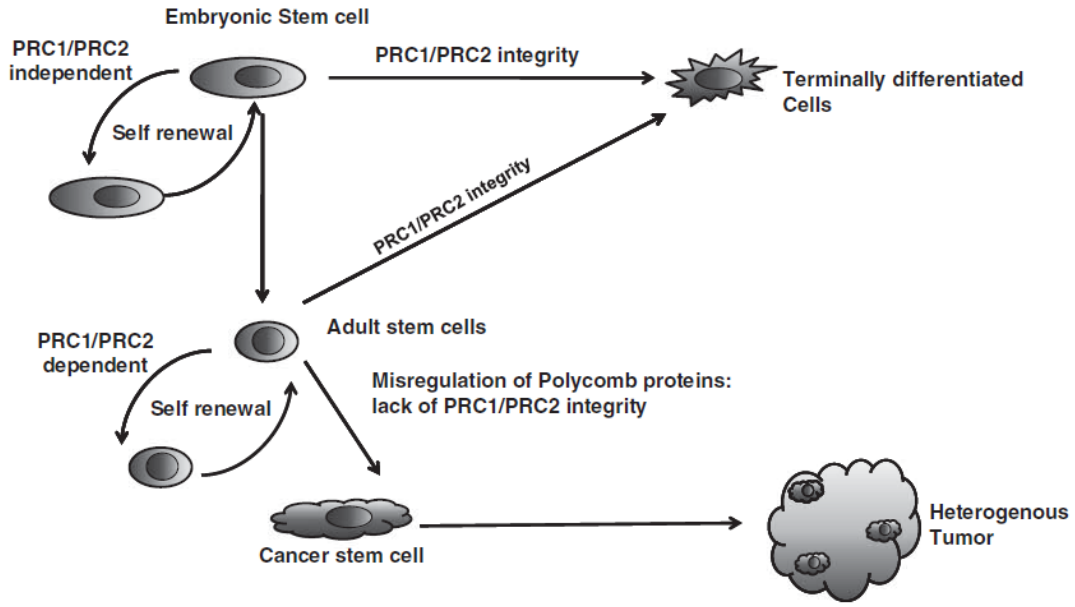

Figure 1.15 ***PRC complexes involved in stem cell maintenance by either activating or repressing specific genes that promote self-renewal or specific cell lineage differentiation.*** *Deregulation of the PRC has been implicated in the formation of cancer stem cells (CSCs). Figure was taken from (Richly et al., 2011).*

BMI1 also has a central role as an epigenetic chromatin modifier capable of regulating a large number of target genes (Richly et al., 2011). Gene expression profiling studies illustrate that *BMI1* modulates self-renewal mechanisms in HSC though regulation of the genes involved in stem cell fate decisions, stem cell-associated genes and survival genes (Park et al., 2004). *BMI1* encodes two tumour suppressor genes known as $p16^{Ink4A}$ (referred to as p16 in this thesis) and $p14^{Arf}$ (referred to as p14 in the thesis) that regulates cell cycle through TP53 and RB pathways (Jacobs et al., 1999a, Sharpless and DePinho, 1999). In cancer development, *BMI1* negatively regulates *p16* suppressing transcription at the promoter region which then initiates the formation of Cyclin dependent kinase 4 and the Cyclin D complex and promotes phosphorylation of Rb and cell progression. Simultaneously, the inhibition of *Mdm2* by *p14* is blocked by *BMI1* thus preventing the activation of the p53 pathway and subsequently cell apoptosis and senescence (Honda and Yasuda, 1999, Weber et al., 1999). In summary, transcriptional regulation by *BMI1*

through suppression of Ink4a/Arf locus promotes extensive self-renewal and cell proliferation while obstructing senescence and the apoptosis pathways. *BMI1* regulates transcriptional silencing of target genes by acting as a cofactor for Ring1/2 through monoubiquitination of lysine 119 of histone H2A, a mark associated with repressive chromatin structure (Richly et al., 2011).

Although numerous studies have illustrated a significant role of *BMI1* in various type of human cancers, very little is known about explicit functions of *BMI1* in cancer development and progression, and the precise involvement of PRC1 in cancer through epigenetic antagonism with SWI/SNF chromatin remodelling complex.

1.3.2 Epigenetic antagonism between SWI/SNF complex and Polycomb Repressive Complex (PRC): Additional mechanism drives the formation of Malignant Rhabdoid Tumour

Approximately 20% of SWI/SNF chromatin components have been found mutated in several human cancers (Alver et al., 2017). Wilson et al. (2010a) proposed that development of cancer can occur through an antagonistic mechanism between the SWI/SNF complex and Polycomb Repressive Complex (PRC). The idea of an antagonistic relationship evolved from genetic experiments in D. *melanogaster*, in which the mutation in subunits of the SWI/SNF chromatin remodelling complex was identified to suppress the defects that were caused by aberrant function of PRC. The SWI/SNF complex was needed for activation of HOX expression while PRC was required for gene silencing through repression of HOX expression.

The mammalian polycomb repressive complex (PRC) consists of two complexes namely PRC1 and PRC2 that together represent the polycomb group complex (PcG). The PRC1 complex consists of two common components which are RING1A/B with BMI1, MEL18 (PCGF2) or NSPC1 (PCGF1) (Margueron and Reinberg, 2011). PRC2 is an evolutionarily conserved complex comprising four components; EZH1/2, SUZ12, EED and RbAp46/48 (also known as RBBP7/4).

The PCG proteins have been shown to be implicated in epigenetic gene silencing during developmental and potentially a role in tumourigenesis. In many cancers such as prostate cancer, PCG protein repressed the expression of tumour suppressors (Dietrich et al., 2007, Gil and Peters, 2006) through methylation on Lys27 of histone H3 thus resulting in DNA hypermethylation (Schlesinger et al., 2007). Additionally, overexpression of PRC along with their histone marks i.e methylation on chromatin can lead to tumourigenesis. For instance, studies have demonstrated bi-allelic inactivation of *SMARCB1*, a core subunit of the SWI/SNF chromatin remodelling complex and tumour suppressors initiate MRT tumourigenesis dependency on a component of the PRC2 complex which is *EZH2* (Knutson et al., 2013, Alimova et al., 2012). Gene expression analysis of primary CNS MRT demonstrated high expression of *EZH2* in these tumours (Wilson et al., 2010a). Mechanistically, mutation of *SMARCB1* mediates the recruitment of *EZH2* of PRC2 to Polycomb target genes that become broadly H3K27-trimethylated and repressed in *Smarcb1*-deficient mouse embryonic fibroblasts. The antagonistic effect between the SWI/SNF complex and PRC was evident as inactivation of *Ezh2* stopped tumour growth following a conditional *Smarcb1* loss (Figure 1.16) however in inactivation of *Ezhw* had no effect on osteosarcomas driven by p53/Rb mutation *in vivo*. The effectiveness of targeting EZH2 as a mean to counteract MRT tumourigenesis was studied using orally bioavailable small molecule inhibibitors of EZH2 enzymatic ((N-((4,6-dimethyl-2-oxo-1,2-dihydropyridin-3-yl)methyl)-5-(ethyl(tetrahydro-2H-pyran-4-yl)amino)-4-methyl-4'-(morpholinomethyl)-[1,1'-biphenyl]-3-carboxamide) (Knutson et al., 2013) and chemical inhibitors of EZH2 (3-deazaneplanocin A (DZNep) (Alimova et al., 2012) in MRT cell lines. Both of the studies demonstrated EZH2 inhibition by the inhibitors suppresses the MRT cells growth, leads to cycle arrest and increases the cell apoptosis, thus establishing attractive therapeutic option for MRT.

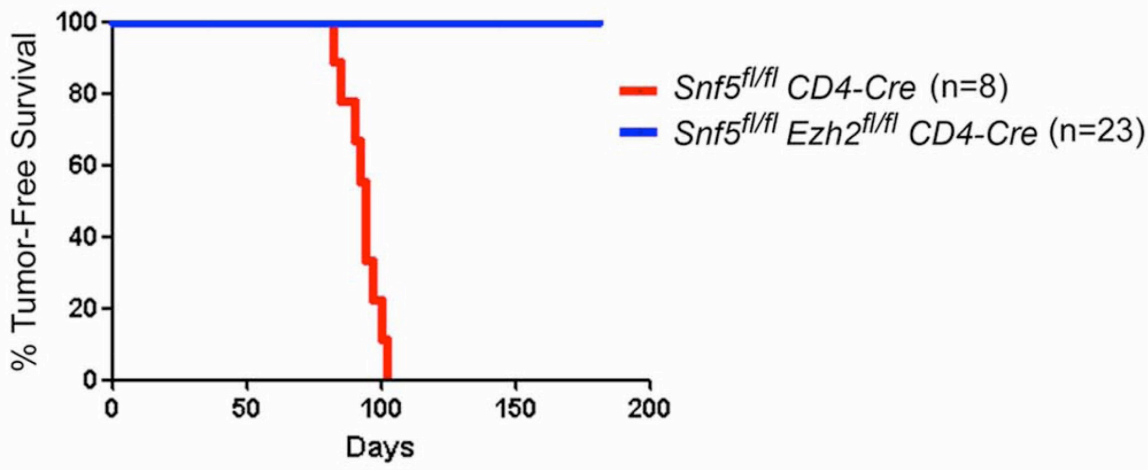

Figure 1.16 ***Ezh2 is essential for rhabdoid tumour development following SMARCB1 inactivation in vivo*** *(Figure was taken from (Wilson et al., 2010a).*

Notably, restoration of *SMARCB1* functionality in MRT cells leads to activation of tumour suppressor *p16*. Wilson et al. (2010a), also reported epigenetic silencing of *p16* by *EZH2* following *SMARCB1* loss in MRT. ChIP analysis showed strong binding of PRC complexes; BMI1, SUZ12 and EZH2 at INK4b-ARF-INK4a locus in the absence of *SMARCB1*. However, the binding of the PRC complexes was greatly reduced following *SMARCB1* re-expression in the cells. This study established the activation of *p16* occurs through displacement of PRC at promoter region in the presence of *SMARCB1*.

Unlike other human cancers which present more frequent genetic alterations, MRT are a good candidate to study the mechanism of epigenetic alterations in driving oncogenesis as its genome is remarkably stable with only one recurrent mutation reported so far (Torchia et al., 2016, Haberler et al., 2006, Lee et al., 2012). A better understanding of an association between SWI/SNF chromatin remodelling and epigenetic in cancer will provide an insight for new therapeutic approaches targeting chromatin remodelling in MRT.

1.4 Research background

MRT are one of the most lethal paediatric cancers known (Brennan et al., 2013b). It is unique not only in terms of its extremely poor prognosis and its occurrence almost entirely in infants but also in its biology. Mutation of a single gene (*SMARCB1* which encodes for a core subunit of the SWI/SNF complex) is minimally sufficient to cause tumourigenesis (Lee et al., 2012) and re-expression of *SMARCB1* in MRT cells is capable of reversing tumourigenesis, provoking growth arrest and differentiation (Caramel et al., 2008, Betz et al., 2002). Although genetically extremely homogeneous, MRT are phenotypically highly heterogeneous. They may occur at almost any part of the body (although with a tendency to occur in the brain and kidney). MRT are teratoid in nature containing cells demonstrating morphology and differentiation markers from multiple lineages even within the same tumour (Ho et al., 2000). Re-expression of *SMARCB1* in MRT cells causes individual cells within a population to become differentiated towards a variety of lineages (epithelial, neural, mesenchymal)(Albanese et al., 2006b, Caramel et al., 2008). Preliminary analysis done by Dr Dan Williamson indicates their expression profiles in this differentiated state most closely resembles that of cells derived from adult multipotent stem cells. Expression profiling of primary MRT tumours shows strong overexpression of a large number of "stemness/self-renewal" genes (e.g *BCL6, BM11, FGF2, GLI2, JAK1*). The Paediatric Brain Tumour Group at NICR and others have shown that a number of these genes are demonstrably deregulated by loss of *SMARCB1* and/or the larger SWI/SNF complex. For instance, RNA-seq profiling showed that *BCL6* is expressed at 6 times greater than related *SMARCB1* positive paediatric tumour types and that upon re-expression of *SMARCB1* in MRT tumour cells *BCL6* is transcriptionally repressed by 9-fold. PcG proteins and SWI/SNF complexes serve antagonistic developmental roles (Wilson et al., 2010b). Upon re-expression of *SMARCB1*, the chromatin environment of the p16 loci is wholesale remodelled, Polycomb silencing complexes removed and histone–marks altered (Kia et al., 2008). Loss of *SMARCB1* in a mouse model leads to elevated expression of the Polycomb gene *EZH2* and H3K27-ME3 remodelling of a large number of repressed genes (Wilson et al., 2010b).

Taken as a whole these facts lead us to hypothesize that not only is mutation of *SMARCB1* itself critical but that the type of cell in which this mutation occurs is also critically important to conferring the aggressive MRT state. Other tumour types such as Choroid Plexus Carcinomas, Schwannomatosis, Epitheliod Sarcoma, etc (Hornick et al., 2009, Hulsebos et al., 2007, Zakrzewska et al., 2005) may possess *SMARCB1* mutations without necessarily demonstrating the aggressive clinical behavior and early onset of disease that makes MRT so difficult to treat. Therefore, I hypothesised in this study that the cell of origin is highly particular and that *SMARCB1* mutation in an early multipotent stem cell provokes genome-wide chromatin remodelling which interrupts normal differentiation. It was further hypothesised that *SMARCB1* mutation in MRT cells is capable of hijacking and aberrantly maintaining the inherent "stemness/self-renewal" programme active in these cells and that this contributes critically to MRT tumourigenesis.

Current therapies for children with MRT are ineffective (Brennan et al., 2013b) and there is a desperate need for novel biological therapies. This study aimed to discover therapeutically targetable "stemness/self-renewal" pathways/genes downstream of *SMARCB1* mutation as the most efficient means to counteract MRT tumourigenesis and induce differentiation/growth arrest in MRT cells.

1.5 Overall objectives and specific aims of the study

This project aims to explore other possible mechanisms that may contribute towards MRT aggressiveness and to use this understanding to identify potential therapeutic targets and cell of origin for this lethal childhood cancer, with the following specific aims:

Aim 1: To identify a likely cell of origin for MRT through bioinformatics analysis and CRISPR/Cas9 SMARCB1 knockout in an appropriate cell of origin. Bioinformatics analysis will provide important data to prioritise the candidate cell of origin for CRISPR/Cas9 experiment. Bioinformatics analysis is presented in chapter 3 while the functional CRISPR/Cas9 experiment is described in chapter 4.

Aim 2: To characterize how *SMARCB1* mutations alter "stemness/self-renewal" programmes in order to affect tumourigenesis. The candidate stemness/self-renewal genes that are *SMARCB1*-dependent and highly expressed in MRT are identified through cross-referencing of curated stemness/self-renewal genes with RNA-seq and CRISPR/Cas9 GeCKO screening data of MRT. The expression of target genes will be studied in MRT cell lines. This part of the study is presented in chapter 2 and 6. This analysis will generate lead "stemness/self-renewal" genes/pathways active in MRT tumourigenesis that will require further validation (aim 3).

Aim 3: To test and validate at least one targetable "stemness/self-renewal" gene/pathway as a potential novel anti-MRT therapy using shRNA and the available small molecular inhibitors. This study is described in chapter 6.

Overview of the project to achieve the specified aims is presented in Figure 1.17

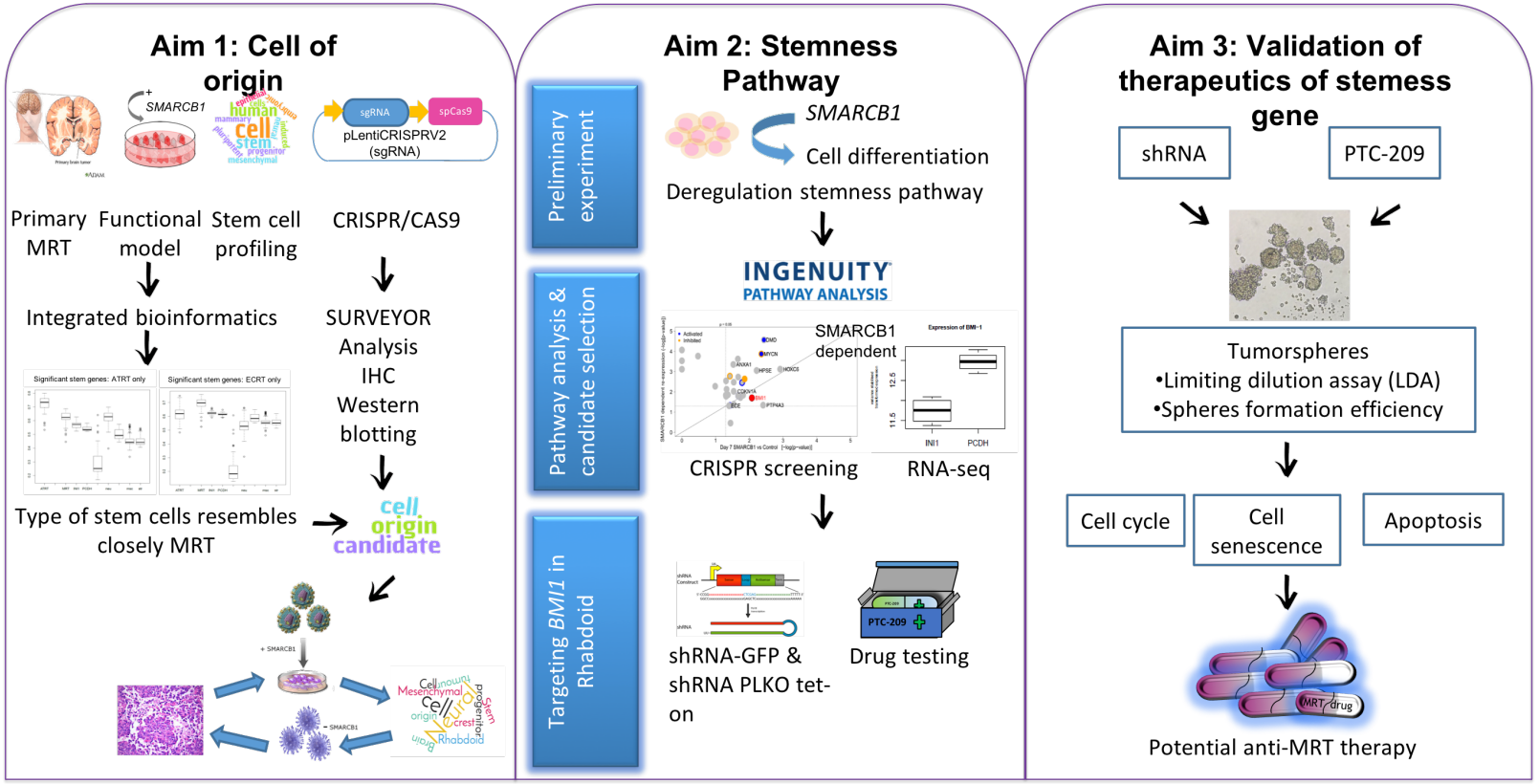

Figure 1.17 ***Illustration showing the overview of the projects for specific aims***

Chapter 2 Materials and Methods

2.1 Introduction

This chapter presents all the material and methods used in this thesis. This chapter is divided into two major sections; “dry lab” and “wet lab”. The “dry lab” section contains the bioinformatics analysis performed to identify a putative cell of origin for MRT (Chapter 3) and stemness/self-renewal candidates in MRT (Chapter 6). Whilst, the “wet lab” section includes all the techniques and materials used to achieve the aims discussed in chapter 4, 5 and 6.

2.2 “Dry lab” methods and materials

2.2.1 Bioinformatics analysis of potential cell of origin for MRT

For identification of cell of origin for MRT, various stem cells profiles were searched and catalogued in this study for identification of the cell of origin for MRT. Details are discussed below:

2.2.1.1 Quantification and Statistical Analysis

The bioinformatics analysis was accomplished using R (version 3.3.1) and Bioconductor (version 3.4).

2.2.1.2 Expression profile analysis of primary tumours

The published Affymetrix HGU133Plus2 expression array datasets for various stem cell types were obtained from NCBI GEO ((https://www.ncbi.nlm.nih.gov/geo/). These datasets were used in cross-referencing analysis with MRT primary and cells RNA-seq data for identification of cellular origin for MRT. Details of GEO accession number for each dataset were tabulated in Appendix 2.1. To generate various stem cell profiles for the analysis, the expression profile was searched for “RNA signature” from various stem cell types. The stem cell types are listed in Appendix 2.1. To identify a stem cell population with potential to become a candidate cell of origin for MRT, the expression profiles were filtered with the following requirement: HGU133plus2 platform, non-cancerous cell line, human expression profiles and no specific treatment that could change the expression of many genes. For instance, GSE32727 contains a dataset for human mammary epithelial cells and breast cancer cells. Therefore, only the expression profiles for epithelial cells were selected for cell of origin analysis. Likewise, there were 16 embryonic stem cell expression profiles in GSE24844, however, the platform that was used to analyse these profiles was Affymetrix human promoter 1.0 Array. Hence, this data was not included in the analysis.

Affymetrix HGU133Plus2 expression array datasets for primary MRT used in this study for the purpose of comparison and/or validation of potential cells of origin for MRT were also obtained from GEO NCBI database. These included 106 ATRT and 20 ECRT Affymetrix HGU133plus2 expression profiles (GEO: GSE35493, GSE64019, GSE70678, GSE73038), 10 ECRT Affymetrix HGU133a expression profiles (GEO: GSE11482). An ECRT RNA-seq dataset comprising gene counts of 65 ECRT was obtained from the open-access component of dbGaP phs000470.

Affymetrix dataset arrays (. cel file) were processed and normalized using the rma package (R/Bioconductor). Differential expression analysis was performed using limma (R/Bioconductor) for array data.

For differential expression tests genes were pre-filtered to remove those for which fold change < 3-fold and/or the range < 300 between maximum and minimum values (with the top/bottom 5% most extreme values removed). Genes were also removed if <40% of samples showed normalized counts of less than 20. Consensus bootstrapped Non-negative Matrix Factorization (NMF) was performed as described by Schwalbe et al. (2013) to determine the optimal number of clusters and to assign individuals to clusters with a given probability/confidence. Optimal metagene solutions were selected based on cluster stability measures of individual NMF runs as well as the average silhouette score obtained from bootstrapped NMF. t-Distributed Stochastic Neighbour Embedding (t-SNE) dimensionality reduction package Rtsne (R/Cran) was used to visualize and confirm NMF consensus clustering assignments. Probes significantly associated with each metagene were identified by carrying out a bootstrapped Pearson correlation with a significance cut-off of $p < 0.001$.

Top discriminatory genes were selected based on the p-value < 0.05 and selecting genes specific for neural using a limma (R/Bioconductor) discriminatory statistical coefficient >2 between embryonic and neural, or mesenchymal and neural stem cells. Mesenchymal specific genes were selected as coefficient greater than 3 compared to neural and embryonal, while embryonal related genes were chosen as those with >3 compared to neural and mesenchymal. Neural crest genes were selected as those with a coefficient greater than 2 compared to mesenchymal cells. In some analyses (to produce

a heatmap), neural crest cell-specific genes were manually curated as previously described (Ishii et al., 2012, Chun et al., 2016). The MRT-specific genes were selected by significant ANOVA F-statistic ($p<0.01$) and selecting only genes whose positive and negative log-fold change exceeded 1.5 for each comparison between MRT and each an embryonal tumour (ET) type.

NMF projection was performed using column-rank normalization, pseudo-inverse method and post-projection normalization as previously described by Tamayo et al. (2007). Pre-filtering of genes was applied to each dataset; either unlogged vst for RNA-seq or unlogged probe intensity for expression array. Genes were pre-filtered by applying a lower threshold of 20 and a ceiling of 10000, a fold change and delta from maximum-minimum of 3 and 300 respectively. Genes/probes were mapped by Ensembl Gene id. Where multiple probes exist for one gene the probe with greatest mean intensity across all samples was used.

2.2.1.3 Gene Set Enrichment Analysis (GSEA)

Gene Set Enrichment Analysis (GSEA) is described as a complete mathematical method to classify correlation between genes and clusters them into uniform classes (Subramanian et al., 2005). GSEA is a method that distinguishes if a pre-ranked gene set shows any statistically significant difference between two experimental conditions, for example, ECRT vs ATRT. The analysis requires a dataset pre-processing step, which ranks genes according to a phenotype or profile defining the distribution of the set of genes across *a priori* predefined gene-sets. The pre-ranked data sets are further processed and for each gene set an enrichment score (ES) is given; ES corresponds to the degree of correlation between the ranked gene list and predefined gene-sets. An empirical phenotype-based permutation test is utilised to measure significance levels of the observed ES, estimating p-values relative to ES null distribution. Finally, ES are normalised to the size of the original set, resulting normalised enrichment scores (NES) and false discovery rate (FDR) for each NES. FDR represents to the projected possibility that identified genes as differentially expressed are false positive. Gene Set Enrichment

Analysis (GSEA) using MSigDB libraries v6.0 C1-7 & Hallmark. was used to examine for differentially regulated pathways.

2.2.1.4 Principle component analysis

The principle component analysis (PCA) is a statistical technique that transforms a number of possibly correlated variables into a limited number of uncorrelated variables known as principle components. This technique can decrease dimensionality of complex data sets and computational costs and error of parameter estimation. PCA is an orthogonal transformation method that is aimed to maximise the component vector variance of the data set. The analysis establishes the direction that corresponds to maximal variance between the data points and projects the obtained data on the hyperplane orthogonal to that direction. Using this mathematical projection, it is possible to achieve a simpler data set, in which the dimensions are reduced. PCA is often used as a tool in explanatory data analysis or making the predictive models. In addition, PCA is utilised for visualisation of genetic distance or relatedness between populations.

2.2.1.5 Non-negative matrix factorisation

Non-negative matrix factorization (NMF) is a mathematical analysis based on an algorithm that decreases the dimension of NGS or microarray data (Brunet et al., 2004, Devarajan, 2008). It has previously been shown to be a useful decomposition of multivariate data. In particular, it allows the characterisation of aggregate patterns of gene expression (metagene) from thousands of genes. In contrast to other clustering methods, NMF groups the genes and samples by factorisation into matrices with non-negative entries; this results in an analysis with higher biological significance than PCA and t-SNE. NMF is more efficient technique for discovery of distinct molecular configurations and offers a robust technique for class identification. Furthermore, NMF is more strategic than t-SNE and PCA in terms of hierarchical clustering or self-organising maps.

NMF is more complex algorithmically, however it allows decomposition of data and also cross-referencing of different dataset (Figure 2.1). Data sets consist of expression levels

of N genes in M samples. The data are compressed into an expression matrix V composed of values N × value M; rows represent expression levels of the N genes in the M samples.

The metagenes (positive linear combination of the N genes) are obtained by factorisation of the matrix A into two matrices characterised by positive entries. Particularly, the two-matrix derived are W (composed by N genes x k metagene) and H (composed by k metagene x M samples), which are approximately equivalent to the matrix A. Each k column of the first matrix illustrates a metagene, while each M column of H matrix corresponds to metagene expression pattern of the corresponding sample.

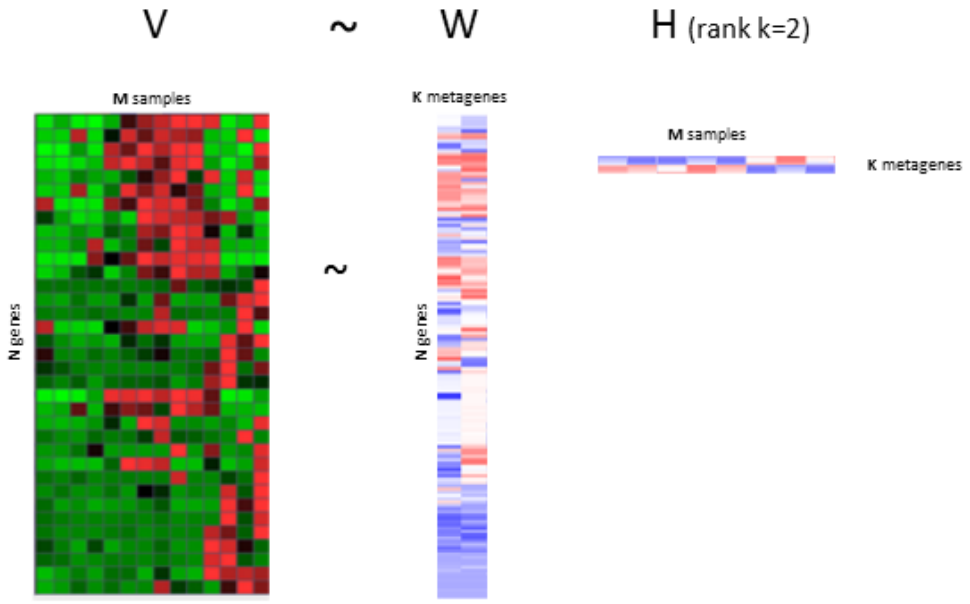

Figure 2.1 ***An example of NMF analysis of expression datasets consists of N genes, M samples and imposed k=2****. Matrix V represents a mock microarray expression data: low expressed genes are coloured in green, with the highly expressed in red while Matrix W is composed of k metagenes and the number of genes and each column corresponds to the expression level of each sample for a given metagene. The matrix H = N sample with k metagenes; in this case, each*

column represents a metagene profile for each sample. Heat colour maps are used to represent the level of metagene expression (dark blue= minimum; dark red= maximum).

2.2.1.6 t-Distributed Stochastic Neighbour Embedding (t-SNE)

t-Distributed Stochastic Neighbour Embedding (t-SNE) is another technique for dimensionality reduction and is particularly suitable for visualisation of high-dimensional datasets, while preserving some features of the original data. This method is efficient for capturing much of the local structure as well as global structure of the high-dimensional data. t-SNE reduces the deviation between two distributions: a distribution that calculates the pairwise similarities of the input objects and a distribution that calculates the pairwise similarities of the corresponding low-dimensional points in the embedding (Maaten and Hinton, 2008). The dimensionality reduction techniques convert the high-dimensional data set X = (x1, x2,...,xn) into two or three-dimensional data Y = (y1,y2,...,yn) which can be presented in a scatterplot. t-SNE plots define a soft border between the local and global structure of the data and for pairs of data that are close together. Furthermore, t-SNE defines the local neighbourhood size for each data distinctly based on the local density of the data (by forcing each conditional probability distribution Pi to have the same perplexity).

Deposited data primary tumours expression profiles			
GEO accession number/Deposited provisional number	**Tumour type**	**Source**	**Number of dataset**
GSE64019	ATRT & ECRT	Gene Expression Omnibus (GEO) NCBI	50
GSE65132	ATRT	Gene Expression Omnibus (GEO) NCBI	9
GSE35493	ATRT	Gene Expression Omnibus (GEO) NCBI	2
GSE70678	ATRT	Gene Expression Omnibus (GEO) NCBI	49
phs000470	ECRT	Database of Genotypes and Phenotypes (dbGaP)	65
GSE11482	ATRT	Gene Expression Omnibus (GEO) NCBI	10
GSE73038	ATRT	Gene Expression Omnibus (GEO) NCBI	5
GSE70421	ECRT	Gene Expression Omnibus (GEO) NCBI	3
GSE28026	ATRT	Gene Expression Omnibus (GEO) NCBI	18

Table 2.1 ***Expression profiles of primary MRT.***

Software and Algorithms		
affy (R/Bioconductor)	(Gautier et al., 2004)	http://bioconductor.org/packages/release/bioc/html/affy.html
Limma (R/Bioconductor)	(Ritchie et al., 2015)	http://bioconductor.org/packages/release/bioc/html/limma.html
Rtsne (R/Cran)	(Maaten and Hinton, 2008)	https://cran.r-project.org/web/packages/Rtsne/index.html
Ingenuity Pathway Analysis (IPA)	Qiagen	https://www.qiagenbioinformatics.com
Gene Set Enrichment Analysis (GSEA)	(Subramanian et al., 2005)	http://software.broadinstitute.org/gsea/index.jsp

Table 2.2 ***Software and algorithms used for analysis of cell of origin for MRT.***

2.2.2 Identification of self-renewal/stemness pathways/genes in MRT

MRT is a highly aggressive disease that occurs predominantly in very young children. There are a few tumour types such as choroid plexus carcinomas, schwannomatosis, epitheliod sarcoma, etc (Hornick et al., 2009, Hulsebos et al., 2007, Zakrzewska et al., 2005) may possess *SMARCB1* mutations without necessarily demonstrating the aggressive clinical behaviour. Therefore, it has been hypothesized in this study that *SMARCB1* mutation in the cell of origin is capable of hijacking and aberrantly maintaining the inherent "stemness/self-renewal" programme active in these cells and that this contributes critically to MRT tumourigenesis. Stemness can be defined as potential of stem cell niches to undergo self-renewal, differentiation and pluripotent (Anton et al., 2007, Leychkis et al., 2009). Cross-platform analysis of CRISPR data and RNA-seq of MRT primary and model lines illustrates pathways that are deregulated by *SMARCB1* such as polycomb, JAK-STAT, stemness and many more (PBTG). JAK-STAT pathway was previously studied in MRT (PBTG).

2.2.2.1 Quantification and Statistical Analysis

The bioinformatics analysis was performed using R (version 3.3.1) and Bioconductor (version 3.4) (Table 2.2).

2.2.2.2 Reconstruction of stemness/self-renewal pathways/genes that are directly affected by SMARCB1 loss in MRT

The genes that involved in stemness/self-renewal was identified through prior knowledge, canonical pathways and ontology (Kegg, GO, etc), ingenuity knowledgebase and direct reference to published literature. As the self-renewal pathways are not readily built on Ingenuity Pathway Analysis (IPA) software, the list of self-renewal genes was manually curated for the purpose of cross-referencing analysis with MRT primary and cell data. The genes were searched for their role in pluripotency and self-renewal.

To identify stemness/self-renewal genes which are active in primary MRT and whose activity is *SMARCB1* dependent, the list of stemness/self-renewal genes was cross-referenced with RNA-seq data of primary MRT and *SMARCB1* re-expression in MRT cells. Analysis of pathways/genes was performed using pathway analysis tools such as ingenuity analysis (Qiagen). Appropriate R/Bioconductor packages such as limma were used to identify statistically significant differentially expression/methylation between Medulloblastoma, and between MRT cells with and without re-expression of *SMARCB1*.

For validation of *SMARCB1* dependency, the list of stemness/self-renewal genes (56 genes) was integrated with whole genome CRISPR/Cas9 GeCKO screening data from 4 MRT cell lines with and without *SMARCB1* expression (Dr Selby, PhD thesis). Potential self-renewal genes that showed *SMARCB1* dependency was selected if the gene present in both cross-referencing analyses (RNA seq and CRISPR).

The workflow for identification of stemness/self-renewal candidate in this study was illustrated in Figure 2.2.

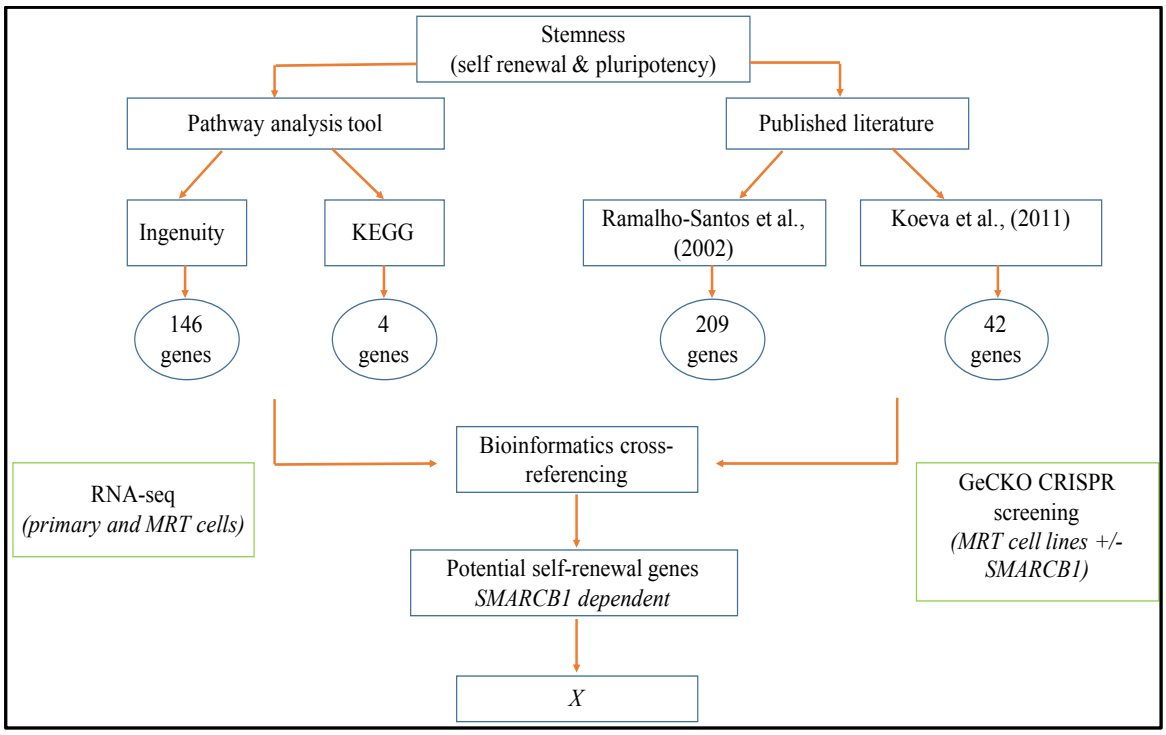

Figure 2.2 ***Workflow to identify stemness/self-renewal genes that are SMARCB1 dependent in MRT.***

2.3 “Wet lab” methods and material

2.3.1 Cell lines

2.3.1.1 Cell line culture

List of cell lines used in this thesis is tabulated in Table 2.3. The role of *Smarcb1* in mediating tumourigenesis in a putative cell of origin for MRT was studied in a neural crest (NC) stem cell and a non-stem cell line NIH3T3. NIH3T3 were used as a control cell line in this study.

Neural crest cells were seeded on Matrigel (Fisher Cat No. CB-40234) coated plate or T75 flask (Corning®) at 200,000 and 1 x 10^6 cells respectively and split every 2-3 days as appropriate.

The effect of downregulation of *BMI1* was evaluated in four different human cell lines; two were Atypical Teratoid Rhabdoid Tumour (BT16 and CHLA-266) and remaining two were Extra Cranial Rhabdoid Tumour (A204 and G401). Cells were seeded at appropriate cell densities in T75 and T175 flasks (Corning®) and were split every 2-3 days as appropriate (Table 2.5). 293T cell line was used as host cells for lentiviral packaging system. *SMARCB1* re-expression in MRT cells were obtained from Dr Finetti (PBTG).

In general, for sub-culturing, cells were washed twice with PBS and treated with either Accumax solution (1x; Millipore Cat No. SCR006) or 0.05% trypsin in 0.5mM EDTA at 37°C for 2-3 minutes. Cell cultures were neutralised inappropriate cell medium (as described in Table 2.4) and centrifuged at 1200rpm for 3-5 minutes to pellet the cells. The cells were gently pipetted and diluted to 5-10 times at the seeding density mentioned in Table 2.5. The cell viability was measured by staining an aliquot of culture with Trypan Blue (Thermo Fisher Scientific) and counted using Countess II FL automated cell counter (Thermo Fisher Scientific). The cells were maintained at 37°C in a 5% CO_2 humidified incubator.

Cells were cryopreserved in cell media with 10% DMSO (Table 2.4) using a Nalgene slow freeze Mr Frosty container at -80°C for the first 24 hours and subsequently transferred to liquid nitrogen.

Cell line	Species	Origin	Disease
A204	Homo sapiens	Kidney	RTK
G401	Homo sapiens	Kidney	RTK
CHLA-266	Homo sapiens	CNS (Posterior fossa)	ATRT
BT16	Homo sapiens	CNS (Posterior fossa)	ATRT
293T	Homo sapiens	Kidney	None
NIH3T3	Mus musculus	Embryo	None
O9-1	Mus musculus	Mouse cranial	None

Table 2.3 ***Information of cell lines used in this thesis***

Media	Cell line	Composition of media	Cryopreservation of cells
ES cell medium	O9-1	15% FBS and mLIF complex ES cell medium (Cat. No. ES-101-B) 25 ng/ml FGF-2 (Cat. No. Milipore GF003)	10% DMSO, 90% ES cell medium
DMEM 10%	NIH3T3, 293T	1% L-glutamine 1% sodium pyruvate 1% penicilin/streptomycin 10% foetal bovine DMEM 5876 (Sigma Aldrich)	10% DMSO, 40% cell media, 50% Foetal calf serum
RPMI 10%	A204, G401	1% L-glutamine 1% penicillin/streptomycin 10% foetal bovine RPMI 1640 (Sigma-Aldrich)	10% DMSO, 40% cell media, 50% Foetal calf serum
IMDM 20%	CHLA-266	1% L-glutamine 1% penicillin/streptomycin 20% foetal bovine IMDM (Thermo Fisher Scientific)	10% DMSO, 40% cell media, 50% Foetal calf serum
DMEM 10%	BT16	1% L-glutamine 1% penicilin/streptomycin 10% foetal bovine DMEM 5876 (Sigma Aldrich)	10% DMSO, 40% cell media, 50% Foetal calf serum

Table 2.4 ***Media used for culturing cell lines***

Cell line	Cell density for culturing	Seeding plate/flask
O9-1	$3x10^6$ in 20 ml media	T175 flask
	$1x10^6$ in 10 ml media	T75 flask
	$2 x10^5$ in 2 ml media	6-well plate
NIH3T3, 293T	$3x10^6$ in 20 ml media	T175 flask
	$1x10^6$ in 10 ml media	T75 flask
	$2 x10^5$ in 2 ml media	6-well plate
	$3.5 x10^6$ in 10 ml media	10 cm^2 plate (for lentiviral)
A204, G401	$3x10^6$ in 20 ml media	T175 flask
	$1x10^6$ in 10 ml media	T75 flask
	$2 x10^5$ in 2 ml media	6-well plate
CHLA-266	$3x10^6$ in 20 ml media	T175 flask
	$1x10^6$ in 10 ml media	T75 flask
	$2 x10^5$ in 2 ml media	6-well plate
BT16	$3x10^6$ in 20 ml media	T175 flask
	$1x10^6$ in 10 ml media	T75 flask
	$2 x10^5$ in 2 ml media	6-well plate

Table 2.5 ***Cell density used for culturing cell lines in various plating formats.***

2.3.1.2 Formation of tumourspheres from Malignant Rhabdoid Tumours (MRT) cell lines and colony formation

MRT cell lines were grown as non-adherent tumourspheres to assess self-renewal capacity. The adherent cells were detached from the flask using 1% trypsin and centrifuged at 1200rpm for 5 minutes. The cells were washed twice with 1x PBS and were dissociated into a single cell suspension by filtering the culture through 70µ cell strainer and were grown in tumoursphere complete media (TSM) at density of 10,000 to 20,000 cells/ml. The spheres were usually formed by day 3-12 and re-fed with TSM media every three days.

The tumoursphere completed media (TSM) was made up of 2% B27 supplement, 20 ng/ml EGF (Peprotech), 30 ng/ml bFGF (Peprotech), 2U/ml heparin (Sigma Aldrich), 0.5 µg/ml hydrocortisone (Sigma Aldrich), 1% sodium pyruvate (Thermo Fisher Scientific), 1% penicillin/streptomycin and 1% non-essential amino acid (Thermo Fisher Scientific) in DMEM/F12 media. Cells were passed through a cell strainer (70 µ) to produce a single cell suspension. The spheres were usually formed by day 3-12. The fresh TS media was refreshed in every three days.

The MRT cells were grown until formation of 100-200 µm spheres to avoid cell differentiation, death and cellular attachment associated with larger spheres. To passage the cells, the cultures were collected and centrifuged at 800 rpm for 10 minutes. The supernatant was gently removed. 500 µl of Accutase solution (Stemcell Technologies) was added to the cells and incubated at 37°C for 5 minutes. The spheres were dissociated by pipetting up and down at least 20 times and 500 µl of warm TS media was added to neutralise the Accutase solution. The culture was centrifuged again at 1200 rpm for 3 min, counted and re-plated at appropriate cell density. Viable cells were then determined by Trypan blue dye exclusion and counted using Countess II FL automated cell counter (Thermo Fisher Scientific). Appropriate numbers of single cells were transferred into 6 and 24 low attachment well plates (Corning®).

2.3.2 SDS-PAGE and Western Blot

2.3.2.1 Protein extraction and quantification

Total protein extracts were prepared from $1x10^6$ cells using cold RIPA buffer (Sigma Aldrich) with 1% cocktail protein inhibitor (Sigma Aldrich). The lysates were kept on ice for 15 minutes followed by sonication in a Diagenode Bioruptor (Denville, NJ) for three 30 second cycles on and three cycles off to ensure complete membrane disruption, and then centrifugation at 15 rcf (relative centrifugal force) for 15 minutes at 4°C.

The protein supernatants were quantified using the BCA™ Protein Assay Kit (Pierce) according to the manufacturer's instructions. Briefly, 25 µl of each standard and 5 µl of protein lysate were loaded into the well of a 96-well plate containing 200 µl of working

reagent. The series of standard protein concentrations were prepared from mixtures of bovine serum albumin (ranging from 2 mg to 0 mg) and 1X PBS according to manufacturer protocol. The plate was incubated for 30 minutes at 37 °C followed by 3 minutes of cooling down at room temperature. The absorbance was measured at 562 nm using FLUOstar Omega (BMG Labtech) plate reader and the standard curve generated.

2.3.2.2 Conventional protein electrophoresis and blotting

Loading buffer (see Appendix) was mixed with 50 µg of protein lysate and the solution was denatured at 99 °C for 5 minutes, briefly centrifuged and kept on ice. The samples and molecular weight marker (Movex Sharp protein standard, Invitrogen) were separated on 4-20% gradient polyacrylamide Amersham ECL Gel (GE Healthcare, UK). The gel was run at a constant 160 mV in Tris-Glycine Running buffer for 60 minutes. The electrophoresed protein was transferred onto nitrocellulose membrane (Amersham) using a semi-dry electroblotting system for 60 minutes at 100 mV. The membrane was stained in Ponceau-S solution 0.1% (Sigma) to check that protein was fully transferred to the membrane and washed with dH_2O to remove leftover staining solution. All solutions are listed in Table 2.6.

Buffer	Composition
Running Buffer	0.3% w/v Tris (Sigma Aldrich) 1.44% w/v Glycine (Sigma Aldrich) 0.1% w/v SDS (Sigma Aldrich) dd H2O
2X Loading Buffer	2% w/v Bromophenol Blue (Biorad) 5% v/v 1 M Tris, pH 7 (Sigma Aldrich) 25% v/v mL 20% SDS (Sigma Aldrich) 2% v/v β-Mercaptoethanol (Sigma Aldrich) ddH2O
Transfer Buffer	0.3 % w/v Tris (Sigma Aldrich) 1.44 % w/v Glycine (Sigma Aldrich) 0.1 % w/v SDS (Sigma Aldrich) 20 % v/v Absolute Ethanol (Sigma Aldrich) dH20
Blocking solution	5% w/v Non-Fat Dry Milk (Sigma Aldrich) 1X TBS 1% v/v Tween-20 (Sigma Aldrich) dH20
TBS pH 7.6	0.24% w/v Tris (Sigma Aldrich) 0.84% w/v NaCl (Sigma Aldrich)
T-TBS	1X TBS (Sigma Aldrich)
	1% v/v Tween-20 (Sigma Aldrich)

Table 2.6 ***Buffers for running Western Blot***

The membrane was blocked in 5% skimmed milk in 1% TBST (10 mM Tris-HCl pH 8.0, 150 mM NaCl, 0.05% Tween 20) overnight at 4°C. The membrane was probed using antibodies against BMI1 (1:250, Abcam), SMARCB1 (1:250, BD Biosciences), SMARCA4 (1:250, Santa Cruz Biotechnology), histone H2A (1:1000, CST), uH2A (1:200, Diagenode), H3 (1: 10,000, ThermoFisher Scientific), RING1A (1:1000, CST) at room temperature for 4 hours or 4 °C overnight followed by another one-hour incubation with specific secondary antibody (1:5000) at room temperature. After rinsing in dH2O three times for 10 minutes, the antibody was detected using enhanced chemiluminescence (ECL) kit (Pierce, France). Immediately after visualisation of antibody using GBox

Chemi XL1.4 (Syngene) imaging system, the membranes were washed three times for 5 minutes with 1x TBST before incubation in Western blot stripping buffer (Thermo Fisher Scientific) for 1 hour at 37°C. The membranes were washed again as before and incubated with β-actin antibody (1:20,000, Abcam) for 30 minutes at room temperature. All antibodies are indicated in Table 2.7.

Antibody	Company	Dilution
Anti-SMARCB1 (BAF47) Cat. No. 612110	BD Biosciences	1:250
Anti-SMARCA4 (BRG1 G-7) Cat. No. sc17796	Santa Cruz Biotechnology	1:250
Anti-Beta Actin Cst. No. ab49900	Abcam	1:50000
Secondary antibody HRP Goat Anti-Rabbit IgG Cat. No. ab6721	Abcam	1:5000
Secondary antibody HRP Rabbit Anti-Mouse IgG Cat. No. ab6728	Abcam	1:5000
Anti-BMI1 ChiP Grade Cat No. ab14389	Abcam	1:250
Anti-BMI1 XP Rabbit Cat. No. 6964	CST Technology	1:250
Anti-p16INK4a/CDKN2A Cat. No. AF5779	R&D Systems	1:50
Anti-CD44 Cat. No. ab157107	Abcam	1:400

Table 2.7 ***Antibodies used in Western Blot***

2.3.2.3 WES simple protein blotting and analysis

Protein lysate was prepared as previously described in Section 2.2.1. For WES analysis, the lysates were separated by an automated capillary-based electrophoresis system (WES, Protein Simple, San Jose, CA). All procedures were performed according to manufacturer's recommendations using supplied reagents. Briefly, after quantification of protein concentration using similar steps described in section 2.2.1, 4 µl of 0.8 to 1.0 µg of protein lysates were mixed with 1 µl of 5x sample fluorescent master mix and were denatured at 95°C for 5 minutes. The samples, blocking reagent, wash buffer, primary antibodies, secondary antibodies and chemiluminescent substrate were added into designated wells in the manufacturer provided microplate. Primary antibodies used as listed in Table 2.7. Plate loading, sample separation and immune detection were carried out automatically using default settings for 3 hours. The data was analysed using Compass software (Protein Simple).

2.3.3 Expression quantification by real-time PCR (RT-PCR)

2.3.3.1 DNA/RNA extraction, purification and quantification

DNA extraction was performed on $1x10^6$ cells using the DNeasy Blood and Tissue Kit (Qiagen) according to the manufacturer's instructions. RNA was extracted from $1x10^6$ cells using the Total RNA Purification Kit (Norgen Biotek). Briefly, the adherent cells were washed twice with 1X PBS and 350 µl of Lysis buffer was added to the cells in a 6-well plate format. The lysate containing DNA or RNA was fixed with 100% methanol and bound to the column. The column was washed twice with a washing buffer followed by centrifugation at 14,000 x g for 1 minute. DNA or RNA was eluted in an appropriate volume of TE buffer or ddH_20 (Invitrogen) respectively. For long-term storage, DNA samples were stored at -20 °C and RNA samples at -80 °C. Quantification of DNA and RNA was carried out using NanoDrop 1000 (Thermo Scientific). The purity and integrity of total RNA was evaluated based on OD ratios at A260/A280 and A260/A230 ranged between 1.8 to 2.

2.3.3.2 cDNA conversion of RNA samples

cDNA was synthesised from 2 µg of total RNA using High-Capacity RNA to cDNA kit ™ (Applied Biosystem). To prepare 20 µl of cDNA, an appropriate volume of RNA (2 µg) was added to 10 µl of 2X reverse transcription buffer mix, 1 µl of reverse transcription enzyme mix and topped up with nuclease-free H_2O. The mixture was incubated at 37 °C for 60 minutes, 95 °C for 5 minutes and held at 4°C. The cDNA was stored at -20°C.

2.3.3.3 Oligonucleotides and Primer design for qRT-PCR

All oligonucleotides were synthesised either by Sigma Aldrich or Eurofins Genomics and re-suspended in nuclease-free H_2O (Invitrogen) to a concentration of 100 µg/mol. Primers used in qRT-PCR (Table 2.8 and Table 2.9) were designed using Primer3Plus software (version 4.0.0 and previously; http://www.bioinformatics.nl/cgi-bin/primer3plus/primer3plus.cgi/) and Primer Express software version 3. The transcripts of the genes were retrieved from the Ensembl (http://www.ensembl.org/index.html). Each of the primers was checked for non-specific binding using NCBI blast nucleotides (https://blast.ncbi.nlm.nih.gov/) and UCSC In-Silico PCR software (https://genome.ucsc.edu/).

Primers	Species	Sequence (5'-3')
GAPDH Fwd	Human	CAGGTCATCCATGACAACTTTG
GAPDH Rev	Human	GTCCACCACCCTGTTGCTGTAG
BMI1 Fwd	Human	TTCATTGATGCCACAACCAT
BMI1 Rev	Human	CAGCATCAGCAGAAGGATGA
p16 Fwd	Human	CCCTCAGACATCCCCGATT
p16 Rev	Human	TCTAAGTTTCCCGAGGTTTCTCA
p14 Fwd	Human	CCCTCGTGCTGATGCTACTG
p14 Rev	Human	CCATCATCATGACCTGGTCTTCT
p21 Fwd	Human	GGCAGACCAGCATGACAGATT
p21 Rev	Human	GCGGATTAGGGCTTCCTCT
CD44 Fwd	Human	TCCAACACCTCCCAGTATGACA
CD44 Rev	Human	GGCAGGTCTGTGACTGATGTACA
CCND1 Fwd	Human	GCCGTCCATGCGGAAGATC
CCND1 Rev	Human	CCTCCTCCTCGCACTTCTGT
CCND2 Fwd	Human	CTGTGTGCCACCGACTTTAAGTT
CCND2 Rev	Human	TGCTCCCACACTTCCAGTTG
CCND3 Fwd	Human	CAGGCCTTGGTCAAAAAGCA
CCND3 Rev	Human	GCGGGTACATGGCAAAGGTA
CCNE1 Fwd	Human	CCAGGAAGAGGAAGGCAAAC
CCNE1 Rev	Human	CCTGTCGATTTTGGCCATTT
CCNE2 Fwd	Human	CCTTGTGCCATTTTACCTCCAT
CCNE2 Rev	Human	CATCCAATCTACACATTCTGAAATACTG
CDK4 Fwd	Human	TGCAGAGATGTTTCGTCGAAA
CDK4 Rev	Human	CCCAACTGGTCGGCTTCA
CDK6 Fwd	Human	CTTCGAGCACCCCAACGT
CDK6 Rev	Human	GGTTTCTCTGTCTGTTCGTGACACT
GLI2 Ex2 Fwd	Human	AAGCAAGAAGCCAAAAGTGG
GLI2 Ex3 Rev	Human	TGGTACCTTCCTTCCTGGTG
GLI3 Ex3 Fwd	Human	CGAACAGATGTGAGCGAGAA
MYC Fwd	Human	AATGAAAAGGCCCCCAAGGTAGTTATCC
MYC Rev	Human	GTCGTTTCCGCAACAAGTCCTCTTC
JARID2 Ex7 Fwd	Human	GTCACGCAGATTCAGCACAT
JARID2 Ex8 Rev	Human	TAATCAGCCGGAAAAAGCAG
SOX2 Fwd	Human	TTGCTGCCTCTTTAAGACTAGGA
SOX2 Rev	Human	CTGGGGCTCAAACTTCTCTC
OCT3/4 Fwd	Human	AGCAAAACCCGGAGGAGT
OCT3/4 Rev	Human	CCACATCGGCCTGTGTATATC

Table 2.8 ***Primers for qRT-PCR to evaluate the differential expression in human cell lines.***

Primers	Species	Sequence (5'-3')
Klf4 Fwd	Mouse	GTACCCCTCTCTCTTCTTC
Klf4 Rev	Mouse	GGCTGCCTCATTAATGT
Sox2 Fwd	Mouse	CTGGACTGCGAACTGGAGAAG
Sox2 Rev	Mouse	TTTGCACCCCTCCCAATTC
Oct4 Fwd	Mouse	TTCCCTCTGTTCCCGTCACT
Oct4 Rev	Mouse	TGGTGCCTCAGTTTGAATGC
Myc Fwd	Mouse	GCAGCTCGCCCAAATCC
Myc Rev	Mouse	CGAGTCCGAGGAAGGAGAGA
Bmi1 Fwd	Mouse	CGCTCTTTCCGGGATCTTTT
Bmi1 Rev	Mouse	GCTCAGTGATCTTGATTCTGGTTGT
Jarid2 Fwd	Mouse	CAGTAGGTCAGCACGGGAGAA
Jarid2 Rev	Mouse	CGGAGTGGCCTCTTTGCTT
Gli2 Fwd	Mouse	CTGCATGCTAGAGGCAAACTTTT
Gli2 Rev	Mouse	TCCATCTCAGAGGCTCATACTCTTT
Ezh2 Fwd	Mouse	CGCTCTTCTGTCGACGAT
Ezh2 Rev	Mouse	CTCTTATATGTGTTGGGTGTTG
P16 Fwd	Mouse	CTCAACTACGGTGCAGATTCGA
P16 Rev	Mouse	CACCGGGCGGGAGAAG
P21 Fwd	Mouse	TTCCGCACAGGAGCAAAGT
P21 Rev	Mouse	CGGCGCAACTGCTCACT
Ccnd1 Fwd	Mouse	GTGCGTGCAGAAGGAGATTGT
Ccnd1 Rev	Mouse	CTCACAGACCTCCAGCATCCA
Ccnd2 Fwd	Mouse	CCATGAATTACCTGGACCGTTT
Ccnd2 Rev	Mouse	GGAGCTGAAGATGGGTCTTAGGA
Ccnd3 Fwd	Mouse	TCCAAGCTGCGCGAAAC
Ccnd3 Rev	Mouse	GGTCCGTATAGATGCAAAGCTTCT
Ccne1 Fwd	Mouse	GGTGGCTCCGACCTTTCAG
Ccne1 Rev	Mouse	GCAAAAACACGGCCACATT
Ccne2 Fwd	Mouse	CTAAGGCGCTTTATGTTTGCAA
Ccne2 Rev	Mouse	ATGTTGACACAGTCCTCATCTCATAAT
Cdk4 Fwd	Mouse	CCTGCCGGTTGAGACCAT
Cdk4 Rev	Mouse	AAGAAAATCCAGGCCGCTTAG
Cdk6 Fwd	Mouse	CCTGAAGCCAGCATGGAGAA
Cdk6 Rev	Mouse	CCACGCACTCATACTGCTGATC
Cd44 Fwd	Mouse	TTCTCCCCACGACCCTTTT
Cd44 Rev	Mouse	GGCGTGCTGGATGAAACG
Gapdh Fwd	Mouse	GTTGTCTCCTGCGACTTCA
Gadh Rev	Mouse	GGTGGTCCAGGGTTTCTTA

Table 2.9 ***Primers for qRT-PCR to evaluate differential expression in mouse cell lines.***

2.3.3.4 Quantitative polymerase chain reaction

The qRT-PCR was performed using a SYBR Green qPCR Supermix-UDG with ROX kit (Invitrogen, USA) on a ViiA7 machine (Applied Biosystems, UK). The qRT-PCR was carried out in a 10 µl reaction containing 4µl of cDNA (1 ng/µl), 0.2 µl of forward primer (100 mM), 0.2 µl of reverse primer (100 mM), 5.1 µl SYBR® Select Master Mix and 0.5 µl dH_2O. The master mix provided is composed of AmpliTaq® DNA Polymerase and SYBR® Green cyanine dye, resulting in binding to DNA that absorbs blue light (λmax = 497 nm) and emits green light (λmax = 520 nm). The reactions were performed in 364-well plate with cycling conditions described in Table 2.10. All qRT-PCR reactions were run in triplicate with GAPDH used as internal control.

Reagent	Final volume (µl)	qPCR cycle run
SYBR Select Master Mix	5.1	50 °C for 2 minutes 95 °C for 10 minutes 45 cycles: 95 °C for 15 minutes 60 °C for 35 minutes 95 °C for 15 minutes 60 °C for 1 minutes
Forward primer (10 mM)	0.2	
Reverse primer (10 mM	0.2	
cDNA (1 ng/µl)	4.0	
dH_2O	0.5	

Table 2.10 ***qRT- PCR reactions and run conditions***

2.3.3.5 Analysis of qRT-PCR data by the comparative CT method

Relative quantification of qRT-PCR data was analysed using $2^{-\Delta\Delta CT}$ to determine changes in gene expression relative to a housekeeping gene, GAPDH. This method is advantageous as it does not require a calibration curve. The $2^{-\Delta\Delta Ct}$ method assumes a uniform PCR amplification efficiency of 100% across all samples.

Differential gene expression (fold change) was calculated as follows:

1) $\Delta Ct = [Ct_{\text{target gene}} - Ct_{\text{reference gene}}]$
2) $\Delta\Delta Ct = [\Delta Ct_{\text{target sample}} - \Delta Ct_{\text{reference sample}}]$
3) $\text{Fold change expression} = 2^{-\Delta\Delta Ct}$

2.3.4 Immunohistochemistry

Cells for immunohistochemistry were harvested and embedded on the slide using the cytospin method. Briefly, 20 µl cell suspension (at a density of 1 $x10^5$ cells) was added into a funnel that attached to the slide. The funnels were loaded in a rotor and centrifuged at 4000 rpm for 5 minutes using Shandon Cytospin Centrifuge instrument. The cells then were fixed in formalin for 10 minutes followed by 95% ethanol for 5 minutes. The cell sections were stained for anti-SMARCB1 and anti-CD44 antibodies (Table 2.7) according to standard protocol (Judkins et al., 2004, Koh, 2013). The images of sections were captured using Aperio Imagescope analysis software.

2.3.5 Flow cytometry

2.3.5.1 Fluorescence-activated cell sorting

For limiting dilution assay, GFP-, RFP- and Tomato-expressing cells were harvested and washed twice with PBS. Cells were centrifuged at 1200 rpm for 5 minutes, re-suspended in 100 µl of PBS for sorting.

For isolation of CD44 high/low cell populations, cells were harvested and washed twice with PBS. Cells were transferred to a 5 ml FACS tube and were mixed with 100 µl of FACS sorting buffer made up from 0.2% BSA in PBS. 5 µl of mouse monoclonal CD44-APC-Cy™7 antibody (BD Pharmingen) was added $1x10^6$ cells and the solution was incubated for 30 minutes at room temperature in the dark. 500 µl of sorting buffer was added after 3 minutes of centrifugation at 450 rcf.

Prior to sorting, cells were passed through a 70 µ cell strainer to obtain single suspension cells. All samples were sorted using FACSAria sorter. DAPI (Sigma Aldrich, 1 µg/ml) was added to exclude dead cells.

2.3.5.2 Cell cycle analysis with Propidium iodide (PI)

Cell cycle stages were determined by measuring the cellular DNA content using flow cytometry. Cells were harvested, washed twice with PBS and fixed with 70% cold ethanol overnight at 4 °C. For cell cycle analysis, the cells were washed twice with cold PBS and centrifuged at 800 rpm for 5 minutes. The cells then were incubated with 100 µg/ml ribonuclease A, RNase (Sigma Aldrich) for 5 minutes followed by 30 minutes staining with 50 µg/ml propidium iodide, PI (Sigma Aldrich). Samples were analysed using a FACSCalibur (BD Biosciences) and FlowJo software.

2.3.5.3 Assessment of different apoptotic stages using FITC AnnexinV

For detection of different apoptotic stages following treatment with shRNA and inhibitor, cells were harvested, washed twice with cold PBS and resuspended in 1X Binding Buffer at a concentration of $1x10^6$ cells/ml. 100 µl of sample was transferred to a 5 ml FACS tube and was mixed with 5 µl of FITC Annexin V and 5 µl PI. The solution was incubated for 15 minutes at room temperature in the dark. 500 µl of 1X Binding Buffer was added to the tube prior to analysing the samples on FACS FortessaX20. The resulting FACS data were analysed with FlowJo.

2.3.6 Lentiviral production, sucrose gradient purification and infection

For lentiviral production, 3.5 x 10^6 293T cells were seeded in 10 cm dish and were co-transfected with 10 µg of expression vector and the packaging vectors 10 µg pCMV-ΔR8.91 and 5 µg pMD2G using Calcium Phosphate Transfection (Calphos Transfection Kit, Clontech). After 12 hours of transfection, media was replaced with fresh media. Lentivirus supernatant was collected 72-hours post-transfection, centrifuged at 4°C for 10 minutes, aliquoted and stored at -80 °C. For transduction of stem cells, the virus was concentrated using the sucrose cushion technique. Briefly, 25 ml of lentivirus medium was added into 37.5 ml Beckman conical tunes and overlaid with 4 ml of 20% sucrose (made in 1X PBS and sterile filtered). The tubes were spun at 26,000 rpm for 2 hours at 4°C in a Beckman Swingle bucket rotor (SW32Ti). After spin, the supernatant was carefully discarded, and the virus pellet was re-suspended with 200 µl of cold 1X PBS.

2.3.6.1 Determining viral titre

Titre of virus particles was calculated by infection of 100,000 293T cells with virus stock in a serial dilution approach from 10^{-3} to 10^{-7}. 24-hours post-infection, the media containing virus was replaced. For Puromycin resistance vector, the cells were split 1:2. Fresh media with 1 µg/ml Puromycin (Invitrogen) was added to all but one well of a 12-well plate which had fresh media only and served as a control. The cells were harvested after 48 hours of Puromycin selection and the cells viability was counted using Countess

II FL automated cell counter (Thermo Fisher Scientific). The virus titer in plaque-forming units (PFU/ml) was calculated by firstly determining the slope of the graph generated from the percentage of viable cells after Puromycin selection at different virus dilutions (with an assumption of MOI 1 = 50%) and then measured PFU/ml according to the formula shown below:

PFU/ml: (slope (x) of graph) / (number of cells seeded for titer)

Virus titre for fluorescently labelled viruses (GFP, RFP and Tomato) was determined using FACS Calibur and the resulting data was used to measure transduction unit per ml (TU/ml) of the virus particle. Briefly, 100,000 of G401 cells was infected with a 10-fold serial dilution of stock virus. 24-hours post infection, the virus-containing media was replaced with fresh media and the cells were harvested three days after infection. The intensity of fluorescence signal for each serial dilution was assessed by FACS and the virus titer (TU/ml) was calculated using the formula as below:

TU/ml: (N x P) / (V x D)

Note:

N = Cell density seeded for titer

P = % of fluorescent positive cells (should be <20%)

V = Virus volume used for infection in each well, in ml

D = Dilution factor

2.3.6.2 Lentivirus transduction with different multiplicity of infection (MOI)

Multiplicity of infection (MOI) is described as number of virions affecting each cell during infection. Theoretically, if 1 million virions are required to infect 1 million cells,

the MOI is one. MOI was determined by infecting the Rhabdoid cell lines with the virus at different MOI ranging from 1 to 20. After 24-hours post infection, the spent media was replaced with fresh media. Three days post-infection, GFP-, RFP- and Tomato-expressing cells were harvested, washed twice with PBS, counted for cell viability using Trypan blue dye and analysed on FACS Calibur for fluorescence signal. RNA was extracted from the samples and cDNA was synthesized from a total RNA to determine the relative quantification of gene expression of *p21, p14, p16, BMI1* and *CD44* (Table 2.8 and Table 2.9). Protein was also extracted from similar cell pellet and was evaluated by Western Blot. The ideal MOI was determined by considering cell culture condition during treatment relative to control and greatest number of infected cells that showed downregulation of *BMI1* and overexpression of other genes *p21, p14, p16* and *CD44*.

MOI for lentiCRISPRv2 virus was determined by infecting stem cells, 293T and NIH3T3 with the unconcentrated or concentrated virus at MOI 1, 3, 5 and 10. Media containing virus was removed next day and replaced with fresh media containing puromycin to a final concentration of 1 μg/ml. Two days after puromycin selection, the cells were harvested, washed twice with PBS and counted for cell viability using Trypan blue staining to determine the MOI.

2.3.7 Bacterial strains

Bacterial strain used in this study was One Shot Stbl3 *Escherichia coli* (*E.coli*) (Invitrogen).

2.3.7.1 Viral vectors

2.3.7.2 shRNA BMI1 and non-silencing (NS)

Two independently designed lentiviral *BMI1* RNAi knockdown and control short hairpins were used. The H1-shRNA-EF-1a-eGFP vector contained shRNA sequences targeting *BMI1* and the Luciferase was a kind gift from Prof John E. Dick. The second hairpin contained pLKO5dSFFVeGFPmiR30n vector (A gift from Prof Olaf T. Heidenreich) (Figure 2.3) had shRNA sequence to *BMI1* and red fluorescent protein (RFP) used as non-

targeting control (NTC). The two *BMI1* short hairpin RNA (shRNA) were designed to target different regions of the *BMI1* transcript.

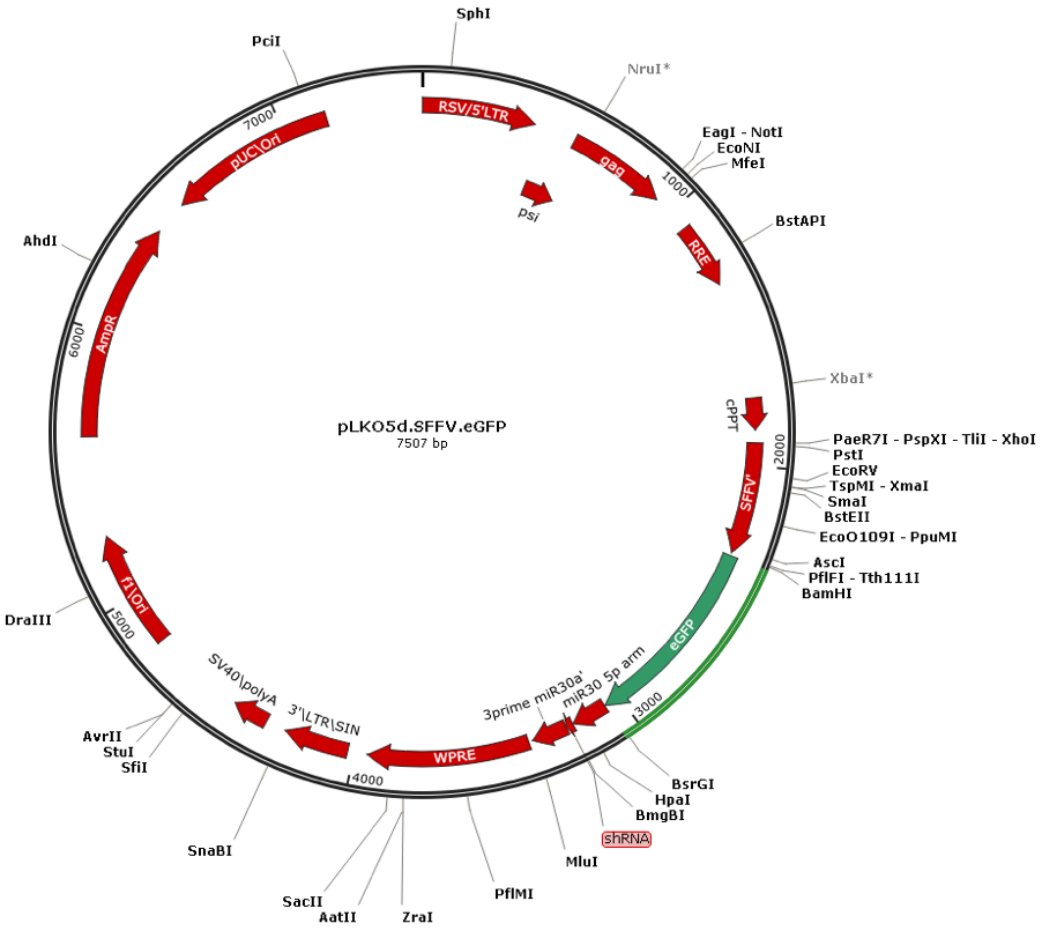

Figure 2.3 ***Full plasmid map of pLKO5dSFFeGFPmiR30n.*** *This plasmid vector is based on a natural human mir-30a backbone. The shRNA sequences were inserted at "shRNA" site on the vector. The SFFV is the promoter region for eGFP and mir-30a. The eGFP is selection marker for the vector.*

2.3.7.3 LentiCRISPRv2 plasmid

LentiCRISPR version 2 (LentiCRISPRv2) was obtained from Addgene (Plasmid #52961) contains Puromycin resistant gene as a selectable marker for transfected cells and Ampicillin resistant gene for selection of the plasmid in *E.coli* (Figure 2.4). LentiCRISPRv2 vector was digested with restriction enzyme BsmBI (NEB) to insert single guide RNA (sgRNA) into the vector.

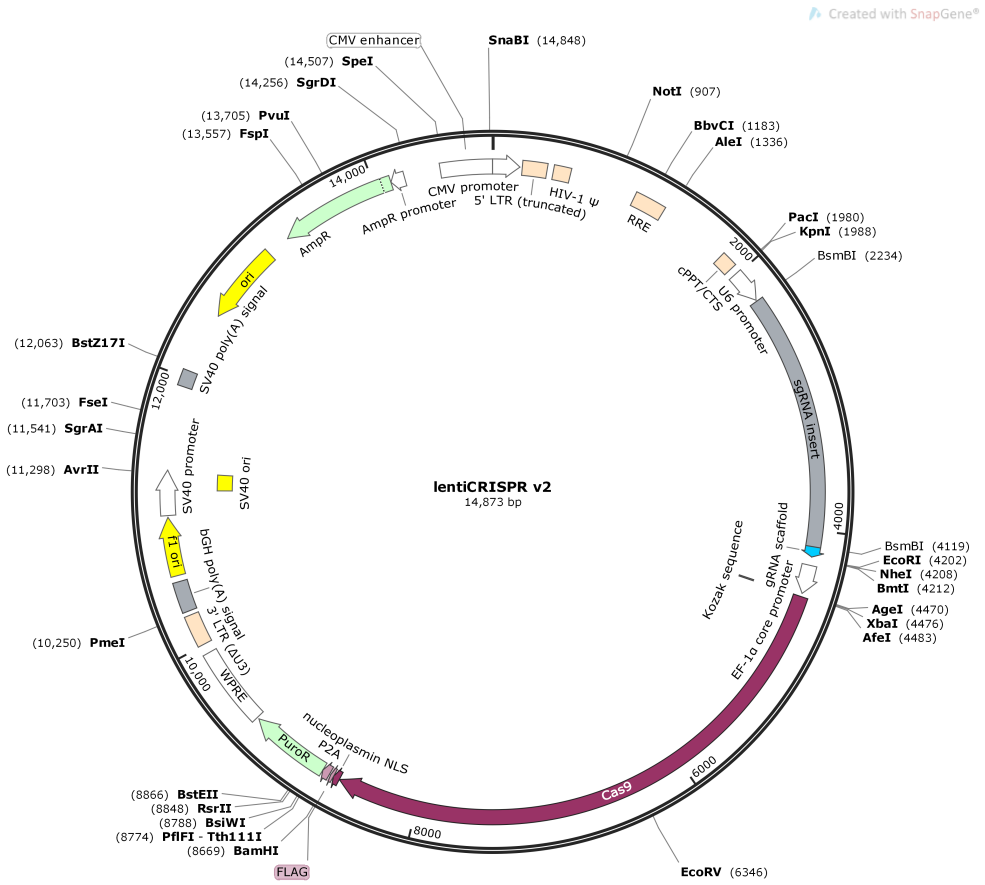

Figure 2.4 ***Full sequence map of LentiCRISPRv2 vector.*** *U6 is a promoter for sgRNA. The sgRNA sequence was inserted at "sgRNA insert" by removing the stuffer (at similar location of sgRNA insert) using BsmBI restriction enzyme. The Cas9 and puromycin selection marker are driven by EF-1a promoter. The co-expression of Cas9 and Puromycin selection marker is linked by P2A.*

2.3.7.4 Packaging plasmids for viral production

Two viral vectors required for generation of lentivirus are packaging plasmid (pCMV-ΔR8.91) and envelope plasmid (pMD2.G) (kindly donated by Dr Paul Sinclair) along with expression vector. The packaging plasmid contains a robust CAG promoter that facilitates the efficient expression of packaging protein during virus production whereas the envelope plasmid contains VSV-G coding sequence which is required to pseudotype the viral envelope.

2.3.8 Bacterial cloning and transformation

2.3.8.1 Ligation and cloning PCR amplicons into digested vectors

Oligo annealing and cloning of the sgRNA into digested LentiCRISPRv2 plasmid was performed according to the protocol provided by Zhang lab and Gecko. Briefly, sgRNA oligos designed for *SMARCB1* and *SMARCA4* were phosphorylated and annealed with T4 PNK enzyme (NEB) at 37 °C for 30 minutes, 95 °C for 5 minutes and then ramped down to 25°C at 5°C /minute in a thermocycler. The annealed oligos were diluted at 1:200 ratio with sterile water. 10 µl ligation reaction included 2.3 µl BsmBI digested vector (50 ng from stock), 1µl diluted oligo duplex, 5 µl 2x Quick Ligase buffer (NEB), ddH_2O water and 1µl Quick Ligase (NEB) was set up and incubated at room temperature for 10 minutes.

Primer sequences targeting *BMI1* was cloned into pLKO5dSFFVeGFPmiR30n (called Plko5d in this thesis) vector according to protocol provided by Thermo Fisher Scientific. T4 DNA ligase (Invitrogen) was used according to Table 2.11. The reaction was incubated overnight at room temperature. The product was stored at -20 °C (5 µl was used for transformation).

Linear vector DNA	50 ng (from stock)
Insert DNA	1:1 to 5:1 molar ratio over vector
10X T4 DNA Ligase buffer	2 µl
Thermo Scientific T4 DNA Ligase	1U
ddH_2O	to 20 µl
Total volume	20 µl

Table 2.11 ***Ligation mixture for sticky-end vector***

2.3.8.2 Transformation

Plasmids were transformed into High-Efficiency One Shot Stbl3 *Escherichia coli* (*E.coli*) bacteria (Invitrogen) according to manufacturer's protocol. 1µl of pUC19 (Invitrogen) and 5 µl of ddH2O were used as positive and negative control respectively. Transformed colonies were selected in Luria-Bertani (LB) plates containing 100 µg/ml Ampicillin.

2.3.8.3 Bacterial cultures

Bacterial strains were cultured in 10 ml of LB growth medium with antibiotic selection from a single colony, overnight on 360° shaker at 37 °C. Microbial LB plate was prepared from LB agar containing specific antibiotic selection. Inoculation was performed using a metal loop into LB plate or LB media. The stock of bacteria was stored at -80 °C in 50% glycerol (v/v) while the LB plates were stored at 4 °C, wrapped in Parafilm.

2.3.8.4 Harvesting of bacteria from LB broth and extraction of nucleic acids

Bacterial cultures were harvested after 18 hours of incubation on a shaker. The mini-cultures (< 1.5 ml) were harvested by centrifugation at 13,000 rpm for 3 min whereas the culture larger than 200 ml (maxi) were harvested at 9,000 rpm for 15 minutes.

Plasmids were extracted from mini and maxi cultures using a miniprep plasmid purification kit (Invitrogen) and Endo-Free Plasmids Maxi kit (Qiagen) respectively, according to manufacturer's protocols. Briefly, the cell pellet was re-suspended in an appropriate volume of Lysis buffer with RNAase and the solution passed through extraction column, leaving the DNA bound to the membrane. At the elution step, DNA was re-suspended first in isopropanol and then in 70% ethanol. The resulting DNA pellets were re-suspended in an appropriate volume of TE buffer.

2.3.8.5 Quantification of nucleic acids by spectroscopy

Total DNA extracted from the plasmid was measured using NanoDrop ND1000 (Thermo Scientific). The purity and integrity of total DNA was evaluated based on OD ratios at A260/A280 ranged between 1.8-2.

2.3.9 DNA manipulation techniques

2.3.9.1 DNA restriction

BsmB1 restriction enzyme (NEB) was used to digest 2 kb stuffer on the LentiCRISPRv2 vector to allow an insertion of sgRNA. Restriction enzyme digests were performed according to manufacturer's instructions. In brief, 5 µg of expression plasmid was digested in a 60 µl reaction mixture containing 3 µl of FastDigest BsmBI (NEB), 3 µl FastAP (Fermentas), 10X FastDigest Buffer and ddH_2O. The digestion reaction was incubated for 30 minutes at 37 °C. Similarly, the same digestion enzyme was used to digest the Plko5d plasmid to create blunt end insertion site.

2.3.9.2 Agarose gel electrophoresis

Digested plasmids required for downstream experiments were separated by agarose gel electrophoresis. The percentage of agarose (Bioline) used in this study varied from 0.8% to 1.5% (w/v) depending on the predicted size of DNA fragments. The agarose powder was suspended in TBE, heated and supplemented with Red gel (Biotium) at a concentration of 0.01% (v/v). Prior to loading the sample into the wells, 5 µl of sample was mixed with 1 µl of DNA loading buffer (Promega). Size of DNA bands on agarose was evaluated using a PCR marker (Promega) and a DNA marker (Promega) depending on the estimated size of the products. The samples were run at constant 100 V for 30 minutes to 1 hours and the DNA bands were visualised using Syngene G-box.

2.3.9.3 Gel extraction and purification of digested DNA

The DNA bands with a correct product size on agarose gel were excised using a clean scalpel and purified using a GeneJET™ Gel Extraction Kit (Thermo Fisher) according to manufacturer's instructions. The gel was dissolved with a binding buffer at 1:1 ratio (v/w) and heated 50 °C for 10 minutes until the gel was completely dissolved. The solution was transferred to column and DNA bound to the membrane. The column was washed twice with a wash buffer and the DNA was eluted in TE buffer.

2.3.9.4 Polymerase chain reaction (PCR)

Target DNA sequences for colony screening or molecular cloning were amplified using PCR (Gene Amp PCR System 9700) thermocycler.

2.3.9.5 Sequencing

To confirm the correct *BMI1*, *SMARCB1* and *SMARCA4* sequences were cloned into various expression vectors and intermediate plasmids, sequencing was carried out using the primers listed in Table 2.12. Sequencing was performed by Eurofins Genomics (Germany) and resulting traces were analysed using FinchTv.

Gene	Species	Vector	Primer sequence
BMI1	*Homo sapiens*	pLKO5d	agcgccctaatactttccagattgattag tgaagccacagatgtaatcaatctggaa agtattaggt
SMARCB1	*Homo sapiens*	lentiCRISPRV2	gaattcgctagctaggtcttgaaaggag tgggaattggctccggtgcccgtcagt gggcagagcgcacatcgcccaca
SMARCA4	*Homo sapiens*	lentiCRISPRV2	gaattcgctagctaggtcttgaaaggag tgggaattggctccggtgcccgtcagt gggcagagcgcacatcgcccaca

Table 2.12 ***Sequencing primers to check for insert in plasmid vectors***

2.3.10 CRISPR/Cas9 mediated knockout of SMARCB1 and SMARCA4

2.3.10.1 Construction of CRISPR/Cas9 single guide RNA (sgRNA)

Single guide RNA (sgRNA) targeting regions in exon 1 and exon 2 of human and murine *SMARCB1* and *SMARCA4* were designed using CRISPR design tool (http://www.e-crisp.org/E-CRISP/designcrispr.html). Two single guide RNAs for each gene for each organism were designed with the least off-target effects that tolerate mismatches and fewer hits. The sgRNA sequences used in the construction of lentiCRISPRv2 vectors are tabulated in Table 2.13.

Platform	Organism	Gene	Sequence
GECKO	Homo sapiens	*SMARCA4*	Oligo 1: CACCG **CTGGCCGAGGAGTTCCGCCC** Oligo 2: **AAACGGGCGGAACTCCTCGGCCAG**C-
		SMARCB1	Oligo 1: CACCG **AACTACCTCCGTATGTTCCG** Oligo 2: **AAACCGGAACATACGGAGGTAGTT**C
	Mus musculus	*SMARCA4*	Oligo1: ACCG**TATGGAGTCCATGCACGAGA** Oligo 2: **AAACTCTCGTGCATGGACTCCATA**C
		SMARCB1	Oligo 1: CACCG **CTAGTCGCCGCCAGAGTGAG** Oligo 2: **AAACCTCACTCTGGCGGCGACTAG**C
E-CRISPR	Homo sapiens	*SMARCA4*	Oligo 1: CACCG**GAGGAGTTCCGCCCAGGGGT** Oligo 2: **AAAC ACCCCTGGGCGGAACTCCTC**C
		SMARCB1	Oligo 1: CACCG**GCCCGTGAAGTTCCAGCTGG** Oligo 2: **AAAC CCAGCTGGAACTTCACGGGC**C
	Mus musculus	*SMARCA4*	Oligo 1: CACCG **GTCTACTCCAGACCCACCCT** Oligo 2: **AAAC AGGGTGGGTCTGGAGTAGAC**C
		SMARCA4	Oligo 1: CACCG **GAGAACCTCGGAACATACGC** Oligo 2: **AAACGCGTATGTTCCGAGGTTCTC**C

Table 2.13 ***List of single guides RNA (sgRNAs) targeting SMARCB1 and SMARCA4 in Homo sapiens and Mus musculus***

2.3.10.2 Non-targeting control single guide RNAs (sgRNA)

sgRNA for non-targeting control was obtained from the Human GECKOv2 library and Mouse GeCKOv2 library (Addgene). The selected 20bp sgRNA was checked for its potential binding to the target genes (i.e *SMARCB1* and *SMARCA4*). Six oligonucleotides were selected for each organism listed in Table 2.14 and Table 2.15. NTCH6 and NTCM1 showed high transduction efficiency and therefore were used in all CRISPR experiments.

Organism	NTC	Sequences
Homo sapiens	NTCH 1	Oligo1: CACCGATCGTTTCCGCTTAACGGCG Oligo2: AAACCGCCGTTAAGCGGAAACGATC
	NTCH 2	Oligo1: CACCGGTAGGCGCGCCGCTCTCTAC Oligo2: AAACGTAGAGAGCGGCGCGCCTACC
	NTCH 3	Oligo1: CACCGGGGCCCGCATAGGATATCGC Oligo2: AAACGCGATATCCTATGCGGGCCCC
	NTCH 4	Oligo1: CACCGCTTACAATCGTCGGTCCAAT Oligo2: AAACATTGGACCGACGATTGTAAGC
	NTCH 5	Oligo1: CACCGTAGACAACCGCGGAGAATGC Oligo2: AAACGCATTCTCCGCGGTTGTCTAC
	NTCH 6	Oligo1: CACCGCTATCTCGAGTGGTAATGCG Oligo2: AAACCGCATTACCACTCGAGATAGC

Table 2.14 ***List of Homo sapiens non-targeting control (NTC) single guide RNAs for CRISPR/Cas9 construction.***

Organism	NTC	Sequences
Mus musculus	NTCM 1	Oligo1:CACCGGACTCCGGGTACTAAATGTC Oligo2:AAACGACATTTAGTACCCGGAGTCC
	NTCM 2	Oligo1:CACCGCCGCGCCGTTAGGGAACGAG Oligo2:AAACCTCGTTCCCTAACGGCGCGGC
	NTCM 3	Oligo1:CACCGACCCATCGGGTGCGATATGG Oligo2:AAACCCATATCGCACCCGATGGGTC
	NTCM 4	Oligo1:CACCGTACAGTTATACGTCGCGGTG Oligo2:AAACCACCGCGACGTATAACTGTAC
	NTCM 5	Oligo1:CACCGCCTTAGACCGGGTGTACCTC Oligo2:AAACGAGGTACACCCGGTCTAAGGC
	NTCM 6	Oligo1:CACCGCTCGGGCTATTCAGCGATAG Oligo2:AAACCTATCGCTGAATAGCCCGAGC

Table 2.15 ***List of Mus musculus non-targeting control (NTC) single guide RNAs for CRISPR/Cas9 construction.***

2.3.10.3 SURVEYOR PCR primers design

Primers for surveyor assays were designed near upstream and downstream of the sgRNA. Ideally, the cleavage site should create two distinct product sizes on an agarose gel. The primers were designed using Primer3web version 4.0.0 website (http://primer3.ut.ee). For efficient amplification, the primers were designed to yield the amplicon length between 400 to 500 bp. The SURVEYOR primers used in CRISPR experiment are listed in Table 2.16 and Table 2.17.

Organism	Name	Sequence: (5' to 3')	Length	Ind. bp	Total bp
Mus musculus	SMARCB1-MME F	GGCATTGTCTCAGTGTGGTG	20	100	403
	SMARCB1-MME R	ACAGTGGAGTACGGGAGACT	20	103	
Mus musculus	SMARCB1-MMG F	GTCTCAGTGTGGTGCTAGGT	20	130	400
	SMARCB1-MMG R	ACAACAGTGGAGTACGGGAG	20	270	
Mus musculus	SMARCA4-MMG F	TCTGTGTGGTCCCCTTTCTC	20	118	405
	SMARCA4-MMG R	CTCTGTCCCACCTGTTCAGT	20	287	
Mus musculus	SMARCA4-MME F	GGACATGCACCATCATTCCC	20	283	490
	SMARCA4-MME R	TGCCTACCTTGTGCATCTGA	20	307	

Table 2.16 ***Mus musculus SURVEYOR assay primers needed for PCR amplification***

Organism	Name	Sequence: (5' to 3')	Length	Ind. bp	Total bp
Homo sapiens	SMARCB1-HSG F	GAGGCCTTGCATTTCTGGAA	20	360	404
	SMARCB1-HSG R	CTAGTCGCCTCCAGAGTGAG	20	44	
Homo sapiens	SMARCB1-HSE F	CGCCGCAATGATGATGATGG	20	65	406
	SMARCB1-HSE R	ATCCCGTTTCTTTGCGTCTG	20	341	
Homo sapiens	SMARCA4-HSG F	TGTGTGCCTGAGATGTAGGA	20	260	450
	SMARCA4-HSG R	GGGATCCCTACCTTGTGCAT	20	190	
Homo sapiens	SMARCA4-HSE F	TGTGTGCCTGAGATGTAGGA	20	260	450
	SMARCA4-HSE R	GGGATCCCTACCTTGTGCAT	20	196	

Table 2.17 ***Homo sapiens SURVEYOR assay primers needed for PCR amplification.***

2.3.10.4 SURVEYOR mutagenesis assay

Detection of InDel mutations generated by CRISPR/Cas9 were validated using the SURVEYOR Nuclease Assay. This assay is commonly used to detect single nucleotide mismatch that is induced by nuclease, a member of CEL family of mismatch specific nucleases. SURVEYOR nuclease recognises and cleaves both strands of a DNA heteroduplex on the 3' side of base substitution or insertion/deletion (InDel), Briefly, there are 4 steps in SURVEYOR mutagenesis assay; PCR amplification of target DNA from both mutant and wild-type reference DNA; (ii) hybridization to form heteroduplexes between mutant and wild-type reference DNA; (iii) cleave of heteroduplexes with Surveyor nuclease to cleave heteroduplexes; and (iv) analysis of digested DNA products using the detection/separation on gel electrophoresis.

Firstly, PCR amplification was performed for control and test samples. Genomic DNA was extracted as described in Section 2.3.3.1 from HEK293T, NIH3T3 and neural crest cells (O9-1) after 48 hours of antibiotic selection. 100 ng of genomic DNA was used to amplify the regions spanning CRISPR CAS9 mutation sites using specific primers (Table 2.16) and AmpliTaq Gold Polymerase (Thermofisher Scientific) as per manufacturer's instructions. Control C and G fragment provided in the Transgenomic SURVEYOR mutation detection kit (Integrated DNA Technologies) were also amplified in parallel. Human male genomic DNA (Promega) and mouse genomic DNA (Promega) were used instead of test sample DNA.

20 µl PCR reactions were prepared as follows; 2µl Gene Amp® 10X Gold Buffer (150 mM Tris-HCl, pH 8.0, 500 mM KCl), 10µl of 10uM forward primer, 10µl of 10uM reverse primer, 0.8µl of 5mM dNTP mix (Vh Bio), 0.8µl of 1.5mM of 25mM magnesium chloride ($MgCl_2$), 0.2µl of AmpliTaq Gold polymerase, 50ng DNA and deionized water. Genomic DNA was substituted with H_20 to serve as a negative control. 50 µl PCR reaction of the two plasmid DNA, Control C and control G provided by the manufacturer were prepared to contain all the PCR components as above except forward primer, reverse primer and genomic DNA as the primers are already incorporated with the plasmid templates. PCR conditions for each primer are shown in Table 2.18 and Table 2.19. PCR products were run on 2% v/w gel electrophoresis with 100bp DNA ladder (Promega) to confirm one single band of the product.

PCR parameter		Temperature (°C)	Time (min)	Ramp down temperature
Hold		95	10	-
5 cycles	Initial denaturation	95	0.5	-
	Annealing	Ta	0.5	(1°C/cycle)
	Extension	72	0.5	-
30 cycles	Denaturation	95	0.5	-
	Annealing (Last Tm from ramp down)	57	0.5	-
	Extension	72	0.5	-
Hold		72	7	-
		4	∞	-

Table 2.18 ***PCR amplification condition for SURVEYOR nuclease analysis***

SURVEYOR primers	Species	Annealing temperature (Ta/°C)
SMARCB1 MMG	*Mus musculus*	55
SMARCB1 MME	*Mus musculus*	55
SMARCB1 HSG	*Homo sapiens*	62
SMARCB1 HSE	*Homo sapiens*	52
SMARCA4 MMG	*Mus musculus*	55
SMARCA4 MME	*Mus musculus*	55
SMARCA4 HSG	*Homo sapiens*	62
SMARCA4 HSE	*Homo sapiens*	58

Table 2.19 ***Annealing temperature for SURVEYOR primers***

After PCR amplification, a DNA hybridisation step was carried out using PCR amplified DNA. Reference DNA (C and G, provided by the company) was mixed at an equal amount to form a reference control. Briefly, 10µl of each PCR amplified DNA (test sample) was mixed with 10µl of negative control (NTC) in 0.2 ml tube. The samples were hybridised on a thermocycler according to manufacturer's protocol. 30 µl of G and C alone were placed in separate tubes to serve as negative control for nuclease treatment. The hybridised product was digested with 2 µl of 0.15M $MgCl_2$ solution, 1µl of SURVEYOR Enhancer S and 1 µl of SURVEYOR Nuclease S. The samples were kept on the ice and properly mixed by gentle vortexing followed by incubation for 60 minutes at 42°C. The reaction was stopped by adding 2µl of Stop solution into the tubes. Finally, the digestion products were analysed by 1.5% w/v agarose gel electrophoresis.

2.3.10.5 IncuCyte® live cell count proliferation assay

Growth curve of cell lines transfected with CRISPR/Cas9 lentivirus was established using IncuCyte® live cell imaging system. The images of cells were captured 24-hours post infection and 24 hours post CD44 sorting for NIH3T3 and O9-1 cell lines respectively. Cell proliferation was measured using an IncuCyte phase only module and the images were collected on IncuCyte Zoom for 14 days. A specific processing definition was applied using IncuCyte mask (goldenrod) and the percentage cell confluency was exported to GraphPad Prism software for statistical analysis.

2.3.10.6 Immunofluorescence imaging of human Rhabdoid tumour markers

The effect of *SMARCB1* knockout on cell migration and cytoskeleton organisation was evaluated using immunofluorescence labelling of phalloidin (F-actin). Additionally, the presence of human Rhabdoid IHC characteristics such as positive vimentin and cytokeratin 8 were also established using this technique. In brief, 20,000 cells were seeded in 8-well chambers (Sigma Aldrich) 24 hours prior to antibody incubation and the cells were fixed with formalin for 30 minutes at room temperature. To permeabilise, the cells were fixed for 5 minutes with 0.1% v/v Triton in PBS followed by 3 x 5 minutes washing steps with PBS. For the evaluation of cytoskeleton organisation, cells were stained with 100µl of 1X of CytoPainter Phalloidin iFlour-488 for 1 hour in the dark at room temperature. Cells were washed with PBS to remove excess conjugate before mounting with Prolong Gold antifade reagent with DAPI staining, sealing with nail polish and imaging with Leica DM6 microscope. For visualisation of vimentin and cytokeratin, cells were incubated with appropriate primary antibodies; anti-rabbit vimentin (CST D21H3) and anti-cytokeratin 8 (Life Technologies MA514428) for 1 hour at room temperature and washed three times 5 minutes each on the rocker to remove the excess antibodies. The cells were then blocked with 1% BSA in PBS for 30 minutes followed by secondary antibody incubation using either goat anti-mouse IgG Alexa Fluor 488 (ThermoFisher A-11001) or goat anti-rabbit IgG Alexa Fluor 568 (ThermoFisher A-11001) for 1 hour in the dark at room temperature. Cells were washed with PBS, mounted with DAPI and sealed for imaging.

2.3.10.7 Cell differentiation

CD44 sorted NC cells were plated on 6-well plate at 200,000 cell density and were cultured in O9-1 media. When the cells reached 90% confluency, the spent media was removed, and the cells were washed once with PBS. To induce osteogenic differentiation, cells were cultured in differentiation medium made up of DMEM, FBS 10%, 50 μg/ml ascorbic acid, 10 mM β-glycerophosphate, 10 nM dexamethasone. The media was changed every three days. After 3 weeks in culture, the cells were washed three times with 1x PBS, fixed with 10% formalin (room temperature) for 30 minutes followed by three times washing step with distilled water. For detection of calcium deposits, alizarin red solution was prepared a day prior to cell staining. 2g alizarin red solution (Sigma Aldrich) was dissolved in 100 ml of distilled water and the pH was adjusted to 4.1-4.3. The dark brown solution was filtered using 0.2 microns and stored in dark at 4°C. To stain the cells, 2 ml of Alizarin red was added to the well and the cells were incubated for 10-15 minutes in dark. Cells were washed with distilled water 3 times. Undifferentiated cells were zero to slightly reddish, whereas differentiated osteoblasts with extracellular calcium deposits cells were bright red.

To induce adipogenic differentiation, the cells were cultured in differentiation medium made up of α-MEM media supplemented with 10% FBS,1% L-glut 1% Pen-Strep, 1μM dexamethasone, 1μM indomethacin, 500 μM 3-isobutyl-1-methylxanthine (IBMX) and 10 μg/ml human recombinant insulin. The media was changed every three days. After 3 weeks in culture, the cells were washed three times with 1x PBS, fixed with 10% formalin (room temperature) for 30 minutes followed by three times washing step with distilled water. Detection of lipid oil droplet was utilized to access adipogenic differentiation. To prepare oil-red-o staining, 300 mg of oil-red-o powder (Sigma Aldrich) was mixed with 100 ml of 99-100% isopropanol. During formalin fixed incubation time, 3 parts of oil-red-o were mixed with 2 part of deionised water and the mixed solution was allowed to sit at room temperature for at least 10 minutes. Prior to staining, oil red o solution was filtered through 0.2-micron filter (Thermo Scientific). To stain the cells, 2 ml of oil-red-o solution was added to the well and the cells were incubated for 10-15 minutes in dark. Cells were washed with distilled water 3 times or until the water becomes clear. For analysis 1 ml of distilled was added to the well and the presence of lipid droplet was assessed by microscope.

2.3.11 Therapeutic targeting BMI1 in Malignant Rhabdoid Tumour (MRT) with shRNA and small inhibitors

2.3.11.1 Oligonucleotides and primers

All oligonucleotides were synthesized and designed as previously described (see section 2.3.3). The primers used to target *BMI1* in Plko5d vector are in Table 2.20.

Sequences for pLKO5d backbone (5' ->3')							
Name	Sigma sequence	Region	TRC library sequence	Forward primer	Reverse primer	Bp fwd	Bp rev
shBMI1_1	CCGGCCTAATACTTTCCAGATTGATCTCGAGATCAATCTGGAAAGTATTAGGTTTTT	CDS	CCTAATACTTTCCAGATTGAT	agcgcCCTAATACTTTCCAGATTGATtagtgaagccacagatgtaATCAATCTGGAAAGTATTAGGt	ggcaaCCTAATACTTTCCAGATTGATtacatctgtggcttcactaATCAATCTGGAAAGTATTAGGg	67	67
shBMI1_2	CCGGCCAGACCACTACTGAATATAACTCGAGTTATATTCAGTAGTGGTCTGGTTTTT	CDS	CCAGACCACTACTGAATATAA	agcgcCCAGACCACTACTGAATATAAtagtgaagccacagatgtaTTATATTCAGTAGTGGTCTGGt	ggcaaCCAGACCACTACTGAATATAAtacatctgtggcttcactaTTATATTCAGTAGTGGTCTGGg	67	67
shBMI1_3	GTACCGGATACTCCTATGGACGTTAATTCTCGAGAATTAACGTCCATAGGAGTATTTTTTTG	3' UTR	ATACTCCTATGGACGTTAATT	agcgcATACTCCTATGGACGTTAATTtagtgaagccacagatgtaAATTAACGTCCATAGGAGTATt	ggcaaATACTCCTATGGACGTTAATTtacatctgtggcttcactaAATTAACGTCCATAGGAGTATg	67	67

Table 2.20 ***shRNA BMI1 design using pLKO5d vector.*** *Primers were designed using the transcript sequence from Ensembl (ENSG00000168283).*

2.3.11.2 shRNA targeting of BMI1 in MRT

MRT cell lines were transfected with shRNA lentivirus from two different vectors as discussed in previous section 2.7.1 at appropriate MOI. Cells were infected with lentivirus for 24 hours and media replaced with fresh media the next day. Cells were harvested 96 hours post infection.

2.3.11.3 Inhibition of BMI1 in MRT cells lines with PTC209

To determine the GI_{50} values, 1000 cells were plated in 96-well plate and 12 different concentrations of *BMI1* inhibitors ranging from 0 to 5.7 nM were added and DMSO was used as a control. The number of visible cells was recorded 96 hours post-transfection in triplicate using CellTiter Glo (Promega) and dose-response curves were fitted to data. For subsequent experiments using PTC209, cells were treated with sub-lethal dose as follows; 1 μM and 3.5 μM for G401, A204 and CHLA-266 whereas 5 μM and 10 μM for BT16.

2.3.11.4 Limiting dilution assay and ELDA analysis

For *in vitro* limiting dilution assay (LDA), transduced MRT cell lines were dissociated into single cells and diluted serially to an appropriate cell density. Prior to cell dissociation, adherent MRT cells were infected with either shRNA lentivirus for 24 hours or PTC209 for 96 hours post infection. Cells transfected with PTC209 were allowed to recover for 120 hours to enable sphere formation.

In 96-well plates, cells were plated at following densities; 50,000, 10,000, 5,000, 1,000, 100, 10 and 1 per well. For each cell density (50,000, 10,000, 5,000), at least 12 wells were seeded with cells whereas 96 wells were seeded with cells for low cell density (1,000, 100, 10 and 1). Wells containing spheres were scored on day 6 and the positive wells were used to measure the frequency of sphere-forming units (SFUs) using the LDA software provided by the Walter and Eliza Hall Institute (http://bioinf.wehi.edu.au/software/elda/index.html). For shRNA-infected cells, positive GFP, RFP and tomato cells were sorted and seeded in the wells.

2.3.11.5 Assessment of cell apoptosis using Caspase 3/7 assay

The effect of BMI1 knockdown using both shRNA and PTC209 on cell apoptosis was assessed using Caspase3/7-Glo apoptosis kit (Promega) according to manufacturer's instructions. Briefly, 1000 MRT cells were seeded in 96-well plate in triplicate and the reading was taken at 24, 72, 120 hours post treatment with shRNA and *BMI1* inhibitors. 25 µl of Caspase3/7 solution was added to the wells and the plate was incubated at 37°C for 30 minutes. The OD at 560 nm was read in a FLUOstar Omega (BMG Labtech) plate reader. Fold increase in Caspase 3/7 activity over time course was determined by comparing these results with that of the simultaneous controls (DMSO or NTC). The background reading from cells and buffers was subtracted from the reading of both MRT-treated and control samples.

2.3.11.6 Cell senescence analysis

To determine senescence following *BMI1* knockdown, MRT cells were seeded at a density of 1 x 10^5 in 6-well plate (Corning) and infected with either shRNA lentivirus at MOI 5 or PTC209 at two drug concentrations and DMSO (1.0%). For A204, G401 and CHLA-266, the cells were treated at 1 and 3.5 µM whereas BT16 cells were treated at 5 and 10 µM. After 96 hours infection, the β-galactosidase was measured using senescence detection kit (Sigma Aldrich) according to manufacturer's protocols. Positive β-galactosidase stained cells (green) were manually counted.

2.4 Appendix

Appendix 2.1: ***Expression profiles of various stem cell types for identification of cell of origin for MRT.***

Deposited data stem cell expression profiles			
GEO accession number	**Stem cell type**	**Source**	**Number of dataset**
GSE40751	NPC	Gene Expression Omnibus (GEO) NCBI	5
GSE40904	Glioma	Gene Expression Omnibus (GEO) NCBI	12
GSE42294	NPC	Gene Expression Omnibus (GEO) NCBI	5
GSE44186	MSC	Gene Expression Omnibus (GEO) NCBI	1
GSE45899	NSC	Gene Expression Omnibus (GEO) NCBI	2
GSE47796	NPC	Gene Expression Omnibus (GEO) NCBI	11
GSE47796	Hepatocytes	Gene Expression Omnibus (GEO) NCBI	4
GSE47796	NPC	Gene Expression Omnibus (GEO) NCBI	10
GSE47796	Neuronal	Gene Expression Omnibus (GEO) NCBI	3
GSE47796	PSC	Gene Expression Omnibus (GEO) NCBI	12
GSE47796	Endoderm	Gene Expression Omnibus (GEO) NCBI	2
GSE48616	Osteogenic	Gene Expression Omnibus (GEO) NCBI	4
GSE54186	ESC	Gene Expression Omnibus (GEO) NCBI	2
GSE54186	EB	Gene Expression Omnibus (GEO) NCBI	2
GSE54186	ESC	Gene Expression Omnibus (GEO) NCBI	2
GSE54186	EB	Gene Expression Omnibus (GEO) NCBI	2
GSE55679	ESC	Gene Expression Omnibus (GEO) NCBI	4
GSE56906	NSC	Gene Expression Omnibus (GEO) NCBI	2

Continued

GSE56906	ESC	Gene Expression Omnibus (GEO) NCBI	2
GSE56906	NPC	Gene Expression Omnibus (GEO) NCBI	2
GSE58475	NSC	Gene Expression Omnibus (GEO) NCBI	2
GSE60740	MSC	Gene Expression Omnibus (GEO) NCBI	2
GSE61050	ESC	Gene Expression Omnibus (GEO) NCBI	3
GSE61266	ESC	Gene Expression Omnibus (GEO) NCBI	3
GSE61266	NPC	Gene Expression Omnibus (GEO) NCBI	3
GSE61842	NPC	Gene Expression Omnibus (GEO) NCBI	8
GSE61842	ESC	Gene Expression Omnibus (GEO) NCBI	4
GSE61842	EB	Gene Expression Omnibus (GEO) NCBI	1
GSE65631	MSC	Gene Expression Omnibus (GEO) NCBI	12
GSE67309	NPC	Gene Expression Omnibus (GEO) NCBI	1
GSE67338	NBS	Gene Expression Omnibus (GEO) NCBI	3
GSE69991	MSC	Gene Expression Omnibus (GEO) NCBI	6
GSE7178	NPC	Gene Expression Omnibus (GEO) NCBI	9
GSE7179	ESC	Gene Expression Omnibus (GEO) NCBI	9
GSE71080	MSC	Gene Expression Omnibus (GEO) NCBI	1
GSE7637	MSC	Gene Expression Omnibus (GEO) NCBI	30
GSE74358	Neuronal	Gene Expression Omnibus (GEO) NCBI	8
GSE74358	NPC	Gene Expression Omnibus (GEO) NCBI	3
GSE7896	ESC	Gene Expression Omnibus (GEO) NCBI	8

Continued

GSE82101	NPC	Gene Expression Omnibus (GEO) NCBI	1
GSE24598	MSC	Gene Expression Omnibus (GEO) NCBI	3
GSE9940	neural epithelial	Gene Expression Omnibus (GEO) NCBI	1
GSE9940	ESC	Gene Expression Omnibus (GEO) NCBI	3
GSE9940	EB	Gene Expression Omnibus (GEO) NCBI	4
GSE9940	neural epithelial	Gene Expression Omnibus (GEO) NCBI	10
GSE10315	MSC	Gene Expression Omnibus (GEO) NCBI	3
GSE10315	Chondrogenic	Gene Expression Omnibus (GEO) NCBI	24
GSE13307	NPC	Gene Expression Omnibus (GEO) NCBI	4
GSE13715	NPC	Gene Expression Omnibus (GEO) NCBI	18
GSE15209	NSC	Gene Expression Omnibus (GEO) NCBI	5
GSE18043	Osteogenic	Gene Expression Omnibus (GEO) NCBI	8
GSE18618	NPC	Gene Expression Omnibus (GEO) NCBI	3
GSE18618	iPSC	Gene Expression Omnibus (GEO) NCBI	6
GSE18618	ESC	Gene Expression Omnibus (GEO) NCBI	6
GSE24530	ESC	Gene Expression Omnibus (GEO) NCBI	8
GSE27313	MSC	Gene Expression Omnibus (GEO) NCBI	1
GSE28618	Glioma	Gene Expression Omnibus (GEO) NCBI	1
GSE29368	Glial	Gene Expression Omnibus (GEO) NCBI	5

Continued

GSE29368	Oligodendrocyte	Gene Expression Omnibus (GEO) NCBI	5
GSE29625	ESC	Gene Expression Omnibus (GEO) NCBI	12
GSE30807	MSC	Gene Expression Omnibus (GEO) NCBI	1
GSE31215	MSC	Gene Expression Omnibus (GEO) NCBI	10
GSE34152	NSC	Gene Expression Omnibus (GEO) NCBI	4
GSE35546	MSC	Gene Expression Omnibus (GEO) NCBI	1
GSE35546	Chondrogenic	Gene Expression Omnibus (GEO) NCBI	6
GSE36923	MSC	Gene Expression Omnibus (GEO) NCBI	3
GSE36923	Adipogenic	Gene Expression Omnibus (GEO) NCBI	3
GSE36923	MSC	Gene Expression Omnibus (GEO) NCBI	11
GSE17312	ESC	Gene Expression Omnibus (GEO) NCBI	1
GSE17312	iPSC	Gene Expression Omnibus (GEO) NCBI	3

Chapter 3 An analysis of putative cell of origin for Malignant Rhabdoid Tumours (MRT)

3.1 Summary

Malignant Rhabdoid Tumours (MRT) are highly aggressive malignancies which occur almost entirely in infants. MRT are caused by biallelic inactivation of *SMARCB1*, a tumour suppressor gene and a core subunit of the SWI/SNF complex (Versteege et al., 2002, Biegel et al., 2000, Roberts and Biegel, 2009). The tumours are highly heterogeneous and can be found at various locations in the body. Knowledge of tumour aetiology especially cell of origin and how it relates to different anatomical locations is still lacking. A few candidates for cell of origin of MRT have been proposed so far by other studies based upon the phenotypic diversity of MRT (Haas et al., 1981, Ota et al., 1993, Suzuki et al., 1997, Okuno et al., 2010, Kato et al., 2003, Parham et al., 1988). However, there is no systematic approach to identify putative cells of origin for MRT as the assumptions of cell of origin were made based on the presence of differentiation markers from multiple lineages such as neural and mesenchymal in primary tumours. Therefore, in this chapter, I seek to shed light on the cell of origin for MRT and whether the cell of origin is common for tumours regardless of anatomical locations. This hypothesis was challenged by performing a meta-analysis, cross-referencing expression profiles from primary MRT (n=119), and functional models in which *SMARCB1* was re-expressed (n=5 lines) with expression profiles from multiple candidate stem cell types including epithelial, embryonic, neural, mesenchymal and neural crest (n=446) suggesting three putative candidate cell populations within the family of neural crest (NC) cells, neural stem cell (NSC) and mesenchymal stem cells (MSC). The extent of transcriptional overlap clearly reflects differences in tumour location and molecular subgroup.

3.2 Introduction

3.2.1 ATRT and ECRT: are they molecularly distinct?

Malignant Rhabdoid Tumours (MRT) are stratified as poor prognosis disease. MRT can be categorised into **A**typical **T**eratoid **R**habdoid **T**umours (ATRT) for which the tumours arise in the brain or central nervous system (CNS) (Rorke et al., 1996, Torchia et al., 2015), and **E**xtra **C**ranial **R**habdoid **T**umours (ECRT) for tumours that are found in the soft tissue, kidney, lung, liver, etc (MacDonald, 2008, Beckwith and Palmer, 1978). MRT are phenotypically highly heterogeneous. Inter-tumoural heterogeneity in each molecular subtype was reported in few studies based on genomic, transcriptomic and epigenomic profiling (Johann et al., 2016, Chun et al., 2016, Torchia et al., 2016, Han et al., 2016, Torchia et al., 2015). In 2015, Torchia et al. (2015) reported two gene expression subgroups within the MRT which correlated with clinical outcome. Their initial study was expanded in 91 primary ATRT and 10 ATRT cell lines (Torchia et al., 2016) demonstrating that ATRT can be segregated into three epigenetic subgroups with distinct epigenomic features, types of *SMARCB1* mutation, transcriptional features and specific therapeutic sensitivities. Molecularly distinguishable subgroups within ATRT also have been reported by Johann et al. (2016), in which ATRT were divided into three subgroups with distinct epigenetic and expression profiles.

Regardless of anatomical location, ATRT and ECRT are caused by biallelic inactivation of *SMARCB1*, a potent tumour suppressor gene and a core subunit of SWI/SNF chromatin remodelling complex (Biegel et al., 2002b, Biegel et al., 2000, Roberts and Biegel, 2009). The question is then raised whether ATRT and ECRT are a single entity with unique genetic and epigenetic expression profiles. To elucidate potential molecular disparities between ATRT and ECRT, Grupenmacher et al. (2013) analysed the global gene expression and microRNA expression of primary MRT (10 RTK and 13 ATRT) and cell lines (G401-RTK and MON-AT/RT) using principal component analysis (PCA). Their work showed two subgroups within MRT related to tumour location (Figure 3.1a). However, analysis based on microRNA expression failed to separate the primary tumours (Figure 3.1b).

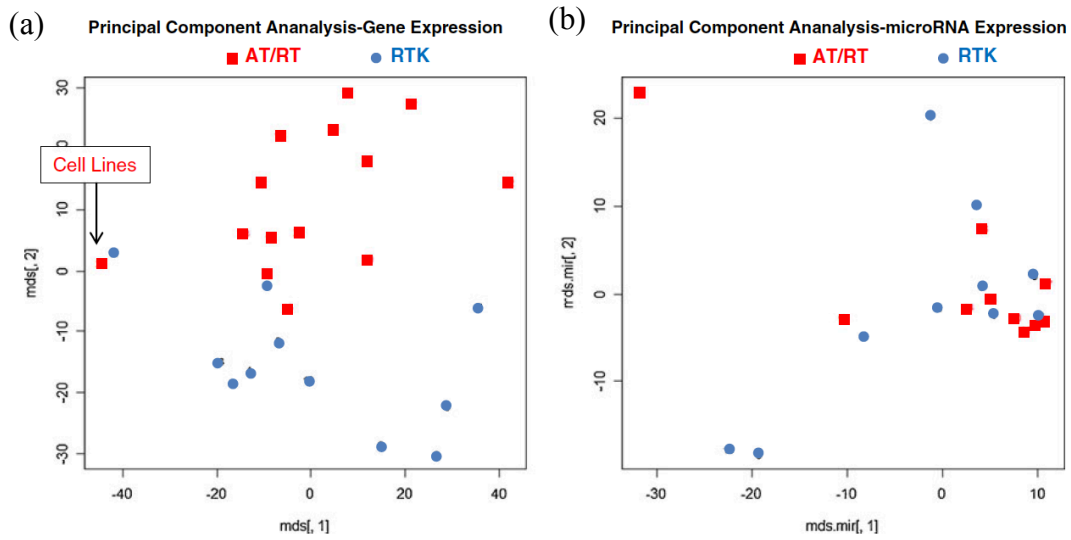

Figure 3.1 ***Principal component analysis of two molecular subgroups in MRT; ATRT and ECRT.*** *Square represented ATRT whereas circle represented RTK (ECRT). (a) The plot shows the separation of two subgroups using unsupervised gene expression analysis. Cell lines clustered as a group and separated from the primary tumour. (b) PCA using microRNA expression showed a major cluster of tumours. The figures were reproduced from Grupenmacher et al. (2013).*

The extent to which ATRT and ECRT overlap also has been studied by PBTG group at NICR (unpublished). RNA-Seq of primary MRT (10 ATRT, 13 ECRT) was compared with 228 paediatric medulloblastoma (MB) and analysed using non-negative matrix factorisation (NMF). Gene expression analysis showed five distinct subgroups consisting of four MB subgroups and one MRT subgroup (irrespective of tumour origin) (Figure 3.2). This finding illustrates that two subgroups within MRT share a closer expression profile than that of the MB subgroups. Additionally, to gain more insight whether there is a common molecular subgroup for MRT, 23 primary MRT RNA-seq (10 ATRT, 13 ECRT) was analysed using NMF. Unsupervised NMF analysis (k=2) of these tumours confirmed the existence of two metagenes associated with primary tumour location, one that broadly but not exclusively defined a group of ECRT while the other group described entirely ATRT (Figure 3.3).

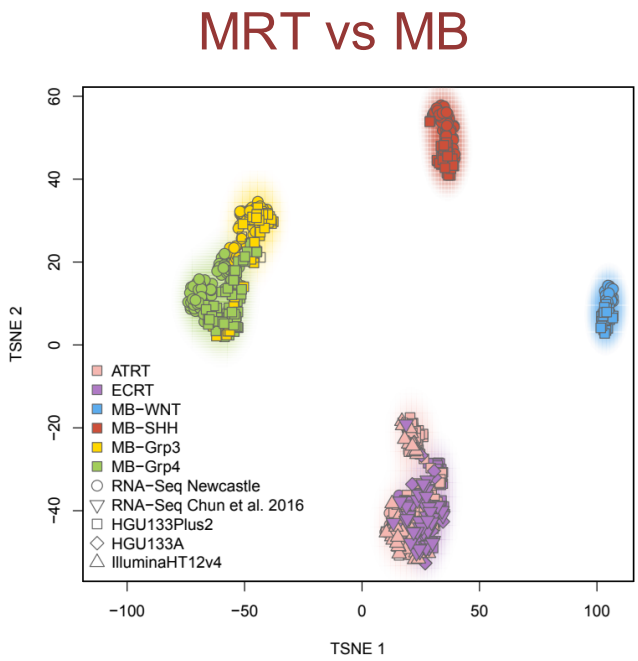

Figure 3.2 ***A t-SNE plot of cross platform projection of consensus NMF metagene expression (k=5) in primary MRT (n=23) vs MB (n=228) showing MRT is a single entity regardless of anatomical location.*** *The figure was reproduced from PBTG group (unpublished).*

Taken together, Grupenmacher et al. (2013) and the PBTG group demonstrated consistent findings in which MRT encompasses two subgroups namely ATRT and ECRT. Of note, a cross-platform projection of 2 metagenes onto four independent published datasets showed a transition of expression profiles from neural (i.e. *GFAP, MAP2, SOX1/2)* to mesenchymal phenotype (*H19, HOXC5/6/8/9/10)* (work done by PBTG group, unpublished) (Figure 3.4). This finding was corroborated by gene set enrichment analysis (GSEA) of these metagenes which showed significant enrichment of neural and mesenchymal genesets e.g. those describing mesenchymal (Normalized Enrichment Score (NES) = 3.48, $p<0.001$) and proneural (NES = 3.09, $p<0.001$) glioblastoma phenotypes respectively. These metagenes are correlated with three subgroups that were previously described by (Johann et al., 2016) as ATRT-MYC which demonstrated a mesenchymal gene signature, ATRT-TYR signifies an intermediate state and ATRT-SHH which associated with a neural signature. These findings, therefore, raise the question as

to whether MRT regardless of tumour location originate from a common type of progenitor cell or if there is more than one cell of origin in MRT.

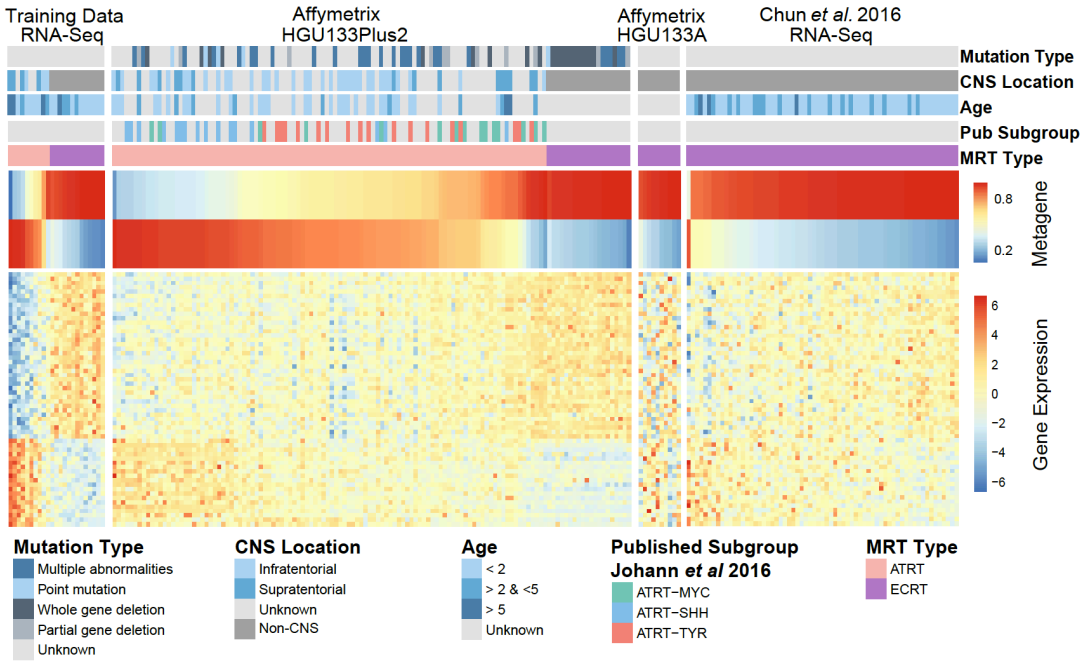

Figure 3.3 ***A heatmap of unsupervised NMF consensus clustering (k=2) of primary MRT RNA-seq (n=23) shows two metagenes within MRT related to primary tumour locations****. Cross-platform projection into previously published dataset that are associated with clinicopathological profiles and gene expression of 58 genes identified within the top 100 genes that related with this metagene and present in all platforms.*

3.2.2 Introduction to cell of origin

3.2.2.1 Cell of origin of CNS embryonal tumours

For many cancer types, the precise identification of cell of origin remains unknown. The cell of origin can be described as normal cells that have undergone oncogenic transformation due to genetic mutations (Rycaj and Tang, 2015). In childhood cancer, cancer may arise as a result of mutation in the embryonal cells or when the mature prenatal cells acquire embryonal properties which favour the survival pre- or post-natal

environment (Marshall et al., 2014). Prenatal oncogenic mutations may occur in early progenitor or stem cells which have extensive self-renewal capacity that is essential for *in utero* development. Therefore, the identification of a cell of origin will allow a better understanding of childhood cancers in terms of why the tumours develop, how to prevent them and what is the best way to treat them.

Several childhood cancers such as infant acute lymphoblastic leukaemia (ALL) and MRT are thought to have an embryonal cell of origin (Marshall et al., 2014). However, there is no clear evidence whether the embryonal tumours arise from the embryonal cells *in utero* or because of mutation in more mature prenatal cells which have the capacity to rapidly evolve towards tumour development.

Neuroblastoma (NB) is also thought to originate from prenatal embryonal cells. Clinical presentations of Neuroblastoma (NB) such as young age at time of diagnosis (<5 years) (Maris, 2010) and multifocal and bilateral tumours in tissue derived from embryonic neural crest cells (Brodeur, 2003) provided evidence of a prenatal origin for this embryonal malignancy. Besides that, normal foetal neuroblasts resemble tumours that derived from neuroblastoma, thus providing an evidence for prenatal origin. NB occurs predominantly in infancy and young children (Brodeur, 2003, Maris, 2010). Analysis of differentiation markers suggests the earliest cell of origin for NB is neural crest cells. Transgenic expression of *Mycn* or *Alk* in JoMa1, a multipotent neural crest progenitor cell line resulted in neuroblastoma like tumours *in vivo* in contrast to wild-type JoMa1 cells (Schulte et al., 2013). Additionally, high expression of Myc in under the control of the rat tyrosine hydroxylase (Th) promoter in Th-MYCN transgenic mice led to NB tumourigenesis (Hansford et al., 2004).

Another type of an embryonal tumour, Medulloblastoma (MB) which consists of four molecular subgroups (Wnt, Shh, Grp3 and Grp4), is thought to have a different type cell of origin for each subgroup. Activation of β-catenin and mutation in Wnt signalling pathway in BLBP+, Olig3+ neural precursor that present in the brainstem of embryonic mice initiated tumour formation which in line with radiological analysis of Wnt MB tumours often found within the fourth ventricle, infiltrating the dorsal surface of the brainstem (Gibson et al., 2010, Takebayashi et al., 2002). Activation of Shh in granule neural progenitor cells predisposed MB at 3 months of age of mice (Yang et al., 2008).

Notably, mutation of Ptch (Shh effector) in neural stem cells led to rapid development of MB with 100% of mice formed tumours by 3-4 weeks. In short, these studies demonstrate that deregulation of Shh in neural progenitor and neural stem cells can serve as origin for Shh subtype of MB.

3.2.3 Cell of origin for Malignant Rhabdoid Tumours

3.2.3.1 Cell of origin for MRT: what we know so far?

MRT are highly heterogeneous tumours however the histological origin of MRT still remains elusive. Nevertheless, significant progress was made to identify the cells of origin that are capable of initiating MRT tumourigenesis. The cell morphology and the presence of multilineage differentiation markers in MRT have led to speculation that the tumours originate from neuroectodermal (Haas et al., 1981, Ota et al., 1993, Suzuki et al., 1997, Okuno et al., 2010), neural (Higashino et al., 2003, Bonnin et al., 1984), epithelial (Parham et al., 1988), or myogenic (Sugimoto et al., 1999). Recent genome-wide analysis of primary MRT (Chun et al., 2016, Torchia et al., 2016) and mouse model experiments (Han et al., 2016, Vitte et al., 2017) point towards mesenchymal, neural crest cells and neural stem cells as potential cells of origin for MRT.

As previously mentioned in section 3.2.1, gene expression analysis of primary MRT (ATRT and ECRT) by the PBTG group demonstrated the transition in gene expression pattern from mesenchymal to neural (Figure 3.4). Transcriptional analysis by Torchia et al. (2016) reported that two genesets related to neural and mesenchymal cell development were highly enriched in ATRT. This raises the possibility that MRT originate from mesenchymal and/or neural stem cells. In support of this view, MRT also exhibit markers involved in myogenesis such as skeletal b-tropomyosin, neutral calponin, NFAT3, and myosin regulatory light chain thus illustrating a mesenchymal stem cell origin of tumours (Pomeroy et al., 2002).

MRT are also postulated to originate from neural crest cells (Chun et al., 2016, Han et al., 2016, Vitte et al., 2017, Gadd et al., 2010). Comparison of 10 MRT with 12 cellular mesoblastic nephromas, 16 clear cell sarcomas of the kidney, and 15 Wilms tumours using RNA-seq showed downregulation of differentially expressed genes associated with neural crest cell and neural development (Gadd et al., 2010). Likewise, a recent genome

study by Chun et al. (2016) in primary ECRT reported significant enrichment of genes expressed during various stages in neural crest development such as neural plate border formation, neural crest cell specification and migration and also neural crest differentiation into various lineages such as cardiac neural crest (Card), myoblast (Myo), and sympathetic neurons (SN). Tamoxifen injection at a specific developmental window (E6-E7) in Smarcb1$^{flox/flox}$; Rosa26-Cre^{ERT2} mice gave rise to tumours at various locations such as soft tissues that phenotypically resembled human MRT (Han et al., 2016). Gene expression analysis of *Smarcb1*-deficient tumours shared closer expression profiles with the expression profiles of neuron progenitors and ectomesenchyme; a cephalic neural crest cell-derived mesoderm. Following this study, Vitte et al. (2017) have reported that conditional knockout of *Smarcb1* at protein zero (P0) in neural crest cells using *Cre* recombinase expression led to tumour formation in cranial nerves and meninges that exhibited histological characteristics and molecular profiles mimicking human MRT.

Although analysis of cell morphology, differentiation markers and gene expression of primary tumours provide clues as to the cell of origin of MRT, such studies have limitations. Expression of specific markers in tumour cells may not reflect the expression at an early developmental stage. Current mouse model experiments by Vitte et al. (2017) and Han et al. (2016) provide the closest clue for cell of origin for MRT, however so far, no tumours were found in CNS. The majority of tumours were developed in meninges, which is a rare location for ATRT (El-Nabbout et al., 2010, Mondal et al., 2011), eyes and head (Vitte et al., 2017). In short, the potential cell of origin and how it can correlate with the location of the primary tumours should be further explored as it will allow development of better mouse models and invention of new targeted therapy for MRT. Having said this, definitive evidence of a cell of origin for each molecular subgroup is critically needed. Here I apply a more systematic approach to accurately identify and characterise potential cells of origin for MRT and the possibility of subgroup-specific cells of origin.

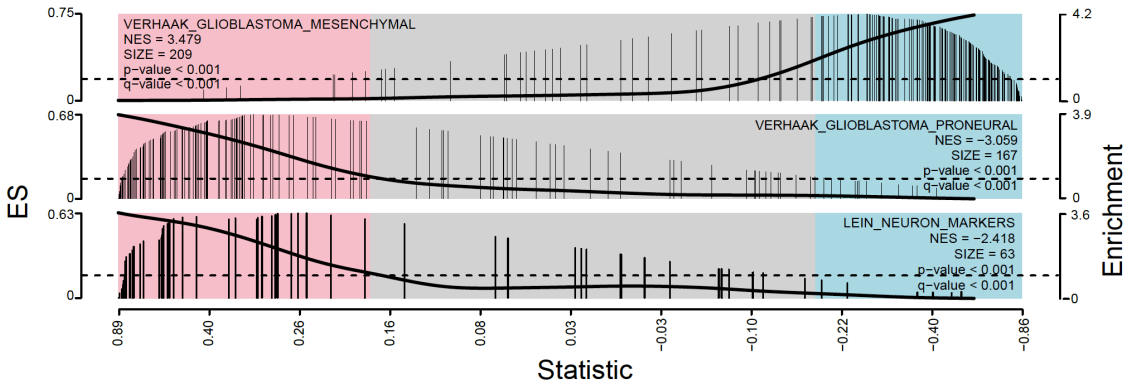

Figure 3.4 ***Transition from neural to mesenchymal geneset observed in primary MRT.*** *GSEA analysis of pre-ranked genes based on correlation with MRT metagenes (k=2) demonstrated significant gene set enrichment associated with neural (on right of plot) and mesenchymal (on the left of plot). Each tick represents the gene within the geneset whereas the height represents the expression score (ES). The loess curve shows enrichment trend. Pink, blue and grey shading represents genes significantly positively negatively, and non-significantly correlated respectively. The figure is adapted from PBTG group (unpublished).*

3.2.3.2 Analysis of expression profiles of MRT cell lines following SMARCB1 re-expression shows resemblance to expression profiles associated with adult multipotent stem cells

Gene expression analysis of *SMARCB1* re-expression profiles in 5 MRT cell lines (A204, G401, KD, SWOH and LM) provides an early indication of potential cell of origin within MRT (Figure 3.5). These expression profiles were generated from time course experiment in which *SMARCB1* expression was forcibly re-expressed in 5 MRT cell lines (Table 3.**1**) using lentiviral transfection of pCDH-EF1-PURO-SMARCB1 plasmid (INI1). The MRT cell lines were also transfected with lentiviral PCDH-CMV-MSC-EF1-Puro plasmid to create control cells (Control). The cell pellets were collected on day 1, 3, 7 and 14 post-transfection and RNA extraction was performed for RNA-sequencing analysis. The initial gene expression analysis using Affymetrix HGU133plus2 array was performed by selecting the genes that were differentially expressed initially between each cell line in the absence of *SMARCB1* expression. The profiles were then projected onto the first three components of a

principle component analysis (Dr Dan Williamson, unpublished). Interestingly, following *SMARCB1* expression over time, the gene expression of all five cell lines converges towards one point in space which resembles most closely that of the cells derived from adult multipotent stem cells. This result provides an insight that MRT, regardless of anatomical origin may possibly originate from the similar cell population. This preliminary analysis was re-evaluated further in this study with addition of a much greater number and range of stem cell profiles and MRT primary tumours.

Cell line	Species	Origin	Disease
A204	Homo sapiens	Kidney	ECRT
G401	Homo sapiens	Kidney	ECRT
SWOH	Homo sapiens	CNS	ATRT
KD	Homo sapiens	Abdomen	ECRT
LM	Homo sapiens	Liver	ECRT

Table 3.1 ***MRT cell lines used in SMARCB1 re-expression experiment***

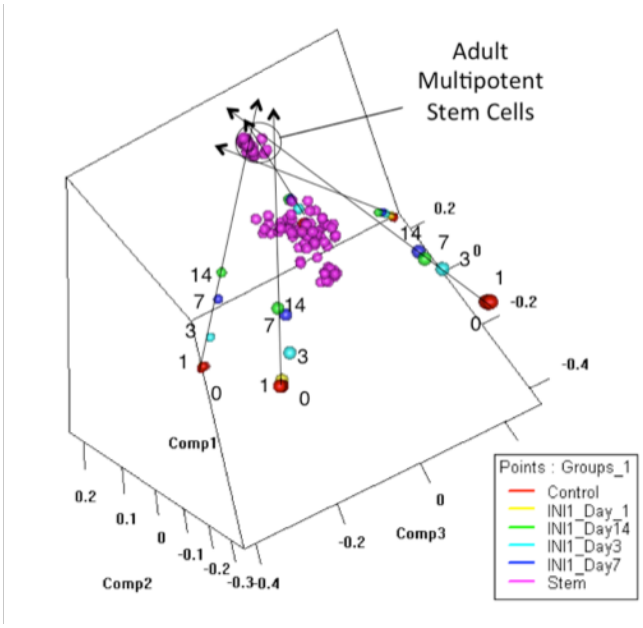

Figure 3.5 ***Analysis of expression profiles of MRT cells from 5 different MRT cell lines following SMARCB1 re-expression after Day 1, 3, 7 and 14****. A principal components analysis of genes, which are differentially expressed in response to SMARCB1 re-expression, shows that expression profiles converge over time to a point in expression space, which most closely resemble adult multipotent stem cells. Included are expression profiles from a variety of multipotent cell types (i.e. neural stem cells, human embryonic stem cells, induced pluripotent stem cells, etc). Expression of these genes separates the adult multipotent stem cells from the other stem cell types.*

3.3 Aims

The study reported in this chapter aimed to identify potential cells of origin within Malignant Rhabdoid Tumours (MRT).

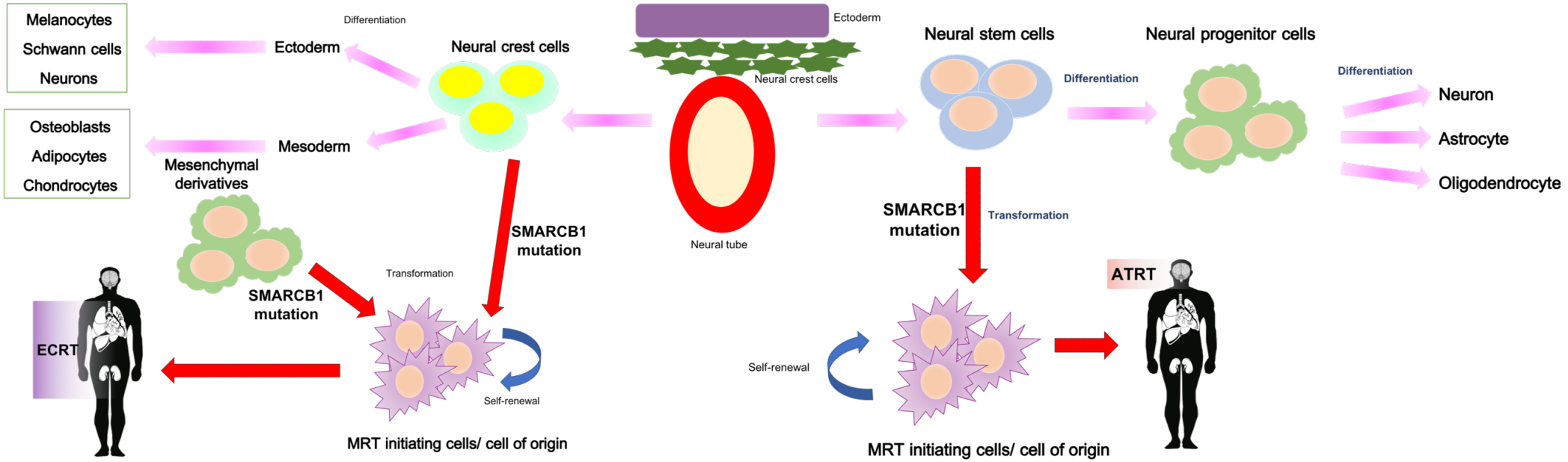

Figure 3.6 ***Schematic diagram showing differentiation of stem cells and how this correlates with identification of potential cell of origin for MRT in this study.***

3.4 Results

3.4.1 Transcriptome analysis of primary Malignant Rhabdoid Tumours (MRT) identifies MRT subgroups and provides an insight into potential cell of origin

MRT can be found at various location in the body including CNS, soft tissues, liver, kidney, etc. Recent genome-wide studies of primary MRT illustrated the existence of molecular subgroups in MRT (Chun et al., 2016, Johann et al., 2016). Transcriptomic analysis of primary MRT (10 ATRT, 13 ECRT) (see detail in section 3.2.1) demonstrated two molecular subgroups within MRT related to bodily location. This finding implies that the cell of origin for each subgroup is distinct. This has led me to hypothesise that MRT have different cells of origin that are linked to primary tumour origin. To explore the molecular subgroups within MRT and how their tumour location correlates to cell of origin, unsupervised cluster analysis was performed on HGU133p2 primary MRT consisting of 113 ATRT and 37 ECRT. All the MRT HGU133p2 profiles were pre-filtered to remove genes for which fold change < 3-fold and/or the range < 300 between maximum and minimum values (with the top/bottom 5% most extreme values removed). t-Distributed Stochastic Neighbour Embedding (t-SNE) showed that despite harbouring a common genetic mutation in *SMARCB1,* MRT are segregated into two subgroups related to tumour location; ECRT and ATRT (Figure 3.7a). The bodily location related to the subgroup in MRT provides the first indication that the cell of origin for MRT is not common and there is a possibility of at least two cellular origins that are specific for each subgroup.

The existence of two subgroups in MRT was further corroborated using t-SNE analysis of the top 1000 most differentially expressed genes between ECRT and ATRT. This t-SNE analysis separated the primary MRT into two distinct subgroups (Figure 3.7b), mainly related to primary tumour location, except for a few ATRT profiles clustered among ECRT. These datasets were from GSE28026 microarray analysis of 18 ATRT (https://www.ncbi.nlm.nih.gov/geo/query/acc.cgi?acc=GSE28026) which showed upregulation of bone morphogenetic protein (BMP), (Birks et al., 2011), a pathway commonly associated with mesenchymal stem cell (MSC) (Beederman et al., 2013) and embryonic stem cell (ESC) differentiation (Zhang et al., 2010).

Initial analysis suggests two different cells of origin for MRT related to the bodily location of primary tumours. To examine the pathways or genes that are specific to the bodily location of each molecular subgroup in MRT, the previously supervised RT HGU133p2 expression profiles were used as the basis for pre-defined gene ranking. The genes were ranked based on ECRT and ATRT related genes. Gene set enrichment analysis (GSEA) was performed on these pre-ranked genes to identify gene signatures that represent well-defined biological states or processes for each subgroup. The pre-ranked genes were analysed against hallmark gene sets (H) and gene ontology gene sets (C5) (both taken from MSigDB) (http://www.broadinstitute.org/gsea/index.jsp).

GSEA analysis against Hallmark MSigDB identified 14 gene sets that were positively enriched (FDR of <25%, 8 of which had a NOM (nominal) p-value of < 1%) in ECRT vs ATRT (cohort of 13 primary ECRT) and 8 gene sets that were negatively enriched (FDR of < 25%; 4 p<1%). Of 14 gene sets identified in this analysis, "hallmark adipogenesis", a subgroup of genes that involve in mesenchymal cell differentiation was positively enriched in ECRT (enrichment score (ES) of 0.22, normalised enrichment score (NES) of 1.17). The adipogenesis associated genes that were upregulated in ECRT includes *FABP4*, *CD36*, *SLC1A5,* etc. Fatty acid binding protein 4 (*FABP4*, also known as *aP2*) is a cytoplasmic fatty acid chaperone which expressed primarily in adipocytes cells. This gene has been widely used as a marker for adipocyte cell differentiation (Shan et al., 2013).

GSEA analysis was also performed against Gene Ontology MSigDB to identify biological signalling pathways associated with two subgroups in MRT; ATRT and ECRT. This analysis has identified 107 gene sets that were positively enriched (FDR of <25%, 66 of which had a NOM (nominal) p-value of < 1%) in ECRT vs ATRT (cohort of 13 primary ECRT) and 45 gene sets that were negatively enriched (FDR of < 25%; 4 p<0.01). These 45 gene sets negatively enriched in ECRT but positively enriched in ATRT are related to brain development and neuronal differentiation. The genesets include "GO neuron differentiation", "neurite development", "neurogenesis", etc. Genes that were upregulated in ATRT includes *Thy1* and *SOX2*.

Both GSEA analyses indicate the enrichment of gene sets related to the anatomical location of the primary tumours; whereby the ECRT subgroup showed enrichment in mesenchymal cell differentiation and ATRT demonstrated upregulation of gene sets

associated with neural cell development. More importantly, results from this study corroborated previous reports whereby the authors identified transitions between neural and mesenchymal gene set in primary MRT (Chun et al., 2016, Torchia et al., 2016). In short, two subgroups differed in genes regulating cell lineage and developmental signalling depending on their primary tumour location. This finding indicates that two cells of origins for MRT are potentially neural for ATRT and mesenchymal for ECRT.

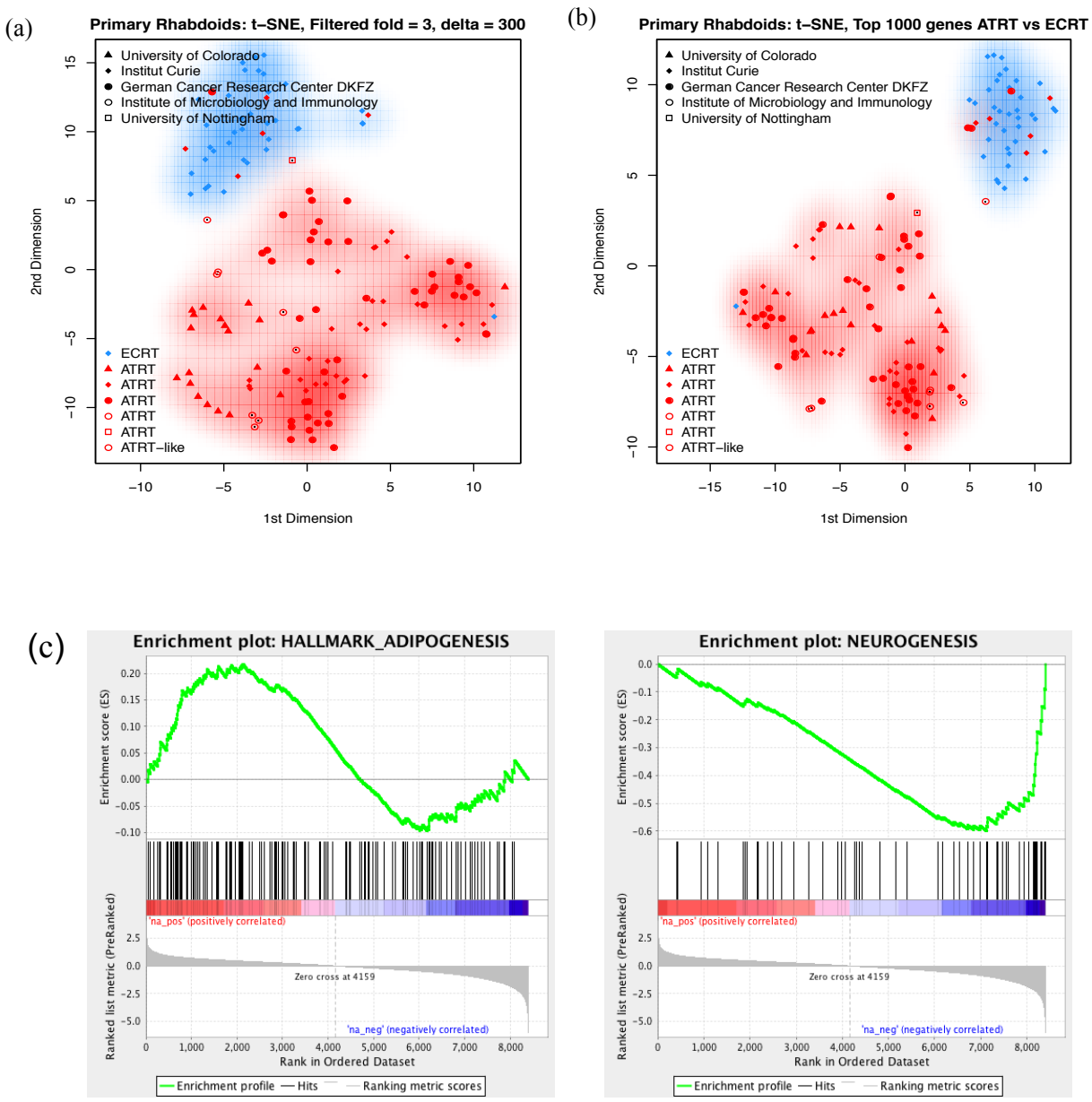

Figure 3.7 ***Bodily location of primary MRT related to molecular subgroups within MRT suggests two possible cells of origin****. t-SNE analysis of HGU133p2 array expression profiles of primary MRT showing two subgroups in MRT known as ATRT (in red) and ECRT (in blue) positively related to bodily location. The genes were pre-filtered in an (a) unsupervised and (b) supervised manner. (c) Example GSEA enrichment plots from the hallmark and gene ontology MSIgDB gene set libraries indicating those positively or negatively enriched in either ECRT or ATRT genesets. The enrichment score (ES) indicates the degree to which the genesets are overrepresented at the top or bottom of the ranked gene list. Positive ES represents the geneset enrichment at the top of the ranked list while negative ES illustrates the geneset enrichment at the bottom of the ranked list. The ranked list that was used in this analysis was ECRT at the top and ATRT*

at the bottom. The leading-edge subset is represented by the vertical line, and it indicates the genes that contribute most to enrichment score within the gene set. Gene set enrichment analysis (GSEA) of pre-ranked data of ECRT vs ATRT shows enrichment of genes linked to adipogenesis in ECRT while genes involved in neural were enriched in ATRT (neurogenesis).

3.4.2 Unsupervised gene expression profiles of various stem cell types

Gene expression analysis in primary MRT provides an initial indication of the possibility of two different cells of origin for MRT; neural stem cell and mesenchymal stem cells (see section 3.4.1). Additionally, gene signatures for neural crest cells and embryonic stem cells have been reported in primary ECRT and ATRT (Richer et al., 2017, Chun et al., 2016, Deisch et al., 2011). To identify putative cells of origin for MRT by considering other stem cell phenotypes that have been reported in MRT such as epithelial, mesenchymal, neuroectodermal, neural etc, the published Affymetrix HGU133Plus2 expression array datasets for various stem cell types were searched using terms "RNA signature" and "non-cancerous stem cells" on NCBI GEO (https://www.ncbi.nlm.nih.gov/geo/)(details of the dataset are presented in Chapter 2, section 2.2.1). These datasets were further filtered to restrict to human expression profiles and the HGU133plus2 platform. The final expression profiles that were retained after the filtering process consists of several progenitor and stem cells. These include embryoid bodies (EB), progenitor stem cells (PSC), embryonic stem cells (ESC), induced pluripotent stem cells (iPSC), mesenchymal stem cells (MSC), stromal (STR), mesodermal cells, epithelial stem cells, hepatocytes, keratinocytes, adipocytes, chondrogenic, osteogenic, neural crest (NC), endoderm, neural epithelial, neurons, neural progenitor cells (NPC) and neural stem cells (NSC).

To identify potential cells of origin for MRT from these various stem cell types, the published HGU133p2 stem cell profiles were initially pre-filtered to remove genes for which fold change < 3-fold and/or the range < 300 between maximum and minimum values (with the top/bottom 5% most extreme values removed) and the data analysed using a principle component analysis (PCA). PCA was performed using the filtered data sets to visualise the clustering of stem cells expression profiles (Figure 3.8). The analysis

showed the tendency of data sets to cluster into three broad groups: neural and its derivates which includes neural epithelia, neuronal stem cell, neuron and neural progenitor cells (in grey), embryonic stem cells (in blue) and mesenchymal with its derivatives which includes stromal, adipocytes, chondrogenic and osteogenic (in orange, yellow and red). (Figure 3.8a). 3D visualisation of PCA shows distinct groups of embryonic/totipotent stem cells separately from neural stem cell profiles. In brief, 3 major groups of stem cell profiles showed in this plot were mesenchymal (MSC) and its derivatives with neural crest (NC), neural stem cells (NSC) and embryonic stem cells (ESC).

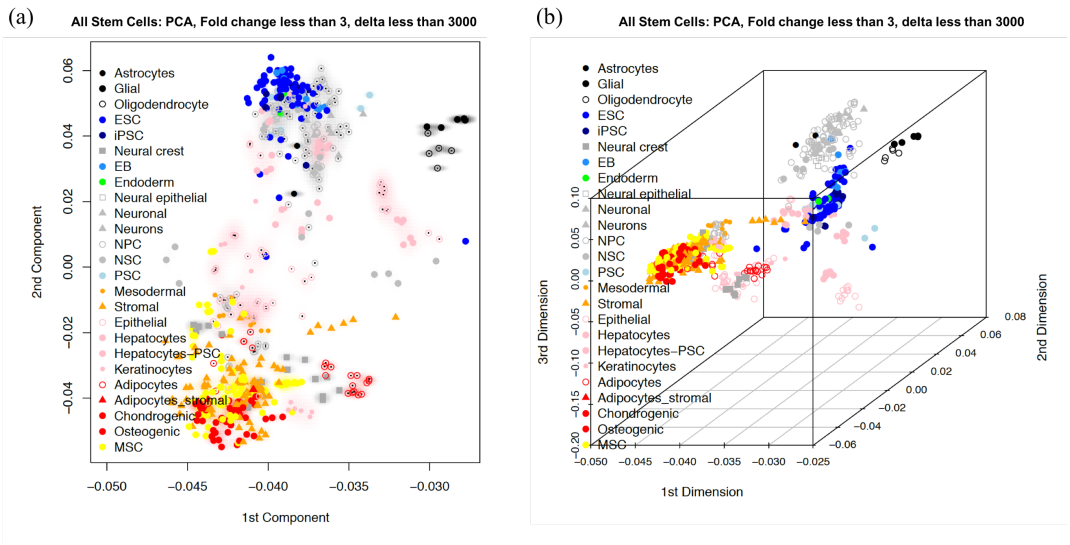

Figure 3.8 ***Unsupervised principle component analysis (PCA) showing HGU133p2 array expression of various stem cell populations****. Colours and shapes are labelled according to broad stem cell types. Black represents group of neuroglia cells of CNS, grey represents neuronal, orange represents stromal, yellow represents mesenchymal stem cells (MSC), red represents MSC derivatives, blue represents embryonic stem cells (ESC) and totipotent progenitor cells. ESC = embryonic stem cells, NSC = neural stem cells, NPC = neural progenitor cells, EB = embryoid bodies, iPSC = induced pluripotent stem cells, MSC = mesenchymal stem cells.*

3.4.3 Unsupervised expression analysis reveals similarities between primary MRT and various stem cell types

In keeping with early onset nature of MRT, *SMARCB1* occurs in the cell of origin for MRT is most likely to be multipotent stem cells. Transcriptomic analysis of primary MRT (113 ATRT and 37 ECRT) shows that MRT are related to the bodily location with enrichment of genes linked to neural (ATRT) and mesenchymal (ECRT) expression phenotype (see section 3.4.1). Hence, the possibility of two cells of origin for MRT. Additionally, various opinions on cells of origin were made based on the presence of differentiation markers (Okuno et al., 2010, Suzuki et al., 1997, Parham et al., 1988), cell morphology (Gonzalez-Crussi et al., 1982, Haas et al., 1981), omics analysis of primary MRT (Torchia et al., 2016, Johann et al., 2016, Chun et al., 2016) and also MRT mouse models (Han et al., 2016, Vitte et al., 2017). I thus sought to explore which stem cell type could give rise to two molecular subgroups in MRT. Transcriptome profiles from stem or progenitor cells that are publicly available (Section 3.4.2) were cross-referenced with primary MRT tumours profiles (Section 3.4.1). Genes were pre-filtered to remove non-varying probes (fold change < 300, absolute delta = 300, after excluding the top 5% most extreme values) in an unsupervised manner and the combined stem cell profiles and primary MRT underwent PCA analysis. The 3D PCA plot shows that primary MRT profiles were located in between NSC, MSC and derivatives; and NSC and derivatives expression profiles (Figure 3.9). The PCA plot demonstrates ECRT clustered close to MSC and NC profiles whereas ATRT clustered close to NSC. This finding corroborated the gene expression analysis of primary MRT mentioned in section 3.4.1. Notably, embryonic stem cell (ESC) profiles formed a distinct cluster separately from other stem cell populations (NSC, NC and MSC). The expression profiles of primary MRT did not overlap with ESC and totipotent stem cells (endoderm, epithelial, hepatocytes, keratinocytes and iPSC). Collectively, the location of primary MRT broadly overlaps with three stem expression profile namely NC, NSC and MSC, indicating that MRT may share a closer expression profiles with these stem cell populations thus possibly cell of origin (Figure 3.9). Secondly, ATRT located close to NSC suggests the potential of similar expression profiles shared between ATRT and NSC, thus the possibility of ATRT originating from NSC. Likewise, ECRT clustered closer to MSC and its derivatives. It is noteworthy that integration of expression profiles of primary MRT with broad stem cell populations in this analysis demonstrates ECRT grouped close to NC ("neural crest" on the PCA). These findings point to the possibility of shared expression profiles between

ECRT and MSC and NC thereby the probability of ECRT to originate either from NC or MSC. The results show consistency with previous analysis in section 3.4.1 that MRT originate from different cell of origin depending on the bodily location of primary tumours.

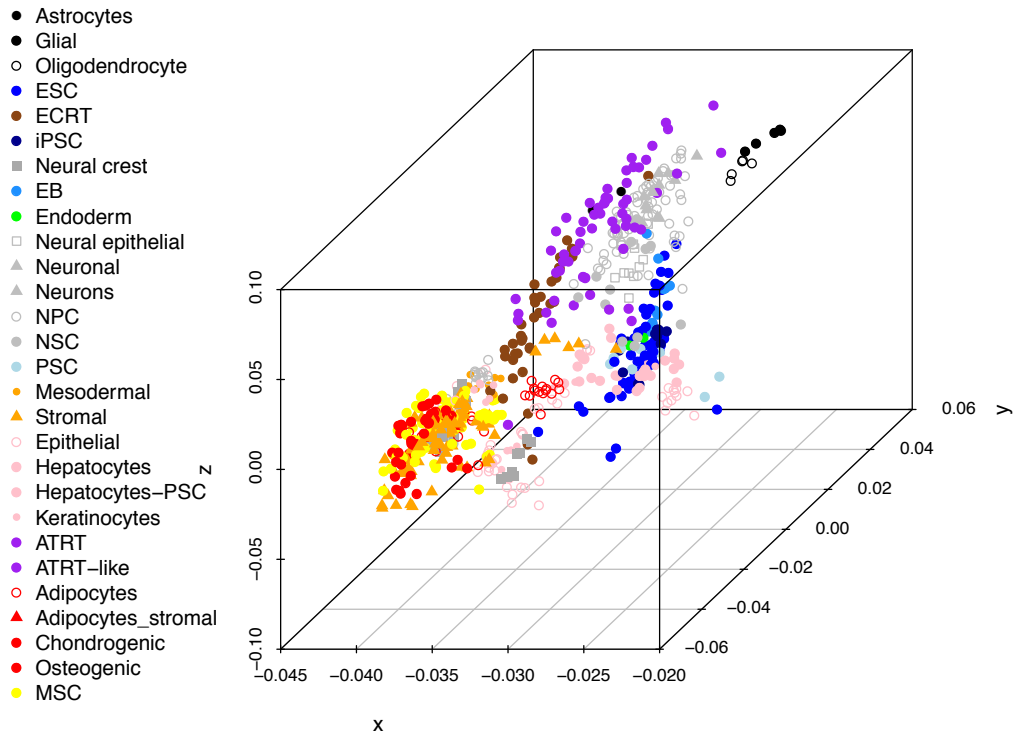

Figure 3.9 ***3D PCA showing unsupervised HGU133p2 array expression of primary MRT clustered close to stem cell profiles of mesenchymal and derivatives (orange, red and yellow), neural (grey) and neural crest cells (grey)****. The stem cell profiles and primary MRT were coloured and labelled according to rough type of stem cell. Embryonic stem cells (blue), endoderm (green) and totipotent progenitor cells (pink) made up a group, away from the primary MRT. This analysis demonstrates primary MRT may share closer expression profiles with stem cell populations (mesenchymal and derivatives; neural and derivatives, and neural crest cells). Notably, ECRT clustered close to neural crest cells and mesenchymal stem cell with its derivatives. Whilst, ATRT were located near neural stem cells and its derivatives. ESC = embryonic stem cells, NSC = neural stem cells, NPC = neural progenitor cells, EB = embryoid bodies, iPSC = induced pluripotent stem cells, MSC = mesenchymal stem cells.*

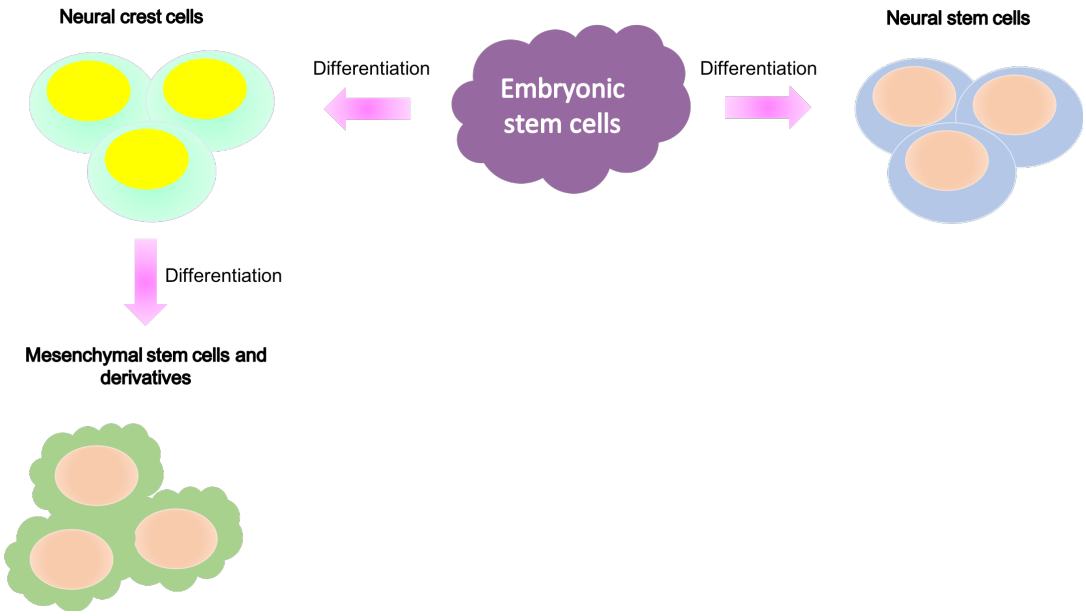

Figure 3.10 ***Hierarchy of stem cell differentiation to support discovery of cell of origin for MRT that are possibly subgroup related.***

3.4.4 Meta-analysis of primary tumour with stem cell profiles suggest three possible cells of origin in MRT

Integration of transcriptome profiles of primary MRT with various stem cell profiles as previously discussed indicates possible three cells of origin in MRT, which related to the location of primary tumours in the body (section 3.4.1, Figure 3.7 and section 3.4.3, Figure 3.9). The findings to this point suggest NSC, NC and MSC as potential cells of origin for MRT. Therefore, the previous stem cell profiles including derivatives were simplified into three groups. EB, PSC, ESC and iPSC were grouped as ESC; MSC, stromal, and endoderm derivatives were clustered as MSC; NPC, NSC and neural epithelial were classified as NSC; and neural crest cells as NC. To further characterise those three potential cells of origin in MRT and how they correlate with the bodily location for each molecular subgroup in MRT, the top 1000 most variably expressed genes between four stem cell profiles ESC, MSC, NSC and NC were selected using limma analysis. Expression of these genes was then integrated into primary MRT. t-SNE analysis showed separation of three stem cell profiles within the family of ESC, NSC and, NC and

MSC (Figure 3.11a). Notably, cross-referencing of genes differentially enriched in stem cell populations (ESC, NSC, NC and MSC) with primary MRT illustrates primary ECRT overlapped with NC and MSC while ATRT overlapped with NSC analysed using PCA (Figure 3.11b). It signifies that primary ECRT may enrich expression of genes that regulate NS and MSC developmental pathway. Likewise, genes that highly expressed in ATRT relative to ECRT tend to relatively highly expressed in NSC compared to other stem cell types.

The presence of MSC and NSC gene signatures in primary MRT have been demonstrated previously in omics studies by Chun et al. (2016), Torchia et al. (2016) and PBTG group (unpublished) in which the authors illustrated the transition between NSC and MSC expression phenotypes in two subgroups of MRT, based on significant enrichment of gene sets that regulate these two pathways as determined by Gene Set Enrichment Analysis. Therefore, it is of interest to examine if similar findings can be achieved using my stem cells cohorts as results point towards MSC and NSC as potential cells of origin for MRT. To achieve this aim, non-negative matrix factorisation (NMF) was applied to MRT primary and stem cell populations; NSC, NC and MSC (STR and MSC) ($k = 2$) (Figure 3.11c). The consensus NMF clustering identifies two metagenes which broadly describe the transition between MSC to NSC. This finding is corroborated by a boxplot of one these metagenes which show ATRT splits into two groups, one group showing expression overlap with NSC and while the remaining ATRT profiles show correlation with MSC and lie on top of an NSC-MSC continuum (Figure 3.11d). These results are compatible with previous observations of MSC-NSC transition in MRT from studies by Chun et al. (2016), Torchia et al. (2016) and PBTG group (unpublished). Two metagenes are broadly related to two subgroups in MRT linked to the location of primary tumours in the body. Consistently, Pearson correlation matrix of genes significantly expressed in either ATRT or ECRT demonstrated ATRT strongly correlated with NSC (Figure 3.11e), while the ECRT correlated with NC and MSC (Figure 3.11f).

Altogether, the analyses further validated three potential cells of origin for MRT; NSC, NC and MSC. The extent of transcriptional overlap between stem cell profiles and primary MRT suggests closer sharing of expression profile that may reflect the occurrence of MRT at different anatomical location.

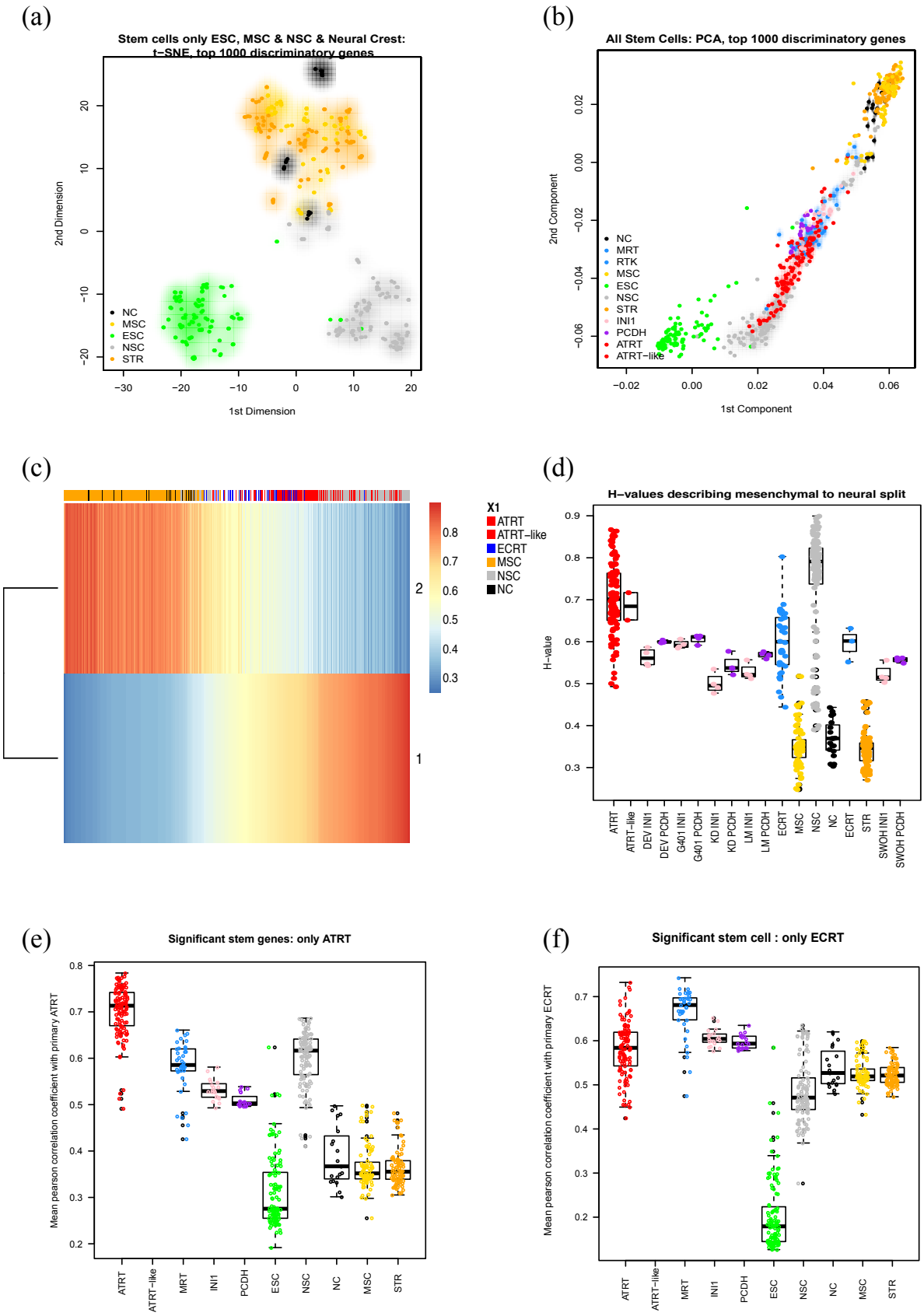

Figure 3.11 ***Degree of transcriptional overlap between primary MRT and stem cell profiles illustrates MRT share a closer expression profile with MSC, NC and NSC thus reflecting different bodily location for subgroups in MRT****. (a) t-SNE showing broad*

grouping of stem cell populations consisting of NSC (grey), MSC (orange and yellow), NC (black) and ESC (green). (b) PCA analysis of integrated expression of top 1000 discriminatory genes between each stem cell population with primary MRT, showing ECRT (blue) clustered close to expression profiles of NC and MSC, while ATRT (red) clustered around NSC. This plot shows the majority of MRT lie in between MSC and NSC. (c) Heatmap showing supervised NMF consensus clustering (k=2) of primary MRT RNA-seq expression profiles and stem cell expression profiles (MSC, STR, NC and NSC) confirming the transition between MSC and NSC. (d) Boxplot of one of the metagenes showing the primary MRT lie on the continuum between MSC and NSC. Also, the boxplot depicts how the SMARCB1 re-expression in the cell lines move the expression profiles towards the mesenchymal. (e and f) Pearson correlation matrix showing genes that are significantly highly expressed in ATRT or ECRT. The boxplot represents the mean pearson correlation between a given sample (f) and all other expression data and the boxplot shows types of stem cells with the greatest correlation with primary MRT. ATRT shows a greatest correlation with NSC (e) relative to other stem cell types, whereas ECRT shows the greatest correlation with MSC and NC (f) relative to NSC. INI1 denotes SMARCB1 re-expressing MRT cells, PCDH denotes SMARCB1-deficient MRT cells. ESC = embryonic stem cells, NSC = neural stem cells, MSC= mesenchymal stem cells, STR = stromal, NC = neural crest cells.

3.4.5 Re-expression of SMARCB1 in MRT cell lines provokes cell differentiation

ATP-dependent SWI/SNF chromatin remodelling complex has a role in a variety of cellular processes including cell differentiation (Roberts and Orkin, 2004). Particularly for MRT, experimental studies demonstrated a requirement for *SMARCB1* in hepatocyte (Gresh et al., 2005) and adipocyte (Caramel et al., 2008) cell differentiation. These studies illustrate that mutation of *SMARCB1* in specific cell types has the capacity to block normal cell differentiation. Evidently, MRT are associated with an undifferentiated phenotype and the differentiation process was restored upon *SMARCB1* re-expression (Caramel et al., 2008). Initial analysis from Dr Dan Williamson manipulating the cell expression models provided the basis for identifying potential cells of origin for MRT (Figure 3.5). The role of *SMARCB1* in cell differentiation as demonstrated in previous studies prompted me to investigate whether *SMARCB1* re-expression in MRT cell lines

will also provide clues to discovery of cell of origin. With this aim, expression profiles of *SMARCB1* re-expressing MRT cell lines (SWOH, KD, A204, G401, WT1) at day 1,3,7 and 14 were analysed. The genes that were differentially expressed amongst cell lines were identified (delta > 6) using supervised clustering analysis of gene expression data and compared against stem cell profiles. In MRT cells in which *SMARCB1* was forcibly re-expressed, cells became gradually more differentiated over time and their expression profile altered from that of an early neural crest to a more differentiated mesenchymal pattern (Figure 3.12). Most of the cell lines were derived from ECRT (A204, G401, WT1, KD) (Table 3.**1**) and this finding is in agreement with my comparison of expression profiles of primary ECRT with stem cell profiles which illustrated the possibility of MSC or NC origin for ECRT. In addition, my assumption that cell line models originate from NC or MSC was corroborated by Pearson correlation matrix which demonstrated *SMARCB1* re-expressing cell lines (denotes as INI1 in Figure 3.11f) correlated most strongly with NC and MSC, as determined by expression of genes that significantly highly expressed in ATRT or ECRT (Figure 3.11f). Comparison of gene expression analysis of MRT cell lines against stem cell profiles indicates that *SMARCB1* expression provokes the cells to differentiate towards NC and MSC, thus confirming that NC or MSC is a potential cell of origin for ECRT.

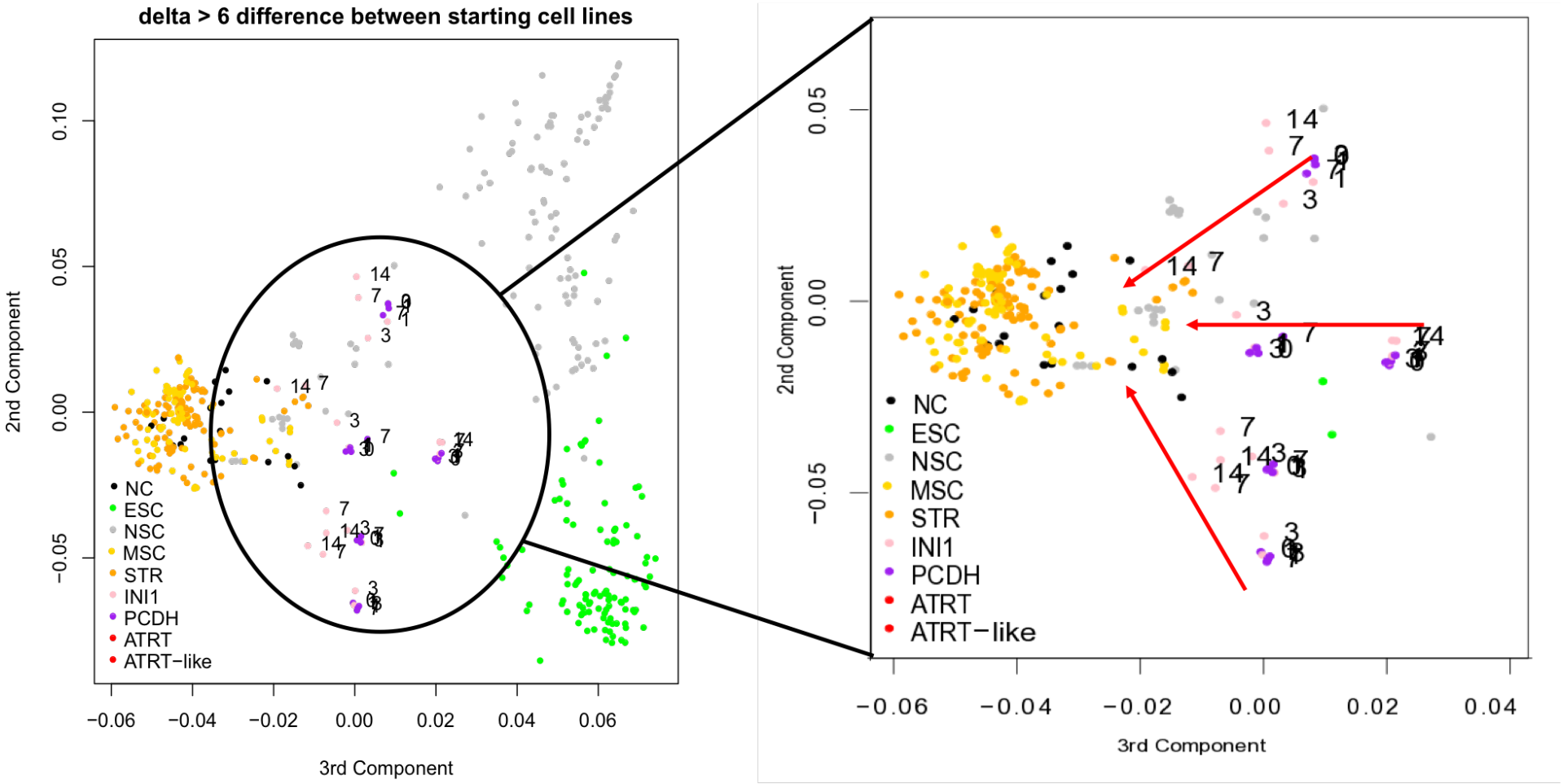
delta > 6 difference between starting cell lines
2nd Component
3rd Component
NC
ESC
NSC
MSC
STR
INI1
PCDH
ATRT
ATRT−like

Figure 3.12 ***PCA of stem cells, primary MRT and SMARCB1 re-expressing cell lines using only genes which were different amongst the cell lines (delta > 6).*** *The PCA plot showing that re-expression of SMARCB1 in MRT cells gradually changed the cells to become more differentiated over time (from day 0, 3, 7 to 14) and their expression profile altered from an early neural crest cells (NC) to more differentiated mesenchymal stem cells (MSC). INI1 represents the RNA-seq data of SMARCB1 re-expression in MRT cell lines while PCDH represents the RNA-seq of SMARCB1-deleted MRT cells. ESC = embryonic stem cells, NSC = neural stem cells, MSC= mesenchymal stem cells, STR = stromal, NC = neural crest cells.*

3.4.6 Expression of stem cell type signature genes illustrates subgroup specific cell of origins within MRT

Integrated gene expression analysis demonstrates the transcription overlap between primary MRT and stem cell types. For instance, ATRT shows a close similarity with NSC, while ECRT illustrates a close expression profile with MSC and NC (Figure 3.11). This may reflect how each subgroup enriches expression of the genes that regulate different biological process. Therefore, I next defined molecular and cellular features of the subgroups, ATRT and ECRT and to what extent these subgroups correlate with a suggested cell of origins i.e NSC for ATRT and MSC/NC for ECRT in order to provide the evidence of bodily location related subgroup. Genes that were significantly differentially expressed in each stem type were selected and compared against primary MRT and cell lines; and other stem cell types. A heatmap of genes differentially expressed in NSC compared to MSC and ESC (defined by discriminatory statistical coefficient >2 between ESC and NSC, and MSC and NSC) illustrates high expression of these genes in ATRT in relative to ECRT (Figure 3.14a). An attempt to examine similarity in gene expression between MRT and NC (defined by a coefficient greater than 2 compared to MSC cells) was unsuccessful due to small number of expression profiles for NC collected in this study (Figure 3.14b). To circumvent this problem, the genes that were linked with NC were manually curated from previously published studies (Chun et al., 2016, Ishii et al., 2012) and compared with expression profiles of other stem cell population (ESC, NSC and MSC), MRT primary (ECRT and ATRT) and cell lines. Additionally, genes that were downregulated in NC were identified and compared against primary MRT, cell model and

other stem cell types. Notably, these gene sets were highly enriched in ATRT (data not shown). Consistently, genes differentially expressed in MSC compared to NSC and ESC (discriminatory statistical coefficient >3 between ESC and NSC) were highly enriched in ECRT relative to ATRT, thus giving strong evidence of MSC as cell of origin for ECRT (Figure 3.13c). In line with these results, genes that are significantly highly expressed in each two subgroups have the greatest correlation with ATRT, while NC and MSC have the greatest correlation with ECRT (Figure 3.11e-f). This analysis demonstrates a degree of similarity in expression profiles between stem cell populations and MRT. High expression of NSC specific genes in ATRT may reflect the possibility of NSC as cell of origin for ATRT subgroup. Likewise, few MSC specific genes are enriched in ECRT, thus describing the incidence of ECRT in mesenchymal metabolically active organ such as liver or kidney.

The initial differential gene expression analysis between ATRT and ECRT in primary MRT cohort (113 ATRT and 37 ECRT) describes two potential cells of origin; NSC and MSC. However, following integrated analysis of transcriptome profiles of these primary MRT with various stem cell expression profiles, I have discovered NC as a potential cell of origin in addition to NSC and MSC. The subsequent analysis illustrates NC and MSC as potential ECRT cells of origin as opposed to NSC for ATRT. To further confirm the subgroup-specific cell of origin from three stem cell types, genes most differentially enriched in each subgroup (ATRT and ECRT) were identified using a supervised analysis of gene expression as previously discussed in section 3.4.1 The heatmap showing expression of ATRT related genes was enriched in NSC (Figure 3.14a). By contrast, expression of ECRT related genes was significantly enriched in NC and MSC (Figure 3.14b). Furthermore, *SMARCB1* re-expressing MRT cell lines (INI1) shared closer expression profiles with ECRT and NC, thereby further corroborating the observations in primary ECRT. Taken together, as demonstrated by consistent gene expression results discussed above, ATRT potentially originates from NSC while ECRT possibly originates either from NC or MSC. Figure 3.14a clearly illustrates two possible cells of origin in MRT which correlate to the bodily location of primary tumours.

To address the relevance of NSC, NC and MSC as candidate cells of origin for MRT, I then sought the examine the expression of *SMARCB1*-dependent genes in these stem cell types. The heatmap illustrates high expression of *SMARCB1*-dependent genes in NSC,

NC and MSC stem cell populations (Figure 3.14b). *SMARCB1* dependent genes which are often associated with ATRT subgroup including *SOX2* and *MYCN* were highly expressed in NSC. Notably, NC and MSC also demonstrate enrichment of *SMARCB1* dependent genes such as *MYC, CDKN2A, CCND1* (Figure 3.14b).

Altogether, the three differential gene expression analyses that were performed in a supervised analysis manner show a positive correlation between ECRT and MSC or NC, and between ATRT and NSC. This finding supports my hypothesis of a subgroup-specific cell of origin in MRT. Importantly, results from this study provide an insight that *SMARCB1* mutation in specific cell types can obstruct normal cell development i.e neural cell differentiation eventually leading to tumour formation in the brain. It may explain the different bodily location associated with each subgroup.

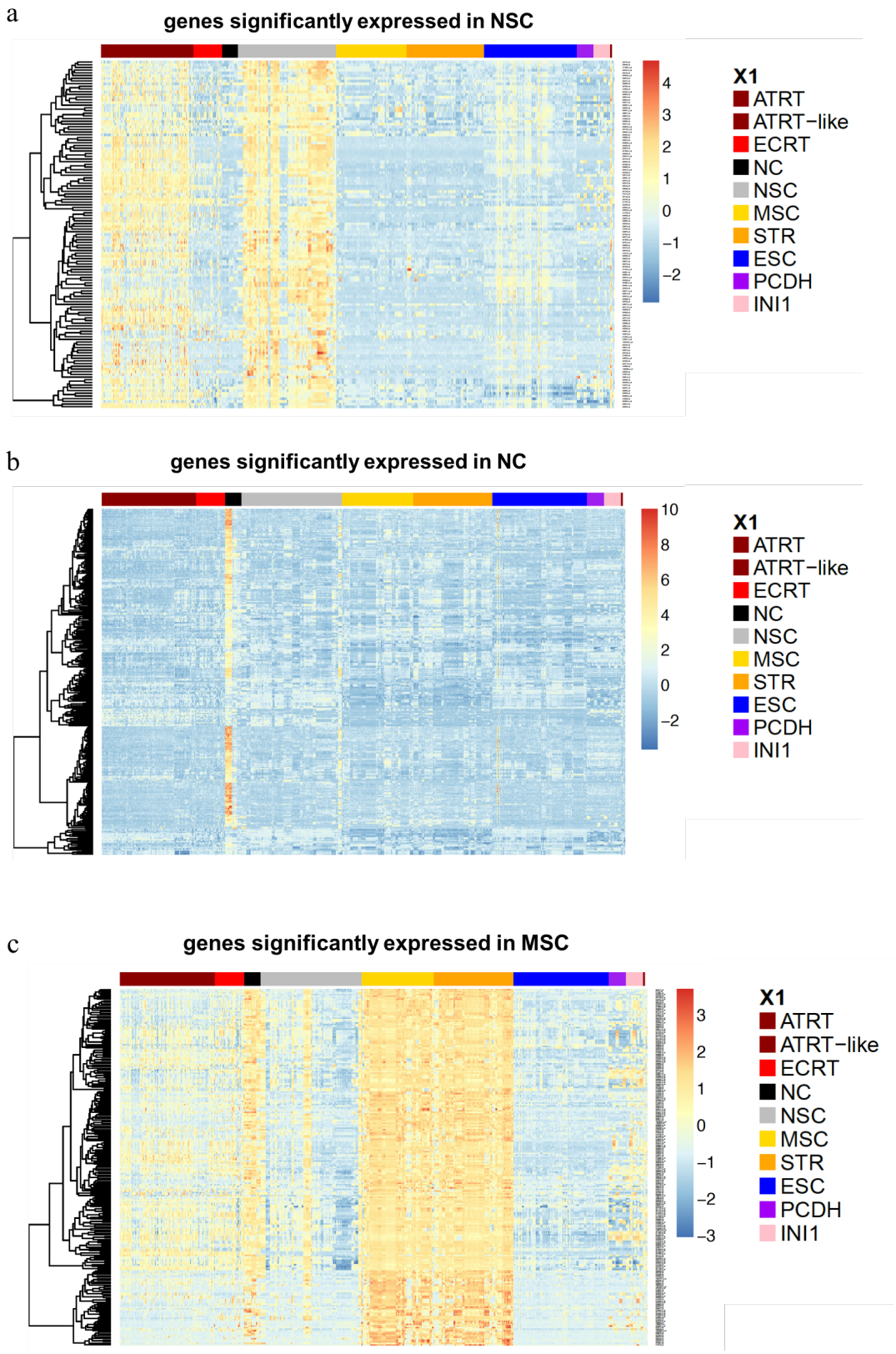

Figure 3.13 ***MRT primary and cell lines share closer expression profiles with MSC, NC and NSC.*** *(a) Heatmap showing NSC specific genes (grey) that are highly expressed in ATRT (crimson), (b) expression of NC specific genes failed to identify in MRT primary*

and cell lines due to limited number of NC specific genes (c) while few MSC (yellow and orange) specific genes are enriched in ECRT (red). ESC = embryonic stem cells, NSC = neural stem cells, MSC= mesenchymal stem cells, STR = stromal, NC = neural crest cells.

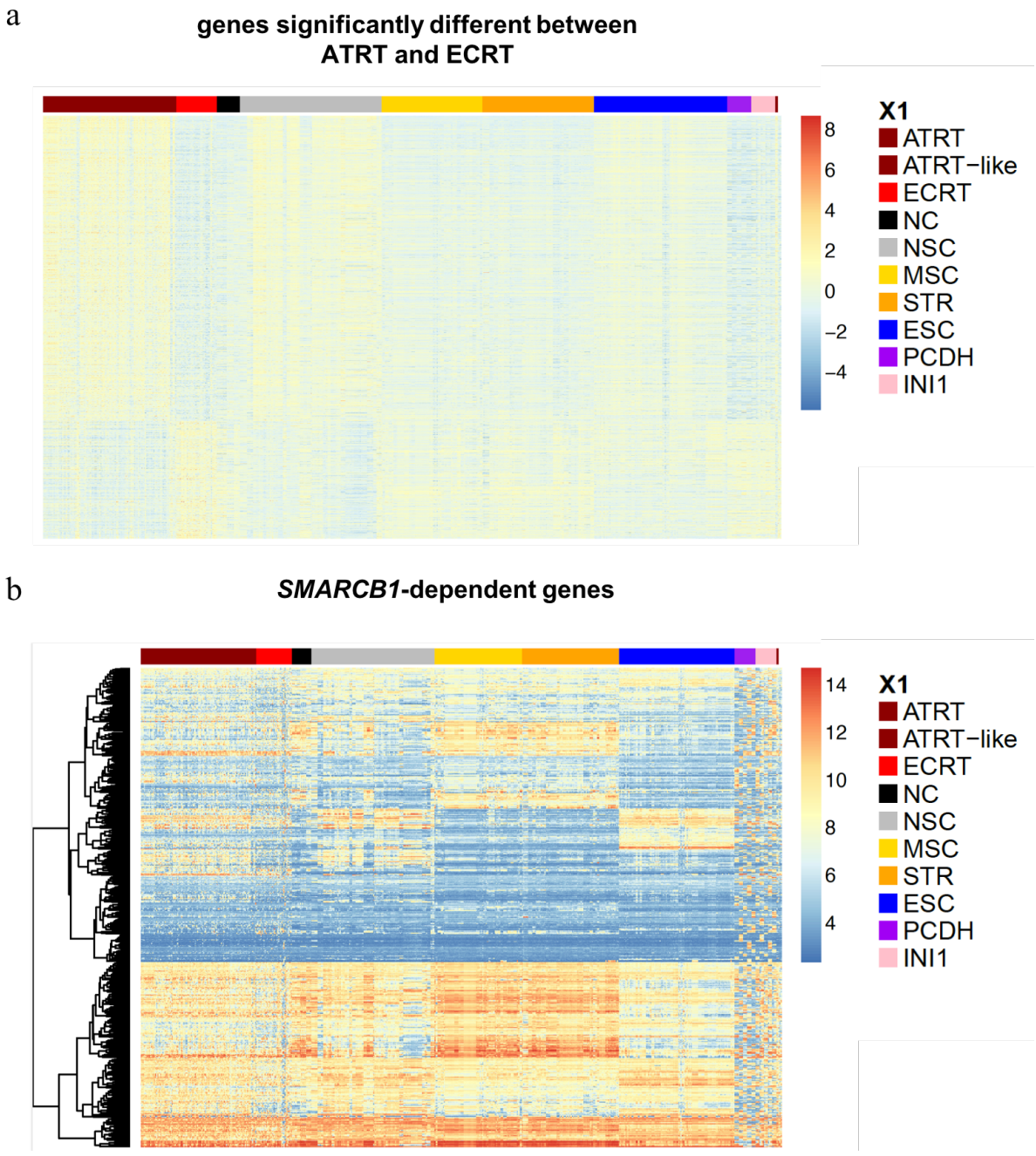

Figure 3.14 ***Heatmap analysis of differential gene expression of MRT primary and cells compared to several stem cell types****. (a)Heatmap analysis of genes significant different*

between ATRT and ECRT illustrates ATRT related genes are enriched in NSC, while ECRT related genes are enriched in MSC and NC, suggesting cell of origin associated with bodily location. (b) Heatmap showing SMARCB1 dependent genes are enriched in MSC, NC and NSC. These genes are associated with two subgroups in MRT. ESC = embryonic stem cells, NSC = neural stem cells, MSC= mesenchymal stem cells, STR = stromal, NC = neural crest cells.

3.4.7 Embryonic stem cells (ESC) are not a cell of origin candidate for MRT

Immunohistochemistry studies and genome-wide analysis of primary MRT have shown the presence of ESC expression markers such as OCT4, NANOG, SOX2, etc thus leading to an assumption that MRT may originate from ESC (Richer et al., 2017, Chun et al., 2016, Deisch et al., 2011). However, the meta-analysis performed in this part of study showed no overlap in expression of ESC with either primary MRT and MRT cell lines (Figure 3.11b, e and f). To confirm these results, genes that were linked with ESC were selected in a supervised manner and were analysed against MRT primary and cell lines. The heatmap shown in Figure 3.13 shows that the expression of ESC specific genes was minimal in MRT primary and cell lines (Figure 3.15), as opposed to the large amount of expression of genes involved in MSC and NSC (Figure 3.13 and Figure 3.14a). The minimal transcriptional overlap between ESC with MRT suggests that ESC is not likely a potential cell of origin for MRT.

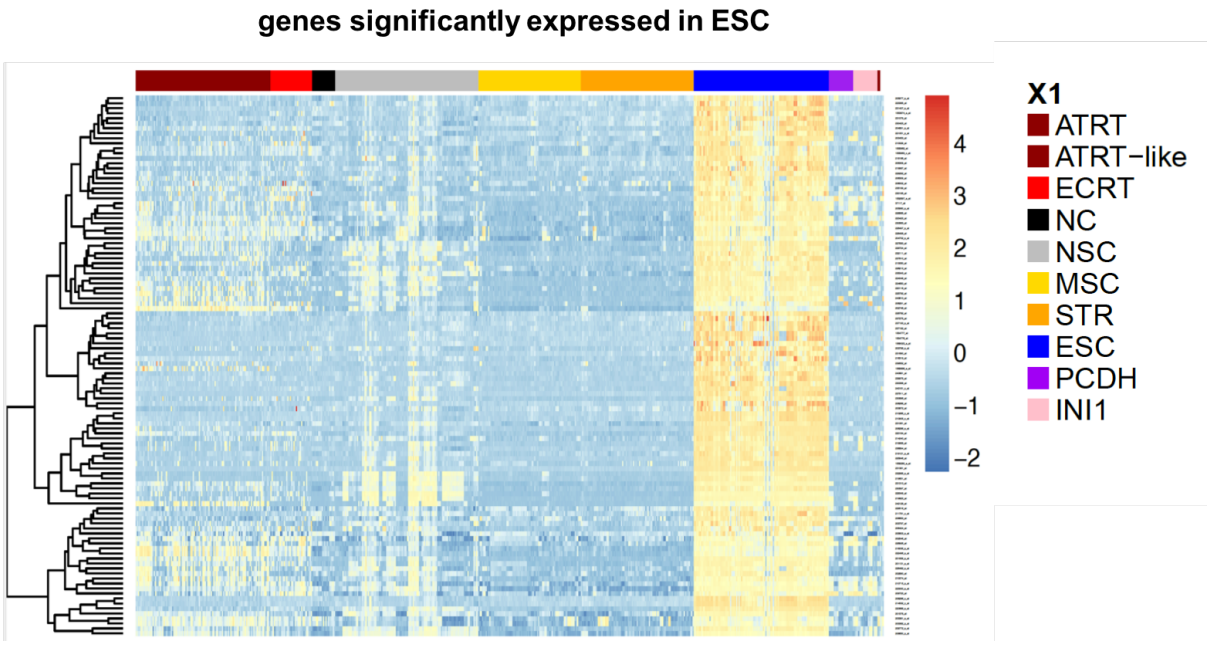

Figure 3.15 ***Heatmap showing expression of embryonic stem cell specific genes are diminished in MRT primary and cell lines signifying that ESC is not likely a cell of origin for MRT****. ESC = embryonic stem cells, NSC = neural stem cells, MSC= mesenchymal stem cells, STR = stromal, NC = neural crest cells*

3.5 Discussion

3.5.1 Gene expression analysis reveals candidates' cell of origin in MRT

MRT can be found at various location in the body but the true cell of origin still remains unknown. Studies reported in this chapter attempted to shed light on the mechanism that leads to MRT occurrence at multiple anatomical sites through identification of putative cells of origin for MRT. I postulated in this chapter that the tumours arise from distinct cell types that serve as a cell of origin and originate from early progenitor cells that have extensive self-renewal capacity due to highly aggressive and early onset nature of MRT (Rorke et al., 1996). Recent genomic studies (Johann et al., 2016, Chun et al., 2016) and mouse model experiments (Vitte et al., 2017, Han et al., 2016) suggest the possibility of neural crest (NC) cell or neural stem cells (NSC) as potential candidates for MRT cell of origin as determined by gene expression profiling and the potential of *SMARCB1* knockout mouse models to develop tumours that molecularly and phenotypically resembling to human MRT. Knockout of *SMARCB1* at specific developmental window (E7-10) *in vivo* is capable of initiating tumourigenesis (Han et al., 2016). In their study, cross-referencing of transcriptome profiles of MRT mouse and human tumours with stem cell expression profiles including embryonic stem cell (GSE44175), neural progenitor (GSE44175 and GSE44175), neuron (GSE46150), oligodendrocytes derived from neural stem cells (GSE9566), astrocytes derived from neural stem cells (GSE9566), ectomesodermal tissue from the palate (GSE9566) and neural crest (GSE11149) suggests neural progenitor and NC as potential cell of origin for MRT. Therefore, their findings are in agreement with results presented in this chapter which demonstrate NSC or NC as possible cell of origin.

Comprehensive gene expression analysis presented in this chapter demonstrated three probable cells of origin which are either NSC, NC or MSC. However, NC is the top candidate for MRT cell of origin in this study as NC progenitors are the earlier migrating cells with multi-lineage differentiation potential. In theory, NC shows the embryonic structural characteristics of vertebrates. It is originally found in the neural plate border region, between presumptive neural epithelium and epidermis. NC possess a high capacity for migration and multipotency (Liu and Cheung, 2016). The cells exhibit stem-like features such as self-renewal and can differentiate into a variety of cell types ranging from craniofacial skeletal tissues to the trunk peripheral nervous system (Dupin and

Coelho-Aguiar, 2013). NC cells that populate in sympathetic, parasympathetic, enteric and partly sensory ganglia can give rise to neurons and glial cells whereas NC cells that reside at head and neck structure can give rise to diversity of mesenchymal cell types. Taken together, NC cells fit the criteria for early onset of MRT and multipotency hence this stem cell type was further studied in Chapter 4 as a potential cell of origin for MRT.

3.5.2 Gene expression analysis indicates the possibility of subgroup specific cell of origin for MRT

Integrated gene expression analysis of primary MRT, cell lines and various stem cell types indicated different cell of origin in MRT related to tumour location of primary tumours. GSEA performed on primary MRT showed enrichment of different biological process in each subgroup found in MRT. In line with previous genome-wide profiling studies (Chun et al., 2016, Johann et al., 2016), ATRT showed enrichment of genes specific for neuronal development whereas ECRT demonstrated upregulation of genes associated with mesenchymal cell processes. These findings are in line with unsupervised analysis of stem cell and primary MRT expression profiles presented in section 3.4.3 which showed a high degree of overlapping expression between ATRT and NSC, and ECRT with NC and MSC as shown in Figure 3.11.

Supervised analysis of differentially expressed genes between ECRT and ATRT confirmed that ATRT shared similar expression profile with NSC whereas ECRT shared a closer expression profiles with NC and MSC. Also, in the absence of *SMARCB1*, the expression profiles of MRT cell lines clustered closely with primary ECRT. However, their expression altered from that of an early NC to a more differentiated MSC pattern upon *SMARCB1* re-expression thus suggesting that ECRT probably originates either from NC or MSC. Transcriptome profiles of primary MRT and mouse models are fully consistent with this finding of potential subgroup-specific origins within MRT (Chun et al., 2016, Han et al., 2016). Previously, Han et al. (2016) profiled tumours developed from their mouse models and compared the transcriptome profiles of these tumours and expression profiles of human MRT with various stem cell profiles. Their analysis of these datasets using Pearson correlation matrix analysis showed mouse and human ATRT were highly correlated with neural progenitor while ECRT were correlated with NC. It was shown that each subgroup enriched different gene sets as shown in genome-wide analysis. ATRT showed enrichment of genes associated with neural such as *OTX2*, a neural

progenitor marker. In contrast, ECRT did not show expression of neural-specific genes but demonstrated enrichment of mesoderm signature genes such as *HOXA/C* and *TXB2*. Taken these as a whole, their results also imply the possibility of subgroup-specific cell of origin which correlated with anatomical location of primary tumours.

Altogether, my study and Han et al. (2016) establish that the cell of origin is subgroup-specific and related to bodily location. The occurrence of MRT at various locations in the body may be due to mutation of *SMARCB1* in a specific cell population that is capable of hijacking normal cell differentiation processes during cell development which leads to tumour development.

Chapter 4 Somatic CRISPR/Cas9 mediated knockout of SMARCB1 in a putative cell of origin: A system for the development of Malignant Rhabdoid Tumours (MRT) models and identification of potential therapeutic targets

4.1 Summary

The poor survival rate of patients with Malignant Rhabdoid Tumours (MRT) who receive conventional chemotherapy or radiotherapy treatment, highlights the need for new targeted therapies. MRT are teratoid in nature and can occur almost anywhere in the body. The development of MRT, in particular, the cell(s) of origin and their relationship to tumour location and molecular subtype is largely unknown. Although biallelic loss of *SMARCB1* is minimally sufficient to initiate tumourigenesis, I hypothesised that this is dependent upon mutation in a particular type of cell; most likely an early pluripotent cell. To provide an effective method for investigating somatic loss of function of *SMARCB1* in a putative cell of origin, CRISPR/Cas9 vectors were generated to target human and mouse *SMARCB1*. Using a lentiviral approach, the phenotype associated with *SMARCB1* mutation in my hypothesised candidate cell of origin, namely neural crest (NC) cells was investigated. Somatic *Smarcb1* loss in NC cells gave rise to cells which resembled human MRT at a histological, immunohistochemical and molecular level, indicating the possible cell of origin for MRT. These studies will pave the way for the development of mouse modelling of MRT and identification of novel therapeutic approaches for treatment of this aggressive childhood cancer.

4.2 Introduction

4.2.1 Loss of SMARCB1 hijacks normal cell proliferation and differentiation thus initiates tumourigenesis

The mechanism by which *SMARCB1* loss contributes to tumourigenesis is complex due to its role as a tumour suppressor gene coding for a core subunit of the SWI/SNF chromatin remodelling complex, which is involved in many normal cellular activities such as differentiation and proliferation. The mechanism by which *SMARCB1* loss promotes cell survival and proliferation is through its interaction with pathways such as the p16(CDKN2A)-Rb-E2F pathway, Wnt signalling pathway, Sonic Hedgehog signalling pathway and the Polycomb group system (Jagani et al., 2010, Knutson et al., 2013, Mora-Blanco et al., 2014, Rimkus et al., 2016, Wilson et al., 2010a, Yang et al., 2016). Several studies have demonstrated the role of *SMARCB1* in cell cycle progression, the re-expression of *SMARCB1* in *SMARCB1*-deficient MRT cells leads to G1 cell cycle arrest, cell senescence and apoptosis (Betz et al., 2002, Versteege et al., 2002)(Figure 4.1). These results are due to the transcriptional activation of *p16* by *SMARCB1* which in turn leads to the phosphorylation of Rb through the repression of cyclin D1-CDK4 activity. Hyper-phosphorylated Rb (pRb) disassociates from *E2F* thus impeding its anti-proliferative activity. *E2F* also regulates genes that are involved in apoptosis and differentiation. In short, *SMARCB1* plays a significant role in regulating cell cycle progression through activation of p16 and repression of Rb pathways.

In addition to being highly aggressive and rapidly proliferating, MRT are teratoid in nature i.e. containing cells with multiple lineages. This phenotype suggests a role for *SMARCB1* in cell differentiation. In Caramel et al. (2008)'s study, the authors reported the re-introduction of *SMARCB1* in MRT cell lines caused the cells to differentiate into adipocytes as measured by Oil-Red-O staining of lipid droplets. To corroborate this finding, qPCR was performed to measure the expression of adipogenic markers LPL, AP2, C/EBPα and PPARγ2 which showed a strong upregulation of these markers in *SMARCB1* re-expressing MRT cells relative to control. These results illustrate the requirement for *SMARCB1* expression in adipogenesis. Additionally, knockdown of *SMARCB1* in hepatoblast-hepatocyte lineage model of cell differentiation impeded glycogen storage and epithelial morphogenesis, which are the criteria of hepatocyte differentiation (Gresh et al., 2005). Besides that, the authors found downregulation of

nearly 70% of genes that are normally upregulated during liver development as assessed from transcriptomic datasets of these cells (Gresh et al., 2005). Results from Gresh et al. (2005) and Caramel et al. (2008) emphasises the role of *SMARCB1* and the SWI/SNF chromatin remodelling complex in the activation of cell-type specific machinery and cell differentiation. In other studies, the SWI/SNF complex is shown to interact with C/EBPβ to regulate the expression of genes specific to the myeloid or adipocyte lineage (Kowenz-Leutz and Leutz, 1999, Pedersen et al., 2001) and MyoD to regulate muscle cell determination (Ivana et al., 2001).

The undifferentiated phenotype of MRT and its high proliferation rate suggest that it is the disruption of the delicate balance between cell proliferation and differentiation that drives MRT tumourigenesis.

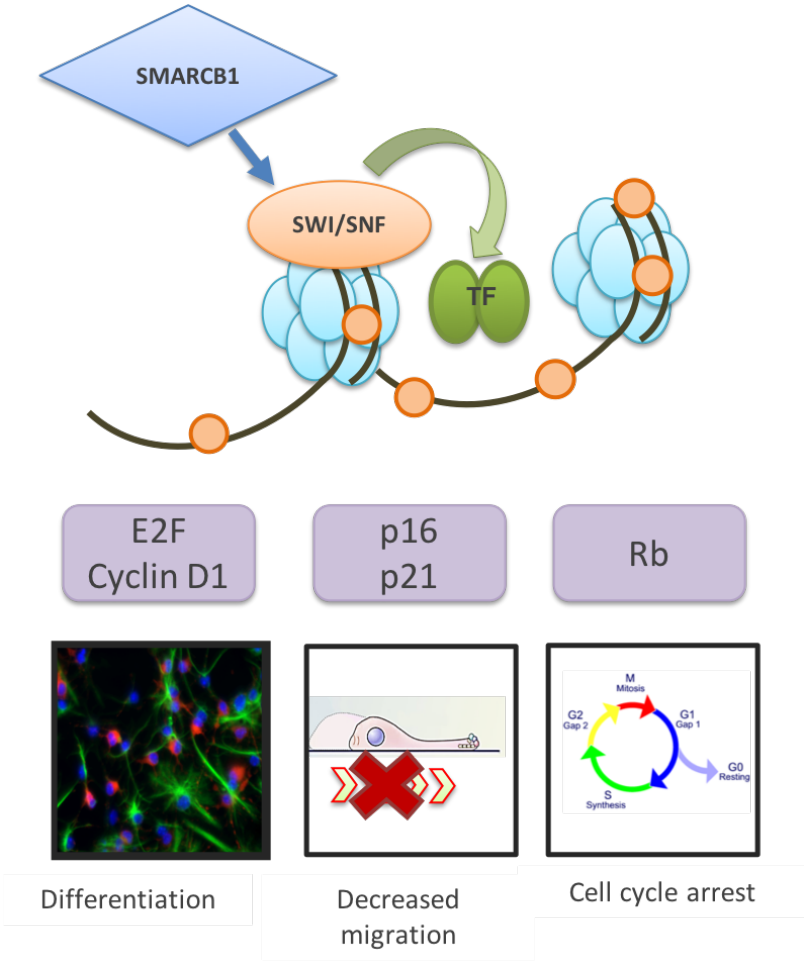

Figure 4.1 ***Role of SMARCB1 in cell differentiation and proliferation****. Re-introduction of SMARCB1 expression in MRT cell lines induces cell differentiation through activation of E2F pathway and decrease cell migration as a result of activation of cell cycle inhibitors; p21 and p16. It also triggers cell cycle arrest and apoptosis via Rb pathway.*

4.1.1 Development of MRT murine disease models: challenges and history

The aggressive nature of MRT and the essential role of *SMARCB1* in multiple pathways poses a major challenge for the development of a disease model. Homozygous deletion of *Smarcb1* in mice results in early embryonic lethality (3.5 – 6.5 days post coitum) (Guidi et al., 2001). To circumvent the problem, mouse models were developed in which *Smarcb1* was heterozygously deleted or subject to conditional deletion. However, these models developed highly aggressive cancers which resembled rhabdoid like tumours and T-cell lymphomas with a median age of onset of 11 months or 3-4 months of age,

depending on the model (Roberts et al., 2000, Roberts et al., 2002, Roberts and Orkin, 2004). Additionally, Han et al. (2016) have developed a Smarcb1$^{/flox}$; Rosa26-Cre^{ERT2} mouse model for MRT by temporal control of tamoxifen injection. Their mouse model showed that tamoxifen injection before E6 in pregnant mice, at the time of birth of the mice, or at 2 months of age of newborn mice were embryonic lethal and these results mimic the embryonic lethality observed in previous mouse models. More importantly, their mouse model demonstrates the appropriate window for injection that leads to a high penetrance of tumours with a median onset of 3 months. Further to this work, comparison of transcriptomic analysis of intra- and inter-species datasets (including data from this mouse model) suggested the possibility of a variety of cells of origin for MRT. A recent mouse model study by (Vitte et al., 2017) exploited the *Smarcb1* deletion in neural crest cells using the *Cre* recombinase vector which was expressed under the control of the P0 promoter. Homozygous deletion of *Smarcb1* in this mouse model leads to the formation of tumours that phenotypically resemble human MRT with an overall median survival of 3.2 months and onset of 1.5-5 months of age.

In general, recent mouse models developed for MRT are promising and able to circumvent embryonic lethality. However, it is worth noting that, while most of the tumours formed resemble human MRT, none of the models was able to provide evidence of tumour formation in other anatomical sites aside from head and brain. These mouse models bear similarities to ATRT tumours, the formation of tumours in extracranial sites such as the kidneys are so far not apparent. To gain a better understanding of MRT disease especially disease arising in different anatomical locations, development of a disease model that represents each molecular subtype within MRT is greatly needed.

4.1.2 CRISPR/Cas9 mediated genome editing technology

CRISPR/Cas9 technology provides a powerful tool for genome editing that has been used widely for functional screenings both *in vivo* and *in vitro*. CRISPR is an acronym for **c**lustered **r**egularly **i**nterspaced **s**hort **p**alindromic **r**epeats and is associated with Cas9 which functions as a nuclease enzyme. CRISPR/Cas9 forms irregular genetic loci in many bacteria and archaea to provide immunity against viruses and plasmids. Three types of CRISPR/Cas9 system (I-III) have been identified in both bacteria and archaea so far but the CRISPR/Cas9 type II from *Streptococcus thermophilus* or *Streptococcus pyogenes* is the most widely adapted in genome engineering technology (Makarova et al., 2011, Rath

et al., 2015, Li et al., 2015). The system works through co-expression of the bacterial endonuclease Cas9 and short guide RNA molecules (sgRNA) (Figure 4.2). The sgRNA directs Cas9 nuclease to the complementary region in the genome. At the recognition site which is usually at the 5' end of gRNA followed by an NGG sequence which is known as protospacer-adjacent motif (PAM), Cas9 nuclease will create double-strand break (DSB) that can be repaired by non-homologous end joining (NHEJ) which often introduces small insertions or deletions (indels) (Figure 4.1). The resulting indels shift the open reading frame, thus leading to loss of function of the gene of interest. CRISPR/Cas9 systems can also be used for gain of function purpose through a homology-directed recombination (HDR) mechanism at the targeted region in the presence of exogenous donor DNA. This can be achieved through introduction of precise DNA mutation or insertion of specific DNA sequence in the targeted site in the genome. However, Cas9 can tolerate the mismatches between sgRNA and complementary region in the genome only up to a certain limit. 3 or more adjacent mismatches at the 5' end of sgRNA can reduce its activity (Anderson et al., 2015), and will produce off-target effects if the mismatch is beyond this threshold. These undesirable effects of the CRISPR/Cas9 system necessitate fresh strategies to reduce the potential for off-target effects.

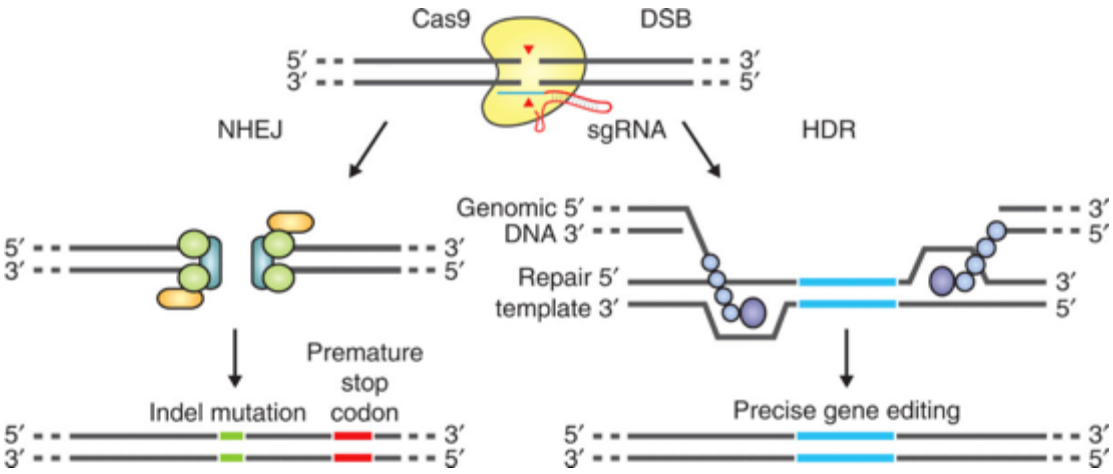

Figure 4.2 ***Schematic diagram of double strand break (DSB) created by Cas9 adapted from (Ran et al., 2013).*** *The DSB can be repaired either by NHEJ or HDR. NHEJ will often create indel mutations.*

4.2.2 Aims

In this chapter, I aimed to:

- construct a CRISPR/Cas9 system targeting *SMARCB1* and *SMARCA4*
- isolate sub-populations cells that will tolerate *Smarcb1* deletion and still retain capacity for prolonged proliferation
- characterise *Smarcb1*-deficient neural crest (NC) cells

4.3 Results

4.3.1 Generation of single guide RNA (sgRNA) for CRISPR/Cas9 genome editing

Four single guide RNA (sgRNA) were designed that specifically target the region in either exon 1 or 2 of *Homo sapiens* (HS) and *Mus musculus* (MM) *SMARCB1* and *SMARCA4* using either optimised CRISPR (http://crispr.mit.edu/) or CRISPR design (http://www.e-crisp.org/E-CRISP/designcrispr.html) web tools. The list of guide RNA generated by the E-CRISPR website is displayed only if the number off-target effect does not exceed a user-specified threshold. The output guide RNA is ranked based on off- and on-target efficiency if more than one design is found in the target locus. On-target efficiency was optimised for 20bp guide with NGG protospacer-adjacent motif (PAM) (Doench et al., 2016) which improved on-target efficiency.

In this study, the 20 nucleotide (nt) sgRNAs were selected due to their specific location near to NGG PAM on 5' sequence, their low off-target effects and high on-target efficiency scores (E-scores). The target sequences should be complementary to the gRNA ending in a NGG 5' (PAM) as this is required to recruit Cas9 nuclease to cut both strands of the DNA (Figure 4.3a). To increase the specificity of Cas9, the location of PAM was specified as a minimum of 8bp and maximum of 12bp of the target sequence (Figure 4.3a)(Hsu et al., 2013). To further optimise the specificity of Cas9 for *SMARCB1* and *SMARCA4* gene editing, the potential off-target effects were considered when choosing the guide RNA. The E-CRISPR website tool was used to evaluate the off-target effects and target site homology using the alignment program Bowtie2 (Heigwer et al., 2014). In addition to this, the guide RNA was not selected if the target sequence with genomic off-target had less than three mismatches. Besides that, the guide RNA sequence was designed to exclude intronic regions, CpG islands and UTRs. A total of 8 guide RNAs were designed in this study (Figure 4.3b). Homo sapiens GeCKO (HSG) or mus musculus GeCKO (MMG) guide RNAs were obtained from human/mouse GeCKO V2 genome-wide library (https://www.addgene.org/pooled-library/#crispr). Whilst, the remaining four guides were designed using the E-CRISPR website and were named as either homo sapiens E-CRISPR (HSE) or mus musculus E-CRISPR (MME). The eight CRISPR constructs were designed to target *SMARCB1* and *SMARCA4* expression in the potential cells of origin for MRT, either from human or mouse derived cell lines.

a)

b)

GENE	SPECIES	ENSEMBL
SMARCB1	Homo sapiens	ENSG00000099956
	Mus musculus	ENSMUSG00000000902
SMARCA4	Homo sapiens	ENSG00000127616
	Mus musculus	ENSMUSG00000032187

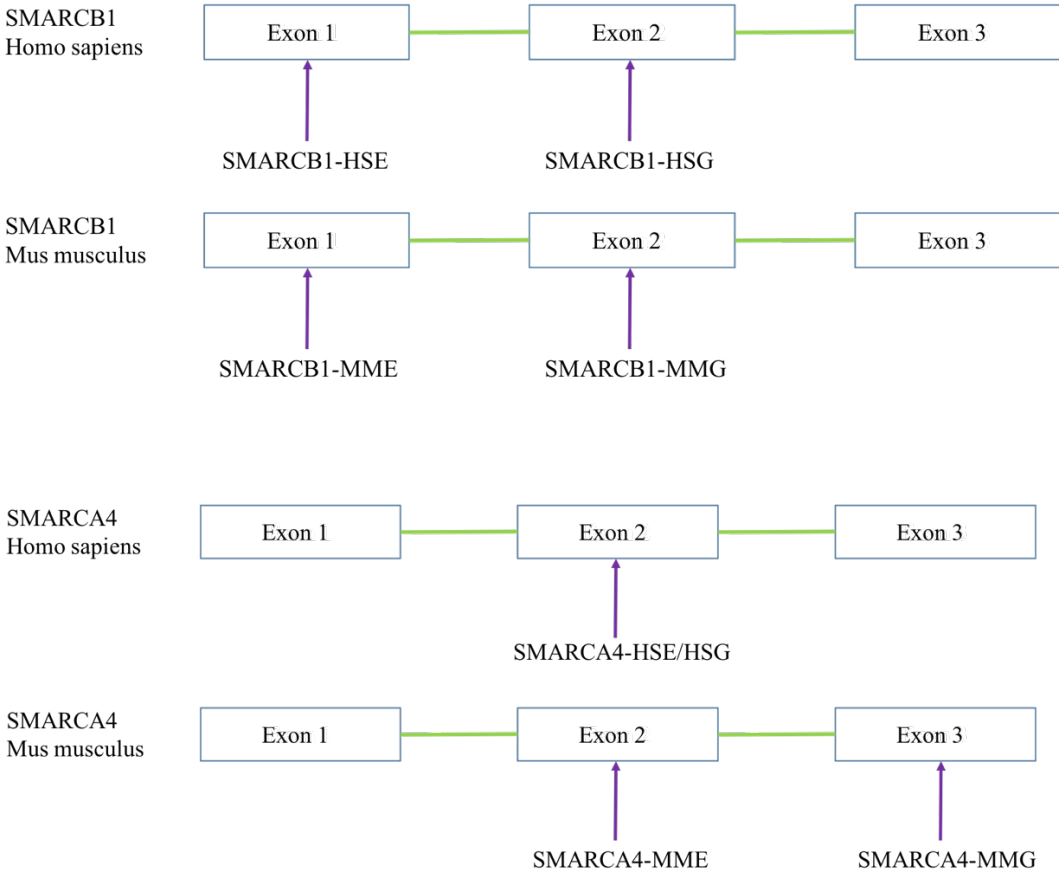

Figure 4.3 ***sgRNA targeting SMARCB1 and SMARCA4 in human and mouse****. (a) schematic of target sequence with NGG PAM in CRISPR/Cas9 construct. (b) The target region of sgRNA for SMARCB1 and SMARCA4. Four sgRNA were manually designed in this study using E-CRISPR website tool here denoted as HSE or MME inducing indels in*

exon 1 for SMARCB1 and exon 2 for SMARCA4. Whilst four sgRNAs were obtained from CRISPR/Cas9 GeCKO library denoted as HSG or MMG.

4.3.2 Optimisation of CRISPR/Cas9 constructs in HEK293T and NIH3T3

To evaluate the efficiency of CRISPR/Cas9 in generating somatic knockout of *SMARCB1* and *SMARCA4*, HEK293T and NIH3T3 cell lines were first infected with the lentiCRISPRV2 virus. Three MOIs initially tested on 293T and NIH3T3 were 1, 5 and 10 using CRISPR SMARCB1 HSE and SMARCA4 HSE. The mutation created by CRISPR/Cas9 was detected using the SURVEYOR nuclease assay which uses endonuclease to cleave DNA with high specificity at sites of base-substitution mismatch (Figure 4.4a). Following infection, the morphologies of *SMARCB1*- and *SMARCA4*-deficient cells differed from the non-targeting control cells. *SMARCB1* knockdown induced cell death 48 hours post puromycin selection and the cutting efficiency increased as the multiplicity of infection (MOI) increased. Cleavage intensity of each PCR amplicon and cleaved bands from SURVEYOR analysis was measured using Image J according to the formula below:

$$f_{cut} = (b + c)/(a + b + c)$$

$$\text{indel } (\%) = 100 \times \left(1 - \sqrt{(1 - fcut)}\right)$$

where a = integrated intensity undigested band, b + c = intensity of cleaved product, the formula adapted from (Ran et al., 2013)

CRISPR/Cas9 targeting SMARCB1 using CRISPR SMARCB1 HSE construct at MOI 5 and 10 in HEK293T yielded 61% of cleavage efficiency in the surveyor mutation detection assay (Figure 4.4b). Lentivirus transfection was less effective at MOI 1 which has 46% cleavage efficiency only. On the other hand, editing (insertion/deletion) efficiency of CRISPR SMARCA4 HSE in 293T cells was more efficient at MOI 10 than

MOI 1 and 5. The cleavage efficiency for MOI 10 was 67% while MOI 1 and 5 have only 35% and 48% cutting efficiency respectively (Figure 4.4b). From this initial surveyor mutation detection analysis, both CRISPR constructs have cleavage activities and the cleavage efficiency is better at MOI 10 for CRISPR SMARCA4 and MOI 5 or MOI 10 for CRISPR SMARCB1 (MOI 5). Hence, the experiments were repeated to examine the cleavage efficiency for other CRISPR sgRNA constructs. Lentivirus transfection at MOI 5 was used for CRISPR SMARCB1 (HSE, HSG. MME and MMG) while MOI 10 was used for CRISPR SMARCA4 (HSE, HSG. MME and MMG) on 293T and NIH3T3 cells. Transfection of 293T and NIH3T3 with CRISPR SMARCB1 at MOI 5 resulted in ~60% cleavage efficiency (Figure 4.4c). Similarly, CRISPR mediated *SMARCA4* knockout in 293T and NIH3T3 at MOI 10 resulted in ~60% cleavage efficiency (Figure 4.4c).

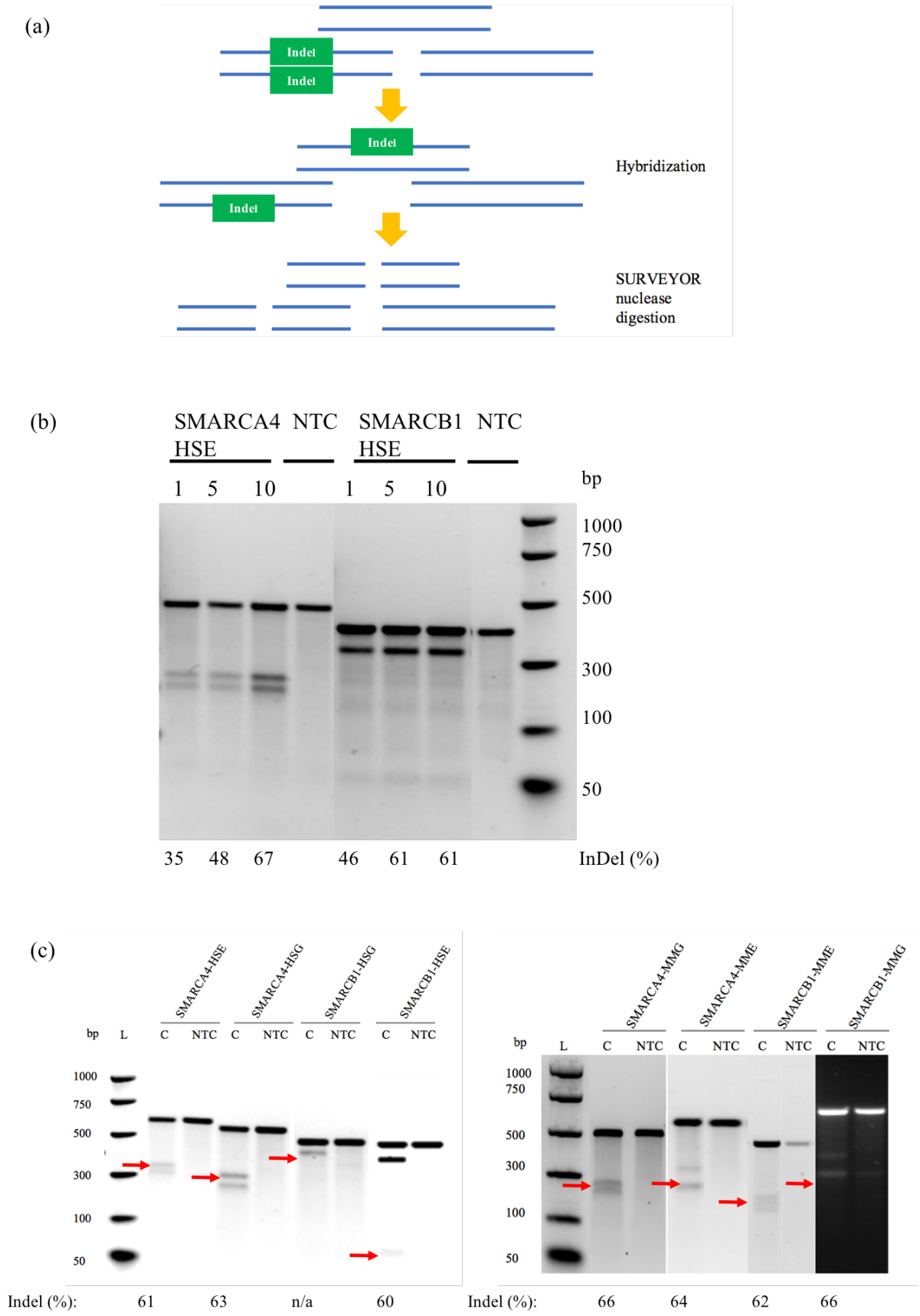

Figure 4.4 ***Efficiency of CRISPR/Cas9 in creating indels in SMARCB1 and SMARCA4 measured by SURVEYOR assay****. (a) Illustration of SURVEYOR mutagenesis assay. Blue*

band represents single strand DNA and indel denotes the mutation created by CRISPR/Cas9 system. First, the genomic DNA from 48 hours post transfection were amplified by PCR. During the hybridisation step, the homoduplex and heteroduplex DNA strands are formed. The assay uses a nuclease enzyme to cut the DNA strand that has mismatch mutation. The CRISPR indel frequency was calculated using the formula and presented above. (b) Optimisation of CRISPR lentivirus infection on 293T cells using two CRISPR construct targeting SMARCB1 and SMARCA4 at MOI 1, 5 and 10. Percentage of Indel represents the cutting efficiency of each CRISPR. (c) Electrophoresis gels showed two cleaved products (indicates with red arrow of). The percentage of indel mutation was calculated using the formula mentioned in the paragraph. C – CRISPR, NTC –No Template Control.

4.3.3 CRISPR/Cas9 can efficiently generate knockout of SMARCB1 and SMARCA4 in HEK293T and NIH3T3

To further analyse the effectiveness of CRISPR/Cas9 in mediating *SMARCB1* and *SMARCA4* knockout, the effect of *SMARCB1* and *SMARCA4* mutation on protein production was studied by an automated western system known as WES and by immunohistochemistry. The HEK293T and NIH3T3 cells were infected with unconcentrated lentiCRISPRv2 virus at MOI of 5 and 10 respectively and the cells were harvested 48 hours post puromycin selection. For detection of SMARCB1 and SMARCA4 protein, the total protein lysate was analysed with anti-SMARCB1 (BAF47) (BD Bioscience, Cat. No. 612110) and anti-SMARCA4 (BRG1 G-7) (Santa Cruz Technology, Cat. No. sc17796) in WES. The band was quantified using the densitometric program on ImageJ, and the percentage of protein loss was calculated using the formula below:

$$y = \frac{SMARCB1}{Vinculin}$$

$$Z = \frac{NTC}{Vinculin}$$

$$\%knockdown = \frac{y}{z} * 100$$

As shown in Figure 4.5a, western blotting illustrated that CRISPR/Cas9 knockout leads to loss of 75% and 44% SMARCB1 protein expression in HEK293T cells infected with HSE and HSG respectively while 88% and 61% SMARCB1 protein loss was observed in NIH3T3 cells infected with MMG and MME respectively as compared to NTC wild-type (WT) (Figure 4.5a). In contrast, WES analysis revealed a loss of 54% and 56% of SMARCA4 protein in HSE and HSG HEK239T cell respectively while 64% and 70% SMARCA4 loss was achieved in MME and MSG NIH3T3 respectively relative to NTC (WT).

To confirm the WES results, immunohistochemical (IHC) staining of SMARCB1 and SMARCA4 deletion was performed in NIH3T3 and HEK293T cells. The cells were stained with anti-SMARCB1 antibody and anti-SMARCA4 antibody at 1:100 and 1:400 dilution respectively. The nuclear staining analysis was performed using Aperio Imagescope software (using nuclear staining algorithm). Loss of nuclear SMARCB1 protein by immunohistochemistry was seen in 60% of *SMARCB1*-deficient HEK293T cells compared to 8.5% of control cells in which the Aperio Imagescope scored them as negative (SMARCA4-HSE cells was used as control for SMARCB1 staining) (Figure 4.5b). In contrast, 71% of cells were scored positive (+3 and +2) for SMARCA4 staining in SMARCA4-HSE transfected cells, as analysed using Aperio Imagescope. This result was not comparable with western blot which showed loss of 56% of SMARCA4 protein expression in HEK293T- deleted SMARCA4A HSE cells. This may be due to SMARCA4 antibody not being optimised for immunohistochemistry analysis. Also, this experiment was performed once only.

Altogether, initial experiments in HEK293T and NIH3T3 showed good knockout was efficiently achieved using CRISPR/Cas9 to target *SMARCB1* and *SMARCA4* as determined by surveyor mutation detection assay, western blot and immunohistochemistry analysis. The CRISPR/Cas9 system containing eight guide RNAs was optimised for ideal MOI and cell density; MOI of 5 for all human and mouse CRISPR SMARCB1 and MOI of 10 for all human and mouse CRISPR SMARCA4.

The following experiments presented in this chapter utilised CRISPR/Cas9 mediated *SMARCB1* knockout in appropriate cells of origin. Although the efficiency of remaining six CRISPR/Cas9 constructs that target human SMARCB1 and SMARCA4, and mouse SMARCA4 was reported in this chapter, I was unable to perform any experiments using these constructs in other candidates' cells of origin due to the time constraints.

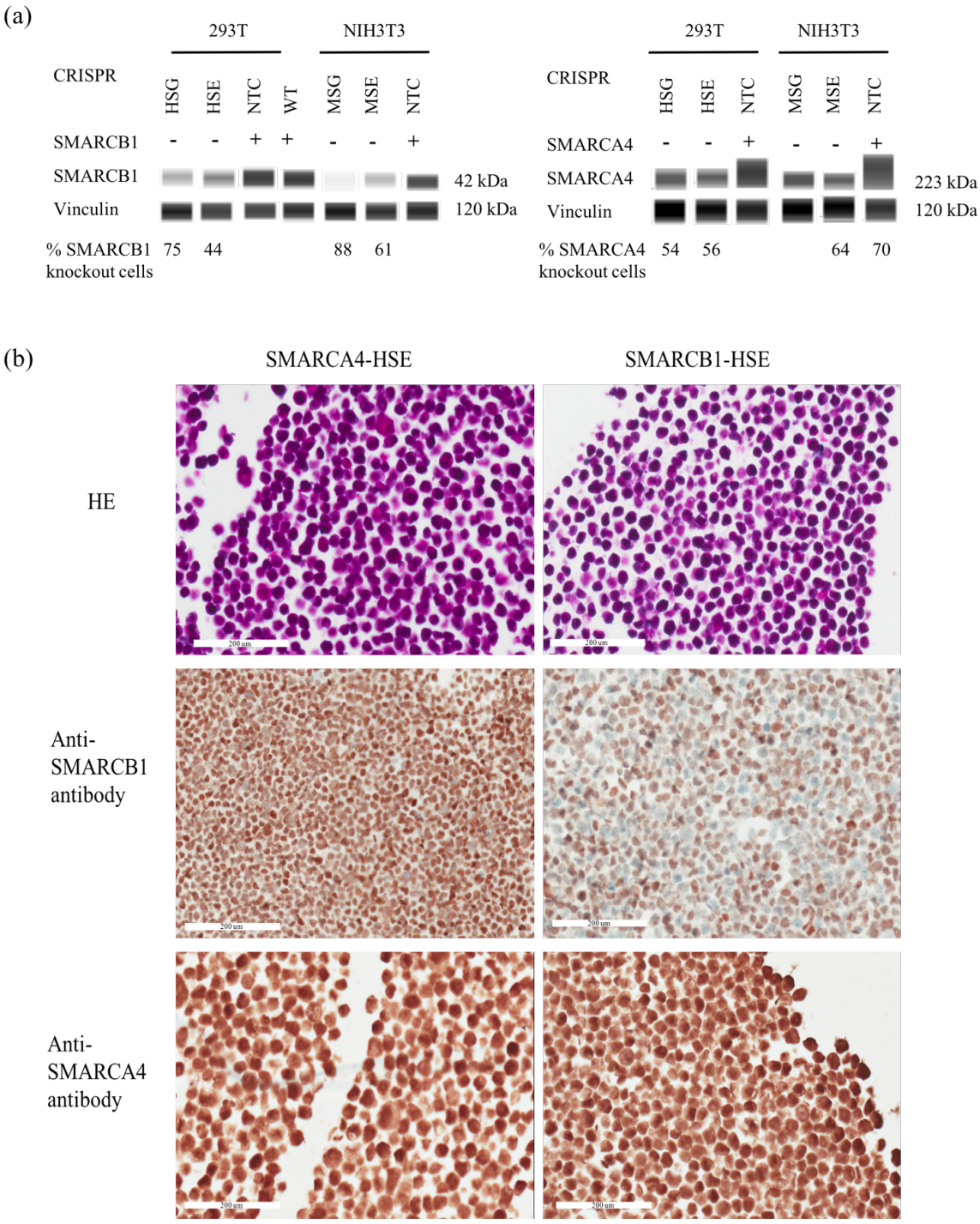

Figure 4.5 ***Validation of SMARCB1 and SMARCA4 protein knockout using CRISPR/Cas9 by western blot and immunohistochemistry****. (a) 0.8 μg of protein lysate was run on WES simple protein western blot for detection of SMARCB1 and SMARCA4 protein. Vinculin antibody serves as loading control. (b) Representative image of immunohistochemistry analysis to further examine the efficiency of CRISPR/Cas9*

knockout system on protein production. Only 293T cells were infected with lentivirus SMARCA4-HSE (MOI 10) and SMARCB1-HSE (MOI 5) were analysed by immunohistochemistry using SMARCB1 (1:100) and SMARCA4 (1:400) antibodies. Knockout using SMARCA4-HSE cells were used as a negative control for SMARCB1 staining whereas SMARCB1-HSE was utilised as a negative control for SMARCA4 staining. The scale bar is 200 μM.

4.3.4 Generation of SMARCB1 knockout in a candidate cell of origin for MRT using CRISPR/Cas9 system

The work in this part of the chapter was performed based on the hypothesis that *SMARCB1* loss in the appropriate cell of origin could provoke genome-wide chromatin remodelling to initiate tumourigenesis and interrupt normal cell differentiation. The aim was to examine whether loss of *SMARCB1* in a putative cell of origin could mimic the phenotype of primary MRT. Previous studies to identify potential cells of origin for MRT (Han et al., 2016, Vitte et al., 2017) and our bioinformatics analysis suggested neural crest (NC) cells as a possible cell of origin for MRT. Therefore, I performed functional studies to create a knockout of *Smarcb1* in this cell population using the CRISPR/Cas9 system. For this project, the NIH3T3 cell line was used as a cell line control and NTC was used as a vector control. Two mouse CRISPRs targeting *Smarcb1* were used and designated as CRISPR SMARCB1 MMG and CRISPR SMARCB1 MME.

4.3.4.1 Validation of CRISPR/Cas9 mediated Smarcb1 knockout in neural crest cells at the protein level

In this study, either exon 1 or 2 of *Smarcb1* was targeted in neural crest (NC) cells using CRISPR/Cas9 (designated CRISPR SMARCB1 MMG and CRISPR SMARCB1 MME respectively) based genome engineering via a lentiviral approach. The NC cells obtained from E8.5 mouse embryos were labelled with Wnt1-Cre; R26R-GFP (Ishii et al., 2012). The cells were obtained from Merck Milipore. The cells exhibited neural crest properties including differentiation capacity, multipotency and expression of neural cell markers. The NC cells were able to differentiate into chondrocyte, osteoblast, smooth muscle cell and glial cells when cultured in specific differentiation media. Furthermore, the cells

exhibited multipotency markers such as CD44, nestin and sca-1 and also showed presence of neural crest markers such as AP-2α, Twist1, and Snail1, as determined by reverse transcriptase polymerase chain reaction (RT-PCR).

For this project, the NC cells were cultured in specialised media supplemented with bFGF, on matrigel and were seeded on a coated plate at a density of 200,000 cells (methods described in Chapter 2, section 2.3.1.2). To determine the appropriate MOI of CRISPR/Cas9 lentivirus, NC cells were infected with lentivirus at MOI 3 and MOI 5. The cell growth was monitored using an EVOS microscope on day 1, 3 and 9 post puromycin selection. Visual inspection revealed a large proportion of dead cells following *Smarcb1* knockout 24 hours post puromycin selection, particularly in CRISPR SMARCB1 MME knocked-out NC cells relative to non-targeting control (NTC) cells (Figure 4.6 and Figure 4.7), however, cell growth was recovered on day 3 and 9. To quantitatively confirm this result, the number of viable cells was counted using the cell images taken using EVOS microscope. The cell images were analysed using Image J analysis software to measure the viable cells. Briefly, the image was converted to 16-bit greyscale and the binary image was analysed using the "analyse particle" programme. The resulting outcome showed the count (number of cells in the image), average size and total area. The bar graph was plotted based on counts for each cell line treated with CRISPR-SMARCB1 or control. Knockout of *Smarcb1* decreased the number of viable cells after 24 hours of puromycin selection. However, the number of cells gradually increased on day 3 and 9. Strikingly, the cell growth was recovered on day 3 for both SMARCB1 MMG and SMARCB1 MME infected cells.

To determine the efficiency of CRISPR *SMARCB1* knockout in NC cells and also to gain an insight that growth recovery was not due to overgrown cells with *Smarcb1* expression, formalin fixed cell blocks were prepared using the cells harvested on day 9. Immunohistochemical staining of sections prepared from these cell blocks allows the assessment of nuclear Smarcb1 protein expression within the NC cell population. The nuclear staining of Smarcb1 in NC cells transfected with CRISPR SMARCB1 MMG and CRISPR SMARCB1 MME at MOI 3 show 92% and 80% of the cells had reduced or negative staining for Smarcb1 expression respectively (Figure 4.9). In contrast, lentivirus transfection at MOI 5 was less efficient for CRISPR SMARCB1 MME where only 40% of cells have lost Smarcb1 expression relative to 81% of cells for CRISPR SMARCB1

MMG. Therefore, MOI 3 was selected for downstream experiments. Notably, Aperio staining failed to detect Smarcb1 expression in 3% of NTC cells and 7% of primary cerebellum tissue section (Figure 4.8).

Importantly, the IHC result of *Smarcb1*-deficient NC cells provides evidence that these cell populations were able to proliferate in the absence of Smarcb1 expression.

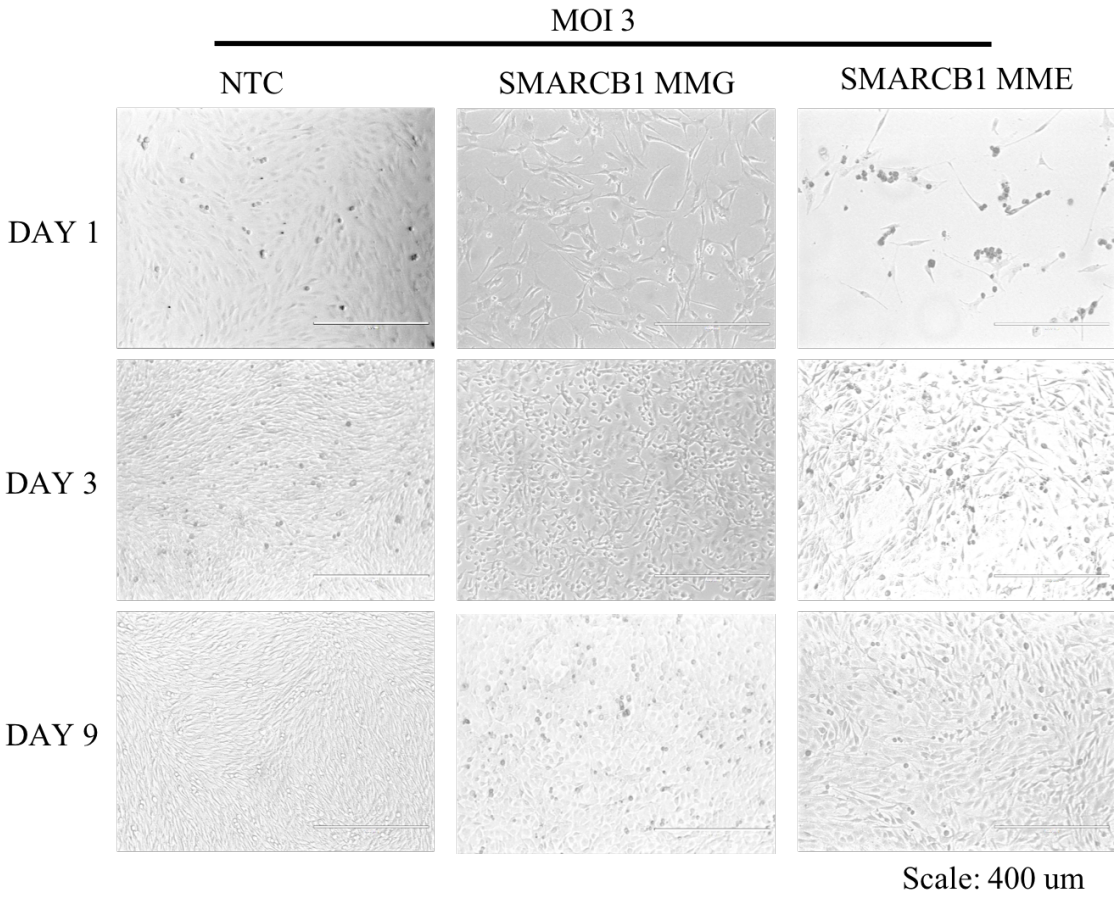

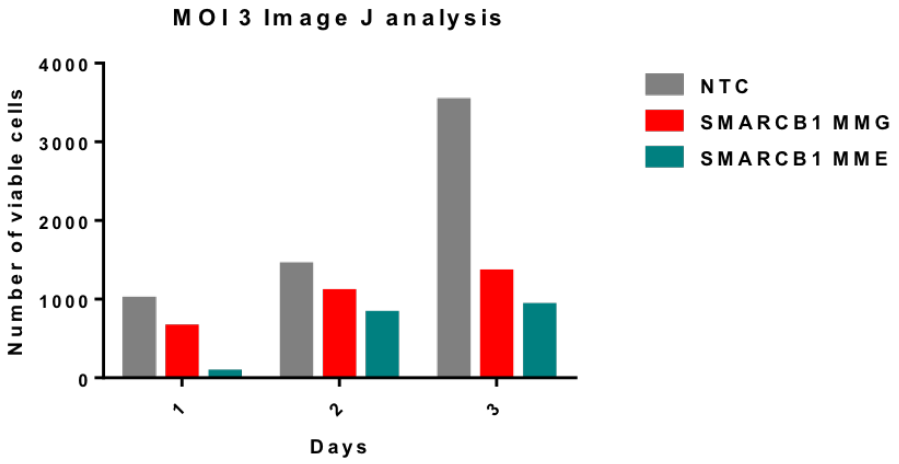

Figure 4.6 ***Optimisation of CRISPR/Cas9 knockout of Smarcb1 in neural crest (NC) cells at MOI 3.*** *The NC cells were seeded at 200,000 cell density in 6 well plate and were infected with concentrated lentivirus CRISPR SMARCB1 MMG and SMARCB1 MME at MOI 3. The images were taken on day 1, 3 and 9 post transfections using an EVOS microscope and the number of viable cells was measured using Image J software. Bar graph showing small number of viable cells counted in CRISPR SMARCB1 MME cells*

using automated cell counter on Image J after 24-hour of puromycin selection (D1 on graph). The growth for SMARCB1 MME and SMARCB1 MMG transfected cells was recovered on the following days.

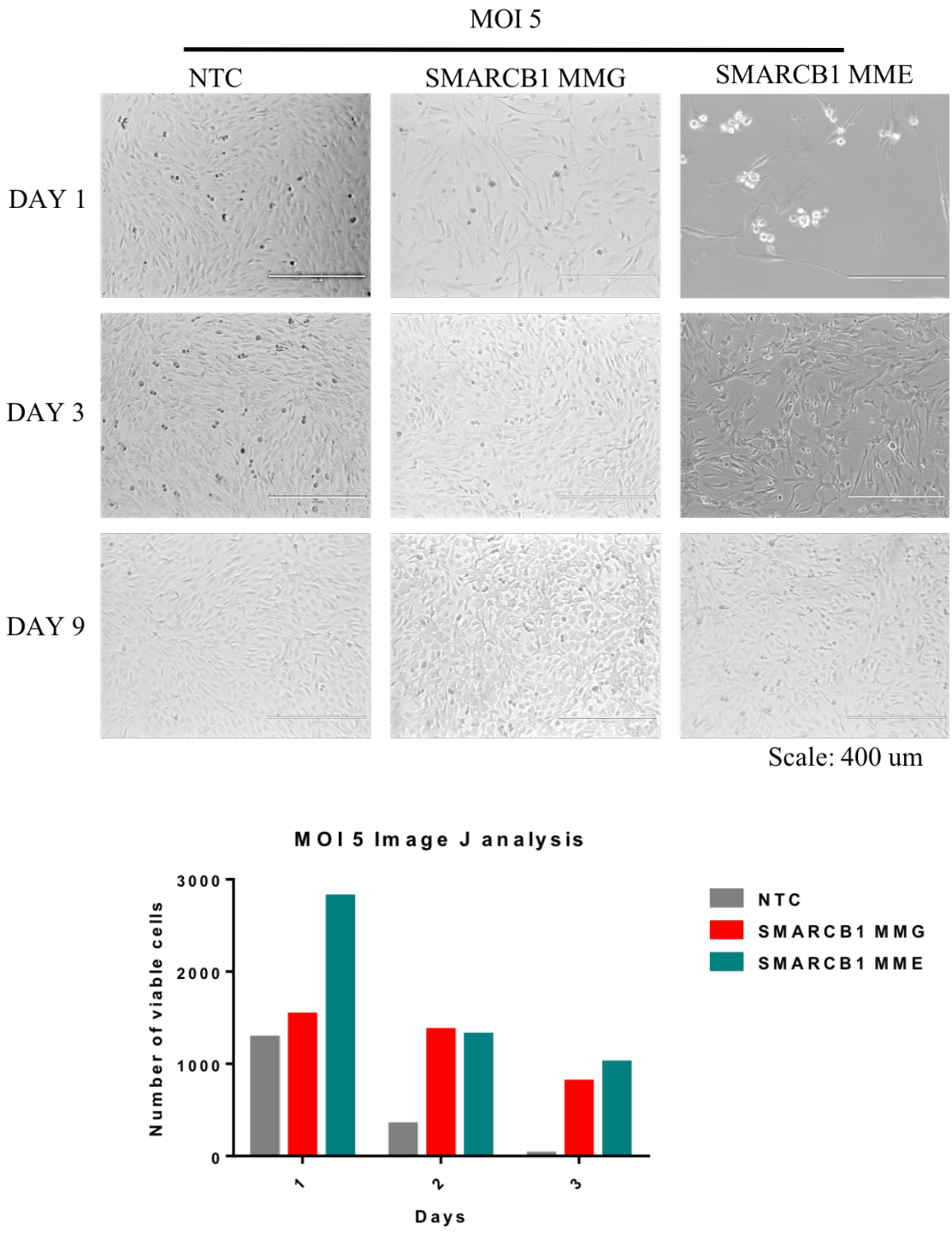

Figure 4.7 ***Optimisation of CRISPR/Cas9 knockout of Smarcb1 in neural crest (NC) cells at MOI 5.*** *The NC cells were seeded at 200,000 cell density in 6 well plate and were infected with concentrated lentivirus CRISPR SMARCB1 MMG and SMARCB1 MME at MOI 5. The images were taken on day 1, 3 and 9 post puromycin selection using EVOS microscope and the number of viable cells was measured using Image J software. Bar graph showing small number of cells counted in CRISPR SMARCB1 MME transfected cells using automated cell counter on Image J after 24-hour of puromycin selection (D1*

on graph). However, the growth for SMARCB1 MME and SMARCB1 MMG transfected cells was recovered on the following days.

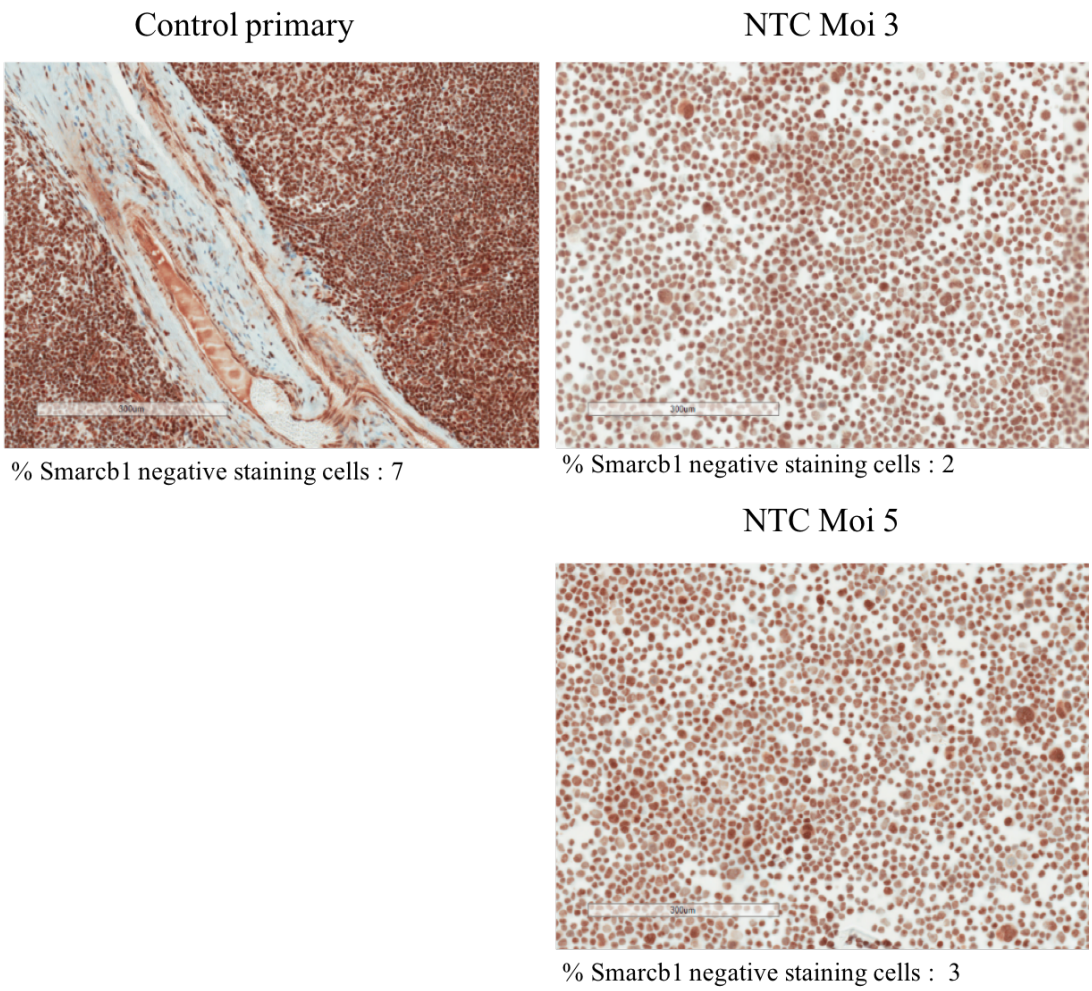

Figure 4.8 ***Immunohistochemical staining of Smarcb1 expression in neural crest (NC) cells and primary tissue****. NC cells used in this analysis were harvested from CRISPR-NTC infected at two different MOIs; MOI 3 and MOI 5. The appropriate MOI to be used in the downstream experiment was selected based on protein knockout efficiency as determined by immunohistochemistry (IHC) analysis. Control primary tissue from cerebellum was included as positive Smarcb1 staining. The percentage of Smarcb1 negative staining cells refers to number of cells in which the Aperio imagescope failed to detect nuclear Smarcb1 staining (algorithm nuclear = 0).*

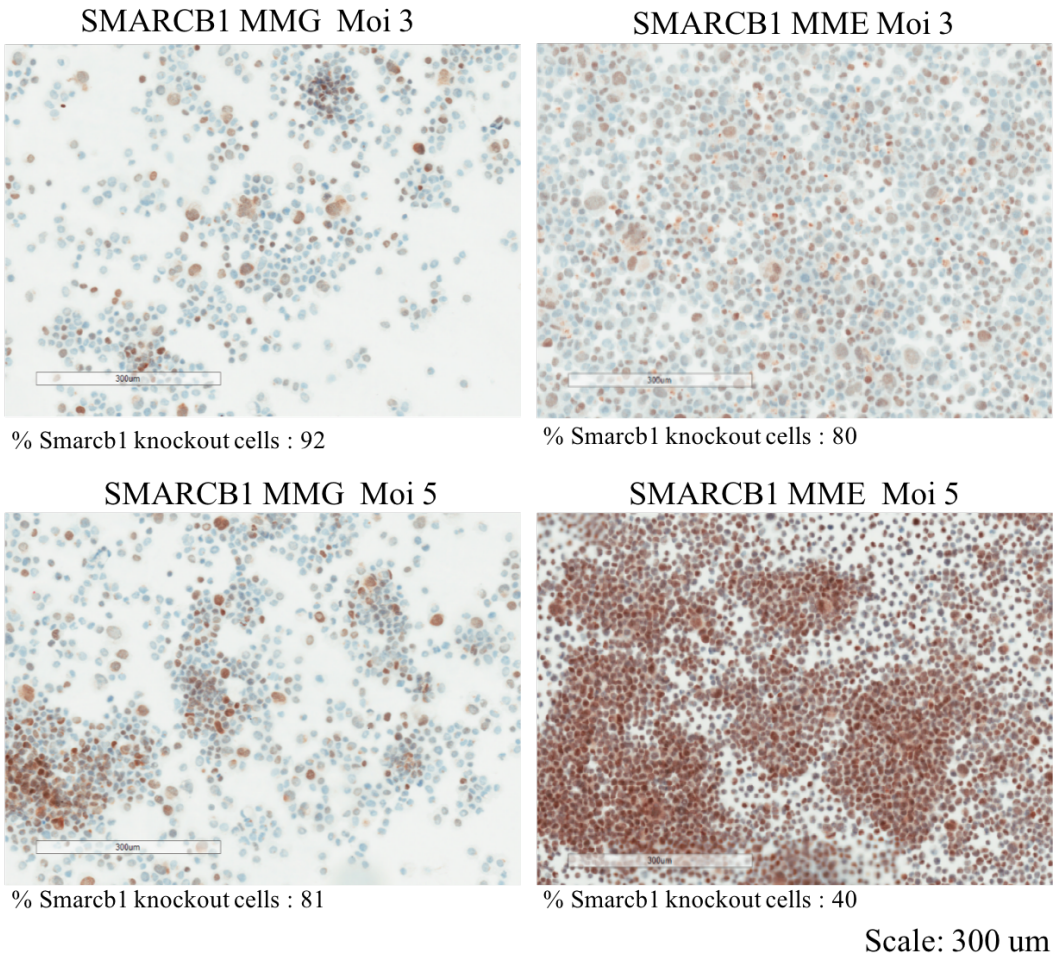

Figure 4.9 ***Immunohistochemical staining of Smarcb1 expression in neural crest (NC) cells and primary tissue****. NC cells used in this analysis were harvested from CRISPR/Cas9 knockout of Smarcb1 at two different MOIs; MOI 3 and MOI 5. The appropriate MOI to be used in the downstream experiment was selected based on protein knockout efficiency as determined by immunohistochemistry (IHC) analysis. Control primary tissue from cerebellum was included as positive Smarcb1 staining.*

4.3.4.2 Selection of the Smarcb1 negative population using CD44 surface marker by FACS sorting

The aim of this study was to establish the characteristics of *Smarcb1*-deficient NC cells. However, IHC analysis of CRISPR SMARCB1 knockout in NC cells demonstrated 50.6% of NC cells were Smarcb1 positive (Figure 4.10a). It was crucial to ensure there

was no masking of effect from *Smarcb1* expressing cells, therefore, we sought to isolate a pure population of *Smarcb1*-deficient cells.

Smarcb1 is a nuclear protein and its expression was knocked out using CRISPR/Cas9 vectors. Thus, it confers a challenge for sampling *Smarcb1* negative cell population. To overcome the problem, I examined the cell surface marker that present in MRT to enrich *Smarcb1* negative cells. In primary MRT, the expression of BAF-SWI/SNF responsive cell surface protein, CD44 was either low or absent (Singhal et al., 2010, Biegel et al., 2002a). Hence, the expression of the Cd44 surface marker protein was exploited to enrich *Smarcb1* negative NC cells by separating the cell population into two groups; Cd44 high (positive *Smarcb1* expression) and Cd44 low (negative *Smarcb1* expression). To achieve this aim, the percentage of Cd44 expression was measured using fluorescence-activated cell sorting (FACS). Briefly, NC cells were transfected with concentrated CRISPR and control (NTC) lentiviruses at MOI 3 and the transfected cells were harvested on day 6, 11 and 13 post-transfections. For sorting, the cells were incubated with CD44-APC-Cy™7 antibody (BD Pharmingen). NC wild-type (WT) cells were used as negative or low Cd44 expression. To enrich the *Cd44* low cell population, the gating strategy was defined as Cd44 high, Cd44 low-high and Cd44 low based on fluorescence intensity of Cd44 protein expression (Figure 4.10b). Analysis of FACS using FlowJo software shows time window for expression of Cd44 cell surface protein expression over time (day 6, 11 and 13) after transfection with the lowest expression recorded on day 13. To examine characteristics of *Smarcb1* negative cells i.e growth, phenotype, etc, *Smarcb1* positive cells (from Cd44 high cell population) were utilised as a control. For comparison between *Smarcb1* negative cells and *Smarcb1* positive cells, cells were sampled based on Cd44 high from Cd44 high gate and Cd44 low from Cd44 high-low and Cd44 low gates. The cut-offs for Cd44 low gating strategy was made as CD44 expression is still present at low percentage in primary MRT (particularly in ECRT) and to maximise sampling of *Smarcb1* negative cells can be obtained from Cd44 low gate.

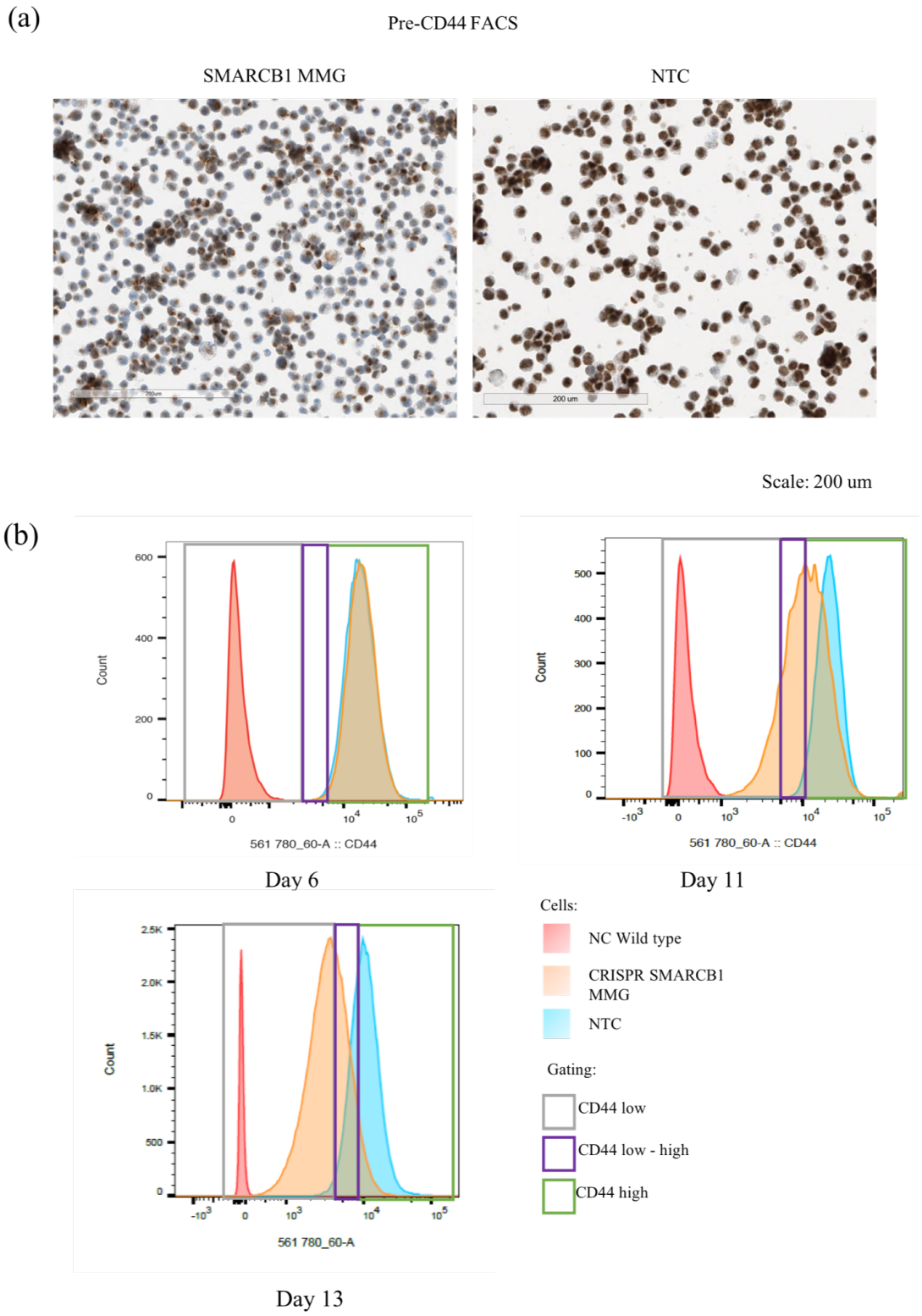

Figure 4.10 ***The optimisation of Cd44 surface marker using FACS for sampling Smarcb1-deficient NC cells.*** *(a) Immunohistochemistry (IHC) showing mixture of Smarcb1 positive and negative cells in NC cells transfected with Smarcb1 (SMARCB1 MMG) CRISPR lentivirus while NTC cells showed total Smarcb1 positive cells. To obtain*

pure Smarcb1-deficient cells, FACS was used to sample cells using Cd44 surface marker. (b) Gating strategy for sorting Cd44 surface marker cells. Three gates were drawn as enrichment strategy to obtain pure Smarcb1-deficient cells, grey denotes Cd44 low, purple denotes Cd44 high-low while green represents Cd44 high. Cells were coloured red for NC wild type, orange for CRISPR targeted cells and blue for NTC. The cells were sorted based on Cd44 high from Cd44 high gate, and Cd44 low from Cd44 low and Cd44 low-high gates. The sorted cells were cultured in 6-well plate for 14 days and were analysed for Smarcb1 and Cd44 expression by IHC.

As I wished to assess the functional relevance of *Smarcb1*-deficient NC cells (Cd44 low) compared to *Smarcb1* positive cells (Cd44 high) in downstream experiments, it was critical to establish that these two cell populations show two distinct *Smarcb1* expressions i.e low/high. To this end, NC cells were transfected with CRISPR SMARCB1 and the cells were sorted based on Cd44 expression on day 13 post-transfection. FACS purified Cd44 low and high were cultured for 14 days and the cells harvested for IHC analysis. Figure 4.11 shows 75% and 77% of NC cells have lost Smarcb1 protein expression obtained from Cd44 low cell populations treated with SMARCB1 MMG and SMARCB1 MME respectively, in comparison to 13% and 13.2% of cells cultured from SMARCB1 MMG and SMARCB1 MME CD44 high respectively. Cells from NTC were included as a positive control of Smarcb1 and Cd44 expression. A totally "pure" population of *Smarcb1* negative cells from Cd44 low gate was unobtainable as a small proportion of cells (~25%) still showed positive nuclear Smarcb1 staining. However, Cd44 high population could still be a useful comparison in the downstream experiment as the two populations showed a 5-fold difference in Smarcb1 protein expression. IHC analysis of Cd44 cytoplasmic staining validated FACS analysis in which Cd44 low demonstrated a low percentage of cells with CD44 staining while Cd44 high showed high proportion of cells with CD44 staining (Figure 4.12). In summary, sorting against the Cd44 surface marker was able to increase the proportion of *Smarcb1* negative cells. More importantly, this experiment indicates that the *Smarcb1* knocked out cells were able to proliferate for 13 days prior sorting and the proliferation persists for a further of 14 days following Cd44 cell sorting (Figure 4.11).

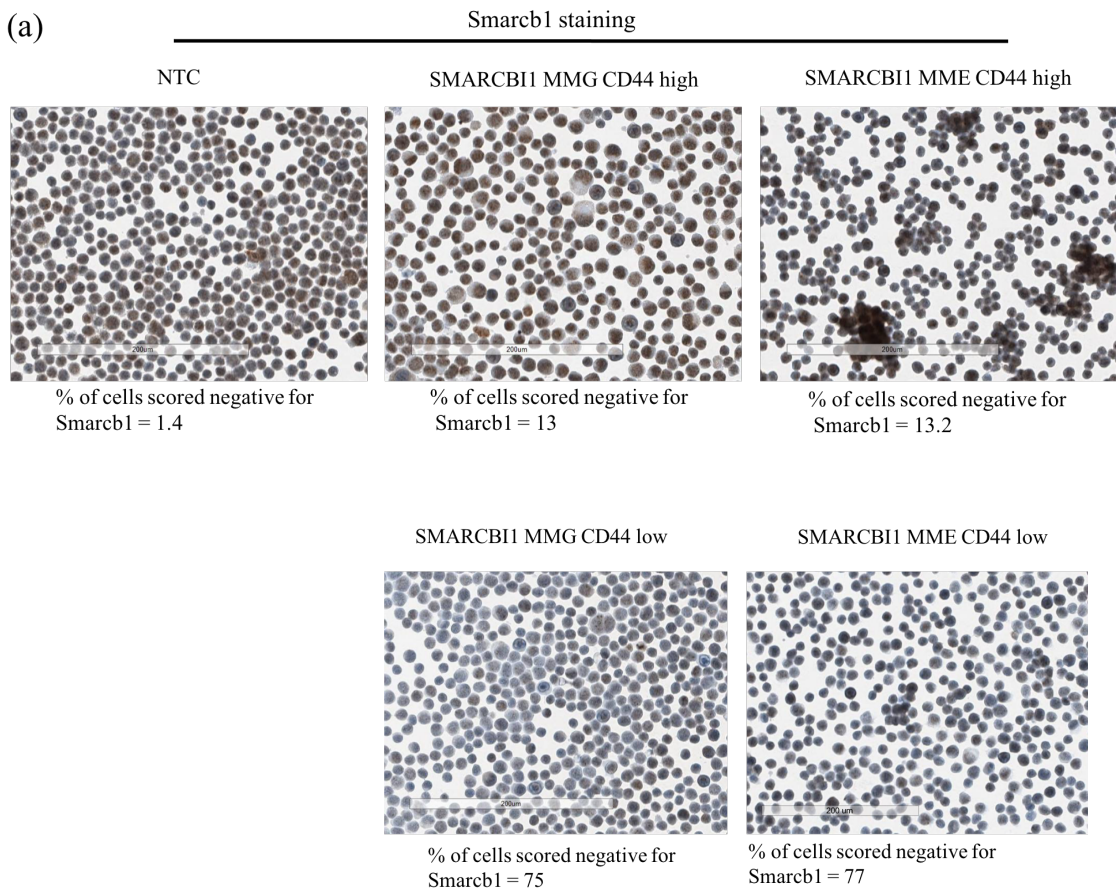

Figure 4.11 ***Immunohistochemical staining for Smarcb1 expression in NC cells to establish positive and negative Smarcb1 cell population from Cd44 surface sorting****. FACS sorted cells were evaluated for by IHC. Pure Smarcb1-deficient cells from Cd44 low sorted cells could not be achieved as a small proportion of cells showed Smarcb1 positive staining. However, there is a marked difference in percentage of positive Smarcb1 cells between Cd44 low and high. Notably, Aperio Imagescope failed to detect nuclear Smarcb1 staining (algorithm nuclear = 0) in 1.4% of NTC cells.*

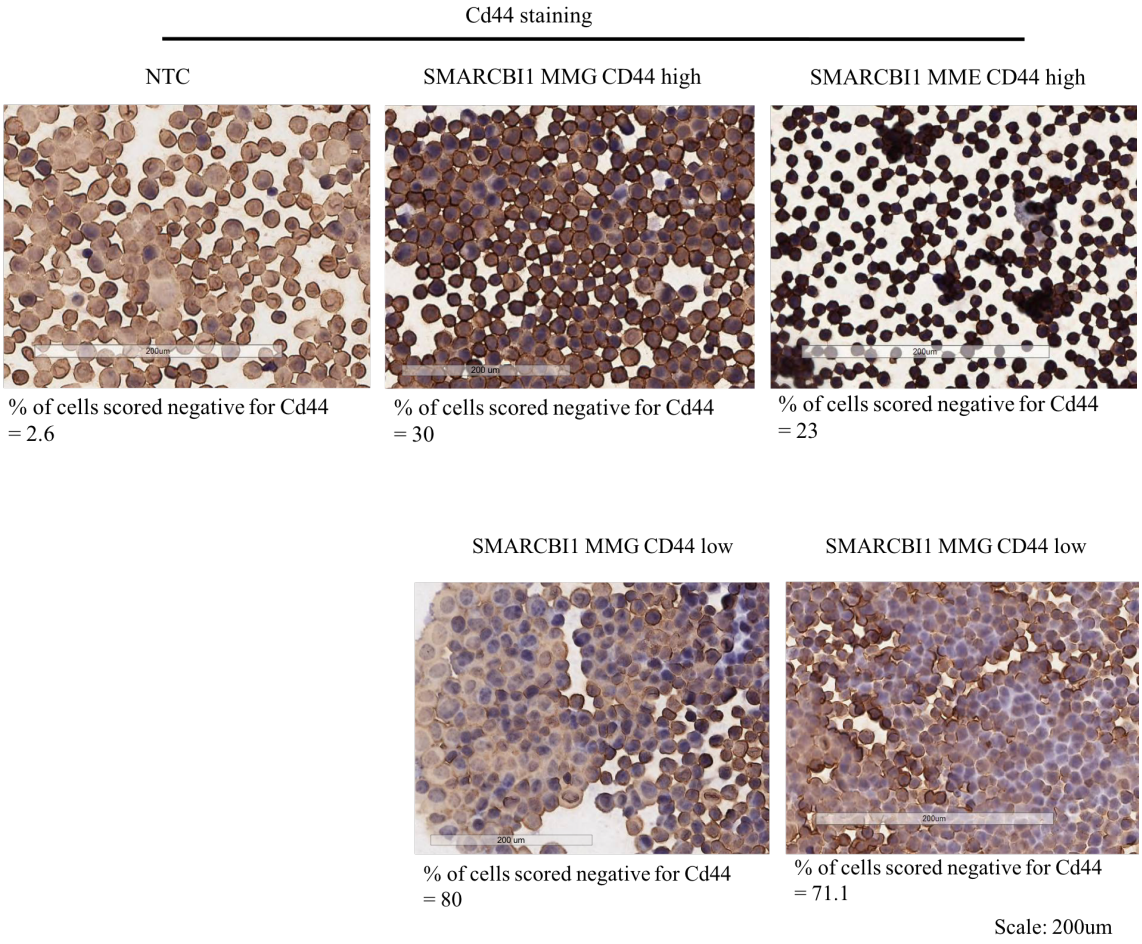

Figure 4.12 ***Immunohistochemical staining for Cd44 expression in NC cells to establish positive and negative Smarcb1 cell population from Cd44 surface sorting****. FACS sorted cells were evaluated for Cd44 cytoplasmic protein expression by IHC. Loss of Cd44 cytoplasmic cells was shown by red arrow. Expression of Cd44 protein was low in Cd44 low and high in Cd44 high, validating FACS analysis. Notably, Aperio Imagescope failed to detect cytoplasmic Cd44 staining (algorithm nuclear = 0) in 2% of NTC cells.*

4.3.4.3 Cell proliferation is sustained in Smarcb1-deficient NC cells

SMARCB1 is ubiquitously expressed in non-cancerous cells and mutation of this gene is not well tolerated in most cell types, consequently, *Smarcb1* loss in mice leads to early embryonic lethality (Roberts et al., 2000, Klochendler-Yeivin et al., 2000, Guidi et al., 2001). To test the hypothesis that loss of *Smarcb1* in neural crest cells leads to MRT tumourigenesis, it was necessary to determine if the NC cells could retain proliferative

capacity without functional *Smarcb1*. The cell growth of transfected cells was monitored pre- and post- Cd44 sorting. The cell density pre-Cd44 sorting was measured using trypan blue whereas post-CD44 sorting was measured using INCUCYTE live imaging microscope.

Prior to Cd44 sorting, 200,000 NC cells were transfected with lentiviral CRISPR targeting *Smarcb1* (SMARCB1 MMG and SMARCB1 MME) and NTC. The number of viable cells was counted on day 2, 4, 7, 9 and 13 post-infection. Although only a small number of viable cells were recorded 48 hours post-transfection, the number was expanded to 2–3 x 10^6 cells by day 13 (Figure 4.13a). Notably, there is no significant difference in number of viable cells measured between *Smarcb1* -deficient cells and NTC. By contrast, *Smarcb1* knockout in NIH3T3 led to cell death as the number of viable cells declined from day 4 onwards. WES analysis on nuclear-extracted samples confirmed the loss of functional Smarcb1 protein expression in NIH3T3 and NC cells (Figure 4.13b).

In short, increased number of viable *Smarcb1*-deficient cells demonstrated that these cells were able to proliferate without functional *Smarcb1*. Furthermore, it indicates that mutation of *Smarcb1* in NC cells does not impede cell survival. More importantly, this experiment established that the effect of *Smarcb1* loss is context dependent as demonstrated by NIH3T3 cells which showed a marked decrease in cell growth and proliferation.

(a)

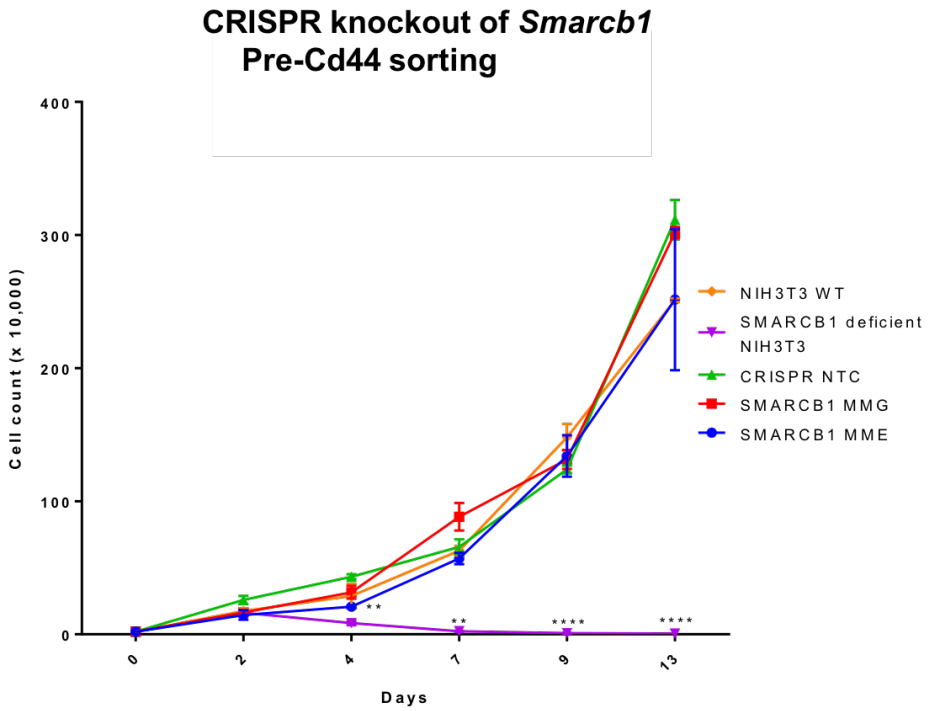

(b)

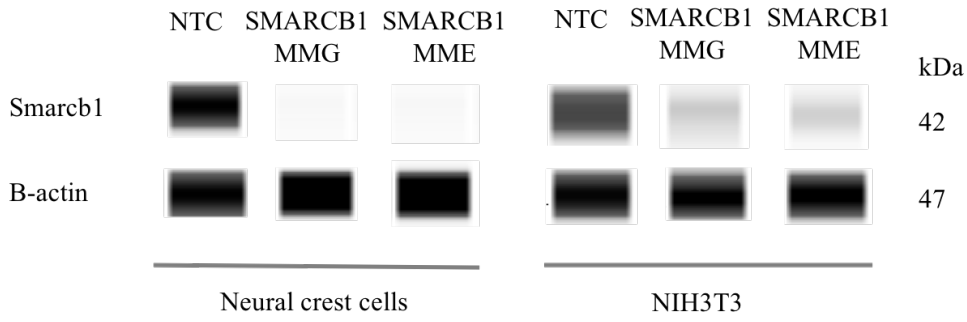

Figure 4.13 ***Smarcb1-deficient NC cells retained proliferative capacity. Loss of Smarcb1 in NTC demonstrated an increase in cell viability over time****. In contrast, loss of Smarcb1 in NIH3T3 has a major impact on the growth rate as cell viability was decreased four days after transfection suggesting this cell type does not tolerate Smarcb1 loss. The results are shown as mean ± SEM of two independent experiments and the significance was determined by unpaired Student's t-test (**p< 0.005 and ****p< 0.0001 vs control of appropriate culture). (b) Automated western blot (WES) analysis of total protein extracted from CRISPR Smarcb1 knockout NC cells confirmed Smarcb1 knockdown in these cells. Smarcb1 knockdown by CRISPR/Cas9 resulted in Smarcb1 protein loss in NC cells and NIH3T3. Beta-actin serves as loading control.*

To gain a better understanding of the growth characteristics of *Smarcb1*-deficient NC cells, I then compared two sorted populations Cd44 low and Cd44 high as these cells exhibited a remarkable difference, more than 50% of cells have lost Smarcb1 expression as shown in Figure 4.11. The cells were sorted on day 13 post-transfection according to Cd44 expression and were cultured for three further passages. The cell growth was monitored using INCUCYTE ZOOM live imaging microscope. Data from INCUCYTE was recorded based on percentage cell confluency and the reading was analysed relative to day 0 of each CRISPR construct i.e. NTC. During passage 1, the cell number of Cd44 high was higher than that of Cd44 low for individual CRISPR (Figure 4.14b). However, Cd44 low cells grew faster than Cd44 high cells in passage 2 for SMARCB1-MME construct as illustrated by percentage of cell confluency in culture (Figure 4.14b). Nevertheless, this was not statistically significant. The increase in proliferation rate was also seen in SMARCB1 MMG Cd44 low and Cd44 high, however, the difference in proliferation rate between these two cell populations was only observed after day 3 (Figure 4.14b). However, during the third passage, SMARCB1 MMG Cd44 low has gained more proliferative capacity than Cd44 high as Cd44 low cells reached approximately 14% cell confluency compared to 7% cell confluency seen in Cd44 high by day 4 (Figure 4.14c). Strikingly, in passage 3, NTC cells showed a decline in proliferation capacity as illustrated by decreased in cell confluency on day 4, compared to SMARCB1 MME CD44 high and low; and SMARCB1 MMG CD44 low (Figure 4.14c). The resulting confluency data indicates *Smarcb1*-deficient cells maintained the cell proliferation and tolerated *Smarcb1* loss.

In short, *Smarcb1* knocked out in NC cells maintained the cell proliferation as seen in all Smarcb1-deficient cell populations. To further understand the role of *Smarcb1*, its effect on cell cycle and self-renewal were assessed in NC Smarcb1 knockout cells.

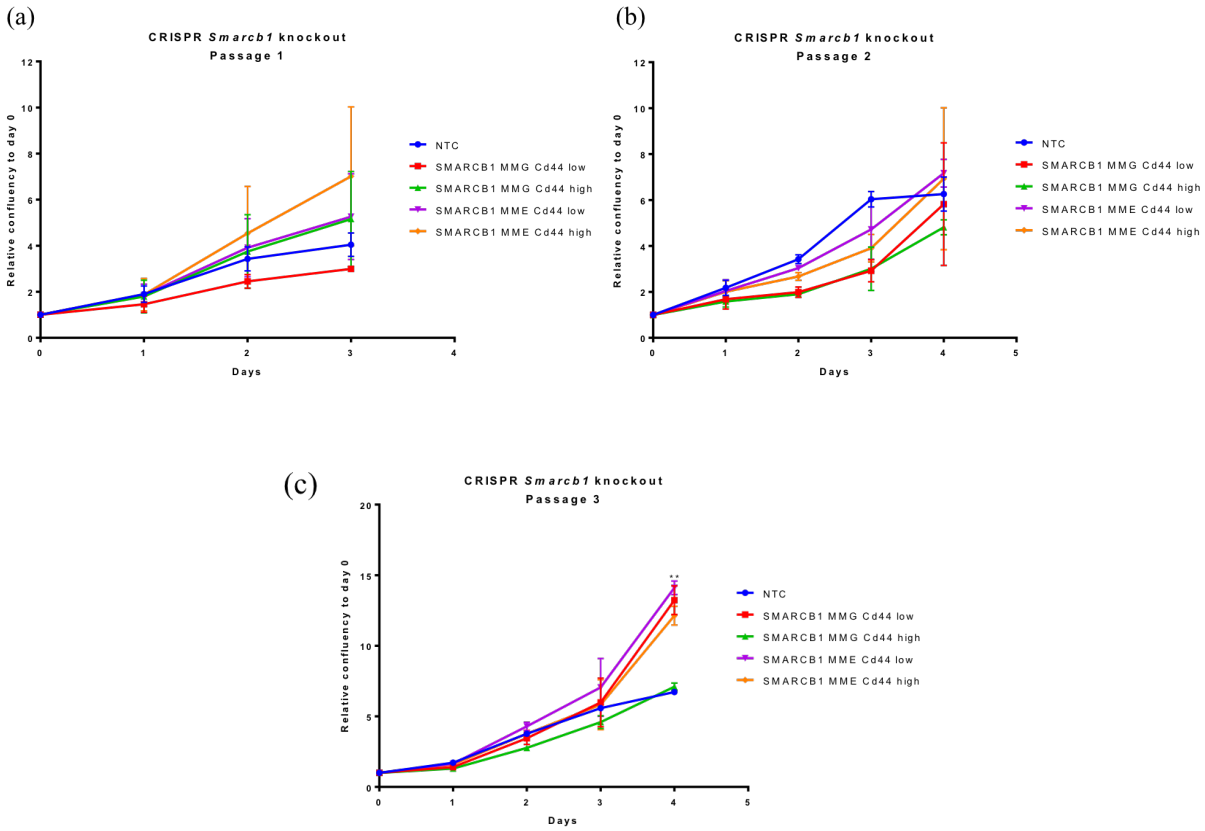

Figure 4.14 ***Time course study of effect of Smarcb1 loss on cell confluency. (a) Cell confluency was measured using INCUCYTE live imaging microscope for three passages.*** *The confluency curves showing Smarcb1-deficient cells maintained cell growth as indicated by cell confluency. (a) Smarcb1 knockout in NC cells increased the proliferation rate as the percentage of cell confluency was higher than that of NTC, with the exception of SMARCB1 MMG Cd44 low. (b) Similar to Passage 1, SMARCB1 Cd44 low cells from CRISPR SMARCB1 MME construct gained proliferative capacity as the percentage of cell confluency was higher than their counterpart in passage 2. Notably, NTC also regained the proliferation rate. (3) The Smarcb1-deficient cells in passage 3 continued to increase the proliferation rate relative to NTC after day 3 in culture. A significant increase in the percentage of cell confluency was seen on day 4 in SMARCB1 MME Cd44 low relative to NTC. There was no statistical different between Cd44 low vs Cd44 high and Smarcb1-deficient NC cells vs NTC. The results are shown as mean ± SEM of two independent experiments and the significance was determined by unpaired Student's t-test (*p< 0.05, **p< 0.005 vs NTC).*

4.3.4.4 Smarcb1 inactivation in neural crest cells dysregulates molecules involved in cell cycle progression and demonstrates the opposite transcriptional effect to that of SMARCB1 re-expression in MRT cells

Smarcb1-deficient NC cells were still able to maintain the proliferation capacity after 26 days of transfection This result suggests a growth suppressive role for *SMARCB1* and supports a causative role of *SMARCB1* loss in MRT tumourigenesis. To elucidate the mechanism by which *Smarcb1* loss in NC drives cellular growth, the effect of *Smarcb1* loss was studied (Figure 4.14) on cell cycle-related genes by qPCR. The cell pellets were harvested from the *Smarcb1*-deficient NC- and NTC cells after day 7 of Cd44 expression sorting. qPCR analysis revealed a significant increase in the expression of genes coding for proteins promoting G1/S phase transition including *Ccnd1*, *Ccnd3, Ccne1, Cdk4* and *Cdk6*. Of note, expression of *Ccnd2* and *Cdk4* is higher in *Smarcb1*-deficient NC cells compared to expression in MRT primary and cell lines which expressed lower *CCND1* and *CDK6*. By contrast, the expression of G1-phase inhibitors such as *p16* and *p21* was downregulated (Figure 4.16) and this mimics the expression level in MRT primary and cell lines. Notably, there were no marked differences in the expression of cell cycle-related genes between Cd44 high and Cd44 low cell populations.

Previous studies have shown reintroduction of *SMARCB1* leads to cell cycle arrest (Betz et al., 2002, Kuwahara et al., 2010). Therefore, in this study, a similar approach was utilised to determine how *Smarcb1* loss drives proliferation in the NC cells. Briefly, MRT cells were transfected with SMARCB1 WT lentivirus containing pCDH-EF1-PURO-SMARCB1 plasmid or PCDH lentivirus carrying pCDH-CMV-MCS-EF1-Puro plasmid. MRT cells were harvested 5 days after puromycin selection and RNA was extracted using the protocol described in 2.3.3.1. Restoration of *SMARCB1* in MRT cells caused downregulation of cell cycle promoting genes such as *CCND1, CCND2, CDK4* and *CDK6* accompanied by decreased expression of *p21* and *p16* (Figure 4.17). By contrast, the transcriptional effects of these genes in *Smarcb1*-deficient NC cells were the reverse. This indicates that *Smarcb1* expression exerts regulation on the cell cycle machinery and its loss increases the proliferative capacity in NC cells. Up to this point, assessment of cell proliferation in Figure 4.13 and the qPCR analysis of cell cycle-related genes did not demonstrate significant differences in transcriptional expression between Cd44 low and Cd44 high of *Smarcb1* -deficient cell populations although more than 50% of cells have

lost SMARCB1 expression as shown in Figure 4.11. Therefore, I sought to examine another mechanism that could provide explanation for similar growth characteristic and transcriptional expression seen in CRISPR SMARCB1 MMG Cd44 high and Cd44 low cell populations.

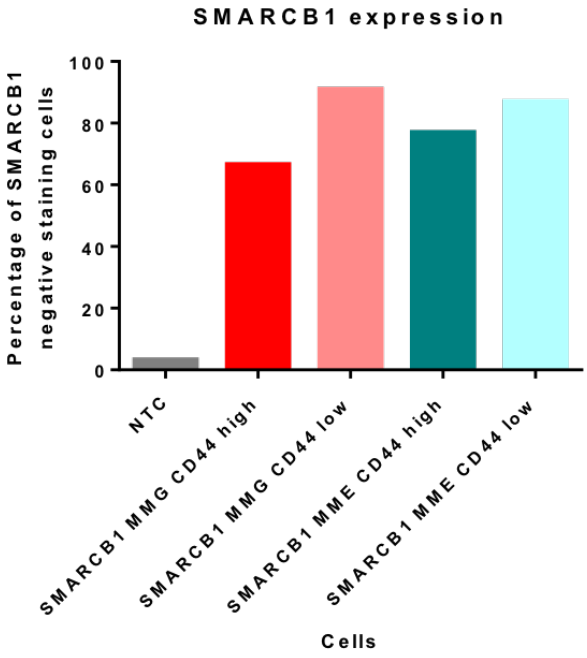

Figure 4.15 ***Percentage of NC cells that have lost Smarcb1 expression measured on day 11 post CD44 sorting by immunohistochemistry analysis (see section 4.2.2).*** *These cells were harvested on day 7 post CD44 sorting for gene expression analysis of cell cycle related genes.*

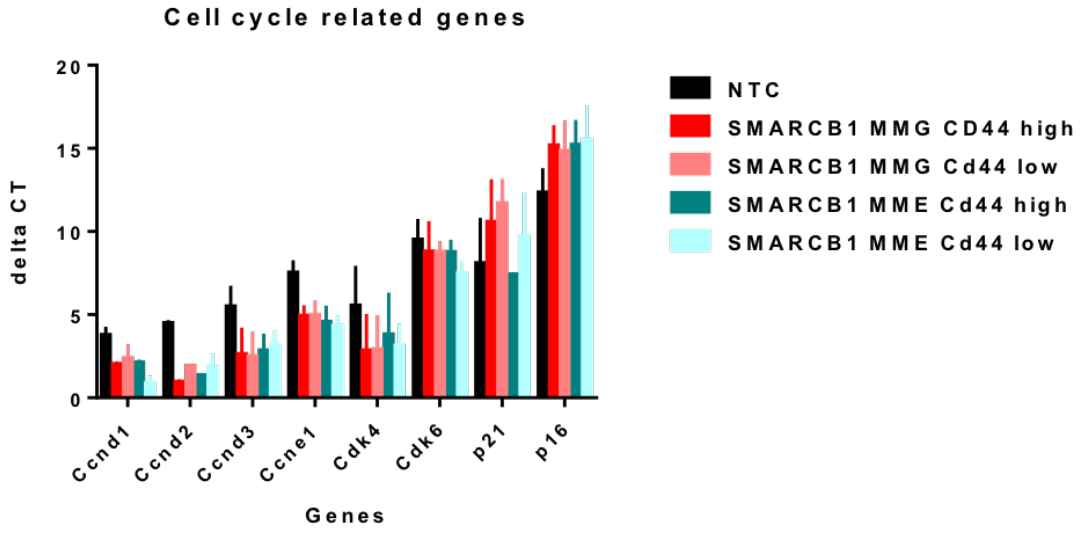

Figure 4.16 ***Smarcb1 loss in neural crest (NC) cells caused deregulation of the expression of cell cycle related genes.*** *Expression analysis of Smarcb1-deficient NC cells demonstrates downregulation of cell cycle inhibitor genes accompanied by upregulation of cell cycle promoting genes, supporting the effect of Smarcb1 loss on cell proliferation of NC cells. Inactivation of Smarcb1 caused upregulation of cell cycle promoting genes including Ccnd1, Ccnd2, Ccnd3, Ccne1, Ccne2, Cdk4 and Cdk6 concomitantly with decreased in expression of two protein inhibitors; p21 and p16. mRNA expression of each genes was normalised to Gapdh. The results are shown as mean ± SEM of two independent experiments.*

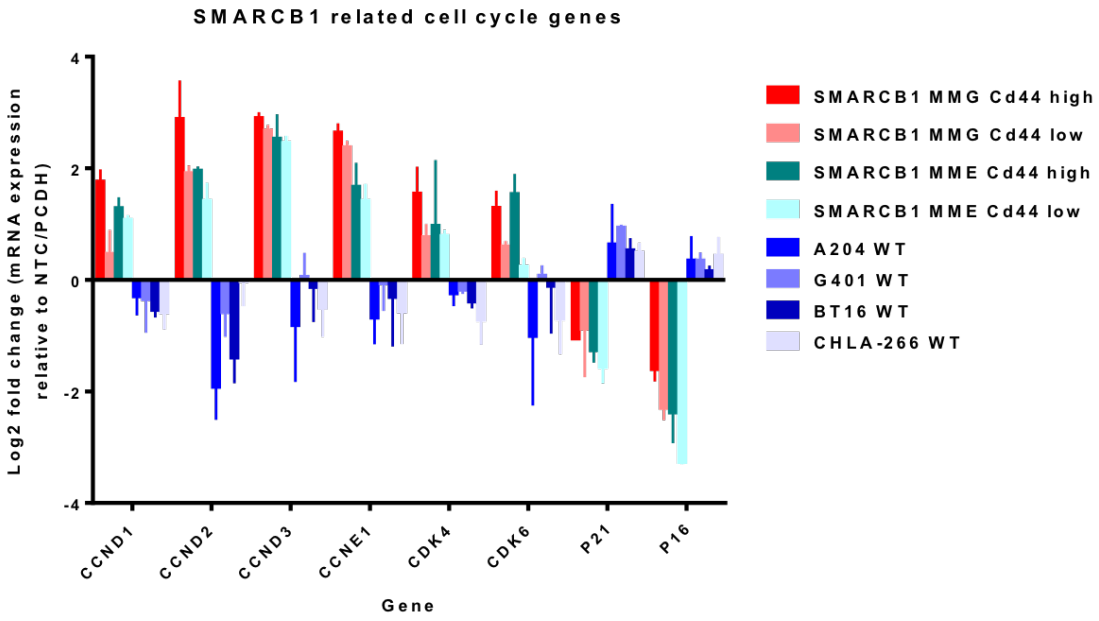

Figure 4.17 ***SMARCB1 re-expression in MRT cells shows the opposite transcriptional effect to that of Smarcb1 loss in NC cells****. RNA was extracted from MRT cells with and without SMARCB1 expression. The mRNA expression of each gene was normalised against GAPDH of MRT cells without SMARCB1. The expression of genes in Smarcb1-deficient NC cells was included for comparison purpose and the mRNA expression was normalised to Gapdh and the expression was presented as relative to control (NTC NC cells for CRISPR and Smarcb1-deficient MRT cells for MRT cells). The bar graph showed SMARCB1 inactivation in human MRT cells caused downregulation of cell cycle promoting genes (CCND1, CCND2, CDK4 and CDK6) along with upregulation of cell cycle inhibitors (p21 and p16). The results are shown as mean ± SEM of two independent experiments.*

4.3.4.5 Mutation of Smarcb1 in neural crest cells causes dysregulation of self-renewal machinery

Primary MRT have a high proliferative rate and *Smarcb1* knockout using CRISPR/Cas9 maintained the proliferation rate of NC cells, the postulated candidate cell of origin. I next examined if *Smarcb1* loss in NC cells impacted self-renewal using a tumoursphere assay. Post Cd44 sorting *Smarcb1*-deficient NC cells were harvested on day 4 and the cells were washed twice with PBS and cultured at a density of 10,000 cells in

tumoursphere media made up of 2% B27 supplement, 20 ng/ml EGF (Peprotech), 30 ng/ml bFGF (Peprotech), 2U/ml heparin (Sigma Aldrich), 0.5 µg/ml hydrocortisone (Sigma Aldrich), 1% sodium pyruvate (Thermo Fisher Scientific), 1% penicillin/streptomycin and 1% non-essential amino acid (Thermo Fisher Scientific) in DMEM/F12 media. The cells were allowed to form spheres for 12 days. Loss of *Smarcb1* in NC cells increased the number of primary tumourspheres as opposed to NTC (Mean ± SEM, 4 ± 1, n=2 technical replicates) (Table 4.1). In short, tumorsphere forming efficiency was not statistically different between Cd44 high and low cell populations although the trend of increase can be observed for Cd44 high cells in two tumoursphere cultures (Figure 4.18).

To further examine the sphere forming efficiency, the secondary tumoursphere cultures derived from primary tumourspheres were established. Briefly, the primary tumourspheres were dissociated into single cells and re-plated in tumoursphere medium at 10,000 cell density and the cells grown in these culture conditions for 12 days. Figure 4.18 shows that *Smarcb1* knockout in NC cells resulted in increased self-renewal potential as illustrated by an increase in the number of secondary tumoursphere when compared to NTC. SMARCB1 MMG Cd44 low cells produced 12.5 tumourspheres while SMARCB1 MMG Cd44 high cells produced 16.5 tumourspheres (n= 2 technical replicates) (Table 4.1). By contrast, seven tumourspheres were counted in NTC culture. The increase in the number of tumoursphere was also seen in SMARCB1 MME Cd44 low and SMARCB1 MME Cd44 high measuring for 11 and 15 respectively. A significant increase of secondary tumoursphere formation was seen in SMARCB1 MMG Cd44 high cell populations only. In line with the formation of primary tumourspheres, the Cd44 high cell population generated more tumourspheres than the Cd44 low cell population, but the data was not significant. CD44 expression has been widely used as cancer stem cell (CSC) marker (Bahena-Ocampo et al., 2016). Thus, selecting for loss of Cd44 expression may be a confounding factor influencing self-renewal mechanisms.

In short, culturing *Smarcb1*-deficient NC cells as tumourspheres demonstrates the capacity of these cells to self-renew as illustrated by an increase in the number of tumourspheres. Intriguingly, the *Smarcb1*-deficient NC cells display increased self-renewal potential as the number of secondary tumourspheres were higher than previously described in primary tumoursphere. More importantly, the proportion of self-renewing

cells within the Cd44 low and Cd44 populations varied, as Cd44 high cell population consistently demonstrated more tumoursphere than Cd44 low, in both primary and secondary tumoursphere assay, although the data were not statistically different.

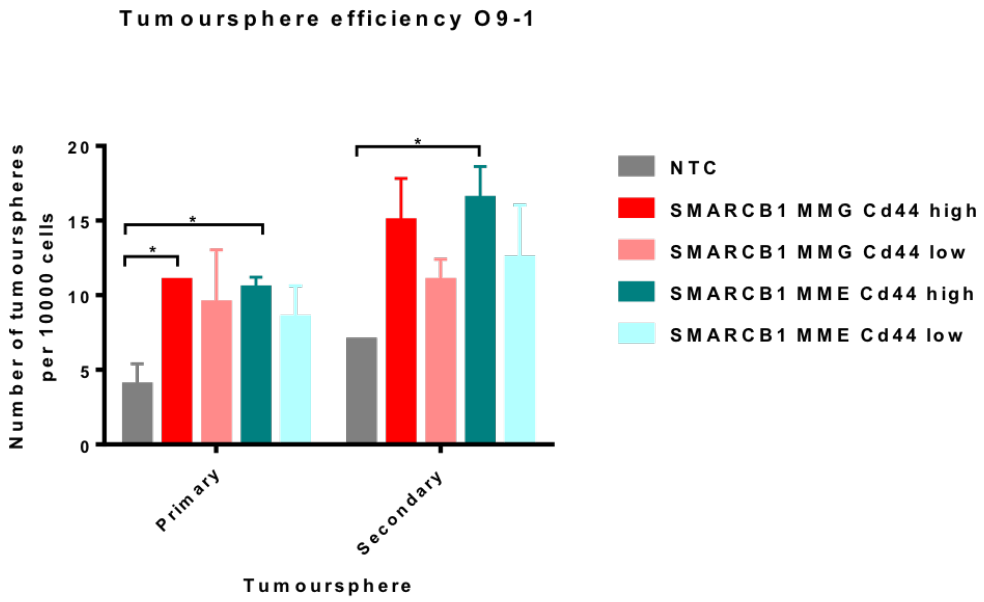

Figure 4.18 ***Smarcb1 loss in NC cells caused dysregulation of self-renewal machinery.*** *To assess the self-renewal potential of these cells, tumoursphere assay was implemented as a self-renewal readout for Smarcb1-deficient cells. Primary tumourspheres were formed from single cells of adherent NC cells (at 10,000 cell density) when cultured in tumoursphere media for 12 days. To further assess self-renewal capacity, the primary tumoursphere was dissociated into single cells and re-plated at 10,000 for formation of secondary tumoursphere. The number of tumourspheres was counted on day 12. Self-renewal capacity of Smarcb1-deficient cells was increased over two serial passage tumoursphere assays, with notable differences in the proportion of self-renewing cells between Cd44 high and Cd44 low. The results are shown as means ± SEM of two independent experiments and the significance was determined by unpaired student's t-test (* $p<0.05$ vs NTC).*

	Primary tumourspheres			Secondary tumourspheres		
	NTC (mean ± SEM)	CRISPR (mean ± SEM)	P-value	NTC (mean ± SEM)	CRISPR (mean ± SEM)	P-value
SMARCB1 MMG CD44 low	10.5 ± 2.50	8.5 ± 1.5, n=2	0.1299	7 ± 1, n=2	12.5 ± 2.5, n=2	0.1588
SMARCB1 MMG CD44 high	10.5 ± 2.50	10.5 ± 0.5, n=2	0.0283	7 ± 1, n=2	16.5 ± 1.5, n=2	0.024
SMARCB1 MME CD44 low	10.5 ± 2.50	9.5 ± 2.5, n=2	0.1778	7 ± 1, n=2	11 ± 1, n=2	0.0572
SMARCB1 MME CD44 high	10.5 ± 2.50	11 ± 0, n=2	0.0198	7 ± 1, n=2	15 ± 2, n=2	0.0572

Table 4.1 ***Effect of Smarcb1 knockout on formation of tumourspheres****. Results are shown as Mean ± SEM and the significance of the results was determined by unpaired student's t-test.*

To gain further insight into the effect of *Smarcb1* loss on self-renewal mechanism and how two cell populations; Cd44 high and Cd44 low showed differences in self-renewal potential, evaluation of the expression of genes involved in self-renewal pathways was carried out using qPCR analysis. The self-renewal genes used in this analysis were selected based on the evidence from published expression profiles of primary MRT (Johann et al., 2016, Deisch et al., 2011, Venneti et al., 2011b) and also *SMARCB1* re-expression cell model (PBTG).

This analysis demonstrated that loss of functional *Smarcb1* in NC cells caused upregulation of the expression of self-renewal genes such as *Sox2, Klf4, Oct4, Bmi1, Gli2* and *Jarid2* by approximately 1.1 to 7 -fold change (Figure 4.19). A small decrease of 0.8-fold in the expression of *Klf4* in CRISPR SMARCB1 MMG Cd44 low was also seen. Although gene expression of self-renewal related genes was broadly similar between Cd44 high and Cd44 low cell populations, a few genes are more highly upregulated in Cd44 high than Cd44 low thus possibly supporting the observation of a higher number of tumourspheres in Cd44 high than Cd44 low cell populations. For instance, expression of *Ezh2* and *Sox2* which have clear roles in self-renewal and pluripotency was significantly higher in Cd44 high cells.

Overall, an increase in expression of self-renewal related genes such as *Sox2, Klf4, Oct4, Bni1, Gli2* and *Jarid2* in *Smarcb1*-deficient NC cells mimics the enrichment of these genes in our expression-profiling of primary MRT (PBTG). In summary, knockout of *Smarcb1* using a CRISPR/Cas9 system in NC cells is associated with an increase in the number of tumourspheres and expression of self-renewal related genes.

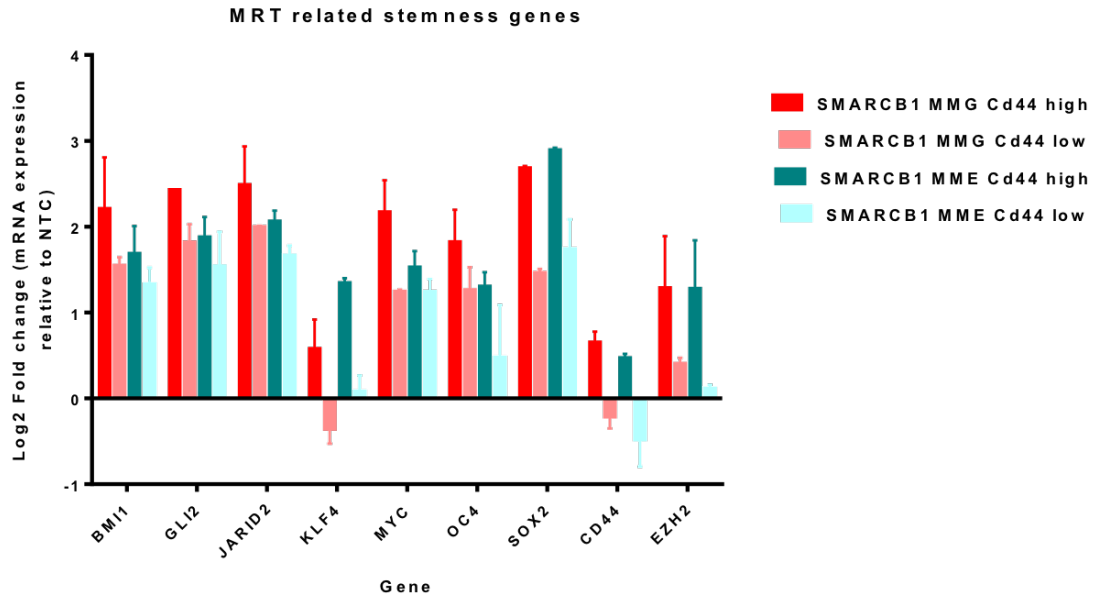

Figure 4.19 ***Increase in the number of tumourspheres is associated with increased expression of self-renewal genes demonstrated by qPCR analysis****. RNA was extracted from NC cells infected with NTC and two different CRISPR constructs targeting Smarcb1 expression in cells. mRNA expression was normalized against Gapdh of NTC NC cells. The expression of self-renewal genes in all Smarcb1 cell populations (CD44 high/low) is largely comparable with the exception of Sox2, Ezh2 and Cd44 which were highly expressed in Cd44 high for both CRISPR construct. The results are shown as means ± SEM of two individual experiments.*

4.3.4.6 Defective cytoskeleton organisation in Smarcb1-deficient NC cells

Knockout of *Smarcb1* in NC cells led to a modification in cell phenotype and morphology. The original spindle shape of NC cells changed upon *Smarcb1* knockdown. In general, the cells demonstrated fibroblastic features. However, this is not obvious from the images taken using phase contrast microscope (Figure 4.20). F-actin distribution can provide an indication of cell morphology (Silveira e Souza et al., 2011, Fernández-Segura et al.,

1995). Hence, the cytoskeleton of cells was examined by immunofluorescence (IF) imaging using phalloidin staining of F-actin filament. Overall, *Smarcb1* knockout in NC cells was associated with dramatic alteration of cell shape including loss of original spindle shape and high cytoplasmic area. Besides that, *Smarcb1*-deficient cells also demonstrated a remarkable increase of the cell size relative to NTC cells, for instance, the area per object measured using ImageJ software for NTC was 4.64 mm^2 whereas SMARCB1 MMG Cd44 low was 19.2 mm^2. The diameter of a nucleus for *Smarcb1*-deficient cells was also bigger than that of NTC cells. The mean size of nucleus for NTC cells was 10.31 ± 0.6988 mm^2 (n = 10 nuclei, n = 4 technical replicates). On the other hand, the mean size of nucleus measured in SMARCB1 MMG Cd44 low was 17.72 ± 1.127 mm^2 (n = 10 nuclei, n = 4 technical replicates, p-value = 0.0014), SMARCB1 MMG Cd44 high was 17.92 ± 0.6864 mm^2 (n = 10 nuclei, n = 4 technical replicates, p-value = 0.0002), SMARCB1 MME Cd44 low was 20.21 ± 1.736 mm^2 (n = 10 nuclei, n = 4 technical replicates, p-value = 0.0018) and SMARCB1 MME Cd44 high was 17.97 ± 0.8892 mm^2 (n = 10 nuclei, n = 4 technical replicates, p-value = 0.0005). The large nucleus seen in *Smarcb1*-deficient NC cells is comparable with morphologic features of proliferating MRT cells which usually show a large nucleus relative to non-cancerous cells. The MRT cells have eccentric nuclei and the cell sometimes may contain two nuclei (Hayat, 2012).

Immunofluorescence imaging of NTC cells showed the majority of F-actin filaments were evenly distributed in the cytoplasm as dense bundles (spindle shape). By contrast, *Smarcb1* knockout in NC cells greatly altered the organisation and distribution of F-actin filaments as seen in CRISPR SMARCB1 MMG Cd44 low *Smarcb1*-deficient NC cells, relative to Cd44 high for the same CRISPR construct, NTC NC cells and NIH3T3 cells (Figure 4.21 and Figure 4.22). CRISPR SMARCB1 MMG Cd44 low cells demonstrated a clear disruption in the cytoskeletal organisation as the F-actin filaments were crossed on top of each other forming a filamentous network within cells. Likewise, NC cells treated with CRISPR SMARCB1 MME also showed disordered distribution of cytoskeletal structures that can be seen in phalloidin staining cells. However, there is no obvious difference in F-actin organisation between Cd44 high and low cells population for the CRISPR SMARCB1 MME construct. Two MRT cell lines; A204 and G401 also showed disruption of the actin organisation compared to NIH3T3, a control cell line

(Figure 4.22) thus supporting observation of F-actin filament arrangement in *Smarcb1*-deficient NC cells.

Smarcb1-deficient cells immunostained with phalloidin antibody also showed localisation of cells within filopodium (Fp) and actin-rich protrusion, microspike. Notably, prominent stress fibre (Sf) was observed in *Smarcb1*-deficient cells and this figure was absent in NTC. The presence of stress fibres in MRT has been reported by (Medjkane et al., 2004). In this study, the authors found that the organisation of stress fibres which were initially present in MRT cell lines was disrupted upon reintroduction of *Smarcb*, causing the change in cell shape. Staining of *Smarcb1*-deficient NC cells with phalloidin antibody also demonstrated the presence of other actin filaments usually involved in cancer progression including diagonal meshwork lamellipodium and filopodium (Arjonen et al., 2011). In summary, these findings suggest that *Smarcb1* loss leads to the alteration in the organisation of actin cytoskeleton and size of cells.

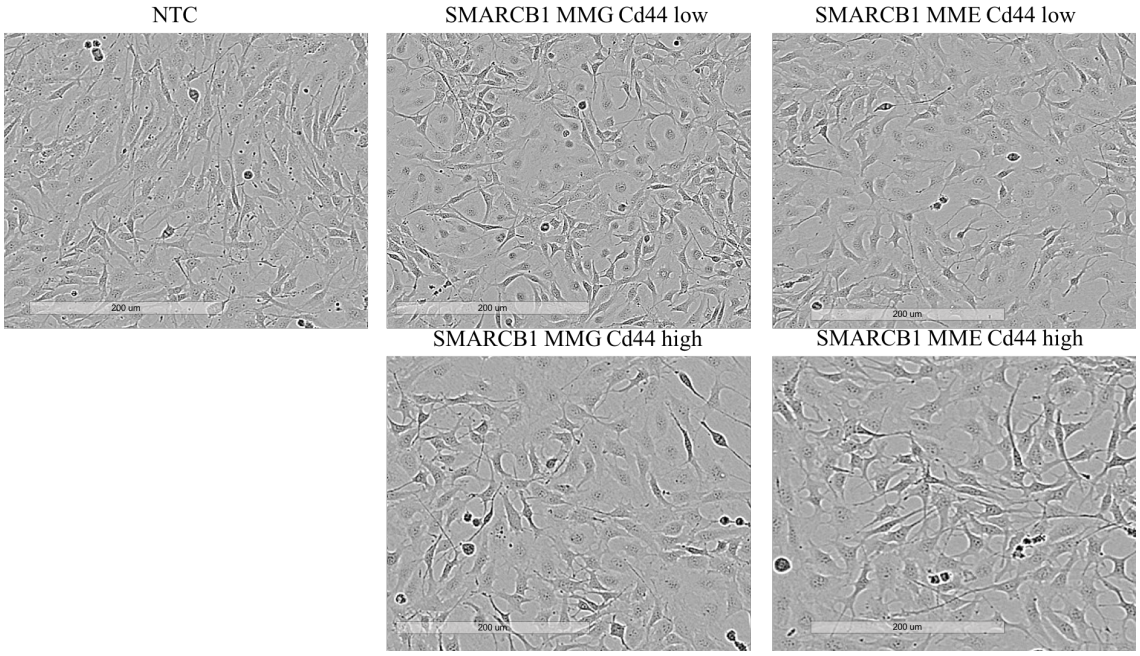

Figure 4.20 ***Smarcb1 loss in NC cells is associated with changes in cell morphology.*** *The sorted cells were cultured in an incubator installed with using INCUCYTE live cell imaging microscope (scale: 200 um). Image of Smarcb1-deficient and NTC cells taken on day 25 post transfection. A phase contrast microscopy showing modification of cell shape of Smarcb1-deficient cells and loss of spindle cell shape, as seen in NTC cells.*

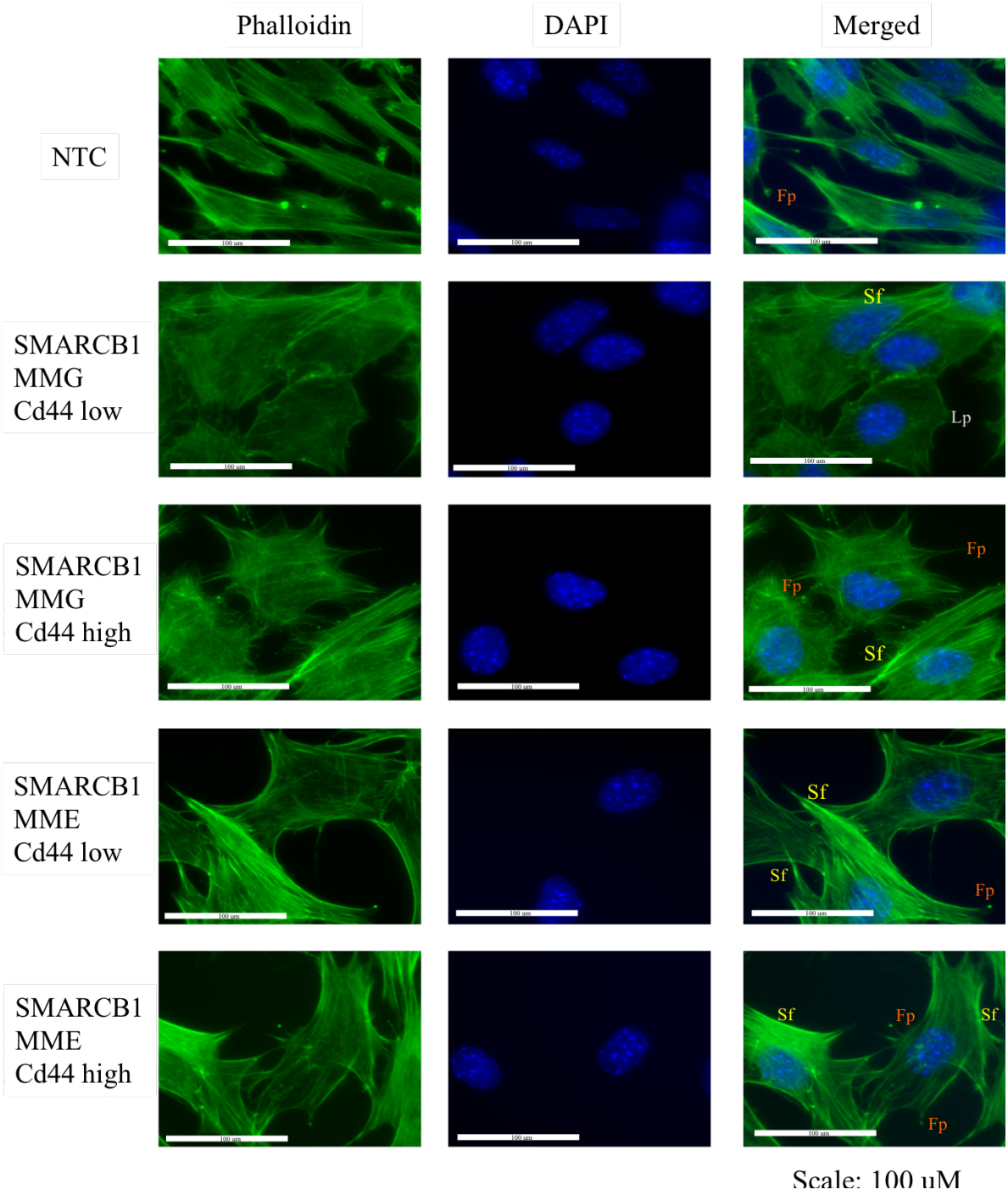

Figure 4.21 ***Smarcb1 loss in NC cells affects the cytoskeletal structure of cells****. The representative fields showing NTC and Smarcb1-deficient NC cells stained for F-actin using fluorescently conjugated phalloidin antibody (in green) and the nuclei were stained with DAPI (in blue). The images were taken using the 40X objective on the Zeiss Leica DM6 microscope. The images showed prominent stress fibre (Sf), diagonal meschwork lamellipodium (Lp) and filopodium (Fp).*

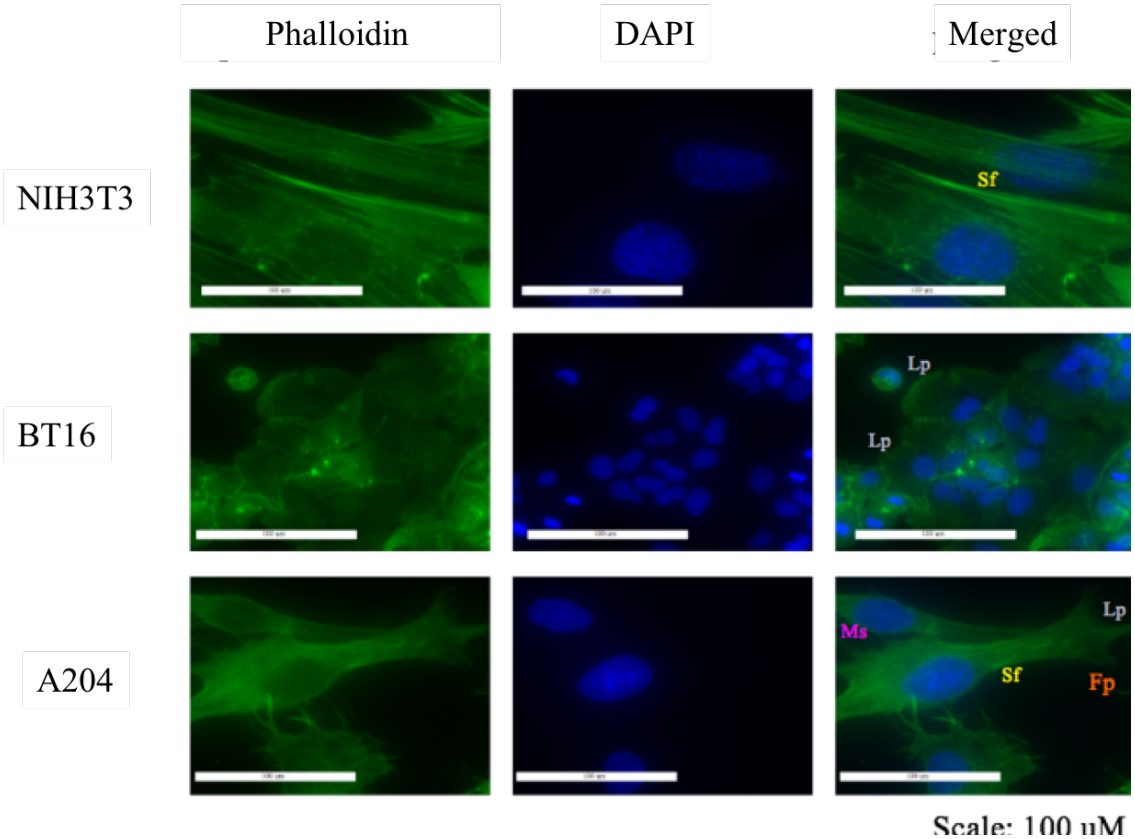

Figure 4.22 ***Smarcb1 loss in NC cells affects the cytoskeletal structure of cells****. The representative fields showing a negative control cells; NIH3T3 and two positive control cells from MRT cell lines; A204 and BT16 stained for F-actin using fluorescently conjugated phalloidin antibody (in green) and the nuclei was stained with DAPI (in blue). The images were taken using the 40X objective on the Zeiss Leica DM6 microscope. The images show prominent stress fibre (Sf)*, actin protusion microspike (Ms), *diagonal meschwork lamellipodium (Lp) and filopodium (Fp)*.

4.3.4.7 Smarcb1 loss in early neural crest cells displays human MRT features

Taking all the findings to this point together, *Smarcb1* loss in NC cells has demonstrated strong evidence supporting the NC cells as a possible cell of origin for MRT. To assess whether *Smarcb1*-deficient NC can phenotypically resemble human MRT, formalin fixed adherent cell were prepared to analyse the typical MRT features such as inclusion bodies and prominent nucleoli in *Smarcb1*-deficient NC cells from day 11 of post Cd44 sorting and control NTC cells using H&E (Haemotoxylin and Eosin) staining (Figure 4.24). The IHC staining of the sections from the cell block could not identify the presence of

prominent nucleoli and inclusion bodies in any *Smarcb1*-deficient NC cells extracted from day 11 post Cd44 sorting (Figure 4.24a), although 91% and 87% of SMARCB1 MMG CD44 low and SMARCB1 MME CD44 low cells respectively have lost Smarcb1 expression (Figure 4.24b).

To further examine if *Smarcb1* loss in NC cells can mimic human MRT, the important markers that are commonly used in MRT diagnosis were examined in knocked out and control NC cells. Human MRT can demonstrate wide-ranging immunoreactivity due to heterogeneous histologic features. For this study, I evaluated the expression of vimentin and cytokeratin 8 (CK8) using immunofluorescence. The immunofluorescence staining revealed positive staining for vimentin in all *Smarcb1*-deficient cells compared to NTC NC cells (Figure 4.26). Notably, the expression of vimentin was stronger in Cd44 low relative to Cd44 high population of cells infected by both CRISPR SMARCB1 MMG and SMARCB1 MME constructs (Figure 4.26). The expression of vimentin was also detected in MRT cell lines; A204 and BT16, thus illustrating the similarity with *Smarcb1*-deficient NC cells (Figure 4.28).

Cytokeratin staining is also used for MRT diagnosis and its expression is usually detected in focal loci of ATRT (Vitte et al., 2017). Therefore, cytokeratin 8 expression was examined in *Smarcb1*-deficient NC cells, MRT cell lines (A204 and BT16) and NTC NC cells. Immunofluorescence staining showed a modest CK8 expression in CRISPR SMARCB1 MME Cd44 low (Figure 4.28). The expression of CK8 was weak in CRISPR SMARCB1 MMG Cd44 low and CRISPR SMARCB1 MME Cd44 high cells. By contrast, expression was absent in NTC NC and NIH3T3, suggesting that *Smarcb1* knockout induces the expression of keratins in cells (Figure 4.28). Furthermore, the modest cytokeratin 8 expression could also be identified in A204 and the expression of cytokeratin 8 was stronger in the BT16 cell line.

Attempt was also made to identify perinuclear inclusion bodies using dual immunofluorescence staining of vimentin and cytokeratin 8 in BT16 cells and SMARCB1-deficient MME Cd44 low cells, however the presence of inclusion bodies was difficult to detect as co-localisation of two intermediate filaments form packed and elongated filaments (Figure 4.29). In summary, *Smarcb1* -deficient NC displayed typical histological and immunophenotype that resemble those found in human MRT but further

work (i.e mice engrafment) should be done to identify the presence of typical rhabdoid cells such as inclusion bodies.

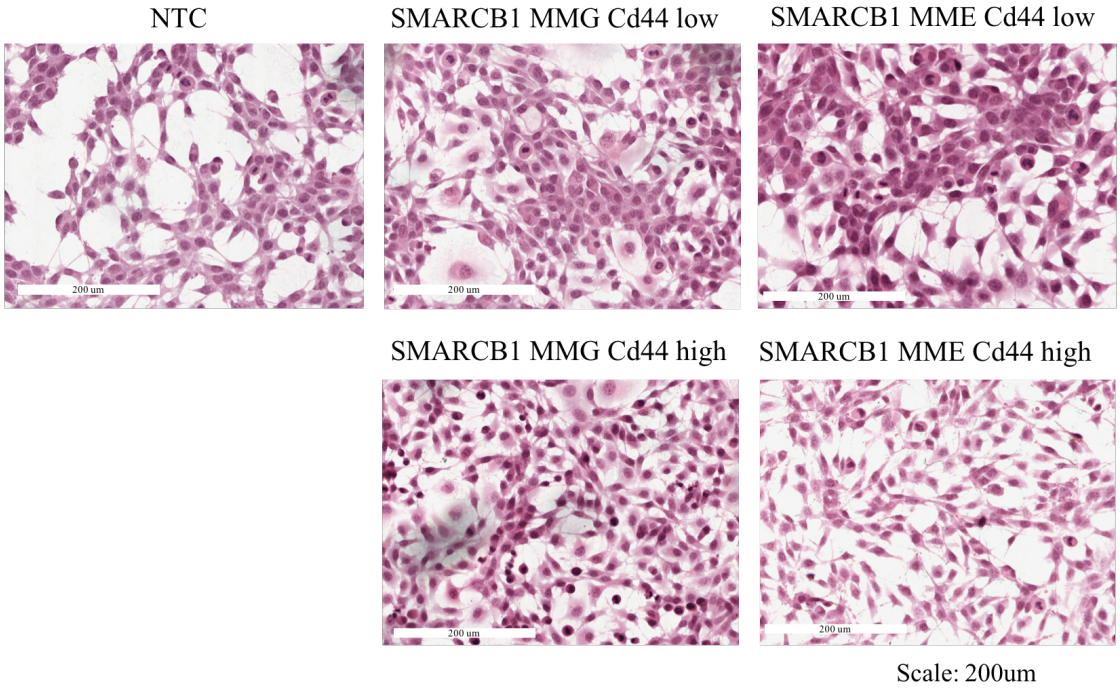

Figure 4.23 ***Identification of human MRT phenotypes in NC cells.*** *The H&E staining was performed on adherent Smarcb1-deficient cells in a chamber of 6 well to identify common phenotypes that are associated with human MRT including eosinophilic inclusion and prominent nuclei.*

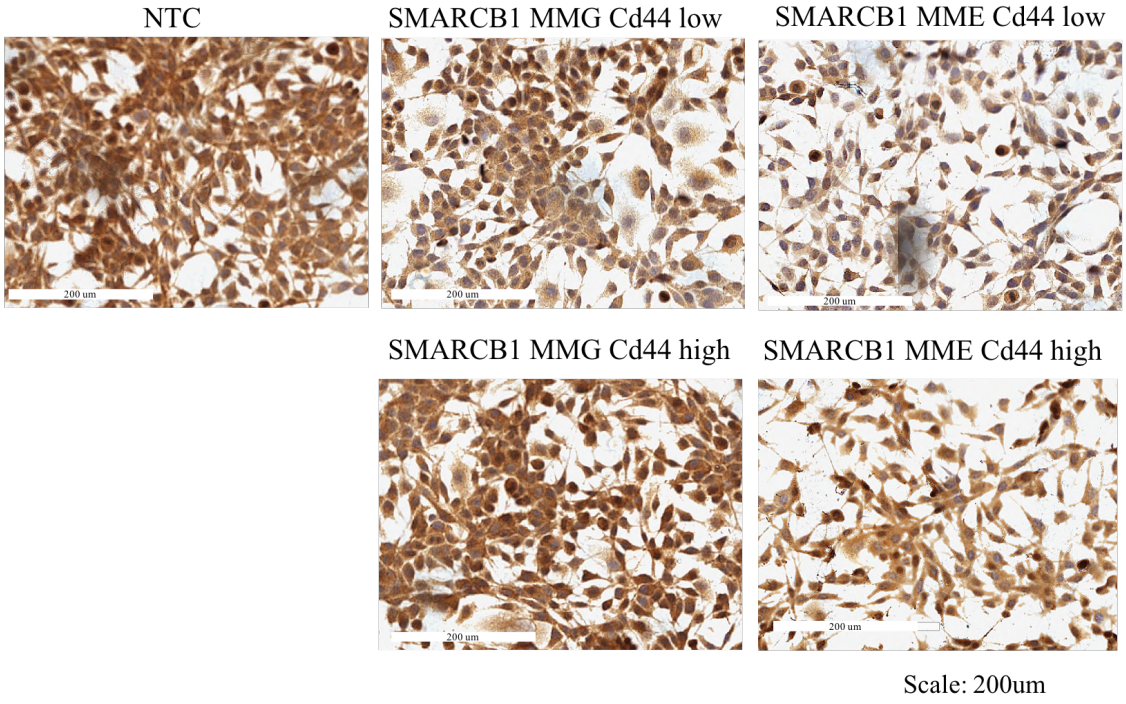

Figure 4.24 ***Immunohistochemical staining for Smarcb1 protein expression in NC cells.*** *The Smarcb1 staining was performed on adherent Smarcb1- deficient cells and NTC cells in a chamber of 6 well. NC cells used in this analysis were harvested 11 days after of Cd44 sorting. Nuclear Smarcb1 staining was scored using Aperio Imagescope using nuclear algorithm. The nuclei were scored negative if algorithm readings were 0 and +1. The nuclei were scored positive if the readings were +2 and +3.*

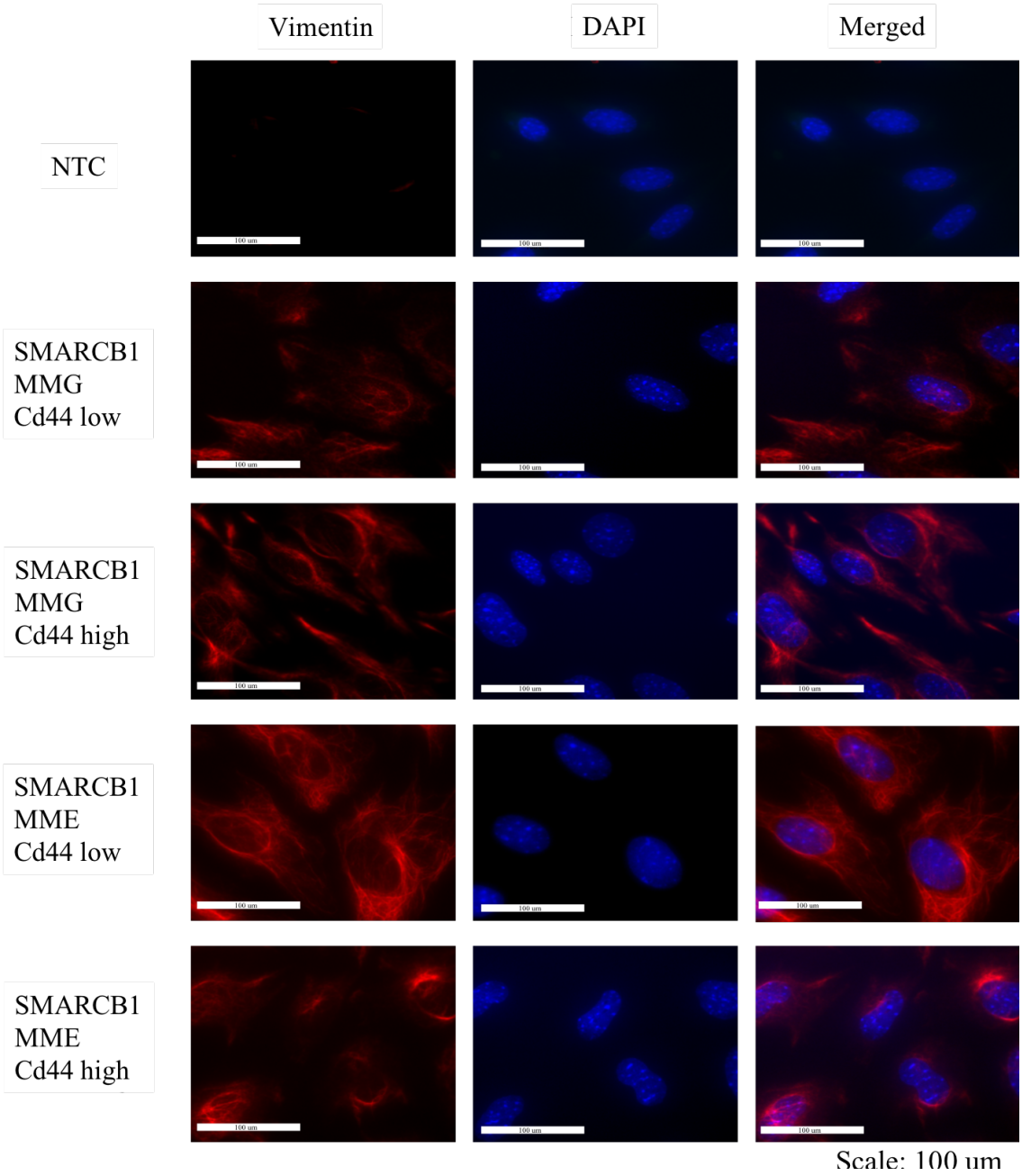

Figure 4.25 ***Smarcb1-deficient cells demonstrates human MRT phenotype****. The representative fields showing Smarcb1-deficient NC cells and NTC cells stained for intermediate filament III using fluorescently conjugated vimentin antibody (in red) and the nuclei were stained with DAPI (in blue). The images were taken using the 40X objective on the Zeiss Leica DM6 microscope.*

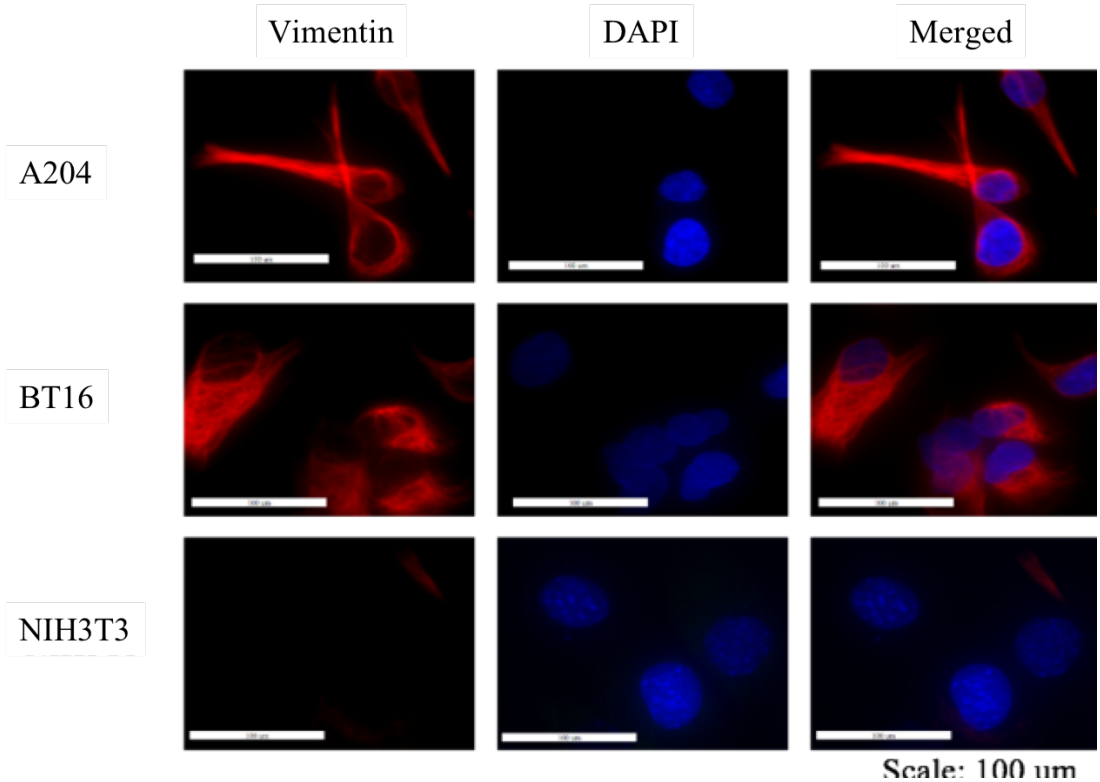

Figure 4.26 ***Smarcb1-deficient cells demonstrates human MRT phenotype.*** *The representative fields showing a negative control cell; NIH3T3 and two positive control cells from MRT cell lines; A204 and BT16 stained for intermediate filament III using fluorescently conjugated vimentin antibody (in red) and the nuclei were stained with DAPI (in blue). The images were taken using the 40X objective on the Zeiss Leica DM6 microscope.*

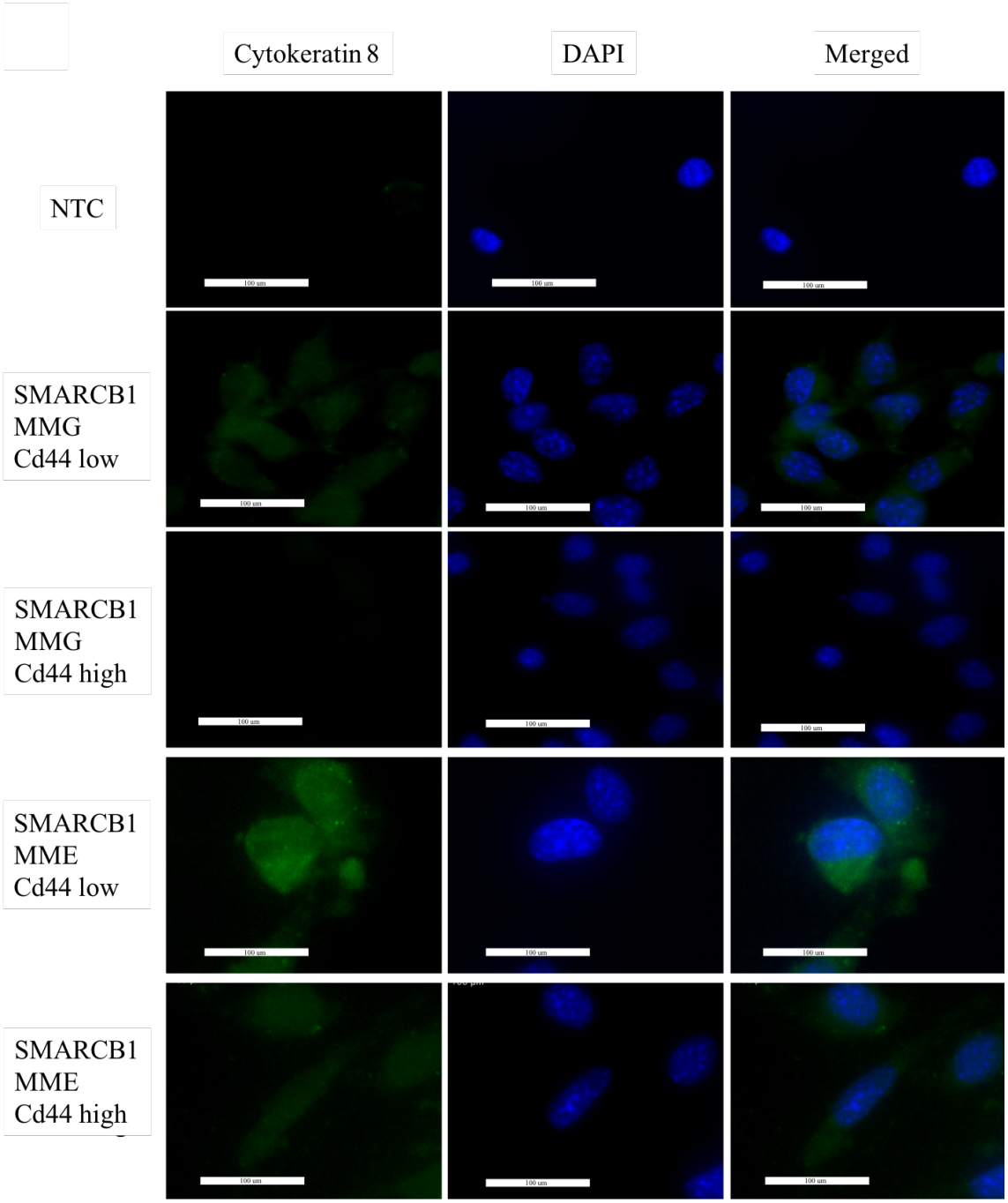

Figure 4.27 ***Smarcb1-deficient cells demonstrates human MRT phenotype.*** *The representative fields showing Smarcb1-deficient NC cells and NTC cells stained for intermediate filament type II keratin using fluorescently conjugated cytokeratin 8 antibody (in green) and the nuclei were stained with DAPI (in blue). The images were taken using the 40X objective on the Zeiss Leica DM6 microscope.*

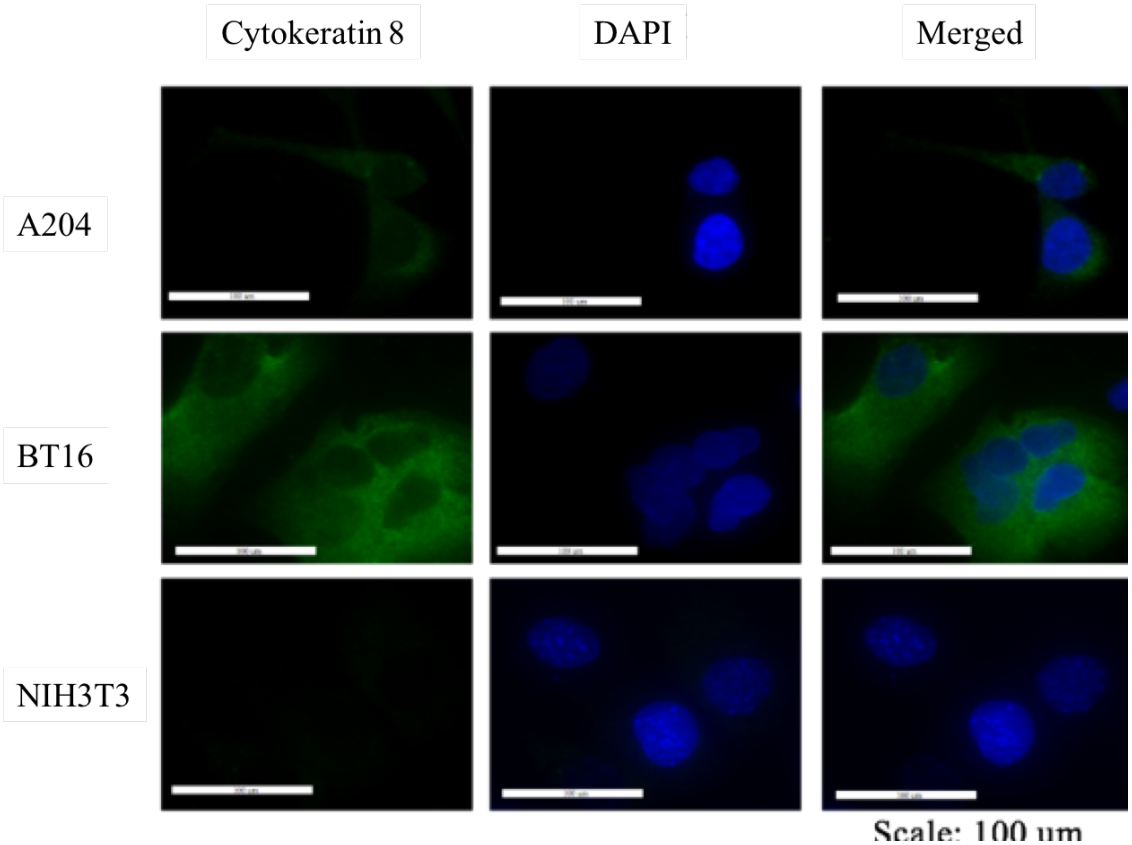

Figure 4.28 ***Smarcb1-deficient cells demonstrates human MRT phenotype.*** *The representative fields showing a negative control cells;, NIH3T3 and two positive control cells from MRT cell lines; A204 and BT16 stained for intermediate filament type II keratin using fluorescently conjugated cytokeratin 8 antibody (in green) and the nuclei were stained with DAPI (in blue). The images were taken using the 40X objective on the Zeiss Leica DM6 microscope.*

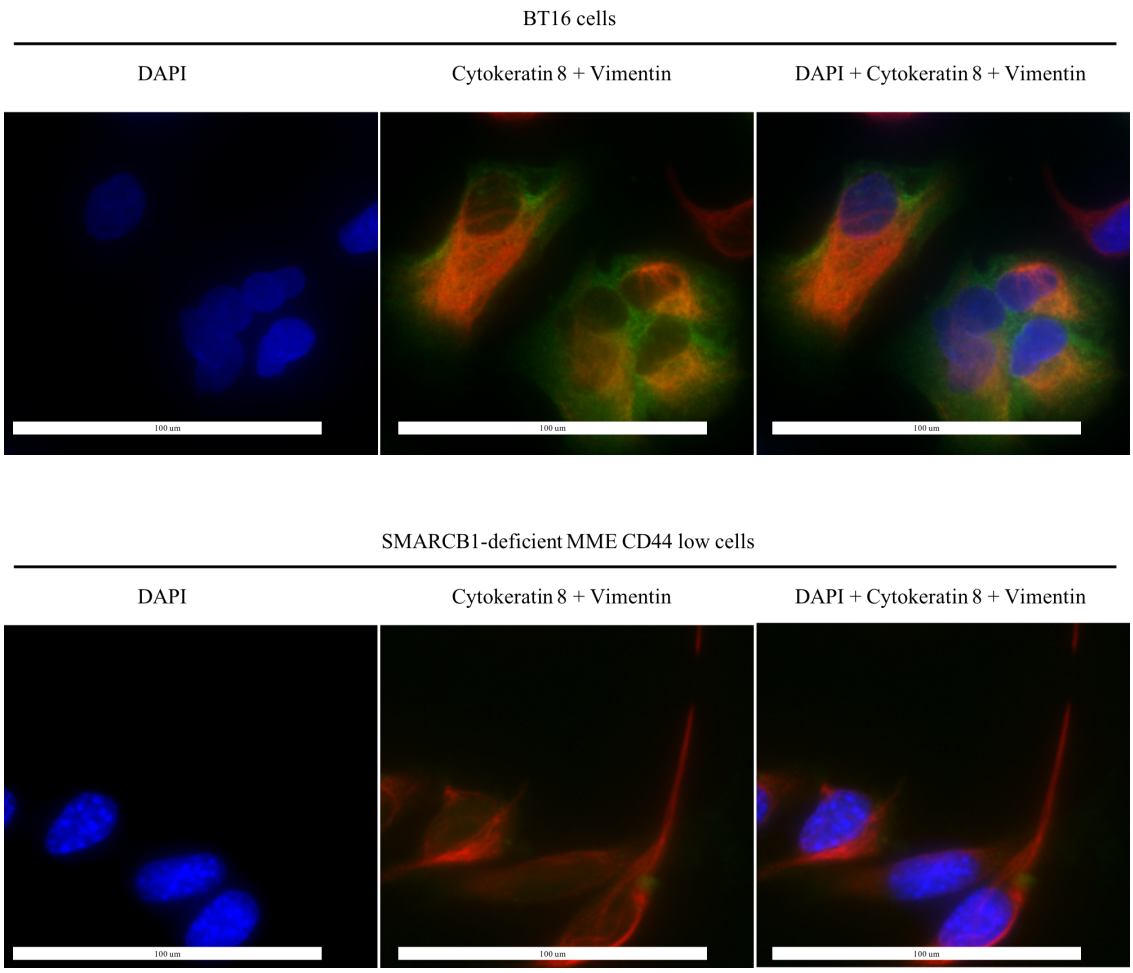

Figure 4.29 ***Immunofluorescence imaging of dual staining of cytokeratin 8 (green) and vimentin (red).*** *Co-localisation of cytokeratin 8 and vimentin was seen in two cells; BT16 and Smarcb1-deficient MME CD44 low cells. However, the perinuclear inclusion bodies could not be detected within the cells. The nuclei were stained with DAPI (in blue). The images were taken using the 40X objective on the Zeiss Leica DM6 microscope.*

4.3.4.8 The effect of Smarcb1 loss on cellular differentiation in neural crest cells

In a previous study, re-expression of *SMARCB1* in MRT cell lines provoked adipogenic cell differentiation (Caramel et al., 2008). Another study showed that loss *Smarcb1* in developing liver impairs the formation of hepatic epithelium accompanied by downregulation of 70% of genes that involve during liver development, thus indicating the requirement of *Smarcb1* for hepatocyte differentiation (Gresh et al., 2005). Furthermore, primary MRT are often associated with an undifferentiated phenotype, thus implying a significant role of *SMARCB1* in cell differentiation.

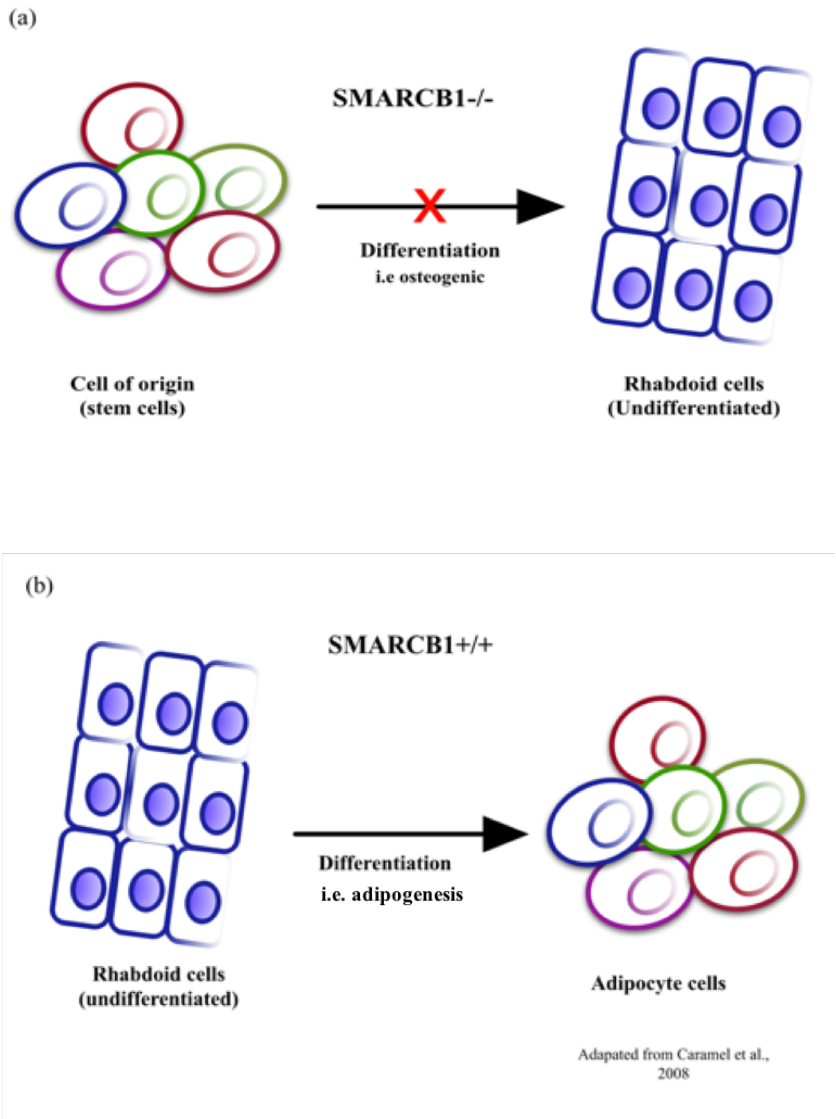

Figure 4.30 ***Experimental model for cell differentiation.*** *It is predicted in this study that SMARCB1 loss could cause defects in cell differentiation. An Experimental study by Caramel et al., (2008) demonstrated that re-expression of SMARCB1 in some MRT cell lines provoked cell differentiation into the adipocyte lineage.*

To investigate this further, *Smarcb1*-deficient NC cells and NTC cells were cultured in two types of differentiation media; adipogenic and osteogenic after 9 days of Cd44 sorting. To induce the cell differentiation, cells were cultured in differentiation media for 3 weeks and the media was changed every two days. In osteogenic cell differentiation, the formation of mineralised nodules in osteogenic cells cultures offers a tool to assess the mature osteoblast cells in culture. Alizarin Red solution was used to stain mineralised

nodules after three weeks in culture. In contrast to the hypothesis of this study that the loss of functional *Smarcb1* in the appropriate cell of origin has the ability to block lineage-specific differentiation, *Smarcb1*-deficient NC cells exhibited osteogenic potential in comparison to NTC cells. Alizarin Red staining showed nearly 70-85% of Cd44 high cells in 6-well plate were stained with Alizarin Red relative to approximately 3-5% of cells in Cd44 high well (Figure 4.31a). Notably, only one mineralised nodule was seen in NTC well.

Likewise, *Smarcb1*-deficient NC cells also differentiated towards an adipogenic lineage when cultured in adipogenic differentiation media (Figure 4.31b). The cells were stained with Oil Red O solution and were analysed for the presence of lipid droplet in the cytoplasm. Figure 4.2b showed the accumulation of lipid droplets in *Smarcb1*-deficient NC cells as well as control NTC. A mean of 38 ± 7 lipid droplets was counted in NTC cells, 52.5 ± 7.5 lipid droplets in SMARCB1 MMG Cd44 high cells, 10 ± 2 lipid droplets in SMARCB1 MMG Cd44 low cells, 68.5 ± 10.5 lipid droplets in SMARCB1 MME Cd44 high and 9.5 ± 4.5 lipid droplets in SMARCB1 MME Cd44 low.

The observations from current study did not support the hypothesis of this study. More repeats should be performed before completely rejecting this hypothesis however it seems from these first experiments that *Smarcb1* loss does not discriminately block cells from differentiating into osteocytes and adipocytes.

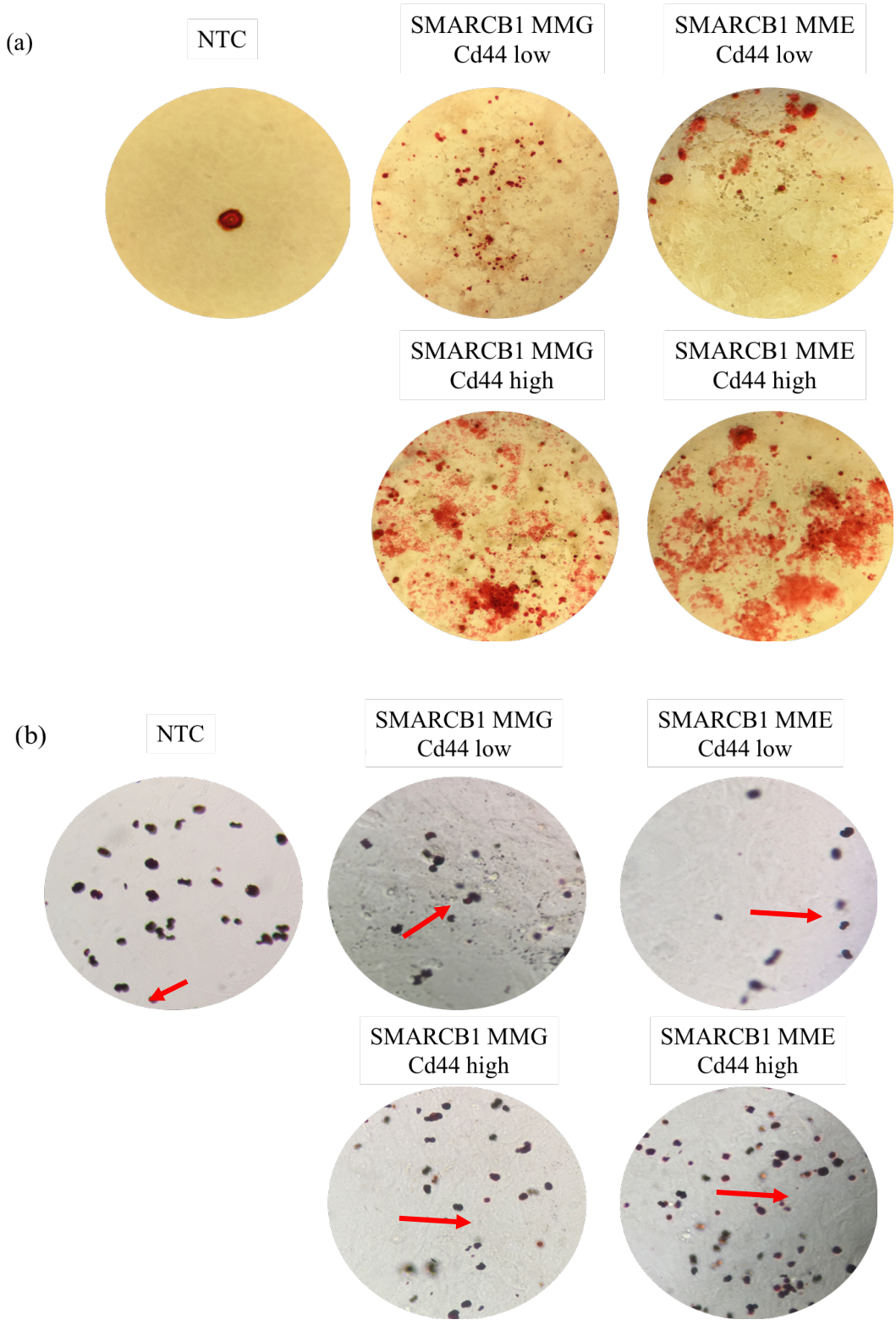

Figure 4.31 ***Osteogenic and adipogenic differentiation experiments to study the potential of Smarcb1-deficient cells to differentiate.*** *Cells were grown in differentiation media (osteogenic and adipogenic) for three weeks before the staining step. (a) Alizarin*

red staining was used to detect accumulation of calcium compounds containing osteocytes in differentiated culture (in red). (b) Oil red O was used to demonstrate the presence of lipid droplet (in red).

4.3.4.9 Summary of the results

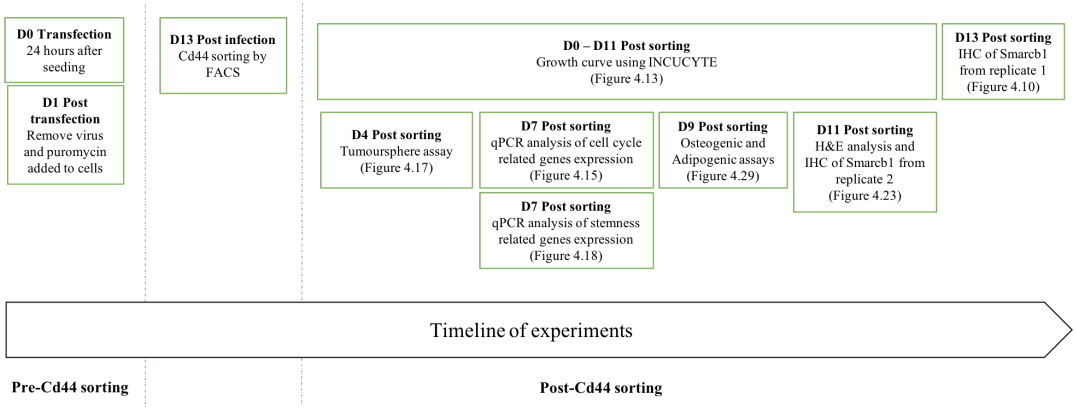

Figure 4.32 ***Timeline of experiments performed in this project.***

Overall, CRISPR/Cas9 can efficiently knock out *Smarcb1* expression in NC cells. The timeline in Figure 4.32 shows the timings of the experiments performed in this project. Smarcb1 expression was checked following the Cd44 cell sorting using IHC analyses on day 13 post-transfection prior to CD44 sorting, day 11 post CD44 sorting and day 13 post Cd44 sorting (Table 4.2 and Table 4.4). IHC analysis of Smarcb1 nuclear expression in *Smarcb1*-deficient NC cells from a second replicate, after 11 days of Cd44 sorting could not be determined accurately due to few problems which I will discuss in detail in Section 4.4.3. Differentiation assays (osteogenic and adipogenic) demonstrated that *Smarcb1*-deficient cells were still capable to differentiate into adipocyte and osteocytes. This is probably due to the fact that small proportion of cells within *Smarcb1*-deficient cells were *Smarcb1* positive. Also, it is worth to note that, there is no significant difference between Cd44 high and Cd44 low cell populations in terms of expression of cell cycle genes, self-renewal potential and growth capacity. The practicability of using Cd44 expression

marker in sampling *Smarcb1* negative cells is further discussed in Section 4.4.2. The summary of results was presented in the table below:

Sorting	Sample transfected with:	Experiment	Negative Smarcb1 expression	Result
Pre	NTC	IHC (Figure 4.9)	0.02% (determined on day 13 post transfection)	
	SMARCB1-MMG		50.6% (determined on day 13 post transfection)	

Table 4.2 ***Summary of results pre CD44 sorting****. ND = not determined*

Sorting	Sample transfected with:	Experiment	Negative Smarcb1 expression	Result
Post	NTC	Growth curve (D0-D11 post sorting)	3.3% Smarcb1-negative cells	* Smarcb1 expression was evaluated by IHC on cells from day 11 post sorting Growth rate of NTC slows down in passage 1 and 3 relative to SMARCB1 MME Cd44 high and low, and SMARCB1 MMG Cd44 low No statistical difference between Cd44 low and high for both CRISPR construct
	SMARCB1-MME		Cd44 high:77 % Smarcb1-negative cells Cd44 low: 87% Smarcb1-negative cells	
	SMARCB1-MMG		Cd44 high: 66.6% Smarcb1-negative cells Cd44 low: 91% Smarcb1-negative cells	
	NTC	Tumoursphere assay (Day 4 post sorting)	ND	Cd44 high cell population produces more tumourspheres than Cd44 low cells for both CRISPR construct. But the reading is not statistically significant *Smarcb1*-deficient cells produces more tumoursphere than NTC cells
	SMARCB1-MME		ND	
	SMARCB1-MMG		ND	

Table 4.3 ***Summary of results post CD44 sorting.*** *ND = not determined*

Sorting	Sample transfected with:	Experiment	Negative Smarcb1 expression	Result
Post	NTC	qPCR analysis of cell cycle related genes	3.3% Smarcb1-negative cells	* Smarcb1 expression was evaluated by IHC on cells from day 11 post sorting No statistical difference of expression of cell cycle genes between Cd44 high and Cd44 low Cell cycle promoting genes were highly expressed in *Smarcb1*-deficient cells compared to NTC cells. The expression of cell cycle inhibitors were downregulated in *Smarcb1*-deficient cells relative to NTC
	SMARCB1-MME		Cd44 high:77 % Smarcb1-negative cells Cd44 low: 87% Smarcb1-negative cells	
	SMARCB1-MMG		Cd44 high: 66.6% Smarcb1-negative cells Cd44 low: 91% Smarcb1-negative cells	
	NTC	qPCR analysis of stemness related genes	3.3% Smarcb1-negative cells	* Smarcb1 expression was evaluated by IHC on cells from day 11 post sorting No statistical difference of expression of cell cycle genes between Cd44 high and Cd44 low. However, a few self-renewal genes such as *Ezh2* and *Sox2* are highly expressed in Cd44 high compared to Cd44 low Cell cycle promoting genes were highly expressed in *Smarcb1*-deficient cells compared to NTC cells. The expression of cell cycle inhibitors were downregulated in *Smarcb1*-deficient cells relative to NTC
	SMARCB1-MME		Cd44 high:77 % Smarcb1-negative cells Cd44 low: 87% Smarcb1-negative cells	
	SMARCB1-MMG		Cd44 high: 66.6% Smarcb1-negative cells Cd44 low: 91% Smarcb1-negative cells	

Table 4.4 ***Summary of results post CD44 sorting****. ND = not determined*

Sorting	Sample transfected with:	Experiment	Negative Smarcb1 expression	Result
Post	NTC	Cell differentiation (day 9 post sorting)	ND	Small population of cells within *Smarcb1*-deficient cells differentiated into adipocytes and osteocytes
	SMARCB1-MME		ND	
	SMARCB1-MMG		ND	
	NTC	IHC analysis (day 11 post sorting) (Figure 4.7) From monolayer cells of 2nd replicate	3.3% Smarcb1-negative cells	
	SMARCB1-MME		Cd44 high:77 % Smarcb1-negative cells Cd44 low: 87% Smarcb1-negative cells	
	SMARCB1-MMG		Cd44 high: 66.6% Smarcb1-negative cells Cd44 low: 91% Smarcb1-negative cells	
	NTC	IHC analysis (day 13 post sorting) (Figure 4.7) From cytospin cells of 1st replicate	1.4% Smarcb1-negative cells	
	SMARCB1-MME		Cd44 high: 13.2% Smarcb1-negative cells Cd44 low: 77% Smarcb1-negative cells	
	SMARCB1-MMG		Cd44 high: 13% Smarcb1-negative cells Cd44 low: 75% Smarcb1-negative cells	

Table 4.5 ***Summary of results post CD44 sorting****. ND = not determined*

4.4 Discussion

4.4.1 CRISPR/Cas9 mediated Smarcb1 genome editing in neural crest cells provides a tool to study MRT tumourigenesis

The early onset of MRT provides an indication of the requirement for a mutational event in early development resulting in tumourigenesis. Loss of *Smarcb1* in granule cell precursors demonstrates a lack of tumourigenic phenotype in Smarcb1$^{flox/flox}$, Atoh-Cre mice model, indicating tumourigenesis of ATRT does not arise from granule cell precursor (Moreno et al., 2014). These observations narrow down the developmental window and the potential candidates for the cell of origin of MRT. Results from the bioinformatics analysis of different cell types (Chapter 3) suggested neural crest (NC) cells as a potential MRT cell of origin, especially for ECRT. This observation is in line with a growing number of reports based on histological, genomics and mouse studies in MRT (Chun et al., 2016, Han et al., 2016, Vitte et al., 2017).

In a MRT mouse model study by Han et al. (2016), the authors found the high penetrance of tumour, mainly intracranial after tamoxifen injection into Rosa26-CreERT2; Smarcb1$^{flox/flox}$ mice were observed between E6 and E10. Injection of tamoxifen after E10 failed to develop tumours. Although their mouse model experiments provides an important piece of information regarding the developmental window at which cells are susceptible to *Smarcb1* loss for the initiation of tumourigenesis, the authors did not specifically perform the injection in specific type of cells to speculate the cell of origin for MRT. Following this study, Vitte et al. (2017) developed P0-CreC; Smarcb1$^{flox/flox}$ mice to study the cell of origin for MRT. In this study, the authors performed deletion of *Smarcb1* in early NC cells at protein zero promoter and reported the tumours demonstrating immunohistological and molecular profiles resemble human MRT. Their mouse model demonstrated loss of *Smarcb1* at a developmental window of E9.5 in early neural crest cells is required for MRT oncogenesis (Vitte et al., 2017). Knockout of *Smarcb1* at a later developmental stage such as E12.5 or E13.5 failed to induce tumourigenesis. However, their hypothesis that early NC cells at P0 is a potential cell of origin raised a question as to whether these cell populations are true cell of origin for MRT since they also speculated that these cell populations are a cell of origin for schwannoma and eventually concluded that some MRT may originate from meninges as most tumours were formed in this region. Furthermore, the authors did not explicitly time

the induction of *Smarcb1* mutation in mice except by inference through the expression of protein zero (P0), which is an active promoter in early NC cells.

In this study, an early NC cell that was derived from the mouse at E8.5 was used as a potential cell of origin for MRT. Previous mouse model studies utilised *Cre* recombinase constructs to specially target *Smarcb1*. Here, I report another technique to knockout *Smarcb1* in cells using CRISPR/Cas9 technology. Inhibition of expression using CRISPR/Cas9 is highly efficient as shown by approximately 80-90% loss of Smarcb1 protein after 27 days of transfection (Figure 4.11). In particular, two CRISPR/Cas9 constructs that targeted different regions in mouse *Smarcb1* has been successfully generated with comparable knockout efficiency. Moreover, the off-target effects were reduced further by choosing the guide RNAs that were distinctive from any other sites in the genome by at least three nucleotides and by adding extra guanines (Kim et al., 2017). Given that, both constructs demonstrated similar results which were distinct from the control (NTC), off-target effects are unlikely to have influenced the findings generated in this part of the study.

This cell model is suitable as a tool to study MRT tumourigenesis and to identify potential therapeutic targets. Transfection of sgRNA and Cas9 plasmid into neural crest cells resulted in high-level expression of these two components, leading to efficient genome editing. Importantly, *Smarcb1*-deficient NC cells could maintain cell proliferation and demonstrated histological and gene expression that resembles human MRT.

4.4.2 The practicality of selecting pure Smarcb1-negative population using Cd44 surface marker

CD44 is a ubiquitously expressed glycoprotein adhesion molecule derived from a gene that contained 18 exons (Shigeishi et al., 2013). CD44 is also known as a SWI/SNF responsive surface protein CD44 (Banine et al., 2005). The expression of CD44 can influence stem cell characteristics through a wide range of mechanism and interaction with its main ligand, hyaluronan can also activate many cell signalling pathways associated with tumour growth and progression (Shigeishi et al., 2013). Particularly in MRT, expression of CD44 is either absent (in ATRT) or low (in ECRT). Hence, its expression was exploited to increase the percentage of pure *Smarcb1*-negative cells. However, a pure *Smarcb1* negative cell population was unobtainable as there were

roughly ~30% *Smarcb1* knocked out cells which were positively stained with Smarcb1 antibody (Figure 4.11). This may explain why *Smarcb1* -deficient cells were still able to differentiate into mesenchymal lineages i.e adipocytes (Figure 4.31). Besides that, there was no significant difference in growth characteristics between Cd44 high and Cd44 low cell population measured for 11 days post Cd44 sorting (Figure 4.13). Moreover, gene expression analysis of cell cycle-related genes also showed no statistical difference between these two cell populations. Hence, the difference in growth characteristics between Cd44 high and Cd44 low cell populations could not clearly be outlined in this project. Failure to obtain *Smarcb1*-negative CD44 cell population may also due to the fact the stability of Cd44 expression following sorting has not been determined in this study. Expression of Cd44 should be re-examined after the first sorting by FACS to ensure Cd44 expression is low in Cd44 low cell population than Cd44 high cell population and therefore may increase significance of the results.

Sampling *Smarcb1*-negative cells using Cd44 expression also presents difficulties as deregulation of Cd44 expression interferes with expression of other stemness genes and capacity of the cells to form tumourspheres. Although the difference in the number of tumourspheres between Cd44 high and Cd44 low cells was not statistically significant, the results can be confounded by Cd44 expression. C44 has a role in stem cell self-renewal. Expression of this gene has been widely used as a cancer stem cell (CSC) marker (Li et al., 2017). High expression of CD44 has been correlated with cell proliferation and tumourigenesis of breast cancer as determined by mammospheres formation and tumourigenesis in xenotransplanted mice experiments. The authors found that the number of mammospheres was higher in CD44 high cell population relative to CD44 low cell population. Their result illustrates the significance of CD44 expression in CSC self-renewal. Furthermore, they found that high expression of CD44 coupled with a high expression of *ALDH* was capable to increase the cell metastasis thus signifying the positive correlation of CD44 with other stemness genes in regulating tumourigenesis.

Given the problems encountered when using Cd44 expression to sample *Smarcb1* negative cells, it is, therefore, necessary to identify other surface markers that can increase the percentage of *Smarcb1* negative cells.

4.4.3 Feasibility of the techniques used to analyse the percentage of Smarcb1-negative NC cells

In this chapter, immunohistochemistry was used to analyse *Smarcb1*-deficient cells in NC cell populations. This technique is commonly used to detect SMARCB1 expression in MRT patient material using anti-SMARCB1 antibody (BD Biosciences). IHC is a useful tool to measure the proportion of *Smarcb1*-deficient NC cells. However, it also confers challenges for image analysis. For instance, the nuclear expression of Smarcb1 was difficult to interpret when the formalin cell blocks were prepared from the monolayer cells (Figure 4.24) as opposed to cytospin cells (Figure 4.8). The cells which grew as monolayers tend to grow on top of each other and were not uniformly spread in the wells, which hindered antigen retrieval and thus antibody staining. The images presented in Figure 4.24 also highlights edge effects which creates challenges to the accuracy of image quantitation and analysis. Thus, preparation of the cell block using cytospin would provide a useful method in evaluating Smarcb1 expression in cells.

4.4.4 Smarcb1 loss in NC cells maintains cell survival and causes deregulation of cell cycle-related genes

Loss of functional *Smarcb1* in other cell lines is often associated with cell death and growth arrest. Knockout of *Smarcb1* using CRISPR/Cas9 resulted in decreased cell proliferation and count after 48 hours of puromycin selection in NIH3T3. However, the proliferative capacity of NC cells was maintained following the loss of *Smarcb1*. *Smarcb1* loss in NC cells also caused dysregulation of cell cycle-related genes. The findings of this study implicating *SMARCB1* in cell cycle regulation in MRT is supported by numerous other studies (Betz et al., 2002, Versteege et al., 2002, Isakoff et al., 2005, Roberts and Biegel, 2009). A study of the role of *SMARCB1* as a tumour suppressor gene in the development of MRT reveals the effect of *SMARCB1* loss on cycle progression through downregulation of *p16* expression and upregulation of *E2F* and *CCND1* expression. Here, I showed that *Smarcb1* knockout reduced the expression of *p16* and *p21* genes concomitantly with an increase in expression of cell cycle promoting genes such as *Ccnd1, Cccnd2* and *Ccnd3* in NC cells, as determined by qPCR analysis. Hence, the effect of *Smarcb1* knockout on cell cycle regulation in NC cells mimics the observations collected from previous studies and also from primary and cell data

available in the group. It is worth noting that the expression of *Ccnd2*, *Ccnd3*, *Cdk6* is higher in *Smarcb1*- deficient cells compared to MRT primary and cell lines.

4.4.5 Smarcb1-deficient cells exhibit phenotypes resembling human features

A few studies have demonstrated that *SMARCB1* re-expression causes a dramatic change in the cell shape such flat cell formation (Dunaief et al., 1994) due to disruption of actin stress fibre organisation associated with increased in expression of genes involved in actin cytoskeleton (Medjkane et al., 2004). A study by Medjkane et al. (2004) provides evidence of *Smarcb1*'s role in cytoskeleton organisation. CRISPR knockout of *Smarcb1* also caused dramatic modifications of cell shape in NC cells and the mechanism that contributes to change in cell shape was investigated using phalloidin antibody staining. This antibody selectively binds to actin filament known as F-actin. Actin is the monomeric subunit of two types of filaments in cells which are microfilaments and thin filaments (Cooper, 2000). It is involved in many cellular activities including cell motility, cell division, cell shape and many more. Indeed, *Smarcb1* knockout in NC cells greatly altered the actin cytoskeleton organisation compared to NTC. Knockout of *Smarcb1* in NC cells also caused the formation of many stress fibres (contractile bundles of actin) within cells. This observation can explain the change in cell shape. Also, the presence of many filopodia, a feature of cell motility, in *Smarcb1*-deficient NC cells relative to the control suggests improved cell propagation in these cells. In the absence of *SMARCB1* expression, many stress fibres were found in the MRT cell line (Medjkane et al., 2004). However, they were diminished upon *SMARCB1* re-expression, thus resulting in a more rounded cell shape. The specific pathway by which *SMARCB1* regulates cytoskeletal arrangement in NC cells can be elucidated through gene expression analysis, though it has been proposed to occur through the Rho pathway in MRT cell line (MON) (Medjkane et al., 2004).

Smarcb1-deficient cells also demonstrated strong positive staining of the intermediate filament vimentin. The immunoreactivity of MRT primary and cell lines with vimentin has been reported in few studies and it serves as a diagnostic marker for MRT (Sugimoto et al., 2016, Itakura et al., 2001). Vimentin usually forms a filamentous network that can vary in size and it can be found at the rim of the cytoplasm or the cell periphery. In some MRT cells, vimentin can co-localise with cytokeratin 8. In this study, *Smarcb1* knocked out in NC cells resulted in weak expression of cytokeratin 8 making it difficult to identify

co-localisation of these two types of intermediate filaments. Nevertheless, the presence of cytokeratin 8 expression still provides the evidence that *Smarcb1*-deficient cells can immunophenotypically resemble human MRT as its expression was absent in NTC NC cells.

Collectively, *Smarcb1* loss altered the cell shape and size and is associated with actin cytoskeleton organisation. *Smarcb1* -deficient cells showed immunoreactivity with two MRT markers; vimentin and cytokeratin 8. In short, data from this study recapitulates the findings from previous studies and human MRT tissue.

4.4.6 Histological characteristics of "Rhabdoid" cells are absent in Smarcb1-deficient NC cells

An attempt was made to identify the main histological characteristics of rhabdoid cells such as prominent nuclei and cytoplasmic inclusion bodies using conventional H&E staining. However, these figures were not detected in *Smarcb1*-deficient NC cells. Of note, classic morphological features and the identification of the rhabdoid cells with characteristics of nuclear and cytoplasmic aspects were also challenging in the primary MRT cells (Bourdeaut et al., 2007). The inclusion bodies and prominent nucleoli can be seen in cells when engrafted in mice. To circumvent the problem mentioned above with immunohistochemistry, the presence of inclusion bodies was further examined using immunofluorescence staining. These inclusions are ultrastructurally characterised by the presence of agglomerates of two intermediate filaments; cytokeratin (CK) or vimentin (Raymond and Leong, 1989, Waelter et al., 2001, Itakura et al., 2001, Parker et al., 2002). The presence of cytokeratin in an MRT cell line, Tm86-16 was described as clusters of globules or clumps if located at the cell periphery (Itakura et al., 2001). Immunofluorescence staining showed weak expression of cytokeratin 8 (CK8) in majority *Smarcb1*-deficient cells which limits the ability to detect inclusion bodies. In this analysis, BT16 and *Smarcb1*-deficient MME Cd44 low cells demonstrated strong positive CK8 and vimentin staining. Hence, dual immunofluorescence staining was performed in these cells to identify perinuclear inclusion bodies (Figure 4.29). The immunofluorescence assessment revealed clear co-localisation of two intermediate filaments in the same area, and CK8 formed packed and elongated filaments. Therefore, it was very difficult to distinguish the inclusion bodies in the cells. Shiratsuchi et al.

(2001) also reported the difficulty to detect inclusions in cells as the filamentous inclusions can vary in size and arrangement from cell to cell.

In short, although classic histological features of rhabdoid cells were not established from these experiments, this may be a result of lack of interaction with a more complex dynamic tissue microenvironment. Thus, establishing a mouse xenograft model with the *Smarcb1*-deficient NC cells will provide a better context to assess histological features and increasing interaction with a more dynamic and complex microenvironment, and potential of NC cells as a cell of origin for MRT.

Chapter 5 Establishing tumoursphere assay of Malignant Rhabdoid Tumours (MRT) cell lines for self-renewal identification and analysis

5.1 Summary

Malignant Rhabdoid Tumours (MRT) are characterised by a biallelic mutation in *SMARCB1*, a component of the SWI/SNF chromatin remodelling complex (Versteege et al., 1998, Biegel et al., 2002b). MRT are aggressive and present a poor disease prognosis (Reinhard et al., 2008, Brennan et al., 2013a). Work done within my group has shown strong overexpression of a large number of "self-renewal/stemness" genes in primary MRT, as determined by gene expression analysis. Other studies also have shown that a number of these genes are deregulated by loss of *SMARCB1* and/or the larger SWI/SNF complex (Deisch et al., 2011, Venneti et al., 2011b, Johann et al., 2016). Therefore, I assume that *SMARCB1* loss is capable of hijacking self-renewal mechanisms and could potentially contribute towards disease aggressiveness. To investigate the mechanism of self-renewal in MRT and to access its potential as a targetable element of MRT tumourigenesis, I have piloted the use of plate-based assays to measure the tumoursphere formation in MRT cells, as a self-renewal readout. The tumourspheres were generated from two MRT cell lines; A204 and G401 in various plating formats. I aimed to identify minimum cell density required to form tumourspheres in order to avoid fusion cells and to determine the conditions for tumoursphere culturing media. Notably, across serial passaging of tumoursphere, MRT cells are able to form tumourspheres and the efficiency of tumoursphere formation is remarkably improved with increased passage number. Identification of cells within MRT that are capable of sustaining multipotency and self-renewal will provide a critical insight into the discovery of tumour origins and the mechanisms that underpin tumourigenic potential.

5.2 Introduction

5.2.1 Malignant Rhabdoid Tumours (MRT) share common biology properties with stem cells

Malignant Rhabdoid Tumours (MRT) are a highly aggressive disease with a poor survival rate (Madigan et al., 2007, Kordes et al., 2010, Reinhard et al., 2008). MRT are heterogeneous tumours consisting of multiple phenotypes such as primitive neuroectodermal, mesenchymal and epithelial features even within the same tumours (Biggs et al., 1987, Tsokos et al., 1989, Kato et al., 2003). In line with this, experimental findings demonstrated the ability of MRT cells to differentiate into adipogenic lineages upon *SMARCB1* re-expression (Caramel et al., 2008) and inhibition of *SMARCB1* with RNAi interference (RNAi) impaired neuronal differentiation *in vivo* (Albanese et al., 2006a). These observations have led to an assumption that MRT originates from multipotent stem cells. Studies to understand MRT biology illustrated a number of stem cell related genes shared between MRT and embryonic stem cells (Deisch et al., 2011). These genes include *SALL4, SOX2, OCT4*, *NANOG* and *KLF4* which regulate the self-renewal pathway. The stem cell-associated gene network often involves the interaction of genes to regulate self-renewal and differentiation. For instance, *SALL4* regulates the expression of *OCT4*, which in turn activates the expression of other genes such as *UTF1*, *TCL1* and *ZFP206*. Of note, *UTF1* and *TCL1* markers were highly expressed in MRT. In line with this, Venneti et al. (2011b) also identified stem cell markers such as NANOG, SOX2, SALL4, MUSASHI, KLF4, T-cell leukaemia/lymphoma 1, undifferentiated embryonic cell transcription factor and ZFP209 in primary MRT using immunohistochemistry analysis. Altogether, the results illustrate the stem cell properties shared between MRT and stem cells.

5.2.2 Tumoursphere assay as in vitro stem cell assay

Tumoursphere assays or sphere-forming assays are a widely used technique to identify stem cells based on their ability to undergo self-renewal and differentiation from a single cell *in vitro*. Tumourspheres are also known in other studies as spheroids, neurospheres (a brain tumour) or mammospheres. Tumourspheres originating from a small number of cells with stem cell characteristics are capable of growing in suspension culture and can

form tumours *in vivo*. They grow as floating clusters of undifferentiated and proliferating cells.

The assay was initially described by Reynolds and Weiss (1992) following the discovery of multipotent precursor from the adult brain. The strial tissue from the periventricular area of the subventricular zone (SVZ) was cultured as tumourspheres (known as neurospheres in their study) in the presence of epidermal growth factor (EGF) in culture (Reynolds and Weiss, 1992, Pastrana et al., 2011). The formed spheres expressed NESTIN which is commonly found in neuroepithelial stem cells in the embryonic brain. Intriguingly, cells differentiated into both neurons and glial cells when cultured in adherent media. Subsequent studies have shown that cells within the SVZ can be cultured as spheres *in vivo*. Use of the tumoursphere assay has led to a breakthrough of surface markers to isolate putative stem cells and to purify stem cells and their progeny for functional studies both *in vitro* and *in vivo*.

Following this study, Dontu et al. (2003) have tailored the neurosphere assay to propagate mammary epithelial stem cells (MaSC) *in vitro*. This assay was later utilised as a surrogate reporter of stem cell activity in the mammary gland (Diaz-Guerra et al., 2012). The assay works based on the principle that only undifferentiated cells derived from mammalian epithelium cells will survive and form tumourspheres while other cell types die from anoikis. The *in vitro* tumoursphere assay also has been used as a tool to select and propagate tumourigenic breast cancer cells from the primary tumours using the surface markers CD44 and CD24 (Ponti et al., 2005).

In addition to the function of tumoursphere as a surrogate tool to measure stem cells within a population, this assay has been used to screen new drugs that target cancer stem cells in tumours (Cioce et al., 2010). Cancer stem cells (CSC) are a subpopulation within the tumours which possess self-renewal and multi-lineage differentiation capacity to maintain the tumourigenicity of cancer cells (Ajani et al., 2015). CSC have been implicated in cancer recurrence and resistance to therapy. CSC are protected from chemotherapy agents through different mechanisms including proficiency in DNA repair machinery, high expression of ATP-binding cassette drug transporters and also activation of signalling pathways such as PI3K/AKT and Wnt (Maugeri-Saccà et al., 2011). In glioblastoma, ionizing radiation caused the inhibition of P13K or AKT which in turn leads to activation of DNA repair, as demonstrated by the delayed clearance of γ-H2AX foci

(Kao et al., 2007). Accordingly, use of an Akt inhibitor can efficiently target glioblastoma stem-like cells, determined by a decrease in the number of viable cells and reduced neurosphere forming efficiency (Eyler et al., 2008). Therefore, development of CSC targeted therapy is considered key for successful cancer treatment with increased cancer recurrence rate and chemoresistance.

To this end, the tumoursphere assay has been used to facilitate the identification of agents that selectively kill CSC. A high throughput screening was performed in a 384-well plate format to identify agents with a strong selective toxicity for breast CSC (Gupta et al., 2009). Using this assay, the authors have identified salinomycin which has the ability to reduce the CSC population by more than 100-fold more than that of paclitaxel, a commonly used breast cancer chemotherapeutic drug. Tumoursphere assays also have been used to screen for chemical compounds that target CSC in triple negative breast cancer cells (Fitzpatrick et al., 2017). Of 989 FDA-approved drugs, three therapeutic compounds with the ability to reduce the breast CSC population of cells in triple-negative breast cancer cell line MDA-MB-231 were identified. This study highlights the practicality of a tumoursphere assay in facilitating the identification of potent anti-cancers for this lethal cancer. Overall, the tumoursphere assay offers a simple, efficient and low-cost culture system and can be widely used in varying types of stem cell research.

5.3 Aims

In this chapter, I aimed to:

1. establish tumoursphere assays from Malignant Rhabdoid Tumours (MRT) to be utilised for identification of self-renewing cells in MRT
2. evaluate stem cell activity in Malignant Rhabdoid Tumours (MRT) cell lines

5.4 Results

5.4.1 Optimisation of tumoursphere assay media composition for culturing adherent MRT cell lines

MRT cell lines are usually grown in adherent culture. This will limit the capacity to identify stem cell properties of these cell lines including self-renewal. As there is currently no publicly available protocol to culture MRT cell lines as tumourspheres, the technique and media condition that are commonly used to culture neurospheres were adapted for this project (Louis and Reynolds, 2009). To establish the tumoursphere condition for MRT, two MRT cell lines that were available at that time (A204 and G401) were cultured on two types of media; homemade media and commercial media, StemXVivo serum-free media from R&D systems which acted as a control. The homemade media was made up from 0.4% BSA, 5 µg/ml Insulin, 1% PenStrep, 1% B27 supplement, 20 ng/ml bFGF and 20 ng/ml EGF in DMEM/F12 medium plus Glutamax. The tumourspheres were allowed to form for 9 days and images were taken every three days using EVOS Cell Imaging microscope (Life Technology).

Overall, there was no statistical difference in the number of tumoursphere between two types of culture media at specific time points, for A204 and G401 cell lines (Figure 5.1,Table 5.1, Figure 5.2). Notably, the number of tumoursphere derived from A204 was significantly increased between day 6 and 9 at a density of 4000 cells per well in homemade media (Figure 5.1 and Figure 5.2). There was no significant increase in the number of tumourspheres in commercial media. Notably, only 20 tumourspheres were counted on day 9 in commercial media as many spheres exceeded the appropriate size for tumoursphere which is no smaller than 50 µm and no larger than 200 µm. This is probably due to the fact the cells proliferated better on 3D Matrigel culture (commercial) in comparison to 2D culture (homemade). The shape of tumourspheres cultured in commercial media was more defined as the cells grew in a tight cluster (Figure 5.2 and Figure 5.3).

For the G401 cell line, the number of tumoursphere was statistically different as measured between day 6 and 9 for homemade media ($p = 0.0248$). The number of tumourspheres increased from 8 to 25 (Figure 5.1 and Figure 5.3). There were marginal differences in the number of tumourspheres on day 6 between a starting density of 4000

and 8000 which recorded for 11 and 8 tumourspheres respectively. In general, the number of tumourspheres was similar between commercial and homemade media suggesting the homemade media can be used for culturing tumoursphere.

Notably, the number of A204 viable cells measured using trypan blue staining on day 9 also increased in homemade culture, as the plating cell density increased. This increase was also seen in the G401 cell line, with the exception of an initial plating cell density of 4000 which recorded a cell count of more than 8000 on day 9 (383000 for 4000 cell density vs 344000 cells for 8000 cell density). The cell count in commercial media could not be measured as the tumourspheres were cultured on sticky methylcellulose which was hard to dissolve in PBS. Overall, although the A204 cell line recorded more cell viability than G401 cell line throughout 9 days of culturing, more tumourspheres were observed with less single cells in G401 cell line compared to A204 cell line. For the future experiment (detailed in Chapter 6), homemade media was used to culture tumoursphere as it was more cost-effective and allows the measurement of viable cells as this could not be achieved when using commercial media. More importantly, tumoursphere forming efficiency measured in this media was almost comparable with commercial media. The culture media was slightly modified with the addition of 4 µg/ml Heparin and 0.5 µg/ml Hydrocortisone. Heparin was added as it helps to stabilise the binding of FGF to its receptor, while hydrocortisone is known to improve cell proliferation (Weiswald et al., 2015).

		Number of viable cells		Number of tumourspheres	
Cell line	Day	Commercial	Homemade	Commercial	Homemade
A204	0	2000	2000	0	0
	6	NA	NA	6	3
	9	NA	244000	21	15
	0	4000	4000	0	0
	6	NA	NA	10	6
	9	NA	586000	25	23
	0	8000	8000	0	0
	6	NA	NA	21	18
	9	NA	751000	20	27
G401	0	2000	2000	0	0
	6	NA	NA	2	5
	9	NA	154000	7	9
	0	4000	4000	0	0
	6	NA	NA	7	11
	9	NA	383000	13	21
	0	8000	8000	0	0
	6	NA	NA	8	8
	9	NA	344000	20	25

Table 5.1 ***Average number of tumourspheres for two MRT cell lines cultured in two different tumoursphere media (n= 2).***

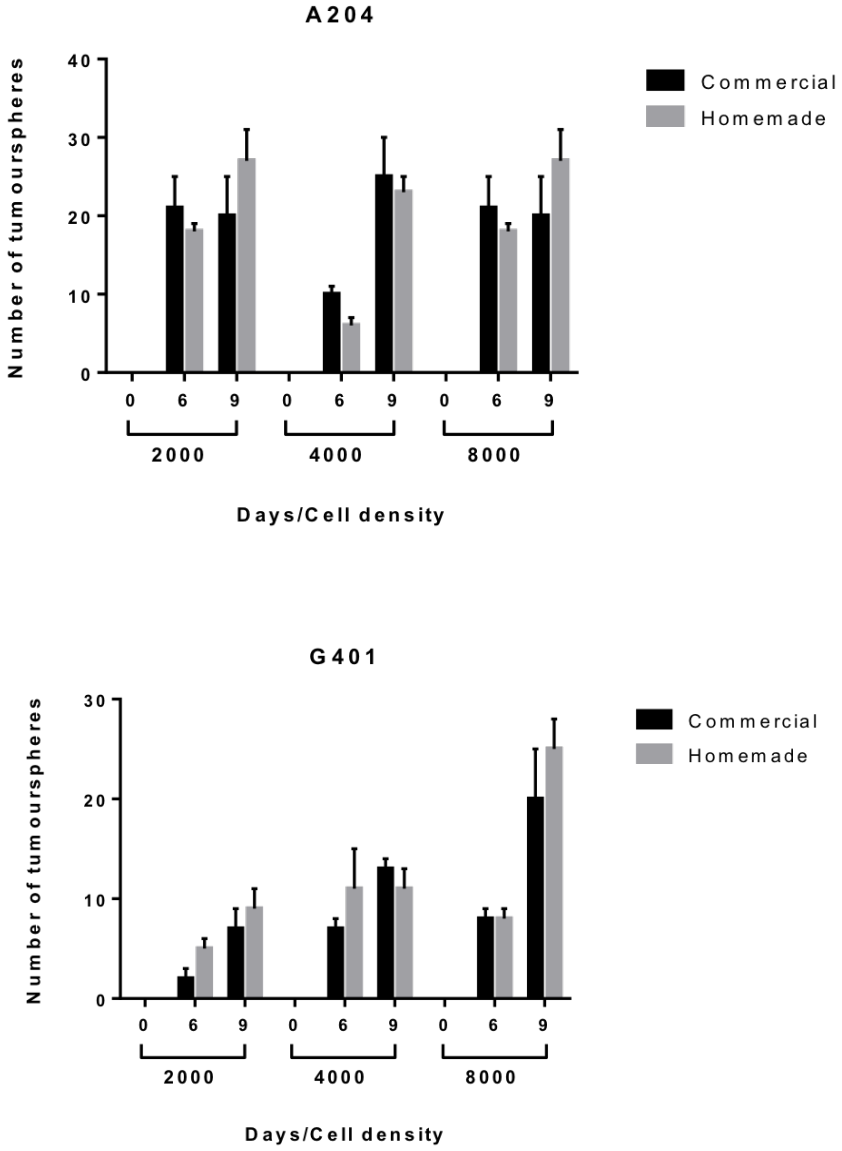

Figure 5.1 ***Culturing tumourspheres from MRT cell lines in two tumoursphere culture medias****. The homemade media was adapted from neurosphere assay with modification and addition of reagent to improve the tumoursphere formation. Adherent MRT cells were dissociated into single cells and seeded at 2000, 4000 and 8000 cell density per well. Bar graph showing the number of tumourspheres measured on day 0,6, and 9 for both media. There was no statistically different in the number of tumourspheres between two cultures at all initial cell seeding density.*

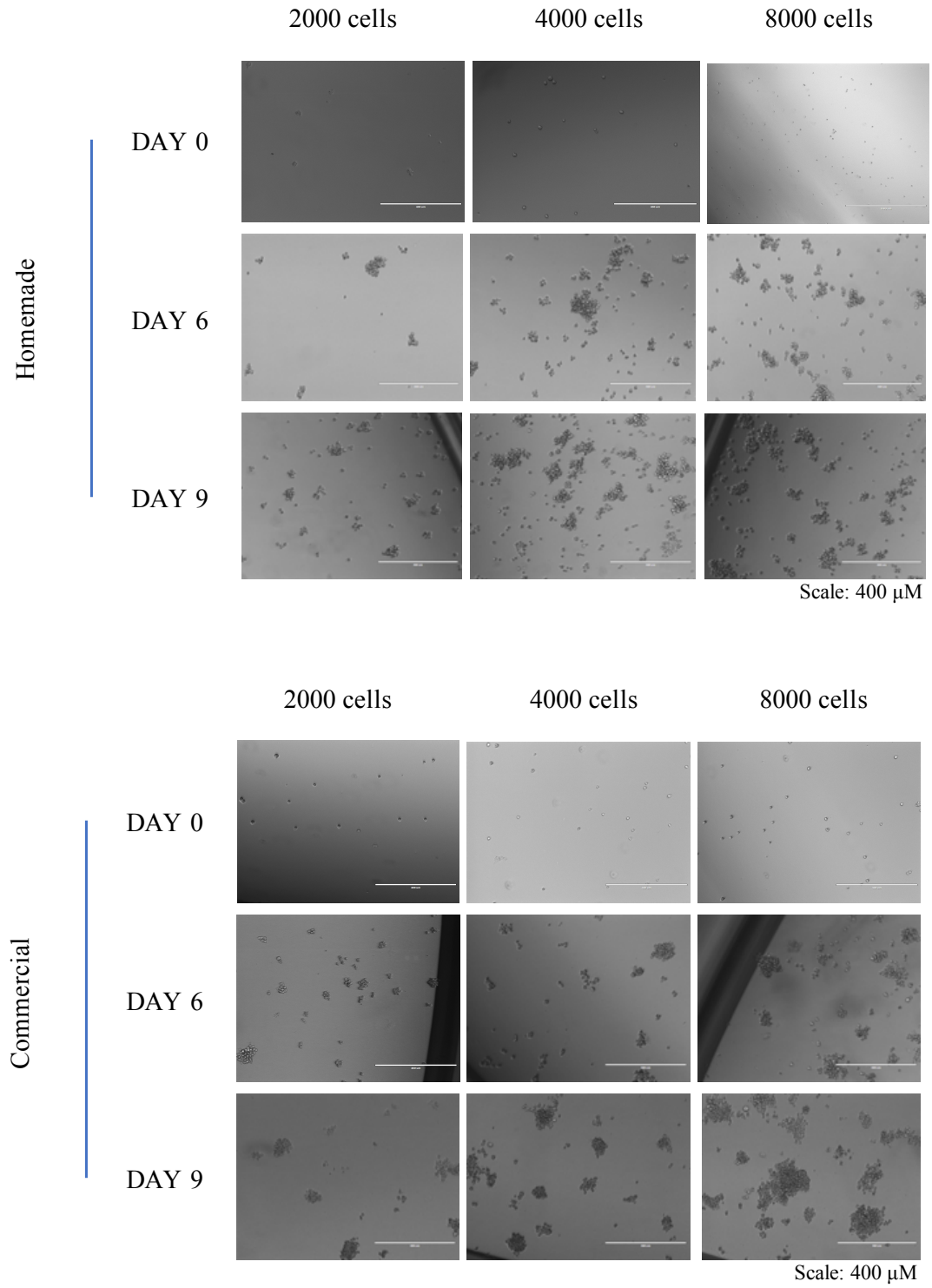

Figure 5.2 ***Phase contrast of tumourspheres from A204 cell lines in two different culture media; homemade and commercial.*** *The cells were seeded at 2000, 4000 and 8000 per well. The number of tumourspheres was counted on day 0, 6 and 9. The images were taken using EVOS microscope. Row represents day of counting the tumourspheres whereas column represent starting initial density of cells in culture.*

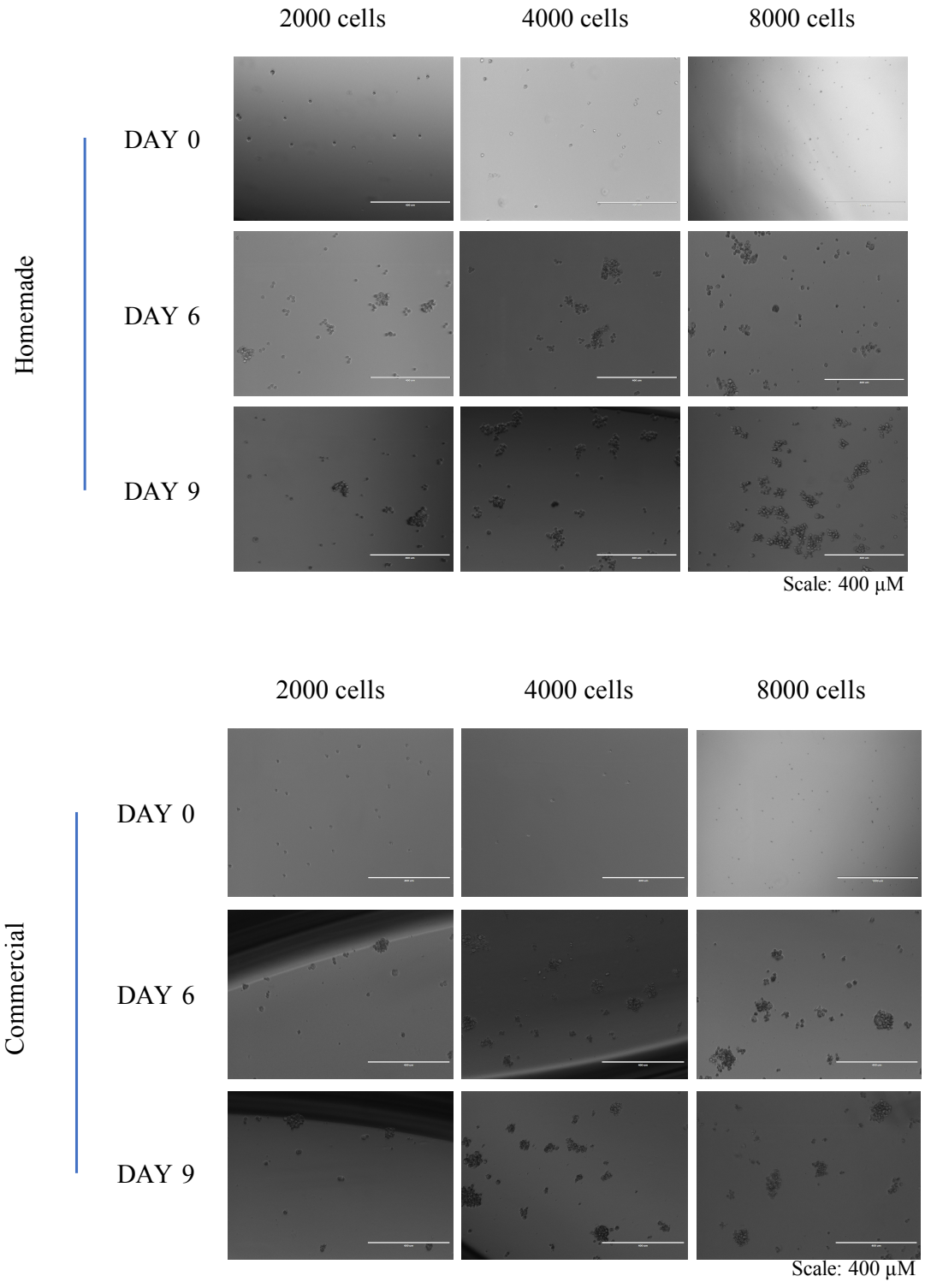

Figure 5.3 ***Example Phase contrast of tumourspheres from G401 cell lines in two different culture media: homemade and commercial.*** *The cells were seeded at 2000, 4000 and 8000 per well. The number of tumourspheres was counted on day 0, 6 and 9. The images were taken using EVOS microscope. Row represents day of counting the tumourspheres whereas column represent starting initial density of cells in culture.*

5.4.2 Cell density and surface area of the culture: Critical parameters when designing tumoursphere assay

Experimental procedures for culturing tumoursphere have undergone a lot of modifications over the years and might be varied between research groups. The modifications include the medium composition, cell density, surface area of culture dish as well as culture length. Amongst all, cell density is the most critical element for the development of clonality of tumoursphere (Pastrana et al., 2011). Since the final readouts of tumoursphere assay are number and size of tumoursphere, it is critical to ensure that the tumourspheres are formed from clonal expansion (proliferation) and not due to cell aggregation. Ideally, each of the tumourspheres is derived from a single cell to become a clone. To examine the ideal cell density for the formation of tumoursphere from MRT cell lines, a range of cell densities were tested in a different surface area of culture plate/flask. Initially, MRT cells were grown in the non-adherent medium at a density of 500 to 8000 cells per ml in a 24-well plate (Figure 5.2 and Figure 5.3). However, the number of tumourspheres obtained at a high cell density was hard to determine due to the fusion of tumourspheres hence false positive results. Likewise, culturing the cells at low density was also problematic as a small number of tumourspheres were observed in the well and the size of clusters of cells did not meet the standard. For tumoursphere assay experiments, the cluster of cells was considered as a tumoursphere if there were at least 10 cells contained within it and the size is no smaller than 50 μM and no larger than 200 μM.

To identify if an increase in surface area of cell dish could improve the number of tumoursphere and avert the problem with tumoursphere fusion, I tried culturing MRT cells in two plating formats; 6-well and T-25 flask for three passages. The number of tumourspheres calculated on day 9 for each passage in a 6-well and T-25 flask was tabulated in Table 5.2. The number of tumourspheres was increased over subsequent passages in both plating formats suggesting a selective increase in self-renewal capacity of MRT cells or at least a greater proportion of spheres initiating cells in culture. The number of tumourspheres was also presented in bar graphs (Figure 5.4).

High-density seeded cultures produced high numbers of tumourspheres when culturing in these two formats (Figure 5.4). Culturing cells in T25 is more practical than plate format as the movement of the plate leads to the cells aggregations either at the centre of

the plate or attached to the wall despite the cells being grown in a low attachment plate. The spheres forming efficiency was significantly increased between passages for both cell lines as indicated by an increase in the number of tumoursphere when culturing in a T25 flask (Figure 5.4a). In A204 cells culture, the formation of tumourspheres was increased by 2 times between passage 0 and 1, and the production of tumourspheres 5 times more between passage 1 and 2 (Figure 5.4a and Table 5.2). Likewise, the number of tumoursphere derived from G401 cells in passage 2 was 5 times higher than that of passage 1 (Figure 5.4a). These results indicate high surface area of T25 flask provided more room for cells to continue to expand without producing cell fusions or aggregations. Nevertheless, production of tumourspheres is also reasonably high in 6-well plates (Figure 5.4c) and the number of tumourspheres continued to increase by 3.4- and 2.8-times between passage 1-2 for A204 and G401 respectively (Figure 5.4c).

In short, high numbers of tumourspheres were achieved when culturing in T25 flask format and the problem with cell aggregation can be avoided if culturing using this format. However, it requires more volume of media than a 6-well plate. On the other hand, the culture of tumoursphere in a 6-well plate can be problematic due to cell aggregation if initial seeding density is high. However, the problem was not pronounced at an initial seeding density of 8000 cells. The presence of tumourspheres can be distinguished from the irregular clump of cells by careful interpretation of size and shape of spheres. The size of tumourspheres is no smaller than 50 μM and no larger than 200 μM and the shape is nearly round.

(a)

Passage	Number of tumoursphere per 10,000 cells			
	A204		G401	
	Replicate 1	Replicate 2	Replicate 1	Replicate 2
0	8	12	6	5
1	24	32	35	26
2	156	174	166	159

(b)

Passage	Number of tumoursphere per 8,000 cells			
	A204		G401	
	Replicate 1	Replicate 2	Replicate 1	Replicate 2
0	7	10	11	14
1	19	15	23	28
2	65	57	77	64

Table 5.2 ***Number of tumourspheres per initial cell density of 10,000 and 8,000 counted in (a) T25 flask and (b) 6-well plate respectively****. The tumourspheres were counted from two replicates.*

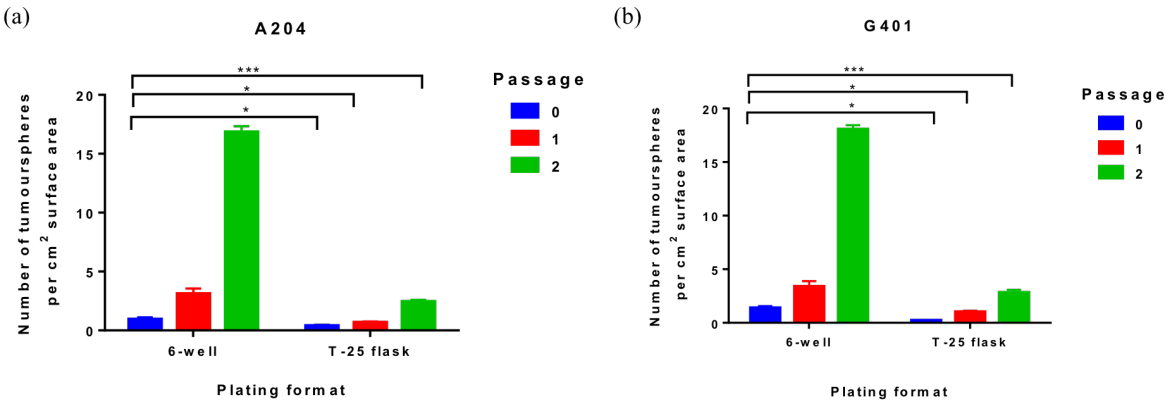

Figure 5.4 ***Tumoursphere formation in T25 flask and 6-well plate.*** *(a) Significant increase in the number of tumourspheres was observed in two MRT cell lines in 3 passages when culturing in T25 flask format. The production of tumourspheres was higher in passage 2 (b) Number of tumoursphere also increased in passage 1 for 6-well plate, but this did not reach statistical significance for both cell lines. Significant increase in number of tumourspheres was observed between passage 1 and 2. The results are shown as means ± SEM of two independent experiments and the significance was determined by unpaired student's t-test (* p< 0.05, ** p<0.01, *** p<0.001, vs plating format in appropriate culture).*

5.4.3 Characterisation of stem cell potential of MRT cell lines

The tumoursphere assay was designed in this study to characterise and define the stem cell potential of MRT cell lines such as self-renewal. This assay will be used in limiting dilution assay (Chapter 6). Ideally, the cells should be plated at an extremely low cell density to investigate self-renewal potential of cells. An attempt was made to culture the MRT cells by plating a single cell per well in 96-well plate by FACS sorting, however, the experiment was not successful. There was no tumoursphere observed when cultured under these conditions. Hence, the cell density was increased to identify minimum cell density that is required to form tumoursphere. MRT cells were plated at 10, 50, 100 per well in triplicate. Three-weeks after FACS sorting in 96-well plate, the tumourspheres were observed in the 96-well plate when cultured under this condition, illustrating that minimum of 10 cells is required to form tumourspheres from MRT cells.

Primary MRT have been shown to express stem cell markers such as SOX2, NANOG, OCT4 and Nestin as determined by immunohistochemistry, genomic and gene expression analyses (Deisch et al., 2011, Venneti et al., 2011b). Therefore, it is of interest to examine if an increase in the number of tumourspheres is correlated with an increase in expression of stem cell markers. To this end, RNA was extracted from the tumourspheres at days 0, 3 and 9. However, due to low numbers of spheres obtained on each harvesting day, it was impossible to perform qPCR to examine the expression of self-renewal genes. The experiment would have to be repeated in the future to identify mechanisms that underly the increase in tumoursphere formation efficiency.

Additionally, the serial passaging assay was performed to examine the self-renewal potential of cells and sphere-forming capacity. The primary tumourspheres were dissociated into a single cell and 8000 cells were plated into a non-adherent medium. After 9 days in culture, the secondary tumourspheres were dissociated and 8000 cells were added to the well for tertiary tumoursphere formation. Of note, MRT cell lines can be passaged up to 4 times (the experiment was purposely stopped at passage 4) (Figure 5.5). The number of tumourspheres was counted on day 9 for passage 1 to 3 and day 5 for passage 4. Of note, the number of tumourspheres was greatly increased accompanied by bigger size of tumoursphere (within the range of preferable diameter) after passage 2 for G401 and A204 cell line cultured in homemade media (Figure 5.5a and b). Interestingly over passages, the time for single cells to form tumourspheres was decreased. For instance, big tumourspheres were observed in culture at passage 4 as early as day 3 but the measurement was performed on day 5.

In theory, during the passaging of the tumourspheres, the majority of the cells do not have the capacity to proliferate and therefore die. A small portion of surviving cells can then expand the progeny and form tumoursphere. I hypothesised that the number of cells that survived and can form tumourspheres increases with passage number. To test the hypothesis, the fold expansion of surviving cells that generated tumourspheres in culture was measured using this formula; initial cell density/end cell density (Deleyrolle et al., 2011). In this study, fold expansion increased over passage time and this finding indicates that tumourspheres possess the self-renewal capacity and display a significant increase in proliferation potential (a characteristic of stem cells) in MRT cells (Figure 5.5c).

Altogether, increase in the number of tumourspheres and the ability of the cells to form tumourspheres in a shorter time (day 3 in passage 4) as opposed to day 9 for earlier passages illustrates an increase in self-renewal capacity of the MRT cells. The number of viable cells was also increased over four passages indicating that tumourspheres possess the self-renewal and proliferation capacity to form clonal.

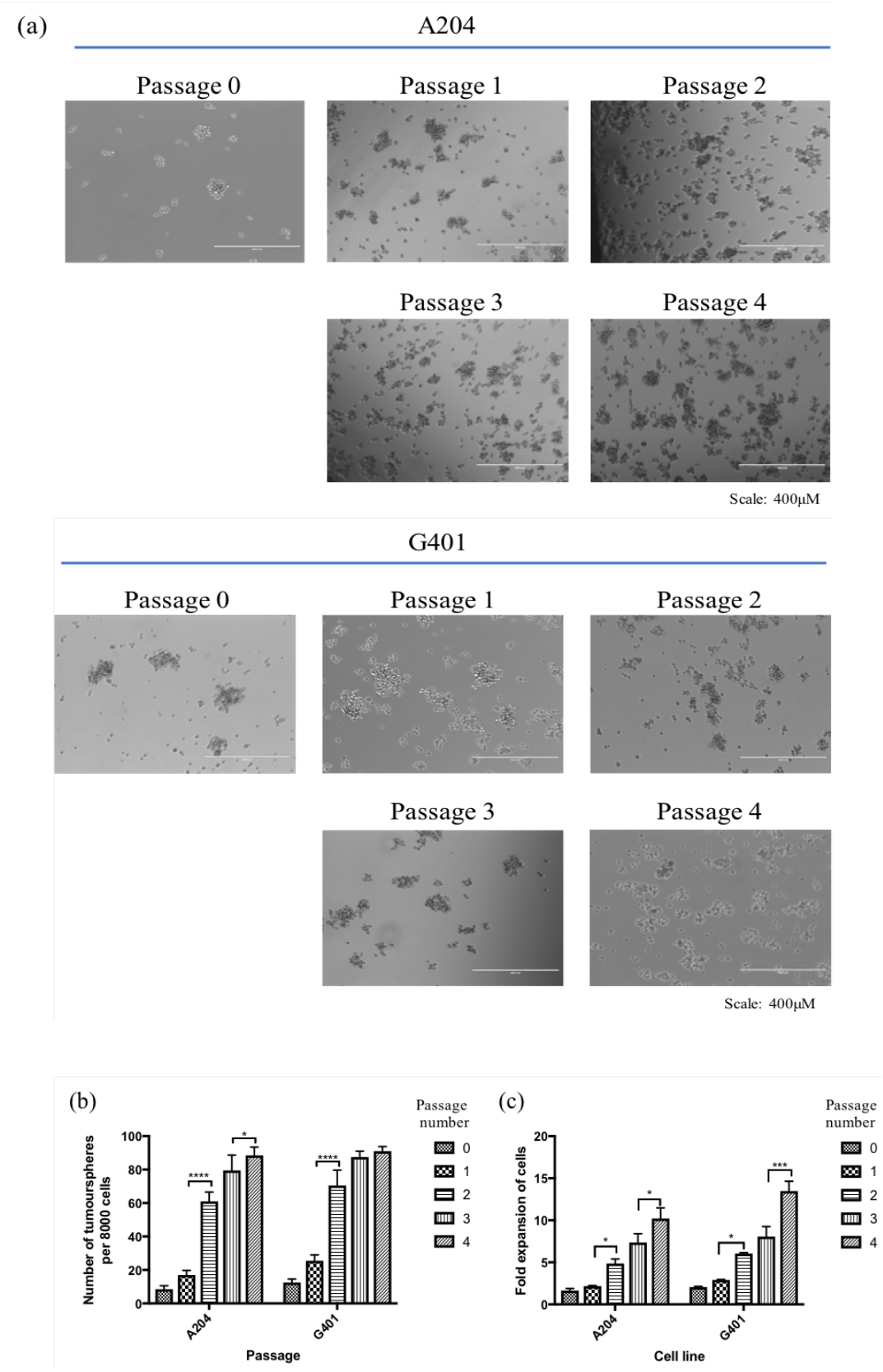

Figure 5.5 ***Increase in self-renewal capacity observed in MRT cell lines is correlated with increase in number of tumourspheres over passages****. (a) Cell images taken on day 9 (except day 5 for P4) showed number and size of tumourspheres. (b) Self-renewal*

capacity increased over passages as indicated by the number of tumourspheres derived from 8000 cells. (c) Fold expansion of cells showed increased cell number (between day 5/9 with day 0) and this finding demonstrated proliferation capacity of tumoursphere. The results are shown as means ± SEM of three individual experiments and the significance was determined by unpaired student's t-test (p< 0.05, ** p<0.01, *** p<0.001, ****p<0.0001 vs earlier passage (i.e passage 2 vs passage 1).*

5.5 Discussion

5.5.1 Practicality of tumoursphere assay as a tool to assess self-renewal capacity of cells

Several immunohistochemistry studies of primary MRT showed that MRT exhibit stem cells markers such as OCT4, NANOG, SOX2 and others (Deisch et al., 2011, Venneti et al., 2011b). Transcriptomic analysis of MRT primary and cells showed upregulation of stem cell self-renewal genes such as *BCL6*, *BMI1, GLI12* etc (PBTG, unpublished). The discovery of these stem cell-associated genes in the MRT primary and cells has led me to the hypothesis that the aggressiveness of MRT is linked to deregulation of stem cell properties such as self-renewal and pluripotency. Investigation of this hypothesis required a method to understand if MRT possess self-renewal capacity and to what extent self-renewal in MRT cells can drive tumourigenesis. Here, the use of the classic tumoursphere assay or spheroid formation assay to assess the ability of MRT cells to self-renew and pluripotent was reported. This technique has been shown to be practical for stem cells and cancer stem cell studies and is widely used in other types of human cancers including leukaemia, breast cancer, brain tumour and others (Ponti et al., 2005, Dontu et al., 2003, Ignatova et al., 2002, Singh et al., 2004). The majority of published studies utilise this method to study cancer stem cells within tumours which commonly rely on specific surface markers to isolate the population of cells of interest. Through a series of experiments presented in this chapter, I have demonstrated that the tumoursphere assay can be used as a MRT self-renewal assay thus allowing the assessment of shRNA and inhibitor that target specific self-renewal pathway in limiting dilution and clonal assay format (Chapter 6).

Although tumourspheres can be generated from MRT cell lines using homemade media and can be grown on non-methylcellulose coated wells, there are a few aspects that need to be considered when using this culture system. Firstly, the size of tumourspheres is inconsistent among different cell lines and there are non-uniform criteria for the size of tumoursphere (Johnson et al., 2013). As this is the first study to culture tumoursphere from MRT cell lines, the size range was determined based on an average of tumoursphere across all cell lines and from previously established protocols (Reynolds and Weiss, 1992, Shaheen et al., 2016). Furthermore, the size can reflect the responsiveness of the cells to growth factor and stage of proliferation/differentiation of parental tumourspheres

(Deleyrolle et al., 2011). This observation is common in the highly heterogeneous tumour as the mixed population of cells at several stages of development can give rise to a different size of tumoursphere. The problem can be solved by growing the cells on an adherent format and by assessing the tumoursphere behaviour based on bulk population analysis (Deleyrolle et al., 2011). Moreover, other confounding factors such as cells that are used to generate tumourspheres should be put into consideration (i.e immediately after thawing vs a week after thawing) as it will interfere with efficiency of the cells to form tumourspheres and growth rate of tumourspheres.

MRT are highly heterogeneous tumours and may be considered as "stem-like" tumours due to the expression of stem cells markers such as NANOG, SOX2, OCT3/4 etc. They possess the ability to differentiate along to multiple stem cell lineages such as adipocytes (Deisch et al., 2011, Okuno et al., 2010, Venneti et al., 2011b, Caramel et al., 2008). Therefore, there is a possibility that a heterogeneous population of cells are composed of cells with (stem-like) and without (progenitor cells) self-renewal potential. The progenitor cells may still have limited proliferation capacity to form tumourspheres, hence leading to underestimation of the number of tumourspheres in culture. This problem, however, can be overcome through serial passaging of tumourspheres as theoretically, only self-renewing cells can form tumoursphere where the other cells cannot. Based on retrospective studies of neurospheres formation, only 6% of all cells can be passaged more than 7 times while the rest of the cells cannot, thus suggesting that a small number of cells have increased the self-renewal capacity (Louis et al., 2008).

Overall, tumourspheres were successfully derived from MRT cell lines grown in homemade media *in vitro*. This assay can be used for self-renewal identification and analysis as serial passaging of tumourspheres demonstrated the increased ability of cells to form tumourspheres. Though more advanced studies such as qPCR, immunofluorescence or sequencing should be done to check the expansion in the expression of self-renewal genes over passing time, serial passaging of tumoursphere assay is able to illustrate a selective increase of self-renewal ability. To establish stem cell properties of MRT, genome-wide studies such as RNA-seq should be performed as it will allow selection of particular genes that govern self-renewal in MRT.

Chapter 6 Therapeutic targeting of the self-renewal machinery as a novel Malignant Rhabdoid Tumour cancer therapy strategy

6.1 Summary

Malignant Rhabdoid Tumours (MRT) are rare paediatric brain tumours caused by mutation of *SMARCB1* which encodes for chromatin remodelling protein (Versteege et al., 2002, Biegel et al., 2000, Roberts and Biegel, 2009). MRT present a challenge for clinical management due to the early onset and highly aggressive nature. Despite intensive multimodal therapy for MRT, overall survival rates are still poor (Reinhard et al., 2008). There is a lack of curative therapeutic interventions available for these patients. To identify potential therapeutic targets for MRT, the mechanisms that may contribute towards MRT aggressiveness were explored in this project. Gene enrichment analysis (GSEA) of integrated functional genomics with primary and cell model MRT identifies stemness as a "less-well evidenced" *SMARCB1*-dependent or MRT tumourigenesis-related pathway as this theme has not previously been studied in detail for MRT. To examine to what extent mutation in stemness/self-renewal pathways/genes can contribute to MRT tumourigenesis, the genes which are highly expressed in MRT and whose expression is *SMARCB1*-dependent were identified by cross-referencing the curated stemness/self-renewal genes with transcriptome profiling of MRT primary and cell lines along with whole-genome CRISPR/Cas9 screening of MRT cell lines (details of the method are described in Chapter 2). This analysis revealed that of 54 curated stemness/self-renewal genes, *BMI1* is highly expressed in primary MRT and its expression is downregulated upon *SMARCB1*-reexpression in MRT cells illustrating its *SMARCB1* dependency. *BMI1* plays a role in the self-renewal machinery for both stem cells and cancer stem cells (Bhattacharya et al., 2015). The function of BMI1 was studied using shRNA and a small molecular inhibitor (PTC209). Knockdown of *BMI1* using shRNA or PTC209 strongly impairs MRT cell growth, induces apoptosis and cell senescence and provokes cell cycle arrest. In addition, PTC209 treatment caused impairment of self-renewal in MRT cells. In short, targeting *BMI1* offers a new strategy for therapeutic targeting in MRT.

6.2 Introduction

6.2.1 Malignant Rhabdoid Tumour (MRT) aggressiveness: potentially linked to stem cell characteristics of tumour

Malignant Rhabdoid Tumours (MRT) are rare, early onset tumours with a median age of diagnosis of ~18 months (Benesch et al., 2014, Varambally et al., 2002). The young age of patients at the time of diagnosis and the aggressive behaviour of the disease provides a real challenge for treatment of the patients. The aggressive behaviour of the malignancy is evidenced by poor patient survival and early onset of disease. The overall survival is less than 25% in infants (≤10 months) and young patients (≤24 months) (Bourdeaut et al., 2008). MRT present immune markers from multiple lineages exhibiting a teratoid phenotype and contains cells with heterogeneous morphology within the same tumour leading to speculation that MRT may arise from multipotent stem cells (Gadd et al., 2010, Deisch et al., 2011, Caramel et al., 2008). Stem-like characteristics of MRT were demonstrated by an immunohistochemistry study showing that MRT primary tumours expressed important stem cell markers such as KLF4, SOX2, NANOG, Mushashi-1 and SALL4 (Deisch et al., 2011). High expression of *EZH2*, a factor that regulates cell proliferation and differentiation has also been found in MRT. Gene expression analysis of primary MRT and *SMARCB1*-deficient mouse embryonic fibroblast (MEF) tumours from a conditional mouse model showed that *SMARCB1* loss caused upregulation of *EZH2* expression which in turn led to increased expression of stem cell-associated genes such as *DNMT3A*, *FGFR1*, *JARID2*, *POU5F1,* etc. (Wilson et al., 2010a). However, the expression of these genes was downregulated in *SMARCB1* and *EZH2* double conditional knockdown in MEF mouse model. Furthermore, recent studies suggest that *SMARCB1* mediates MRT tumourigenesis dependency on *EZH2* (Knutson et al., 2013, Alimova et al., 2012). Their studies showed that inhibition of EZH2 using siRNA and chemical inhibitors suppressed tumour self-renewal and impaired MRT tumour growth. Collectively, their observations suggested the role of *SMARCB1* in stem cell regulation and when mutated can cause the aberrant function of self-renewal and pluripotency machinery.

6.2.2 Role of BMI1 and the impact of its negative regulation in cancer development

The B-cell specific Moloney murine leukaemia virus integration site 1 (*BMI1)* gene in humans is located on the short arm of chromosome 10 (10p11.23) and the protein is universally expressed in almost all tissues, with a tendency to be highly expressed in the brain, kidney, bone marrow, placenta, lungs, blood and oesophagus (Siddique and Saleem, 2012). Studies have demonstrated the role of *BMI1* in a various cellular process such as proliferation, senescence, differentiation and also contributes to the embryonic development and stem cell self-renewal machinery (Cao et al., 2011, Park et al., 2003) (details in Chapter 1). *BMI1* has been shown to exert its role in cell proliferation and senescence by acting as a transcriptional repressor at the INK4a-Arf locus (Jacobs et al., 1999a). An experimental study showed that knockdown of *BMI1* in mouse embryonic fibroblasts (MEF) impaired the cell cycle entry to S phase and led to premature cell senescence. Western blot analysis of the tumour cells obtained from this *Bmi1*-deficient MEF demonstrated upregulation of p19 (Arf) and p16 protein expression. *BMI1* also has the capacity to block cell senescence and immortalisation as overexpression of *BMI1* has been shown to activate human telomerase reverse transcriptase (hTERT) transcription and induction of telomerase activity (Dimri et al., 2002). *BMI1* is also required for self-renewal and maintenance of post-natal haematopoiesis (Park et al., 2003) and neural stem cells (NSC) in the central nervous system and peripheral nervous systems (Molofsky et al., 2005). The number of stem cells present was reported as normal as was cell differentiation in each tissue obtained from $Bmi1^{-/-}$ mice (at time of birth), however, a self-renewal defect was apparent in post-natal $Bmi1^{-/-}$ mice as the number of stem cells was reduced by early adulthood.

Overexpression of *BMI1* and its role in oncogenesis has been reported in several types of human cancers including cervical, breast and ovarian cancers (Gavrilescu et al., 2012). Some studies have also shown a positive correlation between overexpression of *BMI1* with aggressive disease progression and poor prognosis. For instance, overexpression of *BMI1* was reported in 38.7% (29/75) cases of nasopharyngeal carcinoma, in which the 5 year OS was higher in the *BMI1* control group patients (normal expression of *BMI1*) than the *BMI1* overexpression patients (84.2% vs.47.6%)(Song et al., 2006). Similarly, survival analysis of patients with hepatocellular carcinoma also demonstrated short OS in patients with *BMI1* overexpression relative to *BMI1* low expression ($p < 0.0001$) (Zhai

et al., 2016). Furthermore, Yang et al. (2010) also reported a correlation between overexpression of *BMI1* with survival of 179 patients presenting with ovarian carcinoma. The survival of patients with high *BMI1* expression was greatly reduced (mean 49 months) compared to patients with low *BMI1* expression (mean 100 months). Overexpression of *BMI1* has also been associated with paediatric brain tumours (Farivar et al., 2013). qPCR analysis of a cohort of 59 paediatric brain tumours including 20% medulloblastoma, 34% astrocytomas, 28% ependymomas, and 18% others (Primitive Neuro Ectodermal Tumours (PNET), gangliogliomas, and oligodendrogliomas) showed *BMI1* gene expression was 4.85 times higher than normal brain tissue. The univariate survival analysis demonstrated that mean survival time for patients with high *BMI1* expression was 20.3 months compared to 39.6 months in patients with low *BMI1* expression. Furthermore, *BMI1* high expression provided a significant independent prognostic factor determined by multivariate Cox regression analysis.

Altogether, *BMI1* exerts its role in cellular activities including cell proliferation, senescence and self-renewal through transcriptional repression of the Ink4a/Arf locus. In summary, overexpression of *BMI1* has been implicated in the development of various cancers and confers poor disease prognosis.

6.2.3 Specific targeting of BMI1 using PTC209

Recently, a small inhibitor molecule PTC209 that decreases the translation of BMI1, was developed using a drug discovery platform technology called GEMS (Gene Expression Modulation by Small Molecule) by Kreso et al. (2014) and PTC Therapeutics company. In theory, the *BMI1* 3' UTR contains multiple A-U rich elements that significantly upregulate expression of the reporter gene whilst its 5' UTR consists of a strong IRES activity. Therefore, this high throughput technology was employed to selectively identify the compound that could inhibit both 3' and 5' UTR mediated *BMI1* reporter expression.

Evidence has shown that small population of cells within the primary colorectal tumours have the capacity to initiate new tumours and sustain the formation of tumours in transplant experiments. These cells are known as cancer-initiating cells (CICs) and possess the stemness properties including self-renewal. Kreso et al. (2014) found that those CICs functions are dependent on *BMI1*, a self-renewal gene. Thus, the efficacy of PTC209 in inhibiting BMI1 expression was studied in CICs cell lines. They showed that

PTC209 can effectively inhibit expression of endogenous BMI1 in human colorectal HCT116 and human fibrosarcoma HT1080 tumour cells in a dose-dependent manner. Incubation of HEK293 and HT1080 cells with PTC209 overnight and for 48 hours respectively, had no effect upon cell growth or viability. Downregulation of BMI1 using PTC209 inhibits the self-renewal capacity of colorectal cancer initiating cells determined by limiting dilution assay (LDA) *in-vitro* and impaired the ability of these cells to form tumour *in-vivo* long-term, reducing the tumour burden illustrating the potential of targeting self-renewal regulator as means of therapeutic intervention.

The inhibitor has also been tested in other types of cancer such as acute myeloid leukaemia (AML) (Nishida et al., 2015), biliary tract cancer (Mayr et al., 2016) and multiple myeloma (Bolomsky et al., 2016) which also demonstrate similar findings. These authors showed that inhibition of BMI1 using PTC209 reduced cell growth, induced cell apoptosis, senescence and self-renewal defects. Therefore, the therapeutic targeting of BMI1, if achieved, would provide an attractive strategy for the development of cancer therapies for MRT.

This chapter is focused upon exploiting the innate stem cell characteristics of MRT using bioinformatics analysis (detailed in Chapter 2) to identify potential self-renewal genes which are active in MRT and whose activity is *SMARCB1* dependent. Also, in this study, the expression of *BMI1* and the effect of a BMI1 inhibitor, PTC209 in MRT were investigated.

6.3 Aims

In this chapter, I aimed to:

3. Identify self-renewal genes that are active and whose activity is *SMARCB1*-dependent
4. Investigate the effect of targeting BMI1 and how its expression changes following treatment with shRNA and the small molecular inhibitor, PTC209
5. Understand the role of *BMI1* as self-renewal gene in MRT tumourigenesis

6.4 Results

6.4.1 Bioinformatic analysis of candidate self-renewal/stemness genes that drive tumourigenesis in SMARCB1-deficient MRT

Previous studies on MRT presented the consequence of *SMARCB1* loss which included disruption to cycle cell regulation (Betz et al., 2002), aberrant activation of the sonic hedgehog (Shh)-Gli pathway (Jagani et al., 2010), Wnt signalling pathway (Mora-Blanco et al., 2014) etc. Work within my group was performed to further examine other pathways that are deregulated following *SMARCB1* loss and are implicated in *SMARCB1*-dependent tumourigenesis, pathway analysis was performed on RNA-seq data from *SMARCB1* re-expressing, and 5-aza treated MRT cells using Ingenuity (IPA) canonical and upstream regulator analysis. This identifies key regulatory effectors likely to produce the observed changes in expression and Gene Enrichment Analysis (GSEA) using MSigDB libraries C2 (Curated), C3 (Motif), C6 (Oncogenic) and H (Hallmark). The outputs were manually characterised in curated pathway themes (Figure 6.1). Pathway analysis was also performed on CRISPR/Cas9 GeCKO screen data from MRT cell lines with and without *SMARCB1* using Model-based Analysis of Genome-wide CRISPR/Cas9 Knockout (MAGeCK) method. Differentially essential (DEss) genes were identified by comparing per-gene sgRNA abundance at time points across MRT cell lines. For instance, SMARCB1 Day7/14 vs Day0, control Day7/14 vs Day0, SMARCB1 vs control at Day7/14. Pathway analysis was then performed with the ranking and p-value calculated by MAGeCK using IPA analysis and GSEA analysis (MSigDB Hallmarks). To identify genes or pathways that have therapeutic potential to counteract MRT tumourigenesis, functional genomic cell lines and primary tumour data was integrated, and the genes/pathways were prioritized based on these criteria: expression/activation dependent on *SMARCB1* and/or 5-aza, characteristic of primary MRT and essential to cell fitness (GeCKO); preferably in a *SMARCB1*-dependent manner. The data that were functionally analysed using GSEA and IPA included whole genome CRISPR screen including all comparisons as above plus MRT vs MB Day14 (a GeCKO screen comparison of MRT to a panel of 4 medulloblastoma cell lines included as a cell type control), *SMARCB1* re-expression vs control, 5-aza vs control, primary MRT vs MB or ET (embryonic tumour). Pathway analysis of integrated data illustrates pathways that are *SMARCB1*-dependent or associated with MRT tumourigenesis (Paediatric Brain Tumour Group (PBTG) at Newcastle University, unpublished) including MYC/Let7 targets,

Interferon, PLK1, Polycomb (Kim and Roberts, 2014) (Figure 6.1). Amongst these, pathways that have not been recognised as *SMARCB1* related pathways such as stemness were also present in the analysis. Stemness can be defined as the potential of stem cell niches to possess pluripotency and undergo self-renewal and differentiation (Anton et al., 2007, Leychkis et al., 2009).

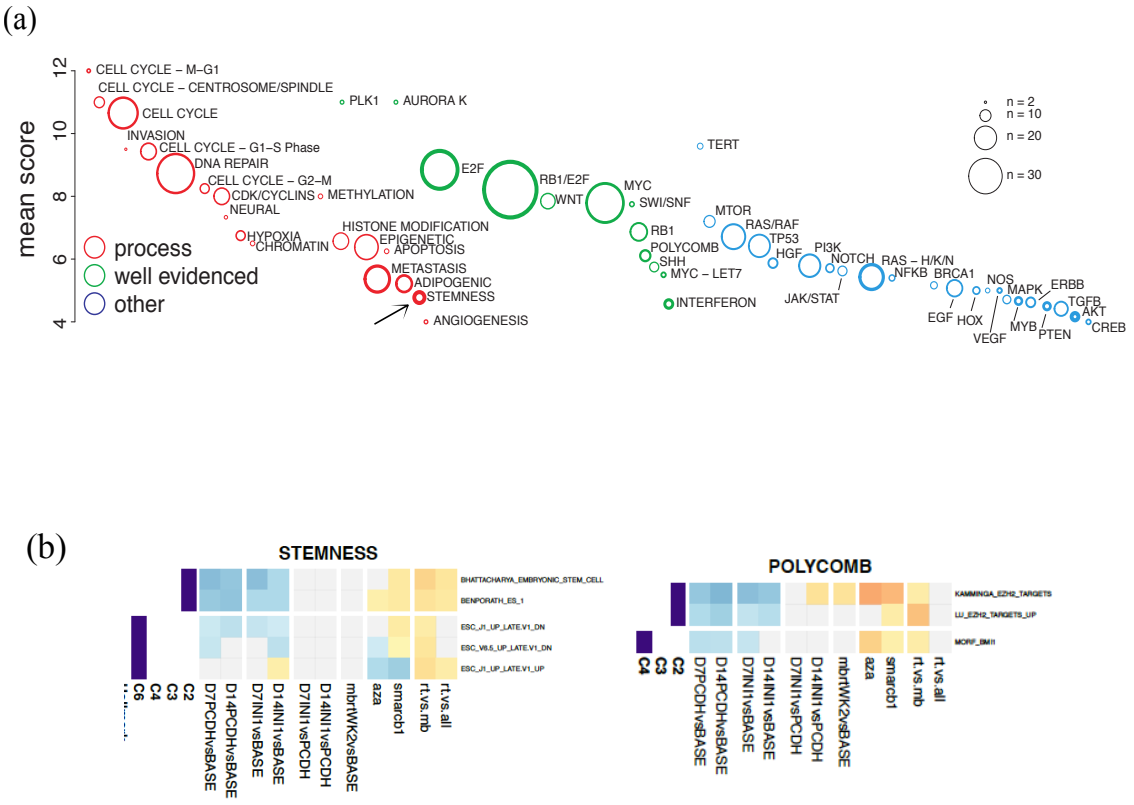

Figure 6.1 ***The multiplatform cross-referencing strategy to identify pathways with potential as therapeutic target to counteract MRT tumourigenesis****.(a) The bubble plot demonstrating the pathway themes that were ranked and prioritized by average score of constituent pathway analyses calculated by rational selection algorithm (strength of evidence. The themes were clustered as processes, those well evidence or poorly evidence to SMARCB1/MRT related pathways. The size of bubble represents number of pathway analyses. (b) Heatmap showing the stemness and polycomb pathways identified by cross-referencing with CRISPR GeCKo screening (D7/D14 Control vs Day 0, D7/D14 SMARCB1 vs Day 0, D7/D14 Control vs D7/D14 SMARCB1 & MRT vs MB Day14), model expression (5-aza vs control, SMARCB1 vs control) and primary expression*

analyses (Primary MRT vs MB, Primary MRT vs Embryonal). Row represents the top 3 events from MSigDB library or analysis type. The heatmaps are colored by normalized enrichment (GSEA) or z-activation score (IPA). Grey shows a non-significant score. Type indicates analysis: blue = GSEA, green = IPA, C2=curated gene sets (GSEA), C4=computational gene sets (GSEA), C6=Oncogenic signatures (GSEA), H=Hallmark gene sets, C=Canonical Pathways (IPA) and U=Upstream regulators (IPA). The figures were reproduced from PTBG (unpublished).

Integrated data analysis of cell line and primary MRT identified stemness as a potential therapeutic target with *SMARCB1*-dependent/related tumourigenesis. However, there has been no systematic genome-wide analysis of how this occurs and which self-renewal pathways are altered by *SMARCB1* mutation and contribute to tumourigenesis. To this end, I implemented a systems biology approach to analyse RNA-Seq data of primary and cell line model data provided by my group (unpublished) to identify the self-renewal/stemness pathways or genes directly affected by the loss of *SMARCB1*. The potential stemness/self-renewal genes were compiled through prior knowledge (canonical pathways and ontology (Kegg and gene ontology (GO)), IPA knowledgebase by searching genes that regulate "stemness", "self-renewal" and "pluripotency" pathways. The stemness/self-renewal genes were also manually profiled from the published literature (Ramalho-Santos et al., 2002, Koeva et al., 2011). The total number of genes that were profiled in this analysis was 210 genes. The stemness genes identified from the aforementioned analysis include *SOX2, POU5F1, TP53* etc while the self-renewal genes include *BMI1, ARID1A, BCL6, CD44,* etc. The pluripotency genes that were listed include *FOXO1, KLF4, SMARCA4* etc. A full list of genes is presented in Appendix 6.1.

To identify which stemness/self-renewal genes are functionally relevant to *SMARCB1*, I next performed integrated data analysis of custom stemness/self-renewal genes with RNA-seq data of primary and cell line MRT using R and IPA analysis. The RNA-seq data that underwent the analysis were; primary MRT (n = 23) vs MB (n = 228), *SMARCB1* re-expression vs control (PCDH) (n = 4), and ATRT (n = 10) vs ECRT (n = 13). Medulloblastoma (MB) was included as a comparison for embryonal tumours. Cross-referencing of stemness gene lists with RNA-seq data of MRT primary and *SMARCB1* re-expression cell model, and embryonal tumours revealed 54 genes that are functionally

relevant to *SMARCB1* expression (stemness genes = 30, self-renewal genes = 25, pluripotency genes = 9). The list of genes is tabulated in Appendix 6.2. The boxplot showing the representation of genes present in three analyses between stemness/self-renewal genes with embryonal tumours, primary MRT and *SMARCB1* re-expression cell models. Cross-referencing of stemness/self-renewal genes with MRT and MB indicates five stemness/self-renewal genes that are activated in these two types of embryonal tumours (Figure 6.2). Similarly, a gene list was also identified when cross-referencing stemness/self-renewal genes with RNAseq of MRT subgroups; ATRT and ECRT. However, of the five genes listed in MRT subgroups, there were only two genes that showed transcriptional activation in response to *SMARCB1* loss and re-expression in MRT cells; *JARID2* and *BMI1*. Expression of *BMI1* was upregulated in the absence of *SMARCB1* (represented by PCDH in boxplot analysis) and its expression was downregulated in response to *SMARCB1* re-expression in MRT cells (denoted by SMARCB1 boxplot). In contrast, the expression of *JARID2* was upregulated in *SMARCB1*-deficient MRT cells and upon restoration of *SMARCB1*, its expression was downregulated.

The genes were described as "functionally relevant to *SMARCB1*" if the gene showed transcriptional evidence of activation in response to *SMARCB1* loss and downregulation in response to *SMARCB1* re-expression in MRT cells and similarly showed high expression in primary MRT. The aforementioned cross-referencing analysis of RNA-seq data from *SMARCB1* re-expression cell model (n = 4) and primary MRT (10 ATRT and 13 ECRT) with the custom stemness/self-renewal gene list revealed two genes that are activated in primary MRT and whose expression is *SMARCB1*-dependent which are *BMI1* and *JARID2*.

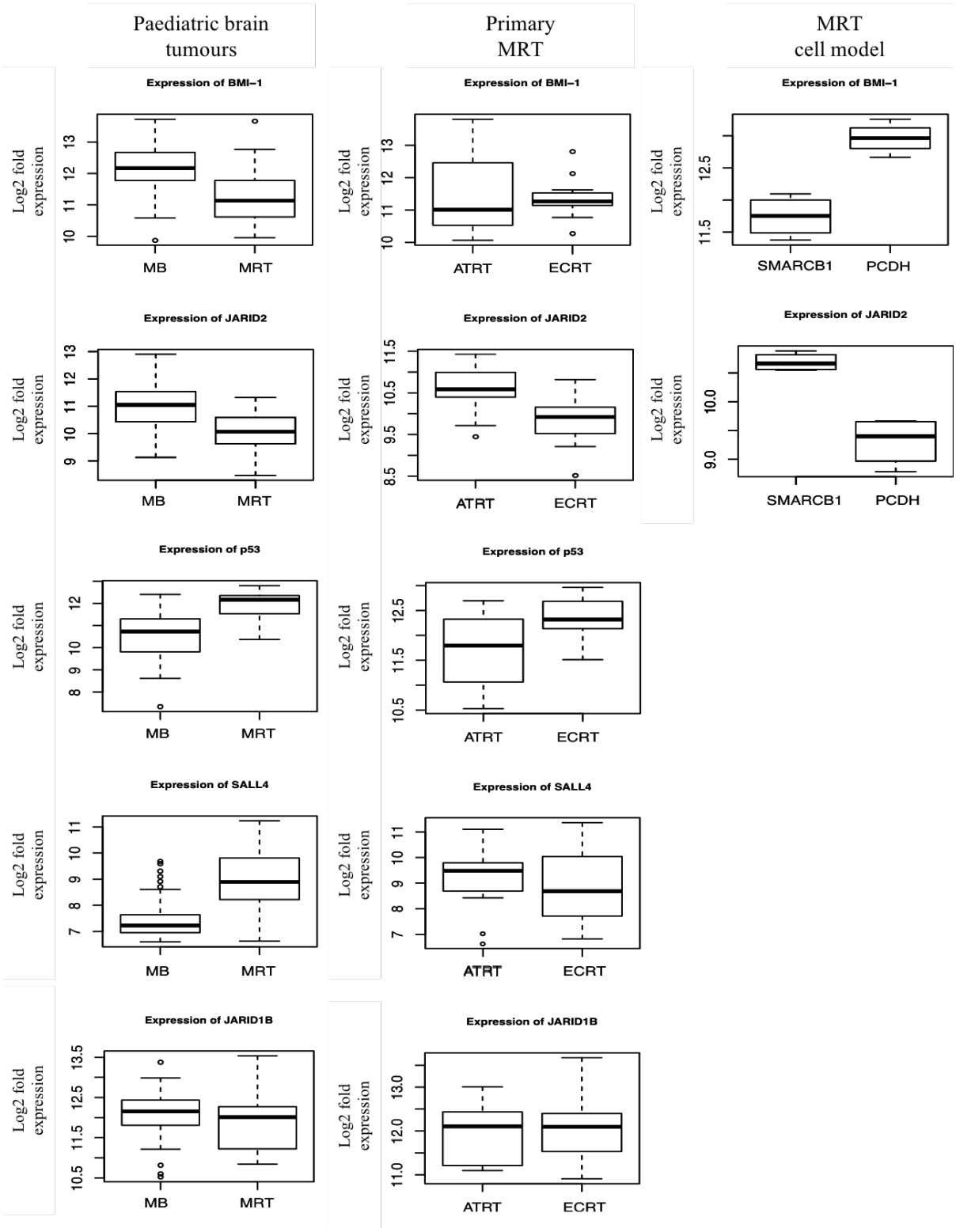

Figure 6.2 ***Boxplots showing representative expression of self-renewal genes in primary tumour and MRT cells****. Integrated analysis between RNA-seq with candidate self-renewal genes showed at least two genes whose expressions are significant in MRT primary and cell models. In cell models, SMARCB1 on the plot represents SMARCB1 re-expression in MRT cells, while PCDH represents MRT cells (without SMARCB1*

expression. Y-axis shows log2 fold expression of gene. The square box denotes interquartile (IQR). Upper whiskers of the boxplot represent the 75% percentile + 1.5 x interquartile (IQR) while lower whiskers represent the 25% percentile – 1.5 x interquartile (IQR). MB = Medulloblastoma.

To further validate the functional relevance of *SMARCB1*-dependent self-renewal/stemness genes, integrated data analysis was performed on 54 self-renewal/stemness genes with a genome-wide CRISPR/Cas9 knockout screen data of 4 MRT cell lines (G401, STA-WT1, A204 & CHLA266) with and without re-expression of *SMARCB1* (PBTG, unpublished). Briefly, CRISPR/Cas9 screening was performed using a GeCKOv2 lentiviral library and the cells were infected with lentivCRISPRv2 virus 2 days before SMARCB1 (INI1) or control lentivirus infection on day 0 (Figure 6.3a). Cells were harvested at days 0, 7 and 14 followed by amplification, sequencing and counting to estimate abundance of integrated sgRNAs. CRISPR/cas9 screening data at day 7 concomitantly with RNA-seq of MRT cells (*SMARCB1* re-expression cell model) were analysed using Ingenuity Pathway Analysis (IPA). The analysis was performed based on upstream regulator analysis (which recognizes key regulatory effectors likely to generate the observed changes in expression) and the result is presented in Figure 6.3b. The upstream regulator analysis showed 31 significant *SMARCB1*-dependent upstream genes at day 7 *SMARCB1* vs control (x-axis) and *SMARCB1* re-expression cell models. Genes that were appeared in two experimental arms includes *CDKN1A, BMI1,* etc.

To identify candidate genes that will be used in a functional stemness/self-renewal experiment for MRT, the genes were prioritised and selected based on their functional significance, establishing *SMARCB1*-dependency in both integrated data analyses (RNA-seq of primary and cell line, and CRISPR/Cas9 GeCKO) and their ability to target non-actionable mutation. Therefore, of 54 genes, *BMI1* was selected as a self-renewal/stemness target as it is druggable, showed *SMARCB1*-dependency and has been implicated in other embryonal tumours such as Medulloblastoma (MB). Furthermore, *Bmi* expression was upregulated following *Smarcb1* loss in candidate cell of origin for MRT, neural crest (NC) cells (details in Chapter 4).

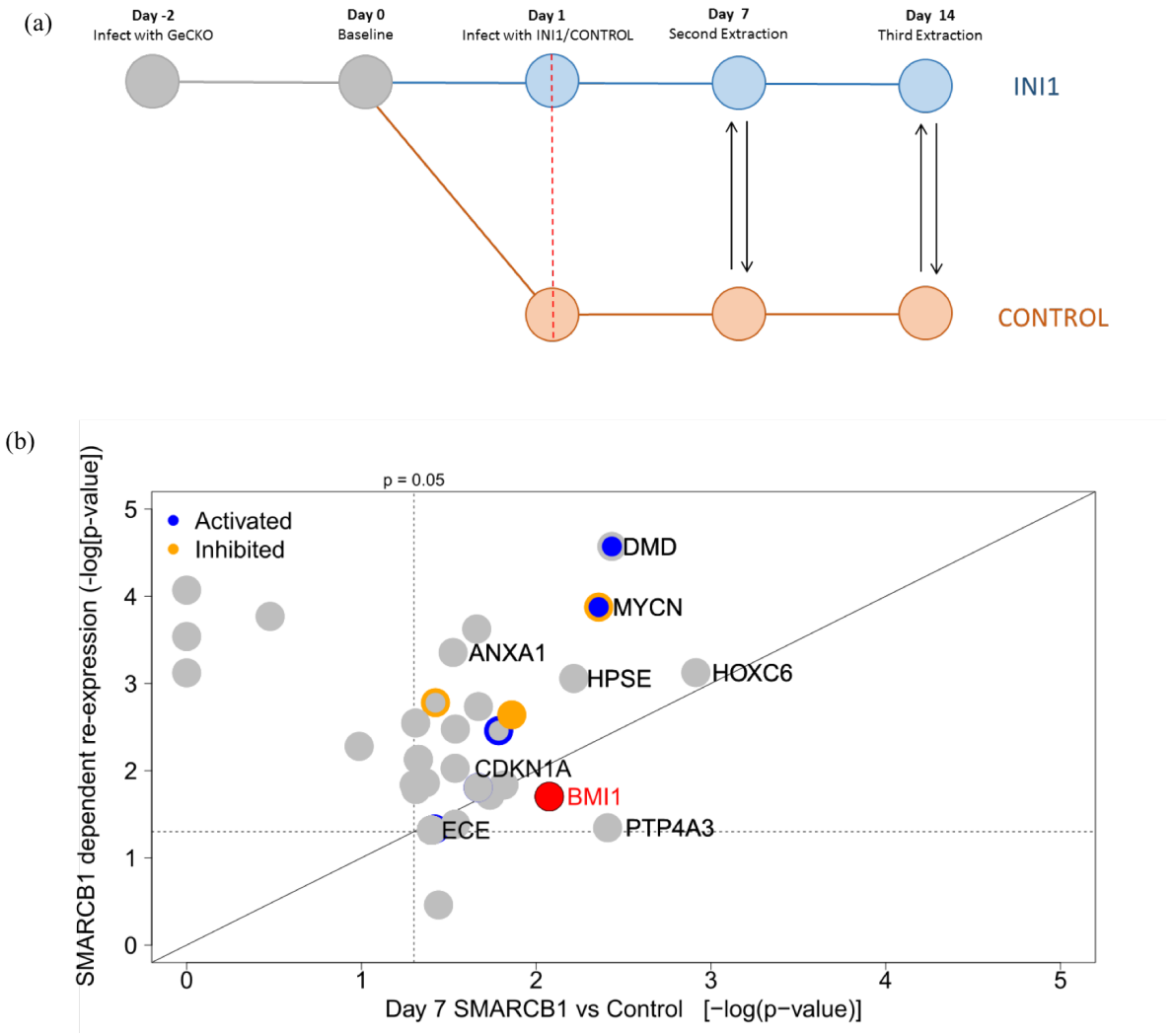

Figure 6.3 ***Stemness/self-renewal genes whose expression are SMARCB1 dependent analysed using CRISPR/Cas9 GeCKO screening****. (a) The experimental set up for whole genome CRISPR/Cas9 screening in 4 MRT cell lines. The cells were infected with GeCKOv2 lentiviral two days prior to SMARCB1 (INI1) or control lentivirus infection on day 0. Cells were collected on day 3, 7 and 14. (b) CRISPR data in combination with RNA seq data of MRT cell model were analysed using IPA based on upstream regulator. The x-axis here represents the dependent knock out in CRISPR screening on Day 7 whereas the Y-axis represent SMARCB1 re-expression model. The figure shows SMARCB1 dependent genes in which SMARCB1 had a clear effect on their expression either by inhibition or activation.*

6.4.2 BMI1 expression in a subset of MRT patient samples and cell lines

Overexpression of *BMI1* has been found in many types of cancers such as Medulloblastoma (MB) (Wang et al., 2012), prostate cancer (Mimeault and Batra, 2011), bladder cancer (Qin et al., 2009) amongst others. *BMI1* overexpression induces cell proliferation, metastasis and has demonstrated significant correlation with poor overall survival of patients (see details in Section 6.2.2) (Wang et al., 2015). As there is no study demonstrating the expression of *BMI1* in MRT, its expression was first evaluated in MRT primary tumours and cell lines; and compared with expression in normal paediatric brain (cortex and cerebellum) using RNA-seq data. As shown in Figure 6.4a, there is no significant difference between primary MRT and normal tissue transcription profiles. Likewise, transcriptional profiling data of human MRT revealed the expression of *BMI1* did not significantly differ between ECRT and ATRT (Figure 6.4a). However, RNA-seq analysis of *SMARCB1* re-expression in MRT cell models demonstrated significant overexpression of *BMI1* in MRT cells (Control vector) and the expression was downregulated upon restoration of *SMARCB1* (SMARCB1+vector) (Figure 6.4).

I next examined the expression of BMI1 in primary tumour tissue at the protein level. The primary MRT tissues (2 ECRT and 1 ATRT) were stained with antibody Anti-BMI1 antibody (Abcam. Cat No. ab14389) for immunohistochemistry analysis. The samples were then analysed for nuclear staining using APERIO Imagescope. Immunohistochemistry analysis demonstrated significant upregulation of BMI1 expression. IHC staining showed BMI1 was highly expressed in ATRT compared to healthy tissues controls extracted from the cerebellum (Figure 6.4b). Of note, BMI1 expression is present at a low level in normal kidney tissue and expression elevated in its corresponding tumour (RTK). To confirm the IHC result, a western blot was performed on total protein lysate to examine the expression of BMI1 in MRT cell lines. The membrane was probed with anti-BMI1 antibody for detection of BMI1 protein. Western blot analysis showed that expression of BMI1 protein was higher in absence of SMARCB1 (control) and the protein was diminished upon *SMARCB1* re-expression (IN1) in MRT cells (Figure 6.4c). Protein lysate from HDMB03, a Medulloblastoma cell line was included as a positive control of BMI1 overexpression as BMI1 has been reported to be upregulated in this tumour (Wang et al., 2012).

Altogether, analyses of MRT primary tissue and cell lines at protein demonstrate overexpression of BMI1 thus indicating the possible involvement of this gene in MRT tumourigenesis. To further elucidate the role of BMI1 in MRT, the expression of this gene was studied using shRNA gene knockdown and pharmacological inhibition of BMI1 inhibitor, PTC209.

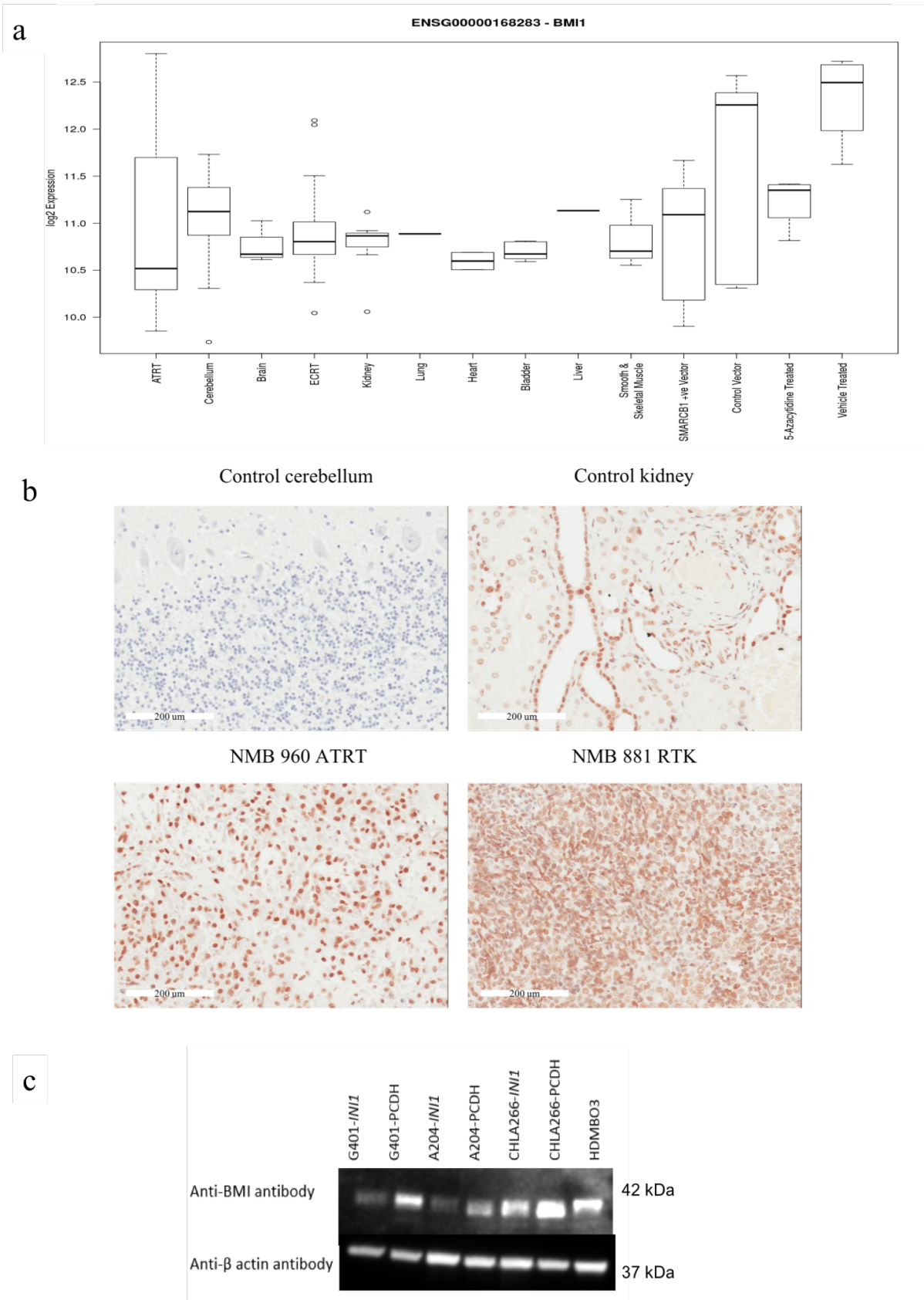

Figure 6.4 ***BMI1 expression in MRT primary tumours and cells****. (a) Boxplot of BMI1 expression in MRT primary, compared with normal tissue from various origins in the*

human body. Data from MRT experimental model was also included (control vector, PCDH) and was compared with SMARCB1 re-expression cells and 5-Azacytidine. Transcriptomic expression of BMI1 is not significantly different between primary MRT and controls. However, high expression of BMI1 was seen in MRT cell lines (control vector) and upon SMARCB1 re-expression in MRT cells, BMI1 expression was reduced. (b) Expression of BMI1 was examined in primary tissue by immunohistochemistry (IHC). Primary MRT tissues consist of two ECRT samples (RTK and ECRT) and one ATRT was analysed for the presence of BMI1 protein using anti-BMI1 antibody. Cerebellum and kidney serve as control. High expression of BMI1 was seen in ATRT tissue compared to cerebellum. Low BMI1 protein expression was observed in control kidney, however the expression level was elevated in RTK tissue, illustrating overexpression of BMI1 in MRT. Overexpression of BMI1 was also seen in ECRT sample (from liver). (c) The BMI1 expression was also examined in MRT cell lines by western blot anlysis. High expression of BMI1 in MRT cell lines (PCDH) compared to control (SMARCB1 re-expression cells, INI1 on figure). Beta-actin serves as a loading control and HDMBO3, a medulloblastoma (MB) cell line was used for comparison as MB has been shown to have high expression of BMI1.

6.4.3 shRNA-mediated knockdown of BMI1 in MRT cells

A few studies illustrated strong association between upregulation of *BMI1* in comparison to normal tissue with rapid tumour progression in other human tumours including Medulloblastoma and Neuroblastoma (Leung et al., 2004, Dahmane and Ruiz-i-Altaba, 1999, Calao et al., 2013). However, there is no study to report the role of BMI1 in MRT tumourigenesis. To address this question, I examined whether the expression of *BMI1* has a functional impact in MRT using two different short hairpin RNA (shRNA) that target different regions of the *BMI1* gene, namely shRNA GFP and shRNA RFP. Two shRNA constructs targeting luciferase (LUC) and a non-silencing (NS) were utilised as controls.

6.4.3.1 Confirmation of BMI1 knockdown at the protein and mRNA level using shRNA

Before exploring the possible biological effect of *BMI1* knockdown in MRT, I first examined the efficiency of shRNA lentivirus in mediating knockdown of BMI1 at the RNA and protein level. To this end, MRT cells were seeded at a density of 200,000 cells in a 6-well plate and were infected with shRNA lentiviral at MOI 5. This MOI was initially determined by the transfection efficiency analysis of GFP/RFP lentivirus evaluated by flow cytometry (FACS) (data not shown). After 48 hours of shRNA transfection, positive GFP/RFP cells (usually 80-90% cells) were harvested, and RNA and protein were extracted for measurement of the mRNA levels by quantitative RT-PCR and analysis of BMI1 protein by immunoblotting against the BMI1 antibody (methods described in Chapter 2). In 4 MRT cell lines, the qPCR analysis showed more than 3 times reduction in *BMI1* transcript was achieved for shRNA-RFP relative to control whereas *BMI1* expression was reduced by 1.5-2.5-fold in shRNA-GFP treated cells compared to control construct.

The automated western blot (WES) analysis also demonstrated efficient knockdown of BMI1 by two shRNA constructs; shRNA-GFP and shRNA-RFP. For shRNA-GFP construct, 25% of BMI1 protein expression reduction was observed in CHLA-266 cell line. In the G401 cell line, about 70% BMI1 protein reduction was achieved. Approximately 60% BMI1 protein knockdown was achieved in A204 and BT16 cell lines. By contrast, shRNA-RFP transfection in A204 and G401 cell lines resulted in minimal BMI1 protein knockdown measured as 26% and 28% respectively. Whilst, 40% BMI1 protein reduction was observed in the CHLA-266 cell line 48 hours post infection. In BT16 cells, more than 50% protein knockdown were achieved.

In short, both qPCR and western blot analyses showed that two shRNA constructs targeting BMI1; GFP and RFP can efficiently knockdown BMI1 in at least three MRT cell lines (A204, G401 and BT16) as demonstrated by a decrease in RNA and protein expression in BMI1-deficient MRT cells in relative to control (LUC/NS) (Figure 6.5a-b). For the rest of the chapter, I present results from shRNA-GFP lentivirus only and any experimental work using shRNA-RFP is included in the appendix.

a

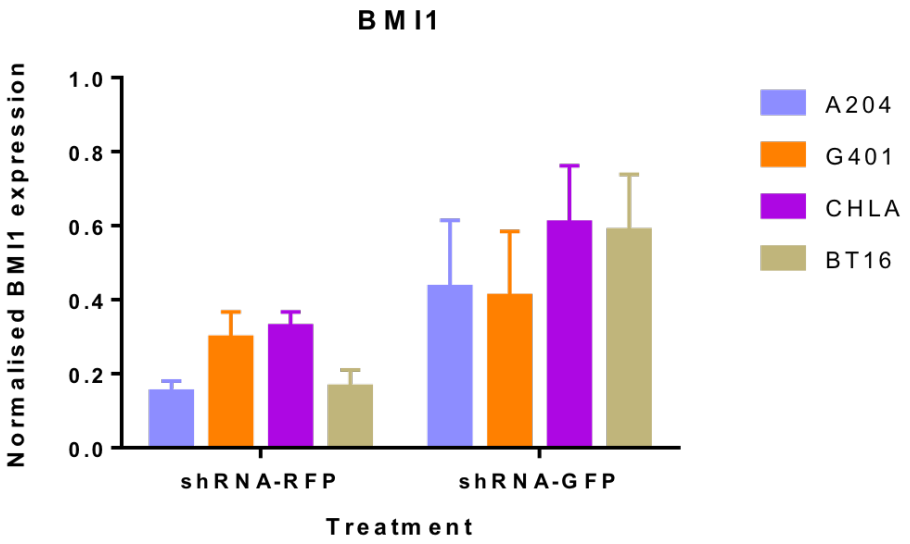
BMI1
Normalised BMI1 expression
1.0
0.8
0.6
0.4
0.2
0.0
shRNA-RFP
shRNA-GFP
Treatment
A204
G401
CHLA
BT16

b

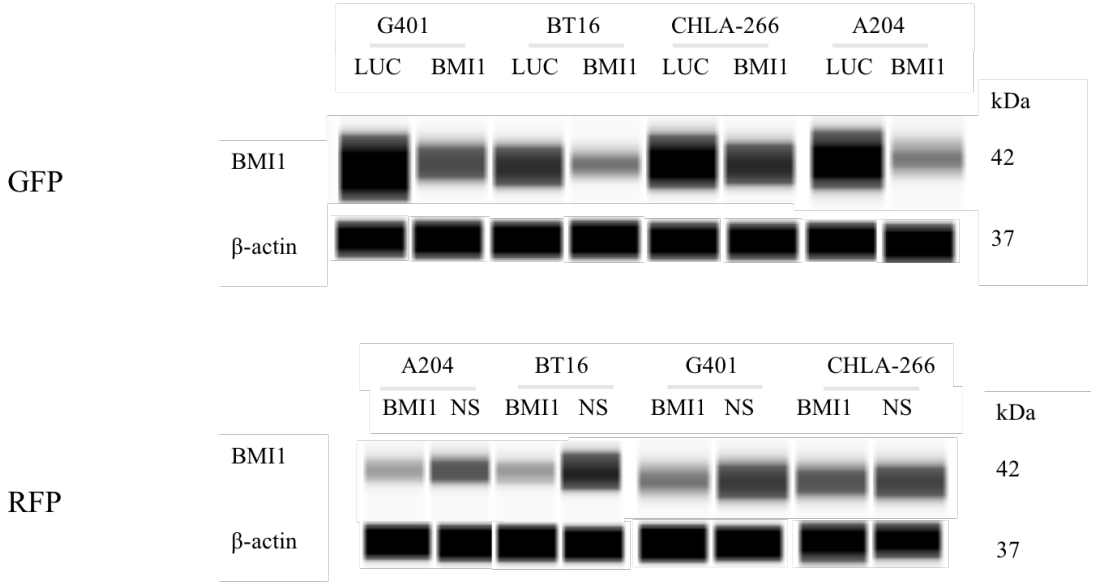
GFP
G401
BT16
CHLA-266
A204
LUC
BMI1
kDa
BMI1
β-actin
42
37
RFP
A204
BT16
G401
CHLA-266
BMI1
NS
kDa
BMI1
β-actin
42
37

c

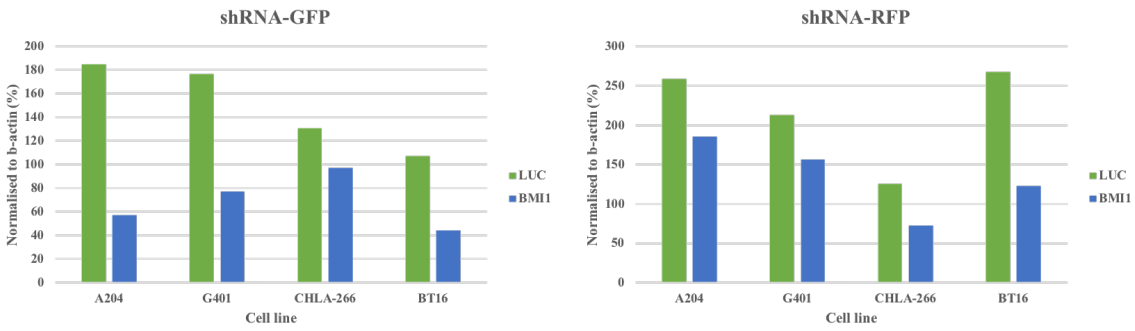
shRNA-GFP
Normalised to b-actin (%)
200
180
160
140
120
100
80
60
40
20
0
A204
G401
CHLA-266
BT16
Cell line
LUC
BMI1
shRNA-RFP
Normalised to b-actin (%)
300
250
200
150
100
50
0
A204
G401
CHLA-266
BT16
Cell line
LUC
BMI1

Figure 6.5 ***shRNA can efficiently knockdown BMI1 at RNA and protein level.*** *Cells were transfected with shRNA lentivirus carrying GFP or RFP construct at MOI 5. (a) BMI1 mRNA level measured by real time qPCR and normalised for GAPDH. The results are shown as mean ± SEM of three independent experiments. (b) Automated western blot (WES) analysis of BMI1 expression in A204, G401, CHLA-266 and BT16 cell line after 48 hours of transfection at MOI 5. β-actin was used as loading control. (c) Densitometry result of WES analysis of A204, G401, CHLA-266 and BT16 cell line following BMI1 knockdown with two shRNA constructs. Densitometry results were normalised to β-actin.*

6.4.3.2 BMI1 is required for MRT cell survival

BMI1 expression has been associated with tumour development and progression (Sparmann and van Lohuizen, 2006). The expression of *BMI1* alone or coupled with other molecules such as Hras, MYC, etc has been shown to initiate tumourigenesis in several types of non-tumourigenic immortalised cells lines through the p16Ink4a mechanism (Chiba et al., 2007, Datta et al., 2007, Jacobs et al., 1999b). *BMI1* has been shown to involve in normal stem cell proliferation via its role as stemness gene. Elevated expression of BMI1 has been observed in many types of cancers including leukaemia, medulloblastoma, gliomas and cancer from other tissues (He et al., 2009). Moreover, overexpression of *BMI1* in culture increased the expression of *p16Ink4a* and *p19Arf* which in turn promoted cell proliferation. In line with this, Liu et al. (2006a) have shown that *BMI1* knockdown by RNA interference (RNAi) in both normal and malignant human cells reduced the survival cancer cells but not of normal cells. Taken as a whole, it raises the question of whether the elevated *BMI1* expression in human malignancies is sufficient to enhance self-renewal activity of cancer cells and therefore increase cell proliferation, I next sought to examine whether *BMI1* loss has an effect on MRT cell growth and proliferation. For this experiment, the MTS based assay, CellTiter96 Aqueous one was used to measure cell proliferation following *BMI1* knockdown with shRNA. The assessment of proliferation was performed 24, 48, 96 and 120 hours post-transfection. Absorbance readings for each time and each condition (BMI1 vs LUC) were normalised to the t_0 absorbance, which was set to 0. The absorbance differences at each time interval

reflect the proliferation rate for each culture, measured by subtraction of normalised absorbance values.

BMI1 knockdown significantly decreased the proliferation rate in all MRT cell lines (Figure 6.6 and Figure 6.7). In A204, transfected with shRNA *BMI1*, the proliferation rate showed a slight decrease, but statistically significant difference was seen relative to LUC at 120 hours post transfection (Figure 6.6a and Figure 6.7a). By contrast, a significant decrease in cell proliferation rate was observed in G401 and CHLA-266 cell lines from 96 hours onwards (Figure 6.6b and Figure 6.7b). *BMI1* knockdown also decreased cell proliferation in the BT16 cell line and significant differences relative to LUC were only observed at 120 hours post-transfection (Figure 6.6a and Figure 6.7b). In all MRT cell lines transfected with shRNA-BMI1, the proliferation rate was significantly slower between 96-120 hours relative to LUC transfected cells (Figure 6.7). Similarly, *BMI1* knockdown with shRNA RFP in four MRT cell lines also reduced the cell proliferation and the proliferation rate was statistically significant between 96 and 120 hours when compared with control NS (Appendix 6.4).

To corroborate the reduced proliferation rate between 96-120 hours, I seeded the transfected cells in a 6-well plate and images of the cells were taken 96 hours after transfection using the EVOS microscope. The cell images were analysed using Image J analysis software to measure the viable cells. Briefly, the image was converted to 16-bit greyscale and the binary image was analysed using the "analyse particle" programme.

The resulting outcome showed the count (number of cells in the image), average size and total area. The bar graph was plotted based on the count for each cell line treated with BMI1 or control. Image J analysis measuring the viable cells of four cell lines is in agreement with this finding which demonstrated significantly less viable cells (approximately 75-80% reduction) measured in *BMI1*-knocked down cells 96 hours post-transfection compared to control (LUC) (Figure 6.8). Knockdown of *BMI1* in G401 and CHLA-266 cells caused a significant reduction in the number of viable cells (Figure 6.8). A small number of viable cells was also observed in A204 and BT16 cell lines following *BMI1* knockdown accounting for 1570 and 1551 cells respectively, compared to 12710 and 12596 respectively for LUC transfected cells. Combining the dataset for all cell lines (n=4 biological replicates) showed a significant reduction in the number of viable cells for BMI1 knocked down cells relative to LUC control cells (paired t-test: p-value <

0.0001, SEM ± 1396). In short, *BMI1* knockdown impaired the MRT cell proliferation implying a role in regulating MRT growth.

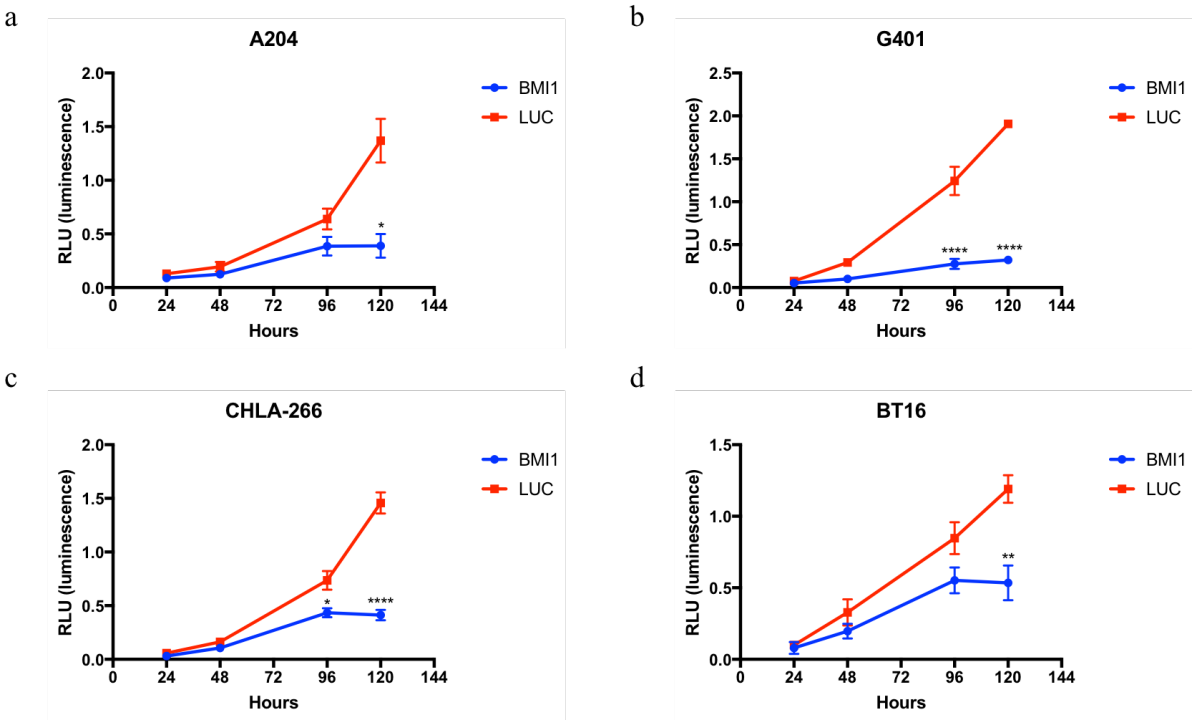

Figure 6.6 ***The effect of BMI1 knockdown on MRT cell proliferation*** *(a) Lentiviral transfection of shRNA significantly reduced the cell proliferation in all MRT cell lines in relative to control (LUC vector) measured using MTS CellTiter Aqueous one solution. The reading was measured 24, 48, 96 and 120 hours post infection. Luminescence unit (RLU): x 10,000. Knockdown of BMI1 reduced the proliferation rate in all MRT cell lines and the readings were more significant at 120 hours post transfection. The results are shown as means ± SEM of three individual experiments and the significance was determined by unpaired student's t-test (* p< 0.05, ** p<0.01, *** p<0.001, ****p<0.0001 vs LUC).*

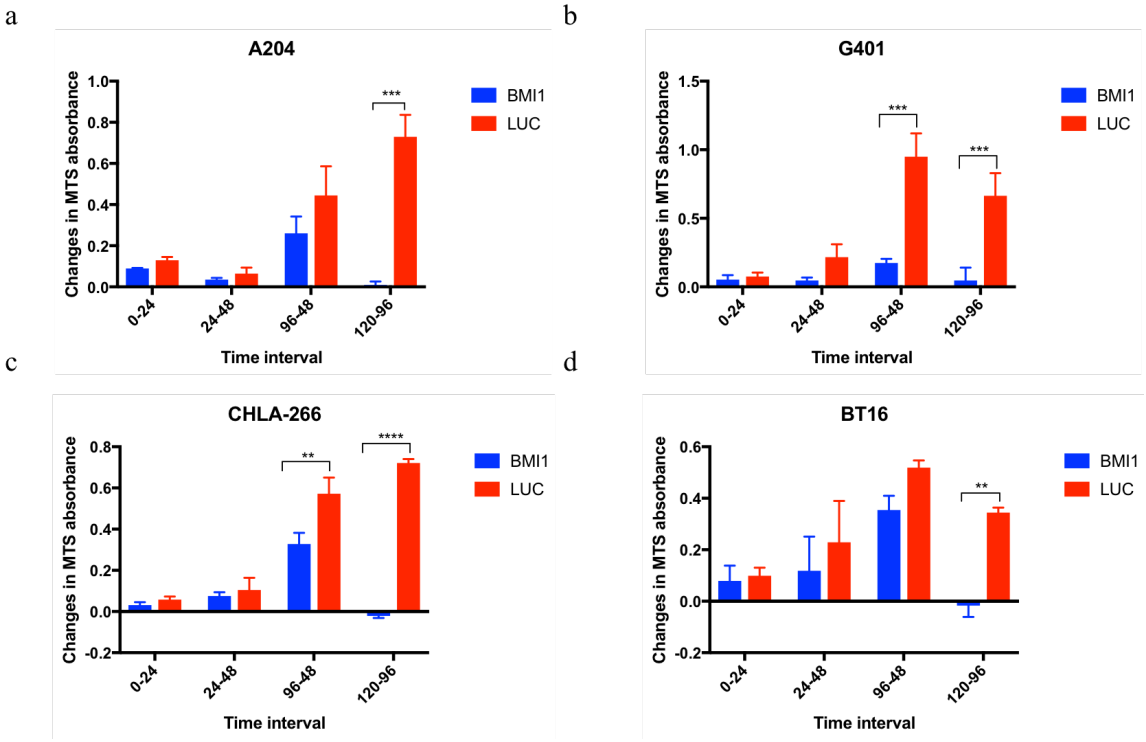

Figure 6.7 ***Knockdown of BMI1 halts MRT cellular growth****. MTS proliferation assay of four MRT cells following transfection with shRNA-BMI1(BMI1) and shRNA-LUC (LUC). (a) Knockdown of BMI1 slows down the cell proliferation in A204 cell lines and more pronounced between 96 – 120 hours relative to LUC. (b-c) BMI1 knockdown in G401 and CHLA-266 resulted in significant of inhibition of proliferation when compared to LUC between 48-96 hours and 96-120 hours time interval. (d) BMI1 knockdown also reduces the growth rate in BT16, however the effect is not statistically different between LUC for three-time intervals; 0.24, 24-48 and 48-96 hours. A significant reduction in cell proliferation was seen only between 96-120 hours. Altogether, these findings suggest BMI1 knockdown slows down the growth rate of four MRT cell lines and the effect is more pronounced at later times (between 96-120 hours). The results are shown as means ± SEM of three individual experiments and the significance was determined by unpaired student's t-test (** $p<0.01$, *** $p<0.001$, **** $p<0.0001$ vs LUC).*

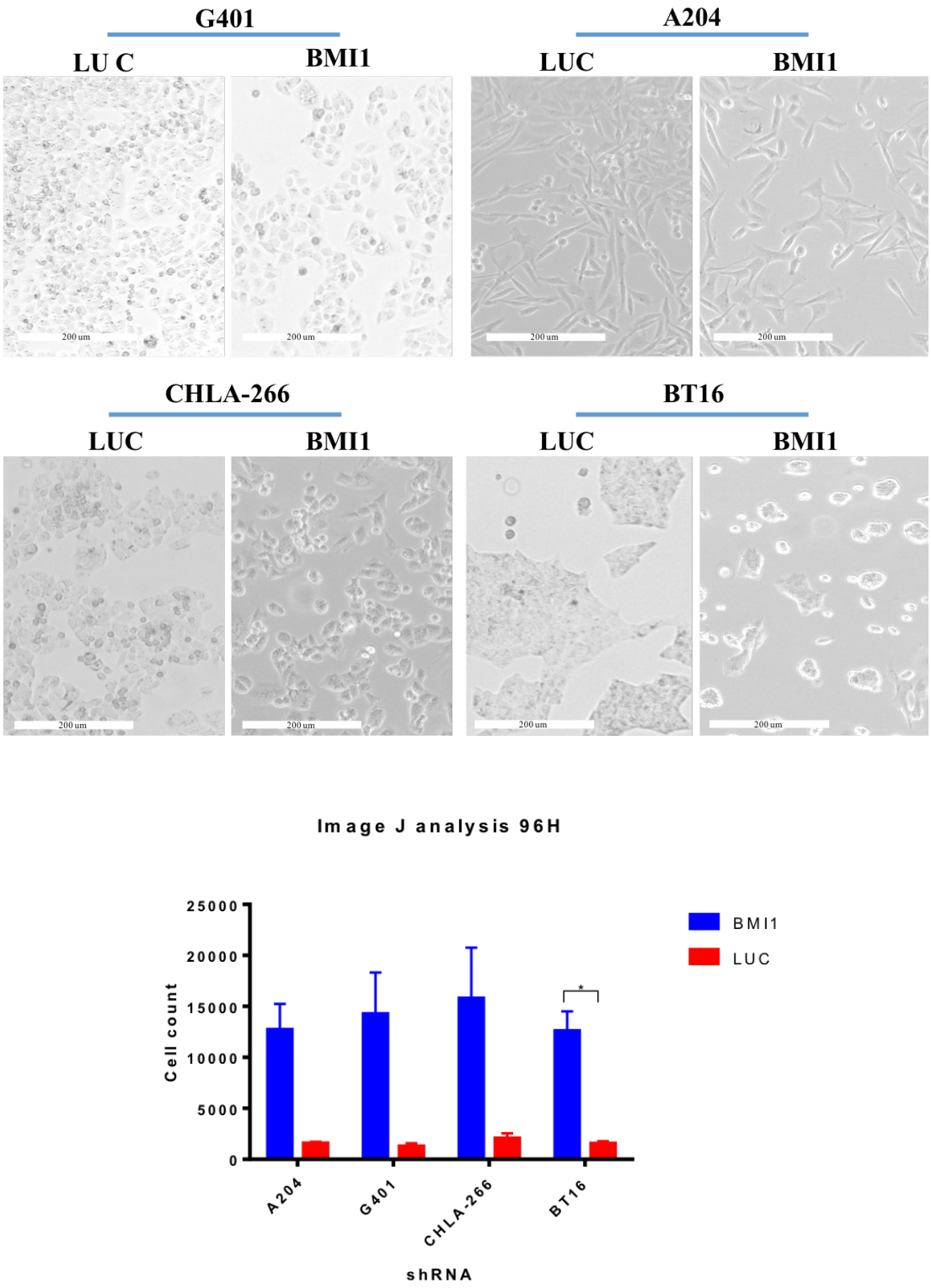

Figure 6.8 ***Phase contrast images of A204, G401, CHLA-266 and BT16 cell lines at 96 hours after transfection with shRNA-BMI1 and shRNA-LUC****. The scale bar is 200 um. Cell images taken at 96 post infection from two independent experiment was analysed using ImageJ software to measure number of viable cells. The image was analysed using "analyse particle" programme and the bar graph was plotted based on outcome from*

"analyse particle" analysis. The bar graph showing decreased in number of viable cells for shRNA BMI compared to LUC) at 96 hours. The results are shown as means ± SEM of two individual experiments and the significance was determined by unpaired student's t-test (p< 0.05 vs LUC).*

6.4.3.3 BMI1 knockdown with shRNA did not significantly induce cell apoptosis but it caused cell senescence

To identify the possible mechanisms by which *BMI1* knockdown slows down cell proliferation, the effect of *BMI1* on cell apoptosis and cell senescence was evaluated. *BMI1* has been associated with enhanced anti-apoptotic ability in many cancers (Teshima et al., 2014, Siddique et al., 2013). To test the induction of apoptosis following *BMI1* loss, the Caspase-Glo 3/7 luminescence assay was used to measure caspase 3- and 7- activities. The reagent has been optimised for measuring caspase activity, luciferase activity and cell lysis. Luminescence was proportional to the amount of caspase activity present in the cells (Promega Corporation). For the apoptosis assay, the MRT cells transfected with shRNA lentivirus were initially seeded in a 6-well plate and were transferred to a 96-well plate after 24 hours of transfection (1000 cells/well).

BMI1 knockdown increased cell apoptosis in G401 cells significantly at 96 and 120 hours post-transfection (> 2-fold increase) (Figure 6.9b). However, no significant increase was seen in two MRT cell lines, A204 and CHLA-266 at similar time points (Figure 6.9a, c and d). A significant increase in apoptosis was observed in BT16 cell line at 120 hours only (approximately 2.5-fold increased over LUC) (Figure 6.9d). The effect of *BMI1* knockdown on cell apoptosis was similar to the effect of *BMI1* knockdown on cell proliferation, i.e. more pronounced from 96 hours onwards. However, combining the datasets from 4 cell lines (n = 4 biological replicates, n= 2 technical replicates each cell lines) demonstrated a significant induction of apoptosis activity as early as 24 hours (24 hours: p-value = 0.0024, SEM ± 0.3587, 48 hours: p-value = 0.045, SEM ± 0.5609, 96 hours: p-value = 0.00279, SEM ± 0.3587, 120 hours: p-value = 0.0526, SEM ± 3.085).

Transfection of MRT cells with shRNA-RFP also induced cell apoptosis at a later time point in the experiment. *BMI1* knockdown significantly caused an increase in apoptosis activity in A204 at 72 and 120 hours when compared to NS (Appendix 6.5). Knockdown

of *BMI1* in G401 resulted in a significant increase in cell apoptosis at 120 hours relative to control. *BMI1* knockdown significantly increased apoptosis in G401, CHLA-266 and BT16 relative to control when measured at 120 hours. A significant increase in apoptosis was observed for all time points; 24, 72 and 120 hours when combining all biological repeats (4 cell lines, 2 technical replicates each cell line) (24 hours: p-value = 0.0022, SEM ± 0.6443, 72 hours: p-value = 0.0042, SEM ± 2.305, 120 hours: p-value = 9.265). Given the variability in apoptosis data for both shRNA constructs, more technical replicates are needed to demonstrate the significance of the datasets.

To fully ascertain whether *BMI1* knockdown can cause significant induction of apoptosis in MRT cells, I, next compared the luminescence reading from *BMI1* knockdown experiment with luminescence reading from Staurosporine-induced apoptosis treatment in MRT cell line (Dr Selby, unpublished). Dr Selby demonstrated that Staurosporine treatment increased apoptosis significantly in G401 cells (n = 2 technical repeats, p-value < 0.0001). The mean luminescence reading was measured at 113,068 (n = 2 technical repeats, SD ± 15,119) Thus, 113,068 was set as a reference point for the massive amount of apoptotic cells in MRT. Comparison of his apoptosis reading with *BMI1* experiment showed that *BMI1* knockdown did not cause massive apoptosis activity in MRT cells. In line with this, later result of cell cycle analysis (Figure 6.11) showed that following *BMI1* knockdown only 2.1% cells accumulated in sub-G0 phase. Thus, supporting the notion that the effect of *BMI1* knockdown on cell apoptosis is less pronounced in MRT cells.

Given the inconsiderable amount of apoptosis in *BMI1* knocked-down cells, I next examined another mechanism that contributes to slow growth rate following *BMI1* knockdown. To further determine if the inhibition of proliferation due to *BMI1* knockdown was also a result of cell senescence, the effect of *BMI1* inhibition by shRNA on cell senescence was studied. A β-galactosidase assay was used to identify senescent cells in culture. One day prior to staining cells with β-galactosidase (staining at 120 hours post-transfection), cells transfected with shRNA-BMI1 and shRNA-LUC were harvested and re-plated at 10,000 cells in a 6-well plate. The senescent cells (in green) were manually counted from 5 random regions per well (6-well plate, 9 cm^2/well) and the mean ± SEM of senescent cells from two independent experiments was presented in Figure 6.10. The senescence-associated β-galactosidase assay showed a high level of β-galactosidase activity in BMI1 knocked out A204 cell lines accounting for 465 positive

β-galactosidase staining compared to 15 positive β-galactosidase staining in LUC transfected cells (Figure 6.10). This result was the highest among other MRT cell lines. In BT16 cells, 300.5 β-galactosidase stained cells were measured for shRNA BMI1, relative to 20 stained cells for shRNA LUC. *BMI1* knockdown in G401 cell line also caused cell senescence, I counted an average of 201 stained cells relative to 24 stained cells for LUC transfection. In contrast, *BMI1* knockdown modestly induced senescence in CHLA cells in which I counted only 105 cells compared to 5 stained cells for LUC. Altogether, *BMI1* knockdown by shRNA did not massive induction of apoptosis, it is however, significantly caused senescence in MRT cells.

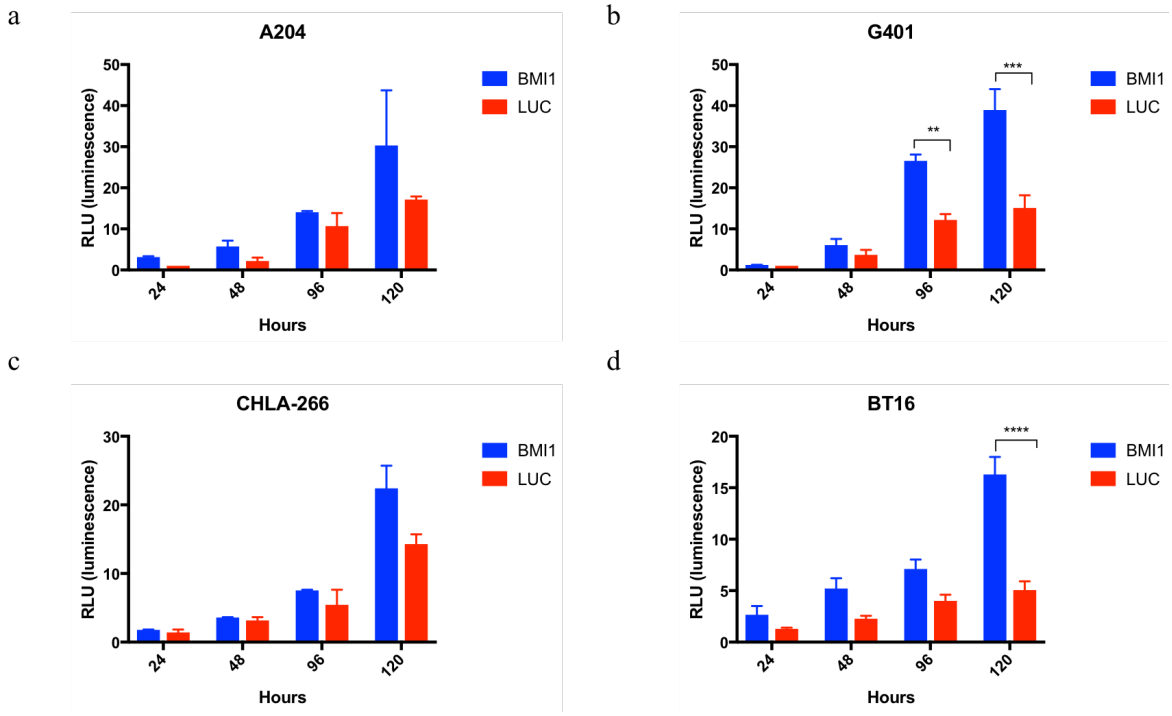

Figure 6.9 ***Effect of BMI1 knockdown on apoptosis in MRT cells****. Time dependent effect of BMI1 knockdown on caspase 3/7 activity in four MRT cell lines (a) A204, (b) G401, (c) CHLA-266 and (d) BT16. BMI1 knockdown did not cause massive apoptosis activity in MRT cells although the trend of increase can be observed in four MRT cell lines.The results are shown as means ± SEM of three individual experiments and the significance was determined by unpaired student's t-test (** p<0.01, *** p<0.001, ****p<0.0001 vs LUC). Luminescence unit (RLU): x 1,000.*

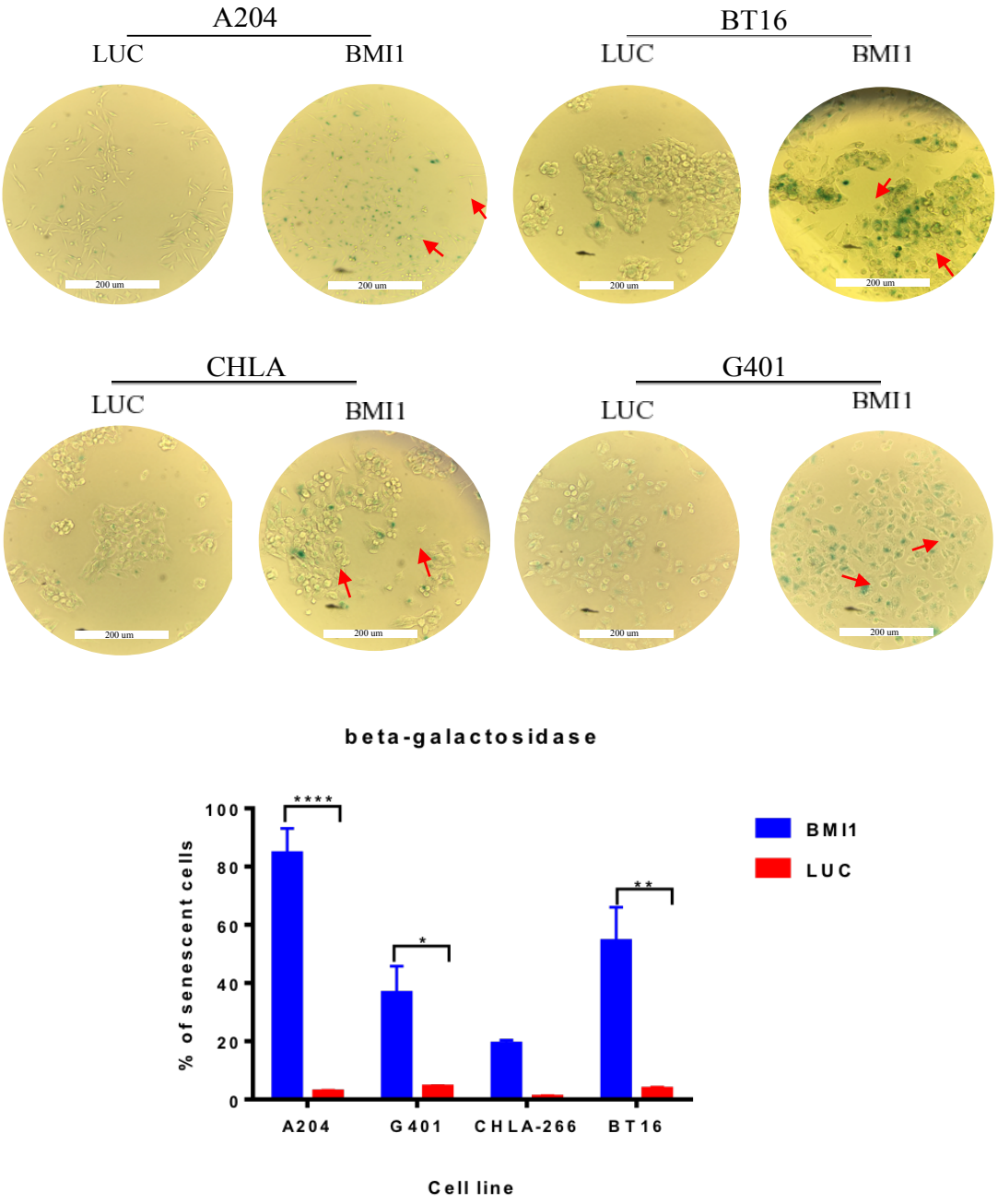

Figure 6.10 ***Silencing of BMI1 using shRNA induced cell senescence in MRT cells****. The presence of senescent cells in culture was identified using senescence associated β-galactosidase staining after 120 hours of lentiviral transfection. The microscopic images represent a region in the well for each culture. Senescent cells shown by red arrows. The number of senescent cells (green coloured cells) was presented as percentage of senescent cells (from a total of 550 cells per well. The bar graph showing the number of senescent cells in each culture measured from two independent experiments. The results are shown as means ± SEM of two independent experiments and the significance was determined by unpaired student's t-test (* p< 0.05 vs control of the appropriate sample).*

6.4.3.4 BMI1 knockdown leads to cell accumulation in G1/G0 phase and alters expression of cell cycle related genes.

Knockdown of *BMI1* in MRT impairs cell growth (section 6.4.3.2). To identify the mechanism that is associated with a reduction in cell proliferation (Figure 6.6), analysis of the cell cycle was performed by flow cytometry (FACS). Analysis of cell cycle distribution was performed on 1x 10^6 *BMI1* knockdown (BMI1-KD) cells and control samples collected at 24 hours and 120 hours post-transfection.

Average accumulation of 2.1% of cells in sub-G0 phase was observed at 120 hours across four cell lines; A204, G401, CHLA-266 and BT16 (2.1 ± 1.3, mean ± SD) (Figure 6.11). *BMI1* knockdown in A204, G401, CHLA-266 and BT16 caused a small but statistically significant increase in the number of cells in G0/G1 phase compared with the control which recorded a significant decrease (Figure 6.11a and b, Appendix 6.10 and 6.11). In G401, CHLA-266 and BT16 cell lines, *BMI1* knockdown resulted in a significant decreased in cell count in S and G2/M phases at 120 hours, compared with LUC (Figure 6.11a and b, Appendix 6.10 and 6.11). The decrease in cell count in G2/M phase was also observed as early as 24 hours but in only two cell lines transfected with shBMI1, G401 (p-value = 0.0007, mean ± SEM: 27.13 ± 2.02) and A204 (p-value = 0.0022, mean ± SEM: 14.9 ± 0.7034). A signification reduction of cells entering S phase was seen in CHLA-266 transfected cells compared with LUC at 24 hours (p-value = 0.0045, mean ± SEM BMI1: 24.8 ± 0.8888, mean ± SEM LUC: 34.23 ± 1.369). Altogether, knockdown of *BMI1* with shRNA disrupts normal cell cycle progression and reduced the fraction of proliferating cells. Notably, a significant accumulation of cells was seen in G0/G1 phase at 120 hours when cell cycle datasets for four cell lines were combined ($p < 0.0001$, n = 4 biological replicates, n = 2 technical replicates, SEM ± 4.186) (Figure 6.12b). Moreover, fraction of cells was significantly reduced in S and G2/M phases for *BMI1* transfected cells relative to control LUC cells (n = 4 biological replicates, n = 2 technical replicates, S phase (p-value < 0.0008, SEM ± 2.982), G2/M phase (p-value < 0.0001, SEM ± 1.608).

To further investigate the effect of *BMI1* inhibition on cell cycle regulatory gene expression, I next performed qPCR analysis to evaluate the change in expression level of seven cell cycle-related genes 96 hours post-transfection with shRNA lentivirus (Figure 6.13). Across four cell lines, the cell cycle promoting G1-S phase genes *CCND1, CCND3,*

CDK4, CDK6, CCNE1 and *CCNE2* were downregulated at an average of 0.81-, 0.91-, 0.79-, 0.88-, 0.89-, 0.61-fold change (Figure 6.13). As expected, *BMI1* knockdown caused upregulation of cell cycle inhibitors including *p21* (an average of 1.67-fold change) and two tumour suppressor genes regulated by *BMI1* which are *p14 and p16* (an average of 1.49 and 1.33-fold change*)*. This data indicates that *BMI1* plays a role in cell cycle regulation. Furthermore, it is worth noting that the expression of *CCND1* was slightly lower than *CCND2* following *BMI1* knockdown in MRT cells. The expression of *CCND1* is higher than *CCND2* in wild type MRT cells and primary (data not shown). This result may indicate the possible role of *BMI1* on cell cycle regulation through regulating *CCND1* expression.

In short, PI staining shows that knockdown of *BMI1* caused growth arrest in G1/G0 phase. Furthermore, the qPCR analysis demonstrated increased expression of cell cycle inhibitor genes; *p21* and *p16* accompanied by downregulation of cell cycle promoting genes. These results may explain the slow proliferation rate in *BMI1* knocked-down MRT cells.

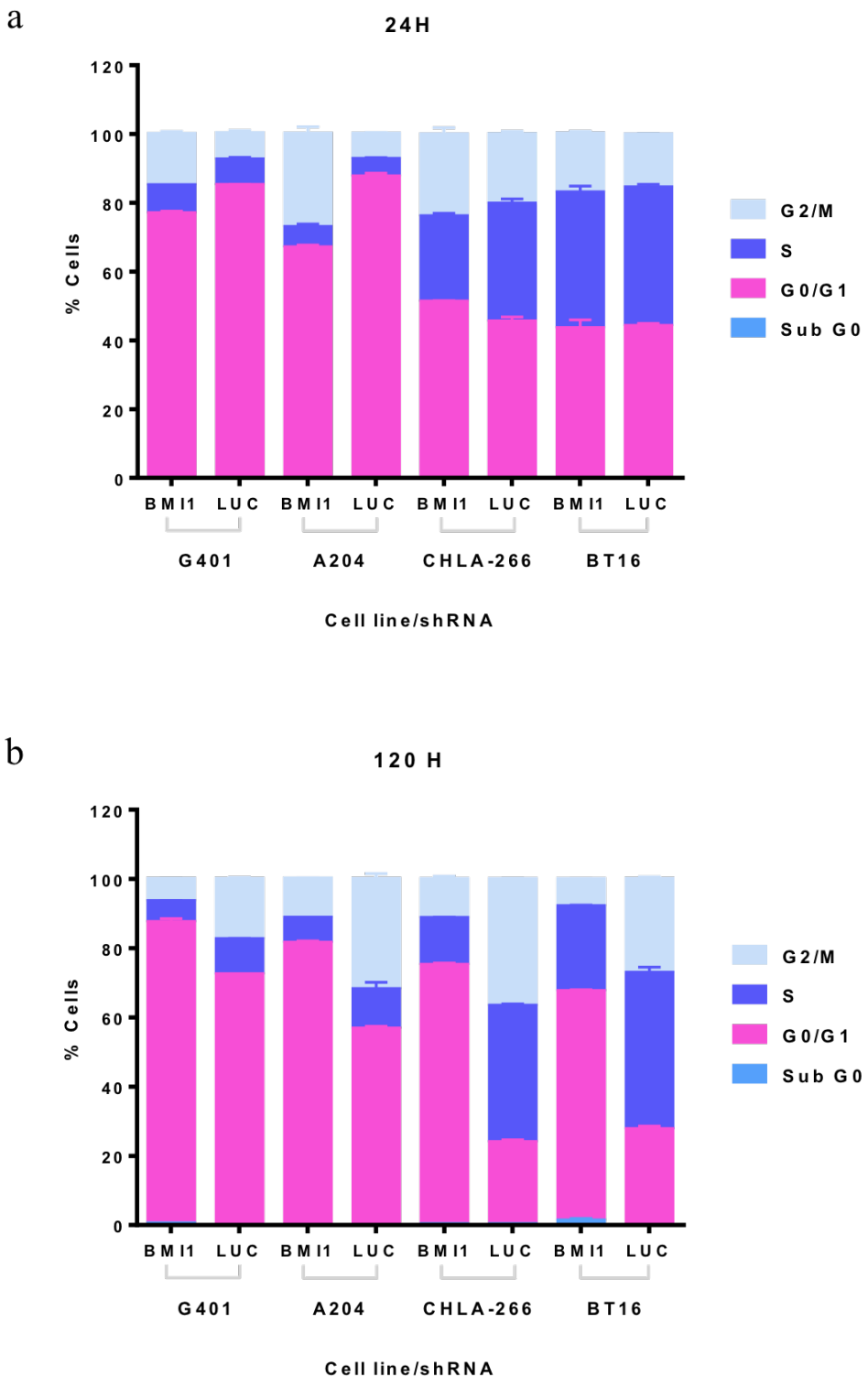

Figure 6.11 ***shRNA mediated silencing of BMI1 resulted in G0/G1 cell cycle arrest in MRT cells****. Cell cycle analysis of MRT cell lines transfected with shRNA-BMI1 and shRNA-LUC. The cells were harvested 24- and 120-hours post transfection, fixed in cold 70% ethanol and stained with propidium iodide (PI). A total number of 15,000 events were counted for each sample and the data were analysed using FlowJo software. Cell*

cycle distribution of BMI1 knocked down cells compared to LUC after (a) 24 hours and (b) 120 hours of transfection. Sub-G0 represents cells with a DNA content less than 2N, G0/G1 represents cells with DNA content 2N, cells in S phase with DNA content more than 2N while G2/M cells with DNA content of 4N. The results are shown as means ± SEM of three individual experiments and the significance was determined by unpaired student's t-test (p< 0.05 ** p<0.01, *** p<0.001, ****p<0.0001 vs LUC).*

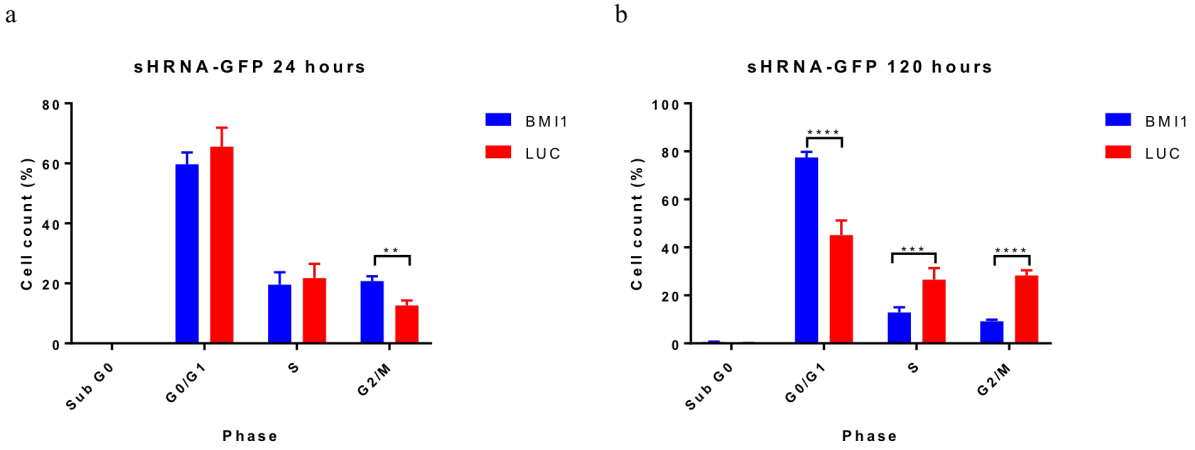

Figure 6.12 ***A significant effect of BMI1 knockdown in cell cycle when datasets were combined.*** *Cell cycle distribution of BMI1 and LUC transfected cells at (a) 24 and (b) 120 hours post lentiviral transfection. The data was presented as combination of four biological replicates (4 MRT cell lines) at two time points. The results are shown as means ± SEM of three independent experiments and the significance was determined by paired student's t-test (** p<0.01, ****p<0.0001 vs LUC).*

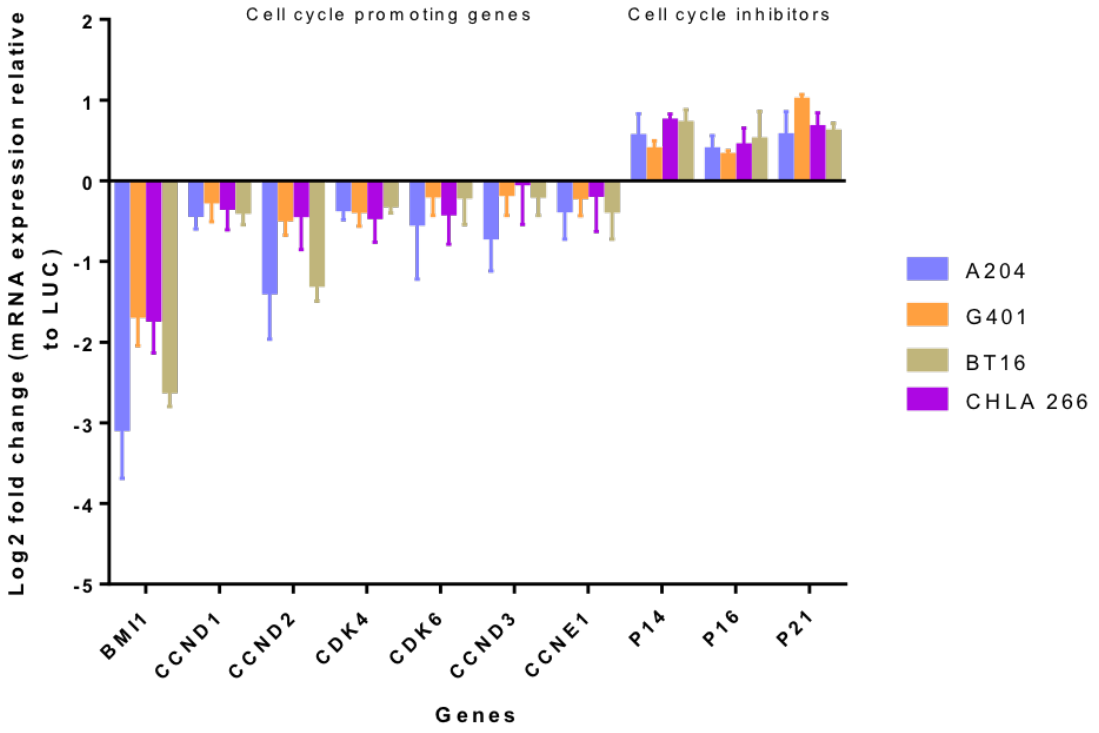

Figure 6.13 ***BMI1 knockdown alters the expression of cell cycle regulatory genes in MRT cells.*** *Accumulation of BMI1-deficient cells in G0/G1 phase was further confirmed with increased in expression of cell cycle inhibitors (p21 and p16) and decreased in cell cycle promoting genes (CCND1, CCCND2, CDK4, CDK6, CCND3 and CCNE1) as determined by qPCR analysis. The expression was presented as relative to control (control is set as 0). The mRNA expression as normalised to GAPDH. Data are presented as mean ± SEM of three independent experiments.*

6.4.3.5 Knockdown of BMI1 depletes the self-renewing cell population in MRT cell lines

The role of *BMI1* as a critical component of the self-renewal machinery has been comprehensively described in many studies (Park et al., 2003, Kreso et al., 2014, Molofsky et al., 2005, Molofsky et al., 2003). I next determined if *BMI1* knockdown could deplete the self-renewing cell population in MRT, which I hypothesised could contribute to MRT tumourigenesis.

As the self-renewal process itself is a complex mechanism to measure, one method that is widely used as self-renewal readout *in vitro* was employed, namely the sphere initiation assay. Briefly, in this assay, the cells are cultured as non-adherent spherical clusters of cells (known as tumourspheres hereafter), which can be dissociated and re-plated to reinitiate the tumourspheres. The self-renewal capacity of cells was studied using a limiting dilution assay (LDA) and re-plating tumourspheres. The adherent MRT cell lines were transfected with shRNA lentivirus for 24 hours and the cells were cultured in appropriate adherent culture media (Details of the media is described in Chapter 2) for another 48 hours. After 72 hours post-transfection, the cells were trypsinised, washed with 1X PBS (3 times) and mechanically dissociated into single cells by pipetting the cells up and down in 1ml PBS. The cells were then passed through a 40 μm filter. The cells were seeded either in a limiting dilution assay format down to one cell per well or 10, 100 and 1000 cells in 6-well plates for serial plating of tumoursphere experiment. At lower cell density, 1 and 10 the cells were seeded in 96-well plate or 6-well plate using FACS while serial dilution was performed to seed cells at cell densities ranging from 50,000 cells to 10 cells per well. The cells were cultured in tumoursphere media for 120 hours.

In the LDA experiment, the wells that contained tumourspheres were recorded as positive. Results from LDA shows no significant difference between shBMI1 and shLUC transfection at a cell density of 1,000 to 50,000 cells as tumourspheres were seen in all 12 wells seeded with control and BMI1 knocked-down cells (Appendix 6.3). The effect of *BMI1* knockdown on tumoursphere initiating efficiency was significant at a seeding density of 10 and 100 cells per well compared to control (Figure 6.14a). Therefore, these data underwent ELDA analysis (http://bioinf.wehi.edu.au/software/elda/) to measure the frequency of active self-renewal cells in MRT cultures following *BMI1* knockdown using shRNA GFP. ELDA limiting dilution analysis from tumoursphere cultures estimated that 1 in 4.69 A204 cells transfected with shLUC lentivirus possessed self-renewal capacity whereas 1 in 58.11 BMI1 knocked-down A204 cells have this ability (p-value= 2.42×10^{-48}, n= 3 technical replicates) (Table 6.1, Figure 6.14b). Knockdown of *BMI1* in A204 reduced the self-renewing cells approximately 12 times more than shLUC A204 cells. *BMI1* knockdown also significantly decreased tumoursphere initiating efficiency in BT16 cells by 9-fold. ELDA analysis demonstrated that the proportion of self-renewing cells in BT16 knocked down cells was 1 in 42.69 cells compared to 1 in 4.69 cells for shLUC

construct (p-value= 1.95 x 10^{-40}, n= 3 technical replicates) (Figure 6.14b). *BMI1* knockdown in CHLA-266 and G401 cell lines significantly reduced the self-renewal capacity of cells by approximately 13.5 times relative to shLUC transfected cells. For G401 cell line, cells that retained self-renewal capacity after transfection with shBMI1 was 1 in 63.15 relative to 1 in 4.69 for shLUC transfected cells (p-value= 2.98 x 10^{-51}, n= 3 technical replicates). This observation was comparable with CHLA-266 cell line in which ELDA analysis estimated 1 in 63.32 self-renewing cells in *BMI1* knocked-down cells compared to 1 in 4.69 in control LUC cells (p-value= 6.90 x 10^{-55}, n= 3 technical replicates). Altogether, these results illustrate that targeting *BMI1* caused self-renewal defects in all MRT cells as the shBMI1 transfected cells have lost the ability to form tumourspheres at an average reduction of 12.25 times compared to shLUC transfected cells, when four datasets from four biological replicates were combined.

BMI1 knockdown using shRNA-RFP also impairs the self-renewal capacity of MRT cells, determined using LDA (Appendix 6.8). Tumourspheres were observed at a plating cell seeding density of 1,000 to 50,000 cells per well for both cells transfected with shRNA-BMI1 and shRNA-NS. The effect of *BMI1* knockdown on tumoursphere forming efficiency was statistically significant at a cell density of 10 and 100 cells per well only for BMI1-knocked down cells relative to control NS cells. The ELDA analysis also demonstrated a significant decrease in sphere-forming efficiency following *BMI1* knockdown in four MRT cell lines compared with NS (Appendix 6.7). The analysis provided an estimate of 1 in 81.77 self-renewing cells in BMI1-knocked-down A204 cells relative to 1 in 4.69 cells for NS transfected cells (p-value= 2.42 x 10^{-48}, n= 3 technical replicates). This observation was comparable with G401 cells line in which the ELDA analysis estimated 1 in 88.68 active self-renewing cells for BMI1 transfected cells compared to 1 in 4.69 for NS transfected cells (p-value= 2.98 x 10^{-51}, n= 3 technical replicates). The number of cells with self-renewal capacity was also small in BMI1 knocked-down BT16 cells, measured for 1 in 90.11 cells relative to 1 in 4.60 for NS transfected cells (p-value= 1.95 x 10^{-40}, n= 3 technical replicates). In the CHLA266 cell line, *BMI1* knockdown reduced the active self-renewing cells, estimated at 1 in 75.92 cells for *BMI1* knocked-down cells compared to 1 in 4.69 for NS control cells (p-value= 6.90 x 10^{-55}, n= 3 technical replicates). These results indicate that *BMI1* knockdown in four MRT cell lines reduced self-renewing population cells at an average reduction of 18 times (mean of four biological replicates).

To fully ascertain the effect of *BMI1* knockdown on self-renewal capacity of MRT cells, I next assessed the tumoursphere forming capacity in MRT cell lines following *BMI1* loss in a re-plating tumoursphere assay. The adherent MRT cells were transfected with shRNA-GFP lentivirus for 24 hours and were dissociated into single cells on the same day. The single cells were seeded in 6-well plate at a density of 1000 cells per well in tumoursphere culture. Formation of primary tumourspheres was counted after 120 hours in culture. Primary tumourspheres were harvested and dissociated into single cells and the cells were re-seeded at 1000 cell per well in tumoursphere culture. Secondary tumourspheres were allowed to form for 120 hours. Results from the serial tumoursphere assay showed that *BMI1* knockdown significantly reduced the mean number of primary tumourspheres in CHLA-266 cells (n = 2 technical replicates, number of tumoursphere =8, p-value = 0.00422) compared with LUC (mean ± SEM: 16.5 ± 1.50) (Figure 6.14c, Appendix 6.15). A decrease was also observed in G401, A204 and BT16 cells transfected with shBMI1, however the number was not statistically different with LUC transfected cells (G401[p-value = 0.1153, mean ± SEM: 9 ± 2], A204 [p-value = 0.4117, mean ± SEM: 10.5 ± 2.50], BT16 [p-value = 0.1425, mean ± SEM: 9.5 ± 1.50].

Knockdown of *BMI1* resulted in a significant reduction in the number of secondary tumourspheres in all MRT cell lines (Figure 6.14c). Formation of secondary tumourspheres was greatly reduced in BT16 cells transfected with shBMI1 (p-value = 0.0068, mean ± SEM: 6.5 ± 0.5). A significant decrease in the number of tumourspheres was also observed in G401, CHLA-266 and A204 (p-value = 0.004). Notably, the number of tumourspheres was not statistically significant over two cultures for all cell lines although the fewer tumourspheres were found in secondary culture than initial primary culture (Figure 6.14 and Appendix 6.15). Combining the datasets from four cell lines (n = 4 biological replicates, n = 2 technical repeats) demonstrated a significant reduction in the number of both primary and secondary tumourspheres in *BMI1* knocked-down cells relative to LUC control cells (primary [p-value < 0.0001)(Figure 6.14d and Table 6.2).

A similar reduction trend was also observed in the formation of secondary tumourspheres as the mean number of tumourspheres across four cell lines was smaller than that of primary tumourspheres for shBMI1 (p-value = 0.0028, mean difference = 2.625, SEM = ± 0.9149). This result indicates that *BMI1* knockdown depletes the self-renewing cells thus corroborating results from ELDA analysis. On the other hand, transfection of shLUC

demonstrated upward trajectory in the formation of tumourspheres (p-value = 0.0006, mean difference = 4.5, SEM = ± 1.065). In conclusion, the reduced number of tumourspheres and abrogation of long-term self-renewal capacity in *BMI1*-deficient cells illustrate the role of *BMI1* in controlling self-renewal in MRT.

Cell line	shRNA construct	p-value (between two groups of treatment)	1/ (active self-renewing cell frequency)	Confidence interval (lower/upper)	Fold reduction of depleted self-renewal cells (relative to LUC)
A204	BMI1	2.42×10^{-48}	58.11	72.41/46.66	12.39
	LUC		4.69	5.74/3.85	
G401	BMI1	2.98×10^{-51}	63.15	78.78/50.63	13.46
	LUC		4.69	5.74/3.85	
CHLA-266	BMI1	6.90×10^{-55}	63.32	78.81/50.70	13.50
	LUC		4.69	5.74/3.85	
BT16	BMI1	1.95×10^{-40}	42.69	53.19/34.29	9.10
	LUC		4.69	5.74/3.85	

Table 6.1 ***Average frequency of sphere forming measured using limiting dilution assay (LDA) in MRT cells transfected with shRNA from three independent experiments.*** *Data was generated using a limdl software provided by Walter and Eliza Hall Institute. P-value represents overall difference in frequency of self-renewing cells between BMI1 and LUC. Active self-renewing cell frequency reflects the efficiency of the cultures to generate spheres.*

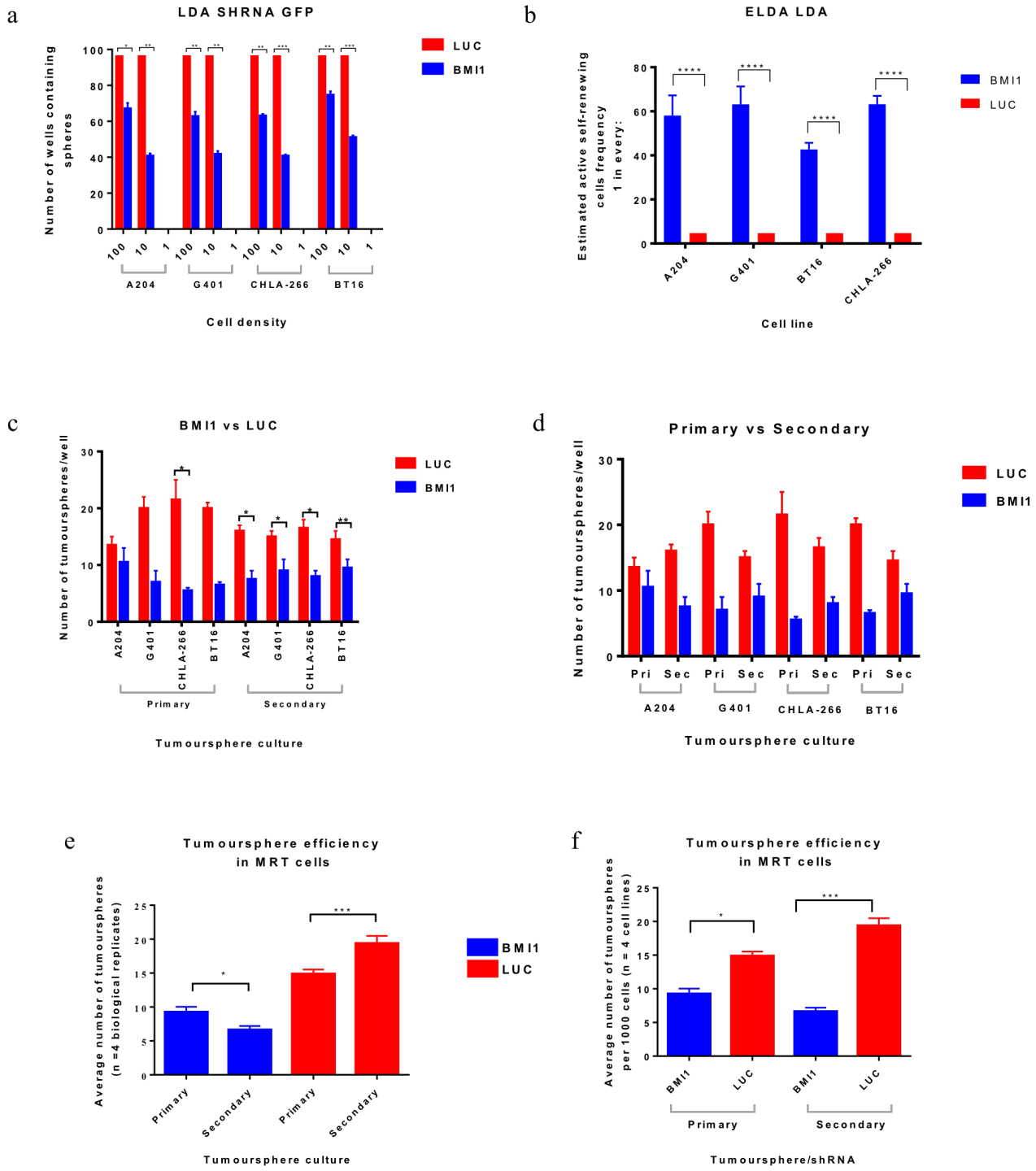

Figure 6.14 ***BMI1 knock-down using shRNA impairs self-renewal capacity of MRT cells****. (a) The effect of BMI1 loss on primary tumourspheres was measured using limiting dilution assay (LDA). The shRNA infected cells were cultured in tumourspheres media at density of 50,000 cells down to one cell per well and tumourspheres were allowed to form for 120h. Knockdown of BMI1 caused significant reduction in the number of tumourspheres at cell density of 10 and 100 cell per well. These results were further*

*analysed using ELDA to measure active self-renewing cells in BMI1-deficient cells. (b) ELDA analysis demonstrates significant decrease in sphere forming efficiency following BMI1 knockdown in four MRT cell lines compared with LUC. The results are shown as means ± SEM of three independent experiments and the significance was determined by unpaired student's t-test (****p<0.0001 vs LUC). (c) BMI1 loss affects the tumoursphere forming efficiency observed in certain MRT cell lines. Knockdown of BMI1 reduced the formation secondary tumourspheres in all MRT cell lines when compared with LUC. The results are shown as means ± SEM of three independent experiments and the significance was determined by paired student's t-test (** p<0.01, *** p<0.001, ****p<0.0001 vs LUC/ primary tumoursphere). (d) Despites a decrease in formation of tumourspheres over two cultures for BMI1 transfected cells, the reading was not statistically significant in all cell lines. (e and f) Number of tumourspheres from four cell lines were combined and paired student t-test analysis was performed on these datasets (n= 4 biological repeats, n= 2 technical repeats,** p<0.01, *** p<0.001, ****p<0.0001 vs LUC/ primary tumoursphere).*

Samples	Tumoursphere	p-value	Significance	± SEM	Mean difference [LUC – BMI1] or [Secondary – Primary]
LUC vs BMI1	Primary	< 0.0001	Yes	1.267	5.625 [BMI1: 9.25 vs LUC: 14.8756]
LUC vs BMI1	Secondary	< 0.0001	Yes	1.946	12.75 [BMI1: 6.625 vs LUC: 19.375]
LUC	Primary vs Secondary	0.0006	Yes	1.065	4.5 [Primary: 14.875 vs Secondary: 19.375]
BMI1	Primary vs Secondary	0.0028	Yes	0.9149	-2.625 [Primary: 9.25 vs Secondary: 6.625]

Table 6.2 ***The effect of BMI1 knockdown on tumoursphere formation efficiency****. The number of tumourspheres for each MRT cell line were combined to access whether BMI1 knockdown on four biological replicates was statistically significant. The results are shown as means ± SEM of two independent experiments and the significance was determined by paired student's t-test*

6.4.4 Targeting self-renewal machinery of BMI1 using small molecule inhibitor, PTC209

Knockdown of *BMI1* mediated by shRNA shows significant effects on MRT cell progression as well as self-renewal potential. These findings imply the value of targeting self-renewal machinery through the therapeutic targeting of *BMI1*. PTC209, a small molecule inhibitor was originally identified by Kreso et al. (2014) in her studies to regulate the survival of colon cancer through inhibition of *BMI1* expression. Recent studies reported potent effects of PTC209 in targeting self-renewing cells in other types of cancer (Bolomsky et al., 2016, Mayr et al., 2016, Alzrigat et al., 2017) which led me to explore the pre-clinical activity of PTC209 in MRT cell lines.

6.4.4.1 PTC209 is a potent anti-MRT agent in vitro

To identify the effect of pharmacological inhibition of BMI1 using PTC209 on cell proliferation, the MRT cell lines (A204, G401, CHLA-266 and BT16) were treated with a concentration ranging from 0.001 to 250 μM. Briefly, the cells were seeded in a 96-well plate (1000 cells/well) in triplicate. The number of viable cells was determined using CelTiter glo and the plate was read at 560 nm in a FLUOstar Omega (BMG Labtech) plate reader. To determine the GI_{50} of PTC209 for each cell line, the reading underwent analysis using GraphPad PRISM to generate a dose-response inhibition curve that fits a non-linear regression model. The curve was presented as log(concentration) vs response. The analysis showed that PTC209 inhibited the growth of four MRT cell lines in a dose-dependent manner (GI_{50}). The effect of PTC209 on the overall cell viability of MRT cell lines after 96 hours was illustrated in a dose-dependent manner as shown in Figure 6.16a. Notably, MRT cell lines showed different responses to PTC209 concentrations as measured by GI_{50}. A204, G401 and CHLA displayed greater sensitivity to the inhibitor (3, 4 and 4.6 μM respectively) in comparison to BT16 (10μM). Altogether, PTC209 mediated a potent anti-MRT activity, reducing the viability of MRT cell lines at concentrations ranging from 1-10 μM and this range is almost equivalent to the study by Mayr et al. (2016) in which the authors reported GI_{50} ranging from 0.52 – 8.33 μM in five biliary tract cancer cell lines. Treatment of PTC209 in eight human myeloma cell lines

showed the different sensitivity of the cell lines to inhibitor with GI_{50} ranging from 0.21 – 5.68 μM (Bolomsky et al., 2016). The GI_{50} reported in eight AML and five ALL cell lines ranging from 0.21 – 0.77 μM to 0.32 – 0.86 μM respectively (Nishida et al., 2015).

To further examine the effect on BMI1 inhibition using PTC209 on cell proliferation, two drug concentrations (sub-lethal dose and GI_{50} dose) were tested in each cell line. For A204, G401 and CHLA, the cells were treated at 1 and 3.5 μM whereas the BT16 cell line was treated at 5 and 10 μM. The cell images were taken after 48 hours of treatment with DMSO and PTC209 using the EVOS microscope. The images then underwent viable cells analysis using ImageJ software. As shown in Figure 6.16c, inhibition of BMI1 by PTC209 reduced the number of viable cells compared with DMSO. PTC209 treatment at the highest concentration tested in this experiment (3.5 and 10 μM) resulted in significant reduction in the number of viable cells seen in all MRT cell lines compared to DMSO. Treatment of PTC209 at 3.5 μM in A204 resulted in a 10 times reduction in the number of cells relative to DMSO (Figure 6.16c). Similarly, the number of viable cells in BT16 treated with 10 μM of PTC209 decreased by 3 times compared with DMSO. The change in the number of viable cells suggests the deficiency in proliferation compared to control DMSO treatment as early as 48 hours (Figure 6.16c).

In the following experiments, two drug concentrations (sub-lethal dose and GI_{50} dose) were tested in each cell line. For A204, G401 and CHLA, the cells were treated at 1 and 3.5 μM whereas the BT16 cell line was treated at 5 and 10 μM.

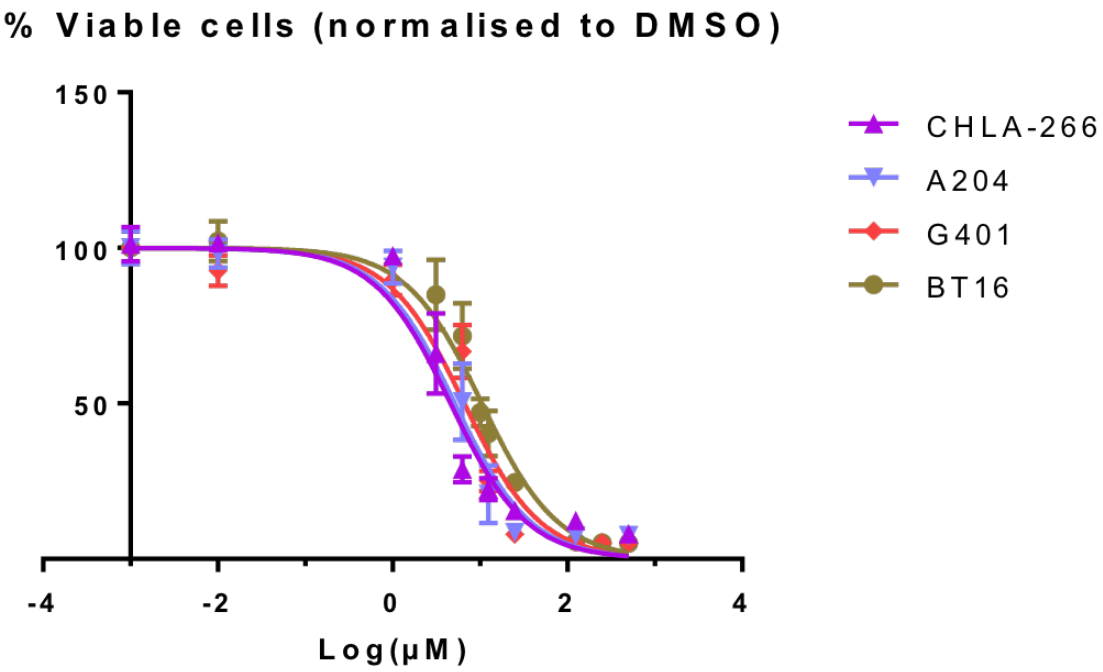

Cell line	GI_{50} (μM)
A204	3.5
G401	4.0
CHLA-266	4.6
BT16	10

Figure 6.15 ***MRT cells demonstrate different responses to concentrations of PTC209****. The GI_{50} of PTC209 in each MRT cell lines was determined using CellTiterGlo assay at 96 hours post treatment and the luminescence readings were analysed using PRISM to generate log(concentration) vs response curve. PTC209 significantly inhibited 4 MRT cell lines in a dose dependent manner ranging from 3.5 to 10 μM.*

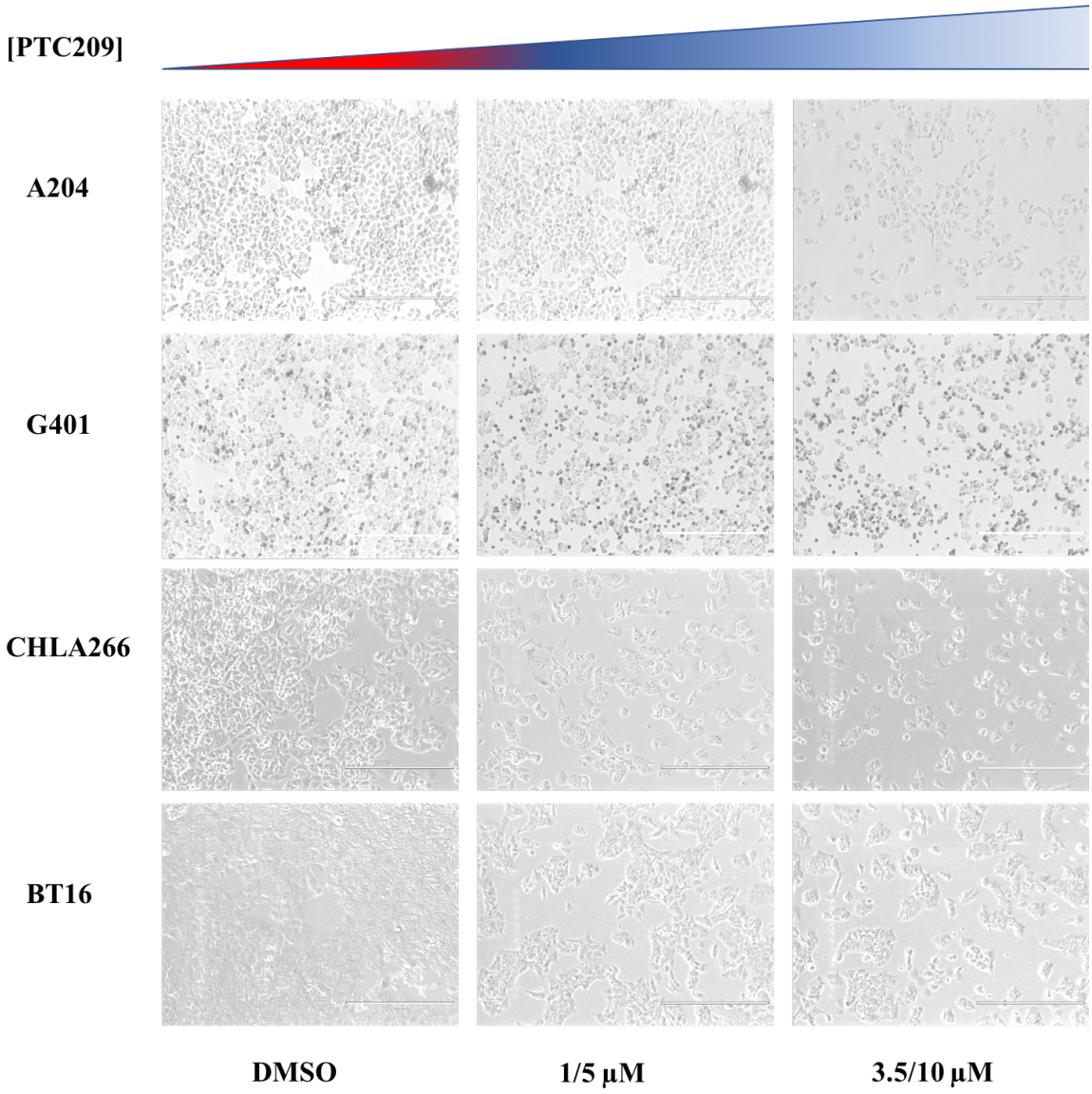
[PTC209]
A204
G401
CHLA266
BT16
DMSO
1/5 µM
3.5/10 µM

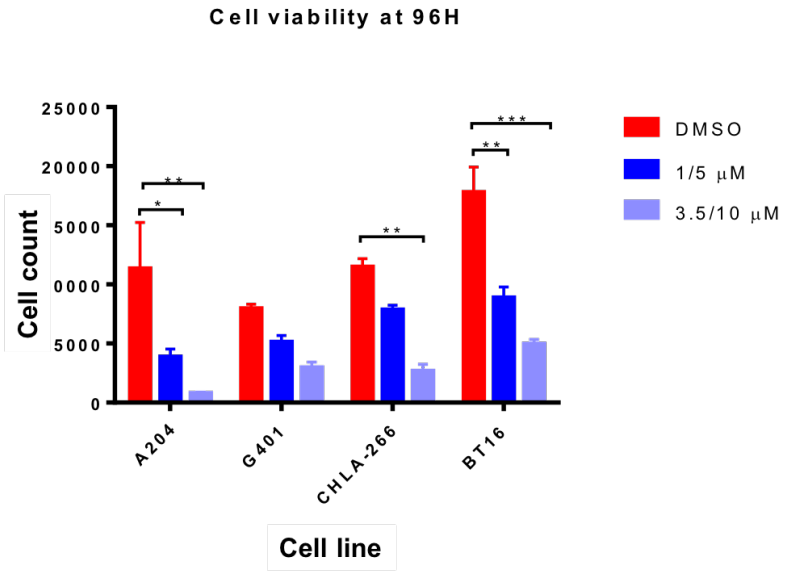
Cell viability at 96H
25000
20000
5000
0000
5000
0
Cell count
A204
G401
CHLA-266
BT16
Cell line
DMSO
1/5 µM
3.5/10 µM

Figure 6.16 ***Pharmacological inhibition of BMI1 reduced cell proliferation*** *(a) Phase contrast images of A204, G401, CHLA-266 and BT16 cell lines at 48 hours after treatment with two concentrations of PTC209 (GI_{50} and sub GI_{50}). The GI_{50} for A204, G401, CHLA-266 was 3.5 μM while BT16 was 10 μM. The sub-GI_{50} for A204, G401, CHLA-266 was 1 μM while BT16 was 5 μM. The cell images were taken using EVOS cell imaging microscope 48hours post treatment. The scale bar is 400um. The images showing the BMI1 inhibition impedes the cell growth as early as 48 hours. Row represents cell lines whereas column represents concentration of drug (b) ImageJ analysis to measure the number of viable cells following treatment with PTC209. To count the viable cells, the images underwent cell count scoring using ImageJ analysis and the number of viable cells was presented in a bar graph. The bar graph showing decreased in cell number of viable cells in PTC209 treated cells compared with DMSO, which serves as control. The results are shown as means ± SEM of two individual experiments and the significance was determined by unpaired student's t-test (* $p< 0.05$, ** $p<0.01$, *** $p<0.001$ vs DMSO).*

6.4.4.2 Pharmacological inhibition of BMI1 did not significantly induce cell apoptosis in MRT cell lines

Treatment of PTC209 in four MRT cell lines impaired cell proliferation as indicated by slow growth rate after PTC209 treatment (Figure 6.16). I next sought to examine other possible mechanisms by which pharmacological inhibition of BMI1 slows down the cell growth. To this end, the effect of BMI1 inhibition by PTC209 on cell apoptosis was studied using a Caspase-Glo 3/7 luminescence assay. This assay measures the caspase 3- and caspase 7- activity within the cells as an indicator for cell apoptosis. BMI1 knockdown by PTC209 did not cause a significant induction of apoptosis in the three MRT cell lines (A204, CHLA-266 and BT16) in a dose-dependent manner, as the apoptosis activity was not statistically significant compared with DMSO (Figure 6.17). A significant increase in apoptosis activity was only seen in G401 cell line at 3.5 μM relative to DMSO treatment. Although apoptosis reading from G401 cell line showed significant apoptosis activity, the luminescence reading was lower than the reference point from Dr Selby's apoptosis dataset (Refer 6.4.3.3). Comparison of the luminescence reading from PTC209 treatment with datasets from Staurosporine treatment in MRT cell lines (Dr

Selby, PhD thesis) indicates that pharmacological inhibition by PTC209 did not cause massive induction of apoptosis in MRT cells. This result was further corroborated by the later result of cell cycle analysis which did not significantly demonstrate accumulation of cells in sub-G0 phase.

To gain more insight into the effect of PTC209 treatment on cell apoptosis, FITC AnnexinV-PI assay was used. In the apoptotic cell, the membrane phospholipid phosphatidylserine (PS) is transported from the inner to the outer space of the plasma membrane, hence showing PS to the external cellular environment. The FITC AnnexinV-PI assay incorporates the AnnexinV, which is a 35-36 kDa Ca2+ dependent phospholipid-binding protein that has a high affinity for phospholipid phosphatidylserine (PS) and binds to cells with exposed PS. AnnexinV is conjugated to FITC for flow cytometry analysis. This assay is used in conjunction with propidium iodide (PI) to identify stages of cell death i.e necrosis. To measure apoptosis using this assay, the cells were harvested 72 hours after the treatment with either DMSO or PTC209) and incubated with FITC Annexin V and PI solution (Details of the method is described in Chapter 2). The cells were analysed using the FACS Canto and measurements were analysed using FlowJo software. Figure 6.18 showing a quadrant plot that represents stages of cell death. The Q4 square represents the viable cells (FITC Annexin V and PI negative), the Q3 square represents the cells in the early apoptosis (FITC Annexin V positive and PI negative. The Q1 and Q2 denote the cells in late apoptosis or already dead.

After 72 hours treatment with PTC209 at 1 and 3.5 μM in A204 cell line, BMI1 inhibition caused accumulation of 2.42% and 10.2% of apoptotic cells in early apoptosis (Q3) stage respectively, and 1.06% and 3.13% of cells in late apoptosis (Q2) stage respectively (Figure 6.18). In the G401 cell line, PTC209 treatment at 1 and 3.5 μM caused less than 1.1% of apoptotic cells in early apoptosis stage. Whilst, 0.93% and 2,13% of cells in late apoptosis stage respectively were measured in G401 cells treated with PTC209 at 1 and 3.5 μM respectively. Similarly, PTC209 treatment at two drug concentrations in other cell CHLA-266 resulted in less than 4% of apoptotic cells measured from late apoptosis Q3 square and less than 1% of apoptotic cells in early apoptosis Q2 square (Figure 6.18). PTC209 treatment in BT16 cells with 1 and 3.5 μM caused 0.81% and 1.12% apoptotic cells in Q2 square respectively whereas less than 2.5% of apoptotic cells were measured in the Q3 square for 1 and 3.5 μM treated cells respectively. Notable, less than 1% of

apoptotic cells were observed in Q2and Q3 squares for DMSO treatment in three MRT cell lines; G401, CHLA-266 and BT16 with an exception of A204 cell line in which 2.09% of apoptotic cells were measured in Q3.

Both apoptosis assays utilised in this study demonstrated that treatment with PTC209 did not significantly induce cell apoptosis in MRT cell lines, although the trend of increase in cell apoptosis can be observed in Caspase-Glo 3/7 luminescence assay. Analysis of cell apoptosis using the Caspase-Glo 3/7 showed a significant increase in apoptosis activity, observed in G401 cells following PTC209 treatment. However, AnnexinV FITC-PI assay showed that pharmacological inhibition of BMI1 only resulted in less than 6% of apoptotic cells. Likewise, PTC209 treatment in A204 at 3.5 μM did not cause significant induction of cell apoptosis as determined by the Caspase-Glo 3/7. However, approximately ~13.77% of apoptotic cells were measured using the Annexin V FITC-PI staining (Figure 6.18). Given the discrepancy in results between two apoptosis assays, more technical replicates are needed to increase the significance of results.

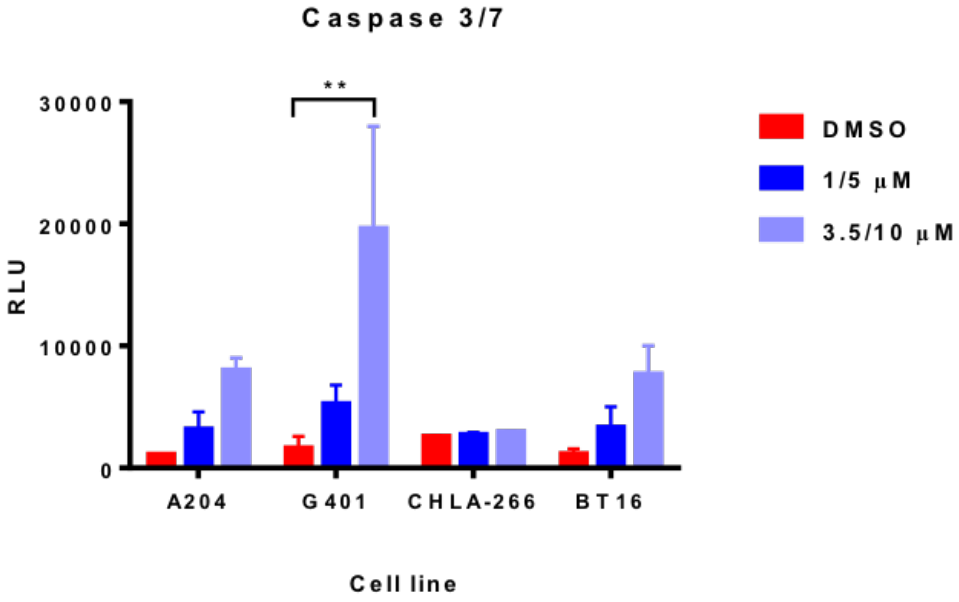

Figure 6.17 ***Pharmacological inhibition of BMI1 on apoptosis in MRT cells after 72 hours treatment with PTC209****. The Caspase-Glo 3/7 assay was used to measure caspase 3- and caspase 7-acitivity within the cells. The luminescence reading was normalised to blank and the measurement was presented as relative to cell only (without any treatment). The results are shown as mean ± SEM of three individual experiments and the significance was determined by unpaired student's t-test (** p<0.01 vs DMSO).*

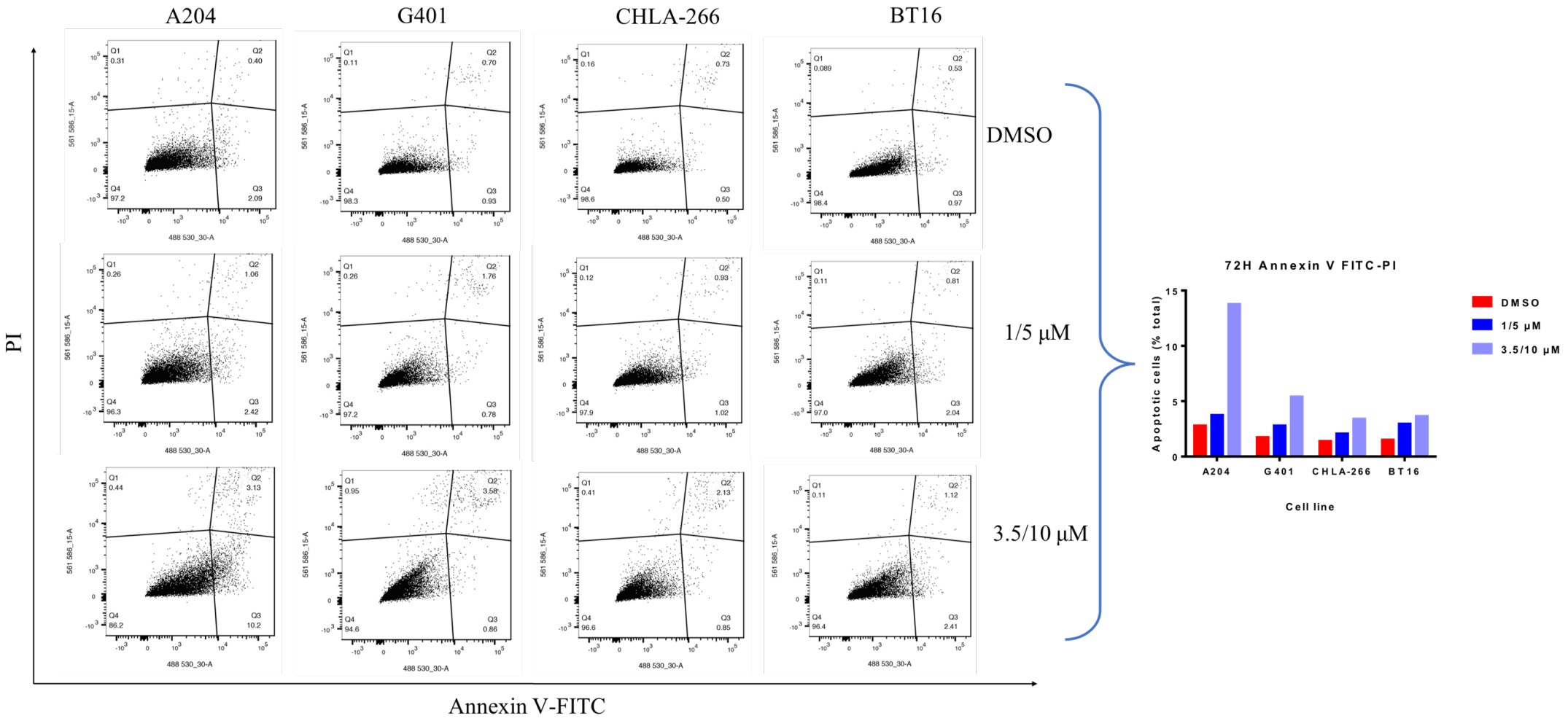
A204
G401
CHLA-266
BT16
DMSO
1/5 µM
3.5/10 µM
PI
Annexin V-FITC
561 586_15-A
488 530_30-A
Q1 0.31
Q2 0.40
Q4 97.2
Q3 2.09
Q1 0.11
Q2 0.70
Q4 98.3
Q3 0.93
Q1 0.16
Q2 0.73
Q4 98.6
Q3 0.50
Q1 0.089
Q2 0.53
Q4 98.4
Q3 0.97
Q1 0.26
Q2 1.06
Q4 96.3
Q3 2.42
Q1 0.26
Q2 1.76
Q4 97.2
Q3 0.78
Q1 0.12
Q2 0.93
Q4 97.9
Q3 1.02
Q1 0.11
Q2 0.81
Q4 97.0
Q3 2.04
Q1 0.44
Q2 3.13
Q4 86.2
Q3 10.2
Q1 0.95
Q2 3.58
Q4 94.6
Q3 0.86
Q1 0.41
Q2 2.13
Q4 96.6
Q3 0.85
Q1 0.11
Q2 1.12
Q4 96.4
Q3 2.41
72H Annexin V FITC-PI
Apoptotic cells (% total)
15
10
5
0
A204
G401
CHLA-266
BT16
Cell line
DMSO
1/5 µM
3.5/10 µM

Figure 6.18 ***FITC Annexin V-PI assay measuring the cell apoptosis in PTC209 treated cells.*** *Cells treated with PTC209 and DMSO were incubated with FITC Annexin V and PI to analyse the percentage of apoptotic cells. Q1 represents necrotic cells (already dead), while Q2 represents late apoptosis. Q3 represents early apoptosis stage. Combination of three squares denotes the apoptotic cells and the number of cells in these squares were combined to generate a bar graph of percentage of apoptotic cells in four MRT cell lines. Statistical analysis could not be performed as the experiment was performed once only.*

To study another mechanism that contributes to inhibition of cell proliferation, I next examined the effect of pharmacological inhibition of PTC209 on cell senescence in four MRT cell lines after 96 hours of treatment. The senescent cells were detected using β-galactosidase staining. The senescent cells (in green) were manually counted from 5 random regions per well (6-well plate, 9 cm^2/well) and the mean ± SEM of senescent cells from two independent experiments was presented in Figure 6.20. The senescence-associated β-galactosidase assay showed a significant effect of BMI1 inhibition in A204 cells treated at 1 μM relative to DMSO (mean 1 μM: 300 cells, mean DMSO: 4, p-value= 0.0019, n= 2 technical replicates) relative to DMSO. PTC209 treatment at 3.5 μM in A204 cell lines also caused significant cell senescence relative to DMSO (mean 3.5 μM: 419 cells, mean DMSO: 4, p-value= 0.0002, n= 2 technical replicates)(Figure 6.20 and Figure 6.20). In BT16 cells, 267.5 and 378 senescent cells were counted for 1 μM and 3.5 μM respectively. These datasets were significant relative to 23.5 senescent cells for DMSO (p-value 5 μM = 0.0051, p-value 10 μM = 0.0026, n= 2 technical replicates). Pharmacological inhibition of BMI1 also caused cell senescence in G401 cell line. 101 and 263.5 senescent cells were measured in PTC209 treated cells at 1 μM and 3.5 μM respectively, relative to 9 senescent cells for DMSO treatment (p-value 1 μM = 0.0144, p-value 3.5 μM = 0.0009, n= 2 technical replicates) (Figure 6.20 and Figure 6.20). In contrast, BMI1 knockdown by PTC209 at 1 μM modestly induced senescence in CHLA-266 cell line recorded for 132.5 senescent cells compared to 6 senescent cells for DMSO (p-value: 0.0253, n= 2 technical replicates) (Figure 6.20). Strikingly, PTC209 treatment at 3.5 μM in CHLA-266 produced less senescent cells than 1 μM (mean 3.5 μM: 94 senescent cells, p-value= 0.0064, n= 2 technical replicates (Figure 6.20 and Figure 6.20).

In short, pharmacological inhibition of BMI1 significantly caused cell senescence in MRT cell lines in a dose-dependent manner, with an exception of CHLA-266 cell lines. More technical replicates are required for CHLA-266 cell line to demonstrate the real effect of BMI1 knockdown on cell senescence at two different drug concentrations.

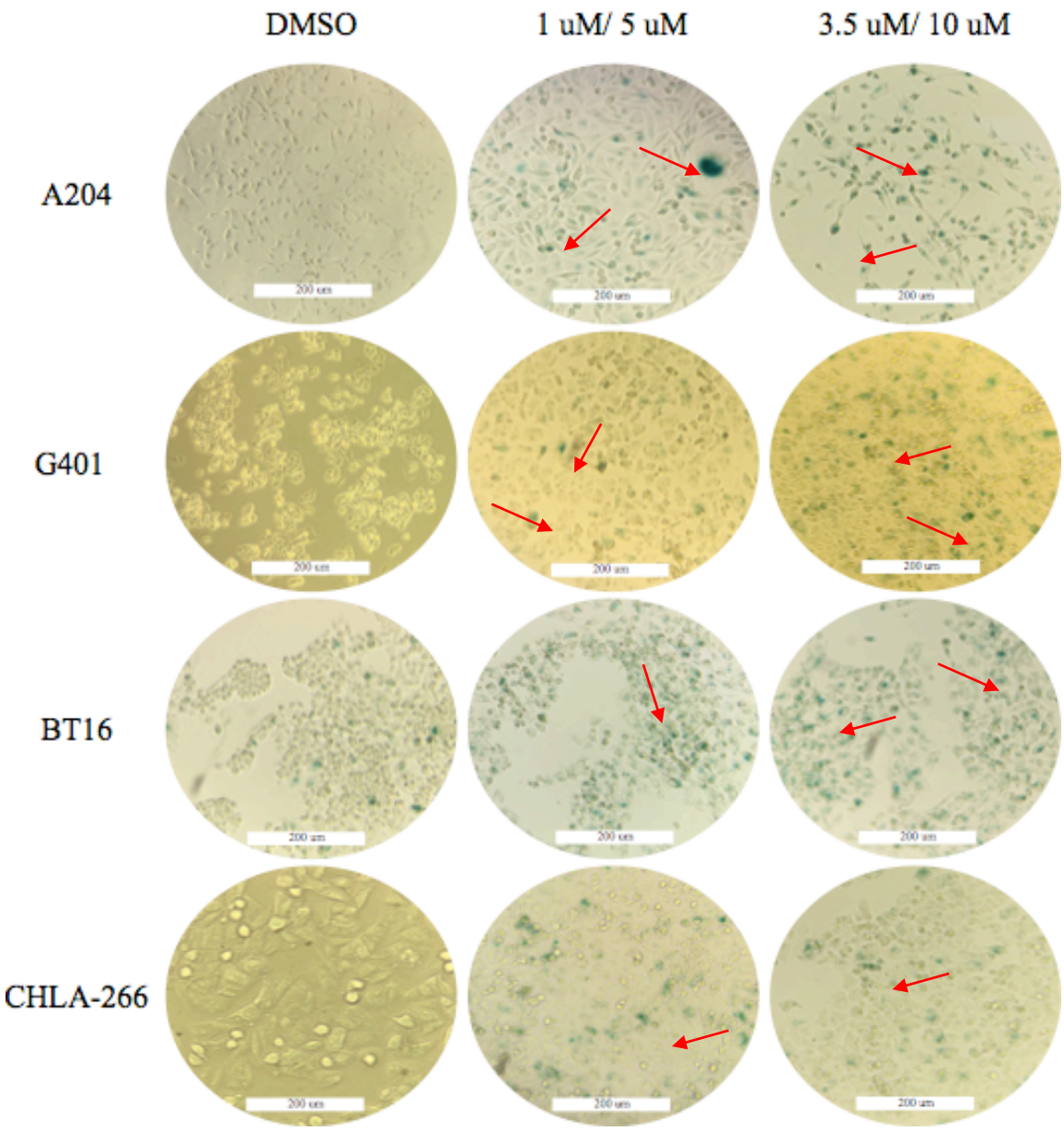

Figure 6.19 ***Pharmacological BMI1 inhibition by PTC209 induces cell senescence in MRT.*** *The presence of senescent cells in culture was identified using senescence associated β-galactosidase staining after 96 hours of treatment. The microscopic images represent a region in the well for each culture of one technical replicate. Senescent cells shown by red arrows.*

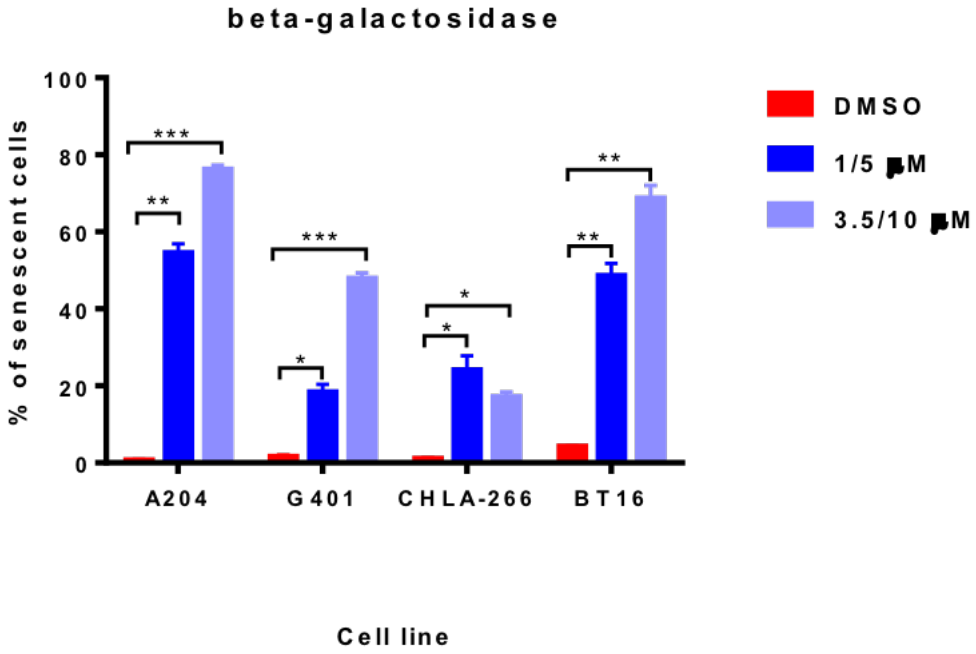

Figure 6.20 ***Pharmacological BMI1 inhibition by PTC209 induces cell senescence in MRT.*** *Knockdown of BMI1 in A204 resulted in significant accumulation of senescent cells at both concentrations (1 and 3.5 μM) after 96 hours of treatment. The number of senescent cells (green coloured cells) was presented as percentage of senescent cells (from a total of 550 cells per wel.. The bar graph showing the number of senescent cells in each culture measured from two independent experiments. The results are shown as means ± SEM of two independent experiments and the significance was determined by unpaired student's t-test (****p<0.0001 vs DMSO).*

Cell line	Treatment	P-value	SE difference
A204	DMSO vs 1 μM	0.0019	13.04
	DMSO vs 3 μM	0.0002	6.083
G401	DMSO vs 1 μM	0.0144	11.18
	DMSO vs 3 μM	0.0009	7.762
CHLA-266	DMSO vs 1 μM	0.0253	20.52
	DMSO vs 3 μM	0.0064	7.071
BT16	DMSO vs 5 μM	0.0051	17.51
	DMSO vs 10 μM	0.0026	18.01

Table 6.3 ***The effect of BMI1 inhibition by PTC209 on cell senescence****. Results show average senescent cells from 5 random regions per well (6-well plate, 9 cm^2/well). The significance was determined using unpaired student t-test.*

6.4.4.3 Targeting BMI1 using PTC209 disrupts normal cell cycle progression

Analysis of senescence-associated β-galactosidase demonstrates the accumulation of senescent cells following treatment with PTC209. This finding may explain the reduced proliferation rate in PTC209 treated cells compared with DMSO. To better understand if slow cell growth is due to cell arrest, cell cycle analysis using Flow Cytometry was performed. The cell cycle analysis was performed to examine if BMI1 inhibition using PTC209 causes a G0/G1 cell cycle arrest. MRT cell lines (1 x 10^6) were treated with PTC209 at two drug concentrations; 1 μM and 3.5 μM for A204, G401 and CHLA-266; and 5 μM and 10 μM for BT16. DMSO was included as a control.

In general, BMI1 knockdown by PTC209 in four MRT cell lines; A204, G401 and CHLA-266 did not alter cell cycle distribution at 24 hours post-treatment (Figure 6.21a-d, Figure 6.22a). A significant result was only measured in BT16. The changes were more pronounced at 72 and 120 hours. There were no fraction of cells in sub-G0 phase for both cell lines when treated at 1 μM. PTC209 treatment in BT16 did not result in an increase

in the number of cells in this phase for two drug concentrations at two-time points (data cannot be clearly seen on the graph due to the small percentage).

Pharmacological inhibition of BMI1 resulted in an increase in the number of cells in the G0/G1 phase for all MRT cell lines. More significant induction of percentage of cells in this phase seen in BT16 measured at 120 hours when compared to DMSO (5 μM [p-value = 0.0129], 10 μM [p-value = 0.0115], n= 2 technical replicates) (Figure 6.21d, Appendix 6.13 and 6.14). The significant increase in the number of cells in G0/G1 phase was also observed in A204 treated with 1 and 3.5 μM, measured at 72 and 120 hours post-treatment (Figure 6.21a, Appendix 6.13 and 6.14). BMI1 inhibition in G401 and CHLA cells also resulted in an increase in the number of cells count in this phase, however, the reading was statistically significant when examined at 120 hours relative to DMSO only (Figure 6.21b-c). When the data were analysed at 120 hours, the increase in the G0/G1 phase of the cycle was more significant suggesting the late effect of PTC209 on cell cycle in these cell lines.

BMI1 inhibition by PTC209 also caused a reduction of cells in S and G2/M phase in all cell lines, A204, G401, CHLA-266 and BT16 (Figure 6.21a-d). The effect of BMI1 knockdown on cell count in these two phases was more significant in BT16, A204 and G401 at two points; 72 and 120 hours. Accumulation of cells in G0/G1 phase was more significant when the data were combined for all cell lines at 72 and 120 hours (Figure 6.22b-c). Furthermore, BMI1 inhibition by PTC209 also resulted in a more significant decrease in the number of cells in the G2/M and S phases. Of note, there were no significant changes observed in cell cycle distribution at 24 hours (Figure 6.22a).

Overall, cell cycle distribution for all MRT cell lines shows that PTC209 treatment causes induction of cells in G0/G1 cell and blocks the cell cycle entry to S and G2/M phases when compared with DMSO. The cell cycle analysis suggests that pharmacological inhibition of BMI1 causes a G1/G0 cell cycle arrest and supports the findings from the cell the senescence analysis.

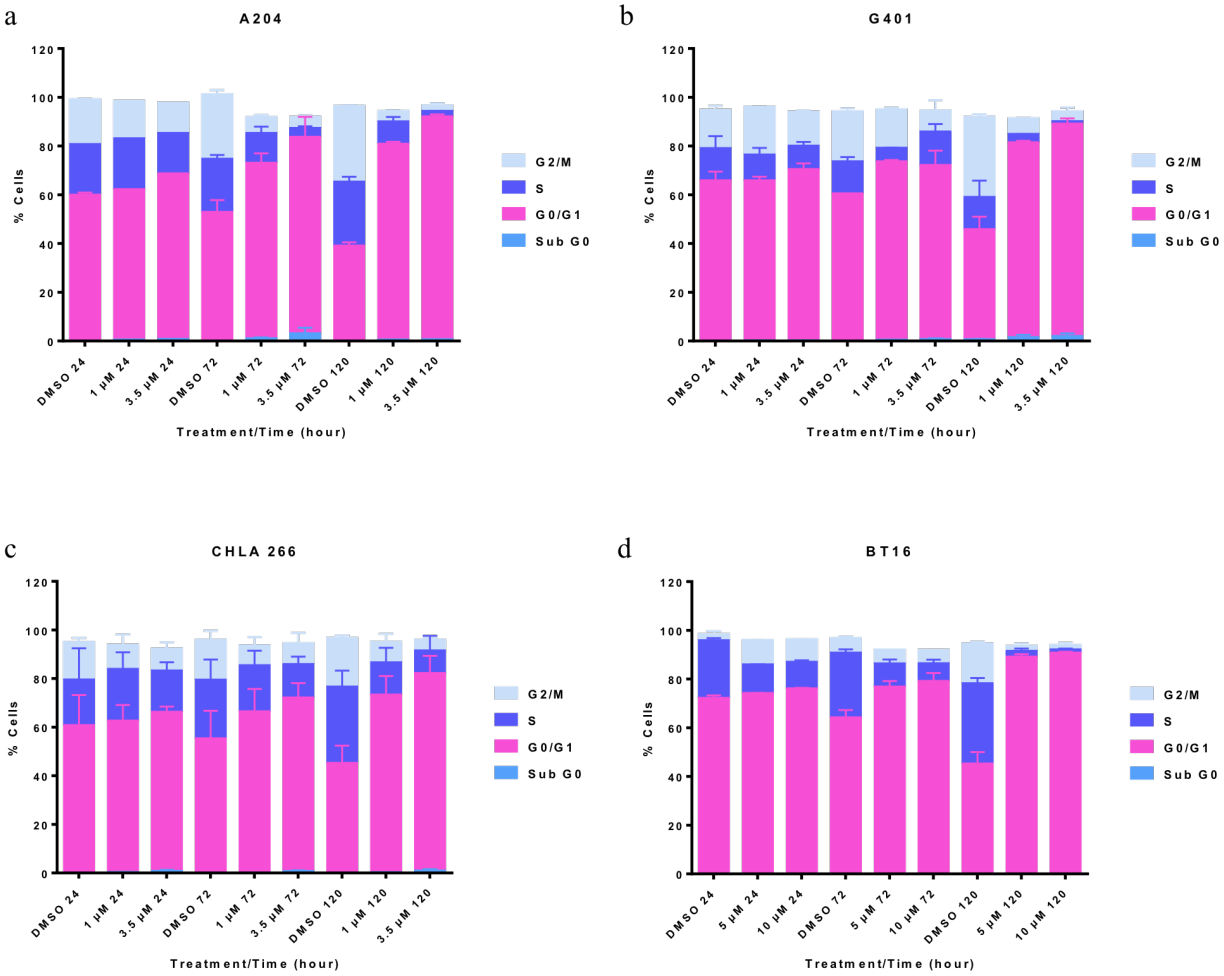

Figure 6.21 ***Pharmacological inhibition of BMI1 causes cell cycle arrest in MRT cell lines.*** *The time dependent effect of PTC209 on cell cycle distributions of four 4 MRT cell line;s (a) A204, (b) G401, (c) CHLA-266 and (d) BT16, after 24, 72 and 120 hours of treatment.. A total number of 15,000 events were counted for each sample and the data were analysed using FlowJo software. Sub-G0 represents cells with a DNA content less than 2N, G0/G1 represents cells with DNA content 2N, cells in S phase with DNA content more than 2N while G2/M cells with DNA content of 4N The results are shown as means ± SEM of two independent experiments and the significance was determined by unpaired student's t-test (* $p<0.05$, ** $p<0.01$, *** $p<0.001$, **** $p<0.0001$ vs DMSO).*

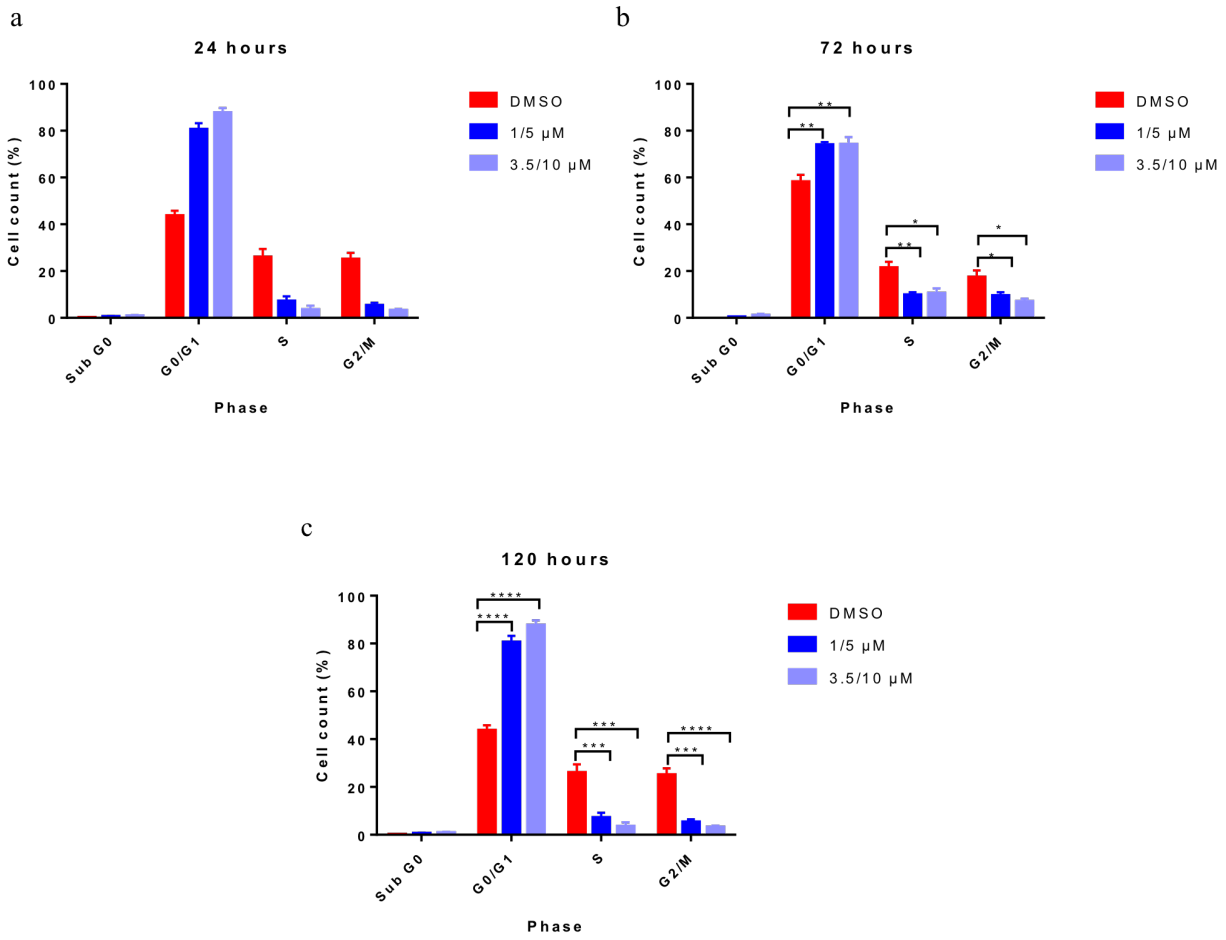

Figure 6.22 ***Effect of BMI1 knockdown on cell cycle seen in MRT cells****. BMI1 knockdown significantly increased cell counts in G0/G1 phase when four datasets (from 4 cell lines) were combined. The decrease in the number of cells in the S and G2/M phase was also observed when datasets were combined for four cell lines. The results are shown as means ± SEM of three independent experiments and the significance was determined by paired student's t-test (* p<0.05, ** p<0.01, *** p<0.001, **** p<0.0001 vs DMSO).*

6.4.4.4 BMI1 inhibition by PTC209 dysregulates the expression of cell cycle regulatory genes.

Flow cytometry analysis of PTC209 treated MRT cells demonstrates cell cycle arrest in which the effect on cell cycle more pronounced from 72 hours onwards. Therefore, the effect of PTC209 on cell cycle regulation was further studied using qPCR analysis of cell cycle-related genes following 96-hours post-treatment with PTC209. Inhibition of BMI1

using PTC209 also caused downregulation of cell cycle promoting G1-phase including *CCND1, CCND3, CCNE1*, *CDK4* and *CDK6* (Figure 6.23). Changes in mRNA expression of these genes were accompanied by increased expression of G1-phase inhibitors such as *CDKN1A* (*p21), CDKN2A (p16* and *p14)*. The gene expression analysis confirms the effect of PTC209 treatment on cell cycle regulation in MRT cell lines.

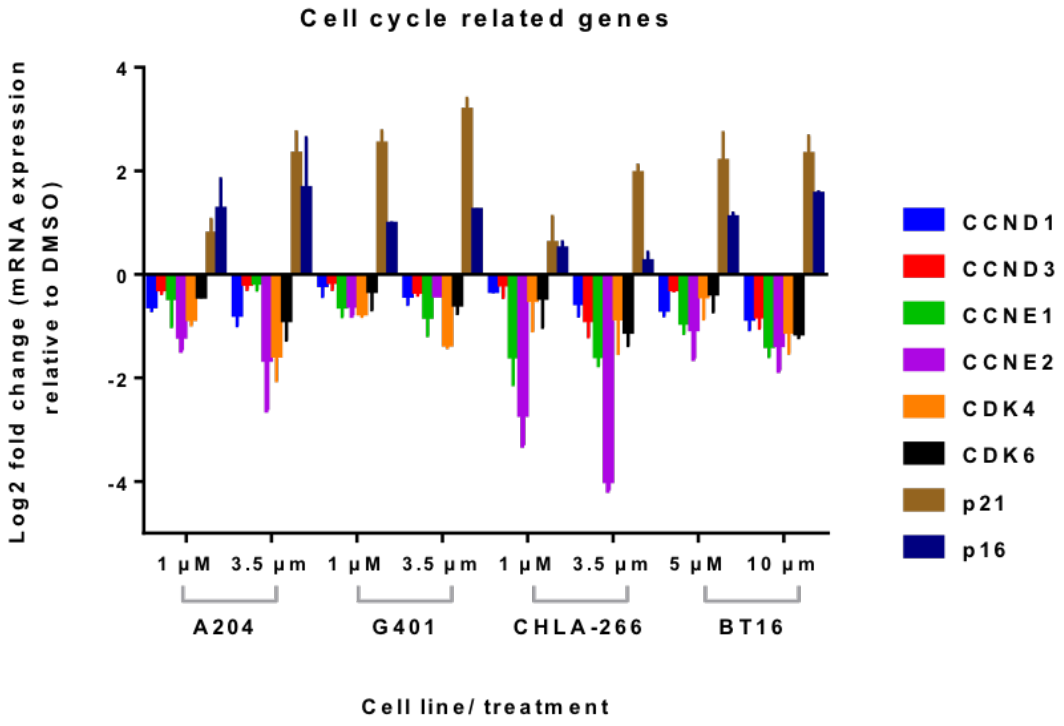

Figure 6.23 ***PTC209 causes deregulation of the expression of cell cycle related genes in MRT cells.*** *qPCR analysis of PTC209 treated samples show deregulation of cell cycle related genes in relation to the DMSO control. Cells were harvested 96 hours post treatment. Pharmacologic inhibition of PTC209 induces expression of cell cycle inhibitors (p14, p16 and p21) accompanied by repression of cell cycle activating genes (CCND1, CCND3, CCNE1, CCNE2, CDK4 and CDK6). The expression was presented relative to DMSO only treatment. Data are presented as mean ± SEM of three independent experiments.*

6.4.4.5 PTC209 effectively depletes MRT self-renewing cells and impairs long-term tumoursphere formation efficiency

To further explore the mechanism by which PTC209 slows down the growth of MRT cells, I continued to examine the pharmacological inhibition of BMI1 on self-renewal. To this end, the limiting dilution assay (LDA) and re-plating tumoursphere experiments were utilised. For the LDA experiment, MRT cell lines were treated with PTC209 at two drug concentrations as adherent cells for 96 hours followed by removal of the drug from the culture. The cells were allowed to recover for 120 hours in an adherent state in culture media that specific for each cell line. The cells were seeded for a limiting dilution assay from 50,000 cells to 1 cell per well in a 96-well plate. Similar to the shRNA experiment, LDA demonstrates no significant difference between DMSO and PTC209 treatment at cell density from 50,000 to 1000 cells as the tumourspheres were observed in all 12 wells for both treatments. The tumourspheres were seen in all 12-wells seeded with the treated cells (Details in Appendix). The effect of BMI1 knockdown on the tumoursphere initiating efficiency was statistically significant at a seeding density of 100 and 10 cell per well relative to DMSO (Figure 6.24a). To estimate the frequency of active self-renewal cells in MRT cells following BMI1 knockdown by PTC209, the number of positive well-containing tumourspheres for 1, 10, 100 and 1000 cells per well underwent ELDA analysis (http://bioinf.wehi.edu.au/software/elda/).

BMI1 inhibition by PTC209 caused a significant reduction in frequency of active self-renewing cells in MRT as shown in Figure 6.24b and Table 6.4. ELDA limiting dilution analysis from tumoursphere culture showed that PTC209 pre-treatment of A204 cells at 1 and 3.5 μM significantly reduced the frequency of self-renewing cells (1 in 32.41 and 1 in 107/36 respectively) when compared to DMSO (1 in 4.69) (p-value = 1.32×10^{-72}, technical replicates, n= 3). The self-renewal capacity of PTC209 treated cells was decreased by 6.9- and 22.8-fold relative to DMSO. The significant reduction of active self-renewal cells following treatment with PTC209 at 1μM was also seen in G401 cell line which shows 1 in 13.3 of frequency active self-renewal compared to 1 in 4.81 for DMSO treatment (p-value = 4.93×10^{-71}, technical replicates, n= 3) (The frequency of active self-renewal cells was more significantly reduced in G401 treated with 3.5 μM of PTC209 (1: 80.48) (p-value = 4.93×10^{-71}, technical replicates, n= 3).

A comparable result was seen in BT16 which shows an active self-renewing cell frequency of 1 in 27.12 and 1 in 81.92 for 5 and 10 μM of PTC209 respectively relative to only 1 in 4.69 cells treated with DMSO (p-value = 1.80 x 10^{-61}, technical replicates, n= 3). ELDA analysis estimated the active self-renewing cells in CHLA-266 was 1 in 31.22 and 1 in 100.3 for 1 and 3.5 μM of PTC209 respectively compared to 1 in 5.03 in DMSO treated cells (p-value = 2.20 x 10^{-66}, technical replicates, n= 3) (Figure 6.24b). The result illustrates that targeting BMI1 caused self-renewal deficiency in MRT cells as the BMI1 infected cells have lost the ability to form tumourspheres by approximately 5 to 23-fold in relative to DMSO.

To confirm the effect of BMI1 knockdown on the self-renewal capacity of MRT cells, I next assessed the effect of PTC209 in four MRT cell lines; A204, G401, CHLA-266 and BT16 in the re-plating tumourspheres assay. The serial re-plating assay reflects the self-renewing cells in culture. To set up this experiment, adherent MRT cells were treated with either DMSO or PTC209 for 96 hours and were dissociated into single cells on the same day (96 hours). The single cells were seeded in 6-well plate at a density of 1000 cells per well in tumoursphere culture. Formation of primary tumoursphere was counted after 120 hours in culture. Primary tumourspheres were harvested and dissociated into single cells, re-seeded at 1000 cells per well in tumoursphere culture. Secondary tumourspheres were allowed to form for 72 hours.

PTC209 treatment caused significant reduction in the mean number of primary tumoursphere at highest concentration tested for this project (3.5 and 10 μM) relative to DMSO (n =2 technical repeats, p-value A204 3.5 μM = 0.0541, p-value G401 3.5 μM = 0.0198, p-value CHLA-266 1 μM = 0.0094, p-value BT16 10 μM = 0.0041) (Figure 6.25a, Appendix 6.5a). A decrease in number of primary tumourspheres also observed in sub-lethal doses (1 and 5 μM), however the number of tumourspheres was significant only in BT16, G401 and CHLA-266 cell lines when compared to DMSO (n =2 technical repeats, p-value BT16 5 μM = 0.0541, p-value G401 1 μM = 0.0282, p-value CHLA-266 1 μM = 0.0077). Pharmacological inhibition of BMI1 at 1 μM in A204 cells also the number of primary tumourspheres, however the data was not significant when compared with DMSO (n = 2 technical repeats, p-value = 0.0541) (Figure 6.25a, Appendix 6.5a). Similarly, formation of secondary tumourspheres was significantly impaired MRT cells treated at GI_{50} and sub-lethal doses of PTC209. (PTC209 GI_{50} doses: n =2 technical

repeats, p-value A204 3.5 μM = 0.0185, p-value G401 3.5 μM = 0.0162, p-value CHLA-266 1 μM = 0.0059, p-value BT16 10 μM = 0.0017, PTC209 sub-lethal doses: n =2 technical repeats, p-value A204 1 μM = 0.0231, p-value G401 1 μM = 0.0233, p-value CHLA-266 1 μM = 0.0081, p-value BT16 5 μM = 0.025).)(Figure 6.25a, Appendix 6.5a).

The effect of BMI1 inhibition by PTC209 on the tumourspheres forming efficiency was more significant when the data for four cell lines were combined. PTC209 treatment caused a significant decrease in the formation of primary tumourspheres (p-value DMSO vs 1/5 μM < 0.0001, SEM 1/5 μM = ± 1.267, p-value DMSO vs 3.5/10 μM < 0.0001, SEM 3.5/10 μM = ± 1.133) and secondary tumourspheres (p-value DMSO vs 1/5 μM < 0.0001, SEM 1/5 μM = ± 1.946, p-value DMSO vs 3.5/10 μM < 0.0001, SEM 3.5/10 μM = ± 2.133) (n = 4 biological replicates, n= 2 technical repeats) (Table 6.5, Figure 6.26). A significant decrease in tumoursphere number was observed in PTC209 treated cells over two passages (n = 4 biological replicates, n= 2 technical repeats, p-value 1/5 μM = 0.0006, SEM 1/5 μM = ± 1.065, p-value 3.5/10 μM < 0.0028, SEM 3.5/10 μM = ± 1.946).

Taken all together my results show that PTC209 can efficiently reduce the self-renewing capability in MRT cell lines. Besides that, self-renewal capacity of MRT cells was sustained following 120 hours recovery period even only with a sub-lethal dose. In the serial re-plating experiment, pharmacological inhibition of PTC209 caused a persistent decrease in the number of tumourspheres suggesting self-renewal defects. The effect of BMI1 knockdown on tumoursphere forming efficiency is more significant when the datasets for individual cell line were combined.

Cell line	Treatment	p-value (between two groups of treatment)	1/ (active self-renewing cell frequency)	Confidence interval (lower/upper)	Fold reduction of depleted self-renewal cells (relative to DMSO)
A204	DMSO	1.32×10^{-72}	4.69	3.85/5.47	N/A
	1 μM		32.41	25.81/40.43	6.90
	3.5 μM		107.36	84.21/136.93	22.80
G401	DMSO	4.93×10^{-71}	4.81	3.95/5.80	N/A
	1 μM		13.30	10.40/17.00	2.77
	3.5 μM		80.48	64.06/101.17	16.73
CHLA-266	DMSO	2.20×10^{-66}	5.03	3.85/5.47	N/A
	1 μM		31.22	21.11/33.93	6.2
	3.5 μM		100.3	68.59/109.02	19.94
BT16	DMSO	1.80×10^{-61}	4.69	4.24//6.16	N/A
	5 μM		27.12	24.05/38.14	5.78
	10 μM		81.92	77.82/125.14	17.47

Table 6.4 ***Average frequency of sphere forming measured using limiting dilution assay (LDA) in MRT cells transfected with PTC209 from three independent experiments****. Data was generated using a limdl software provided by Walter and Eliza Hall Institute. P-value represents overall difference in frequency of self-renewing cells between PTC209 treatment and DMSO. Active self-renewing cell frequency reflects the tumoursphere forming efficiency of the cultures to generate spheres.*

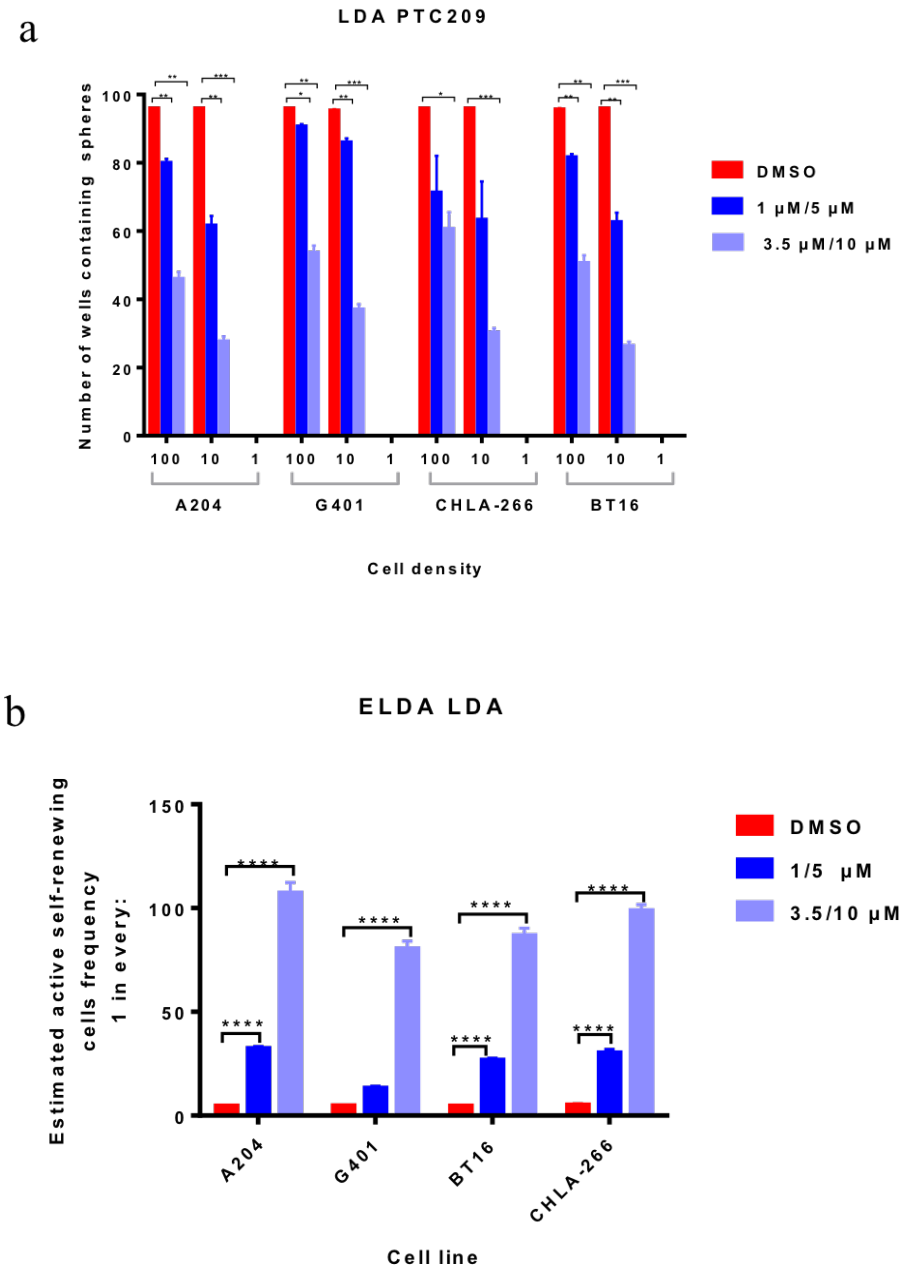

Figure 6.24 ***BMI1 silencing using PTC209 impairs self-renewal capacity of MRT cells.*** *(a) The effect of BMI1 loss on primary tumoursphere was measured using LDA. The PTC209 and DMSO treated cells were cultured in tumourspheres media at density of 50,000 cells down to one cell per well after 120 hours of recovery time (after removal of drug) and tumoursphere were allowed to form for 72h. Knockdown of BMI1 caused significant reduction in the number of tumourspheres at cell density of 10 and 100 cell per well. These results were further analysed using ELDA to measure active self-renewing cells in BMI1-deficient cells (b) ELDA analysis demonstrated significant decrease in sphere forming efficiency following BMI1 knockdown in four MRT cell lines*

*compared with LUC. The results are shown as means ± SEM of three independent experiments and the significance was determined by unpaired student's t-test (****p<0.0001 vs DMSO or primary tumourspheres in appropriate culture).*

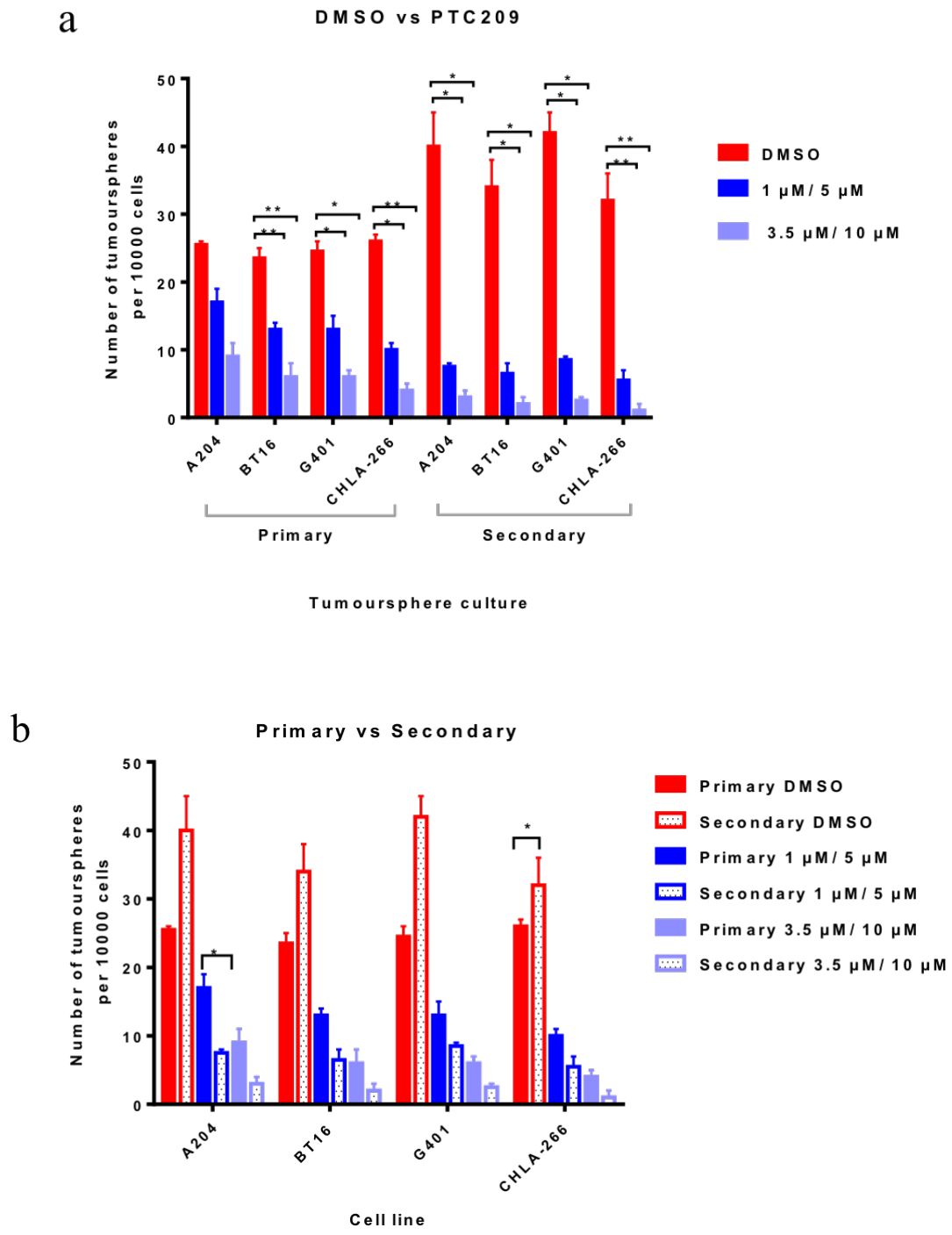

Figure 6.25 ***The effect of PTC209 on self-renewal is corroborated by re-plating assay.*** *Knockdown of BMI1 significantly reduced the formation of primary and secondary tumourspheres in four MRT cell lines in comparison to control (DMSO). The results are shown as means ± SEM of two independent experiments and the significance was determined by unpaired student's t-test (* p< 0.05, ****p<0.0001 vs DMSO or primary tumourspheres in appropriate culture).*

a

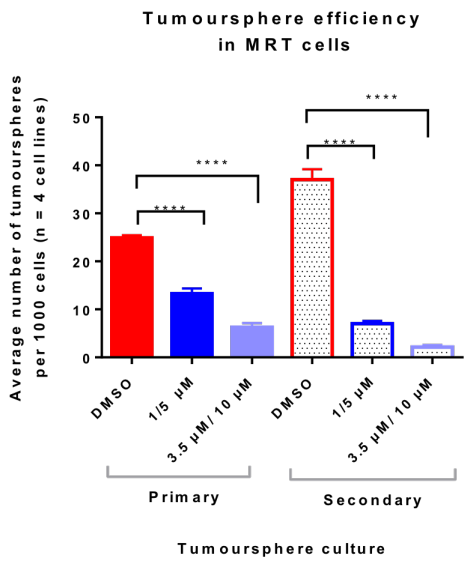

b

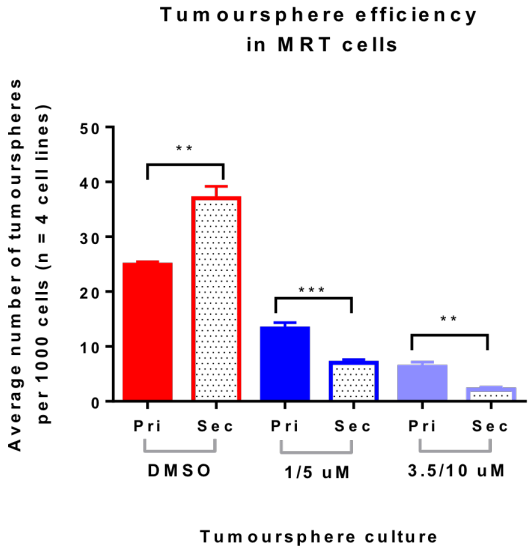

Figure 6.26 ***Significant effect of BMI1 knockdown on formation of tumourspheres****. The decrease in the number of tumourspheres over two passages was more significant when the data was combined. The results are shown as means ± SEM of two independent experiments and the significance was determined by unpaired student's t-test (* p< 0.05, ****p<0.0001 vs DMSO or primary tumourspheres in appropriate culture).*

Samples	Tumoursphere	p-value	Significance	± SEM
DMSO vs 1/5 µM	Primary	< 0.0001	Yes	1.267
DMSO vs 3.5/10 µM	Primary	< 0.0001	Yes	1.133
DMSO vs 1/5 µM	Secondary	< 0.0001	Yes	1.946
DMSO vs 3.5/10 µM	Secondary	< 0.0001	Yes	2.133
DMSO	Primary vs Secondary	0.0017	Yes	2.467
1/5 µM	Primary vs Secondary	0.0006	Yes	1.065
3.5/10 µM	Primary vs Secondary	0.0028	Yes	0.9149

Table 6.5 ***The effect of BMI1 knockdown on tumoursphere formation efficiency****. The number of tumourspheres for each MRT cell line were combined to access whether BMI1 knockdown on four biological replicates was statistically significant. The results are shown as means ± SEM of two independent experiments and the significance was determined by paired student's t-test.*

6.4.4.6 PTC209 reduces the expression of BMI1 possibly through protein degradation

PTC209 treatment in MRT cell lines reduces cell viability, induces cell senescence and cycle arrest in G0/G1 phase, and attenuates self-renewal potential. However, the underlying mechanism of the drug action is not fully understood. Gene expression analysis of BMI1 in PTC209 treated cells shows that PTC209 treatment did not reduce the mRNA expression of *BMI1* but rather caused upregulation of *BMI1* expression (Figure 6.27a). However, significant protein expression reduction was observed following treatment with PTC209 (Figure 6.27b). Conversely, shRNA-mediated knockdown of BMI1 shows significant downregulation of expression at both RNA and protein levels (Figure 6.27a and c). These data suggest PTC209 pharmacologically inhibited BMI1 expression presumably through post-transcriptional repression (ubiquitination). These findings are comparable with studies by Mayr et al. (2016) and Alzrigat et al. (2017) in which the authors also reported increased expression of *BMI1* at the RNA level and reduced BMI1 protein expression in western blot analysis following PTC209 treatment. The authors further showed that downregulation of BMI1 protein expression was accompanied by decreased in H2AK119ub protein levels in multiple myeloma cells. Their findings illustrate that PTC209 pharmacologically inhibited BMI1 expression presumably through post-transcriptional repression and protein degradation.

.

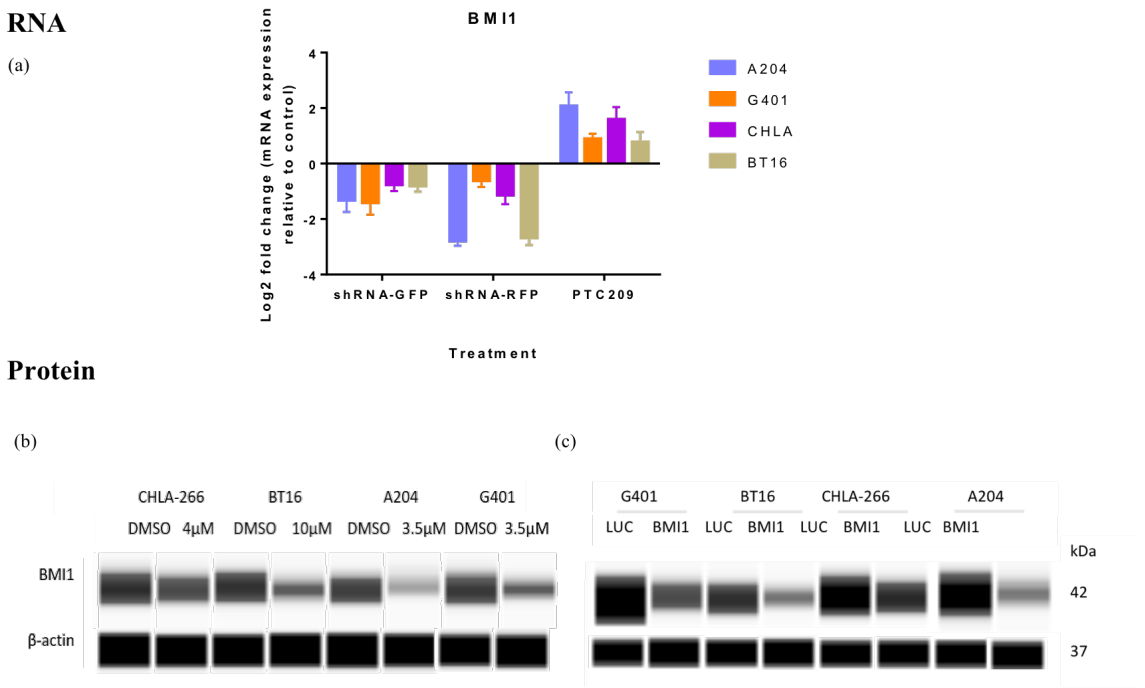

Figure 6.27 ***PTC209 inhibits the BMI1 expression in MRT cells through protein degradation.*** *(a) Treatment with PTC209 increased the transcript level of BMI1 but resulted in degradation of BMI1 protein 48 hours post treatment (b). The expression was normalised to DMSO (control) and each bar represents the expression of BMI1 at* IC_{50} *concentration (3.5 μM for A204, G401 and CHLA-266 whilst 5 μM for BT16). On the other hand, (a-c) shRNA mediated knockdown of BMI1 showed downregulation at both transcript and protein level thus suggesting degradation of BMI1 using PTC209 possibly through protein degradation. Beta-actin serves as control in western blot analysis.*

6.4.4.7 BMI1 knockdown using shRNA and BMI1-inhibitor, PTC209 mimics the effects of SMARCB1 re-expression in MRT cell lines: criteria for an attractive drug target

BMI1 regulates the cell survival, proliferation and expression of stem cells associated genes. In many human cancers, expression of *BMI1* enhances tumour survival through alteration of cell cycle regulatory protein expression. With respect to MRT tumourigenesis, loss of *SMARCB1* is associated with deregulation of cell cycle-related genes such as *p21*, *p16* and *CCND1* and re-expression of *SMARCB1* caused G1 cell cycle arrest (Zhang et al., 2002, Reincke et al., 2003). Since *SMARCB1* is not directly targetable, it is of interest to examine if targeting *BMI1* could mimic the effect of *SMARCB1* re-expression on cell cycle regulation. The expression of *BMI1* downstream genes associated with cell cycle was examined in the qPCR analysis. Kuwahara et al. (2010), Betz et al. (2002) and Versteege et al. (2002) have shown in their studies that reintroduction of *SMARCB1* in MRT cells caused upregulation of *CD44*, *p21* and *p16*. Therefore, the qPCR analysis was performed in MRT cells to identify if *BMI1* knockdown can recapitulate their results.

BMI1 regulates the expression of p16, which is a critical gene associated with MRT tumourigenesis. Analysis of gene expression by qPCR showed an elevation of *p16* mRNA expression in *BMI1*-deficient MRT cells. Additionally, knockdown of BMI1 by PTC209 increased the expression of *SMARCB1* related genes including *p21* and *CD44*. The findings recapitulate the effect of *SMARCB1* re-expression in MRT cells. In line with this, both pharmacologic inhibition and gene silencing of *BMI1* also demonstrated commonalities in cell phenotype i.e. growth and cell cycle pattern. Taking the observations as a whole, *BMI1* presents a new avenue in pharmacological targeting for MRT.

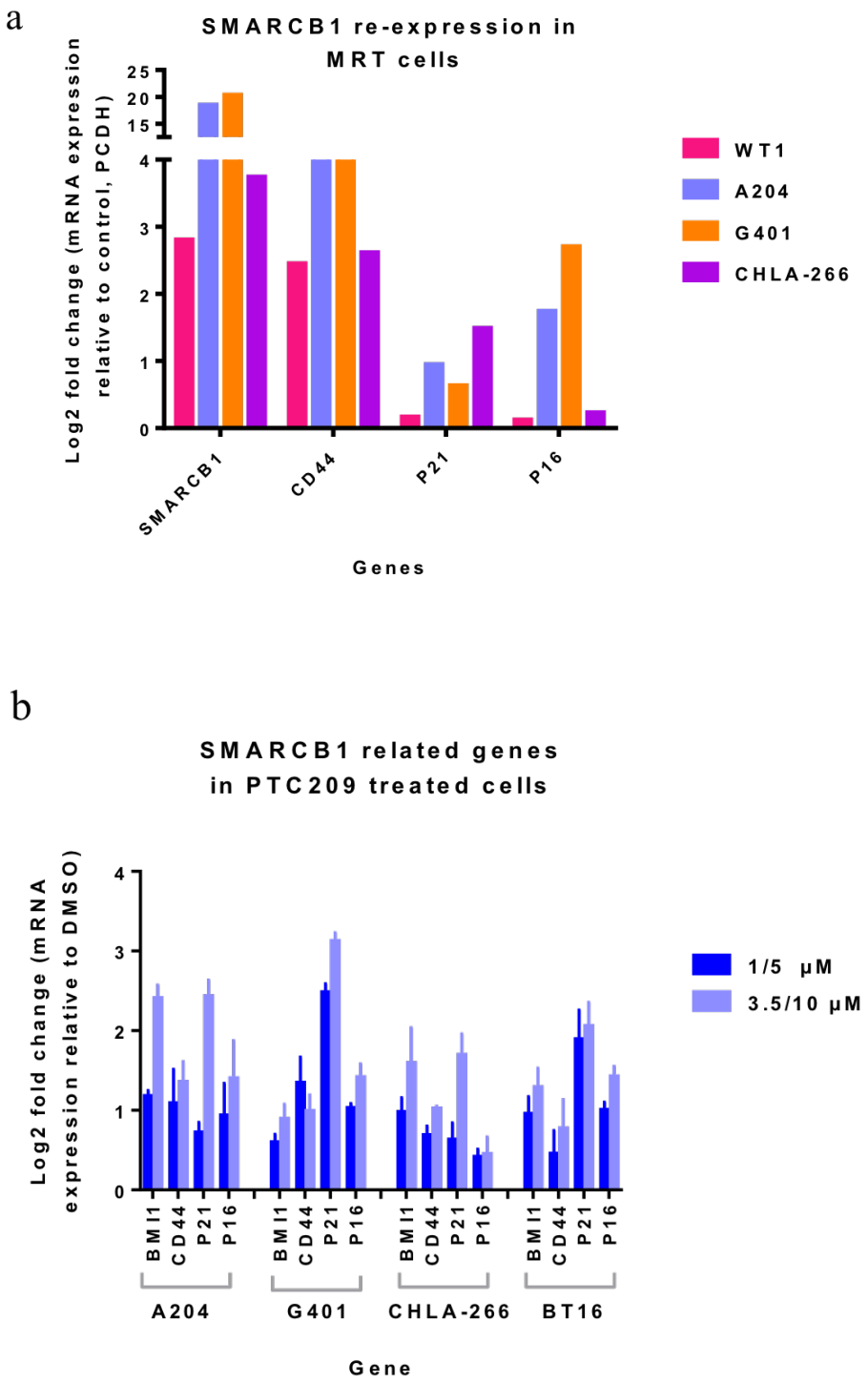

Figure 6.28 ***Knocking down BMI1 transcriptionally activates the expression of critical genes for MRT and recapitulates the effect of SMARCB1 re-expression in MRT cell lines****. (a) qPCR analysis of SMARCB1 related genes in SMARCB1 re-expression MRT cells. The expressions of CD44, p21 and p16 were upregulated following SMARCB1 re-introduction in cells. The mRNA expression was normalised to GAPDH and was presented as relative to PCDH. (b) qPCR analysis of SMARCB1 related genes CDK2A*

(p16), CDKN1A (p21) and CD44 was performed to validate the effect of BMI1 inhibition on expression of these genes in MRT. The bar graph showing p16, p21 and CD44 were following PTC209 treatment. The mRNA expression was normalised to GAPDH and the data was presented as relative to DMSO (which was set at 0). Data are presented as mean ± SEM of three independent experiments.

6.5 Discussion

6.5.1 Effects of BMI1 knockdown in MRT using shRNA and PTC209

For this project, selection of candidate self-renewal gene was performed through a cross-referencing analysis of curated stemness/self-renewal genes with the available genomics within the group which included RNA-seq of MRT primary and cells and CRISPR GeCKO screening of MRT cells with and without *SMARCB1*. Through this systematic biological approach, *BMI1* was selected from 54 stemness/self-renewal genes as it shows *SMARCB1* dependency, has been implicated in cancer development and is druggable.

To explore the therapeutic potential of *BMI1* as a means to counteract MRT tumourigenesis, the effect of BMI1 knockdown was studied in four MRT cell lines using shRNA and small molecule inhibitor, PTC209. shRNA targeting BMI1 inhibited the expression of BMI1 at both RNA and protein levels which significantly impaired cell proliferation 72 hours post-transfection. Treatment with PTC209 reduced BMI1 expression at protein level only and which reflects to the mode of action of PTC209 as post-translational modificator. Nevertheless, *BMI1* knockdown using shRNA and PTC209 resulted in an induction of senescence in MRT cell lines. The slow proliferation rate was seen after 72 hours and increase in the number of β-galactosidase senescent cells after 120 hours were correlated with G0/G1 cell cycle arrest. *SMARCB1* loss is also associated with deregulation of key cell cycle regulatory proteins. Experimental studies by (Kuwahara et al., 2010) and (Betz et al., 2002) showed that re-expression of *SMARCB1* in MRT cell lines leads to G0/G1 cell cycle arrest accompanied by increased expression of cell cycle inhibitors; *p21* and *p16*. RNA inhibition of these genes reversed the cycle arrest (Kuwahara et al., 2010). In this study, *BMI1* knockdown caused cell cycle arrest associated with upregulation of *p16* and *p21* gene expression, thus mimicking the effect of *SMARCB1* re-expression in MRT cells. It is worth noting that, apoptosis was low in PTC209 treated cells and shRNA knocked down cells, and this almost comparable with DMSO. These results are corroborated by small percentage of cells in sub-G0 phase. Of note, previous studies have demonstrated some variable effects of PTC209 on cell apoptosis. Mayr et al. (2016) observed a slight increase in caspase activity in biliary tract cancer cells. However, in additional PTC209 studies by Alzrigat et al. (2017) and Bolomsky et al. (2016) a high level of induction of apoptosis in PTC209 treated multiple

myeloma cells was observed. Thus, the effect of PTC209 on apoptosis is likely context dependent.

For this project, I hypothesised that MRT tumourigenesis and aggressiveness is correlated with its stemness/self-renewal properties. In order to investigate the stemness properties within MRT and how it could be exploited to counteract MRT tumourigenesis, it was critical to determine if knocking down *BMI1* has a significant effect on self-renewal machinery. Limiting dilution assay (LDA) and re-plating tumourspheres experiments showed that inhibition of BMI1 expression using shRNA and PTC209 significantly reduced the self-renewing cell population within MRT. This result is comparable with previous observations made by Kreso et al. (2014) on the effect of *BMI1* knockdown in reducing self-renewal potential in colorectal cancer cells.

Taking all the data together, results from shRNA and PTC209 studies indicate the potential of BMI1 as a future therapeutic target in MRT. Since BMI1 inhibition using PTC209 shows the transcriptional results mimicking the effect of *SMARCB1* re-expression in cells, PTC209 deserves further evaluation in organoids or *in vivo* for its potential as an anti-MRT therapy.

6.5.2 PTC209 modulates post-translational modification of BMI1 expression

PTC209 was primarily described to reduce the BMI1 expression in a human colorectal cancer cell line (Kreso et al., 2014). Subsequent pre-clinical studies tested PTC209 as a means to inhibit self-renewal capacity (Bolomsky et al., 2016, Alzrigat et al., 2017, Mayr et al., 2016, Nishida et al., 2015). I show that PTC209 treatment in MRT cell lines resulted in significant protein loss while elevating the transcript level. The findings were in contrast with shRNA mediated *BMI1* knockout where I achieved downregulation at both RNA and protein levels. Studies of PTC209 in multiple myeloma and biliary tract cancers also showed the downregulation of BMI1 at the protein level only but expression at the RNA level was not affected (Bolomsky et al., 2016, Mayr et al., 2016). Therefore, it was postulated that PTC209 possibly alters post-translational expression of BMI1. BMI1 inhibition using another BMI1 inhibitor, PTC596 in Acute Myeloid Leukaemia (AML) proposed that protein degradation is the principal mechanism of drug action (Nishida et al., 2017). The role of *BMI1* and other subunits of PRC1 namely *RING1A* in ubiquitination was previously studied by Cao et al. (2005) in which the authors reported

the role of *BMI1* and *RING1A* in *HOX* gene silencing. Knock out of these two genes resulted in reduced expression of *HOX* as determined by qPCR analysis. Additionally, ChIP analysis showed knock out of *BMI1* caused significant reduction of H2A ubiquitination at the *HOX* promoter region relative to wild-type cells. Thus, their findings illustrate the PTC209 inhibits expression of *BMI1* through ubiquitination process.

6.6 Appendix

Stemness genes
DNMT1
ERK1/2
FGF2
FGF4
FGFR1
FOXD3
HES1
KIT
LIF
MCFD2
MTF2
NANOG
NODAL
POU5F1
SOX2
STAT3
TBX3
TP53
UTF1
Wnt

Self-renewal genes				
ABCB1	EGFR	IFNG	Meis1	PRRX1
APC	ERBB2	IFNGR1	mir-15	PTEN
ARID1A	ERK	IGF1R	mir-218	Rab11
ARTN	EXT1	Igtp	MUC1	RARA
BATF	FGFR2	IL11	MYB	RBPJ
BCL2	FLT3	IL12 (family)	N-cor	SHH
BCL6	FLT3LG	Il3	Notch	SKP2
BMI1	FOXG1	IL3	NOTCH1	SMAD5
BMP4	FOXO3	IMPDH	NPM1	SMAD7
CD44	FOXO4	IRF8	NRG1	SMARCA4
CDKN1A	FZD4	Irgm1	P38 MAPK	SMO
CDKN2A	GLI1	ITGB3	PCGF2	SS18
CLEC11A	GLI2	JAG1	PD98059	ST8SIA1
COCH	GLI3	JAK2	PIK3R1	STAT5A
COMMD3-BMI1	GMI-1070	KITLG	PIN1	STAT5a/b
CSF3	GNL3	KLF4	Pkc(s)	STAT5B
CTNNB1	Hmga2	KMT2A	POU2F2	TBX1
DHH	Hmgb3	LAMTOR3	PPM1D	TDGF1
DPPA4	HOXB4	LEF1	PRMT1	TERC
E2F4	ID1	LY294002	PROM1	TFCP2L1
TGFBR	THPO	TP63	TRNP1	U0126
VAMP3	WLS	WNT5A	WWTR1	ZBTB16

Pluripotency genes			
APC	GATA6	MED6	SALL4
BMPR1A	GMNN	MED7	SETD1A
CDC73	GRB2	METTL14	SMAD2
CEBPA	HNF4A	METTL3	SMARCA4
CETN2	Id	MYC	SMC1A
CTR9	IGF1	NIPBL	SMC3
DICER1	JAK1	NKAP	SOX1
DIS3L2	KLF4	NOTCH2	SOX3
DMRT1	LEO1	PAF1	SOX7
DPPA2	LIN28A	Panct2	SPP1
DUSP2	MED10	PAX1	STAG2
DUSP7	MED12	PBX1	TCL1A
EOMES	MED14	PDPK1	TET1
ESRRB	MED15	PHF19	TFAP2C
FBXO15	MED17	POU2F1	TGFBR1
FN1	MED21	PPARG	TPT1
FOXO1	MED24	Pramel7	TRIM28
FZD7	MED27	RAD23B	TRIM8
GATA3	MED28	RIF1	XPC
GATA4	MED30	RTF1	ZCCHC11

Appendix 6.1 List of stemness, self-renewal and pluripotency genes for identification candidate self-renewal genes in MRT. The genes were manually curated from previously published studies and IPA.

Genes are functionally relevant to SMARCB1			
Stemness (self-renewal and pluripotency)	CKS2	STAT3	FKBP9
	MCM2	P53	ITGA6
	CDT1	MCM4	ITGB1
	PCNA	HELLS	LAPTM4A
	TOP2A	COL18A1	MSH2
	CSRP2	SFRS3	MTMR10
	ACAT2	BUB1	FGF2
	CBR3	SHROOM3	FGFR1
	CCND1	CDC6	HES1
	EIF4EBP1	TTK	LIF
Self renewal	CD44	GLI1	BCL6
	CDKN2A	GLI2	BMI1
	EXT1	IGF1R	JARID2
	FOXO4	ITGB3	JARID1B
	FZD4	KLF4	CDKN1A
Pluripotency	DUSP2	MYC	TET1
	FN1	NOTCH2	TGFBR1
	JAK1	SPP1	MED12

Appendix 6.2 ***Genes that are functionally relevant to SMARCB1****. Integrated data analysis of curated gene list in Appendix 6.1 with RNA-seq data of MRT primary, MB primary and SMARCB1 re-expression in MRT cell model revealed 54 genes whose expression are active in MRT.*

	Cell density/well	Number of wells	LUC	BMI1
A204	50,000	15	15	15
	10,000	15	30	30
	5,000	30	30	30
	1,000	96	96	96
	100	96	96	67
	10	96	96	40
	1	96	0	0
G401	50,000	15	15	15
	10,000	15	30	30
	5,000	30	30	30
	1,000	96	96	96
	100	96	96	62
	10	96	96	41
	1	96	0	0
CHLA-266	50,000	15	15	15
	10,000	15	30	30
	5,000	30	30	30
	1,000	96	96	96
	100	96	96	63
	10	96	96	40
	1	96	0	0
BT16	50,000	15	15	15
	10,000	15	30	30
	5,000	30	30	30
	1,000	96	96	96
	100	96	96	74
	10	96	96	51
	1	96	0	0

Appendix 6.3 ***In-vitro limiting dilution assay of BMI1-deficient MRT cells and control (LUC) measured on day 5 (120 h) post-lentiviral transfection****.*

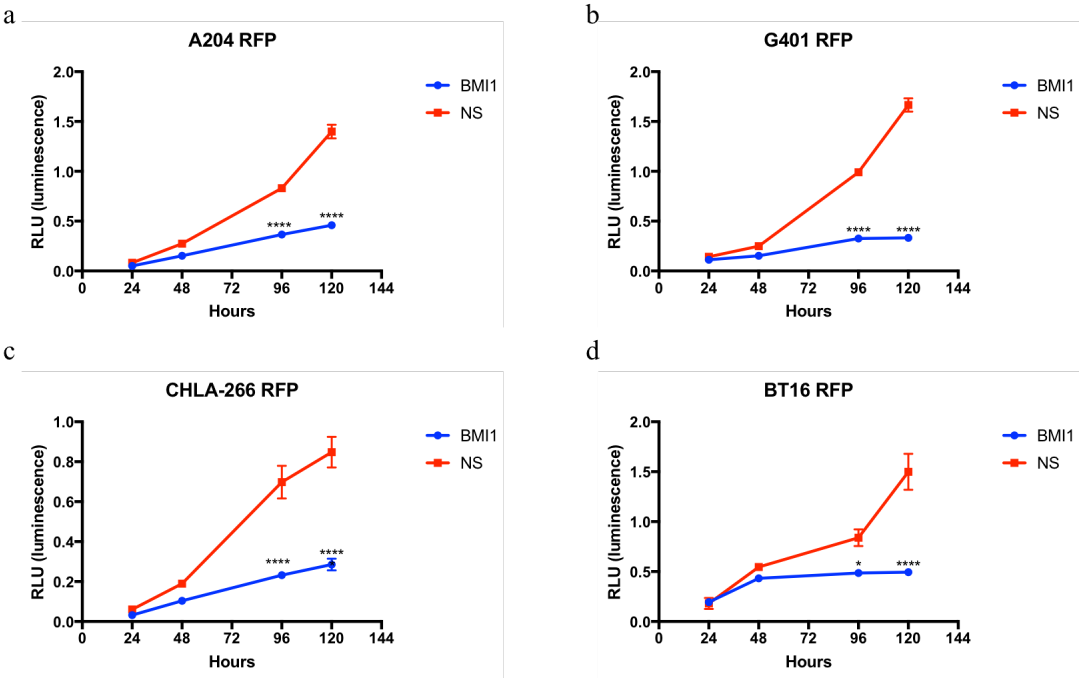

Appendix 6.4 ***The effect of BMI1 knockdown on MRT cell proliferation.*** *Lentiviral transfection of shRNA significantly reduced the cell proliferation in all MRT cell lines relative to control (Non-silencing (NS) vector) measured using MTS CellTiter Aqueous one solution. The reading was measured 24, 48, 96 and 120 hours post infection (a). Knockdown of BMI1 significantly reduced the proliferation rate in A204 from 96 hours onwards compared to NS. (b-c) Similarly, BMI1 knockdown in G401 and CHLA-266 cells resulted in significant decrease in cell proliferation at 96 and 120 hours post transfection when compared to NS. (a) A decrease in proliferate rate was also observed in BT16 and significant decrease was seen at 120 hours relative to NS. The results are shown as means ± SEM of three individual experiments and the significance was determined by unpaired student's t-test (* p< 0.05, ****p<0.0001 vs NS).*

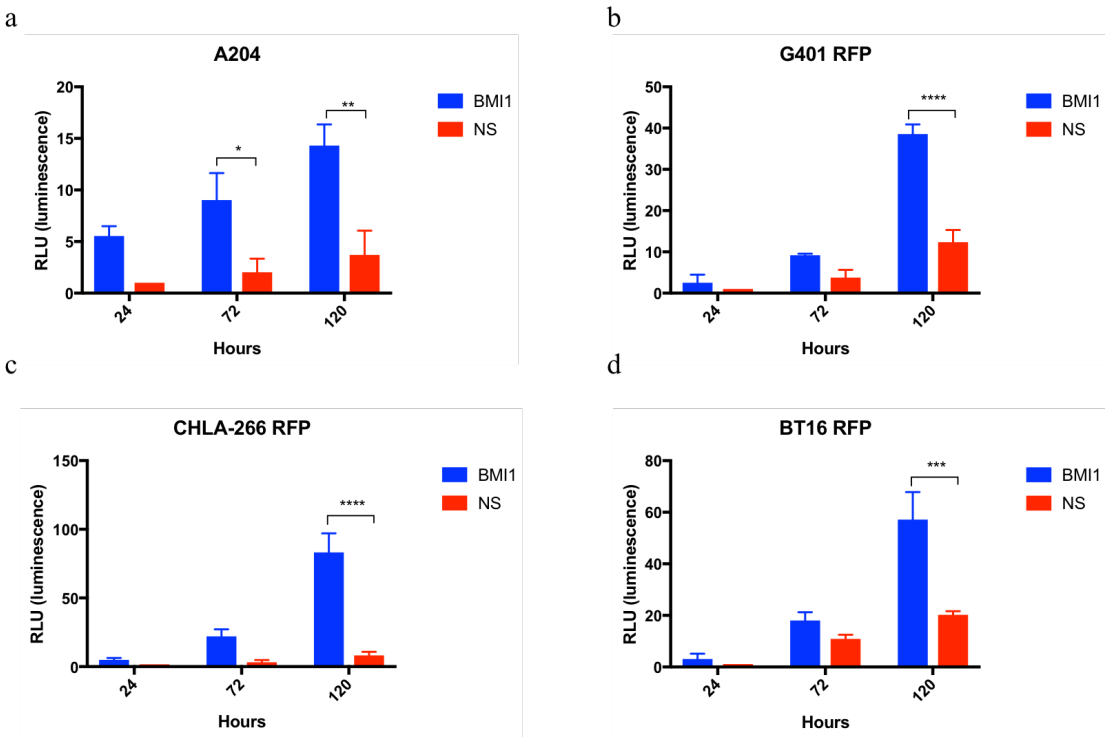

Appendix 6.5 ***Effect of BMI1 silencing on apoptosis in MRT cells****. (a) BMI1 knockdown significantly induced the apoptosis activity in A204 at 72 and 120 hours when compared to NS. (b) Knockdown of BMI1 in G401 resulted in significant increase in cell apoptosis at 120 hours relative to control. (c) Similarly to G401, BMI1 knockdown caused apoptosis in CHLA-266 and statistically different with NS was measured at 120 hours. (d) BMI1 knockdown in BT16 resulted in an induction of apoptosis activity and more significant at 120 post transfection when compared to control. The results are shown as means ± SEM of two individual experiments and the significance was determined by unpaired student's t-test (* p< 0.05, ** p<0.01, *** p<0.001, ****p<0.0001 vs NS of appropriate sample).*

	Cell density/well	Number of wells	NS	BMI1
A204	50,000	15	15	15
	10,000	15	30	30
	5,000	30	30	30
	1,000	96	96	96
	100	96	96	58
	10	96	96	28
	1	96	0	0
G401	50,000	15	15	15
	10,000	15	30	30
	5,000	30	30	30
	1,000	96	96	96
	100	96	96	52
	10	96	96	32
	1	96	0	0
CHLA-266	50,000	15	15	15
	10,000	15	30	30
	5,000	30	30	30
	1,000	96	96	96
	100	96	96	55
	10	96	96	39
	1	96	0	0
BT16	50,000	15	15	15
	10,000	15	30	30
	5,000	30	30	30
	1,000	96	96	96
	100	96	96	53
	10	96	96	29
	1	96	0	0

Appendix 6.6 ***In-vitro limiting dilution assay of BMI1-deficient MRT cells and control (NS) measured on day 5 (120 h) post-lentiviral transfection***.

Cell line	shRNA construct	p-value (between two groups of treatment)	1/ (active self-renewing cell frequency)	Confidence interval (lower/upper)	Fold reduction of depleted self-renewal cells (relative to NS)
A204	BMI1	2.42×10^{-48}	81.77	102.86/65.03	17.43
	NS		4.69	5.74/3.85	
G401	BMI1	2.98×10^{-51}	88.68	111.98/70.25	18.90
	NS		4.69	5.74/3.85	
CHLA-266	BMI1	6.90×10^{-55}	75.92	95.19/60.58	16.19
	NS		4.69	5.74/3.85	
BT16	BMI1	1.95×10^{-40}	90.11	113.88/71/33	19.21
	NS		4.69	5.74/3.85	

Appendix 6.7 ***Average frequency of sphere forming measured using limiting dilution assay (LDA) in MRT cells transfected with shRNA-RFP from three independent experiments****. Data was generated using a limdl software provided by Walter and Eliza Hall Institute. P-value represents overall difference in frequency of self-renewing cells between BMI1 and NS. Active self-renewing cell frequency reflects the cloning efficiency of the cultures to generate spheres.*

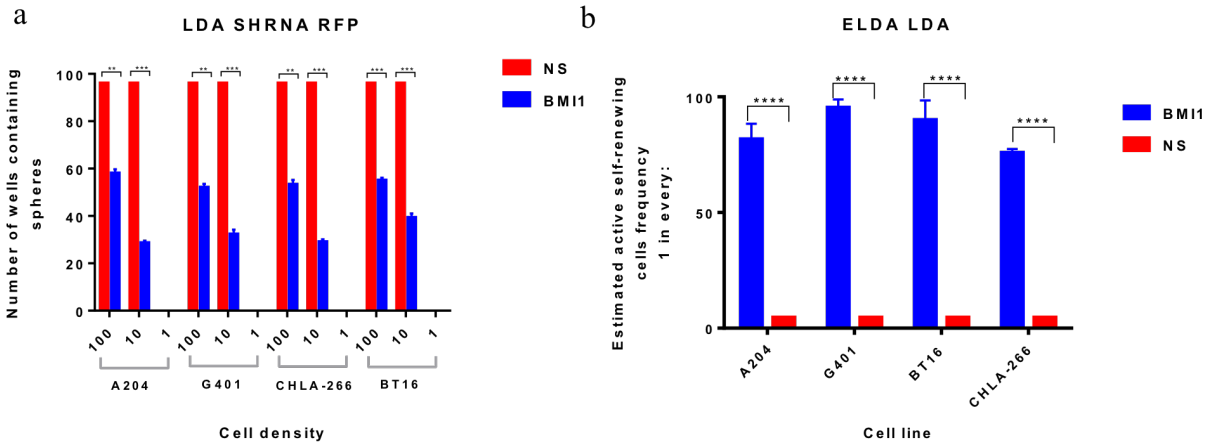

Appendix 6.8 ***BMI1 knock-down using shRNA impairs self-renewal capacity of MRT cells.*** *(a) The effect of BMI1 loss on primary tumoursphere was measured using limiting dilution assay (LDA). The shRNA infected cells were cultured in tumourspheres media at density of 50,000 cells down to one cell per well and tumourspheres were allowed to form for 120h. Knockdown of BMI1 caused significant reduction in the number of tumourspheres at cell density of 10 and 100 cell per well. These results were further analysed using ELDA to measure active self-renewing cells in BMI1-deficient cells. (b) ELDA analysis demonstrate significant decrease in sphere forming efficiency following BMI1 knockdown in four MRT cell lines compared with NS. The results are shown as means ± SEM of three individual experiments and the significance was determined by unpaired student's t-test (****p<0.0001 vs NS of appropriate sample).*

	Cell density/well	Number of wells	DMSO	1/5 µM	3.5/10 µM
A204	50,000	15	15	15	15
	10,000	15	15	15	15
	5,000	30	30	30	30
	1,000	96	96	96	96
	100	96	96	80	46
	10	96	96	59	27
	1	96	0	0	0
G401	50,000	15	15	15	15
	10,000	15	15	15	15
	5,000	30	30	30	30
	1,000	96	96	96	96
	100	96	96	90	53
	10	96	95	86	37
	1	96	0	0	0
CHLA-266	50,000	15	15	15	15
	10,000	15	15	15	15
	5,000	30	30	30	30
	1,000	96	96	96	96
	100	96	96	81	57
	10	96	96	74	30
	1	96	0	0	0
BT16	50,000	15	15	15	15
	10,000	15	15	15	15
	5,000	30	30	30	30
	1,000	96	96	96	96
	100	96	96	81	50
	10	96	96	62	26
	1	96	0	0	0

Appendix 6.9 ***In-vitro limiting dilution assay of BMI1-deficient MRT cells and control (DMSO) measured on day 5 (120 h) after recovery time of PTC209 treatment****.*

Phase		G0/G1		S		G2/M	
Cell line	Construct	p- value	Mean ± SEM	p- value	Mean ± SEM	p- value	Mean ± SEM
A204	BMI1	0.0002	76.96 ± 0.6	0.3167	8.13 ± 0.05292	0.0022	14.9 ± 0.7034
	LUC		85.15 ± 0.1202		7.403 ± 0.6334		7.657 ± 0.7552
G401	BMI1	<0.0001	66.97 ± 0.6984	0.4504	5.933 ± 0.9062	0.0007	27.13 ± 2.02
	LUC		87.6 ± 0.9849		5.1 ± 0.4163		7.333 ± 0.3844
CHLA-266	BMI1	0.0122	51.27 ± 0.2667	0.0045	24.8 ± 0.8888	0.1623	23.83 ± 1.938
	LUC		45.5 ± 1.3		34.23 ± 1.369		20.23 ± 0.8212
BT16	BMI1	0.8333	43.57 ± 2.39	0.6949	39.4 ± 1.909	0.0701	17.17 ± 0.6438
	LUC		44.13 ± 0.809		40.3 ± 0.9539		15.43 ± 0.2906

Appendix 6.10 ***The effect of BMI1 knockdown on cell cycle in MRT cells at 24 hours.*** *Results are shown as mean ± SEM*

Phase		G0/G1		S		G2/M	
Cell line	Construct	p- value	Mean ± SEM	p- value	Mean ± SEM	p- value	Mean ± SEM
A204	BMI1	<0.0001	81.5 ± 0.5132	0.1085	7.2 ± 0.1528	0.0002	11.3 ± 0.2646
	LUC		56.77 ± 0.6642		11.37 ± 2.017		31.9 ± 1.493
G401	BMI1	0.0002	87.07 ± 1.097	0.0002	6.053 ± 0.2569	<0.0001	6.467 ± 0.1186
	LUC		72.39 ± 0.1667		10.18 ± 0.191		17.42 ± 0.4041
CHLA-266	BMI1	<0.0001	74.87 ± 0.5608	<0.0001	13.57 ± 0.2728	<0.0001	11.27 ± 0.8293
	LUC		23.7 ± 0.6429		39.37 ± 0.5667		36.6 ± 0.2082
BT16	BMI1	<0.0001	66.3 ± 0.4163	0.0003	24.57 ± 0.3283	<0.0001	7.833 ± 0.1453
	LUC		27.67 ± 0.9597		45.17 ± 1.713		27.2 ± 0.5508

Appendix 6.11 ***The effect of BMI1 knockdown on cell cycle in MRT cells at 120 hours****. Results are shown as mean ± SEM*

24 hours					
		G401	A204	CHLA-266	BT16
G0/G1	Mean ± SEM of DMSO	65.75 ± 3.750	60.65 ± 12.550	48.5 ± 10.40	72.1 ± 1.20
	P-Value	0.9827	0.9206	0.3795	0.2526
	Mean ± SEM of 1/3.5µM	65.65 ± 1.650	62.25 ± 6.650	60.25 ± 1.450	74.05 ± 0.250
	P-Value	0.4256	0.7431	0.2549	0.0911
	Mean ± SEM of 5/10µM	70.25 ± 2.550	65.45 ± 2.350	65.4 ± 2.50	76 ± 0.40
S	Mean ± SEM of DMSO	13.22 ± 5.080	18.75 ± 13.050	31.4 ± 10.70	23.7 ± 10
	P-Value	0.6993	0.8791	0.481	0.0073
	Mean ± SEM of 1/3.5µM	10.62 ± 2.8850	21.3 ± 70	22.15 ± 1.250	11.8 ± 0.20
	P-Value	0.57	0.9115	0.368	0.0099
	Mean ± SEM of 5/10µM	9.615 ± 1.6850	17.05 ± 3.550	18.8 ± 2.20	10.9 ± 0.80
G2/M	Mean ± SEM of DMSO	15.8 ± 1.70	15.5 ± 1.80	17.95 ± 0.050	2.52 ± 1.320
	P-Value	0.1544	0.3593	0.0021	0.0308
	Mean ± SEM of 1/3.5µM	19.65 ± 0.250	10.02 ± 4.280	15.5 ± 0.10	9.975 ± 0.2250
	P-Value	0.4232	0.1893	0.0156	0.0365
	Mean ± SEM of 5/10µM	14 ± 0.60	9.03 ± 2.770	11.6 ± 0.80	9.265 ± 0.1250

Appendix 6.12 ***The effect of BMI1 knockdown on cell cycle in MRT cells at 24 hours****. Results are shown as mean ± SEM.*

72 hours					
		G401	A204	CHLA-266	BT16
G0/G1	Mean ± SEM of DMSO	60.4 ± 0.2	55.2 ± 11.5	52.8 ± 5	64.1 ± 3.2
	P-Value	0.0037	0.2083	0.0955	0.0902
	Mean ± SEM of 1/3.5µM	73.15 ± 0.75	76.75 ± 2.45	72 ± 4	74.05 ± 0.25
	P-Value	0.2133	0.4746	0.1046	0.0864
	Mean ± SEM of 5/10µM	71.4 ± 6.1	65.45 ± 2.35	80.6 ± 8.4	79.05 ± 3.45
S	Mean ± SEM of DMSO	13.15 ± 1.95	24.15 ± 8.45	21.8 ± 1.7	26.55 ± 1.55
	P-Value	0.0616	0.232	0.098	0.011
	Mean ± SEM of 1/3.5µM	5.605 ± 0.245	9.5 ± 1.8	12.25 ± 2.75	11.8 ± 0.2
	P-Value	0.8783	0.5196	0.0109	0.0135
	Mean ± SEM of 5/10µM	13.8 ± 3.2	17.05 ± 3.55	3.645 ± 0.865	7.25 ± 1.65
G2/M	Mean ± SEM of DMSO	20.5 ± 1.4	16.4 ± 3.9	26.49 ± 1.885	6.005 ± 0.735
	P-Value	0.1021	0.1108	0.0111	0.0355
	Mean ± SEM of 1/3.5µM	15.7 ± 0.9	5.68 ± 0.06	6.555 ± 0.955	9.975 ± 0.225
	P-Value	0.1247	0.2633	0.0083	0.6263
	Mean ± SEM of 5/10µM	8.545 ± 4.455	9.03 ± 2.77	4.63 ± 0.67	5.585 ± 0.055

Appendix 6.13 ***The effect of BMI1 knockdown on cell cycle in MRT cells at 72 hours****. Results are shown as mean ± SEM*

120 hours					
		G401	A204	CHLA-266	BT16
G0/G1	Mean ± SEM of DMSO	45.2 ± 5.30	45.1 ± 7.30	39 ± 1.50	45.1 ± 4.90
	P-Value	0.0229	0.121	0.0019	0.0129
	Mean ± SEM of 1/3.5µM	79.95 ± 0.750	73.05 ± 7.850	80.3 ± 10	89 ± 1.20
	P-Value	0.0186	0.0723	0.0011	0.0115
	Mean ± SEM of 5/10µM	87.15 ± 2.350	81.25 ± 7.250	91.45 ± 0.950	90.65 ± 0.550
S	Mean ± SEM of DMSO	13.23 ± 6.8750	31.45 ± 6.750	26.2 ± 2.20	33 ± 2.30
	P-Value	0.2903	0.1861	0.0293	0.0069
	Mean ± SEM of 1/3.5µM	3.43 ± 0.070	13.32 ± 6.180	9.2 ± 20	2.4 ± 1.10
	P-Value	0.2182	0.1367	0.0083	0.0056
	Mean ± SEM of 5/10µM	1.035 ± 0.0250	9.33 ± 6.170	2.2 ± 0.10	1.325 ± 0.5750
G2/M	Mean ± SEM of DMSO	32.83 ± 1.2750	20 ± 1.20	31.09 ± 0.50	16.35 ± 0.950
	P-Value	0.0024	0.0861	0.0007	0.0108
	Mean ± SEM of 1/3.5µM	6.41 ± 0.30	8.49 ± 3.410	4.22 ± 0.50	2.06 ± 1.160
	P-Value	0.0059	0.0096	0.0015	0.0102
	Mean ± SEM of 5/10µM	4.005 ± 1.8150	4.46 ± 0.960	2.3 ± 10	1.78 ± 1.140

(a)

	Primary tumourspheres			Secondary tumourspheres		
	BMI1 (mean ± SEM)	LUC (mean ± SEM)	P-value	BMI1 (mean ± SEM)	LUC (mean ± SEM)	P-value
A204	10.5 ± 2.50	13.5 ± 1.50	0.4117	7.5 ± 1.50	16 ± 10	0.0422
G401	9 ± 20	15 ± 10	0.1153	7 ± 20	20 ± 20	0.0442
CHLA-266	8 ± 10	16.5 ± 1.50	0.0422	5.5 ± 0.50	21.5 ± 3.50	0.0455
BT16	9.5 ± 1.50	14.5 ± 1.50	0.1425	6.5 ± 0.50	20 ± 10	0.0068

(b)

	BMI1			LUC		
	Primary tumourspheres (mean ± SEM)	Secondary tumourspheres (mean ± SEM)	P-value	Primary tumourspheres (mean ± SEM)	Secondary tumourspheres (mean ± SEM)	P-value
A204	10.5 ± 2.50	7.5 ± 1.50	0.4117	13.5 ± 1.50	16 ± 10	0.2999
G401	9 ± 20	7 ± 20	0.5528	15 ± 10	20 ± 20	0.1548
CHLA-266	8 ± 10	5.5 ± 0.50	0.1548	16.5 ± 1.50	21.5 ± 3.50	0.3196
BT16	9.5 ± 1.50	6.5 ± 0.50	0.1982	14.5 ± 1.50	20 ± 10	0.0927

Appendix 6.15 ***The effect of BMI1 knockdown on formation of tumourspheres in serial re-plating experiments****. (a) Decrease in the number of primary and secondary tumourspheres in BMI1 knocked down cells. (b) Differences in the number of tumourspheres over two cultures Results are shown as mean ± SEM*

(a)

	Primary tumourspheres				Secondary tumourspheres			
	1/5 µM (mean ± SEM)	P-value (1/5 µM vs DMSO)	3.5/10 µM (mean ± SEM)	P-value (3.5/10 µM vs DMSO)	1/5 µM (mean ± SEM)	P-value (1/5 µM vs DMSO)	3.5/10 µM (mean ± SEM)	P-value (3.5/10 µM vs DMSO)
A204	17 ± 2	0.0541	17 ± 2	0.0541	7.5 ± 0.5	0.0231	3 ± 1	0.0185
G401	13 ± 1	0.0282	6 ± 2	0.0198	6.5 ± 1.5	0.0233	2 ± 1	0.0162
CHLA-266	13 ± 2	0.0442	6 ± 1	0.0094	8.5 ± 0.5	0.0081	2.5 ± 0.5	0.0059
BT16	10 ± 1	0.0077	4 ± 1	0.0041	5.5 ± 1.5	0.025	1 ± 1	0.0172

(b)

	DMSO			1/5 µM			3.5/10 µM		
	Primary (mean ± SEM)	Secondary (mean ± SEM)	P-value	Primary (mean ± SEM)	Secondary (mean ± SEM)	P-value	Primary (mean ± SEM)	Secondary (mean ± SEM)	P-value
A204	25.5 ± 0.5	40 ± 5	0.102	17 ± 2	7.5 ± 0.5	0.044	9 ± 2	3 ± 1	0.1153
G401	23.5 ± 1.5	34 ± 4	0.1332	13 ± 1	6.5 ± 1.5	0.0691	6 ± 2	2 ± 1	0.2155
CHLA-266	24.5 ± 1.5	42 ± 3	0.0348	13 ± 2	8.5 ± 0.5	0.1607	6 ± 1	2.5 ± 0.5	0.0887
BT16	26 ± 1	32 ± 4	0.2829	13 ± 2	8.5 ± 0.5	0.1607	4 ± 1	1 ± 1	0.1679

Appendix 6.16 ***Effect of pharmacological inhibition of BMI1 on formation of tumourspheres in serial re-plating experiments****. (a) Decrease in the number of primary and secondary tumourspheres in BMI1 knocked down cells. (b) Differences in the number of tumourspheres over two cultures Results are shown as mean ± SEM.*

Chapter 7 Conclusion

7.1 Introduction

Malignant Rhabdoid Tumours (MRT) are rare and aggressive cancers that occur primarily in infants and children less than 3 years old (Woehrer et al., 2010). These tumours are not restricted to one anatomical location but can be found almost everywhere in the body. MRT that arise in soft tissue and outside of the brain are known as extra-cranial rhabdoid tumour (ECRT) whereas the tumours that occur in the brain and spinal cord are called Atypical Teratoid Rhabdoid Tumour (ATRT) (Biggs et al., 1987, Parham et al., 1994, Rorke et al., 1996). MRT present a unique feature which is often described as "simple genome" due to the one recurrent genomic alteration which is characteristic of these tumours type regardless of tumour origins (Lee et al., 2012, Hasselblatt et al., 2013, Johann et al., 2016). Histological and genome-wide studies report a consistent biallelic inactivation at chromosome 22 of *SMARCB1* (Versteege et al., 1998, Biegel et al., 2002a). Patients with MRT are treated with multimodal therapies which involve the combination of few treatments including surgery, radiotherapy and chemotherapy. Despite the advancement in cancer therapy, patients with MRT have very poor prognosis due to inefficacious treatment, most patients survived less than 1 year after treatment (Chi et al., 2009, Hilden et al., 2004, Tekautz et al., 2005).

The role of *SMARCB1* has been previously established both *in vivo* and *in vitro*. Several studies have illustrated the tumourigenic effects of *SMARCB1* loss in MRT on various pathways such as cell cycle, epigenetic mechanism, and lineage-specific cell development and differentiation (Wilson and Roberts, 2011, Betz et al., 2002). Additionally, the effect of *SMARCB1* loss in tumourigenesis was previously studied in a limited number of MRT mouse models (Roberts et al., 2000, Roberts et al., 2002, Han et al., 2016). Although *SMARCB1* loss can initiate tumour formation, there is little evidence as to how this single genomic abnormality results in a highly aggressive disease which is almost exclusive to very young children.

Despite having little genetic variability, MRT vary histologically containing cells with different morphology and differentiation markers from multiple lineages even intratumourally (Okuno et al., 2010, Fischer et al., 1989, Harris et al., 1987, Kato et al., 2003). Various cell of origin has been suggested due to the phenotypic diversity of MRT such as neural, neural crest cells, mesenchymal, etc (Harris et al., 1987, Fischer et al., 1989, Ota et al., 1993, Parham et al., 1988). The aetiology of MRT regarding its cell of origin and how this relates to tumour location and molecular subtype is largely unknown. Attempts to

identify cellular origins for MRT showed variable findings. Deletion of either *Smarcb1* or *Smarca4* in granule neurons and their progenitors; which had been postulated to be the origin of ATRT, failed to generate tumours *in vivo* (Moreno et al., 2014). Genome-wide analyses suggested neural crest (NC) cells or neural stem cells (NSC) as cells of origin for MRT based on deregulation of many genes involved in development of these two cell types following *SMARCB1* loss (Chun et al., 2016, Johann et al., 2016, Gadd et al., 2010). MRT are characterised as an early onset disease, with a peak incidence at 0-3 years of age (Margol and Judkins, 2014). Also in rare circumstances MRT have been reported occurring as a congenital subcutaneous mass (White et al., 1999, Toth et al., 2011). Hence, it is more likely that *SMARCB1* loss occurs in early progenitor cells which are later transformed into MRT.

As a member of the SWI/SNF chromatin remodelling complex and tumour suppressor gene, expression of *SMARCB1* is associated with deregulation of pathways that are involved in stem cell regulation and maintenance (Gadd et al., 2010). MRT have been proposed to have "stem-like cells" within the tumours due to expression of various stem cell markers and also phenotypes that resemble mesenchymal, neural and epithelial stem cells (Hollmann and Hornick, 2011, Kohashi et al., 2016, Okuno et al., 2010, Biswas et al., 2016, Venneti et al., 2011b, Deisch et al., 2011). Genome-wide analyses of primary MRT patient samples also demonstrated overexpression of genes that regulate self-renewal and pluripotency which are common features of stem cells. Collectively, these findings suggest that deregulated stem cell processes may significantly impact upon MRT tumourigenesis.

This research study was performed to provide a better understanding of MRT tumourigenesis through identification of cell of origin and stem cell self-renewal pathways/genes that drive disease aggressiveness. Given the lack of appropriate MRT mouse models, the data collected from cell of origin study were analysed in such a way as to understand which stem cell types are potentially the cell of origin of MRT and whether knocking down *SMARCB1* in the putative cell of origin can be a strategy for the development of a more disease appropriate mouse model. My research study also aimed to investigate the stemness/self-renewal properties of MRT and its potential to counteract MRT tumourigenesis. To examine the effect of manipulating stemness/self-renewal genes/proteins in MRT and to what extent their role in MRT can be manipulated for development of new therapeutic targets for MRT.

7.2 Summary

7.2.1 Identification of cell of origin for MRT

7.2.1.1 Integrated bioinformatics analysis reveals potentially different cell of origin(s) for each subtype within MRT

For many cancer types, the precise identification of tumour initiating cells remains unknown. Unlike other human cancers which can be found locally, MRT can arise almost anywhere in the body and exhibit multiple phenotypes, thus posing challenges for specific discovery of cell of origin for this childhood malignancy. Few studies have tried to establish the potential cell of origin for MRT (Harris et al., 1987, Fischer et al., 1989, Ota et al., 1993, Parham et al., 1988) and the subtypes within MRT (Chun et al., 2016, Johann et al., 2016, Torchia et al., 2016). However, these studies showed several technical limitations in which the findings were concluded solely based on either gene expression profiles of primary tumours or existence of stem cell surface markers. Preliminary bioinformatic analysis of MRT cell models performed by Dr Williamson suggested that MRT possibly originate from early pluripotent stem cells. However, this analysis had a limited number of stem cell expression profiles and no primary MRT profiles were included. This result was studied further in this project.

To shed light on a potential cell of origin for MRT, a system for ranking putative cells of origin was described in chapter 3 through the integrated bioinformatics analysis of expression profiles of various stem cells types that were publicly available on the GEO NCBI database with primary and model data of MRT. Expression profiles from neural, neural crest, stromal, mesenchymal and embryonic stem cells, as well as iPSC, were included (n=446). Additionally, a time course experiment in which *SMARCB1* was re-expressed in MRT cell lines, was utilised in the analysis. This data provided extra information on the potential cell of origin for MRT as restoration of *SMARCB1* in MRT cells caused the expression profiles to converge over time to a point that was closer to neural crest (NC) cells and mesenchymal stem cell (MSC) expression profiles. The data were analysed based on differential gene expression between MRT primary and *SMARCB1* re-expression cell model with various stem cell expression profiles using NMF, heatmap and PCA clustering analyses.

Results from this study indicate that three candidate cells of origin within the family of neural crest (NC), neural (NSC) and mesenchymal stem (MSC) cells. Expression profiles of ATRT resemble NSC whilst ECRT resembles NC and MSC. The results were further interrogated to understand the possibility of subtype-specific cell of origin in MRT. Gene expression profiling characterised three potential cells of origin within MRT based on developmental gene expression that related to the bodily location of primary tumours. ATRT showed significant enrichment of genes associated with neuronal development while ECRT demonstrated upregulation of genes associated with mesenchymal cell type development. These findings were in line with previous studies (Chun et al., 2016, Gadd et al., 2010) in which the authors reported the expression of genes associated with MSC and NSC in primary MRT. Additionally, the extent of transcriptional overlap clearly reflects differences in tumour location and molecular subgroup. Of note, embryonic stem cells demonstrated a very small similarity with expression profiles of MRT subtypes.

In conclusion, the bioinformatics analysis performed in this study illustrated that MRT might not arise from the same progenitor cells. Consistent with other previous studies (Chun et al., 2016, Gadd et al., 2010, Han et al., 2016, Vitte et al., 2017), MRT possibly derive either from NSC, NC or MSC. Notably, the current study shows that there are possible subtype specific cells of origin within MRT which should be explored further as it can feed on current knowledge of clinicopathological features and the development of disease models.

7.2.1.2 CRISPR/Cas9 mediated knockout of Smarcb1 in putative cell of origin: A tool for future development of MRT mouse models and identification of therapeutic targets ex-vivo

To develop targeted therapies for MRT, more knowledge is required about the cellular origin of these tumours and how *SMARCB1* loss results in malignant transformation of these cells. Such studies should be first conducted *in vivo* or *ex vivo* as it is challenging to isolate the cell of origin from patient material. A previous MRT mouse model used in a cell of origin study relied on multiple stages of chemically induced *Smarcb1* knockdown (Han et al., 2016). Although this study presented high penetrance, the standard dose of tamoxifen also led to embryonic lethality due to excessive *Smarcb1* deletion. Besides that, the authors did not perform the knockout *Smarcb1* in a specific cell type in mice to provide evidence of cell of origin as the chemical tamoxifen were present everywhere in the mice's body. In the second cell of origin mouse model study, *Smarcb1* was inactivated in protein zero (P0) of

NC cells using *Cre* recombinase system which resulted in tumour development which molecularly, phenotypically and immunohistochemically mimics to human MRT (Vitte et al., 2017). However, the majority of tumours resemble meningeal tumours and developed in the head, and the authors also speculated that protein zero of NC as a cell of origin for Schwannomas. Hence, their results raise a question to which extent neural crest cells is a cell of origin for MRT as the authors did not explicitly time the induction of *Smarcb1* knockout except through P0. Besides that, their results did not link to particular subgroups within MRT.

For this project, the NC cells derived from an E8.5 mice embryo was used to investigate the prospect of these cells as an MRT cell of origin, as it has been postulated by many studies (Vitte et al., 2017, Han et al., 2016, Johann et al., 2016). The expression of *Smaarcb1* was targeted using CRISPR/Cas9 technology in NC cells. Here, the effect *Smarcb1* knockdown was studied in *ex vivo* before evaluating its tumourigenic capacity *in vivo*. Although the findings generated from this part of the study are insufficient to establish neural crest cell as the cell of origin for MRT specifically ECRT, this study demonstrates that CRISPR/Cas9 system is proficient to inactivate nuclear expression of *Smarcb1* and with a very small discrepancy between two CRISPR/Cas9 constructs. Here, we show the CRISPR/Cas9 mediated *Smarcb1* gene editing achieves over 85% efficiency of generating NC cells that do not express Smarcb1 protein. In this study, stable cell line that permanently knockout of *Smarcb1* expression was successfully created thus circumventing the limitations found in aforementioned mouse models. The CRISPR/Cas9 system is often associated with unfavourable off-target events. Such effects were not pronounced as both constructs generated almost similar findings in the current studies.

Data generated from current study demonstrated that *Smarcb1* loss in NC cells was able to maintain the proliferation capacity even one month after lentiviral transfection, differing from studies in other cell types such as NIH3T3 (Detailed in Chapter 4, Section 4.4.4.3). Furthermore, in this study, *Smarcb1*-deficient cells were shown to gain the self-renewal capacity when growing as tumoursphere under clonogenic conditions and the findings were corroborated by qPCR analysis of self-renewal gene expression (Detailed in Chapter 4, Section 4.4.4.5). Strikingly, genetically modified NC cells presented in this study revealed gene expression and phenotypes that resemble human MRT. Most importantly, most of the data generated from in this cell model including the presence of vimentin and cytokeratin 8

protein expression are in line with previous findings from the *in vivo* study of targeting *Smarcb1* in early NC cells (Vitte et al., 2017). Besides that, *Smarcb1* knockout in NC cells resulted in opposing gene expression profiles i.e cell cycle to that of *SMARCB1* re-expression in MRT cells. This result implies that functional NC cells are a potential cell of origin for MRT.

Though this cell model still requires further validation, it will pave a path to development of a model system in which the disease is initially originated. In summary, this study reported a system to efficiently knock down *Smarcb1* in NC cells as a potential cell of origin for MRT. This will be useful for researchers aiming to utilise gene editing in NC cell applications. Also, researchers will be able to study how MRT tumourigenesis could be linked to tumour origin *ex vivo*. The *ex vivo* model can allow one to investigate the role of specific gene alterations in disease initiation and progression. Such knowledge can provide the basis for an improved subgrouping of MRT and for identification of targeted therapies for patients with MRT. Furthermore, utilizing CRISPR/Cas9 mediated genome knockout can rapidly induce mutation in the gene of interest and has been shown to create higher gene inactivation in many *in vivo* studies.

7.2.2 Self-renewal genes as potential therapeutic targets in Malignant Rhabdoid Tumours (MRT)

Malignant Rhabdoid Tumours (MRT) are genetically defined by inactivation of *SMARCB1* which has a role as a tumour suppressor gene and a member of the SWI/SNF chromatin remodelling complex (Biegel et al., 2002a, Versteege et al., 1998). In experimental systems, *SMARCB1* re-expression leads to activation of the *p16* and *p21* pathway leading to cell cycle arrest. *SMARCB1* expression in the cells restricts the activity of cyclin D-CDK4/6 through transcriptional repression of *CCND1* accompanied by increase in the expression of cell cycle inhibitors; *p21* and *p16*. Therefore, efficacy of targeting CDK4/6 expression in MRT was studied in few pre-clinical studies using CDK4/6 inhibitor, Ribociclib (Infante et al., 2016) and PD 0332991, a potent inhibitor for CDK4 (Katsumi et al., 2011). Treatment with PD in MRT cell lines impaired cell proliferation and induced cell arrest. Phase I clinical trial of Ribociclib demonstrated single agent treatment was well tolerated in mrt patients, with a similar safety profiles observed in adult patients. Nevertheless, the authors suggested combination of ribociclib agent with other targeted therapies such as MAPK/ERK inhibitors should be considered in future trials.

Recent study showed that cell cycle alteration is not a sole driver in MRT tumourigenesis. It has been postulated that MRT tumourigenesis is not only driven by alteration in *SMARCB1* but dependency on Enhancer of Zeste 2 (*EZH2)*, an enzymatic subunit of the Polycomb Repressive Complex 2 (PRC2) (Knutson et al., 2013). *EZH2* has been implicated in invasive tumour growth and poor prognosis in many types of human cancers (Bracken et al., 2003, Kleer et al., 2003, Varambally et al., 2002). The role of EZH2 in stem cell maintenance such as self-renewal and differentiation in MRT was studied in few chemical inhibition studies *in vivo* and *in vitro* (Knutson et al., 2013, Alimova et al., 2012). These studies investigated the pharmacological properties of different EZH2 inhibitors such as EPZ-6438 and DZNep in MRT cell lines and the authors showed comparable results that EPZ-6438 and DZNep treatment in MRT cells induced cell apoptosis, altered cell cycle regulatory and also abrogated sphere formations. These studies illustrated deregulation of stem cell genes that regulate self-renewal and differentiation and may have a critical impact on MRT tumourigenesis.

The impact of targeting self-renewal machinery as a revenue for future MRT therapies was also studied by Shabab et al., 2018. In this study, the authors inhibit the expression of Lin28 which is also a known regulator for the let-7 family of miRNAs. The expression of Lin28 was found to be upregulated following *SMARCB1* loss in MRT samples and the authors found that knockdown of Lin28 in two MRT cell lines increased the cell apoptosis and impaired cell growth.

To gain more insight into the impact of targeting self-renewal machinery to counteract MRT tumourigenesis, I aimed to identify and assess the stemness/self-renewal genes as new therapeutic targets for MRT. Firstly, the self-renewal genes which are active and whose activity is *SMARCB1* dependent in models and primary MRT samples were assessed by comparing of transcriptomic data with a list of self-renewal genes generated from Ingenuity Pathway Analysis (IPA). In particular, the stemness/self-renewal genes whose expression was commonly implicated in brain tumour progression were identified including *BMI1* and *JARID2*. Overexpression of these genes is required to mediate tumourigenesis for the hedgehog (Hh) subgroup of Medulloblastoma (Wang et al., 2012). Through cross-referencing analysis between stemness/self-renewal candidate genes with RNA-seq and CRISPR screening data, *BMI1* was selected as a target gene. Although the mechanism of

BMI1 in stem cell self-renewal has been established in other human cancers, its role in MRT is still not clear.

The expression of *BMI1* in MRT was studied in this project using shRNA constructs and the small molecule inhibitor, PTC209. As MRT occur predominantly in infants and children, the administration of anti-cancer agents at low dose is desirable. Here, we identified sub-lethal, low doses of PTC209 as a potent inhibitor of cell proliferation and self-renewal in MRT. Treatment of MRT cell lines with sub-lethal doses of PTC209 inhibits cell growth, induces cell cycle arrest and senescence and more importantly impairs long-term MRT self-renewal capacity as assessed by limiting dilution assay. Notably, knockdown of *BMI1* using shRNA and an inhibitor in MRT cell lines generated data such as cell cycle profiles, gene expression and cell senescence that recapitulates the findings from *SMARCB1* re-expressing cell studies (PBTG, unpublished).

Targeting *BMI1* using PTC209 significantly impedes protein production while maintaining RNA expression. This suggests the possible effect of PTC209 on *BMI1* post-translation modification thus conferring its attractive therapeutic effect. Here, this study reports the potential of *BMI1* to act as a therapeutic target for MRT and the efficacy of PTC209 in inhibiting BMI1 expression. While the cytotoxic effect of PTC209 and detailed mechanism by which this inhibitor can impair cell growth and self-renewal capacity at low doses need to be determined *in vivo*, it may offer an effective and well-tolerated therapeutic option for young patients diagnosed with MRT and possibly other types of tumours as well. Besides that, *BMI1* which is also a component of Polycomb Repressive Complex 1 (PRC1) has been reported to have a synergetic role with *EZH2* in modulating transcriptional silencing. Therefore, it can offer a new drug combination for MRT treatment.

7.3 Limitations

7.3.1 Identification of cell of origin for MRT

The initial aim of the study was to identify the cell of origin for MRT through knock out of *SMARCB1* and *SMARCA4* using CRISPR/Cas9 system in candidate cells. Meta-analysis of RNA-seq data of primary and cell line model with various stem cell profiles revealed three possible cells of origin for MRT related to location of primary tumours; neural stem cell (NSC) for ATRT whilst neural crest (NC) cells and mesenchymal stem cells (MSC) for ECRT. It is worth noting that gene expression analysis performed to identify cell of origin for MRT and how it correlates with bodily location may confound the results as niche environment may influence the tumour cell growth and variable activities (i.e expression of the genes). Genes may be expressed in one microenvironment, but not in another, therefore will lead to false positive results. Therefore, analysis of other datasets that have less variance (i.e effect of tumour microenvironment such as paracrine) such as genome wide DNA methylation profiles may provide clues for cell of origin for MRT. Our detailed methylation profiles of primary tumours (work done by Yura Grabvoska) revealed differences in methylation status i.e hypomethylation among different regions of CpG island. Although use of methylation profiles may be of limited value as the data can also show hypo- or hyper-methylated status, the difference seen in our primary and cell lines may reflect different cell of origin for MRT and further work should be done to identify a cohort of developmentally regulated sequence elements i.e CpG island to uncover transcriptional regulators in lineage differentiation.

From the bioinformatics analysis, three potential cells of origin were identified from a family of neural crest (NC) cells, mesenchymal stem cells (MSC) and neural stem cells (NSC). However, due to time constraint, the effect of *SMARCB1* knockdown in neural crest cells was only reported in this study. Although *Smarcb1*-deficient NC cells demonstrated phenotypic similarities with human MRT, they cannot be definitively stated as the only cell of origin for MRT and particularly ECRT, since experiments were not carried out on the other candidates. Besides, though qPCR analysis and tumoursphere assay showed an increase in cell cycle regulation and self-renewal capacity in *Smarcb1* knockout cells, this study has not provided definitive evidence that deletion of *Smarcb1* in this cell type confers tumourigenesis. Xenograft of *Smarcb1*-deficient cells may provide an insight into *SMARCB1* driven MRT tumourigenesis dependency on cell of origin, though previous

mouse model study illustrates *Smarcb1* loss in P0 expressing cells is tumourigenic and capable to initiate tumour formation (Vitte et al., 2017).

Attempts were made to characterise *Smarcb1*-deficient NC cells based on histological characteristics of rhabdoid cells such as abundance of mitotic figure, inclusion bodies and prominent nuclei. However, I failed to detect cells with these characteristics. One possible explanation is most studies which have previously demonstrated the MRT phenotypes have done so using tissue sections. Hence, *in vivo* study of *Smarcb1*-deficient NC cells may provide better assessment of MRT histological phenotypes if the tumours are successfully formed.

7.3.2 Self-renewal genes as potential therapeutic targets in Malignant Rhabdoid Tumours (MRT)

Current therapies for infants and children with MRT are still ineffective. Hence, this part of the project aimed to discover therapeutically targetable self-renewal pathways/genes downstream of *SMARCB1* mutation as the most efficient means to counteract MRT tumourigenesis and induce differentiation/growth arrest in MRT cells. Reduced expression of BMI1 using small inhibitor, PTC209 was able to demonstrate remarkable findings that mimic the effect of *SMARCB1* re-expression in MRT cell lines. However, further investigation of this inhibitor should be performed to identify the utility of BMI1 inhibitor for MRT treatment. The cytotoxicity and efficacy of PTC209 in inhibiting MRT tumourigenesis *in vivo* cannot be established as the effect of this small inhibitor was only studied *in vitro*. Besides that, data for self-renewal efficiency was generated from *in vitro* limiting dilution assay. Though inhibition of BMI1 with PTC209 and shRNAs demonstrated impairment of long-term self-renewal capacity of MRT cells growing in 3D tumoursphere, such effect should be studied further *in vivo*.

7.4 Future work

7.4.1 Molecular profiling of Smarcb1-deficient cells on cell of origin within MRT

The present study attempted to identify potential cells of origin for MRT. Bioinformatics analysis suggests that the cell of origin for MRT is potentially molecular subtype specific. Despite comprehensive bioinformatics analysis, further investigation is required to support this finding. Besides that, results from bioinformatics analysis showed neural crest (NC) cells as one of the potential cells of origin for MRT. To further investigate if NC cells are the cell of origin in MRT, CRISPR/Cas9 knock out of *Smarcb1* was performed in NC cells. However, due to time constraint, the experiment was performed only in neural crest cells and non-stem cells (NIH3T3 cell line) was used as a control. Knockout of *SMARCB1* should also be performed in other candidates of cell of origin; neural stem cells and mesenchymal stem cells. Furthermore, from the bioinformatics analysis, embryonic stem cells (ESC) showed no potential as cell of origin for MRT. Use of ESC as control may be useful to validate this result. To determine if there is a common or specific cell of origin for MRT, RNA-seq and 450K methylation of *SMARCB1*-deficient cells will be performed and compared with human MRT and previous mouse model data. Though *SMARCB1* loss led to tumour formation in previous mouse models of MRT, the majority of the tumours were observed in head or meninges (Vitte et al., 2017). For this project, I hypothesised that cell of origin for MRT in subtype-specific which related to the bodily location of primary tumours. Therefore, it is necessary to determine if tumours or *Smarcb1*-deficient NC cells (if *Smarcb1*-deficient cells can transform into tumours) can preferentially recapitulate molecular subgroups seen in primary human tumours. To this end, across species comparative genome-wide studies between *Smarcb1*-deficient NC cells with published expression profiles of human and mouse MRT tumours (Han et al., 2016, Vitte et al., 2017, Chun et al., 2016, Johann et al., 2016) can be done to examine their molecular analogy.

7.4.2 Characterisation of cell of origin for development of MRT mouse models and therapeutic intervention

Recent mouse models have shown the potency to develop tumours that mimicking human MRT (Han et al., 2016, Vitte et al., 2017). However, majority of the tumours were found in the rare regions such as meninges. To date, there is no study that reported the occurrence of the tumours in other parts of mice's body including kidney. To address this issue,

development of mouse model that can represent each molecular subgroup is anticipated through identification of cell of origin. To this end, *Smarcb1* knock out was performed in a candidate cell of origin for ECRT using CRISPR/Cas9 technology. The *ex vivo* study of *Smarcb1* loss in early NC cells suggests that *Smarcb1* inactivation is sufficient to promote cell proliferation and induce phenotypes that resemble human MRT Hence, xenograft of *Smarcb1*-deficient cells in mice will provide a better model for understanding the role of cell of origin in mediating MRT tumourigenesis and aggressive behaviour of MRT. Besides that, transcriptomic profiling of *Smarcb1*-deficient cells obtained from mouse model will be performed by RNAseq and the data will be integrated with primary human and mouse model data to investigate the potential of NC cells as the cell of origin for MRT before the attempts to translate the functional cell of origin as relevant mouse model for pre-clinical drug testing for MRT.

This study demonstrates the phenotype of *Smarcb1*-deficient NC cells mimicking human MRT based on the presence of two commonly associated markers in MRT; vimentin and cytokeratin. It is important to note that, *SMARCB1* loss can also be found in other types of tumours such as Schwanomma. Therefore, staining the cells preferably tumour cells with S100, epithelial membrane antigen, or smooth muscle will differentiate MRT cells from non-rhabdoid tumours. Characterisation of *SMARCB1* loss in cells of origin will uncover the molecular factors within the cell of origin that supports the mutation in *SMARCB1* is transforming particular cells to become cancerous.

Our ultimate goal of studying cell of origin is to discover new therapeutic targets that could effectively cure MRT. To develop effective therapies for MRT, there is a need to understand better how the cell of origin can affect the characteristics and behaviour of MRT cells. Analysis of differential gene expression between primary human tumours with candidate cell of origin and normal cells should be implemented to identify “gene signature” that associated with cancer transformation and drug sensitivity. The identification of the genes that implicated in MRT tumourigenesis will facilitate the development of new targeted therapies for MRT.

7.4.3 Understanding the role of BMI1 as histone m.odification protein in MRT as potential therapeutic target for MRT

Post-translation modifications (PTM) of core histone protein of chromatin play a critical role in controlling the dependability of transcription regulatory machinery in cells. PTM includes methylation, acetylation, ubiquitination, phosphorylation, lipidation, SUMOylation, hydroxylation, glycosylation and disulphide bonds (Witze et al., 2007, Liddy et al., 2013). Studies have illustrated aberrant function of PTM can cause disruption in normal biological process such as cell signalling, DNA repairs, cell differentiation, cell proliferation which eventually can lead to tumour progression and drug resistance (Chandrasekaran et al., 2017, Okamoto and Lipton, 2015, Eisenberg-Lerner et al., 2016, Khan et al., 2015). Post-translation modifiers have demonstrated the potential as therapeutic target for human cancers in several studies (Lu et al., 2016, Krueger and Srivastava, 2006, Martín-Bernabé et al., 2017). The most common type of modifications is methylation processes which are catalysed by histone methyltransferase. The most common gene that is linked to methylation events on histone modification is *EZH2*, which is a member of Polycomb Repressive Complex 2 (PRC2).

It has been shown that histone modifications are also regulated by SWI/SNF complexes (Alver et al., 2017). Deregulation of enzymes that regulate the epigenome often results in global consequences on chromatin. For instance, experimental studies have illustrated *SMARCB1* loss in MRT causes upregulation of trimethylase on histone H3K27 and repression of p16Ink4a (Kia et al., 2008). In line with these findings, studies have demonstrated the efficacy of selective inhibitors for EZH2 as a mean of MRT treatment (Knutson et al., 2013, Alimova et al., 2012).

In this study, we report a potential therapeutic target for MRT which is BMI1. Inhibition of BMI1 using small molecular inhibitor, PTC209 demonstrated the possible mechanism of post-translation modification. It has been demonstrated in other studies that BMI1 regulates the transcriptional silencing through catalysing mono-ubiquitination of lysine 119 on histone H2A (Kreso et al., 2014, Bolomsky et al., 2016, Alzrigat et al., 2017). Similarly, to the methylation process, ubiquitination proteins have been shown to play a significant crucial role in several drug responses and therefore disease prognosis. Interestingly, impaired BMI1 protein production resulted in growth suppression of *SMARCB1*-deleted cells accompanied by downregulation of cell cycle promoting genes and upregulation of cell cycle inhibitors

including p16. Study of PTC209 in squamous cell carcinoma demonstrated suppression of ubiquitination of histone H2A following BMI1 inactivation (Wang et al., 2015). Therefore, ChIP analysis of BMI1-deficient MRT cells will determine to what extent *BMI1* loss can affect global histone modification and interaction with another member of the SWI/SNF complex in impeding MRT cell growth.

7.4.4 BMI1 knockdown mimics the effect of SMARCB1 re-expression in MRT cells: a way to counteract MRT tumourigenesis

Despite minimal gene expression analysis presented in this study, findings demonstrated remarkable similarity between BMI1-deficient MRT cells with *SMARCB1* re-expression in MRT cells, suggesting that BMI1 might represent an ideal target for therapeutic intervention. Therefore, more comprehensive genome-wide studies with primary and model MRT data should be performed to verify the observations from the current study and also to illustrate an effect of BMI1 loss on transcriptomic or methylation profiles. Given this study was able to provide proof-of-concept for inhibitor targeting expression of BMI1 *in vitro*, the efficacy of this drug should be further evaluated in Phase I clinical trials.

PRC proteins have been shown to have antagonistic effects with SWI/SNF chromatin remodelling (Wilson et al., 2010a). The PRC2 complex is commonly linked with MRT tumourigenesis due to the significant role of EZH2 in catalysing methylation on histones. However, there is no single study reporting the potential impact of PRC1 complex on regulatory of SWI/SNF complex in MRT. Previous ChIP analysis illustrated the co-occupancy of both PRC complexes at a promoter region in mediating transcriptional silencing of p16Ink4a (Kia et al., 2008), a critical gene that is associated with MRT tumourigenesis. Therefore, investigation of deregulation of genes expression following BMI1 loss in MRT cells by RNAseq may provide knowledge of anti-tumour activity of PTC209 and also canonical PRC1 complex in MRT tumourigenesis. More importantly, this will highlight the potential synergistic drug development of PRC proteins for MRT treatment.

7.5 Final conclusion

The aims of this study were to identify the cell of origin and "stemness" of Malignant Rhabdoid Tumours as new therapeutic approach for these lethal childhood malignancies.

The first aim of this study is to identify the cell of origin for MRT. Through comparative genomic studies of stem cell population with primary and model MRT, I have identified important findings that there is no common cell of origin within MRT and that cellular origins are possibly subtype specific. Moreover, cross-referencing between these datasets was applied to identify gene signatures within primary and model MRT that resemble to stem cell populations. Importantly, the analysis demonstrated dysregulation of developmental genes that differed between subtypes within MRT. From the bioinformatics analysis, three potential cells of origins have been identified; neural crest (NC) cells, mesenchymal stem cells (MSC) and neural stem cells (NSC). To further investigate the relevance of these cells as cell of origin for MRT, CRISPR/Cas9 system was utilised in experimental studies to knock out functional *Smarcb1* in NC cells. This investigation has made a substantial contribution to knowledge in the cell of origin for MRT research through characterisation of cell phenotypes and gene expression profiles (i.e cell cycle) that resembles human MRT. Furthermore, this study has demonstrated that whilst the majority of cell types do not tolerate having *Smarcb1* loss except neural crest cells which grew, and display increased the proliferative capacity. Altogether, a system for ranking putative cells of origin was established and a practical means for testing *Smarcb1* mutation *ex vivo* was carried out using CRISPR/Cas9 technology.

Besides that, this study was also aimed to characterize how *SMARCB1* mutations alter "stemness/self-renewal" programmes in order to affect tumourigenesis. To achieve this aim, assessment of the expression of self-renewal genes that are deregulated in MRT cells was performed through comparative studies of self-renewal genes with RNA-seq data of primary and cells, and CRISPR GeCKO screening of MRT cells. From this analysis, I've identified *BMI1* as SMARCB1-dependent gene in MRT. The third and final aim of this study was to test and validate at least one targetable "stemness/self-renewal" gene/pathway as a potential novel anti-MRT therapy. To this end, expression of BMI1 was further studied in four MRT cell lines using shRNA and small molecular inhibitor, PTC209. Of note, BMI1 knockdown mimics the effect of SMARCB1 re-expression in MRT. Therefore, this study illustrates

BMI1 is one potential therapeutic target for MRT, but its expression needs to be explored further.

Chapter 8 Reference

ABDOUH, M., FACCHINO, S., CHATOO, W., BALASINGAM, V., FERREIRA, J. & BERNIER, G. 2009. BMI1 sustains human glioblastoma multiforme stem cell renewal. *Journal of Neuroscience,* 29**,** 8884-8896.

AGAIMY, A. 2014. The expanding family of SMARCB1 (INI1)-deficient neoplasia: implications of phenotypic, biological, and molecular heterogeneity. *Advances in anatomic pathology,* 21**,** 394-410.

AJANI, J. A., SONG, S., HOCHSTER, H. S. & STEINBERG, I. B. Cancer stem cells: the promise and the potential. Seminars in oncology, 2015. Elsevier, S3-S17.

ALBANESE, P., BELIN, M.-F. & DELATTRE, O. 2006a. The tumour suppressor hSNF5/INI1 controls the differentiation potential of malignant rhabdoid cells. *European journal of cancer,* 42**,** 2326-2334.

ALBANESE, P., BELIN, M. F. & DELATTRE, O. 2006b. The tumour suppressor hSNF5/INI1 controls the differentiation potential of malignant rhabdoid cells. *Eur J Cancer,* 42**,** 2326-34.

ALIMOVA, I., BIRKS, D. K., HARRIS, P. S., KNIPSTEIN, J. A., VENKATARAMAN, S., MARQUEZ, V. E., FOREMAN, N. K. & VIBHAKAR, R. 2012. Inhibition of EZH2 suppresses self-renewal and induces radiation sensitivity in atypical rhabdoid teratoid tumor cells. *Neuro-oncology,* 15**,** 149-160.

ALKEMA, M., WIEGANT, J., RAAP, A. K., BEMS, A. & VAN LOHUIZEN, M. 1993. Characterization and chromosomal localization of the human proto-oncogene BMI-1. *Human molecular genetics,* 2**,** 1597-1603.

ALVER, B. H., KIM, K. H., LU, P., WANG, X., MANCHESTER, H. E., WANG, W., HASWELL, J. R., PARK, P. J. & ROBERTS, C. W. 2017. The SWI/SNF chromatin remodelling complex is required for maintenance of lineage specific enhancers. *Nature communications,* 8**,** 14648.

ALZRIGAT, M., PÁRRAGA, A. A., MAJUMDER, M. M., MA, A., JIN, J., ÖSTERBORG, A., NAHI, H., NILSSON, K., HECKMAN, C. A. & ÖBERG, F. 2017. The polycomb group protein BMI-1 inhibitor PTC-209 is a potent anti-myeloma agent alone or in combination with epigenetic inhibitors targeting EZH2 and the BET bromodomains. *Oncotarget,* 8**,** 103731.

AMMERLAAN, A., ARAROU, A., HOUBEN, M., BAAS, F., TIJSSEN, C., TEEPEN, J., WESSELING, P. & HULSEBOS, T. 2008. Long-term survival and transmission of INI1-mutation via nonpenetrant males in a family with rhabdoid tumour predisposition syndrome. *British journal of cancer,* 98**,** 474.

ANDERSON, E. M., HAUPT, A., SCHIEL, J. A., CHOU, E., MACHADO, H. B., STREZOSKA, Ž., LENGER, S., MCCLELLAND, S., BIRMINGHAM, A. & VERMEULEN, A. 2015. Systematic analysis of CRISPR–Cas9 mismatch tolerance reveals low levels of off-target activity. *Journal of biotechnology,* 211**,** 56-65.

ANTON, R., KESTLER, H. A. & KÜHL, M. 2007. β-Catenin signaling contributes to stemness and regulates early differentiation in murine embryonic stem cells. *FEBS letters,* 581**,** 5247-5254.

AOYAGI, S. & HAYES, J. J. 2002. hSWI/SNF-catalyzed nucleosome sliding does not occur solely via a twist-diffusion mechanism. *Molecular and cellular biology,* 22**,** 7484-7490.

ARJONEN, A., KAUKONEN, R. & IVASKA, J. 2011. Filopodia and adhesion in cancer cell motility. *Cell adhesion & migration,* 5**,** 421-430.

ATHALE, U. H., DUCKWORTH, J., ODAME, I. & BARR, R. 2009. Childhood atypical teratoid rhabdoid tumor of the central nervous system: a meta-analysis of observational studies. *Journal of pediatric hematology/oncology,* 31**,** 651-663.

BAHENA‐OCAMPO, I., ESPINOSA, M., CEBALLOS‐CANCINO, G., LIZARRAGA, F., CAMPOS‐ARROYO, D., SCHWARZ, A., MALDONADO, V. & MELENDEZ‐ZAJGLA, J. 2016. miR‐10b expression in breast cancer stem cells supports self‐renewal through negative PTEN regulation and sustained AKT activation. *EMBO reports,* 17**,** 648-658.

BANINE, F., BARTLETT, C., GUNAWARDENA, R., MUCHARDT, C., YANIV, M., KNUDSEN, E. S., WEISSMAN, B. E. & SHERMAN, L. S. 2005. SWI/SNF chromatin-remodeling factors induce changes in DNA methylation to promote transcriptional activation. *Cancer research,* 65**,** 3542-3547.

BANSAL, K. & GOEL, D. 2007. Atypical teratoid/rhabdoid tumors of central nervous system. *Journal of Pediatric Neurosciences,* 2**,** 1.

BECKWITH, J. & PALMER, N. 1978. Histopathology and prognosis of Wilms tumor Results from the first national wilms' tumor study. *Cancer,* 41**,** 1937-1948.

BEEDERMAN, M., LAMPLOT, J. D., NAN, G., WANG, J., LIU, X., YIN, L., LI, R., SHUI, W., ZHANG, H. & KIM, S. H. 2013. BMP signaling in mesenchymal stem cell differentiation and bone formation. *Journal of biomedical science and engineering,* 6**,** 32.

BENESCH, M., BARTELHEIM, K., FLEISCHHACK, G., GRUHN, B., SCHLEGEL, P., WITT, O., STACHEL, K., HAUCH, H., URBAN, C. & QUEHENBERGER, F. 2014. High-dose chemotherapy (HDCT) with auto-SCT in children with atypical teratoid/rhabdoid tumors (AT/RT): a report from the European Rhabdoid Registry (EU-RHAB). *Bone marrow transplantation,* 49**,** 370.

BETZ, B. L., STROBECK, M. W., REISMAN, D. N., KNUDSEN, E. S. & WEISSMAN, B. E. 2002. Re-expression of hSNF5/INI1/BAF47 in pediatric tumor cells leads to G 1 arrest associated with induction of p16ink4a and activation of RB. *Oncogene,* 21**,** 5193.

BHATTACHARYA, R., MUSTAFI, S. B., STREET, M., DEY, A. & DWIVEDI, S. K. D. 2015. Bmi-1: At the crossroads of physiological and pathological biology. *Genes & diseases,* 2**,** 225-239.

BIEGEL, J. A. 2006. Molecular genetics of atypical teratoid/rhabdoid tumors. *Neurosurgical focus,* 20**,** 1-7.

BIEGEL, J. A., BUSSE, T. M. & WEISSMAN, B. E. SWI/SNF chromatin remodeling complexes and cancer. American Journal of Medical Genetics Part C: Seminars in Medical Genetics, 2014. Wiley Online Library, 350-366.

BIEGEL, J. A., FOGELGREN, B., ZHOU, J.-Y., JAMES, C. D., JANSS, A. J., ALLEN, J. C., ZAGZAG, D., RAFFEL, C. & RORKE, L. B. 2000. Mutations of the INI1 rhabdoid tumor suppressor gene in medulloblastomas and primitive neuroectodermal tumors of the central nervous system. *Clinical cancer research,* 6**,** 2759-2763.

BIEGEL, J. A., KALPANA, G., KNUDSEN, E. S., PACKER, R. J., ROBERTS, C. W., THIELE, C. J., WEISSMAN, B. & SMITH, M. 2002a. The role of INI1 and the SWI/SNF complex in the development of rhabdoid tumors: meeting summary from the workshop on childhood atypical teratoid/rhabdoid tumors. AACR.

BIEGEL, J. A., TAN, L., ZHANG, F., WAINWRIGHT, L., RUSSO, P. & RORKE, L. B. 2002b. Alterations of the hSNF5/INI1 gene in central nervous system atypical teratoid/rhabdoid tumors and renal and extrarenal rhabdoid tumors. *Clinical Cancer Research,* 8**,** 3461-3467.

BIEGEL, J. A., ZHOU, J.-Y., RORKE, L. B., STENSTROM, C., WAINWRIGHT, L. M. & FOGELGREN, B. 1999. Germ-line and acquired mutations of INI1 in atypical teratoid and rhabdoid tumors. *Cancer research,* 59**,** 74-79.

BIGGS, P. J., GAREN, P. D., POWERS, J. M. & GARVIN, J. J. 1987. Malignant rhabdoid tumor of the central nervous system. *Human pathology,* 18**,** 332-337.

BIRKS, D. K., DONSON, A. M., PATEL, P. R., DUNHAM, C., MUSCAT, A., ALGAR, E. M., ASHLEY, D. M., KLEINSCHMIDT-DEMASTERS, B., VIBHAKAR, R. & HANDLER, M. H. 2011. High expression of BMP pathway genes distinguishes a subset of atypical teratoid/rhabdoid tumors associated with shorter survival. *Neuro-oncology,* 13**,** 1296-1307.

BISWAS, A., KASHYAP, L., KAKKAR, A., SARKAR, C. & JULKA, P. K. 2016. Atypical teratoid/rhabdoid tumors: challenges and search for solutions. *Cancer management and research,* 8**,** 115.

BOLOMSKY, A., SCHLANGEN, K., SCHREINER, W., ZOJER, N. & LUDWIG, H. 2016. Targeting of BMI-1 with PTC-209 shows potent anti-myeloma activity and impairs the tumour microenvironment. *Journal of hematology & oncology,* 9**,** 17.

BONNIN, J. M., RUBINSTEIN, L. J., PALMER, N. F. & BECKWITH, J. B. 1984. The association of embryonal tumors originating in the kidney and in the brain. A report of seven cases. *Cancer,* 54**,** 2137-2146.

BOURDEAUT, F., FRÉNEAUX, P., THUILLE, B., BERGERON, C., LAURENCE, V., BRUGIÈRES, L., VÉRITÉ, C., MICHON, J., DELATTRE, O. & ORBACH, D. 2008. Extra‐renal non‐cerebral rhabdoid tumours. *Pediatric blood & cancer,* 51**,** 363-368.

BOURDEAUT, F., FRENEAUX, P., THUILLE, B., LELLOUCH‐TUBIANA, A., NICOLAS, A., COUTURIER, J., PIERRON, G., SAINTE‐ROSE, C., BERGERON, C. & BOUVIER, R. 2007. hSNF5/INI1‐deficient tumours and

rhabdoid tumours are convergent but not fully overlapping entities. *The Journal of pathology,* 211**,** 323-330.

BOURDEAUT, F., LEQUIN, D., BRUGIÈRES, L., REYNAUD, S., DUFOUR, C., DOZ, F., ANDRÉ, N., STEPHAN, J.-L., PÉREL, Y. & OBERLIN, O. 2011. Frequent hSNF5/INI1 germline mutations in patients with rhabdoid tumor. *Clinical Cancer Research,* 17**,** 31-38.

BOYD, C., SMITH, M. J., KLUWE, L., BALOGH, A., MACCOLLIN, M. & PLOTKIN, S. R. 2008. Alterations in the SMARCB1 (INI1) tumor suppressor gene in familial schwannomatosis. *Clinical genetics,* 74**,** 358-366.

BRACKEN, A. P., PASINI, D., CAPRA, M., PROSPERINI, E., COLLI, E. & HELIN, K. 2003. EZH2 is downstream of the pRB‐E2F pathway, essential for proliferation and amplified in cancer. *The EMBO journal,* 22**,** 5323-5335.

BRENNAN, B., STILLER, C. & BOURDEAUT, F. 2013a. Extracranial rhabdoid tumours: what we have learned so far and future directions. *The Lancet Oncology,* 14**,** e329-e336.

BRENNAN, B., STILLER, C. & BOURDEAUT, F. 2013b. Extracranial rhabdoid tumours: what we have learned so far and future directions. *Lancet Oncol,* 14**,** e329-36.

BRODEUR, G. M. 2003. Neuroblastoma: biological insights into a clinical enigma. *Nature Reviews Cancer,* 3**,** 203.

BRUGGERS, C. S., BLEYL, S. B., PYSHER, T., BARNETTE, P., AFIFY, Z., WALKER, M. & BIEGEL, J. A. 2011. Clinicopathologic comparison of familial versus sporadic atypical teratoid/rhabdoid tumors (AT/RT) of the central nervous system. *Pediatric blood & cancer,* 56**,** 1026-1031.

BRUNET, J.-P., TAMAYO, P., GOLUB, T. R. & MESIROV, J. P. 2004. Metagenes and molecular pattern discovery using matrix factorization. *Proceedings of the National Academy of Sciences,* 101**,** 4164-4169.

BULTMAN, S., GEBUHR, T., YEE, D., LA MANTIA, C., NICHOLSON, J., GILLIAM, A., RANDAZZO, F., METZGER, D., CHAMBON, P. & CRABTREE, G. 2000. A Brg1 null mutation in the mouse reveals functional differences among mammalian SWI/SNF complexes. *Molecular cell,* 6**,** 1287-1295.

BUSCARIOLLO, D. L., PARK, H. S., ROBERTS, K. B. & YU, J. B. 2012. Survival outcomes in atypical teratoid rhabdoid tumor for patients undergoing radiotherapy in a surveillance, epidemiology, and end results analysis. *Cancer,* 118**,** 4212-4219.

CALAO, M., SEKYERE, E., CUI, H., CHEUNG, B., THOMAS, W., KEATING, J., CHEN, J., RAIF, A., JANKOWSKI, K. & DAVIES, N. 2013. Direct effects of Bmi1 on p53 protein stability inactivates oncoprotein stress responses in embryonal cancer precursor cells at tumor initiation. *Oncogene,* 32**,** 3616.

CAO, L., BOMBARD, J., CINTRON, K., SHEEDY, J., WEETALL, M. L. & DAVIS, T. W. 2011. BMI1 as a novel target for drug discovery in cancer. *Journal of cellular biochemistry,* 112**,** 2729-2741.

CAO, R., TSUKADA, Y.-I. & ZHANG, Y. 2005. Role of Bmi-1 and Ring1A in H2A ubiquitylation and Hox gene silencing. *Molecular cell,* 20**,** 845-854.

CARAMEL, J., MEDJKANE, S., QUIGNON, F. & DELATTRE, O. 2008. The requirement for SNF5/INI1 in adipocyte differentiation highlights new features of malignant rhabdoid tumors. *Oncogene,* 27**,** 2035-44.

CHAI, J., CHARBONEAU, A. L., BETZ, B. L. & WEISSMAN, B. E. 2005. Loss of the hSNF5 gene concomitantly inactivates p21CIP/WAF1 and p16INK4a activity associated with replicative senescence in A204 rhabdoid tumor cells. *Cancer research,* 65**,** 10192-10198.

CHANDRASEKARAN, A. P., SURESH, B., KIM, H. H., KIM, K. S. & RAMAKRISHNA, S. 2017. Concise review: fate determination of stem cells by deubiquitinating enzymes. *Stem Cells,* 35**,** 9-16.

CHEN, Y.-W., WONG, T.-T., HO, D. M.-T., HUANG, P.-I., CHANG, K.-P., SHIAU, C.-Y. & YEN, S.-H. 2006. Impact of radiotherapy for pediatric CNS atypical teratoid/rhabdoid tumor (single institute experience). *International Journal of Radiation Oncology• Biology• Physics,* 64**,** 1038-1043.

CHENN, A. & WALSH, C. A. 2002. Regulation of cerebral cortical size by control of cell cycle exit in neural precursors. *Science,* 297**,** 365-369.

CHI, S. N., ZIMMERMAN, M. A., YAO, X., COHEN, K. J., BURGER, P., BIEGEL, J. A., RORKE-ADAMS, L. B., FISHER, M. J., JANSS, A. & MAZEWSKI, C. 2009. Intensive multimodality treatment for children with newly diagnosed CNS atypical teratoid rhabdoid tumor. *Journal of Clinical Oncology,* 27**,** 385-389.

CHI, T. H., WAN, M., ZHAO, K., TANIUCHI, I., CHEN, L., LITTMAN, D. R. & CRABTREE, G. R. 2002. Reciprocal regulation of CD4/CD8 expression by SWI/SNF-like BAF complexes. *Nature,* 418**,** 195.

CHIBA, T., ZHENG, Y.-W., KITA, K., YOKOSUKA, O., SAISHO, H., ONODERA, M., MIYOSHI, H., NAKANO, M., ZEN, Y. & NAKANUMA, Y. 2007. Enhanced self-renewal capability in hepatic stem/progenitor cells drives cancer initiation. *Gastroenterology,* 133**,** 937-950.

CHUN, H.-J. E., LIM, E. L., HERAVI-MOUSSAVI, A., SABERI, S., MUNGALL, K. L., BILENKY, M., CARLES, A., TSE, K., SHLAFMAN, I. & ZHU, K. 2016. Genome-wide profiles of extra-cranial malignant rhabdoid tumors reveal heterogeneity and dysregulated developmental pathways. *Cancer cell,* 29**,** 394-406.

CIOCE, M., GHERARDI, S., VIGLIETTO, G., STRANO, S., BLANDINO, G., MUTI, P. & CILIBERTO, G. 2010. Mammosphere-forming cells from breast cancer cell lines as a tool for the identification of CSC-like-and early progenitor-targeting drugs. *Cell cycle,* 9**,** 2950-2959.

COOPER, G. 2000. Structure and organization of actin filaments. *The cell: a molecular approach*.

DAHMANE, N. & RUIZ-I-ALTABA, A. 1999. Sonic hedgehog regulates the growth and patterning of the cerebellum. *Development,* 126**,** 3089-3100.

DATTA, S., HOENERHOFF, M. J., BOMMI, P., SAINGER, R., GUO, W.-J., DIMRI, M., BAND, H., BAND, V., GREEN, J. E. & DIMRI, G. P. 2007. Bmi-1 cooperates with H-Ras to transform human mammary epithelial cells via dysregulation of multiple growth-regulatory pathways. *Cancer research,* 67**,** 10286-10295.

DAWSON, M. A. & KOUZARIDES, T. 2012. Cancer epigenetics: from mechanism to therapy. *Cell,* 150**,** 12-27.

DEISCH, J., RAISANEN, J. & RAKHEJA, D. 2011. Immunohistochemical expression of embryonic stem cell markers in malignant rhabdoid tumors. *Pediatric and Developmental Pathology,* 14**,** 353-359.

DELEYROLLE, L. P., ERICKSSON, G., MORRISON, B. J., LOPEZ, J. A., BURRAGE, K., BURRAGE, P., VESCOVI, A., RIETZE, R. L. & REYNOLDS, B. A. 2011. Determination of somatic and cancer stem cell self-renewing symmetric division rate using sphere assays. *PloS one,* 6**,** e15844.

DEVARAJAN, K. 2008. Nonnegative matrix factorization: an analytical and interpretive tool in computational biology. *PLoS Comput Biol,* 4**,** e1000029.

DIAZ-GUERRA, E., LILLO, M. A., SANTAMARIA, S. & GARCIA-SANZ, J. A. 2012. Intrinsic cues and hormones control mouse mammary epithelial tree size. *The FASEB Journal,* 26**,** 3844-3853.

DIETRICH, N., BRACKEN, A. P., TRINH, E., SCHJERLING, C. K., KOSEKI, H., RAPPSILBER, J., HELIN, K. & HANSEN, K. H. 2007. Bypass of senescence by the polycomb group protein CBX8 through direct binding to the INK4A‐ARF locus. *The EMBO journal,* 26**,** 1637-1648.

DIMRI, G. P., MARTINEZ, J.-L., JACOBS, J. J., KEBLUSEK, P., ITAHANA, K., VAN LOHUIZEN, M., CAMPISI, J., WAZER, D. E. & BAND, V. 2002. The Bmi-1 oncogene induces telomerase activity and immortalizes human mammary epithelial cells. *Cancer research,* 62**,** 4736-4745.

DOENCH, J. G., FUSI, N., SULLENDER, M., HEGDE, M., VAIMBERG, E. W., DONOVAN, K. F., SMITH, I., TOTHOVA, Z., WILEN, C. & ORCHARD, R. 2016. Optimized sgRNA design to maximize activity and minimize off-target effects of CRISPR-Cas9. *Nature biotechnology,* 34**,** 184.

DONTU, G., ABDALLAH, W. M., FOLEY, J. M., JACKSON, K. W., CLARKE, M. F., KAWAMURA, M. J. & WICHA, M. S. 2003. In vitro propagation and transcriptional profiling of human mammary stem/progenitor cells. *Genes & development,* 17**,** 1253-1270.

DUNAIEF, J. L., STROBER, B. E., GUHA, S., KHAVARI, P. A., ÅLIN, K., LUBAN, J., BEGEMANN, M., CRABTREE, G. R. & GOFF, S. P. 1994. The retinoblastoma protein and BRG1 form a complex and cooperate to induce cell cycle arrest. *Cell,* 79**,** 119-130.

DUPIN, E. & COELHO‐AGUIAR, J. M. 2013. Isolation and differentiation properties of neural crest stem cells. *Cytometry Part A,* 83**,** 38-47.

EATON, K. W., TOOKE, L. S., WAINWRIGHT, L. M., JUDKINS, A. R. & BIEGEL, J. A. 2011. Spectrum of SMARCB1/INI1 mutations in familial and sporadic rhabdoid tumors. *Pediatric blood & cancer,* 56**,** 7-15.

EISENBERG-LERNER, A., CIECHANOVER, A. & MERBL, Y. 2016. Post-translational modification profiling–A novel tool for mapping the protein modification landscape in cancer. *Experimental biology and medicine,* 241**,** 1475-1482.

EL-NABBOUT, B., SHBAROU, R., GLASIER, C. M. & SAAD, A. G. 2010. Primary diffuse cerebral leptomeningeal atypical teratoid rhabdoid tumor: report of the first case. *Journal of neuro-oncology,* 98**,** 431-434.

EYLER, C. E., FOO, W. C., LAFIURA, K. M., MCLENDON, R. E., HJELMELAND, A. B. & RICH, J. N. 2008. Brain cancer stem cells display preferential sensitivity to Akt inhibition. *Stem cells,* 26**,** 3027-3036.

FARIVAR, S., ZATI KEIKHA, R., SHIARI, R. & JADALI, F. 2013. Expression of bmi-1 in pediatric brain tumors as a new independent prognostic marker of patient survival. *BioMed research international,* 2013.

FEINBERG, A. P. & VOGELSTEIN, B. 1983. Hypomethylation distinguishes genes of some human cancers from their normal counterparts. *Nature,* 301**,** 89.

FERNÁNDEZ‐SEGURA, E., GARCÍA, J. M., SANTOS, J. L. & CAMPOS, A. 1995. Shape, F‐actin, and surface morphology changes during chemotactic peptide‐induced polarity in human neutrophils. *The Anatomical Record,* 241**,** 519-528.

FISCHER, H.-P., THOMSEN, H., ALTMANNSBERGER, M. & BERTRAM, U. 1989. Malignant rhabdoid tumour of the kidney expressing neurofilament proteins: immunohistochemical findings and histogenetic aspects. *Pathology-Research and Practice,* 184**,** 541-547.

FITZPATRICK, P., AKRAP, N., SÖDERBERG, E., HARRISON, H., THOMSON, G. J. & LANDBERG, G. 2017. Robotic Mammosphere Assay for High-Throughput Screening in Triple-Negative Breast Cancer. *SLAS DISCOVERY: Advancing Life Sciences R&D,* 22**,** 827-836.

FLAUS, A. & OWEN-HUGHES, T. 2004. Mechanisms for ATP-dependent chromatin remodelling: farewell to the tuna-can octamer? *Current opinion in genetics & development,* 14**,** 165-173.

FRASER, S. E. & BRONNER-FRASER, M. 1991. Migrating neural crest cells in the trunk of the avian embryo are multipotent. *Development,* 112**,** 913-920.

FRÜHWALD, M. C., HASSELBLATT, M., WIRTH, S., KÖHLER, G., SCHNEPPENHEIM, R., SUBERO, J. I. M., SIEBERT, R., KORDES, U., JÜRGENS, H. & VORMOOR, J. 2006. Non‐linkage of familial rhabdoid tumors to SMARCB1 implies a second locus for the rhabdoid tumor predisposition syndrome. *Pediatric blood & cancer,* 47**,** 273-278.

GADD, S., SREDNI, S. T., HUANG, C.-C. & PERLMAN, E. J. 2010. Rhabdoid tumor: gene expression clues to pathogenesis and potential therapeutic targets. *Laboratory investigation,* 90**,** 724.

GAMA-SOSA, M. A., SLAGEL, V. A., TREWYN, R. W., OXENHANDLER, R., KUO, K. C., GEHRKE, C. W. & EHRLICH, M. 1983. The 5-methylcytosine content of DNA from human tumors. *Nucleic acids research,* 11**,** 6883-6894.

GARDNER, S. L., ASGHARZADEH, S., GREEN, A., HORN, B., MCCOWAGE, G. & FINLAY, J. 2008. Intensive induction chemotherapy followed by high dose chemotherapy with autologous hematopoietic progenitor cell rescue in young children newly diagnosed with central nervous system atypical teratoid rhabdoid tumors. *Pediatric blood & cancer,* 51**,** 235-240.

GAVRILESCU, M., TODOSI, A., ANIȚEI, M., FILIP, B. & SCRIPCARIU, V. 2012. Expression of bmi-1 protein in cervical, breast and ovarian cancer. *Revista medico-chirurgicala a Societatii de Medici si Naturalisti din Iasi,* 116**,** 1112-1117.

GIBSON, P., TONG, Y., ROBINSON, G., THOMPSON, M. C., CURRLE, D. S., EDEN, C., KRANENBURG, T. A., HOGG, T., POPPLETON, H. & MARTIN, J. 2010. Subtypes of medulloblastoma have distinct developmental origins. *Nature,* 468**,** 1095.

GIDWANI, P., LEVY, A., GOODRICH, J., WEIDENHEIM, K. & KOLB, E. A. 2008. Successful outcome with tandem myeloablative chemotherapy and autologous peripheral blood stem cell transplants in a patient with atypical teratoid/rhabdoid tumor of the central nervous system. *Journal of neuro-oncology,* 88**,** 211-215.

GIL, J. & PETERS, G. 2006. Regulation of the INK4b–ARF–INK4a tumour suppressor locus: all for one or one for all. *Nature reviews Molecular cell biology,* 7**,** 667.

GONZALEZ‐CRUSSI, F., GOLDSCHMIDT, R. A., HSUEH, W. & TRUJILLO, Y. P. 1982. Infantile sarcoma with intracytoplasmic filamentous inclusions: distinctive tumor of possible histiocytic origin. *Cancer,* 49**,** 2365-2375.

GRESH, L., BOURACHOT, B., REIMANN, A., GUIGAS, B., FIETTE, L., GARBAY, S., MUCHARDT, C., HUE, L., PONTOGLIO, M. & YANIV, M. 2005. The SWI/SNF chromatin‐remodeling complex subunit SNF5 is essential for hepatocyte differentiation. *The EMBO journal,* 24**,** 3313-3324.

GRUPENMACHER, A. T., HALPERN, A. L., DE FÁTIMA BONALDO, M., HUANG, C.-C., HAMM, C. A., DE ANDRADE, A., TOMITA, T. & SREDNI, S. T. 2013. Study of the gene expression and microRNA expression profiles of malignant rhabdoid tumors originated in the brain (AT/RT) and in the kidney (RTK). *Child's Nervous System,* 29**,** 1977-1983.

GUIDI, C. J., SANDS, A. T., ZAMBROWICZ, B. P., TURNER, T. K., DEMERS, D. A., WEBSTER, W., SMITH, T. W., IMBALZANO, A. N. & JONES, S. N. 2001. Disruption of Ini1 leads to peri-implantation lethality and tumorigenesis in mice. *Molecular and cellular biology,* 21**,** 3598-3603.

GUPTA, P. B., ONDER, T. T., JIANG, G., TAO, K., KUPERWASSER, C., WEINBERG, R. A. & LANDER, E. S. 2009. Identification of selective inhibitors of cancer stem cells by high-throughput screening. *cell,* 138**,** 645-659.

HAAS, J. E., PALMER, N. F., WEINBERG, A. G. & BECKWITH, J. B. 1981. Ultrastructure of malignant rhabdoid tumor of the kidney: a distinctive renal tumor of children. *Human pathology,* 12**,** 646-657.

HABERLER, C., LAGGNER, U., SLAVC, I., CZECH, T., AMBROS, I. M., AMBROS, P. F., BUDKA, H. & HAINFELLNER, J. A. 2006. Immunohistochemical analysis of INI1 protein in malignant pediatric CNS tumors: lack of INI1 in atypical teratoid/rhabdoid tumors and in a fraction of primitive neuroectodermal tumors without rhabdoid phenotype. *The American journal of surgical pathology,* 30**,** 1462-1468.

HADJIMICHAEL, C., CHANOUMIDOU, K., PAPADOPOULOU, N., ARAMPATZI, P., PAPAMATHEAKIS, J. & KRETSOVALI, A. 2015. Common stemness regulators of embryonic and cancer stem cells. *World journal of stem cells,* 7**,** 1150.

HAN, Z.-Y., RICHER, W., FRÉNEAUX, P., CHAUVIN, C., LUCCHESI, C., GUILLEMOT, D., GRISON, C., LEQUIN, D., PIERRON, G. & MASLIAH-PLANCHON, J. 2016. The occurrence of intracranial rhabdoid tumours in mice depends on temporal control of Smarcb1 inactivation. *Nature communications,* 7**,** 10421.

HANSFORD, L. M., THOMAS, W. D., KEATING, J. M., BURKHART, C. A., PEASTON, A. E., NORRIS, M. D., HABER, M., ARMATI, P. J., WEISS, W. A. & MARSHALL, G. M. 2004. Mechanisms of embryonal tumor initiation: distinct roles for MycN expression and MYCN amplification. *Proceedings of the National Academy of Sciences of the United States of America,* 101**,** 12664-12669.

HARRIS, M., EYDEN, B. P. & JOGLEKAR, V. 1987. Rhabdoid tumour of the bladder: a histological, ultrastructural and immunohistochemical study. *Histopathology,* 11**,** 1083-1092.

HASSELBLATT, M., GESK, S., OYEN, F., ROSSI, S., VISCARDI, E., GIANGASPERO, F., GIANNINI, C., JUDKINS, A. R., FRÜHWALD, M. C. & OBSER, T. 2011. Nonsense mutation and inactivation of SMARCA4 (BRG1) in an atypical teratoid/rhabdoid tumor showing retained SMARCB1 (INI1) expression. *The American journal of surgical pathology,* 35**,** 933-935.

HASSELBLATT, M., ISKEN, S., LINGE, A., EIKMEIER, K., JEIBMANN, A., OYEN, F., NAGEL, I., RICHTER, J., BARTELHEIM, K. & KORDES, U. 2013. High‐resolution genomic analysis suggests the absence of recurrent genomic alterations other than SMARCB1 aberrations in atypical teratoid/rhabdoid tumors. *Genes, Chromosomes and Cancer,* 52**,** 185-190.

HASSELBLATT, M., NAGEL, I., OYEN, F., BARTELHEIM, K., RUSSELL, R. B., SCHÜLLER, U., JUNCKERSTORFF, R., ROSENBLUM, M., ALASSIRI, A. H. & ROSSI, S. 2014. SMARCA4-mutated atypical teratoid/rhabdoid tumors are associated with inherited germline alterations and poor prognosis. *Acta neuropathologica,* 128**,** 453-456.

HAYAT, M. A. 2012. *Pediatric Cancer, Volume 2: Teratoid/Rhabdoid, Brain Tumors, and Glioma*, Springer Science & Business Media.

HE, S., IWASHITA, T., BUCHSTALLER, J., MOLOFSKY, A. V., THOMAS, D. & MORRISON, S. J. 2009. Bmi-1 over-expression in neural stem/progenitor cells increases proliferation and neurogenesis in culture but has little effect on these functions in vivo. *Developmental biology,* 328**,** 257-272.

HEIGWER, F., KERR, G. & BOUTROS, M. 2014. E-CRISP: fast CRISPR target site identification. *Nature methods,* 11**,** 122.

HIGASHINO, K., NARITA, T., TAGA, T., OHTA, S. & TAKEUCHI, Y. 2003. Malignant rhabdoid tumor shows a unique neural differentiation as distinct from neuroblastoma. *Cancer science,* 94**,** 37-42.

HILDEN, J. M., MEERBAUM, S., BURGER, P., FINLAY, J., JANSS, A., SCHEITHAUER, B. W., WALTER, A. W., RORKE, L. B. & BIEGEL, J. A. 2004. Central nervous system atypical teratoid/rhabdoid tumor: results of therapy in children enrolled in a registry. *Journal of clinical oncology,* 22**,** 2877-2884.

HIRSCHHORN, J. N., BROWN, S. A., CLARK, C. D. & WINSTON, F. 1992. Evidence that SNF2/SWI2 and SNF5 activate transcription in yeast by altering chromatin structure. *Genes & development,* 6**,** 2288-2298.

HO, D. M., HSU, C. Y., WONG, T. T., TING, L. T. & CHIANG, H. 2000. Atypical teratoid/rhabdoid tumor of the central nervous system: a comparative study with primitive neuroectodermal tumor/medulloblastoma. *Acta Neuropathol,* 99**,** 482-8.

HO, L., JOTHI, R., RONAN, J. L., CUI, K., ZHAO, K. & CRABTREE, G. R. 2009a. An embryonic stem cell chromatin remodeling complex, esBAF, is an essential component of the core pluripotency transcriptional network. *Proceedings of the National Academy of Sciences,* 106**,** 5187-5191.

HO, L., RONAN, J. L., WU, J., STAAHL, B. T., CHEN, L., KUO, A., LESSARD, J., NESVIZHSKII, A. I., RANISH, J. & CRABTREE, G. R. 2009b. An embryonic stem cell chromatin remodeling complex, esBAF, is essential for embryonic stem cell self-renewal and pluripotency. *Proceedings of the National Academy of Sciences,* 106**,** 5181-5186.

HODGES, C., KIRKLAND, J. G. & CRABTREE, G. R. 2016. The many roles of BAF (mSWI/SNF) and PBAF complexes in cancer. *Cold Spring Harbor perspectives in medicine,* 6.

HOLLMANN, T. J. & HORNICK, J. L. 2011. INI1-deficient tumors: diagnostic features and molecular genetics. *The American journal of surgical pathology,* 35**,** e47-e63.

HONDA, R. & YASUDA, H. 1999. Association of p19ARF with Mdm2 inhibits ubiquitin ligase activity of Mdm2 for tumor suppressor p53. *The EMBO journal,* 18**,** 22-27.

HONG, C. R., KANG, H. J., JU, H. Y., LEE, J. W., KIM, H., PARK, S.-H., KIM, I. H., PARK, K. D. & SHIN, H. Y. 2015. Extra-cranial malignant rhabdoid tumor in children: A single institute experience. *Cancer research and treatment: official journal of Korean Cancer Association,* 47**,** 889.

HORNE, G. A. & COPLAND, M. 2017. Approaches for targeting self-renewal pathways in cancer stem cells: implications for hematological treatments. *Expert opinion on drug discovery,* 12**,** 465-474.

HORNICK, J. L., DAL CIN, P. & FLETCHER, C. D. 2009. Loss of INI1 expression is characteristic of both conventional and proximal-type epithelioid sarcoma. *Am J Surg Pathol,* 33**,** 542-50.

HSU, P. D., SCOTT, D. A., WEINSTEIN, J. A., RAN, F. A., KONERMANN, S., AGARWALA, V., LI, Y., FINE, E. J., WU, X. & SHALEM, O. 2013. DNA targeting specificity of RNA-guided Cas9 nucleases. *Nature biotechnology,* 31**,** 827.

HULSEBOS, T. J., PLOMP, A. S., WOLTERMAN, R. A., ROBANUS-MAANDAG, E. C., BAAS, F. & WESSELING, P. 2007. Germline mutation of INI1/SMARCB1 in familial schwannomatosis. *Am J Hum Genet,* 80**,** 805-10.

IGNATOVA, T. N., KUKEKOV, V. G., LAYWELL, E. D., SUSLOV, O. N., VRIONIS, F. D. & STEINDLER, D. A. 2002. Human cortical glial tumors contain neural stem‐like cells expressing astroglial and neuronal markers in vitro. *Glia,* 39**,** 193-206.

IMBALZANO, A. N. & JONES, S. N. 2005. Snf5 tumor suppressor couples chromatin remodeling, checkpoint control, and chromosomal stability. *Cancer cell,* 7**,** 294-295.

INFANTE, J. R., CASSIER, P. A., GERECITANO, J. F., WITTEVEEN, P. O., CHUGH, R., RIBRAG, V., CHAKRABORTY, A., MATANO, A., DOBSON, J. R. & CRYSTAL, A. S. 2016. A phase I study of the cyclin-dependent kinase 4/6 inhibitor ribociclib (LEE011) in patients with advanced solid tumors and lymphomas. *Clinical Cancer Research***,** clincanres. 1248.2016.

ISAKOFF, M. S., SANSAM, C. G., TAMAYO, P., SUBRAMANIAN, A., EVANS, J. A., FILLMORE, C. M., WANG, X., BIEGEL, J. A., POMEROY, S. L. & MESIROV, J. P. 2005. Inactivation of the Snf5 tumor suppressor stimulates cell cycle progression and cooperates with p53 loss in oncogenic transformation. *Proceedings of the National Academy of Sciences of the United States of America,* 102**,** 17745-17750.

ISHII, M., ARIAS, A. C., LIU, L., CHEN, Y.-B., BRONNER, M. E. & MAXSON, R. E. 2012. A stable cranial neural crest cell line from mouse. *Stem cells and development,* 21**,** 3069-3080.

ITAKURA, E., TAMIYA, S., MORITA, K., SHIRATSUCHI, H., KINOSHITA, Y., OSHIRO, Y., ODA, Y., OHTA, S., FURUE, M. & TSUNEYOSHI, M. 2001. Subcellular distribution of cytokeratin and vimentin in malignant rhabdoid tumor: three-dimensional imaging with confocal laser scanning microscopy and double immunofluorescence. *Modern Pathology,* 14**,** 854.

IVANA, L., CARLSON, K. A. & IMBALZANO, A. N. 2001. Mammalian SWI/SNF complexes promote MyoD-mediated muscle differentiation. *Nature genetics,* 27**,** 187.

IWAMA, A., OGURO, H., NEGISHI, M., KATO, Y., MORITA, Y., TSUKUI, H., EMA, H., KAMIJO, T., KATOH-FUKUI, Y. & KOSEKI, H. 2004. Enhanced self-renewal

of hematopoietic stem cells mediated by the polycomb gene product Bmi-1. *Immunity,* 21**,** 843-851.

JACKSON, E. M., SIEVERT, A. J., GAI, X., HAKONARSON, H., JUDKINS, A. R., TOOKE, L., PERIN, J. C., XIE, H., SHAIKH, T. H. & BIEGEL, J. A. 2009. Genomic analysis using high-density single nucleotide polymorphism-based oligonucleotide arrays and multiplex ligation-dependent probe amplification provides a comprehensive analysis of INI1/SMARCB1 in malignant rhabdoid tumors. *Clinical cancer research,* 15**,** 1923-1930.

JACOBS, J. J., KIEBOOM, K., MARINO, S., DEPINHO, R. A. & VAN LOHUIZEN, M. 1999a. The oncogene and Polycomb-group gene bmi-1 regulates cell proliferation and senescence through the ink4a locus. *Nature,* 397**,** 164.

JACOBS, J. J., SCHEIJEN, B., VONCKEN, J.-W., KIEBOOM, K., BERNS, A. & VAN LOHUIZEN, M. 1999b. Bmi-1 collaborates with c-Myc in tumorigenesis by inhibiting c-Myc-induced apoptosis via INK4a/ARF. *Genes & development,* 13**,** 2678-2690.

JAGANI, Z., MORA-BLANCO, E. L., SANSAM, C. G., MCKENNA, E. S., WILSON, B., CHEN, D., KLEKOTA, J., TAMAYO, P., NGUYEN, P. T. & TOLSTORUKOV, M. 2010. Loss of the tumor suppressor Snf5 leads to aberrant activation of the Hedgehog-Gli pathway. *Nature medicine,* 16**,** 1429.

JANSON, K., NEDZI, L. A., DAVID, O., SCHORIN, M., WALSH, J. W., BHATTACHARJEE, M., PRIDJIAN, G., TAN, L., JUDKINS, A. R. & BIEGEL, J. A. 2006. Predisposition to atypical teratoid/rhabdoid tumor due to an inherited INI1 mutation. *Pediatric blood & cancer,* 47**,** 279-284.

JANUARIO, T., YE, X., BAINER, R., ALICKE, B., SMITH, T., HALEY, B., MODRUSAN, Z., GOULD, S. & YAUCH, R. L. 2017. PRC2-mediated repression of SMARCA2 predicts EZH2 inhibitor activity in SWI/SNF mutant tumors. *Proceedings of the National Academy of Sciences,* 114**,** 12249-12254.

JIANG, L., LI, J. & SONG, L. 2009. Bmi-1, stem cells and cancer. *Acta Biochim Biophys Sin,* 41**,** 527-534.

JOHANN, P. D., ERKEK, S., ZAPATKA, M., KERL, K., BUCHHALTER, I., HOVESTADT, V., JONES, D. T., STURM, D., HERMANN, C. & WANG, M. S. 2016. Atypical teratoid/rhabdoid tumors are comprised of three epigenetic subgroups with distinct enhancer landscapes. *Cancer cell,* 29**,** 379-393.

JOHNSON, S., CHEN, H. & LO, P. 2013. In vitro tumorsphere formation assays. *Bio-protocol,* 3**,** e325.

JUDKINS, A. R., MAUGER, J., HT, A., RORKE, L. B. & BIEGEL, J. A. 2004. Immunohistochemical analysis of hSNF5/INI1 in pediatric CNS neoplasms. *The American journal of surgical pathology,* 28**,** 644-650.

KADOCH, C., HARGREAVES, D. C., HODGES, C., ELIAS, L., HO, L., RANISH, J. & CRABTREE, G. R. 2013. Proteomic and bioinformatic analysis of mammalian

SWI/SNF complexes identifies extensive roles in human malignancy. *Nature genetics,* 45**,** 592.

KAO, G. D., JIANG, Z., FERNANDES, A. M., GUPTA, A. K. & MAITY, A. 2007. Inhibition of phosphatidylinositol-3-OH kinase/Akt signaling impairs DNA repair in glioblastoma cells following ionizing radiation. *Journal of Biological Chemistry,* 282**,** 21206-21212.

KATO, H., OHTA, S., KOSHIDA, S., NARITA, T., TAGA, T., TAKEUCHI, Y. & SUGITA, K. 2003. Expression of pericyte, mesangium and muscle markers in malignant rhabdoid tumor cell lines: Differentiation‐induction using 5‐azacytidine. *Cancer science,* 94**,** 1059-1065.

KATSUMI, Y., IEHARA, T., MIYACHI, M., YAGYU, S., TSUBAI-SHIMIZU, S., KIKUCHI, K., TAMURA, S., KUWAHARA, Y., TSUCHIYA, K. & KURODA, H. 2011. Sensitivity of malignant rhabdoid tumor cell lines to PD 0332991 is inversely correlated with p16 expression. *Biochemical and biophysical research communications,* 413**,** 62-68.

KHAN, S. A., REDDY, D. & GUPTA, S. 2015. Global histone post-translational modifications and cancer: Biomarkers for diagnosis, prognosis and treatment? *World journal of biological chemistry,* 6**,** 333.

KIA, S. K., GORSKI, M. M., GIANNAKOPOULOS, S. & VERRIJZER, C. P. 2008. SWI/SNF mediates polycomb eviction and epigenetic reprogramming of the INK4b-ARF-INK4a locus. *Molecular and cellular biology,* 28**,** 3457-3464.

KIDDER, B. L., PALMER, S. & KNOTT, J. G. 2009. SWI/SNF‐Brg1 regulates self‐renewal and occupies core pluripotency‐related genes in embryonic stem cells. *Stem cells,* 27**,** 317-328.

KIM, H. S., LEE, K., BAE, S., PARK, J., LEE, C.-K., KIM, M., KIM, E., KIM, M., KIM, S. & KIM, C. 2017. CRISPR/Cas9-mediated gene knockout screens and target identification via whole-genome sequencing uncover host genes required for picornavirus infection. *Journal of Biological Chemistry,* 292**,** 10664-10671.

KIM, T. H., BARRERA, L. O., ZHENG, M., QU, C., SINGER, M. A., RICHMOND, T. A., WU, Y., GREEN, R. D. & REN, B. 2005. A high-resolution map of active promoters in the human genome. *Nature,* 436**,** 876.

KLEER, C. G., CAO, Q., VARAMBALLY, S., SHEN, R., OTA, I., TOMLINS, S. A., GHOSH, D., SEWALT, R. G., OTTE, A. P. & HAYES, D. F. 2003. EZH2 is a marker of aggressive breast cancer and promotes neoplastic transformation of breast epithelial cells. *Proceedings of the National Academy of Sciences,* 100**,** 11606-11611.

KLOCHENDLER-YEIVIN, A., PICARSKY, E. & YANIV, M. 2006. Increased DNA damage sensitivity and apoptosis in cells lacking the Snf5/Ini1 subunit of the SWI/SNF chromatin remodeling complex. *Molecular and cellular biology,* 26**,** 2661-2674.

KLOCHENDLER‐YEIVIN, A., FIETTE, L., BARRA, J., MUCHARDT, C., BABINET, C. & YANIV, M. 2000. The murine SNF5/INI1 chromatin remodeling factor is essential for embryonic development and tumor suppression. *EMBO reports,* 1**,** 500-506.

KNUTSON, S. K., WARHOLIC, N. M., WIGLE, T. J., KLAUS, C. R., ALLAIN, C. J., RAIMONDI, A., SCOTT, M. P., CHESWORTH, R., MOYER, M. P. & COPELAND, R. A. 2013. Durable tumor regression in genetically altered malignant rhabdoid tumors by inhibition of methyltransferase EZH2. *Proceedings of the National Academy of Sciences,* 110**,** 7922-7927.

KOEVA, M., FORSBERG, E. C. & STUART, J. M. 2011. Computational integration of homolog and pathway gene module expression reveals general stemness signatures. *PLoS One,* 6**,** e18968.

KOH, C. M. 2013. Preparation of cells for microscopy using cytospin. *Methods in enzymology.* Elsevier.

KOHASHI, K., TANAKA, Y., KISHIMOTO, H., YAMAMOTO, H., YAMADA, Y., TAGUCHI, T., IWAMOTO, Y. & ODA, Y. 2016. Reclassification of rhabdoid tumor and pediatric undifferentiated/unclassified sarcoma with complete loss of SMARCB1/INI1 protein expression: three subtypes of rhabdoid tumor according to their histological features. *Modern Pathology,* 29**,** 1232.

KORDES, U., BARTELHEIM, K., MODENA, P., MASSIMINO, M., BIASSONI, V., REINHARD, H., HASSELBLATT, M., SCHNEPPENHEIM, R. & FRÜHWALD, M. C. 2014. Favorable outcome of patients affected by rhabdoid tumors due to rhabdoid tumor predisposition syndrome (RTPS). *Pediatric blood & cancer,* 61**,** 919-921.

KORDES, U., GESK, S., FRÜHWALD, M. C., GRAF, N., LEUSCHNER, I., HASSELBLATT, M., JEIBMANN, A., OYEN, F., PETERS, O. & PIETSCH, T. 2010. Clinical and molecular features in patients with atypical teratoid rhabdoid tumor or malignant rhabdoid tumor. *Genes, Chromosomes and Cancer,* 49**,** 176-181.

KOWENZ-LEUTZ, E. & LEUTZ, A. 1999. AC/EBPβ isoform recruits the SWI/SNF complex to activate myeloid genes. *Molecular cell,* 4**,** 735-743.

KRESO, A., VAN GALEN, P., PEDLEY, N. M., LIMA-FERNANDES, E., FRELIN, C., DAVIS, T., CAO, L., BAIAZITOV, R., DU, W. & SYDORENKO, N. 2014. Self-renewal as a therapeutic target in human colorectal cancer. *Nature medicine,* 20**,** 29.

KRUEGER, K. E. & SRIVASTAVA, S. 2006. Posttranslational protein modifications current implications for cancer detection, prevention, and therapeutics. *Molecular & Cellular Proteomics,* 5**,** 1799-1810.

KRUGER, G. M., MOSHER, J. T., BIXBY, S., JOSEPH, N., IWASHITA, T. & MORRISON, S. J. 2002. Neural crest stem cells persist in the adult gut but undergo changes in self-renewal, neuronal subtype potential, and factor responsiveness. *Neuron,* 35**,** 657-669.

KURAS, L. & STRUHL, K. 1999. Binding of TBP to promoters in vivo is stimulated by activators and requires Pol II holoenzyme. *Nature,* 399**,** 609.

KUWAHARA, Y., CHARBONEAU, A., KNUDSEN, E. S. & WEISSMAN, B. E. 2010. Reexpression of hSNF5 in malignant rhabdoid tumor cell lines causes cell cycle arrest through a p21CIP1/WAF1-dependent mechanism. *Cancer research,* 70**,** 1854-1865.

LAFAY-COUSIN, L., HAWKINS, C., CARRET, A., JOHNSTON, D., ZELCER, S., WILSON, B., JABADO, N., SCHEINEMANN, K., EISENSTAT, D. & FRYER, C. 2012. Central nervous system atypical teratoid rhabdoid tumours: the Canadian Paediatric Brain Tumour Consortium experience. *European journal of cancer,* 48**,** 353-359.

LEE, R. S., STEWART, C., CARTER, S. L., AMBROGIO, L., CIBULSKIS, K., SOUGNEZ, C., LAWRENCE, M. S., AUCLAIR, D., MORA, J. & GOLUB, T. R. 2012. A remarkably simple genome underlies highly malignant pediatric rhabdoid cancers. *The Journal of clinical investigation,* 122**,** 2983-2988.

LEUNG, C., LINGBEEK, M., SHAKHOVA, O., LIU, J., TANGER, E., SAREMASLANI, P., VAN LOHUIZEN, M. & MARINO, S. 2004. Bmi1 is essential for cerebellar development and is overexpressed in human medulloblastomas. *Nature,* 428**,** 337.

LEYCHKIS, Y., MUNZER, S. R. & RICHARDSON, J. L. 2009. What is stemness? *Studies in History and Philosophy of Science Part C: Studies in History and Philosophy of Biological and Biomedical Sciences,* 40**,** 312-320.

LI, W., MA, H., ZHANG, J., ZHU, L., WANG, C. & YANG, Y. 2017. Unraveling the roles of CD44/CD24 and ALDH1 as cancer stem cell markers in tumorigenesis and metastasis. *Scientific Reports,* 7**,** 13856.

LI, Y., PAN, S., ZHANG, Y., REN, M., FENG, M., PENG, N., CHEN, L., LIANG, Y. X. & SHE, Q. 2015. Harnessing Type I and Type III CRISPR-Cas systems for genome editing. *Nucleic acids research,* 44**,** e34-e34.

LIDDY, K. A., WHITE, M. Y. & CORDWELL, S. J. 2013. Functional decorations: post-translational modifications and heart disease delineated by targeted proteomics. *Genome medicine,* 5**,** 20.

LIU, J. A. & CHEUNG, M. 2016. Neural crest stem cells and their potential therapeutic applications. *Developmental biology,* 419**,** 199-216.

LIU, L., ANDREWS, L. & TOLLEFSBOL, T. 2006a. Loss of the human polycomb group protein BMI1 promotes cancer-specific cell death. *Oncogene,* 25**,** 4370.

LIU, S., DONTU, G., MANTLE, I. D., PATEL, S., AHN, N.-S., JACKSON, K. W., SURI, P. & WICHA, M. S. 2006b. Hedgehog signaling and Bmi-1 regulate self-renewal of normal and malignant human mammary stem cells. *Cancer research,* 66**,** 6063-6071.

LOGAN, C. Y. & NUSSE, R. 2004. The Wnt signaling pathway in development and disease. *Annu. Rev. Cell Dev. Biol.,* 20**,** 781-810.

LOUIS, D. N., OHGAKI, H., WIESTLER, O. D., CAVENEE, W. K., BURGER, P. C., JOUVET, A., SCHEITHAUER, B. W. & KLEIHUES, P. 2007. The 2007 WHO classification of tumours of the central nervous system. *Acta neuropathologica,* 114**,** 97-109.

LOUIS, S. A. & REYNOLDS, B. A. 2009. Neurosphere and neural colony-forming cell assays. *Protocols for Neural Cell Culture.* Springer.

LOUIS, S. A., RIETZE, R. L., DELEYROLLE, L., WAGEY, R. E., THOMAS, T. E., EAVES, A. C. & REYNOLDS, B. A. 2008. Enumeration of neural stem and progenitor cells in the neural colony‐forming cell assay. *Stem Cells,* 26**,** 988-996.

LU, H., LI, G., ZHOU, C., JIN, W., QIAN, X., WANG, Z., PAN, H., JIN, H. & WANG, X. 2016. Regulation and role of post-translational modifications of enhancer of zeste homologue 2 in cancer development. *American journal of cancer research,* 6**,** 2737.

MAATEN, L. V. D. & HINTON, G. 2008. Visualizing data using t-SNE. *Journal of machine learning research,* 9**,** 2579-2605.

MACDONALD, T. J. 2008. Aggressive infantile embryonal tumors. *Journal of child neurology,* 23**,** 1195-1204.

MADIGAN, C. E., ARMENIAN, S. H., MALOGOLOWKIN, M. H. & MASCARENHAS, L. 2007. Extracranial malignant rhabdoid tumors in childhood. *Cancer,* 110**,** 2061-2066.

MAKAROVA, K. S., HAFT, D. H., BARRANGOU, R., BROUNS, S. J., CHARPENTIER, E., HORVATH, P., MOINEAU, S., MOJICA, F. J., WOLF, Y. I. & YAKUNIN, A. F. 2011. Evolution and classification of the CRISPR–Cas systems. *Nature Reviews Microbiology,* 9**,** 467.

MARGOL, A. S. & JUDKINS, A. R. 2014. Pathology and diagnosis of SMARCB1-deficient tumors. *Cancer genetics,* 207**,** 358-364.

MARGUERON, R. & REINBERG, D. 2011. The Polycomb complex PRC2 and its mark in life. *Nature,* 469**,** 343.

MARIS, J. M. 2010. Recent advances in neuroblastoma. *New England Journal of Medicine,* 362**,** 2202-2211.

MARSHALL, G. M., CARTER, D. R., CHEUNG, B. B., LIU, T., MATEOS, M. K., MEYEROWITZ, J. G. & WEISS, W. A. 2014. The prenatal origins of cancer. *Nature Reviews Cancer,* 14**,** 277.

MARTÍN-BERNABÉ, A., BALCELLS, C., TARRAGÓ-CELADA, J., FOGUET, C., BOURGOIN-VOILLARD, S., SEVE, M. & CASCANTE, M. 2017. The importance of post-translational modifications in systems biology approaches to identify therapeutic targets in cancer metabolism. *Current Opinion in Systems Biology,* 3**,** 161-169.

MAUGERI-SACCÀ, M., VIGNERI, P. & DE MARIA, R. 2011. Cancer stem cells and chemosensitivity. *Clinical Cancer Research,* 17**,** 4942-4947.

MAYR, C., WAGNER, A., LOEFFELBERGER, M., BRUCKNER, D., JAKAB, M., BERR, F., DI FAZIO, P., OCKER, M., NEUREITER, D. & PICHLER, M. 2016. The BMI1 inhibitor PTC-209 is a potential compound to halt cellular growth in biliary tract cancer cells. *Oncotarget,* 7**,** 745.

MCGOVERN, S. L., GROSSHANS, D. & MAHAJAN, A. 2014. Embryonal brain tumors. *The Cancer Journal,* 20**,** 397-402.

MEDINA, P. P. & SANCHEZ-CESPEDES, M. 2008. Involvement of the chromatin-remodeling factor BRG1/SMARCA4 in human cancer. *Epigenetics,* 3**,** 64-68.

MEDJKANE, S., NOVIKOV, E., VERSTEEGE, I. & DELATTRE, O. 2004. The tumor suppressor hSNF5/INI1 modulates cell growth and actin cytoskeleton organization. *Cancer research,* 64**,** 3406-3413.

MIMEAULT, M. & BATRA, S. K. 2011. Frequent gene products and molecular pathways altered in prostate cancer–and metastasis-initiating cells and their progenies and novel promising multitargeted therapies. *Molecular medicine,* 17**,** 949.

MODENA, P., SARDI, I., BRENCA, M., GIUNTI, L., BUCCOLIERO, A. M., POLLO, B., BIASSONI, V., GENITORI, L., ANTONELLI, M. & MAESTRO, R. 2013. Case report: long-term survival of an infant syndromic patient affected by atypical teratoid-rhabdoid tumor. *BMC cancer,* 13**,** 100.

MOLOFSKY, A. V., HE, S., BYDON, M., MORRISON, S. J. & PARDAL, R. 2005. Bmi-1 promotes neural stem cell self-renewal and neural development but not mouse growth and survival by repressing the p16Ink4a and p19Arf senescence pathways. *Genes & development,* 19**,** 1432-1437.

MOLOFSKY, A. V., PARDAL, R., IWASHITA, T., PARK, I.-K., CLARKE, M. F. & MORRISON, S. J. 2003. Bmi-1 dependence distinguishes neural stem cell self-renewal from progenitor proliferation. *nature,* 425**,** 962.

MONDAL, D., JANA, M. & JULKA, P. 2011. Supratentorial atypical teratoid rhabdoid tumor: An uncommon childhood tumor. *Journal of pediatric neurosciences,* 6**,** 90.

MORA-BLANCO, E. L., MISHINA, Y., TILLMAN, E. J., CHO, Y.-J., THOM, C. S., POMEROY, S. L., SHAO, W. & ROBERTS, C. W. 2014. Activation of β-catenin/TCF targets following loss of the tumor suppressor SNF5. *Oncogene,* 33**,** 933.

MORENO, N., SCHMIDT, C., AHLFELD, J., PÖSCHL, J., DITTMAR, S., PFISTER, S. M., KOOL, M., KERL, K. & SCHÜLLER, U. 2014. Loss of Smarc proteins impairs cerebellar development. *Journal of Neuroscience,* 34**,** 13486-13491.

MORRISON, S. J., WHITE, P. M., ZOCK, C. & ANDERSON, D. J. 1999. Prospective identification, isolation by flow cytometry, and in vivo self-renewal of multipotent mammalian neural crest stem cells. *Cell,* 96**,** 737-749.

NEIGEBORN, L. & CARLSON, M. 1984. Genes affecting the regulation of SUC2 gene expression by glucose repression in Saccharomyces cerevisiae. *Genetics,* 108**,** 845-858.

NISHIDA, Y., MAEDA, A., CHACHAD, D., ISHIZAWA, J., QIU, Y. H., KORNBLAU, S. M., KIMURA, S., ANDREEFF, M. & KOJIMA, K. 2015. Preclinical activity of the novel B‐cell‐specific Moloney murine leukemia virus integration site 1 inhibitor PTC‐209 in acute myeloid leukemia: Implications for leukemia therapy. *Cancer science,* 106**,** 1705-1713.

NISHIDA, Y., MAEDA, A., KIM, M., CAO, L., KUBOTA, Y., ISHIZAWA, J., ALRAWI, A., KATO, Y., IWAMA, A. & FUJISAWA, M. 2017. The novel BMI-1 inhibitor PTC596 downregulates MCL-1 and induces p53-independent mitochondrial apoptosis in acute myeloid leukemia progenitor cells. *Blood cancer journal,* 7**,** e527.

ODA, Y. & TSUNEYOSHI, M. 2006. Extrarenal rhabdoid tumors of soft tissue: clinicopathological and molecular genetic review and distinction from other soft‐tissue sarcomas with rhabdoid features. *Pathology international,* 56**,** 287-295.

OKAMOTO, S.-I. & LIPTON, S. A. 2015. S-Nitrosylation in neurogenesis and neuronal development. *Biochimica et Biophysica Acta (BBA)-General Subjects,* 1850**,** 1588-1593.

OKUNO, K., OHTA, S., KATO, H., TAGA, T., SUGITA, K. & TAKEUCHI, Y. 2010. Expression of neural stem cell markers in malignant rhabdoid tumor cell lines. *Oncology reports,* 23**,** 485-492.

ORUETXEBARRIA, I., VENTURINI, F., KEKARAINEN, T., HOUWELING, A., ZUIJDERDUIJN, L. M., MOHD-SARIP, A., VRIES, R. G., HOEBEN, R. C. & VERRIJZER, C. P. 2004. P16INK4a is required for hSNF5 chromatin remodeler-induced cellular senescence in malignant rhabdoid tumor cells. *Journal of Biological Chemistry,* 279**,** 3807-3816.

OSTROM, Q. T., CHEN, Y., M. DE BLANK, P., ONDRACEK, A., FARAH, P., GITTLEMAN, H., WOLINSKY, Y., KRUCHKO, C., COHEN, M. L. & BRAT, D. J. 2014. The descriptive epidemiology of atypical teratoid/rhabdoid tumors in the United States, 2001–2010. *Neuro-oncology,* 16**,** 1392-1399.

OTA, S., CRABBE, D. C., TRAN, T. N., TRICHE, T. J. & SHIMADA, H. 1993. Malignant rhabdoid tumor. A study with two established cell lines. *Cancer,* 71**,** 2862-2872.

PANANDIKER, A. S. P., MERCHANT, T. E., BELTRAN, C., WU, S., SHARMA, S., BOOP, F. A., JENKINS, J. J., HELTON, K. J., WRIGHT, K. D. & BRONISCER, A. 2012. Sequencing of local therapy affects the pattern of treatment failure and survival in children with atypical teratoid rhabdoid tumors of the central nervous system. *International Journal of Radiation Oncology• Biology• Physics,* 82**,** 1756-1763.

PARHAM, D., PEIPER, S., ROBICHEAUX, G., RIBEIRO, R. & DOUGLASS, E. 1988. Malignant rhabdoid tumor of the liver. Evidence for epithelial differentiation. *Archives of pathology & laboratory medicine,* 112**,** 61-64.

PARHAM, D. M., WEEKS, D. A. & BECKWITH, J. B. 1994. The clinicopathologic spectrum of putative extrarenal rhabdoid tumors. An analysis of 42 cases studied with immunohistochemistry or electron microscopy. *The American journal of surgical pathology,* 18**,** 1010-1029.

PARK, I.-K., MORRISON, S. J. & CLARKE, M. F. 2004. Bmi1, stem cells, and senescence regulation. *The Journal of clinical investigation,* 113**,** 175-179.

PARK, I.-K., QIAN, D., KIEL, M., BECKER, M. W., PIHALJA, M., WEISSMAN, I. L., MORRISON, S. J. & CLARKE, M. F. 2003. Bmi-1 is required for maintenance of adult self-renewing haematopoietic stem cells. *Nature,* 423**,** 302.

PARKER, J. S., BROERING, T. J., KIM, J., HIGGINS, D. E. & NIBERT, M. L. 2002. Reovirus core protein μ2 determines the filamentous morphology of viral inclusion bodies by interacting with and stabilizing microtubules. *Journal of virology,* 76**,** 4483-4496.

PASTRANA, E., SILVA-VARGAS, V. & DOETSCH, F. 2011. Eyes wide open: a critical review of sphere-formation as an assay for stem cells. *Cell stem cell,* 8**,** 486-498.

PATIL, S., PERRY, A., MACCOLLIN, M., DONG, S., BETENSKY, R. A., YEH, T. H., GUTMANN, D. H. & STEMMER‐RACHAMIMOV, A. O. 2008. Immunohistochemical analysis supports a role for INI1/SMARCB1 in hereditary forms of schwannomas, but not in solitary, sporadic schwannomas. *Brain pathology,* 18**,** 517-519.

PEDERSEN, T. Å., KOWENZ-LEUTZ, E., LEUTZ, A. & NERLOV, C. 2001. Cooperation between C/EBPα TBP/TFIIB and SWI/SNF recruiting domains is required for adipocyte differentiation. *Genes & development,* 15**,** 3208-3216.

POMEROY, S. L., TAMAYO, P., GAASENBEEK, M., STURLA, L. M., ANGELO, M., MCLAUGHLIN, M. E., KIM, J. Y., GOUMNEROVA, L. C., BLACK, P. M. & LAU, C. 2002. Prediction of central nervous system embryonal tumour outcome based on gene expression. *Nature,* 415**,** 436.

PONTI, D., COSTA, A., ZAFFARONI, N., PRATESI, G., PETRANGOLINI, G., CORADINI, D., PILOTTI, S., PIEROTTI, M. A. & DAIDONE, M. G. 2005. Isolation and in vitro propagation of tumorigenic breast cancer cells with stem/progenitor cell properties. *Cancer research,* 65**,** 5506-5511.

PROUST, F., LAQUERRIERE, A., COSTANTIN, B., RUCHOUX, M., VANNIER, J. & FREGER, P. 1999. Simultaneous presentation of atypical teratoid/rhabdoid tumor in siblings. *Journal of neuro-oncology,* 43**,** 63-70.

QIN, Z.-K., YANG, J.-A., YE, Y.-L., ZHANG, X., XU, L.-H., ZHOU, F.-J., HAN, H., LIU, Z.-W., SONG, L.-B. & ZENG, M.-S. 2009. Expression of Bmi-1 is a prognostic marker in bladder cancer. *Bmc Cancer,* 9**,** 61.

RAMALHO-SANTOS, M., YOON, S., MATSUZAKI, Y., MULLIGAN, R. C. & MELTON, D. A. 2002. " Stemness": transcriptional profiling of embryonic and adult stem cells. *Science,* 298**,** 597-600.

RAN, F. A., HSU, P. D., WRIGHT, J., AGARWALA, V., SCOTT, D. A. & ZHANG, F. 2013. Genome engineering using the CRISPR-Cas9 system. *Nature protocols,* 8**,** 2281.

RATH, D., AMLINGER, L., RATH, A. & LUNDGREN, M. 2015. The CRISPR-Cas immune system: biology, mechanisms and applications. *Biochimie,* 117**,** 119-128.

RAYMOND, W. A. & LEONG, A. S. Y. 1989. Co‐expression of cytokeratin and vimentin intermediate filament proteins in benign and neoplastic breast epithelium. *The Journal of pathology,* 157**,** 299-306.

REINCKE, B. S., ROSSON, G. B., OSWALD, B. W. & WRIGHT, C. F. 2003. INI1 expression induces cell cycle arrest and markers of senescence in malignant rhabdoid tumor cells. *Journal of cellular physiology,* 194**,** 303-313.

REINHARD, H., REINERT, J., BEIER, R., FURTWÄNGLER, R., ALKASSER, M., RUTKOWSKI, S., FRÜHWALD, M., KOSCIELNIAK, E., LEUSCHNER, I. & KAATSCH, P. 2008. Rhabdoid tumors in children: prognostic factors in 70 patients diagnosed in Germany. *Oncology reports,* 19**,** 819-823.

REPPAS, N. B., WADE, J. T., CHURCH, G. M. & STRUHL, K. 2006. The transition between transcriptional initiation and elongation in E. coli is highly variable and often rate limiting. *Molecular cell,* 24**,** 747-757.

REYA, T. & CLEVERS, H. 2005. Wnt signalling in stem cells and cancer. *Nature,* 434**,** 843.

REYNOLDS, B. A. & WEISS, S. 1992. Generation of neurons and astrocytes from isolated cells of the adult mammalian central nervous system. *science,* 255**,** 1707-1710.

RICHER, W., MASLIAH-PLANCHON, J., CLEMENT, N., JIMENEZ, I., MAILLOT, L., GENTIEN, D., ALBAUD, B., CHEMLALI, W., GALANT, C. & LAROUSSERIE, F. 2017. Embryonic signature distinguishes pediatric and adult rhabdoid tumors from other SMARCB1-deficient cancers. *Oncotarget,* 8**,** 34245.

RICHLY, H., ALOIA, L. & DI CROCE, L. 2011. Roles of the Polycomb group proteins in stem cells and cancer. *Cell death & disease,* 2**,** e204.

RIMKUS, T. K., CARPENTER, R. L., QASEM, S., CHAN, M. & LO, H.-W. 2016. Targeting the sonic hedgehog signaling pathway: review of smoothened and GLI inhibitors. *Cancers,* 8**,** 22.

ROBERTS, C. & BIEGEL, J. 2009. The role of SMARCB1/INI1 in the development of rhabdoid tumors. *Cancer biology & therapy,* 8**,** 412-416.

ROBERTS, C. W., GALUSHA, S. A., MCMENAMIN, M. E., FLETCHER, C. D. & ORKIN, S. H. 2000. Haploinsufficiency of Snf5 (integrase interactor 1) predisposes to malignant rhabdoid tumors in mice. *Proceedings of the National Academy of Sciences,* 97**,** 13796-13800.

ROBERTS, C. W., LEROUX, M. M., FLEMING, M. D. & ORKIN, S. H. 2002. Highly penetrant, rapid tumorigenesis through conditional inversion of the tumor suppressor gene Snf5. *Cancer cell,* 2**,** 415-425.

ROBERTS, C. W. & ORKIN, S. H. 2004. The SWI/SNF complex—chromatin and cancer. *Nature Reviews Cancer,* 4**,** 133.

RORKE, L. B., PACKER, R. J. & BIEGEL, J. A. 1996. Central nervous system atypical teratoid/rhabdoid tumors of infancy and childhood: definition of an entity. *Journal of neurosurgery,* 85**,** 56-65.

RYAN, M. P., JONES, R. & MORSE, R. H. 1998. SWI-SNF complex participation in transcriptional activation at a step subsequent to activator binding. *Molecular and cellular biology,* 18**,** 1774-1782.

RYCAJ, K. & TANG, D. G. 2015. Cell-of-origin of cancer versus cancer stem cells: assays and interpretations. *Cancer research,* 75**,** 4003-4011.

SAHA, A., WITTMEYER, J. & CAIRNS, B. R. 2005. Chromatin remodeling through directional DNA translocation from an internal nucleosomal site. *Nature Structural and Molecular Biology,* 12**,** 747.

SAHA, A., WITTMEYER, J. & CAIRNS, B. R. 2006. Chromatin remodelling: the industrial revolution of DNA around histones. *Nature reviews Molecular cell biology,* 7**,** 437.

SCHLESINGER, Y., STRAUSSMAN, R., KESHET, I., FARKASH, S., HECHT, M., ZIMMERMAN, J., EDEN, E., YAKHINI, Z., BEN-SHUSHAN, E. & REUBINOFF, B. E. 2007. Polycomb-mediated methylation on Lys27 of histone H3 pre-marks genes for de novo methylation in cancer. *Nature genetics,* 39**,** 232.

SCHNEPPENHEIM, R., FRÜHWALD, M. C., GESK, S., HASSELBLATT, M., JEIBMANN, A., KORDES, U., KREUZ, M., LEUSCHNER, I., SUBERO, J. I. M. & OBSER, T. 2010. Germline nonsense mutation and somatic inactivation of SMARCA4/BRG1 in a family with rhabdoid tumor predisposition syndrome. *The American Journal of Human Genetics,* 86**,** 279-284.

SCHULTE, J., LINDNER, S., BOHRER, A., MAURER, J., DE PRETER, K., LEFEVER, S., HEUKAMP, L., SCHULTE, S., MOLENAAR, J. & VERSTEEG, R. 2013. MYCN and ALKF1174L are sufficient to drive neuroblastoma development from neural crest progenitor cells. *Oncogene,* 32**,** 1059.

SCHWALBE, E. C., WILLIAMSON, D., LINDSEY, J. C., HAMILTON, D., RYAN, S. L., MEGAHED, H., GARAMI, M., HAUSER, P., DEMBOWSKA-BAGINSKA, B. & PEREK, D. 2013. DNA methylation profiling of medulloblastoma allows robust subclassification and improved outcome prediction using formalin-fixed biopsies. *Acta neuropathologica,* 125**,** 359-371.

SÉVENET, N., SHERIDAN, E., AMRAM, D., SCHNEIDER, P., HANDGRETINGER, R. & DELATTRE, O. 1999. Constitutional mutations of the hSNF5/INI1 gene predispose to a variety of cancers. *The American Journal of Human Genetics,* 65**,** 1342-1348.

SHAHEEN, S., AHMED, M., LORENZI, F. & NATERI, A. S. 2016. Spheroid-formation (Colonosphere) assay for in vitro assessment and expansion of stem cells in colon cancer. *Stem Cell Reviews and Reports,* 12**,** 492-499.

SHAIN, A. H. & POLLACK, J. R. 2013. The spectrum of SWI/SNF mutations, ubiquitous in human cancers. *PloS one,* 8**,** e55119.

SHAN, T., LIU, W. & KUANG, S. 2013. Fatty acid binding protein 4 expression marks a population of adipocyte progenitors in white and brown adipose tissues. *The FASEB Journal,* 27**,** 277-287.

SHARPLESS, N. E. & DEPINHO, R. A. 1999. The INK4A/ARF locus and its two gene products. *Current opinion in genetics & development,* 9**,** 22-30.

SHENGHUI, H., NAKADA, D. & MORRISON, S. J. 2009. Mechanisms of stem cell self-renewal. *Annual Review of Cell and Developmental,* 25**,** 377-406.

SHIGEISHI, H., BIDDLE, A., GAMMON, L., EMICH, H., RODINI, C. O., GEMENETZIDIS, E., FAZIL, B., SUGIYAMA, M., KAMATA, N. & MACKENZIE, I. C. 2013. Maintenance of stem cell self‐renewal in head and neck cancers requires actions of GSK3β influenced by CD44 and RHAMM. *Stem Cells,* 31**,** 2073-2083.

SHIRATSUCHI, H., OSHIRO, Y., SAITO, T., ITAKURA, E., KINOSHITA, Y., TAMIYA, S., ODA, Y., KOMIYAMA, S. & TSUNEYOSHI, M. 2001. Cytokeratin subunits of inclusion bodies in rhabdoid cells: immunohistochemical and clinicopathological study of malignant rhabdoid tumor and epithelioid sarcoma. *International journal of surgical pathology,* 9**,** 37-48.

SIDDIQUE, H. R., PARRAY, A., TARAPORE, R. S., WANG, L., MUKHTAR, H., KARNES, R. J., DENG, Y., KONETY, B. R. & SALEEM, M. 2013. BMI1 polycomb group protein acts as a master switch for growth and death of tumor cells: regulates TCF4-transcriptional factor-induced BCL2 signaling. *PloS one,* 8**,** e60664.

SIDDIQUE, H. R. & SALEEM, M. 2012. Role of BMI1, a stem cell factor, in cancer recurrence and chemoresistance: preclinical and clinical evidences. *Stem cells,* 30**,** 372-378.

SIGAUKE, E., RAKHEJA, D., MADDOX, D. L., HLADIK, C. L., WHITE III, C. L., TIMMONS, C. F. & RAISANEN, J. 2006. Absence of expression of SMARCB1/INI1 in malignant rhabdoid tumors of the central nervous system, kidneys and soft tissue: an immunohistochemical study with implications for diagnosis. *Modern pathology,* 19**,** 717.

SILVEIRA E SOUZA, A. M. M., MAZUCATO, V. M., JAMUR, M. C. & OLIVER, C. 2011. Lipid rafts in mast cell biology. *Journal of lipids,* 2011.

SINGH, S. K., HAWKINS, C., CLARKE, I. D., SQUIRE, J. A., BAYANI, J., HIDE, T., HENKELMAN, R. M., CUSIMANO, M. D. & DIRKS, P. B. 2004. Identification of human brain tumour initiating cells. *nature,* 432**,** 396.

SINGHAL, N., GRAUMANN, J., WU, G., ARAÚZO-BRAVO, M. J., HAN, D. W., GREBER, B., GENTILE, L., MANN, M. & SCHÖLER, H. R. 2010. Chromatin-remodeling components of the BAF complex facilitate reprogramming. *Cell,* 141**,** 943-955.

SOKPOR, G., XIE, Y., ROSENBUSCH, J. & TUOC, T. 2017. Chromatin remodeling BAF (SWI/SNF) complexes in neural development and disorders. *Frontiers in molecular neuroscience,* 10**,** 243.

SONG, L.-B., ZENG, M.-S., LIAO, W.-T., ZHANG, L., MO, H.-Y., LIU, W.-L., SHAO, J.-Y., WU, Q.-L., LI, M.-Z. & XIA, Y.-F. 2006. Bmi-1 is a novel molecular marker of nasopharyngeal carcinoma progression and immortalizes primary human nasopharyngeal epithelial cells. *Cancer research,* 66**,** 6225-6232.

SPARMANN, A. & VAN LOHUIZEN, M. 2006. Polycomb silencers control cell fate, development and cancer. *Nature Reviews Cancer,* 6**,** 846.

SREDNI, S. T. & TOMITA, T. 2015. Rhabdoid tumor predisposition syndrome. *Pediatric and Developmental Pathology,* 18**,** 49-58.

SRINIVASAN, M., BHARALI, D. J., SUDHA, T., KHEDR, M., GUEST, I., SELL, S., GLINSKY, G. V. & MOUSA, S. A. 2017. Downregulation of Bmi1 in breast cancer stem cells suppresses tumor growth and proliferation. *Oncotarget,* 8**,** 38731.

SUBRAMANIAN, A., TAMAYO, P., MOOTHA, V. K., MUKHERJEE, S., EBERT, B. L., GILLETTE, M. A., PAULOVICH, A., POMEROY, S. L., GOLUB, T. R., LANDER, E. S. & MESIROV, J. P. 2005. Gene set enrichment analysis: a knowledge-based approach for interpreting genome-wide expression profiles. *Proc Natl Acad Sci U S A,* 102**,** 15545-50.

SUGIMOTO, M., KOHASHI, K., ITSUMI, M., SHIOTA, M., ABE, T., YAMADA, Y., KUROIWA, K., NAITO, S. & ODA, Y. 2016. Epithelial to mesenchymal transition in clear cell renal cell carcinoma with rhabdoid features. *Pathobiology,* 83**,** 277-286.

SUGIMOTO, T., HOSOI, H., HORII, Y., ISHIDA, H., MINE, H., TAKAHASHI, K., ABE, T., OHTA, S. & SAWADA, T. 1999. Malignant rhabdoid‐tumor cell line showing neural and smooth‐muscle‐cell phenotypes. *International journal of cancer,* 82**,** 678-686.

SULTAN, I., QADDOUMI, I., RODRÍGUEZ‐GALINDO, C., NASSAN, A. A., GHANDOUR, K. & AL‐HUSSAINI, M. 2010. Age, stage, and radiotherapy, but not primary tumor site, affects the outcome of patients with malignant rhabdoid tumors. *Pediatric blood & cancer,* 54**,** 35-40.

SUNG, K. W., DO HOON LIM, E. S. Y., CHOI, Y. B., LEE, J. W., YOO, K. H., KOO, H. H., KIM, J. H., SUH, Y.-L., JOUNG, Y. S. & SHIN, H. J. 2016. Tandem high-dose chemotherapy and autologous stem cell transplantation for atypical teratoid/rhabdoid tumor. *Cancer research and treatment: official journal of Korean Cancer Association,* 48**,** 1408.

SUVÀ, M. L., RIGGI, N. & BERNSTEIN, B. E. 2013. Epigenetic reprogramming in cancer. *Science,* 339**,** 1567-1570.

SUZUKI, A., OHTA, S. & SHIMADA, M. 1997. Gene expression of malignant rhabdoid tumor cell lines by reverse transcriptase-polymerase chain reaction. *Diagnostic molecular pathology: the American journal of surgical pathology, part B,* 6**,** 326-332.

TAIPALE, J. & BEACHY, P. A. 2001. The Hedgehog and Wnt signalling pathways in cancer. *nature,* 411**,** 349.

TAKEBAYASHI, H., OHTSUKI, T., UCHIDA, T., KAWAMOTO, S., OKUBO, K., IKENAKA, K., TAKEICHI, M., CHISAKA, O. & NABESHIMA, Y.-I. 2002. Non-overlapping expression of Olig3 and Olig2 in the embryonic neural tube. *Mechanisms of development,* 113**,** 169-174.

TAMAYO, P., SCANFELD, D., EBERT, B. L., GILLETTE, M. A., ROBERTS, C. W. & MESIROV, J. P. 2007. Metagene projection for cross-platform, cross-species characterization of global transcriptional states. *Proceedings of the National Academy of Sciences,* 104**,** 5959-5964.

TANG, L., NOGALES, E. & CIFERRI, C. 2010. Structure and function of SWI/SNF chromatin remodeling complexes and mechanistic implications for transcription. *Progress in biophysics and molecular biology,* 102**,** 122-128.

TAYLOR, M. D., GOKGOZ, N., ANDRULIS, I. L., MAINPRIZE, T. G., DRAKE, J. M. & RUTKA, J. T. 2000. Familial posterior fossa brain tumors of infancy secondary to germline mutation of the hSNF5 gene. *The American Journal of Human Genetics,* 66**,** 1403-1406.

TAYLOR, M. D., NORTHCOTT, P. A., KORSHUNOV, A., REMKE, M., CHO, Y.-J., CLIFFORD, S. C., EBERHART, C. G., PARSONS, D. W., RUTKOWSKI, S. & GAJJAR, A. 2012. Molecular subgroups of medulloblastoma: the current consensus. *Acta neuropathologica,* 123**,** 465-472.

TEKAUTZ, T. M., FULLER, C. E., BLANEY, S., FOULADI, M., BRONISCER, A., MERCHANT, T. E., KRASIN, M., DALTON, J., HALE, G. & KUN, L. E. 2005. Atypical teratoid/rhabdoid tumors (ATRT): improved survival in children 3 years of age and older with radiation therapy and high-dose alkylator-based chemotherapy. *Journal of Clinical Oncology,* 23**,** 1491-1499.

TEN BERGE, D., KUREK, D., BLAUWKAMP, T., KOOLE, W., MAAS, A., EROGLU, E., SIU, R. K. & NUSSE, R. 2011. Embryonic stem cells require Wnt proteins to prevent differentiation to epiblast stem cells. *Nature cell biology,* 13**,** 1070.

TESHIMA, K., NARA, M., WATANABE, A., ITO, M., IKEDA, S., HATANO, Y., OSHIMA, K., SETO, M., SAWADA, K. & TAGAWA, H. 2014. Dysregulation of BMI1 and microRNA-16 collaborate to enhance an anti-apoptotic potential in the side population of refractory mantle cell lymphoma. *Oncogene,* 33**,** 2191.

TOLSTORUKOV, M. Y., SANSAM, C. G., LU, P., KOELLHOFFER, E. C., HELMING, K. C., ALVER, B. H., TILLMAN, E. J., EVANS, J. A., WILSON, B. G. & PARK, P. J. 2013. Swi/Snf chromatin remodeling/tumor suppressor complex establishes nucleosome occupancy at target promoters. *Proceedings of the National Academy of Sciences,* 110**,** 10165-10170.

TOMLINSON, G. E., BRESLOW, N. E., DOME, J., GUTHRIE, K. A., NORKOOL, P., LI, S., THOMAS, P. R., PERLMAN, E., BECKWITH, J. B. & D'ANGIO, G. J. 2005. Rhabdoid tumor of the kidney in the National Wilms' Tumor Study: age at diagnosis as a prognostic factor. *Journal of clinical oncology,* 23**,** 7641-7645.

TORCHIA, J., GOLBOURN, B., FENG, S., HO, K. C., SIN-CHAN, P., VASILJEVIC, A., NORMAN, J. D., GUILHAMON, P., GARZIA, L. & AGAMEZ, N. R. 2016.

Integrated (epi)-genomic analyses identify subgroup-specific therapeutic targets in CNS rhabdoid tumors. *Cancer cell,* 30**,** 891-908.

TORCHIA, J., PICARD, D., LAFAY-COUSIN, L., HAWKINS, C. E., KIM, S.-K., LETOURNEAU, L., RA, Y.-S., HO, K. C., CHAN, T. S. Y. & SIN-CHAN, P. 2015. Molecular subgroups of atypical teratoid rhabdoid tumours in children: an integrated genomic and clinicopathological analysis. *The lancet oncology,* 16**,** 569-582.

TOTH, G., ZRALY, C. B., THOMSON, T. L., JONES, C., LAPETINO, S., MURASKAS, J., ZHANG, J. & DINGWALL, A. K. 2011. Congenital anomalies and rhabdoid tumor associated with 22q11 germline deletion and somatic inactivation of the SMARCB1 tumor suppressor. *Genes, Chromosomes and Cancer,* 50**,** 379-388.

TSOKOS, M., KOURAKLIS, G., CHANDRA, R., BHAGAVAN, B. & TRICHE, T. 1989. Malignant rhabdoid tumor of the kidney and soft tissues. Evidence for a diverse morphological and immunocytochemical phenotype. *Archives of pathology & laboratory medicine,* 113**,** 115-120.

VAN DER LUGT, N., DOMEN, J., LINDERS, K., VAN ROON, M., ROBANUS-MAANDAG, E., TE RIELE, H., VAN DER VALK, M., DESCHAMPS, J., SOFRONIEW, M. & VAN LOHUIZEN, M. 1994. Posterior transformation, neurological abnormalities, and severe hematopoietic defects in mice with a targeted deletion of the bmi-1 proto-oncogene. *Genes & development,* 8**,** 757-769.

VARAMBALLY, S., DHANASEKARAN, S. M., ZHOU, M., BARRETTE, T. R., KUMAR-SINHA, C., SANDA, M. G., GHOSH, D., PIENTA, K. J., SEWALT, R. G. & OTTE, A. P. 2002. The polycomb group protein EZH2 is involved in progression of prostate cancer. *Nature,* 419**,** 624.

VENNETI, S., LE, P., MARTINEZ, D., EATON, K. W., SHYAM, N., JORDAN-SCIUTTO, K. L., PAWEL, B., BIEGEL, J. A. & JUDKINS, A. R. 2011a. p16INK4A and p14ARF tumor suppressor pathways are deregulated in malignant rhabdoid tumors. *Journal of Neuropathology & Experimental Neurology,* 70**,** 596-609.

VENNETI, S., LE, P., MARTINEZ, D., XIE, S. X., SULLIVAN, L. M., RORKE-ADAMS, L. B., PAWEL, B. & JUDKINS, A. R. 2011b. Malignant rhabdoid tumors express stem cell factors, which relate to the expression of EZH2 and Id proteins. *The American journal of surgical pathology,* 35**,** 1463-1472.

VERSTEEGE, I., MEDJKANE, S., ROUILLARD, D. & DELATTRE, O. 2002. A key role of the hSNF5/INI1 tumour suppressor in the control of the G1-S transition of the cell cycle. *Oncogene,* 21**,** 6403.

VERSTEEGE, I., SÉVENET, N., LANGE, J., ROUSSEAU-MERCK, M.-F., AMBROS, P., HANDGRETINGER, R., AURIAS, A. & DELATTRE, O. 1998. Truncating mutations of hSNF5/INI1 in aggressive paediatric cancer. *Nature,* 394**,** 203.

VITTE, J., GAO, F., COPPOLA, G., JUDKINS, A. R. & GIOVANNINI, M. 2017. Timing of Smarcb1 and Nf2 inactivation determines schwannoma versus rhabdoid tumor development. *Nature communications,* 8**,** 300.

VON HOFF, K., HINKES, B., DANNENMANN‐STERN, E., VON BUEREN, A. O., WARMUTH‐METZ, M., SOERENSEN, N., EMSER, A., ZWIENER, I., SCHLEGEL, P. G. & KUEHL, J. 2011. Frequency, risk‐factors and survival of children with atypical teratoid rhabdoid tumors (AT/RT) of the CNS diagnosed between 1988 and 2004, and registered to the German HIT database. *Pediatric blood & cancer,* 57**,** 978-985.

WAELTER, S., BOEDDRICH, A., LURZ, R., SCHERZINGER, E., LUEDER, G., LEHRACH, H. & WANKER, E. E. 2001. Accumulation of mutant huntingtin fragments in aggresome-like inclusion bodies as a result of insufficient protein degradation. *Molecular biology of the cell,* 12**,** 1393-1407.

WANG, M. C., LI, C. L., CUI, J., JIAO, M., WU, T., JING, L. & NAN, K. J. 2015. BMI-1, a promising therapeutic target for human cancer. *Oncology letters,* 10**,** 583-588.

WANG, X., SANSAM, C. G., THOM, C. S., METZGER, D., EVANS, J. A., NGUYEN, P. T. & ROBERTS, C. W. 2009. Oncogenesis caused by loss of the SNF5 tumor suppressor is dependent on activity of BRG1, the ATPase of the SWI/SNF chromatin remodeling complex. *Cancer research,* 69**,** 8094-8101.

WANG, X., VENUGOPAL, C., MANORANJAN, B., MCFARLANE, N., O'FARRELL, E., NOLTE, S., GUNNARSSON, T., HOLLENBERG, R., KWIECIEN, J. & NORTHCOTT, P. 2012. Sonic hedgehog regulates Bmi1 in human medulloblastoma brain tumor-initiating cells. *Oncogene,* 31**,** 187.

WEBER, J. D., TAYLOR, L. J., ROUSSEL, M. F., SHERR, C. J. & BAR-SAGI, D. 1999. Nucleolar Arf sequesters Mdm2 and activates p53. *Nature cell biology,* 1**,** 20.

WEISWALD, L.-B., BELLET, D. & DANGLES-MARIE, V. 2015. Spherical cancer models in tumor biology. *Neoplasia,* 17**,** 1-15.

WHITE, F. V., DEHNER, L. P., BELCHIS, D. A., CONARD, K., DAVIS, M. M., STOCKER, J. T., ZUPPAN, C. W., BIEGEL, J. A. & PERLMAN, E. J. 1999. Congenital disseminated malignant rhabdoid tumor: a distinct clinicopathologic entity demonstrating abnormalities of chromosome 22q11. *The American journal of surgical pathology,* 23**,** 249-256.

WILSON, B. G. & ROBERTS, C. W. 2011. SWI/SNF nucleosome remodellers and cancer. *Nature reviews Cancer,* 11**,** 481.

WILSON, B. G., WANG, X., SHEN, X., MCKENNA, E. S., LEMIEUX, M. E., CHO, Y.-J., KOELLHOFFER, E. C., POMEROY, S. L., ORKIN, S. H. & ROBERTS, C. W. 2010a. Epigenetic antagonism between polycomb and SWI/SNF complexes during oncogenic transformation. *Cancer cell,* 18**,** 316-328.

WILSON, B. G., WANG, X., SHEN, X., MCKENNA, E. S., LEMIEUX, M. E., CHO, Y. J., KOELLHOFFER, E. C., POMEROY, S. L., ORKIN, S. H. & ROBERTS, C. W. 2010b. Epigenetic antagonism between polycomb and SWI/SNF complexes during oncogenic transformation. *Cancer Cell,* 18**,** 316-28.

WITZE, E. S., OLD, W. M., RESING, K. A. & AHN, N. G. 2007. Mapping protein post-translational modifications with mass spectrometry. *Nature methods,* 4**,** 798.

WOEHRER, A., SLAVC, I., WALDHOER, T., HEINZL, H., ZIELONKE, N., CZECH, T., BENESCH, M., HAINFELLNER, J. A. & HABERLER, C. 2010. Incidence of atypical teratoid/rhabdoid tumors in children. *Cancer,* 116**,** 5725-5732.

YANG, G.-F., HE, W.-P., CAI, M.-Y., HE, L.-R., LUO, J.-H., DENG, H.-X., GUAN, X.-Y., ZENG, M.-S., ZENG, Y.-X. & XIE, D. 2010. Intensive expression of Bmi-1 is a new independent predictor of poor outcome in patients with ovarian carcinoma. *BMC cancer,* 10**,** 133.

YANG, K., WANG, X., ZHANG, H., WANG, Z., NAN, G., LI, Y., ZHANG, F., MOHAMMED, M. K., HAYDON, R. C. & LUU, H. H. 2016. The evolving roles of canonical WNT signaling in stem cells and tumorigenesis: implications in targeted cancer therapies. *Laboratory investigation,* 96**,** 116.

YANG, Z.-J., ELLIS, T., MARKANT, S. L., READ, T.-A., KESSLER, J. D., BOURBOULAS, M., SCHÜLLER, U., MACHOLD, R., FISHELL, G. & ROWITCH, D. H. 2008. Medulloblastoma can be initiated by deletion of Patched in lineage-restricted progenitors or stem cells. *Cancer cell,* 14**,** 135-145.

ZAKRZEWSKA, M., WOJCIK, I., ZAKRZEWSKI, K., POLIS, L., GRAJKOWSKA, W., ROSZKOWSKI, M., AUGELLI, B. J., LIBERSKI, P. P. & RIESKE, P. 2005. Mutational analysis of hSNF5/INI1 and TP53 genes in choroid plexus carcinomas. *Cancer Genet Cytogenet,* 156**,** 179-82.

ZECHNER, D., FUJITA, Y., HÜLSKEN, J., MÜLLER, T., WALTHER, I., TAKETO, M. M., CRENSHAW III, E. B., BIRCHMEIER, W. & BIRCHMEIER, C. 2003. β-Catenin signals regulate cell growth and the balance between progenitor cell expansion and differentiation in the nervous system. *Developmental biology,* 258**,** 406-418.

ZHAI, R., TANG, F., GONG, J., ZHANG, J., LEI, B., LI, B., WEI, Y., LIANG, X., TANG, B. & HE, S. 2016. The relationship between the expression of USP22, BMI1, and EZH2 in hepatocellular carcinoma and their impacts on prognosis. *OncoTargets and therapy,* 9**,** 6987.

ZHANG, K., LI, L., HUANG, C., SHEN, C., TAN, F., XIA, C., LIU, P., ROSSANT, J. & JING, N. 2010. Distinct functions of BMP4 during different stages of mouse ES cell neural commitment. *Development,* 137**,** 2095-2105.

ZHANG, Z.-K., DAVIES, K. P., ALLEN, J., ZHU, L., PESTELL, R. G., ZAGZAG, D. & KALPANA, G. V. 2002. Cell cycle arrest and repression of cyclin D1 transcription by INI1/hSNF5. *Molecular and cellular biology,* 22**,** 5975-5988.

ZOFALL, M., PERSINGER, J., KASSABOV, S. R. & BARTHOLOMEW, B. 2006. Chromatin remodeling by ISW2 and SWI/SNF requires DNA translocation inside the nucleosome. *Nature Structural and Molecular Biology,* 13**,** 339.

ZURAWEL, R. H., CHIAPPA, S. A., ALLEN, C. & RAFFEL, C. 1998. Sporadic medulloblastomas contain oncogenic β-catenin mutations. *Cancer research,* 58**,** 896-899.